BEST AVAILABLE IMAGES

Defective images within this document are accurate representations of the original documents submitted by the applicant.

Defects in the images may include (but are not limited to):

- BLACK BORDERS
- TEXT CUT OFF AT TOP, BOTTOM OR SIDES
- FADED TEXT
- ILLEGIBLE TEXT
- SKEWED/SLANTED IMAGES
- COLORED PHOTOS
- BLACK OR VERY BLACK AND WHITE DARK PHOTOS
- GRAY SCALE DOCUMENTS

IMAGES ARE BEST AVAILABLE COPY.

As rescanning documents *will not* correct images, please do not report the images to the Image Problem Mailbox.

PATENT
Docket No.: **201487/1070 (KUV-101PCT-US)**

IN THE UNITED STATES PATENT AND TRADEMARK OFFICE

Applicant(s) :	Amagai et al.	)	Examiner: Q. Janice Li
Serial No. :	09/937,739 based on PCT/JP00/02023	)	Art Unit: 1632
Cnfrm. No. :	5390	)	
Filed :	March 30, 2000	)	
For :	AUTOIMMUNE DISEASE MODEL ANIMAL	)	

SECOND DECLARATION OF MASAYUKI AMAGAI UNDER 37 CFR § 1.132

Mail Stop **RCE**
Commissioner for Patents
P.O. Box 1450
Alexandria, VA 22313-1450

Sir:

I, MASAYUKI AMAGAI, pursuant to 37 C.F.R. § 1.132, declare that:

1. I received an M.D. from Keio University School of Medicine, Tokyo, Japan, and a Ph.D. from Keio University Graduate School of Medicine, Tokyo, Japan.

2. I was a Visiting Research Fellow at Dermatology Branch, National Cancer Institute, National Institutes of Health, USA, from 1989 to 1992, and an Instructor at the Department of Dermatology, Ehime University School of Medicine, Japan, from January, 1996 to July, 1996.

3. I am currently an Assistant Professor in the Department of Dermatology, Keio University School of Medicine, Tokyo, Japan.

4. I am a co-inventor of the above-identified patent application.

5. I present this declaration to demonstrate that it is possible to practice my invention as taught in the above-referenced application, and furthermore, that a skilled scientist would be able to do so without undue experimentation. In particular, I will show that it is well within the ability of a skilled scientist to prepare an animal deficient in an

antigen related to an autoimmune disease, *i.e.*, a "autoantigen knockout" animal, using routine techniques well-known in the art, and thus, having read my patent application, a skilled scientist would be fully able to make and use my invention as claimed.

6. For example, the autoantigen knockout mouse line lacking desmoglein 3 ("Dsg3"), the target antigen for pemphigus vulgaris disclosed in the working examples in my patent application, was prepared by a method well-known in the art (*see* Koch *et al.*, "Targeted Disruption of the Pemphigus Vulgaris Antigen (Desmoglein 3) Gene in Mice Causes Loss of Keratinocyte Cell Adhesion with a Phenotype Similar to Pemphigus Vulgaris," *J Cell Biology* 137(5):1091-1102 (1997), attached hereto as Exhibit 1). Briefly, this involved creating a target vector to delete the coding sequence from the first exon of the *Dsg3* gene by homologous recombination, thereby inactivating the gene (*Id.* at p. 1095, left col. 1st two full para.). To carry this out, a vector containing a neo-cassette was inserted in place of a portion of the 3' end of the first exon of *DSG3* molecule in a mouse embryonic stem ("ES") cell (*Id.*). An ES clone with a targeted allele was injected into a mouse blastocyst (*Id.* at p. 1095, left col., 3rd full para.). Chimeric F1 mice were produced from the ES clone. F1 mice detected by Southern blot to be positive for the targeted mutation (*i.e.*, Dsg3+/-) were intercrossed to produce F2 mice homozygous for the mutation (*i.e.*, *Dsg3*-/-) (*Id.*). mRNA, expression tests for Dsg3 and immunofluorescence western blots using antibodies to Dsg3 were carried out to demonstrate that the *Dsg3*-/- homozygous mice did not produce any detectable Dsg3 protein. (*Id.* 1095, para. bridging left and right col.). Because the *Dsg3*-/- homozygous mice produce no Dsg3 protein, they are highly suitable for use in my invention.

7. The working example disclosed in my patent application is sufficiently illustrative such that other autoimmune/autoantigen combinations would be readily apparent to one skilled in the art. Furthermore, this approach is widely applicable to various antibody-mediated and T cell-mediated autoimmune diseases. For example, many autoimmune diseases were well characterized at the time of invention. Indeed, at the tune my invention was made, numerous autoantigens and their genes had been positively identified. Examples of specific autoimmune disease/autoantigen combinations known in the art at the time my invention was made are shown in Table 1, attached hereto as Exhibit 2. The references listed in Table 1 for autoantigens are attached hereto as Exhibit 3. In addition, a knockout animal deficient in each of the genes described in Table 1 has been made and shown to be viable. The references listed in Table 1 for autoantigen knockouts (several of which were known at

the time my invention was made), are attached hereto as Exhibit 4. This list, while not exhaustive, is indicative of the advanced state of the art in autoimmune disease identification, as well as that of applicable knockout technology, at the time my invention was made.

8. Furthermore, the ability to create knockout animals has been known and practiced for many years (*see, e.g.*, Walinski, H., "Studying Gene Function: Creating Knockout Mice," http://www.bioteach.ubc.ca/CellBiology/StudyingGeneFunction, attached hereto as Exhibit 5; Pray, L., "Refining Transgenic Mice," *The Scientist* 16(13): 34-36 (2002), attached hereto as Exhibit 6; "The Life History of the Mouse in Genetics," *Nature* 420:510-511 (2002) attached hereto as Exhibit 7, describing the history of the knockout mouse in the 1970's and 80's, and the significant improvements in the technology to date). In addition to several of the references cited above, a multitude of publications were available at the time my invention was made that describe, in detail, successful procedures for producing knockout animals (*see, e.g.*, Smith, Christopher M., "Technical Knockout," *The Scientist* 14(15):32-34 (2000), attached hereto as Exhibit 8; Rajewsky *et al.*, "Molecular Medicine in Genetically Engineered Animals," *J Clin Invest* 98(3):600-603 (1996), attached hereto as Exhibit 9; Wu *et al.*, "Double Replacement: Strategy for Efficient Introduction of Subtle Mutations into the Murine *Col1a-1* Gene by Homologous Recombination in Embryonic Stem Cells," *Proc Natl Acad Sci USA* 91:2819-2823 (1994), attached hereto as Exhibit 10; Nagy *et al.*, "Derivation of Completely Cell Culture-Derived Mice from Early Passage Embryonic Stem Cells," *Proc Natl Acid Sci USA* 90:8424-8428 (1993), attached hereto as Exhibit 11; and Orban *et al.*, "Tissue- and Site-Specific DNA Recombination in Transgenic Mice," *Proc Natl Acad Sci USA* 89:6861-6865 (1992), attached hereto as Exhibit 12). Rajewsky, fox example, teaches a method of producing knockout animals by mutagenesis that involves the use of the bacteriophage *Cre*-loxP recombination system to produce gene deletions, replacements, insertions, and even cell- and tissue-specific mutations that has been shown to work well in mice (*see* Rajewsky at 601, left col., 1st full para.). Given the detailed guidance for making knockout animals that was available when my invention was made, combined with the high degree of success described therein, it is apparent that a skilled scientist would have known how to make other autoantigen donor animals with which to practice my invention.

9. The production of knockout animals, mice and rats in particular, is a technique that is highly valuable for studying genetic function and the process of disease (*see*

Walinski, para. bridging pp. 4-5). Furthermore, given the refinement of genetic engineering techniques over the last 20 years, it is expected that knockout mice will continue to be an invaluable experimental tool in basic and applied research (*Id.*).

10. Turning to the question of whether the effect of the knockout on the viability of the resulting phenotype creates a barrier to practicing my invention, it is clear that my invention is not applicable to the study of all autoimmune diseases and/or all autoantigens. Indeed, some autoantigen knockout animals may not be viable. However, one skilled in the art would readily recognize that the "antigen of an autoimmune disease" cannot constitute an essential protein if the knockout animal is to be viable. Furthermore, two generalizations have emerged from examining knockout mice: 1) knockout mice are often surprisingly unaffected by their deficiency, as many genes turn out not to be indispensable; 2) most genes are pleotropic, *i.e.*, they are expressed in different tissues in different ways and at different times in development (*see* Kimball, J., *Transgenic Animals*, pg. 5 of 6, viewed April 14, 2004 at http://users.com/jkimball.ma.ultranet/BiologyPages/T/TransgenicAnimals.html, attached hereto as Exhibit 13). Thus, one skilled in the art would have a high expectation of producing a viable knockout animal using the techniques known in the art. Moreover, a skilled scientist can distinguish between operative and inoperative embodiments with only minimal effort. A skilled scientist would also know that the problem of lethal homozygous knockouts can be addressed using a modification of the *Cre*-lox recombination method, a technique that involves introducing a construct into the null background to rescue the developmental defect, but not the downstream functions of the deleted gene (*see* Smith at pg. 34, para. bridging middle to right col.). In addition, because the *Cre*-lox system removes the need for the selection marker DNA sequence(s) required by the classical homologous recombination method of knockout production, the potential for unexpected mutant phenotypes can be reduced or removed by using the *Cre*-lox knockout production technique as an alternative to homologous recombination (Rajewsky at pg. 600, last full para. to top of pg. 601).

11. The technique of "adoptive transfer," in which immune cells from a donor of interest are transplanted to a host in which the immune responsiveness has been eliminated, is a well-known method used for the study of immune cells and of the cellular interactions required in an immune response (*see* Kuby, J., *Immunology* Chap. 2, pg. 24, Freeman and Company, New York (1992), attached hereto as Exhibit 14). The literature is replete with reports in which adoptive transfer has been used to transfer immune cells to a

host individual for immunological investigations of disease conditions and for *in vivo* therapeutic treatment. (*See, e.g.*, abstracts of numerous articles using the adoptive transfer methodology from 1983 to 2001, attached hereto as Exhibit 15). Therefore, one of ordinary skill in the art would have been fully familiar with adoptive transfer techniques and would have a high expectation of success for this technique when used in accordance with the disclosure of my patent application.

12. Moreover, the claimed recipient animal need not exhibit a phenotype corresponding to a particular autoimmune disease. Rather, all that is required by the claimed invention is that the recipient animal "produces an antibody reactive to the antigen protein and/or has activated T cells reactive to the antigen protein" (*see* claims 2 and 3). Therefore, the display of symptoms or characteristics of a particular autoimmune disease is not an element of the claimed invention. Rather, an essential feature of the present invention is the creation of an animal that produces an antibody against a self-antigen and the use of such an animal in the study of autoimmune conditions. Even in autoimmune diseases that involve multiple antigens, my invention remains applicable for producing antibodies against one or a few autoantigens, thereby inducing an autoimmune response against these antigens in the recipient. Therefore, in this respect, autoimmune animal models made according to the present invention would have great utility in the investigation of disease states and potential treatments thereof.

13. In assessing the degree of experimentation required to practice my invention, it should be considered, first of all, that the preparation of knockout animals has reached a level of high predictability as evidenced by the availability of specific vectors designed for the preparation of knockouts, the rise of commercial enterprises that offer preparation of knockout animals on an as-needed basis (*see e.g.*, the web pages of inGenious Targeting Laboratory, Inc.; genOway; and Genomatix, Ltd., offering knockout vectors and knockout mice and rat provider services, attached hereto as Exhibits 16-18, respectively, and Smith at pg. 33, "Products and Services for Knockout Technology" chart), and the numerous peer review journals that describe making and/or using knockout animals, including, but limited to, those named herein above. Secondly, it is important to note that a major hurdle in developing animal models of autoimmune diseases has been overcoming the self-tolerance component of the homeostatic system (*see, e.g.*, Amagai *et al.*, "Use of Autoantigen Knockout Mice in Developing an Active Autoimmune Disease Model for Pemphigus," *J Clin Invest* 105(5):25-631 (2000), at pg. 625, left col., 1st full para., attached hereto as Exhibit 19).

An example of this problem is provided in my patent application at Example 2, which describes my initial failure in producing an autoimmune response using the conventional multiple injection technique in a wild-type (*i.e.*, *Dsg3*+/+) mouse. My invention circumvents this long-standing problem by immunizing autoantigen knockout mice with the autoantigen, then transferring their splenocytes to mice that express the autoantigen. Thus, the effort in making an autoantigen knockout animal is offset by the tremendous advantage to be gained over prior art methods in using my invention for making an autoimmune model without the complications of antigen self-tolerance.

14. Therefore, given the knowledge of a skilled scientist at the time my invention was made as to the identification and characterization of numerous autoimmune diseases and the responsible autoimmune/autoantigen combinations, the availability of successful, predictable methods for production of knockout animals, rodents in particular, I believe a skilled scientist, having read my patent application, would be fully able to prepare or obtain, without undue experimentation, an autoimmune antigen knockout animal suitable for use in my invention.

15. I hereby declare that all statements made herein of my own knowledge are true; and further that these statements were made with the knowledge that willful false statements and the like so made are punishable by fine or imprisonment, or both, under Section 1001 of Title 18 of the United States Code and that any such willful false statements may jeopardize the validity of the application or any patent issued thereon.

Date : June 24, 2004

Masayuki Amagai

Masayuki Amagai, M.D., Ph.D.

Targeted Disruption of the Pemphigus Vulgaris Antigen (Desmoglein 3) Gene in Mice Causes Loss of Keratinocyte Cell Adhesion with a Phenotype Similar to Pemphigus Vulgaris

Peter J. Koch,* Mỹ G. Mahoney,* Hiroyasu Ishikawa,‡ Leena Pulkkinen,‡ Jouni Uitto,‡ Leonard Shultz,§ George F. Murphy,* Diana Whitaker-Menezes,* and John R. Stanley*

*Department of Dermatology, University of Pennsylvania School of Medicine, Philadelphia, Pennsylvania 19104; ‡Department of Dermatology and Cutaneous Biology, Jefferson Medical College, Philadelphia, Pennsylvania 19107; and §The Jackson Laboratory, Bar Harbor, Maine 04609

Abstract. In patients with pemphigus vulgaris (PV), autoantibodies against desmoglein 3 (Dsg3) cause loss of cell–cell adhesion of keratinocytes in the basal and immediate suprabasal layers of stratified squamous epithelia. The pathology, at least partially, may depend on protease release from keratinocytes, but might also result from antibodies interfering with an adhesion function of Dsg3. However, a direct role of desmogleins in cell adhesion has not been shown. To test whether Dsg3 mediates adhesion, we genetically engineered mice with a targeted disruption of the *DSG3* gene. DSG3 −/− mice had no DSG3 mRNA by RNase protection assay and no Dsg3 protein by immunofluorescence (IF) and immunoblots. These mice were normal at birth, but by 8–10 d weighed less than DSG3 +/− or +/+ littermates, and at around day 18 were grossly runted. We speculated that oral lesions (typical in PV patients) might be inhibiting food intake, causing this runting. Indeed, oropharyngeal biopsies showed erosions with histology typical of PV, including suprabasilar acantholysis and "tombstoning" of basal cells. EM showed separation of desmosomes. Traumatized skin also had crusting and suprabasilar acantholysis. Runted mice showed hair loss at weaning. The runting and hair loss phenotype of DSG3 −/− mice is identical to that of a previously reported mouse mutant, balding (*bal*). Breeding indicated that *bal* is coallelic with the targeted mutation. We also showed that *bal* mice lack Dsg3 by IF, have typical PV oral lesions, and have a DSG3 gene mutation. These results demonstrate the critical importance of Dsg3 for adhesion in deep stratified squamous epithelia and suggest that pemphigus autoantibodies might interfere directly with such a function.

DESMOSOMES are cell–cell adhesion junctions that are found in epithelia and a small number of other tissues (for review see Schwarz et al., 1990). These junctions have two basic functions: in addition to mediating cell–cell coupling, they provide anchorage for intermediate filaments via their cytoplasmic plaque and therefore function as organizational centers for part of the cytoskeleton. Given these structural features and the abundance of desmosomes in certain tissues, especially in stratified squamous epithelia, it is assumed that desmosomes are critical in providing mechanical stability to these tissues.

Two types of transmembrane proteins, desmogleins (Dsg)[1] and desmocollins (Dsc), are constitutive components of desmosomes. Both represent small families of type 1 transmembrane glycoproteins (Dsg1, Dsg2, Dsg3; Dsc1, Dsc2, Dsc3, for nomenclature see Buxton et al., 1993) that are sequence related to the previously characterized family of calcium-dependent cell adhesion molecules, the cadherins (Koch et al., 1990, 1991*a*,*b*, 1992; Goodwin et al., 1990; Amagai et al., 1991; Collins et al., 1991; Mechanic et al., 1991; Nilles et al., 1991; Parker et al., 1991; Wheeler et al., 1991; King et al., 1993; Theis et al., 1993; Troyanovsky et al., 1993; Schäfer et al., 1994; for reviews see Koch and Franke, 1994; Schmidt et al., 1994).

The members of the desmoglein and desmocollin subfamily of desmosomal cadherins show a tissue- and cell

Please address all correspondence to John R. Stanley, Department of Dermatology, University of Pennsylvania School of Medicine, 211 CRB, 415 Curie Blvd., Philadelphia, PA 19104. Tel.: (215) 898-3240. Fax: (215) 573-2033. e-mail: jrstan@mail.med.upenn.edu

G.F. Murphy and D. Whitaker-Menezes' present address is Department of Pathology, Anatomy, and Cell Biology, Jefferson Medical College, Philadelphia, PA 19107.

1. *Abbreviations used in this paper:* aa, amino acid; Dsc, desmocollin; Dsg, desmoglein; ES, embryonic stem; neo, neomycin resistance; PV, pemphigus vulgaris; PVA, PV antigen.

type–specific expression pattern (e.g., Koch et al., 1992; Arnemann et al., 1993; Theis et al., 1993; Schäfer et al., 1994, 1996; Schmidt et al., 1994; Nuber et al., 1995, 1996; Amagai et al., 1996; North et al., 1996). Some tissues, e.g., simple epithelia, express Dsg2 and Dsc2 only. In stratified squamous epithelia, however, all three desmoglein and desmocollin isoforms are present, although the expression of some of these proteins is restricted to certain strata. In human skin, for example, Dsg1 is expressed in suprabasal cell layers, Dsg2 in the basal cell layer only, and Dsg3 in the basal as well as the immediate suprabasal cell layer (Amagai et al., 1996; Schäfer et al., 1996).

In this study we focused on the biological function of one member of the desmoglein family, Dsg3. This protein has been shown to be the antigen recognized by autoantibodies from patients with the disease pemphigus vulgaris (PV), and therefore is also referred to as PV antigen (PVA) (Amagai et al., 1991).

PV is a life-threatening, autoantibody-mediated, blistering disease of the skin and mucous membranes (Stanley, 1993*a*). Blisters in these patients result from loss of keratinocyte cell-to-cell adhesion in the basal and immediate suprabasal level of stratified squamous epithelia. The typical histology of an early lesion in PV shows detachment of the epithelium just above the basal cells, usually with a few acantholytic (detached and rounded-up) cells in the blister cavity. There is no, or minimal, inflammation in an early lesion. In addition, the basal cells may detach slightly from one another while maintaining their attachment to the basement membrane, a histologic pattern referred to as a "row of tombstones" (Lever, 1965; also shown schematically in Stanley, 1993*b*). Besides the resemblance of the individual basal cells to tombstones, this designation of the histologic appearance also reflected the dismal prognosis of the disease which, before the advent of corticosteroid therapy, was almost uniformly fatal. Without therapy, patients died because these blisters rapidly lost the superficial epithelia, resulting in large areas of erosions on mucous membranes and skin. The mucous membrane lesions prevented adequate food and fluid intake, while erosions on the skin resulted in protein and electrolyte loss as well as infection. Histology of older lesions shows erosions with inflammation (which is characteristically seen in mucous membrane or skin eroded from any cause, probably secondary to infection, colonization with microbes, and/or irritation due to loss of the barrier function) and attempts at reepithelialization.

IgG autoantibodies against the cell surface of keratinocytes of stratified squamous epithelia are present in the skin and sera of PV patients, as detected by direct and indirect immunofluorescence, respectively (Stanley, 1993*a*). These antibodies are pathogenic, i.e., they cause blister formation, as proven by several lines of evidence (for review see Stanley, 1990). In general, autoantibody titer, as determined by indirect immunofluorescence, correlates with disease activity. That is, the higher the antibody titer, the more severe the disease. Furthermore, neonatal PV has been reported in infants born to mothers with active PV. As the passively transferred maternal IgG is catabolized, the infant recovers. Similarly, PV IgG passively transferred to neonatal mice causes clinically and histologically typical blisters. Finally, normal skin in organ culture incubated with PV IgG develops typical blisters, without the addition of complement or inflammatory cells.

Screening of a keratinocyte λgt11 expression library with patient sera was used to isolate cDNA encoding PVA (Amagai et al., 1991). Analysis of the predicted amino acid sequence defined PVA as Dsg3 (Buxton et al., 1993). Antibodies raised in rabbits to recombinant Dsg3, as well as patient sera, localized it, like the other desmogleins, to desmosomes, in particular to their extracellular face (Akiyama et al., 1991; Karpati et al., 1993). Recent studies have shown that antibodies against the extracellular domain of Dsg3 can cause suprabasilar blisters in neonatal mice (Amagai et al., 1992) and that the extracellular domain of Dsg3, expressed by baculovirus in Sf9 insect cells, can adsorb out all pathogenic antibodies from PV sera (Amagai et al., 1994*a*; Memar et al., 1996). Therefore, the antibodies against Dsg3 in patient sera are pathogenic. Finally, it has recently been shown that Dsg3 mRNA and antibodies to Dsg3 in patients' sera localize in epidermis to the basal and immediate suprabasal layer, exactly where blisters occur in PV (Arnemann et al., 1993; Shimizu et al., 1995; Amagai et al., 1996).

It is unclear exactly how PV autoantibodies cause loss of cell–cell adhesion. One possibility is that Dsg3 functions in cell–cell adhesion in the deep stratified squamous epithelia, and that autoantibodies from PV patients might interfere with its adhesive function. However, several points do not support such a hypothesis. First, it has been suggested that PV autoantibodies do not directly cause loss of cell adhesion, but function through stimulating release of proteases (specifically, plasminogen activator) from keratinocytes (Schiltz et al., 1978, 1979; Farb et al., 1978; Hashimoto et al., 1983, 1989; Morioka et al., 1987; Naito et al., 1989). Furthermore, although the classical cadherins (e.g., E-cadherin, N-cadherin, P-cadherin) have been directly shown to be calcium-dependent cell adhesion molecules, the desmogleins have not. Expression of classical cadherins in transfected L cells (mouse fibroblasts) mediates calcium-dependent aggregation (Nagafuchi et al., 1987). However, experiments with desmogleins do not show similar aggregation (Kowalczyk et al., 1996) nor do studies using desmocollins (Chidgey et al., 1996). Even a chimeric molecule of the extracellular domain of Dsg3 with the cytoplasmic domain of E-cadherin, which allows for proper interaction with the actin cytoskeleton through catenins (an interaction shown to be critical for E-cadherin function), mediates only weak aggregation when expressed in L cells (Amagai et al., 1994*b*). These studies suggest that Dsg3 might mediate adhesion but only does so effectively when organized with other desmosomal molecules.

Another approach to investigate whether Dsg3 is important for adhesion of keratinocytes would be to eliminate it from desmosomes in tissue. Therefore, in this study we genetically engineered a mouse with a targeted disruption of the desmoglein 3 gene (*DSG3*). We hypothesized that if the PV autoantibodies directly interfere with an adhesion function of this molecule then such a mouse might have a phenotype resembling human disease. Our findings demonstrate that Dsg3 is critical for cell adhesion in the basal and immediate suprabasilar keratinocytes, especially in the oral mucous membrane, thereby showing a differentiation- and tissue-specific adhesion function of one of the

desmogleins. Furthermore, because the pathology of these mice strikingly resembles that of humans with PV, our findings are consistent with the idea that PV autoantibodies directly interfere with this adhesive function.

Materials and Methods

Cloning and Characterization of 129/Sv DSG3 Gene

We have previously cloned partial cDNAs corresponding to mouse Dsg3 (Ishikawa et al., 1994). To initiate the cloning of the mouse *DSG3* gene, three different cDNA probes corresponding to mouse cDNA sequences were used for screening of a mouse 129/Sv genomic λFixII library (Stratagene, La Jolla, CA) (Sambrook et al., 1989). These three cDNAs, 413, 405, and 404 bp in size, respectively, corresponded to the amino-terminal, central, and carboxyl-terminal regions of the coding sequences. (These sequence data are available from EMBL/Genbank/DDBJ under accession number U86016.) A total of nine unique genomic clones were isolated and characterized by restriction enzyme digestions and Southern analysis with synthetic oligonucleotides based on exon sequences derived from the cDNA. The endonuclease digestion products were fractionated by electrophoresis on 1% agarose gels, and the sizes were estimated by comparison with standard DNA markers (New England Biolabs, Beverly, MA). Subcloning and sequencing of the genomic DNA, in comparison with cDNA sequences, allowed identification of the intron–exon borders. The sizes of the introns in the genomic DNA were determined by direct nucleotide sequencing, estimated by generating PCR products using synthetic nucleotide primers placed on the flanking exons, or by Southern blot analysis. (These sequence data [for exon 1/intron 1/exon 2] are available from EMBL/Genbank/DDBJ under accession number U86015.)

Construction of Targeting Vector

The plasmid pPNT (Tybulewicz et al., 1991), which contains a neomycin resistance (neo) and a herpes simplex virus thymidine kinase (HSV-tk) minigene (both under the control of the phosphoglycerate kinase promoter), was used to construct the targeting vector (Fig. 1 *B*). *DSG3* gene fragments were derived from two overlapping λFixII clones, both of which contained portions of exon 1. In the targeting vector the neo-cassette is flanked by a 2.1-kb DNA fragment (5′ arm, derived from ~400 bp of the 5′ end of exon 1 and ~1.7 kb of sequences upstream of exon 1) inserted into the BamHI and EcoRI sites of pPNT and a 5-kb DNA fragment (3′ arm, derived from intron 1) inserted into the XhoI and NotI sites of pPNT. This targeting vector, through homologous recombination with the *DSG3* gene locus, is predicted to delete exon 1 coding sequences for amino acids 1–16, 164 bp upstream of this coding sequence, and ~500 bp of intron 1.

Targeting of Embryonic Stem Cells and Generation of DSG3-deficient Mice

The embryonic stem (ES) cell line RW4 (Genome Systems, St. Louis, MO) was cultured according to the recommendations of the supplier. In a typical electroporation experiment, 30 μg of the NotI-linearized targeting vector was mixed with 8×10^6 RW4 cells suspended in 10 mM Hepes in PBS, pH 7.5, and electroporated with a single pulse (960 μF, 0.22 kV) using a BioRad Gene Pulser II (Hercules, CA). Electroporated cells were grown on neomycin-resistant mouse embryonic feeder cells (MEF; Genome Systems) in selection medium containing 220 μg/ml G418 and 2 μM gancyclovir (Mansour et al., 1988) for 9 d. With procedures previously described (Ramirez-Solis et al., 1992, 1993), G418/gancyclovir-resistant ES cell clones were cultured in duplicate; one set of cultures was frozen while the duplicate set was screened by Southern analysis. In the initial Southern blot screening, BamHI-digested DNA was hybridized to the probe shown in Fig. 1 *B*. Out of 628 clones tested, one clone had undergone homologous recombination (Fig. 1 *C*). Additional Southern blot analysis with additional restriction enzymes and a probe located in the *DSG3* gene just 3′ to the homologous sequences used in the targeting vector confirmed the targeting event in this cell line (data not shown.). A neo-derived probe indicated the presence of a single copy of the neo-minigene in the recombinant ES cell clone (data not shown). The targeted ES cells were found to possess a normal male karyotype (Hogan et al., 1994) and had no detectable mycoplasma infection (Mycoplasma PCR Primer Set; Stratagene). The recombinant ES cells were injected into C57Bl/6J blastocysts. Chimeric offspring were crossed with C57Bl/6J mice. DNA from agouti offspring was prepared from tail or, if mice were killed, other organs (Hogan et al., 1994) and tested for the presence of the targeted allele by Southern blot hybridization. Mice heterozygous for the targeted mutation were intercrossed to obtain homozygous DSG3 mutants.

Southern Blots

Labeled DNA probes were synthesized using a random primer labeling kit with [^{32}P]dCTP (Prime-It Rmt; Stratagene). The blots were hybridized for 2 h at 65°C with labeled probes in "rapid hybridization buffer" (Amersham, Little Chalfont, UK). Blots were washed twice (15 min each time) in 2× SSC, 0.1% SDS at room temperature and twice (15 min each time) in 0.2× SSC, 0.1% SDS at 65°C, and then exposed to X-Omat films (Eastman Kodak Co., Rochester, NY) for autoradiography.

Genomic DNA was extracted from 1 cm of mouse tails by digesting the tails overnight at 55°C in 700 μl tail buffer containing 50 mM Tris, pH 8.0, 100 mM EDTA, 100 mM NaCl, 0.4 mg/ml proteinase K, and 1% SDS. The lysate was extracted by phenol, 1:1 phenol/choroform, and then chloroform, and DNA was precipitated with isopropanol. Genomic DNA (10–20 μg) was digested overnight with restriction enzymes and electrophoresed in 0.8% agarose gels. DNA was transferred to Nytran membranes by the alkaline transfer method according to Schleicher and Schuell (Keene, NH) and was cross-linked with 120 mJ of UV light.

RNase Protection

The following cDNAs were used to synthesize biotinylated RNA antisense and sense probes with the Biotinscript kit (Ambion, Austin, TX): B9 (338 bp of mouse Dsg3 cDNA starting from 63 bp upstream of the translation initiation site), Dsg2.mc580 (mouse desmoglein 2 cDNA, provided by Werner W. Franke, German Cancer Research Center, Heidelberg, Germany), mDsg1exon15A (mouse desmoglein 1 exon 15), and pTRI-β-actin (mouse β-actin; Ambion). Tissue lysates from the skin of 2–4-d-old pups or the tongue of adult animals were prepared (Direct Protect; Ambion). Products of the protection assay were separated in 6% Tris-borate-EDTA-urea gels (Novex, San Diego, CA), and then transferred to nylon membranes (BrightStar Plus; Ambion). Biotin-labeled RNA fragments were detected with a chemiluminescent detection system (BrightStar Biodetect; Ambion).

Antibodies

A rabbit antiserum was raised against a synthetic peptide, HQWGIEGAHPEDKEITNIC (single letter amino acid code) (amino acids 667–685 [Amagai et al., 1991]), from the "intracellular anchor" domain of Dsg3, coupled to keyhole limpet hemocyanin (Imject Activated Immunogen Conjugation Kit; Pierce Chemical Co., Rockford, IL) (Tanaka et al., 1990). The rabbit antiserum was affinity purified on the peptide (ImmunoPure Ag/Ab Immobilization Kit 2; Pierce Chemical Co.) and concentrated to 0.3 mg/ml. On immunoblots, the resulting antibody identified the 130-kD Dsg3, but not the 160-kD Dsg1 or Dsg2, extracted from mouse (Fig. 2 *C*) or human (not shown) stratified squamous epithelia. In addition, two sera from PV patients, Nos. 1172 and 1409, were used to identify Dsg3 by immunofluorescence of mouse tissue.

The anti–desmoglein 1 and 2 mouse mAb DG3.10 was generously provided by W.W. Franke. We also used mAbs against desmoplakin I + II (Biodesign, Kennebunk, ME) and plakoglobin (15F11 generously provided by M. Wheelock, University of Toledo, OH).

Anti–rabbit IgG, anti–human IgG, and anti–mouse IgG antibodies coupled to fluorescent dyes (FITC, Texas red) or enzymes (HRP) were purchased from Biosource (Camarillo, CA), Bio Rad Laboratories, and Molecular Probes (Eugene, OR).

Immunofluorescence Microscopy

Cryosections were fixed for 10 min in acetone or a 1:1 mixture of acetone/methanol at −20°C, and then washed in PBS. In some experiments, tissue samples were washed for 5 min in PBS with 1% Triton X-100 after fixation, followed by several washes in PBS. The tissue samples were incubated with the first antibody at the appropriate dilution in 1% BSA in PBS for 1 h. After washing three times for 5 min each in PBS, samples were incubated with a fluorescent dye–coupled antibody diluted in 1%

BSA/PBS for 30 min and washed as described above. Stained sections were examined and photographed with a BX60 photomicroscope (Olympus Corp., Lake Success, NY).

Western Blotting

Whole tissue extracts were prepared by homogenizing mouse tongue in lysis buffer (10 mM Tris-HCl, pH 7.4, 5 mM EDTA, 420 mM NaCl, 1% Triton X-100, 100 μg/ml leupeptin, 0.5 mM PMSF, 50 μg/ml aprotinin) on ice. The lysates were centrifuged for 10 min (4°C 16,000 *g*). The pellet was suspended in Laemmli buffer (Bio Rad Laboratories), incubated for 5 min at 100°C, and then centrifuged for 5 min at 16,000 *g*. The proteins from these supernatants were separated in 8% Tris-glycine gels (Novex) and then transferred to nitrocellulose (Trans-Blot; Bio Rad Laboratories). The membranes were incubated for 1 h in blocking buffer (5% fat-free milk powder, 1% BSA, 0.1% Tween-20 in PBS).The first antibody (diluted in blocking buffer) was incubated overnight at 4°C. The membranes were washed three times, for 15 min each, in 0.1% Tween-20/PBS, and then incubated with the secondary antibody (goat anti–mouse-HRP or goat anti–rabbit-HRP, 1:1,000 dilution in PBS/0.1% Tween-20). The membranes were washed as described above. Binding of the secondary antibody was detected with the ECL system (Amersham Corp., Arlington Heights, IL).

Histology and EM

Paraffin-embedded, microtome-sectioned tissues were stained with hematoxylin and eosin by routine methods (Lavker et al., 1991). We used routine, previously described methods to examine the ultrastructure of lesional mouse skin by transmission EM (Lavker et al., 1991).

Detection and Verification of a DSG3 Mutation in bal Mice

Information on the intron–exon organization of the mouse *DSG3* gene allowed us to develop a strategy to screen for sequence variants by heteroduplex analysis using conformation-sensitive gel electrophoresis (Ganguly et al., 1993). For heteroduplex analysis, total DNA isolated from homozygous *bal/bal*, heterozygous *bal/+*, or wild-type mice (+/+) was used as template for amplification of exons within DSG3. Oligonucleotide primers spanning each of the 15 exons were synthesized on the basis of intronic sequences and used to generate PCR products spanning the exons. Specifically, to amplify exon 14 containing the mutation, the following primers were used: sense, 5′-GCCATAGCATGAACTGTTAG-3′; antisense, 5′-GTTGGCTTGTCTTGTGAGTT-3′.

For PCR amplification, 250 ng of genomic DNA was used as a template in the amplification buffer containing 20 pmol of each primer, 100 nmol $MgCl_2$, 20 mmol of each nucleotide, and 2.5 U of Taq polymerase (GIBCO BRL, Gaithersburg, MD), in a total vol of 50 μl. The amplification conditions were 94°C for 5 min, followed by 35 cycles of 94°C for 45 s, 55°C for 45 s, and 72°C for 45 s. Aliquots of 5 μl of the PCR products were analyzed on 2% agarose gel electrophoresis, and 10 μl of the sample was prepared for heteroduplex analysis. The PCR products demonstrating heteroduplex formation were sequenced using an ABI automated sequencer.

Since the mutation in the *DSG3* gene did not create or abolish a restriction endonuclease site, its presence was verified by allele-specific oligonucleotide hybridization. The oligonucleotide probes used for hybridization were, for the wild-type (WT) sequence, 5′-TTGAAGGACTATGCTGCGC-3′, and, for the mutant (M) allele, 5′-TGAAGGACTTATGCTGCGC-3′. These oligomers were end labeled with [γ-^{32}P]ATP and hybridized to PCR-amplified DNAs that had been immobilized to Zetabind nylon membrane. Hybridizations were carried out in 5× SSPE, 0.5% SDS, 0.1% BSA, 0.1% polyvinyl pyrrolidone/Ficoll, at 37°C for 1 h, followed by washing in 2× SSPE, 0.1% SDS at 58°C. Radioactive oligomer DNA hybrids were visualized by autoradiography on exposure to x-ray film.

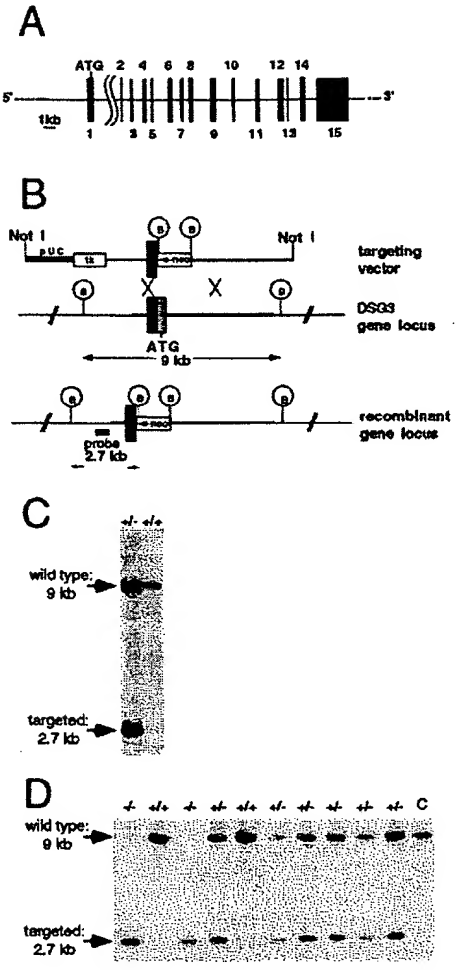

Figure 1. Targeting strategy and Southern blot confirmation of targeted alleles. (*A*) Intron–exon organization of the mouse *DSG3* gene. The exons (*vertical blocks*) and introns (*horizontal lines*) are drawn to scale, with the exception of intron 1 that is >6 kb in size. (*B*) Targeting strategy. Vertical box indicates exon 1 (lighter shading indicates part of exon 1 that is deleted in targeting strategy). *neo*, neomycin-resistance cassette; *tk*, herpes thymidine kinase cassette; *B*, BamHI sites; *NotI*, restriction site used to linearize vector; (*bold horizontal lines*) portions of the *DSG3* gene that were used in targeting vector; (*thickest horizontal line*) pUC vector sequences. Probe indicated was used in Southern blots described below. (*C*) Southern blot of DNA from wild type (+/+) and targeted (+/−) ES cell clones. DNA was digested with BamHI. Targeted allele shows a 2.7-kb band; wild-type allele shows a 9-kb band. (*D*) Southern blot of tail DNA from pups of DSG3 +/− × DSG3 +/− mating. −/−, both DSG3 alleles are targeted, resulting in only a 2.7-kb band. +/− animals show both a recombinant (2.7 kb) and wild-type (9 kb) allele, whereas +/+ animals only show a wild-type allele. Lane *C* shows control ES cell DNA.

Results

Cloning of the 129/Sv Mouse DSG3 Gene

To obtain homologous DNA sequences to target the *DSG3* gene in embryonic stem cells derived from 129/Sv mice, we cloned the gene from a 129/Sv λFixII genomic library and determined the intron–exon structure, which revealed 15 exons spanning ~25 kb of DNA (Fig. 1 *A*). The smallest exon (13) was 64 bp in size, while the last exon (15) consisted of 3,677 bp, including a segment corresponding to the 3′ untranslated sequence ending at the

polyadenylation signal. Exon 1 contained the putative translation initiation codon, ATG, as well as an upstream 5′ untranslated region.

Generation of Mice with a Targeted Disruption of the DSG3 Gene

The strategy underlying the experiments described below was to delete the coding sequence from the first exon of the *DSG3* gene, thereby functionally inactivating the gene.

We constructed a targeting vector to delete, by homologous recombination, about one-third of the 3′ end of exon 1 from one DSG3 allele in mouse 129/Sv ES cells (Fig. 1 *B*) (Horie et al., 1994; Thomas et al., 1992; Zhang et al., 1994). This part of exon 1 was replaced by a neo-cassette in the recombinant locus. The deleted part of exon 1 encodes the first 16 amino acids (aa) of the Dsg3 signal peptide and 164 bp upstream of this coding sequence (see above and Ishikawa et al., 1994). The next methionine in the aa sequence is located at position 177 (encoded by exon 6) in the second extracellular domain (EC2) of Dsg3 (Ishikawa et al., 1994; Amagai et al., 1991). Therefore, even if the neo-cassette would be spliced out of a primary transcript generated at a targeted gene locus, the resulting mRNA would encode a truncated polypeptide lacking signal sequences necessary for insertion into the cell membrane. Furthermore, the first extracellular domain of Dsg3 (EC1; Amagai et al., 1991) would be missing in this polypeptide. Although the specific function of EC1 in desmogleins is unknown, it has been shown for other cadherins (e.g., E-cadherin) that this domain of the protein is crucial for homophilic interactions (Nose et al., 1990; Blaschuk et al., 1990).

An ES clone with a targeted allele (Fig. 1 *C*) was injected into C57Bl/6J blastocysts and seven male chimeras were generated, three of which showed germline transmission of the ES cell genome as determined by the agouti coat color of offspring from chimera × C57Bl/6J breedings. As expected, Southern blot analysis revealed that ~50% of the agouti animals were heterozygous (+/−) for the targeted mutation. The DSG3+/− animals were healthy and indistinguishable from wild-type (+/+) littermates. Heterozygous mice (F1 generation) were then intercrossed to produce offspring homozygous (−/−) for the targeted allele. 132 pups derived from these intercrosses were genotyped (example in Fig. 1 *D*). Of those, 23% were +/+, 54% +/−, and 23% −/−, indicating inheritance of the targeted mutation according to Mendel's laws with no indication of significant embryonic lethality of the homozygous state. The litter size in the F2 generation was normal, and, at birth, +/+, +/−, or −/− animals could not be distinguished by visual inspection.

Taken together, these findings indicated that the targeted mutation did not significantly interfere with prenatal development. Furthermore, so far one male and one female homozygous mutant mouse were able to breed, demonstrating fertility of the mutants.

Mice Homozygous for the Targeted Mutation Do Not Synthesize Dsg3

To demonstrate that the gene targeting resulted in a functional null mutation, we studied the Dsg3 mRNA expression and protein synthesis in pups derived from intercrosses between +/− animals. Dsg3 mRNA was absent in −/− animals, whereas the mRNA was detected in +/+ and +/− animals, as determined by an RNase protection assay. (Fig. 2 *A*). The levels of Dsg1 and Dsg2 mRNA expression were not affected by the targeted mutation and were similar in +/+, +/−, and −/− mice (data not shown). Immunofluorescence microscopy on tongue epithelium using antibodies against extracellular or cytoplasmic epitopes of Dsg3 indicated the absence of the protein in −/− mutants (Fig. 2 *B*). Control antibodies against other desmogleins (e.g., mAb 3.10 that recognizes Dsg1 and Dsg2) (Fig. 2 *B*), as well as antibodies against the desmosomal plaque proteins plakoglobin (Fig. 2 *B*) or desmoplakin (not shown), showed no difference in the staining patterns in samples derived from +/+, +/−, and −/− mice. Furthermore, Western blot analysis of tongue extracts from −/− mutants demonstrated the absence of the Dsg3 polypeptide but the presence of Dsg1 and Dsg2, as indicated by mAb 3.10 (Fig. 2 *C*).

These data indicate that the targeted mutation indeed represented a functional null mutation.

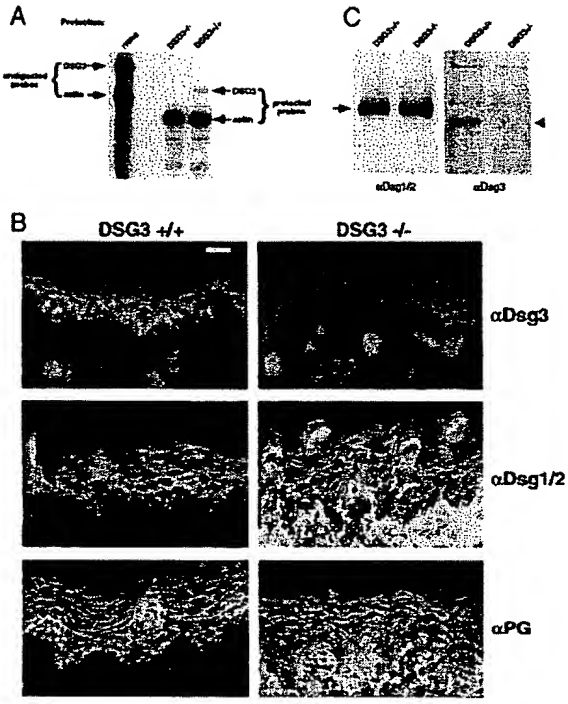

Figure 2. Lack of Dsg3 RNA and protein in homozygous targeted mice. (*A*) RNase protection assay of tongue lysates from wild type (+/+) and targeted (−/−) mice. (*B*) Immunofluorescence of tongue from wild-type and targeted mice shows absence of Dsg3 from −/− mice, but presence of Dsg 1 and 2 (*Dsg1/2*, identified by mAb DG3.10), and plakoglobin. The submucosa of −/− mice shows increased nonspecific fluorescence probably as a result of inflammation. (*C*) Western blot of tongue lysates. Dsg3 is absent in −/− mice (*arrowhead*), but Dsg1 and 2 are present (*arrow*) to the same degree as in +/+ mice. Bar, 25 μm.

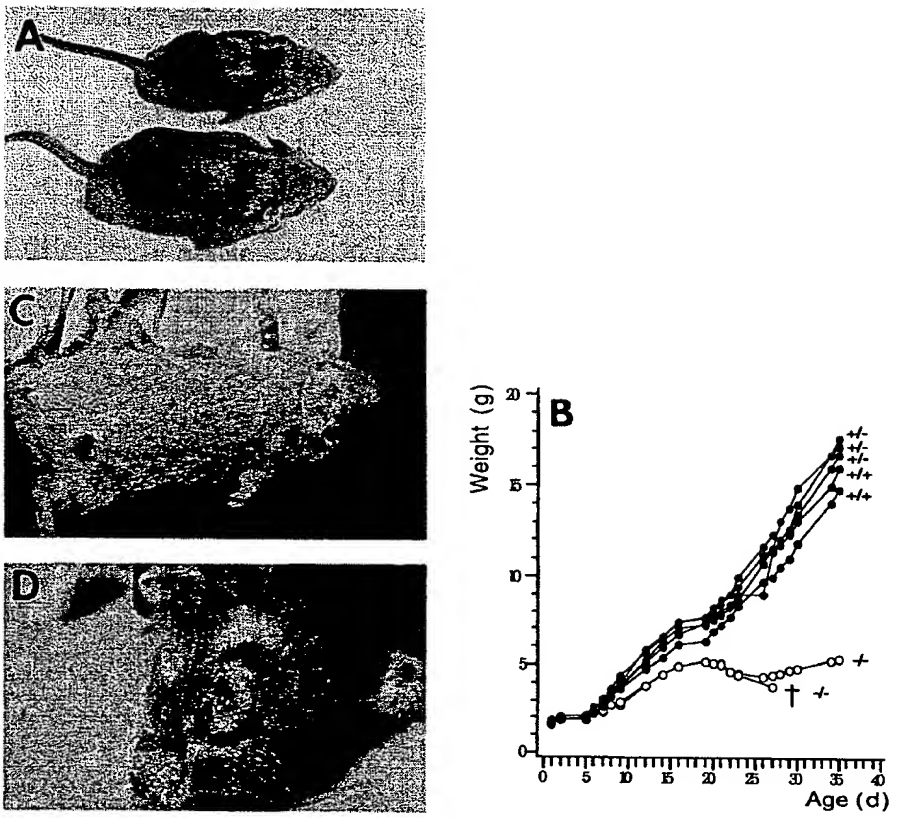

Figure 3. DSG3 −/− mice are runts and have skin erosions and eye lesions. (*A*) DSG3 −/− mice are runts. Upper mouse is DSG3 −/−; lower mouse is a +/+ littermate. (*B*) Weight graph shows that −/− mice (*open circles*), compared with +/+ and +/− littermates (*filled circles*), are born with equal weight but by about day 8–10 are lagging in weight gain. Weight loss is seen about day 20, approximately the time of weaning and start of solid food. (*C*) Nipple erosions in a DSG3 −/− nursing mother. (*D*) Snout erosion and conjunctivitis in a DSG3 −/− mouse.

DSG3 −/− Mice Show Loss of Keratinocyte Cell Adhesion Resulting in a Phenotype That Resembles That of Patients with PV

Around 15–20 d after birth, −/− animals differed in size from +/− and +/+ animals. The −/− mutants were much smaller than their littermates (Fig. 3 *A*). Autopsies revealed a dramatic reduction in body fat in the −/− animals that resembles what is seen in starvation.

Runting of the pups consistently sorted with the targeted mutation and was never observed in animals that were wild type or heterozygous for the mutant allele. A closer analysis revealed that at birth all pups showed similar weights, but, at 8–10 d after birth, −/− animals showed reduced bodyweight (Fig. 3 *B*). In the following days, the mutants grew at a much slower rate than +/− and +/+ mice. Between days 18 and 25, the growth of −/− animals slowed down even more with most mutants losing weight and a few dying (Fig. 3 *B*). However, >80% of mutants survived and again started to gain weight, but they were still clearly smaller than their littermates. No significant weight difference between +/− and +/+ mice was observed.

Since the most characteristic lesions in pemphigus vulgaris patients are painful oral erosions that may interfere with eating, we speculated that the DSG3 −/− animals might have similar lesions preventing them from feeding sufficiently that would, in turn, result in runting. Indeed, histological examination of the oral mucosa in DSG3 −/− mice showed a full spectrum of the types of lesions typical of PV. The most common lesion was an inflammatory erosion, sometimes seen with reepithelialization (Fig. 4 *A*). This is typical of a late PV blister after the superficial epidermis is lost and the resulting irritation and/or colonization of the erosion results in acute inflammation and loss of the basal cells (Fig. 4 *B*). Further examination showed intermediate lesions with the superficial epidermis lost, leaving the basal cells still attached to the basement membrane, but slightly detached from each other (Fig. 4 *C*). This appearance has been called the "row of tombstones" in patients with PV (Fig. 4 *D*). Finally, we could also detect the earliest lesion of PV in the DSG3 −/− mice, namely a suprabasilar split in the epithelium, with minimal inflammation (Fig. 4 *E*). Oropharyngeal biopsies of essentially all DSG3 −/− mice, examined at ages 3 d–5 mo, showed these changes, but DSG3 +/− and +/+ mice never showed them. We speculate from this data that suckling resulted in the trauma necessary to cause these lesions initially, with the beginning of solid food at 16–20 d exacerbating them. The resulting lesions presumably decreased food intake enough to result in the runting of these mice.

Interestingly, the epidermis of these mice did not show extensive spontaneous lesions. However, when a female DSG3 −/− mouse delivered pups, their suckling caused erosions around the nipples (Fig. 3 *C*) and some mice

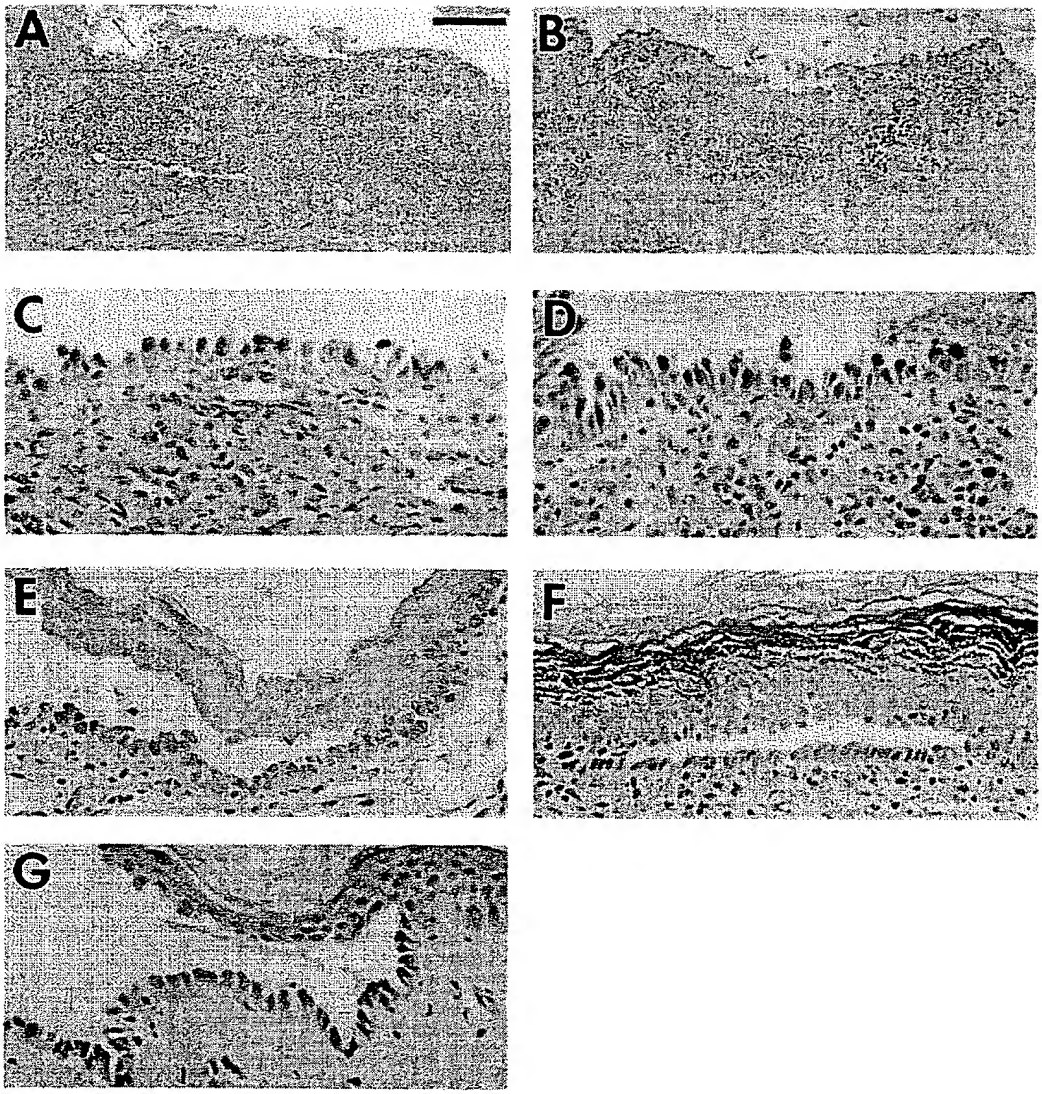

Figure 4. Histology of oral mucous membranes and skin in DSG3 −/− mice and human PV patients. (*A*) DSG3 −/−: inflammatory oral erosion of the tongue. (*B*) Human PV: inflammatory oral erosion. (*C*) DSG3 −/−: oral lesion shows basal cells are separated from each other and the suprabasilar epithelium is lost. This is a characteristic histology called a "row of tombstones." (*D*) Human PV: oral lesion shows a "row of tombstones." (*E*) DSG3 −/−: early oral lesion shows suprabasilar acantholysis with intact suprabasilar epithelium separated from basal cells. (*F*) DSG3 −/−: early skin lesion on dorsum of foot near where skin was traumatized by cutting. (*G*) Human PV: skin lesion shows typical suprabasilar acantholysis. Bar: (*A* and *B*) 160 μm; (*C–G*) 40 μm.

showed crusting on the skin around the eyes and snout (Fig. 3 *D*), areas that are normally traumatized by scratching. Histology of traumatized skin also showed typical suprabasilar blisters (Fig. 4 *F*), similar to the histology of skin lesions in pemphigus vulgaris patients (Fig. 4 *G*). Some DSG3 −/− mice also showed suppurative conjunctivitis (Fig. 3 *D*) with suprabasilar blisters of eyelids and mucocutaneous conjunctiva, similar to what has been reported in patients (Hodak et al., 1990).

Among the other stratified epithelia examined, only the vaginal epithelium of a DSG3 −/− mouse showed suprabasilar blistering. Histology of the esophagus, the cardiac portion of the stomach, and the thymus (for Dsg3 expression in thymus see Schäfer et al., 1994) revealed no abnormalities.

EM of nonlesional epidermis and lingual mucosa in DSG3 −/− mice showed normal differentiation. Desmosomes were present, and individual desmosomes appeared indistinguishable from those of unaffected littermates: both had well-defined membrane lipid bilayers, intracellular dense plaques anchored to aggregated intermediate filaments, and extracellular domains with typical central,

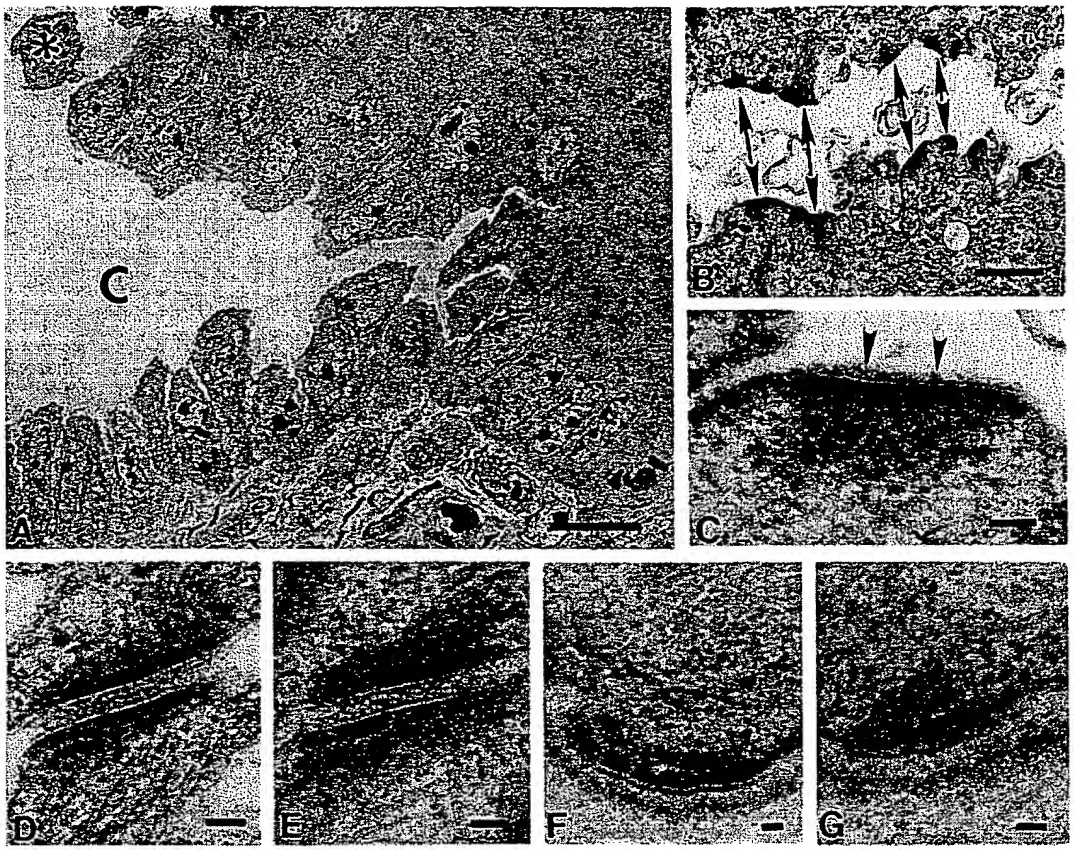

Figure 5. Ultrastructure of lesional posterior lingual epithelium in DSG3 −/− mice. (*A*) An edge of a blister cavity, denoted by "C" in a DSG3 −/− mouse. The base is formed by a single layer of basal keratinocytes with a characteristic "tombstone" cytoarchitecture. The roof consists of intact suprabasal epithelium with occasional associated acantholytic keratinocytes (*). (*B*) Blister in a DSG3 −/− mouse shows separation of desmosomes which form half-desmosomes (*double arrows*) with tonofilaments still attached. (*C*) Higher magnification of a half-desmosome shows an intact intracytoplasmic dense plaque and its associated tonofilaments. There is residual flocculent material (*arrowheads*) along the cell membrane. (*D*) Desmosome in DSG3 +/+ littermate. (*E*) Desmosome in DSG3 −/− mouse has normal appearance. (*F*) Hemidesmosome in DSG3 +/+ littermate. (*G*) Hemidesmosome in DSG3 −/− mouse shows normal appearance. Bars: (*A*) 10 μm; (*B*) 0.5 μm; (*C–G*) 50 nm.

electron-dense disks formed by flocculent material (Fig. 5, *D* and *E*). The extracellular domains were consistently 20–25 nm thick in both control and affected animals. Our general impression was that the number of desmosomes in DSG3 −/− mice may have been diminished focally along the lateral and apical surfaces of basal cells, but, as a result of the focal nature of this finding, we could not quantitate it convincingly. EM of lesions in DSG3 −/− mice showed cellular detachment primarily at the apical and lateral surfaces of the basal cells (Fig. 5, *A* and *B*). Accordingly, the acantholytic cleft was formed as a result of separation of basal cells from suprabasal cells and from each other at the cell membranes. Hemidesmosomes were structurally normal (Fig. 5, *F* and *G*). Separated acantholytic cells retained "half" desmosomes, containing the intracytoplasmic dense plaque with attached intermediate filaments, along the plasma membrane that abutted the cleavage plane (Fig. 5 *C*). These half desmosomes contained a finely flocculent material (i.e., desmoglea) on their extracellular surface. These residual half desmosomes were particularly prominent along the apical surfaces of basal cells and tended to aggregate and coalesce. Individual intact desmosomes directly adjacent to acantholytic areas appeared normal.

An additional, and unexpected, phenotype developed at around the time of weaning (3–4 wk after birth) in DSG3 −/− mice. They started to lose their hair and developed completely bald areas, first on the forehead, and then proceeding onto the entire back (Fig. 6 *A*). This phenomenon was observed whether the mutants were housed in groups or alone. The ventral coat at this age seemed thin but basically intact. New hair regrowth started from the head to the back. These cycles of hair loss and regrowth occurred repeatedly, but after two to three cycles they lost the head to tail synchronization and occurred as bald patches with regrowth, involving both the ventral and dorsal coats. As hair loss is not a major finding in PV patients, this phenotype either is specific for a genetic loss of Dsg3 or is peculiar to mice as opposed to humans.

There were no phenotypic abnormalities of any kind observed in DSG3 +/− mice.

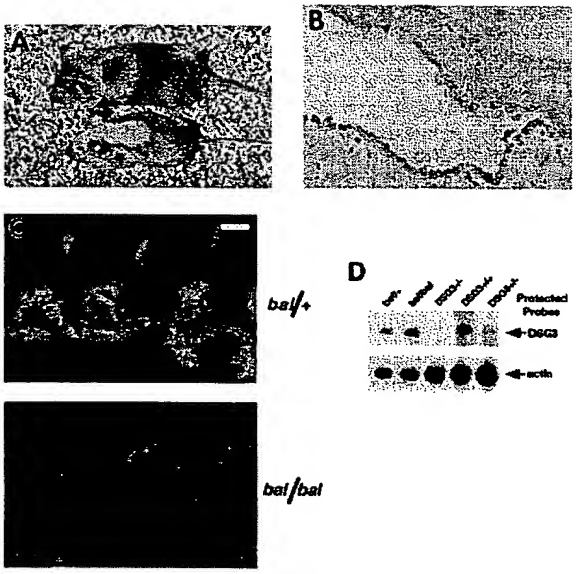

Figure 6. Analysis of balding mice compared with DSG3 −/− mice. (*A*) Balding phenotype of a 1-mo-old DSG3 −/− mouse compared with a normal littermate (above). (*B*) Histology of an oral mucosal blister in a *bal/bal* mouse shows suprabasilar acantholysis. (*C*) Immunofluorescence of *bal/bal* tongue shows no Dsg3 compared with control littermate. (*D*) RNase protection assay of tongue lysates demonstrates that *bal/bal* mice synthesize DSG3 mRNA, as compared with DSG3 −/− mice that do not. Note that DSG3 +/− mice demonstrate about half of the mRNA of wild-type mice.

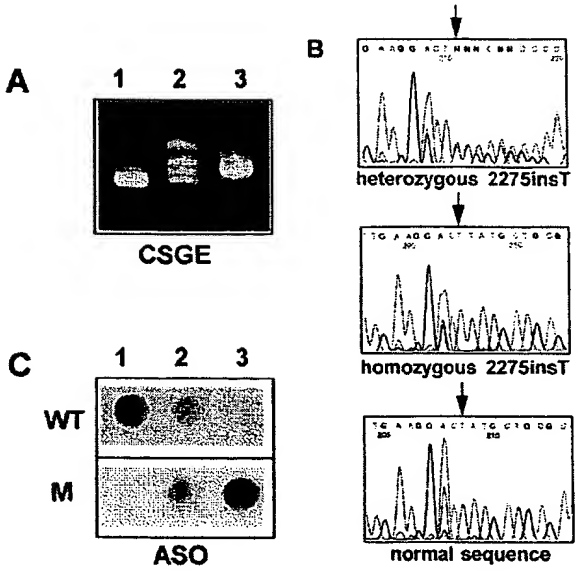

Figure 7. Analysis of the DSG3 mutation in balding mice. (*A*) Heteroduplex analysis of a 400-bp segment of PCR-amplified mouse DSG3, containing exon 14 and flanking intronic sequences, revealed heteroduplex bands in case of a heterozygous *bal/+* mouse (lane *2*), while control mouse (lane *1*) and a homozygous *bal/bal* (lane *3*) showed a homoduplex band only. (*B*) Direct nucleotide sequencing of DNA shown on lane *2* in *A* revealed a heterozygous 1-bp insertion, 2275insT, which resulted in frame-shift (*upper panel*), in comparison with normal sequence in DNA obtained from a control mouse shown on lane *1* in *A* (*lower panel*). Sequencing of DNA on lane *3* revealed that *bal/bal* mouse was homozygous for the 2275insT mutation (*middle panel*). (*C*) Allele-specific oligonucleotide hybridization (*ASO*) was used to verify the presence of the mutation in balding mice. Specifically, PCR-amplified DNA from the control mouse hybridized with the wild-type oligomer (*WT*) only (lane *1*), while homozygous *bal/bal* mouse hybridized with the mutant (*M*) probe only (lane *3*). DNA from *bal/+* mouse hybridized with both the WT and M probes, indicating that these mice were heterozygous for the mutation (lane *2*).

Balding (bal) Mice Have the Same Phenotype as DSG3 −/− Mice and Have a Null Mutation in the DSG3 Gene

The phenotype of runting and hair loss around the time of weaning seen in the DSG3 −/− mutants has been described in mice with a spontaneous mutation termed *bal* (Sundberg, 1994). This recessive mutation has recently been mapped to a position close to the DSG3 locus on mouse chromosome 18 (Davisson et al., 1994). We therefore speculated that *bal* might be a DSG3 null mutation.

Histological analysis revealed the presence of suprabasilar blisters on the tongue of *bal/bal* mice, indistinguishable from those found in our DSG3 −/− mice (Fig. 6 *B*). These lesions were never found in *bal/+* or +/+ littermates.

We then determined whether the balding mutation and our targeted mutation were coallelic. A mouse heterozygous for the targeted mutation (DSG3 +/−) was bred to a mouse heterozygous for the *bal* mutation (*bal/+*). Two of the seven pups obtained from these crosses were runts. Furthermore, histological analysis demonstrated the presence of multiple lesions in the oropharynx of the runts (but not the normal size littermates) with the typical PV-like morphology (data not shown). By Southern blot analysis, we showed that one runt possessed a targeted DSG3 allele, and mutation analysis (see below) demonstrated the presence of the heterozygous balding mutation as well (data not shown). Additionally, at the time of weaning, these runts lost their hair in a pattern identical to that described above for the mice with the targeted DSG3 mutation. We conclude that the runt had inherited the targeted allele from one parent and the *bal* mutation from the other, and developed the same phenotype as DSG3 −/− and *bal/bal* mice. These data demonstrate that the targeted mutation and the balding mutation are coallelic.

Further analysis of the balding mice by immunofluorescence microscopy on tongue epithelium from mice heterozygous (*bal/+*) and homozygous (*bal/bal*) for the balding mutation was done using antibodies against extracellular and intracellular epitopes of Dsg3. Whereas *bal/+* epithelium clearly stained with these antibodies, no staining was observed in the *bal/bal* epithelium (Fig. 6 *C*). Control antibodies against desmoglein 1 and 2, desmoplakin and plakoglobin stained both *bal/+* and *bal/bal* epithelia equally well (data not shown). However, using an RNase protection assay, we were able to detect a transcript derived from the DSG3 locus (Fig. 6 *D*). Given the fact that we did not detect Dsg3 by immunofluorescence analysis, we hypothe-

sized that a mutation within the *DSG3* gene of the *bal/bal* mutants leads to a transcript that is either not translated or that directs the synthesis of a truncated polypeptide that is rapidly degraded. We therefore screened the *DSG3* gene for putative mutations by heteroduplex analysis. Band shifting of PCR products derived from exon 14 of the obligate heterozygous *bal/+* mouse suggested the presence of a mutation in the *DSG3* gene (Fig. 7 *A*). Sequence analysis of this aberrant PCR fragment identified heterozygous insertion of a thymidine residue at a position that would correspond to nucleotide 2,418 in the human cDNA (Amagai et al., 1991), as determined by the nucleotide and aa homology in this region with the mouse sequence (Fig. 7 *B*). This insertion causes a frame-shift resulting in a premature stop codon 78 bp downstream from the site of insertion. The *bal/bal* mouse was homozygous for the insertion (Fig. 7 *B*). The presence of the insertion mutation was verified by allele-specific oligonucleotide hybridization (Fig. 7 *C*). By homology to the reported human sequence, the mutated transcript would encode a polypeptide that lacks most of the intracellular domain of Dsg3 (after aa 778 [Amagai et al., 1991]), in particular the amino acid sequence to which plakoglobin binds (Mathur et al., 1994; Troyanovsky et al., 1994; Roh and Stanley, 1995; Chitaev et al., 1996; Kowalczyk et al., 1996). The fact that the Dsg3 antibodies used in this study (e.g., those that bind extracellular epitopes and an intracellular epitope encoded upstream of the frame-shift mutation) did not stain *bal/bal* epithelium strongly suggests that a truncated Dsg3 polypeptide, if synthesized in these mice, is not inserted into the plasma membrane and/or is rapidly degraded.

Both the absence of Dsg3 immunostaining and the presence of suprabasilar blisters indicate that the balding mouse represents a functional DSG3 null mutation.

Histology of the bald area in DSG3 −/− mice shows slightly cystic telogen hair follicles that lack a hair shaft (Fig. 8). Further detailed analysis will be needed to determine the exact cause of this hair loss.

Figure 8. Histology of bald back skin from a 24-d-old DSG3 −/− mouse. Note dilated telogen hair follicle containing a clump of pigment but no hair shaft. Bar, 35 μm.

Discussion

It has proven difficult, using in vitro methods, to demonstrate whether desmogleins mediate cell adhesion because they normally are organized in the desmosome with multiple other proteins that may affect their function. A direct way to analyze their function in vivo is to determine what happens to cell adhesion if one desmoglein is eliminated. We therefore genetically engineered a mouse with a targeted disruption of DSG3.

The phenotype of this mouse resembled in many, but not all, ways that of patients with PV who have autoantibodies directed against DSG3. Painful oral mucous membrane erosions resulting from suprabasilar acantholysis are the most characteristic lesions of PV (Lever, 1965). Patients often present with oral mucous membrane lesions, and these may persist, without skin lesions, for months. Some patients only have oral lesions. Patients may lose weight and become dehydrated because these painful lesions often interfere with normal food and fluid intake. Similarly, the major lesions in DSG3 −/− mice were oral mucous membrane erosions. As in PV patients, early lesions showed suprabasilar acantholysis with later lesions showing inflammatory erosions. We presume that these lesions interfered with oral intake, as these mice, which were born with normal weights, became runts once they relied on oral intake for food. We noticed individual variations in the severity of the mutant phenotype; i.e., a few animals died whereas most reached adulthood. These variations were not unexpected and might be, at least in part, due to the presence of "modifier genes" in this outbred line. Finally, electron microscopic analysis of a blister in DSG3 −/− mice reveals very similar findings to those of patients' lesions. In both, separating desmosomes are seen, with acantholytic cells showing single attachment plaques to which tonofilaments insert (Lever, 1979).

Unlike some patients, these mice did not develop extensive spontaneous skin lesions, but did develop some crusted lesions around the eyes, on the snout, and on the nipples of a nursing mother, resulting presumably from trauma. The skin and mucocutaneous junction of the eyelids also showed histologically typical pemphigus lesions as did some biopsies near the edges where skin was traumatized in cutting. An analogous phenomenon, called the Nikolski sign, occurs in patients with active PV in whom rubbing on normal skin may cause erosions with resultant crusting (Lever, 1965). The findings of conjunctivitis and PV-like lesions in the eyes of DSG3 −/− mice have also been reported in patients (Hodak et al., 1990).

The fact that skin of mice is very different from that of humans, with many more hair follicles, may account for the finding that most skin areas in mice do not develop extensive erosions. Furthermore, mice may not develop skin erosions as extensive as those sometimes seen in humans because, as discussed in the Introduction, autoantibody binding to human skin might stimulate release of proteases that could amplify blister formation. In addition, the hair phenotype of these mice may be a reflection of the

difference in hair in rodents and humans, as humans with PV usually do not develop a balding phenotype. Preliminary analysis of the hair phenotype in these mice shows a normal first hair cycle but loss of hair after this cycle. In bald areas, histology of the skin reveals dilated telogen follicles lacking a hair shaft. Previous analysis of balding mice has shown necrosis immediately above the hair matrix leading to some scattered generalized follicular necrosis (Sundberg, 1994). Additional analysis will be required to better define the pathophysiology of hair loss in these DSG3 −/− and balding mice.

Moreover, considering the major difference in mouse and human stratified squamous epithelia and adnexal structures, it is remarkable how similar the phenotype of DSG3 −/− mice is to PV patients.

The phenotype of Dsg3 −/− mice is quite different from that of a recently described transgenic mouse that expresses an amino-terminal deleted Dsg3 under the control of the K14 promoter (Allen et al., 1996). The transgene used consisted of the cytoplasmic and transmembrane domain as well as part of the extracellular domain of Dsg3 and was expressed mainly in the lower layers of the epidermis. The transgenic mice, thought to express a dominant negative effect of the truncated Dsg3, showed swelling of paws and digits, focal flakiness of the skin, and necrotic changes on the tips of the tails that ultimately resulted in tail degeneration. Furthermore, histological analysis revealed epidermal thickening and widening of the intercellular space between keratinocytes but did not show loss of cell–cell adhesion (i.e., acantholysis). At the ultrastructural level, a reduction in the number of desmosomes and the occurrence of aberrant desmosomes were reported. Although these mice were noted to have a wet and matted hair coat (probably because of excess grooming), they did not show an obvious loss of hair. Our DSG3 −/− mice clearly had a different phenotype and distinct histologic and ultrastructural abnormalities. DSG3 −/− mice did not show any tail abnormality and did not have flaky skin, but they developed crusted erosions in areas of trauma. They also had a striking balding phenotype. Histologically these mice showed obvious acantholysis. Finally, ultrastructurally, the DSG3 −/− mice showed normally appearing desmosomes in intact skin and "half"-desmosomes where cells were acantholytic. We conclude from these differences between the transgenic and DSG3 −/− mice that the truncated Dsg3 did not act in a dominant negative fashion to totally inactivate DSG3 function.

The phenotype of DSG3 knockout mice underscores the importance of Dsg3 for cell adhesion and mechanical stability in the deepest layers of stratified epithelia. The other transmembrane adhesion molecules present, such as Dsg2, desmocollins, E-cadherin, and P-cadherin, apparently cannot compensate for the loss of Dsg3. In addition, Dsg3 seems to be particularly important for adhesion in the oral mucous membrane, where lesions always occurred in DSG3 −/− mice, and less so in other stratified squamous epithelia such as esophagus where lesions were never seen. The importance of Dsg3 in skin seems intermediate because lesions were mainly seen secondary to trauma. These studies, then, show that specific desmogleins may have tissue- and differentiation-specific adhesion functions.

Finally, the phenotype of the Dsg3 knockout mice not only demonstrates the importance of Dsg3 for cell adhesion in the deep stratified squamous epithelia, but also is consistent with the idea that, at least in part, PV autoantibodies cause loss of cell adhesion by directly interfering with the adhesive function of Dsg3.

We thank Dr. Chin Howe for valuable discussions and advice regarding knockout technology; Dr. Victor Tybulewicz for providing the targeting vector; Daniela Simon who did karyotyping; Dr. Jean Richa, from the University of Pennsylvania Transgenic Facility, who performed the ES cell injections; Qi Tian, Drs. Stephan Schäfer, and Werner Franke for providing Dsg2 cDNA and antibodies; Dr. Margaret Wheelock for plakoglobin antibodies; Dr. Kehua Li for assistance in cloning the mouse *DSG3* gene; and Dr. Sarolta Karpati for helping with anti-Dsg3 antibody preparation.

This work was supported by National Institutes of Health grants 1RO1AR43776, PO1AR38923, and CA20408. P. Koch was supported by The Thyssen Foundation and a research fellowship from the Dermatology Foundation.

Received for publication 3 February 1997 and in revised form 20 March 1997.

References

Akiyama, M., T. Hashimoto, M. Sugiura, and T. Nishikawa. 1991. Ultrastructural localization of pemphigus vulgaris and pemphigus foliaceus antigens in cultured human squamous carcinoma cells. *Br. J. Dermatol.* 125:233–237.

Allen, E., Q.C. Yu, and E. Fuchs. 1996. Mice expressing a mutant desmosomal cadherin exhibit abnormalities in desmosomes, proliferation, and epidermal differentiation. *J. Cell Biol.* 133:1367–1382.

Amagai, M., V. Klaus-Kovtun, and J.R. Stanley. 1991. Autoantibodies against a novel epithelial cadherin in pemphigus vulgaris, a disease of cell adhesion. *Cell.* 67:869–877.

Amagai, M., S. Karpati, R. Prussick, V. Klaus-Kovtun, and J.R. Stanley. 1992. Autoantibodies against the amino-terminal cadherin-like binding domain of pemphigus vulgaris antigen are pathogenic. *J. Clin. Invest.* 90:919–926.

Amagai, M., T. Hashimoto, N. Shimizu, and T. Nishikawa. 1994*a*. Absorption of pathogenic autoantibodies by the extracellular domain of pemphigus vulgaris antigen (Dsg3) produced by baculovirus. *J. Clin. Invest.* 94:59–67.

Amagai, M., S. Karpati, V. Klaus-Kovtun, M.C. Udey, and J.R. Stanley. 1994*b*. The extracellular domain of pemphigus vulgaris antigen (desmoglein 3) mediates weak homophilic adhesion. *J. Invest. Dermatol.* 102:402–408.

Amagai, M., P.J. Koch, T. Nishikawa, and J.R. Stanley. 1996. Pemphigus vulgaris antigen (Desmoglein 3) is localized in the lower epidermis, the site of blister formation in patients. *J. Invest. Dermatol.* 106:351–355.

Arnemann, J., K.H. Sullivan, A.I. Magee, I.A. King, and R.S. Buxton. 1993. Stratification-related expression of isoforms of the desmosomal cadherins in human epidermis. *J. Cell Sci.* 104:741–750.

Blaschuk, O.W., R. Sullivan, S. David, and Y. Pouliot. 1990. Identification of a cadherin cell adhesion recognition sequence. *Dev. Biol.* 139:227–229.

Buxton, R.S., P. Cowin, W.W. Franke, D.R. Garrod, K.J. Green, I.A. King, P.J. Koch, A.I. Magee, D.A. Rees, J.R. Stanley, and M.S. Steinberg. 1993. Nomenclature of the desmosomal cadherins. *J. Cell Biol.* 121:481–483.

Chidgey, M.A., J.P. Clarke, and D.R. Garrod. 1996. Expression of full-length desmosomol glycoproteins (desmocollins) is not sufficient to confer strong adhesion on transfected L929 cells. *J. Invest. Dermatol.* 106:689–695.

Chitaev, N.A., R.E. Leube, R.B. Troyanovsky, L.G. Eshkind, W.W. Franke, and S.M. Troyanovsky. 1996. The binding of plakoglobin to desmosomal cadherins: patterns of binding sites and topogenic potential. *J. Cell Biol.* 133: 359–369.

Collins, J.E., P.K. Legan, T.P. Kenny, J. MacGarvie, J.L. Holton, and D.R. Garrod. 1991. Cloning and sequence analysis of desmosomal glycoproteins 2 and 3 (desmocollins): cadherin-like desmosomal adhesion molecules with heterogeneous cytoplasmic domains. *J. Cell. Biol.* 113:381–391.

Davisson, M.T., S.A. Cook, K.R. Johnson, and E.M. Eicher. 1994. Balding: a new mutation on mouse chromosome 18 causing hair loss and immunological defects. *J. Hered.* 85:134–136.

Farb, R.M., R. Dykes, and G.S. Lazarus. 1978. Anti-epidermal-cell-surface pemphigus antibody detaches viable epidermal cells from culture plates by activation of proteinase. *Proc. Natl. Acad. Sci. USA.* 75:459–463.

Ganguly, A., M.J. Rock, and D.J. Prockop. 1993. Conformation-sensitive gel electrophoresis for rapid detection of single base differences in double-stranded PCR products and DNA fragments: evidence for solvent-induced bends in DNA heteroduplexes. *Proc. Natl. Acad. Sci. USA.* 90:10325–10329.

Goodwin, L., J.E. Hill, K. Raynor, L. Raszi, M. Manabe, and P. Cowin. 1990. Desmoglein shows extensive homology to the cadherin family of cell adhesion molecules. *Biochem. Biophys. Res. Commun.* 173:1224–1230.

Hashimoto, K., K.M. Shafran, P.S. Webber, G.S. Lazarus, and K.H. Singer.

1983. Anti-cell surface pemphigus autoantibody stimulates plasminogen activator activity of human epidermal cells. *J. Exp. Med.* 157:259–272.

Hashimoto, K., T.C. Wun, J. Baird, G.S. Lazarus, and P.J. Jensen. 1989. Characterization of keratinocyte plasminogen activator inhibitors and demonstration of the prevention of pemphigus IgG-induced acantholysis by a purified plasminogen activator inhibitor. *J. Invest. Dermatol.* 92:310–314.

Hodak, E., I. Kremer, M. David, B. Hazaz, A. Rothem, P. Feuerman, and M. Sandbank. 1990. Conjunctival involvement in pemphigus vulgaris: a clinical, histopathological and immunofluorescence study. *Br. J. Dermatol.* 123:615–620.

Hogan, B., R. Beddington, F. Costantini, and E. Lacy. 1994. Manipulating the Mouse Embryo. Cold Spring Harbor Laboratory, Cold Spring Harbor, NY. 497 pp.

Horie, K., S. Nishiguchi, S. Maeda, and K. Shimada. 1994. Structures of replacement vectors for efficient gene targeting. *J. Biochem. (Tokyo).* 115:477–485.

Ishikawa, H., S.A. Silos, K. Tamai, N.G. Copeland, D.J. Gilbert, N.A. Jenkins, and J. Uitto. 1994. cDNA cloning and chromosomal assignment of the mouse gene for desmoglein 3 (Dsg3), the pemphigus vulgaris antigen. *Mamm. Genome.* 5:803–804.

Karpati, S., M. Amagai, R. Prussick, K. Cehrs, and J.R. Stanley. 1993. Pemphigus vulgaris antigen, a desmoglein type of cadherin, is localized within keratinocyte desmosomes. *J. Cell Biol.* 122:409–415.

King, I.A., J. Arnemann, N.K. Spurr, and R.S. Buxton. 1993. Cloning of the cDNA (DSC1) coding for human type 1 desmocollin and its assignment to chromosome 18. *Genomics.* 18:185–194.

Koch, P.J., and W.W. Franke. 1994. Desmosomal cadherins: another growing multigene family of adhesion molecules. *Curr. Opin. Cell Biol.* 6:682–687.

Koch, P.J., M.J. Walsh, M. Schmelz, M.D. Goldschmidt, R. Zimbelmann, and W.W. Franke. 1990. Identification of desmoglein, a constitutive desmosomal glycoprotein, as a member of the cadherin family of cell adhesion molecules. *Eur. J. Cell Biol.* 53:1–12.

Koch, P.J., M.D. Goldschmidt, M.J. Walsh, R. Zimbelmann, and W.W. Franke. 1991*a*. Complete amino acid sequence of the epidermal desmoglein precursor polypeptide and identification of a second type of desmoglein gene. *Eur. J. Cell Biol.* 55:200–208.

Koch, P.J., M.D. Goldschmidt, M.J. Walsh, R. Zimbelmann, M. Schmelz, and W.W. Franke. 1991*b*. Amino acid sequence of bovine muzzle epithelial desmocollin derived from cloned cDNA: a novel subtype of desmosomal cadherins. *Differentiation.* 47:29–36.

Koch, P.J., M.D. Goldschmidt, R. Zimbelmann, R. Troyanovsky, and W.W. Franke. 1992. Complexity and expression patterns of the desmosomal cadherins. *Proc. Natl. Acad. Sci. USA.* 89:353–357.

Kowalczyk, A.P., J.E. Borgwardt, and K.J. Green. 1996. Analysis of desmosomal cadherin-adhesive function and stoichiometry of desmosomal cadherin-plakoglobin complexes. *J. Invest. Dermatol.* 107:293–300.

Lavker, R.M., G. Dong, P. Zheng, and G.F. Murphy. 1991. Hairless micropig skin. A novel model for studies of cutaneous biology. *Am. J. Pathol.* 138: 687–697.

Lever, W.F. 1965. Pemphigus and Pemphigoid. Charles C. Thomas, Springfield, IL. 266 pp.

Lever, W.F. 1979. Pemphigus and pemphigoid. *J. Am. Acad. Dermatol.* 1:2–31.

Mansour, S.L., K.R. Thomas, and M.R. Capecchi. 1988. Disruption of the proto-oncogene int-2 in mouse embryo-derived stem cells: a general strategy for targeting mutations to non-selectable genes. *Nature (Lond.).* 336:348–352.

Mathur, M., L. Goodwin, and P. Cowin. 1994. Interactions of the cytoplasmic domain of the desmosomal cadherin dsg1 with plakoglobin. *J. Biol. Chem.* 269:14075–14080.

Mechanic, S., K. Raynor, J.E. Hill, and P. Cowin. 1991. Desmocollins form a distinct subset of the cadherin family of cell adhesion molecules. *Proc. Natl. Acad. Sci. USA.* 88:4476–4480.

Memar, O.M., S. Rajaraman, R. Thotakura, S.K. Tyring, J.L. Fan, G.S. Seetharamaiah, A. Lopez, R.E. Jordon, and B.S. Prabhakar. 1996. Recombinant desmoglein 3 has the necessary epitopes to adsorb and induce blister-causing antibodies. *J. Invest. Dermatol.* 106:261–268.

Morioka, S., G.S. Lazarus, and P.J. Jensen. 1987. Involvement of urokinase-type plasminogen activator in acantholysis induced by pemphigus IgG. *J. Invest. Dermatol.* 89:474–477.

Nagafuchi, A., Y. Shirayoshi, K. Okazaki, K. Yasuda, and M. Takeichi. 1987. Transformation of cell adhesion properties by exogenously introduced E-cadherin cDNA. *Nature (Lond.).* 329:341–343.

Naito, K., S. Morioka, S. Nakajima, and H. Ogawa. 1989. Proteinase inhibitors block formation of pemphigus acantholysis in experimental models of neonatal mice and skin explants: effects of synthetic and plasma proteinase inhibitors on pemphigus acantholysis. *J. Invest. Dermatol.* 93:173–177.

Nilles, L.A., D.A.D. Parry, E.E. Powers, B.D. Angst, R.M. Wagner, and K.J. Green. 1991. Structural analysis and expression of human desmoglein: a cadherin-like component of the desmosome. *J. Cell Sci.* 99:809–821.

North, A.J., M.A. Chidgey, J.P. Clarke, W.G. Bardsley, and D.R. Garrod. 1996. Distinct desmocollin isoforms occur in the same desmosomes and show reciprocally graded distributions in bovine nasal epidermis. *Proc. Natl. Acad. Sci. USA.* 93:7701–7705.

Nose, A., K. Tsuji, and M. Takeichi. 1990. Localization of specificity determining sites in cadherin cell adhesion molecules. *Cell.* 61:147–155.

Nuber, U.A., S. Schäfer, A. Schmidt, P.J. Koch, and W.W. Franke. 1995. The widespread human desmocollin Dsc2 and tissue-specific patterns of synthesis of various desmocollin subtypes. *Eur. J. Cell Biol.* 66:69–74.

Nuber, U.A., S. Schäfer, S. Stehr, H.R. Rackwitz, and W.W. Franke. 1996. Patterns of desmocollin synthesis in human epithelia: immunolocalization of desmocollins 1 and 3 in special epithelia and in cultured cells. *Eur. J. Cell Biol.* 71:1–13.

Parker, A.E., G.N. Wheeler, J. Arnemann, S.C. Pidsley, P. Ataliotis, C.L. Thomas, D.A. Rees, A.I. Magee, and R.S. Buxton. 1991. Desmosomal glycoproteins II and III. Cadherin-like junctional molecules generated by alternative splicing. *J. Biol. Chem.* 266:10438–10445.

Ramirez-Solis, R., J. Rivera-Perez, J.D. Wallace, M. Wims, H. Zheng, and A. Bradley. 1992. Genomic DNA microextraction: a method to screen numerous samples. *Anal. Biochem.* 201:331–335.

Ramirez-Solis, R., A.C. Davis, and A. Bradley. 1993. Gene targeting in embryonic stem cells. *Methods Enzymol.* 225:855–879.

Roh, J.Y., and J.R. Stanley. 1995. Plakoglobin binding by human Dsg3 (pemphigus vulgaris antigen) in keratinocytes requires the cadherin-like intracytoplasmic segment. *J. Invest. Dermatol.* 104:720–724.

Sambrook, J., E.F. Fritsch, and T. Maniatis. 1989. Molecular Cloning: A Laboratory Manual. Cold Spring Harbor Laboratory, Cold Spring Harbor, NY. 545 pp.

Schäfer, S., P.J. Koch, and W.W. Franke. 1994. Identification of the ubiquitous human desmoglein, Dsg2, and the expression catalogue of a subfamily of desmosomal cadherins. *Exp. Cell Res.* 211:391–399.

Schäfer, S., S. Stumpp, and W.W. Franke. 1996. Immunological identification and characterization of the desmosomal cadherin Dsg2 in coupled and uncoupled epithelial cells and in human tissues. *Differentiation.* 60:99–108.

Schiltz, J.R., B. Michel, and R. Papay. 1978. Pemphigus antibody interaction with human epidermal cells in culture. *J. Clin. Invest.* 62:778–788.

Schiltz, J.R., B. Michel, and R. Papay. 1979. Appearance of "pemphigus acantholysis factor" in human skin cultured with pemphigus antibody. *J. Invest. Dermatol.* 73:575–581.

Schmidt, A., H.W. Heid, S. Schäfer, U.A. Nuber, R. Zimbelmann, and W.W. Franke. 1994. Desmosomes and cytoskeletal architecture in epithelial differentiation: cell type-specific plaque components and intermediate filament anchorage. *Eur. J. Cell Biol.* 65:229–245.

Schwarz, M.A., K. Owaribe, J. Kartenbeck, and W.W. Franke. 1990. Desmosomes and hemidesmosomes: constitutive molecular components. *Annu. Rev. Cell Biol.* 6:461–491.

Shimizu, H., T. Masunaga, A. Ishiko, A. Kikuchi, T. Hashimoto, and T. Nishikawa. 1995. Pemphigus vulgaris and pemphigus foliaceus sera show an inversely graded binding pattern to extracellular regions of desmosomes in different layers of human epidermis. *J. Invest. Dermatol.* 105:153–159.

Stanley, J.R. 1990. Pemphigus: skin failure mediated by autoantibodies. *JAMA (J. Am. Med. Assoc.).* 264:1714–1717.

Stanley, J.R. 1993*a*. Pemphigus. *In* Dermatology in General Medicine. T.B. Fitzpatrick, A.Z. Eisen, K. Wolff, I.M. Freedberg, and K.F. Austen, editor. McGraw-Hill, New York. 606–615.

Stanley, J.R. 1993*b*. Cell adhesion molecules as targets of autoantibodies in pemphigus and pemphigoid, bullous diseases due to defective epidermal cell adhesion. *Adv. Immunol.* 53:291–325.

Sundberg, J.P. 1994. The balding (bal) mutation, chromosome 18. In Handbook of Mouse Mutations with Skin and Hair Abnormalities: Animal Models and Biomedical Tools. J.P. Sundberg, editor. CRC Press, Boca Raton. 187–191.

Tanaka, T., N.J. Korman, H. Shimizu, R.A.J. Eady, V. Klaus-Kovtun, K. Cehrs, and J.R. Stanley. 1990. Production of rabbit antibodies against carboxy-terminal epitopes encoded by bullous pemphigoid cDNA. *J. Invest. Dermatol.* 94:617–623.

Theis, D.G., P.J. Koch, and W.W. Franke. 1993. Differential synthesis of type 1 and type 2 desmocollin mRNAs in human stratified epithelia. *Int. J. Dev. Biol.* 37:101–110.

Thomas, K.R., C. Deng, and M.R. Capecchi. 1992. High-fidelity gene targeting in embryonic stem cells by using squence replacement vectors. *Mol. Cell. Biol.* 12:2919–2923.

Troyanovsky, S.M., L.G. Eshkind, R.B. Troyanovsky, R.E. Leube, and W.W. Franke. 1993. Contributions of cytoplasmic domains of desmosomal cadherins to desmosome assembly and intermediate filament anchorage. *Cell.* 72:561–574.

Troyanovsky, S.M., R.B. Troyanovsky, L.G. Eshkind, V.A. Krutovskikh, R.E. Leube, and W.W. Franke. 1994. Identification of the plakoglobin-binding domain in desmoglein and its role in plaque assembly and intermediate filament anchorage. *J. Cell Biol.* 127:151–160.

Tybulewicz, V.L.J., C.E. Crawford, P.K. Jackson, R.T. Bronson, and R.C. Mulligan. 1991. Neonatal lethality and lymphopenia in mice with a homozygous disruption of the c-abl proto-oncogene. *Cell.* 65:1153–1163.

Wheeler, G.N., A.E. Parker, C.L. Thomas, P. Ataliotis, D. Poynter, J. Arnemann, A.J. Rutman, S.C. Pidsley, F.M. Watt, D.A. Rees et al. 1991. Desmosomal glycoprotein DGI, a component of intercellular desmosome junctions, is related to the cadherin family of cell adhesion molecules. *Proc. Natl. Acad. Sci. USA.* 88:4796–4800.

Zhang, H., P. Hasty, and A. Bradley. 1994. Targeting frequency for deletion vectors in embryonic stem cells. *Mol. Cell. Biol.* 14:2404–2410.

TABLE 1

Autoimmune Disease	Autoantigen	Autoantigen Reference	Knockout Reference
Autoimmune Polyglandular Syndrome Type 1	P450 1A2	Clement et al., *J Clin. Endocrinol. & Metabol.* 82:1353-1361 (1997)	Liang et al., *Proc. Natl Acad. Sci. USA* 93:1671-1676 (1996)
Halothane Hepatitis	P450 2E1	Eliasson et al., *Mol. Pharmacol.* 50:573-582 (1996)	Lee et al., *J. Biol. Chem.* 271:12063-12067 (1996).
Autoimmune Polyendocrine Syndrome	Tryptophan hydroxylase	Ekwall et al., *Lancet* 352:279-283 (1998)	Walther et al., *Science*, 299:76 (2003)
Celiac Disease	Tissue trans-glutaminase 2	Dieterich et al., *Nat. Med.* 3:797-801 (1997)	Laurenzi et al., *Mol. Cell. Biol.* 21:148-155 (2001)
Systemic Lupus Erythematosus	Ro	McCauliffe et al., *J. Invest. Dermatol.* 100:73S-79S (1993)	Xue et al., *Proc. Natl. Acad. Sci. USA* 100:7503-7508 (2003)
Insulin-dependent Diabetes Mellitus	Islet cell auto-antigen 69 (ICA69)	Pietropaolo et al., *J. Clin. Invest.* 92:359-371 (1993)	Winer et al., *J. Immunol.* 168:475-482 (2002)
Insulin-dependent Diabetes Mellitus	IA-2	Lan et al., *Proc. Natl. Acad. Sci. USA* 93:6367-6370 (1996)	Saeki et al., *Diabetes* 51:1842-1850 (2002)
Insulin-dependent Diabetes Mellitus	GAD65	Kaufman et al., *J. Clin. Invest.* 89:283-292 (1992)	Asada et al., *Biochem. Biophys. Res. Commun.* 229:891-895(1996)
IgA Pemphigus	Desmocollin 1	Hashimoto et al., *J. Invest. Dermatol.* 109:127-131 (1997)	Chidgey et al., *J. Cell Biol.* 155:821-832 (2001)
Stiff-Man Syndrome	Amphiphysin 1	De Camilli et al., *J. Exp. Med.* 178:2219-2223 (1993)	Di Paolo et al., *Neuron* 33:789-804 (2002)
Rasmussen's Encephalitis	GluR3	Rogers et al., *Science* 265:648-651 (1994)	Meng et al., *Neuron* 39:163-176 (2003)

0021-972X/97/$03.00/0
Journal of Clinical Endocrinology and Metabolism

Vol. 82, No. 5
Printed in U.S.A.

Cytochrome P450 1A2 Is a Hepatic Autoantigen in Autoimmune Polyglandular Syndrome Type 1*

MARIA GRAZIA CLEMENTE, PETRA OBERMAYER-STRAUB, ANTONELLA MELONI, CHRISTIAN P. STRASSBURG, VINCENZO ARANGINO, ROBERT H. TUKEY, STEFANO DE VIRGILIIS, AND MICHAEL P. MANNS

Department of Gastroenterology and Hepatology (M.G.C., P.O.-S., C.P.S., M.P.M.), Hannover Medical School, 30625 Hannover, Germany; Institute of Clinica e Biologia dell'eta evolutiva (M.G.C., A.M., S.D.V.), Universita degli Studi di Cagliari, Cagliari, Italy 09121; Patologia Medica II (V.A.), Universita degli Studi di Cagliari, Cagliari, Italy; and University of California at San Diego Cancer Center (R.H.T.), Department of Medicine and Pharmacology, San Diego, La Jolla, California 92093

ABSTRACT

Autoantibodies directed against proteins of the adrenal cortex and the liver were studied in 88 subjects of Sardinian descent, namely six patients with autoimmune polyendocrine syndrome type 1 (APS1), 22 relatives of APS1 patients, 40 controls with other autoimmune diseases, and 20 healthy controls. Indirect immunofluorescence, using tissue sections of the adrenal cortex, revealed a cytoplasmatic staining pattern in 4 of 6 patients with APS1. Western blotting with adrenal mitochondria identified autoantigens of 54 kDa and 57 kDa. Western blotting with placental mitochondria revealed a 54-kDa autoantigen. The 54-kDa protein was recognized by 4 of 6 patients with APS1 both in placental and adrenal tissue, whereas the 57-kDa protein was detected only by one serum. Using recombinant preparations of cytochrome P450 proteins, the autoantigens were identified as P450 scc and P450 c17.

One of six APS1 patients suffered from chronic hepatitis. In this patient, immunofluorescence revealed a centrolobular liver and a proximal renal tubule staining pattern. Western blots using microsomal preparations of human liver revealed a protein band of 52 kDa. The autoantigen was identified as cytochrome P450 1A2 by use of recombinant protein preparations. P450 1A2 represents the first hepatic autoantigen reported in APS1. P450 1A2 usually is not detected by sera of patients with isolated autoimmune liver disease and might be a hepatic marker autoantigen for patients with APS1. (*J Clin Endocrinol Metab* 82: 1353–1361, 1997)

AUTOIMMUNE polyendocrine syndrome type 1 (APS1) is a rare autosomal recessive disorder characterized by a variable combination of disease components (1–3). The first clinical manifestation of APS1 usually occurs in childhood, and progressively new components appear throughout life, the majority (63%) of the patients suffering from three to five of them (2). The most frequent components in APS1 are chronic mucocutaneous candidiasis, hypoparathyroidism, adrenocortical failure, and gonadal failure in females (2, 3). Hepatitis is a serious, but less frequent, disease component (1–3). Defects in immunoregulation were suggested to play a role in the disease mechanism, and the presence of organ-specific autoantibodies was demonstrated repeatedly (4–12; also see Ref. 14).

Recently, progress was made in the study of APS1-related Addison's disease, which affects more than 60% of APS1 patients (1–3). Adrenal autoantigens in APS1 are cytochromes P450 c17, P450 scc, and P450 c21, which are all enzymes involved in steroidogenesis (5–13). P450 c21 is reported to be present in the adrenal cortex; expression of P450 c17 is found in adrenal tissue and steroid-producing cells of testis and ovary; and P450 scc is expressed in adrenals, gonads, and placenta (8). It was shown previously that autoantibodies directed against the adrenal cortex alone correlate with a high risk of adrenocortical failure, and antibodies directed against steroidal cells in females, in addition, correlate with a high risk of ovarian failure (14).

Chronic hepatitis is a serious disease component present in 10–18% of patients with APS1 (1–3), and occasional deaths related to hepatitis are reported in APS1 (2, 15). However, hepatitis as a disease component of APS1 still is poorly investigated. Autoantibodies associated with autoimmune hepatitis as part of APS1 were not described before, and the corresponding antigens accordingly remained unidentified.

Here we report the characterization of six patients with APS1 and confirm P450 scc and P450 c17 as adrenal autoantigens in APS1 in patients from Sardinia. We present the first characterization of hepatic autoantibodies in patients with APS1 and the molecular identification of a hepatic autoantigen in APS 1. The molecular target, cytochrome P450 1A2, is different from the targets of LKM1 and LKM3 autoantibodies that are found in autoimmune hepatitis type 2. Potential diagnostic consequences of this finding are discussed.

Subjects and Methods

Patients

We studied six patients with APS1 (Table 1). Patient 1 suffered from liver disease. Patient 1 is female and lacks markers for hepatitis B, C, and

Received November 21, 1995. Revision received May 9, 1996. Rerevision received December 20, 1996. Accepted January 31, 1997.

Address all correspondence and requests for reprints to: Prof. M. P. Manns, Department of Gastroenterology and Hepatology, Hannover Medical School Carl-Neuberg Strasse 30625 Hannover, Germany.

* This work was supported by Grant SFB 244 of the Deutsche Forschungsgemeinschaft and USPHS Grant GM-49135 (to R.H.T.).

D viruses and HIV. Serum ceruloplasmin and α-1 antitrypsin levels are normal. She presented at the clinic at the age of 6 yr with acute hepatitis that subsequently turned chronic. Four years after the onset of hepatitis, she developed adrenal failure and chronic mucocutaneous candidiasis. A percutaneous liver biopsy revealed the histologic picture of chronic active hepatitis.

We also studied sera of 22 first-degree relatives of APS1 patients, of 40 patients with other autoimmune diseases (namely 1 with isolated Addison's disease, 10 with Hashimoto disease, 10 with insulin-dependent diabetes mellitus (IDDM), 3 with IDDM and celiac disease, 4 with autoimmune hepatitis type 1 and type 2, 10 with chronic hepatitis C virus, 1 with primary billiary cirrhosis, 1 with systemic lupus erythematosus) and of 20 healthy controls (Table 2). All subjects were of Sardinian descent. As shown in Fig. 1, the 6 APS1 patients belong to 5 different families. In family 3 and in family 5, 1 sister affected by APS1 died of acute adrenal failure (at 8 yr old and 15 yr old, respectively). None of the other 22 relatives had evidence of an autoimmune disorder.

Materials

Human liver tissue was obtained during liver transplantation from a patient's liver that was removed because of hepatocellular carcinoma. The tissue otherwise would have been discarded.

For the immunofluorescence studies, a goat antihuman IgM, IgG, IgA polyclonal FITC-conjugated antiserum was used (Dianova, Hamburg, Germany). The antibody used for Western blots was an alkaline phosphatase conjugated anti-IgG, IgA, and IgM antiserum (Dianova). The complementary DNA (cDNA) construct pBS/1A2, used for subcloning the cDNA of P450 1A2, was provided by one of us (R. H. Tukey, UC San Diego). The cDNA constructs, pUC18-scc and PUC 18-c17, containing the cDNAs of P450 scc and P450 c17, were a kind gift of Walter Miller, UC San Francisco (16, 17). The DH5α FIQ cells were from GIBCO-BRL (Eggenstein, Germany).

Nitro blue tetrazolium chloride/5-bromo-chloro-3 indolyl phosphate substrates and isopropylthiogalactoside (IPTG) for bacterial induction were from Promega (Madison, WI). Vectors for the expression of bacterial proteins were from the pQE 30 series of Quiagen (Hilden, Ger-

TABLE 1. Disease components and analytical results of six patients with APS1

Patients	Disease components in APS1	IF Adrenals (Human)	WB Adrenal mitoch. (Human)	WB Placental mitoch. (Human)	WB P450 scc	WB P450 c17	IF Liver (Rat)	IF Kidney (Rat)	WB Liver micros. (Human)	WB P4501A2
Patient 1	M. candidiasis Addison's disease (11) Chronic hepatitis (15) Pernicious anemia	1:40	54 kD	54 kD	+		1:1000	1:320	52 kD	+
Patient 2	M. candidiasis Hypoparathyroidism Addison's disease (8)	1:1000	54 kD 57 kD	54 kD	+	+				
Patient 3	Hypoparathyroidism									
Patient 4	M. candidiasis Hypoparathyroidism Addison's disease (7) Fat malabsorption Polyneuropathy	1:1000	54 kD	54 kD	+					
Patient 5	M. candidiasis Hypoparathyroidism Addison's disease (19) Pernicious anemia	1:40	54 kD	54 kD	+					
Patient 6	M. candidiasis Hypoparathyroidism Addison's disease (7)									

Listed in parentheses in the column of disease components is the time interval between the first occurrence of chronic active hepatitis or Addison's disease and the time point of blood sampling. M. candidiasis, mucocutaneous candidiasis; IF, indirect immunofluorescence; WB, Western blot.

TABLE 2. Diseases and analytical results of the control subjects

	Addison's disease	IDDM	IDDM & celiac disease	Hashimoto's disease	AIH	HCV	PBC	SLE	APS1 Relatives	Healthy controls
No. subjects	1	10	3	10	4	10	1	1	22	20
IF/WB human adrenals										
IF rat liver/kidney										
LKM					2	2				
SMA (F-actin)					2					
ANA				8	1	5		1		
AMA							1			
WB human liver microsomes:										
LKM (50 kDa)					1	2				
LKM (50 kDa + 68 kDa)					1					
WB—P450 c17										
WB—P450 scc										
WB—P450 1A2										

IDDM, Insulin-dependent diabetes mellitus; AIH, autoimmune hepatitis; HCV, hepatitis C virus; PBC, primary biliary cirrhosis; SLE, systemic lupus erythematosus; IF, indirect immunofluorescence; WB, Western blot; LKM, liver kidney microsomal autoantibodies; SMA, smooth muscle antibodies; ANA, antinuclear antibodies; AMA, antimitochondrial antibodies.

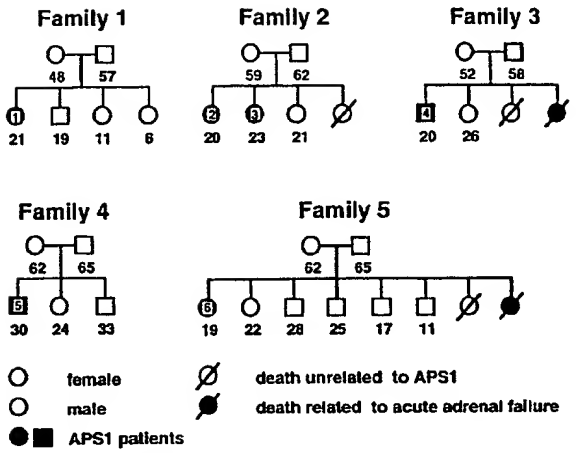

FIG. 1. Families of the APS1 patients studied. The *number below* each *symbol* indicates the age in years. *Numbers in a black square* or *circle* indicate the number for this APS1 patient used in this paper. The dead relatives of APS1 patients are not included in this study.

many). Restriction enzymes were purchased from New England Biolabs (Schwalbach/Taunus, Germany), and the sequencing kit was from Pharmacia (Freiburg, Germany). All other chemicals used were of the highest degree available and purchased from Sigma (Heidelberg, Germany).

Methods

Indirect immunofluorescence. Frozen sections of rat liver and kidney and of human adrenals were incubated at room temperature for 30 min with patient sera at dilutions of 1:40, 1:80, 1:160, 1:320, 1:640, and 1:1280 in phosphate buffered saline (PBS). The sections were washed twice in PBS and incubated with a goat antihuman anti-IgM, IgA, and IgG FITC-conjugated antiserum at a dilution of 1:100 in PBS for 30 min at room temperature. The sections were washed twice in PBS and embedded in 90% vol/vol glycerol in PBS. For analysis of the results, we used an Olympus IMT2 microscope (Olympus, Hamburg, Germany) fitted with an Olympus SC 35 type 12 camera.

Antigen preparations. One gram of frozen tissue was homogenized with 20 strokes of a homogenisator in 3 mL ice-cold solution of 0.25 mol/L sucrose containing 0.1 mmol/L phenylmethylsulfonylfluoride. Cellular debris and nuclei were removed by centrifugation (Sigma SK15 centrifuge, 1000 × *g*, 4 C, 15 min). The supernatant was fractionated by centrifugation (Sigma SK15 centrifuge, 3000 × *g*, 4 C, 15 min) into a mitochondrial pellet and the supernatant containing microsomes and the soluble liver proteins.

Mitochondrial preparation. For mitochondrial preparations, the pellet was resuspended in the sucrose solution, and the mitochondria were washed three times, as described above. The washed pellet was frozen on dry ice and stored at −80 C. The resulting fraction is enriched in mitochondria.

Microsomal preparation. The supernatant containing microsomes and soluble liver proteins was subjected to ultracentrifugation (Beckman ultracentrifuge, TLA 100 rotor, 100,000 × *g*, 4 C, 1 h). The supernatant was discarded, and the microsomal pellet was resuspended in 0.5 ml sucrose solution. The subcellular fractions were frozen on dry ice and stored at −80 C. The resulting preparation is enriched in microsomal proteins.

Western blotting. Fifty micrograms of tissue antigens and bacterial extracts containing recombinant proteins were separated on a 10% polyacrylamide gel and transferred to nitrocellulose (18, 19). The blots were blocked in PBS containing 0.1% Tween 20 and 5% nonfat dry milk and incubated for 1 h with a 1:100 dilution of the patient's or control sera in PBS-Tween. The blots were then washed three times for 10 min with PBS-Tween and incubated for 1 h with a 1:1000 dilution of an alkaline phosphatase conjugated antihuman IgM, IgA, IgG antiserum in PBS-Tween. After washing three times with PBS-Tween and two times in alkaline phosphatase buffer, the blots were developed using the nitro blue tetrazolium chloride/5-bromo-chloro-3 indolyl phosphate detection system (20).

Cloning and expression of recombinant cytochromes P450s. The primers used for amplification and modification of cytochromes P450 according to Waterman (21) had the following sequences: P450 scc-primers: 5′ GTGAGGTACCGCTCTGTTATTAGCAGTTTTCTGTCAGTCCTGGTCAAAGGCTAC 3′ and 5′ GCTCAAGCTTTGATCACTGCTGGGTTGCTTC 3′; P450 c17-primers: 5′ GTGAGGTACCGCTCTGTTATTAGCAGTTTTCTGCTTACCCTAGCTTATTTGTTT 3′ and 5′ GCTCAAGCTTTGATCACTGCTGGGTTGCTTC 3′; P450 1A2-primers: 5′ GTGAGGTACCGCTCTGTTATTAGCAGTTTTTCTGTTCTGCCTGGTATTCTGGGTG 3′ and 5′ GCTCAAGCTTCAATTGATGGAGAACG 3′.

The cDNAs were amplified by the Vent polymerase according to the manufacturers recommendations (New England Biolabs) (Fig. 2A). Denaturation was performed for 1 min at 94 C, annealing for 2 min at 62 C, and the elongation for 3 min at 72 C. Twenty cycles were applied for the amplification of the cDNA, with a final elongation step of 7 min. After PCR, the modified cDNAs were purified by the Quiagen PCR-purification kit, digested with *Hin*dIII and *Kpn*I, and inserted into the respective restriction sites of the pQE 30 vector. All constructs were confirmed by several restriction digests and by sequence analysis of the N- and C-termini, using the T7 sequencing kit, according to the manufacturer's recommendations. For expression of the recombinant cytochrome P450 proteins, all cDNA-expression vectors were transfected into DH5αFIQ cells. The expression of the recombinant proteins was induced by the addition of IPTG to a final concentration of 2 mmol/L for 3 h after the cells were grown to late-log phase. The cells were harvested by centrifugation, lysed in SDS-sample buffer, and the proteins were analyzed by SDS-PAGE and Western blotting. The expression of cytochrome P450 1A2 was further confirmed by Western blotting using a polyclonal rabbit antihuman P4501A2 antibody that was a kind gift from Prof. P. Beaune of the University of Paris.

Absorption studies. For absorption experiments, all sera were incubated with total proteins from *Escherichia coli* (*E. coli*) cells, carrying the expression vector alone or expressing the recombinant cytochromes P450 c17, P450 scc, or P450 1A2, according to the method described by Uibo *et al.* (8). Experiments of indirect immunofluorescence and immunoblotting (of human adrenal, human liver antigen preparations, and recombinant P450 enzymes) were performed with nonadsorbed and absorbed sera.

Results

Indirect immunofluorescence on human adrenal sections

Indirect immunofluorescence studies of the sera were performed on cryosections of human adrenal tissue (Table 1). Four of six APS1 sera detected tissue antigens in all three layers (zona glomerulosa, the zona fasciculata, and the zona reticularis) of the human adrenal cortex. None of the 82 other sera, including the serum from a patient with idiopathic Addison's disease, recognized adrenal antigens.

Immunoblotting with human adrenal antigens

To further characterize the adrenal autoantigens involved, we prepared mitochondrial subfractions of human adrenal and placental tissues. Western blotting, with patient sera 1, 2, 4, and 5, revealed a protein band at 54 kDa in both tissues (Fig. 3, A and B). In addition to the 54-kDa protein, patient serum no. 2 recognized a second band at 57 kDa in adrenal but not in placental tissue. In contrast, none of the sera from the patients' first-degree relatives, from patients with other autoimmune diseases, or from healthy controls showed pro-

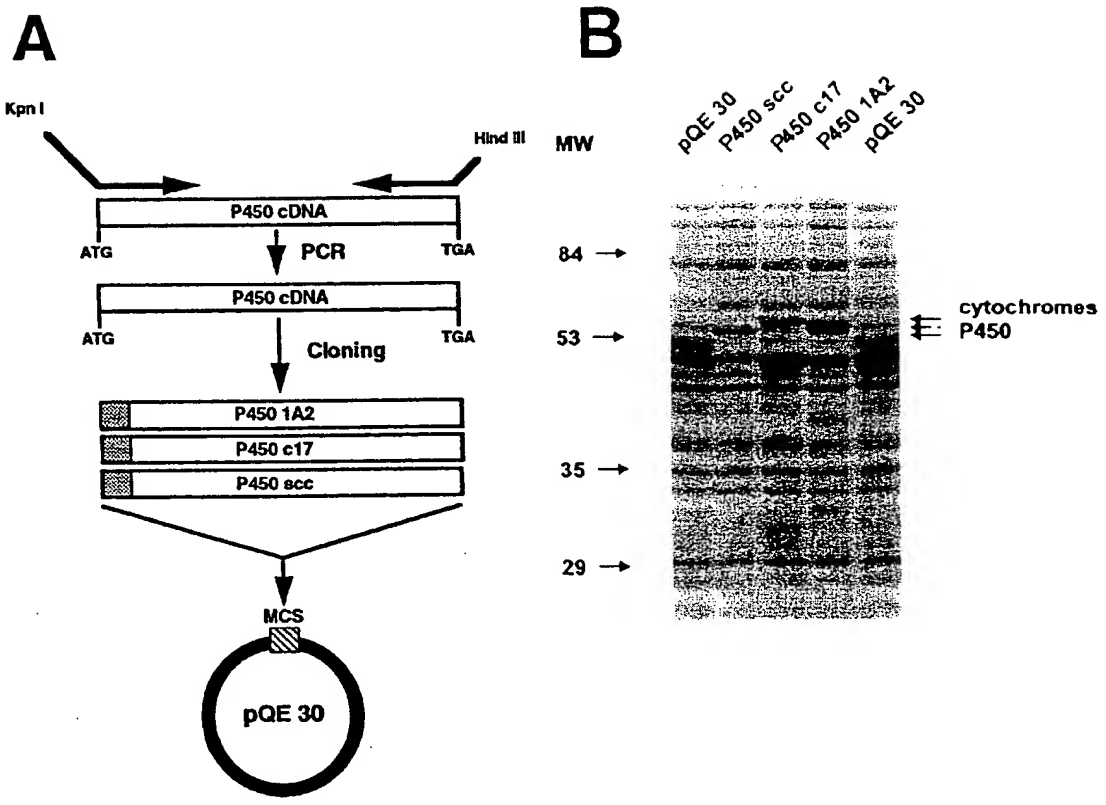

FIG. 2. Expression of recombinant cytochromes P450 scc, P450 c17, and P450 1A2 in *E. coli*. A, Construction of the expression vectors; B, the figure shows a typical result after Coomassie Blue staining of *E. coli* lysates expressing cytochromes P450 1A2, P450 scc, and P450 c17. *Arrows* on the *left* indicate the position of the molecular weight standards, *arrows* on the *right* mark the positions of the recombinant cytochrome P450 proteins.

tein bands at the levels of 54 or 57 kDa (Fig. 3, A and B, Table 2). Also, the serum of the patient with isolated Addison's disease failed to recognize any of these autoantigens. This result is in accordance with the working hypothesis that the autoantigenes recognized in immunofluorescence are the 54-kDa and 57-kDa protein bands found in Western blotting.

Immunoblotting with recombinant cytochromes P450 scc and P450 c17

Bacterial lysates of clones expressing cytochromes P450 scc and P450 c17 were used to test for the presence of autoantibodies directed against these two proteins. Sera 1, 2, 4, and 5, which also reacted with the 54-kDa adrenal and placental autoantigens, recognized the recombinant P450 scc (Fig. 3C). Serum 2, which in addition detected a 57-kDa adrenal antigen, recognized P450 c17 (Fig. 3D). In contrast, none of 82 sera from the patients' first-degree relatives, patients with other autoimmune diseases, and healthy controls recognized P450 scc or P450 c17 (Fig. 3, C and D and Table 2).

Control experiments with lysates from bacteria expressing the empty pQE vector were performed with all patient and control sera, demonstrating the specificity of the reaction by the absence of the specific 54-kDa and 57-kDa bands (data not shown).

Absorption studies were performed with recombinant preparations of P450 scc and P450 c17 (data not shown). As expected, recombinant P450 scc absorbed the bands at 54 kDa and P450 c17 the band at 57 kDa, in Western blots with human adrenal mitochondria, demonstrating the identity of the molecular targets. Interestingly, using P450 scc for absorption, no other signal was left in blots with patient sera 1, 4, and 5, whereas only the 57-kDa band remained in blots using serum 2.

Also, the signals in immunofluorescence could be absorbed by the recombinant preparations of P450 scc and P450 c17, if P450 scc were used for sera 1, 4, and 5 and a combination of P450 scc and P450 c17 was used for patient serum 2 (data not shown). These results clearly demonstrate that the immunofluorescence is caused by autoantibodies directed against cytochromes P450 scc and P450 c17. They further show that no autoantibodies directed against cytochrome P450 c21 are present that would not have been absorbed by the recombinant antigens.

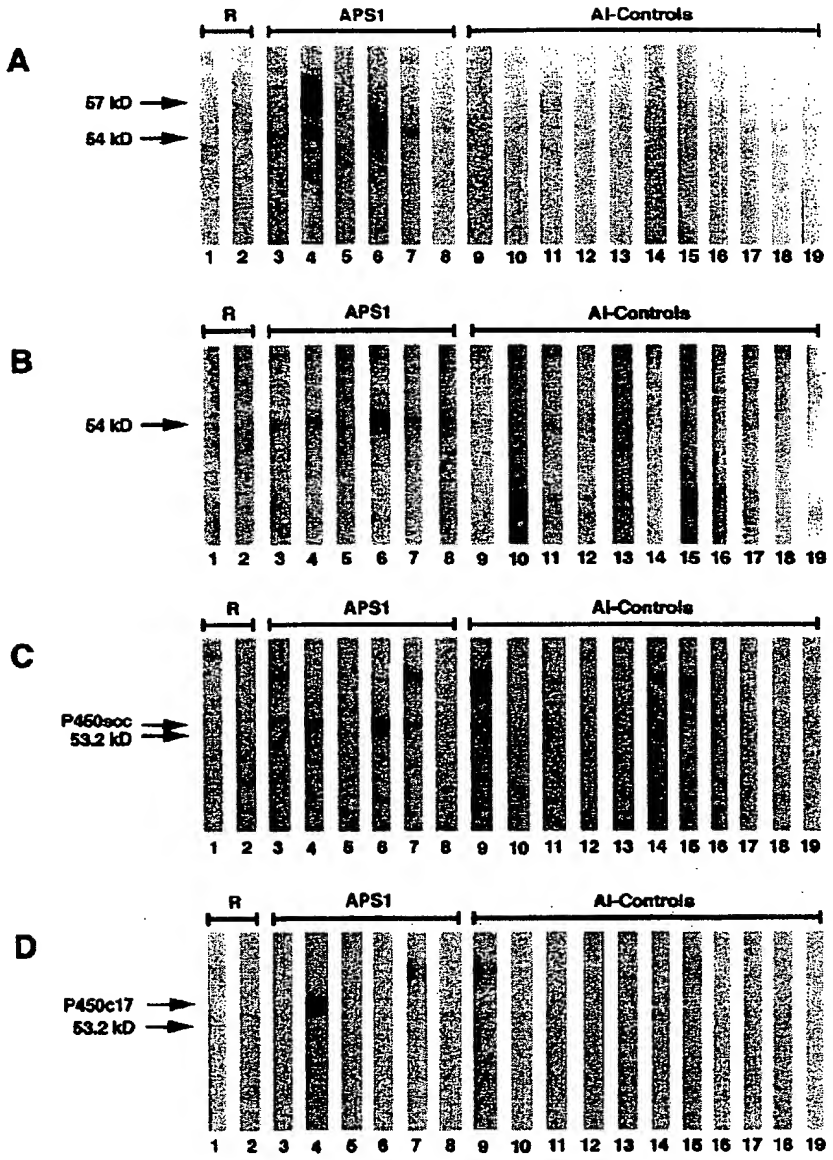

FIG. 3. Western blots with adrenal antigens, placental antigens, and recombinant cytochromes P450 scc and P450 c17. A, Western blots with mitochondrial antigens of human adrenals; B, Western blots with mitochondrial antigens of human placenta; C, Western blots with P450 scc expressed in *E. coli*; D, Western blots with P450 c17 expressed in *E. coli*; Lanes 1 and 2, first-degree APS1 patients' relatives; lanes 3–8, APS1 patients 1–6; lane 9, patient with isolated Addison's disease; lanes 10–12, patients with Hashimoto disease; lane 13, LKM1-positive patient with autoimmune hepatitis; lane 14, LKM1-positive patient with hepatitis C virus; lane 15, patient with primary biliary cirrhosis; lanes 16–18, patients with IDDM and celiac disease; lane 19, patient with systemic lupus erythematosus.

Indirect immunofluorescence on rat liver and kidney sections

To investigate the hepatic autoantigens involved in chronic autoimmune hepatitis associated with APS1, indirect immunofluorescence was performed (Tables 1 and 2). Six out of 88 sera tested revealed immunostaining of liver and kidney sections. These sera were the serum of patient 1, who suffered from chronic hepatitis and APS1, two sera from patients with LKM-1 positive autoimmune hepatitis, two sera from patients with LKM-1 positive hepatitis C, and one serum from a patient with primary biliary cirrhosis, who was positive for antimitochondrial antibodies. The staining pattern of the serum of patient 1 (Fig. 4) was characterized by a predominant staining of the perivenous hepatocytes (titer > 1:1000) and of the proximal renal tubules (titer 1:320). This pattern differs from the homogeneous staining pattern found in patients with isolated autoimmune hepatitis, suggesting that the serum of patient 2 recognizes an autoantigen that is different from LKM1 (anticytochrome P450 2D6) and LKM3 (anti-UDP-glucuronosyltransferase) autoantigenes that were described earlier to be targets for autoimmunity in patients with autoimmune and virus hepatitis (22, 23).

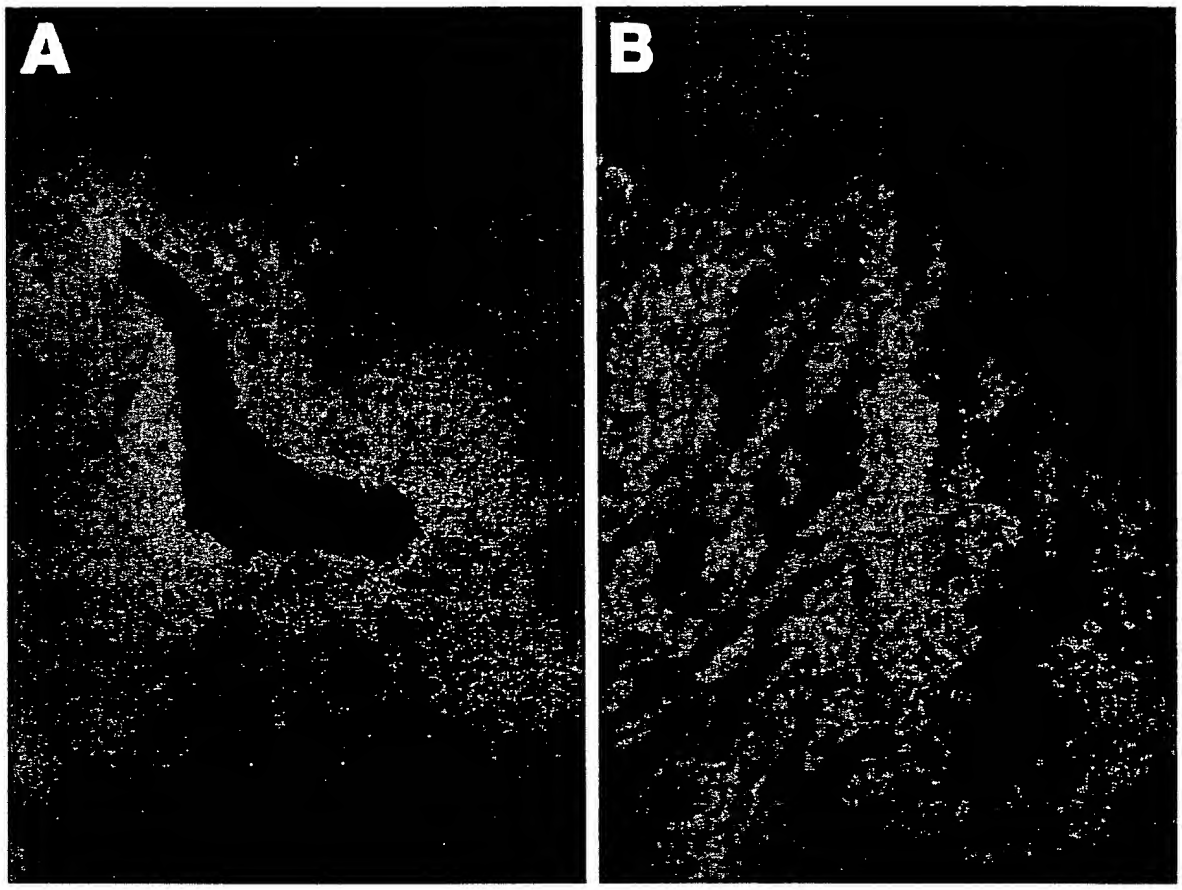

FIG. 4. Indirect immunofluorescence of rat liver and rat kidney sections. Patient serum 2 was diluted 1:320 in PBS, and indirect immunofluorescence was performed on cryosections on rat liver (A) and rat kidney (B). For immunostaining, a goat antihuman anti-IgM, IgA, and IgG FTC-conjugated antiserum was used at a dilution of 1:100.

Immunoblotting with human liver antigens

To further characterize the hepatic antigens involved, the microsomal fraction of human liver tissue was handled under nonreducing conditions and tested by immunoblotting. As shown in Fig. 5A, a protein band of approximately 52 kDa was detected by the serum of patient 1. Bands of 50 kDa and 68 kDa were detected by the LKM1-positive patients, the 50-kDa band representing an autoantibody directed against cytochrome P450 2D6 (22). The patient with PBC shows a band at about 70 kDa, which is caused by a high-titer antimitochondrial antibody produced by this patient.

Immunoblotting with P450 1A2

To identify the hepatic autoantigen recognized by patient 1, we expressed cytochrome P450 1A2 in *E. coli* (Fig. 2). Preparations of the recombinant cytochrome P450 1A2 were used in Western blotting experiments. All of the 88 sera were tested; however, only the serum of patient 1 was positive (Fig. 5B). This result demonstrates that P450 1A2 is an autoantigen in autoimmune hepatitis associated with APS1. To demonstrate the specificity of the reaction, a Western blot of serum 1 was performed, using *E. coli* extracts of clones carrying the empty vector alone, in parallel with preparations containing recombinant P450 1A2. No band appeared in the control extract, whereas a clear signal was visible in the lane containing P450 1A2 (Fig. 5C).

P450 1A2 is expressed in liver, but not in kidney, and therefore, antibodies directed against P450 1A2 were described before as LM autoantibody in patients with dihydralazine-induced hepatitis (24). There are two potential explanations for the renal immunofluorescence pattern. The first explanation consists of a cross-reaction of the autoantibody with a kidney antigen. A cross-reaction also would explain why the signal is only detected at lower serum dilutions. The second explanation is the presence of an unrelated second autoantibody present at a lower titer. To distinguish between these possibilities, absorption studies were performed.

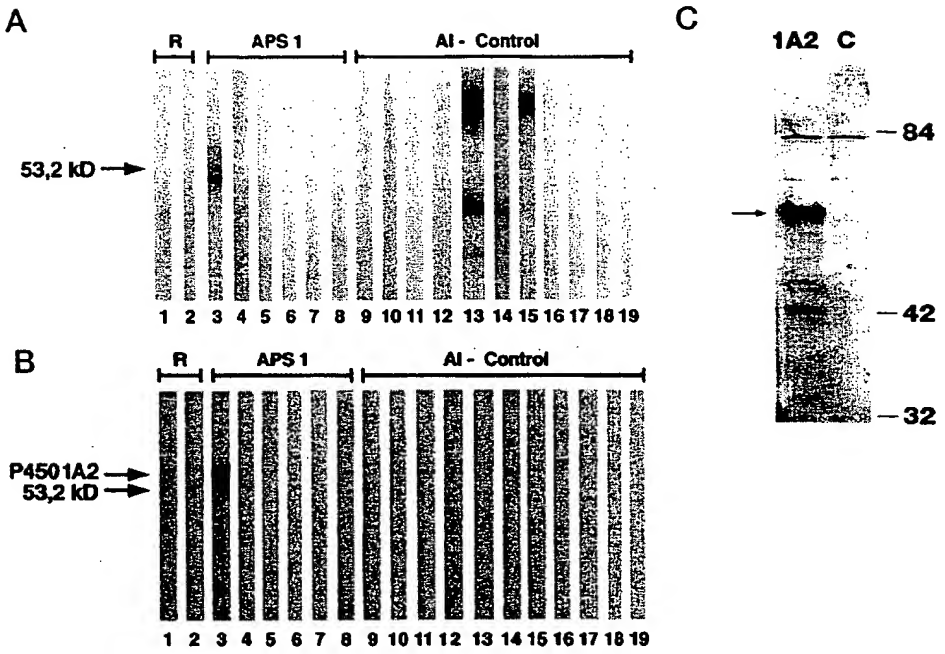

FIG. 5. Western blotting of microsomal antigens of human liver and recombinant P450 1A2. The numbering of patient sera is the same as in Fig. 3, A–C. A, Western blotting of microsomal antigens of human liver; B, Western blotting of a recombinant preparation of P450 1A2. The *arrow* on the *left* indicates the position of the recombinant cytochrome P450 1A2. C, Lysates from cells induced by IPTG carrying the empty vector (control) and expression vector for cytochrome P450 1A2 were analyzed by Western blot using the serum of patient 1, who is suffering fom APS1-related autoimmune hepatitis. The *arrow* on the *left* indicates the position of the recombinant cytochrome P450 1A2, the *arrows* on the *right* indicate the molecular mass in kDa.

Absorption studies

After absorption with preparations of recombinant P450 1A2, the immunofluorescence studies shown in Fig. 4 were repeated (data not shown). In three independent experiments, the immunofluorescence disappeared in liver and in kidney. In control experiments performed with LKM1 positive control sera, the immunofluorescence patterns persisted after absorption with the recombinant P450 1A2.

Figure 6A shows a result after Western blotting with liver microsomes. The serum of patient 1 revealed a clear signal at 52 kDa in a Western blot with liver microsomes before absorption (Fig. 6A, lane 1) the signal almost completely disappeared after absorption with P450 1A2 (Fig. 6A, lane 2). The third lane of Fig. 6A shows that the signals of an LKM1-positive serum that are not related to P450 1A2 persist after absorption with P450 1A2. Figure 6B shows a result after Western blotting using recombinant P450 1A2.

Based on these results, we conclude that the 52-kDa band detected in Western blotting experiments with liver microsomes is caused by an autoantibody directed against P450 1A2. The fact that the immunostaining of kidney sections that was found at lower serum dilutions could be absorbed sug-

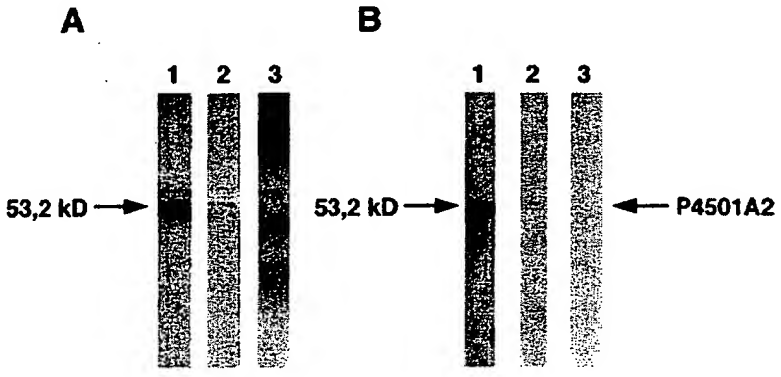

FIG. 6. Absorption experiments with recombinant P450 1A2. A, Immunoblotting using liver microsomes; B, immunoblotting using recombinant P450 1A2; Lane 1, serum of patient 1 before absorption with cytochrome P450 1A2; lane 2, serum of patient 1 after absorption with cytochrome P450 1A2; lane 3, LKM1-positive control serum after absorption with P4501A2.

gests that the autoantibody directed against P450 1A2 shows some cross-reactivity with renal autoantigens.

Discussion

APS1 is characterized by the progressive manifestation of a multitude of endocrine and nonendocrine disease components (1, 2, 3). Frequent disease components, Addison's disease, and premature ovarian failure in females are linked to the presence of adrenal and steroidal cell autoantibodies (9, 14, 25–27). Autoantigens detected by these autoantibodies in APS1 patients are P450 c21, P450 scc, and P450 c17 (5–12). In our study, four of six Sardinian patients with APS1 recognized cytochrome P450 scc, and one patient's serum detected cytochrome P450 c17. This result is in accordance with studies showing that autoantibodies directed against cytochrome P450 scc are produced with a high frequency in Scandinavian patients with APS1 (7, 8, 12); however, other investigators failed to detect autoantibodies directed against P450 scc (10). Differing results also are reported concerning the frequency of detection of P450 c17. Whereas Krohn and his colleges reported the presence of P450 c17 autoantibodies in a substantial fraction of their patients (5, 8, 9), others failed to detect reactivity directed against cytochrome P450 c17 (7, 10, 12). In our study, we confirm that cytochrome P450 c17 is recognized by sera from patients with APS1, albeit at a lower frequency than P450 scc. The identification of the autoantigens was based on apparent molecular weight in SDS-PAGE and on the use of recombinant preparations expressed in *E. coli* (Fig. 3, A–D). There also is some disagreement as to whether P450 c21 is an autoantigen in APS1. Although Uibo *et al.* (8) report P450 c21 being an autoantigen in 15/50 patients with APS1, Winqvist *et al.* (7, 12) failed to detect this autoantibody in APS1. In our group of six patients with APS1, we also did not detect other adrenal autoantigens than P450 scc and P450 c17.

The most important aspect of this paper, however, is the detection and identification of a hepatic autoantigen in patients with APS1. Ten to eighteen percent of APS1 patients develop chronic hepatitis (1–3), and occasionally, patients are reported to have died within only a few days from hepatitis, which occurred unexpectedly and without signs of prewarning (2, 15). However, in contrast to the wealth of information collected by the researchers working on adrenal and gonadal failure in APS1, very little is known about hepatitis as a disease component in APS1. Here we report for the first time the characterization of hepatic autoantigens and the identification of cytochrome P450 1A2 as hepatic autoantigen in APS1. The identification of the autoantigen was facilitated by an immunofluorescence pattern that was different from the patterns resulting from LKM1 and LKM3 autoantibodies. When Western blots were performed with rat microsomes, we failed to detect a specific protein recognized by the antiserum (data not shown). However, using human liver microsomes, a protein band of 52 kDa appeared. This is in accordance with observations published by P. Beaune and his colleges (24), who identified cytochrome P450 1A2 as hepatic autoantigen in dihydralazine hepatitis. In addition, control experiments with intestinal microsomes were performed (data not shown), demonstrating by the absence of the 52-kDa signal that an organ specific autoantigen is detected by the serum of patient 1. To prove that cytochrome P450 1A2 also is an autoantigen in APS1, P450 1A2 was expressed in *E. coli*. The serum not only specifically recognized cytochrome P450 1A2 in Western blot experiments, but absorption with recombinant P450 1A2 resulted in a complete disappearance of the immunofluorescence pattern and the reactivity in Western blots with human liver microsomes. At lower dilutions of the serum, immunofluorescence also was detected in kidney sections, in spite of the fact that P450 1A2 is not expressed in kidney. This result seems to be caused by a cross-reaction of the antibody, because the renal immunofluorescence also could be absorbed with the recombinant cytochrome P450 1A2.

Cytochrome P450 1A2 was described earlier by our group as autoantigen in an unusual case of autoimmune hepatitis (28, 29). This patient suffered from vitiligo, alopecia, and nail dystrophy and had a brother who had died from Addison's disease at the age of 8 yr. We now believe that in accordance with the criteria for diagnosis of APS1 from Neufeld (1), this patient also suffered from APS1. Adding the present patient to that previous one, we now have two patients on record suffering from autoimmune hepatitis in APS1 with cytochrome P450 1A2 as hepatic autoantigen.

Extensive control studies were performed. A total of 40 patient sera with other autoimmune diseases and 22 first-degree relatives of the patients were tested for autoantibodies directed against hepatic antigens and cytochrome P450 1A2. However, only patient serum 1 and 4 sera from patients with other liver diseases reacted with human hepatic microsomes (Fig. 5, Tables 1, 2). When extracts of expression clones containing the recombinant P450 1A2 were used, reaction of only patient serum 1 was detected, showing that the detection of the hepatic autoantibodies and P450 1A2 did not represent false positive results caused by elevated IgG-levels that are typical for patients with autoimmune diseases. Most patients with autoimmune hepatitis type 2 recognize P450 2D6, and about 10% recognize UGT 1 proteins. Of 15 German patients with autoimmune hepatitis type 2, none was found to recognize cytochrome P450 1A2 (data not shown). Determination of the exact molecular target of autoimmunity in patients with autoimmune hepatitis could help to distinguish patients with autoimmune hepatitis-2 from patients with hepatitis in APS1. The later patients should be closely monitored for the development of further disease manifestations.

Acknowledgments

We thank Prof. W. Miller for providing the cDNAs for P450 scc and P450 c17. We also thank Dr. B. Lüttig, S. Loges, and E. Schmidt for their help in the indirect immunofluorescence studies of the patient sera used in this work.

References

1. Neufeld M, Maclaren N, Blizzard R. 1980 Autoimmune polyglandular syndromes. Pediatr Ann. 9:154–162.
2. Ahonen P, Myllärniemi S, Sipilä I, Perheentupa J. 1990 Clinical variation of autoimmune polyendocrinopathy-candidiasis-ectodermal dystrophy (APECED) in a series of 68 patients. N Engl J Med. 322:1829–1836.
3. Riley WJ. 1992 Autoimmune polyglandular syndromes. Horm Res. [Suppl 38]2:9–15.
4. Arulantham K, Dwyer JM, Genel M. 1979 Evidence for defective immuno-

regulation in the syndrome of familial candidiasis endocrinopathy. N Engl J Med. 300:164–168.
5. Krohn K, Uibo R, Aavik E, Peterson P, Savilahti K. 1992 Identification by molecular cloning of an autoantigen associated with Addison's disease as steroid 17α-hydroxylase. Lancet. 339:770–773.
6. Winqvist O, Karlsson FA, Kämpe O. 1992 21-hydroxylase, a major autoantigen in idiopathic Addison's disease. Lancet. 339:1559–1562.
7. Winqvist O, Gustafsson J, Rorsman F, Karlsson F, Kampe O. 1994 Two different cytochrome P450 enzymes are the adrenal antigens in autoimmune polyendocrine syndrome type 1 and Addison's disease. J Clin Invest. 92:2377–2385.
8. Uibo R, Aavik E, Peterson P, Perheentupa J, Aranko S, Pelkonen R, Krohn K. 1994 Autoantibodies to cytochrome P450 enzymes P450 scc, P450 c17 and P450 c21 in autoimmune polyglandular diseases types I and II and in isolated Addison's disease. J Clin Endocrinol Metab. 78:323–328.
9. Uibo R, Perheentupa J, Ovod V, Krohn KJE. 1994 Characterization of adrenal autoantigens recognized by serta from patients with autoimmune polyglandular syndrome (APS) type 1. J Autoimmun. 7:399–411.
10. Song YH, Connor EL, Muir A, et al. 1994 Autoantibody epitope mapping in autoimmune Addison's disease. J Clin Endocrinol Metab. 78:1108–1112.
11. Peterson P, Krohn JE. 1994 Mapping of B cell epitopes on steroid 17a-hydroxylase, an autoantigen in autoimmune polyglandular syndrome type I. Clin Exp Immunol. 98:104–109.
12. Winqvist O, Gebre-Mehedin G, Gustafsson J, et al. 1995 Identification of the main gonadal autoantigens in patients with adrenal insufficiency and associated ovarian failure. J Clin Endocrinol Metabol. 80:1717–1723.
13. Nebert DW, Gonzalez FJ. 1987 P450 genes: structure, evolution, and regulation. Annu Rev Biochem. 56:945–993.
14. Ahonen P, Miettinen A, Perheentupa J. 1987 Adrenal and steroidal cell antibodies in patients with autoimmune polyglandular disease type I and risk of adrenocortical and ovarian failure. J Clin Endocrinol Metab. 64:494–500.
15. Michele TM, Fleckenstein J, Sgrignoli AR, Tuluvath PJ. 1994 Chronic active hepatitis in the type I polyglandular autoimmune syndrome. Postgrad Med J. 70:128–131.
16. Chung BC, Matteson KJ, Voutilainen R, Mohandas TK, Miller WL. 1986 Human cholesterol side-chain cleavage enzyme P450 scc; cDNA cloning, assignment of the gene to chromosome 15 and expression in the placenta. Proc Natl Acad Sci USA. 83:8962–8966.
17. Chung BC, Picardo-Leonard J, Haniu H, et al. 1987 Cytochrome P450 c17 (steroid 17 hydroxylase-17,20 lyase): cloning of human adrenal and testis cDNAs indicates the same gene is expressed in both tissues. Proc Natl Acad Sci USA. 84:407–411.
18. Laemmli UK. 1970 Cleavage of structural proteins during the assembly of the head of bacteriophage T4. Nature. 227:680–685.
19. Towbin HT, Staehelin T, Gordon J. 1979 Electrophoretic transfer of proteins from polyacrylamide gels to nitrocellulose sheets: procedure and some application. Proc Natl Acad Sci USA 76:4350–4354.
20. Sambrook J, Fritsch EF, Maniatis T. 1989 Molecular cloning. A laboratory manual. 2nd ed. New York: Cold Spring Harbor Laboratory Press; 18.67–18.74.
21. Barnes HJ, Arlotto MP, Waterman MR. 1991 Expression and enzymatic activity of recombinant cytochrome P450 c17 hydroxylase in *E. coli*. Proc Natl Acad Sci USA. 88:5597–5601.
22. Manns MP, Griffin KJ, Sullivan KF, Johnson EF. 1991 LKM1 autoantibodies recognize a short linear sequence in P450 IID6, a cytochrome P450 monooxygenase. J Clin Invest. 88:1370–1378.
23. Philipp T, Durazzo M, Trautwein C, et al. 1994 Recognition of uridine-diphosphate-glucuronosyl-transferases by LKM3 antibodies in chronic hepatitis D. Lancet. 344:578–581.
24. Bourdi M, Larrey D, Nataf J, et al. 1991 Anti-liver endoplasmatic reticulum autoantibodies are directed against human cytochrome P450 1A2. J Clin Invest. 85:1967–1973.
25. Irvine WJ, Chan MMW, Scarth L. 1969 The further characterization of autoantibodies reactive with extra-adrenal steroid-producing cells in patients with adrenal disorders. Clin Exp Immunol. 4:489–503.
26. Elder M, Maclaren N, Riley W. 1981 Gonadal autoantibodies in patients with hypogonadism and/or Addison's disease. J Clin Endocrinol Metab. 52:1137–1142.
27. Betterle C, Rossi A, Pria SD, et al. 1993 Premature ovarian failure: autoimmunity and natural history. Clin Endocrinol (Oxf). 389:35–43.
28. Sacher M, Blumel P, Thaler H, Manns M. 1990 Chronic active hepatitis associated with vitiligo, nail dystrophy, alopecia and a new variant of LKM antibodies. J Hepatol. 10:364–369.
29. Manns MP, Griffin KJ, Quattrochi L, et al. 1990 Identification of cytochrome P450 IA2 as a human autoantigen. Arch Biochem Biophys. 280:229–232.

0026-895X/96/030573-10$3.00/0

MOLECULAR PHARMACOLOGY, 50:573–582 (1996).

Cytochrome P450 2E1 Is a Cell Surface Autoantigen in Halothane Hepatitis

ERIK ELIASSON and J. GERALD KENNA

Department of Pharmacology and Toxicology, Imperial College School of Medicine at St. Mary's, London W2 1PG, UK

Received March 14, 1996; Accepted May 29, 1996

SUMMARY

Recent studies have shown that cytochrome P450 2E1 (CYP2E1) is a major catalyst of formation of trifluoroacetylated proteins, which have been implicated as target antigens in the mechanism of halothane hepatitis. In the present investigation, trifluoroacetylated CYP2E1 was detected immunochemically in livers of rats treated with halothane. Furthermore, high levels of autoantibodies that recognized purified rat CYP2E1 but not purified rat CYP3A were detected by enzyme-linked immunosorbent assay in 14 of 20 (70%) sera from patients with halothane hepatitis. Only very low levels of such antibodies were detected in sera from healthy controls, from patients anesthetized with halothane without developing hepatitis, or from patients with other liver diseases. The intracellular distribution of CF_3CO-adducts was studied in highly differentiated FGC4 rat hepatoma cell cultures. High levels of adducts were found after 22-hr culture in the presence of halothane, and their generation was dependent on the expression of CYP2E1. Adducts were predominantly located in the endoplasmic reticulum but also, to a minor extent, on the cell surface, as detected by immunofluorescence. A very similar distribution was found for CYP2E1 in FGC4 cells, and immunoprecipitation experiments performed in cultures of FGC4-related Fao hepatoma cells suggest that surface immunoreactivity originates from a small fraction of intact CYP2E1 apoprotein. Human CYP2E1, expressed in V79 cells after cDNA transfection, was also detected to a minor extent in the plasma membrane, whereas no immunofluorescence was evident in parental V79 cells. It is suggested that immune responses to cell surface CYP2E1 could be involved in the pathogenesis of halothane hepatitis.

The anesthetic halothane (2-bromo-2-chloro-1,1,1-trifluoroethane) is associated with a severe and sometimes fatal hepatitis in approximately one in several thousand anesthetized patients and also with a mild form of liver injury that occurs in ~25% of patients (1). The great majority of patients (>80%) who develop the severe form of liver injury, termed halothane hepatitis, have been exposed to halothane on two or more occasions, and these patients frequently exhibit rash, arthralgia, eosinophilia, and a variety of autoantibodies, which are characteristics of immune-mediated drug hepatotoxicity (1). Furthermore, a series of investigations have directly implicated immune responses to novel antigens, halothane metabolite-modified protein adducts, in the mechanism of liver injury.

Initial investigations showed that patients with halothane hepatitis exhibited cellular and humoral immune sensitization to novel antigens expressed in livers of halothane-dosed rabbits. In particular, antibodies that recognized the novel antigens were shown to be highly specific for patients with halothane hepatitis and could not be detected in various control groups, including halothane-anesthetized individuals who do not develop halothane hepatitis, patients anesthetized with halothane who develop liver injury attributable to other causes (2), and patients with the mild form of halothane-induced liver dysfunction (1). The novel halothane-induced antigens have been detected on the surface of isolated rabbit hepatocytes, and it has been shown that such hepatocytes are susceptible to antibody-mediated cytotoxic killing by normal human lymphocytes *in vitro* (2). This suggests that the antibodies could be responsible for and/or contribute to liver injury in patients *in vivo*.

Halothane is oxidized by hepatic P450 to the highly reac-

Portions of this work were presented at meetings of the British Toxicological Society and the International Society for the Study of Xenobiotics and have been published in abstract form [*Hum. Exp. Toxicol.* 14:755 (1995); *ISSX Proc.* 8:229 (1995)].

E.E. was Visiting Research Fellow from the Department of Medical Biochemistry and Biophysics, Karolinska Institutet, Stockholm, Sweden, and was supported by the Swedish Medical Society, Magnus Bergvalls Stiftelse, the Swedish Society for Medical Research 1994, and a Wellcome/Swedish Medical Research Council Travelling Fellowship (1995).

ABBREVIATIONS: SDS, sodium dodecyl sulfate; PAGE, polyacrylamide gel electrophoresis; ELISA, enzyme-linked immunosorbent assay; IP, immunoprecipitation; ER, endoplasmic reticulum; PM, plasma membrane; P450 or CYP, cytochrome P450; HRP, horseradish peroxidase; PDI, protein disulfide isomerase; FITC, fluorescein isothiocyanate; DAS, diallylsulfide; PBS, phosphate-buffered saline; BSA, bovine serum albumin; FBS, fetal bovine serum; TBS, Tris-buffered saline; PMSF, phenylmethylsulfonyl fluoride; PEST, penicillin/streptomycin; RT, room temperature; HEPES, 4-(2-hydroxyethyl)-1-piperazineethanesulfonic acid.

tive metabolite trifluoroacetylchloride, which either reacts with water to yield trifluoroacetate or binds covalently to hepatic proteins and lipids to produce trifluoroacetyl adducts (CF_3CO adducts) (3). The novel antigens recognized by antibodies from patients with halothane hepatitis have been shown to comprise a range of CF_3CO-protein adducts, which are expressed in livers of halothane-exposed rabbits, rats, and humans and are concentrated in the liver microsomal fraction (1). Studies performed using the technique of SDS-PAGE and immunoblotting (4, 5) have identified at least eight distinct CF_3CO-modified polypeptide antigens, of which all except one are derived from the lumen of the ER (4–6). In addition, a second group of antigens was identified recently that could be detected by ELISA but not by immunoblotting (7). It seems that these comprise one or more CF_3CO-modified integral membrane proteins of the ER and that the epitopes recognized by the antibodies of patients are conformational (7).

Studies undertaken *in vivo* in rats and *in vitro* in rat and human liver microsomes have shown that the P450 isozyme primarily responsible for generation of the CF_3CO adducts detectable by immunoblotting is CYP2E1 (8).[1] The major CF_3CO adduct(s) formed *in vitro* exhibited a subunit molecular mass of 55 kDa, and so could constitute CYP2E1 adducts.[1] In the current report, we demonstrate expression of CF_3CO-CYP2E1 adducts in livers of rats treated with halothane *in vivo* and the presence of autoantibodies to CYP2E1 in sera from patients with halothane hepatitis. In addition, by the use of cell model systems that express CYP2E1, we demonstrate expression of a fraction of cellular CYP2E1 and CF_3CO adducts on the cell surface. These findings indicate that CYP2E1 is a cell surface autoantigen in halothane hepatitis and suggest that this enzyme plays a dual role in the mechanism of liver injury.

Materials and Methods

Chemicals

BSA (fraction V), casein (Hammarsten grade), DAS, dithio-bis-(propionic-*N*-hydroxysuccinimide ester, protein A/Sepharose CL-4B, iodoacetamide, PMSF, Nonidet P-40 (octylphenoxy polyethoxy ethanol), Tween 20 (polyoxy ethylenesorbitan monolaurate), Triton X-100 (*t*-octylphenoxy polyethoxy ethanol), *o*-phenylenediamine, and streptavidin-agarose were purchased from Sigma Chemical (Poole, UK). Halothane was purchased from Aldrich Chemical (Gillingham, UK) and distilled to eliminate thymol (a stabilizer). Imidazole was obtained from BDH Chemicals (Merck, Lutterworth, UK). Chlormethiazole was from Astra Arcus AB (Södertälje, Sweden) and was provided by Prof. Magnus Ingelman-Sundberg (Karolinska Institutet, Stockholm, Sweden). SDS and EDTA were obtained from Koch-Light (Haverhill, UK). Protein A-HRP, acrylamide/bis (40%), polymerization initiators, and molecular mass standards were from BioRad Lab (Hemel Hempstead, UK). Ham's F12 medium [including 0.86 mg of ($ZnSO_4 \times 7H_20$)/liter], Dulbecco's modified Eagle's medium (including 4500 mg of glucose/liter), fetal bovine serum, PEST (5000 IU of penicillin/ml, 5000 μg of streptomycin/ml), geneticin sulfate (G-418), and Dulbecco's PBS were from GIBCO BRL (Life Technologies, Paisley, UK). Biotinylation reagent and Sephadex G-25 was included in a protein biotinylation module from Amersham Life Sciences (Amersham, UK). Enhanced chemiluminescent HRP substrates were also obtained from Amersham Life Sciences or from Pierce & Warriner (Chester, UK). Vectashield anti-bleach was from Vector Lab (Bretton, UK).

Purified Enzymes

CYP2E1 and P450 reductase were purified to homogeneity from livers of starved and acetone-treated male Sprague-Dawley rats in the laboratory of Prof. M. Ingelman-Sundberg (Karolinska Institutet, Stockholm, Sweden) according to a published protocol (9). Purified rat CYP3A (PCNb) was a gift from Prof. J. R. Halpert (University of Arizona, Tucson, AZ) and was purified as described previously (10).

Sera

Human sera were obtained from healthy individuals (25 sera), patients anesthetized with halothane on multiple occasions who did not develop hepatitis (six sera), patients with halothane hepatitis (20 sera), patients with primary biliary cirrhosis (seven sera), or patients with other liver disorders [i.e., chronic autoimmune hepatitis (six sera), alcoholic liver disease (four sera), and chronic viral hepatitis C (seven sera)]. Rabbit anti-CF_3CO adduct antiserum, which was produced as described in detail elsewhere (11), has been shown to recognize specifically CF_3CO-modified rat and human liver proteins in immunoblots and ELISA (5).[1] Polyclonal goat anti-human IgG/HRP or anti-rabbit IgG/HRP conjugate was from Tago Immunochemicals (Serotech, Kidlington, UK). Polyclonal goat anti-rabbit IgG/FITC conjugate was from Sigma. Polyclonal rabbit anti-CYP2E1 antiserum, raised against rat liver CYP2E1 (9) but also recognizing human CYP2E1 (12), was a gift from Magnus Ingelman-Sundberg (Stockholm, Sweden). Antiserum to PDI was obtained from a rabbit that had been immunized with rat PDI, purified essentially as described previously (13). This antiserum was shown by immunoblotting to recognize purified rat PDI (subunit molecular mass, 57 kDa) and to recognize a single 57-kDa polypeptide expressed in rat liver microsomes (results not shown).

Animals

Male Sprague-Dawley rats (200–250 g) were administered halothane (10 mmol/kg) in a single dose by intraperitoneal injection of a 21.5% (v/v) solution in sesame oil. Control rats received sesame oil only. After the indicated time intervals (see Fig. 4), rats were killed, and the livers were removed, homogenized, and subjected to differential centrifugation to obtain isolated liver microsomes (5).

Cell Cultures

FGC4 rat hepatoma cells (14) were obtained from Dr. M. Weiss (Institute Pasteur, Paris, France). These cells originated from a H4IIEC3 clone of the Reuber H35 rat hepatoma (14). Batches of FGC4 cells (2×10^6/ml) were kept frozen at −70° in 1.5 ml of Ham's F12 medium, including 25% (v/v) fetal bovine serum, 16% (v/v) dimethylsulfoxide, and 2% (v/v) PEST. Before each experiment, cells were quickly thawed at +37°, diluted into 15 ml of Ham's F12 medium [including 5% (v/v) fetal bovine serum and 2% (v/v) PEST], and cultured in 75-cm^2 plastic flasks (Corning; Costar, Cambridge, MA, or Falcon; Becton & Dickinson, Parsippany, NJ) in humidified atmosphere with 5% CO_2 at 37°. Medium was renewed after 24 hr and every second day thereafter. Rat hepatoma Fao cells (15), originating from the same H4IIEC3 clone as FGC4, were obtained from M. Ingelman-Sundberg and cultured under the same conditions as FGC4 cells. V79MZ Chinese hamster cells were provided by Prof. J. Doehmer (Technische Universität München, Munich, Germany). These cells exhibited a stable expression of human CYP2E1 after transfection with an simian virus 40 early promoter-controlled expression vector, which included human CYP2E1 cDNA (12). Both the transfected, CYP2E1-expressing V79MZh2E1 cells and the non-transfected, parental V79MZ cells were cultured in Dulbecco's mod-

[1] E. Eliasson, H. Hume-Smith, I. Gardner, I. de Waziers, P. Beaune, and J. G. Kenna. Cytochrome P450 2E1-dependent generation of trifluoroacetyl protein adducts recognized by antibodies from patients with halothane hepatitis. Submitted for publication.

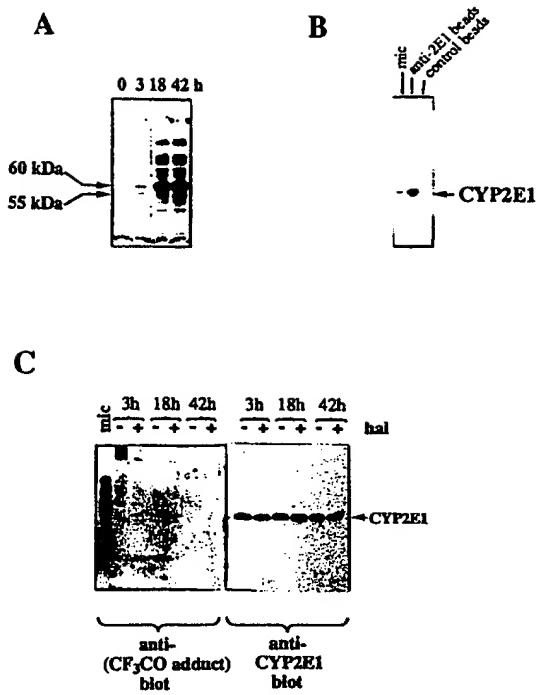

Fig. 1. Identification of CF_3CO-modified CYP2E1 in livers of rats treated with halothane. Microsomes were prepared from pooled livers of groups of four rats given an intraperitoneal dose of either halothane (10 mmol/kg) or sesame oil and killed after 3, 18, or 42 hr. A, Time-dependent formation of CF_3CO adducts. Liver microsomal proteins, corresponding to 5 μg/lane, were resolved by SDS-PAGE (8.5% gels) under reducing conditions, and immunoblots were developed using an anti-CF_3CO adduct rabbit antiserum, with final detection by peroxidase-generated chemiluminescence. B, IP of CYP2E1. Rabbit IgG specific for CYP2E1 or nonimmune IgG was cross-linked to protein A/Sepharose beads and used for precipitation of CYP2E1 from solubilized liver microsomes. Precipitates were subjected to SDS-PAGE (anti-2E1 beads and control beads, respectively), as were intact rat liver microsomes (*mic*) and CYP2E1 was detected by immunoblotting. C, Detection of CF_3CO-CYP2E1 formed in rat liver *in vivo*. CYP2E1 was immunoprecipitated from the various liver microsomes using the anti-2E1 beads; then, immunoprecipitates were resolved by SDS-PAGE (10% gels), and immunoblots were probed using anti-CYP2E1 antiserum (right) or anti-CF_3CO adduct antiserum (*left*), as was a reference sample of liver microsomes from halothane-treated animal (*mic*; 18 hr time point). Similar results were obtained in three separate experiments.

ified Eagle's medium (4500 mg/liter glucose), including 10% fetal bovine serum and 2% PEST, but geneticin sulfate (G-418, 200 μg/ml) was also included in the V79MZh2E1 cultures.

Formation of CF_3CO Adducts in FGC4 Cells

Within 5 weeks after initial thawing and reseeding, FGC4 cells were challenged with imidazole (0.5 mM, 2 days) or chlormethiazole (20 μM, 2 days) and thereafter washed twice in PBS and incubated in fresh medium for 60 min. Medium was exchanged once again, and flasks were closed air-tight with the use of silicone stoppers and parafilm. Halothane (5 μl of a 1:10 dilution in methanol) was injected through the stopper onto a strip of filter paper positioned inside the cell flask (16). This dose of halothane has been shown in a previous investigation to result in maximal generation of CF_3CO adducts in primary cultures of rat hepatocytes and has been estimated to give a final halothane concentration of ~20 μM in the culture medium (16). After the indicated incubation time (Figs. 4 and 5) at 37°, cells were washed three times in cold PBS and scraped off the plastic into Eppendorff tubes. The cells were pelleted by low-speed centrifugation and frozen in 100 μl of PBS at −20° before preparation of microsomes.

Isolation of Microsomes

Cell microsomes were isolated essentially as described previously (17) with minor modifications. The FGC4 samples (~5 × 10^6 cells) were thawed and sonicated in 1 ml of ice-cold 0.25 M sucrose, 1 mM EDTA, and 50 mM HEPES, pH 7.4. The homogenate was centrifuged at 10,000 × *g* for 10 min at +5°, and the resulting supernatant was ultracentrifuged at 109,000 × *g* for 60 min at +4° with a Beckman Optima TL ultracentrifuge with a TLA45 rotor (Beckman Instruments, Columbia, MD). Microsomal pellets were homogenized with a tight-fitting pestle in 200 μl of ice-cold centrifugation buffer. Protein concentration was determined according to the Lowry method using BSA as standard.

SDS-PAGE and Immunoblotting

Microsomal aliquots, corresponding to 150 μg (FGC4 cells) or 15 μg (rat liver), were diluted to 75 μl in water, mixed with 75 μl of SDS sample buffer [0.125 M Tris·HCl, ph 6.8, including 8% SDS (w/v), 20% glycerol (v/v), 0.002% bromphenol blue (w/v)] containing dithiotreitol (10 mg/ml), and boiled for 3 min. Thereafter, aliquots (specified in figure legends) were resolved by SDS-PAGE (using BioRad minigels with 8.5% or 10% acrylamide in the resolving gel) and transferred to nitrocellulose sheets. The sheets were incubated for 90 min at RT (20–25°) in blocking solution consisting of TBS, Tween 20 [0.05% (v/v)], fat-free dry milk [5% (w/v)], and fetal bovine serum [2% (v/v)]. Anti-CF_3CO protein antiserum was used at a 1:5000 dilution in blocking buffer and incubated for 3 hr or overnight at RT, after which blots were washed with 1% milk/TBS-Tween and incubated with goat anti-rabbit IgG/HRP conjugate at 1:5000 dilution in 1% milk/TBS-Tween for 2 hr. Primary antibody incubations with anti-CYP2E1 antiserum were performed using a 1:5000 dilution in 1% milk/TBS-Tween for 90 min at RT, followed by a thorough wash in TBS-Tween and incubation at RT for 90 min with protein A-HRP (1:3000) in 1% milk/TBS-Tween. Thereafter, sheets were washed again in TBS-Tween, and antibody reactivity was visualized using enhanced chemiluminescence HRP substrates and Hyperfilm (Amersham Life Sciences). The intensity of immunoblot signals was determined using a Molecular Dynamics scanner (Sunnyvale, CA) and ImageQuant software. The apparent molecular masses of protein adducts were estimated by comparison of their electrophoretic mobilities with those of molecular mass standards.

ELISA

Aliquots of PBS (96 μl) were added to wells of polystyrene microtiter plates (Immulon 4; Dynatech Lab, Billinghurst, UK). Subsequently, 5-μl aliquots of purified rat CYP2E1, which previously had been diluted to a final concentration of 1.8 pmol of CYP2E1/5 μl in 0.2% (w/v) sodium cholate, 50 mM HEPES, pH 7.4, were added to the wells (yielding a final protein concentration of ~1 μg/ml). Control wells received the same volumes of PBS and cholate dilutent buffer. Plates were incubated for 16 hr at +5°; then wells were washed four times in washing buffer [TBS, casein (0.5% (w/v), 0.02% (w/v) thimerosal] using a Titertek SA/12 Microplate washer (Flow Lab, ICN Biomedical, Thame, UK) at RT. Human sera (100 μl, diluted 1:100 in washing buffer) were added to the wells and plates were incubated for 3 hr at +4°. After another wash step, 100 μl of anti-human IgG/HRP conjugate (dilution 1:1000 or 1:3000 in washing buffer) was added to the wells, and plates were incubated for 2 hr at +4°. After a final wash (four times with washing buffer, then twice with TBS alone), bound HRP activity was determined by reaction with *o*-phenylenediamine (7) and determinations of absorbance at 490 nm (performed using a Titertek Multiskan Plus MkII Plate Reader; Flow Lab). The same protocol was used in ELISA studies of antibody binding to rat CYP3A and purified P450 reductase.

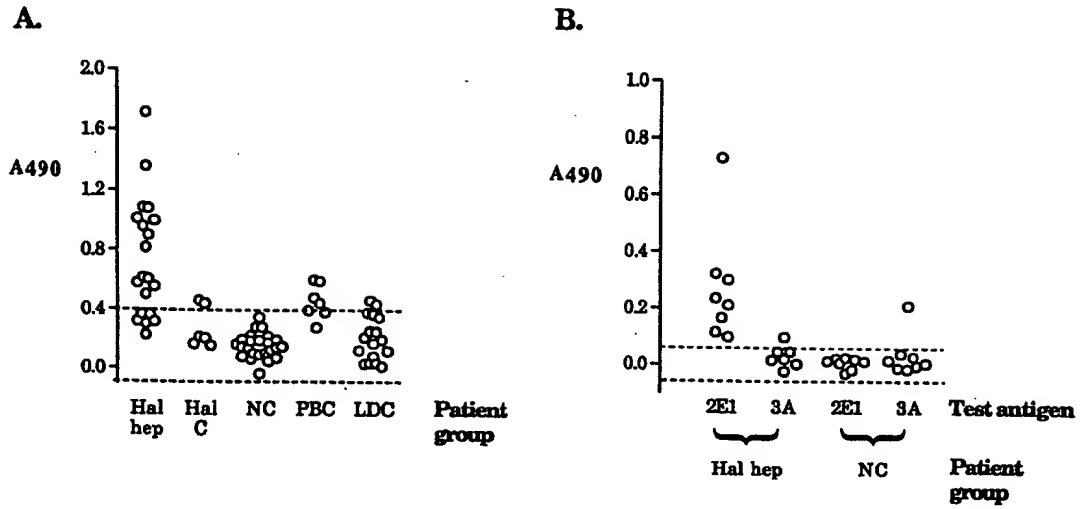

Fig. 2. Expression of anti-CYP2E1 antibodies in the sera of patients with halothane hepatitis. Binding of human antibodies (serum dilution 1:100) to purified rat CYP2E1 (A) or rat CYP2E1 and rat CYP3A (B) was investigated by ELISA. The dilutions of secondary antibody (goat anti-human IgG/HRP conjugate) were 1:1000 for A and 1:3000 for B. Sera were from patients with halothane hepatitis (*Hal hep*, 20 sera), patients undergoing multiple halothane anesthesia without hepatitis (*Hal C*, six sera), healthy controls (*NC*, 25 sera), patients with primary biliary cirrhosis (*PBC*, seven sera), or patients with other liver disorders (*LDC*, 17 sera). The background reactivity of each serum against wells coated with PBS was subtracted from each presented value. The analysis was repeated twice, with similar results.

Immunofluorescence

FGC4 cells were reseeded in 3 ml of complete F12 medium (described above) in Slide-Flasks (Nunc, Roskilde, Denmark) and grown to 40–50% confluency. The medium was replaced, and FGC4 cells were incubated with or without halothane, as described above. The cells were washed (2 × 5 min) in PBS and fixed in 2.5 ml of 5% (v/v) formaldehyde in PBS for 25 min at RT. After another wash in PBS, cells were treated by slow shaking for 20 min at RT in PBS, with or without 0.2% (v/v) Triton X-100, and then incubated without shaking for 15 hr at +5° with 10% (v/v) FBS in PBS. Subsequently, the Slide-Flasks were washed briefly in PBS and incubated (gentle shaking) for 3 hr at RT with 1 ml of primary antibody solution [either anti-CYP2E1 antiserum, diluted 1:2000 in 3% (w/v) BSA in PBS, or nonimmune rabbit antiserum or anti-CF_3CO adduct antiserum, diluted 1:400 in 1% (w/v) BSA in PBS]. Cell specimens were then washed in 3 ml of 3% (w/v) BSA (3 × 10 min) and incubated with goat anti-rabbit IgG/FITC conjugate [diluted 1:200 in 0.8 ml of 3% (w/v) BSA in PBS] for 1.5 hr at RT. Finally, specimens were washed in BSA/PBS (3 × 10 min) and once in H_2O, before being mounted in Vectashield anti-bleach under a glass coverslip. The specimens were analyzed by immunofluorescence microscopy using a Zeiss Axioskop and photographed using a Nikon UFX-DX camera, with the same exposure time for all samples. The same immunofluorescence protocol was used for V79 cells. Confocal microscopy was performed using a BioRad MRC600 with a krypton/argon laser.

IP of CYP2E1 from Liver Microsomes

Coupling of IgG to insoluble beads. Protein A/Sepharose CL-4B beads (80 mg) were equilibrated in 1 ml of IP buffer [0.15 M NaCl, 0.2% (v/v) Nonidet P-40, 1 mM EDTA, 50 mM HEPES, pH 7.4], including 2% (w/v) BSA, to yield a 20% (v/v) suspension. This was incubated with 4 mg of anti-CYP2E1 IgG (9) or 200 μl of nonimmune rabbit serum by shaking on ice for 2 hr. Beads were pelleted and washed once in IP buffer/BSA and twice in PBS and then incubated with 1.5 ml of dithio-bis(propionic-*N*-hydroxysuccinimide ester (1 mM in PBS) for 45 min during shaking on ice. Beads were washed three times with glycine (2 mM) in PBS and stored in this buffer at +5°.

IP of CYP2E1. Liver microsomes (300 μg) were solubilized in 1 ml of ice-cold IP buffer including 0.5% (w/v) BSA, 1% (w/v) deoxycholate, 1 mM PMSF, and 1 mM iodoacetamide and then incubated with 75 μl of a 10% (v/v) suspension of IgG beads for 2.5 hr on ice, with continuous shaking. The beads were pelleted by centrifugation and washed three times in solubilization buffer and then three times in IP buffer. Beads were boiled for 15 min in 100 μl of SDS sample buffer without DTT and then analyzed by SDS-PAGE and immunoblotting. Sample loading was 10 μl/well, and immunoblotting was performed using either anti-CYP2E1 or anti-CF_3CO adduct antiserum.

IP of CYP2E1 from Hepatoma Cells

Biotinylation of IgG. Anti-CYP2E1 IgG (2.5 mg) was biotinylated in 2.5 ml of sodium bicarbonate buffer (40 mM, pH 8.6) using 60 μl of biotinylation reagent from Amersham Life Sciences, according to the manufacturer's recommendation. The biotinylated IgG was separated from free biotin on a Sephadex G-25 column, resulting in an approximate protein concentration of 0.8 mg/ml in PBS.

Precipitation of CYP2E1. Fao cells were grown to 90% confluency under the conditions described above for FGC4 cells and then washed in PBS at RT (3 × 5 ml) and cooled to +5° in 10 ml of PBS containing 5% (v/v) FBS. This buffer was replaced with a further 10 ml of FBS in PBS, with or without digitonin (50 μg/ml). Biotinylated anti-CYP2E1 IgG was added (approximate concentration, 4 or 16 μg/ml), and incubation was conducted for 75 min at +5°, with very gentle agitation. Cell integrity, or permeabilization of cells in the presence of digitonin, was verified in separate flasks by investigation of trypan blue uptake. Essentially all of digitonin-treated cells (>99%) took up trypan blue, compared with <0.5% of cells incubated in PBS. The antibody solution was then discarded, and cells were washed once in 10 ml of PBS containing 10% (v/v) FBS, once in 20 ml of PBS supplemented with 5% FBS, and once in 20 ml of PBS. Cells were lysed by shaking on ice for 15 min in 2.5 ml of 1% Nonidet P-40, 0.15 M NaCl, 50 mM Tris, pH 7.8, including 1 mM EDTA, 1 mM PMSF, and 1 mM iodoacetamide. The lysate was further disrupted by vortex mixing, incubation on ice for 20 min, and then centrifugation at 2500 × *g* for 5 min. The supernatant was incubated on ice for 2 hr with streptavidin-agarose (60-μl beads, pre-equilibrated in lysis buffer), and then CYP2E1 bound to biotinylated IgG was pelleted by

centrifugation. The agarose pellet was washed in lysis buffer (3 × 1 ml) and once in PBS before boiling in SDS sample buffer (60 μl), without DTT, for 5 min. Aliquots (20 μl of each sample) were subjected to SDS-PAGE and immunoblotted with anti-CYP2E1 antiserum.

Results

Identification of CF_3CO-modified CYP2E1 in livers of halothane-treated rats. Liver microsomes were isolated from rats killed at 3, 18, or 42 hr after an *in vivo* dose of halothane (10 mmol/kg, in sesame oil) and from rats killed at the same time intervals after administration of the vehicle alone. Initially, formation of microsomal CF_3CO adducts was evaluated by immunoblotting, using a specific anti-CF_3CO adduct rabbit antiserum. Although only a very low of expression of two adducts (55 and 60 kDa) was evident at 3 hr after administration of halothane (Fig. 1A), much higher levels of many different CF_3CO adducts were detected after 18 hr and after 42 hr (Fig. 1A). Subsequently, IP experiments were undertaken using anti-CYP2E1 IgG antibodies coupled to insoluble beads (see Materials and Methods) to investigate expression of CF_3CO-modified CYP2E1. This procedure resulted in efficient precipitation of CYP2E1 from detergent-solubilized microsomes (Fig. 1B). Analyses of the immunoprecipitates by immunoblotting with anti-CF_3CO adduct serum revealed the presence of CF_3CO-modified CYP2E1 in livers of halothane-dosed rats but not in livers of control rats (Fig. 1C, *left*). Expression of CF_3CO-CYP2E1 could be detected in livers at 3 hr after halothane and was maximal at 18 hr (Fig. 1C). In contrast to the expression of the majority of other CF_3CO adducts (Fig. 1A), no CF_3CO-CYP2E1 was detectable after 42 hr. No significant differences between the expression of CYP2E1 apoprotein in the liver microsomes from halothane-treated and control rats were noted (Fig. 1C, *right*).

Autoantibodies to CYP2E1 in sera of patients with halothane hepatitis. The finding that CYP2E1 was modified by reactive metabolites of halothane raised the possibility that the protein could evoke an immune response in halothane hepatitis. To investigate this, purified rat CYP2E1 was used as test antigen in ELISA studies. Only low levels of antibody binding were detected using a control group of 25 sera from healthy blood donors (Fig. 2A). In contrast, levels of antibody binding that exceeded the normal range (defined as the mean plus three standard deviations of the values obtained for the healthy blood donors) were detected in 14 of 20 (70%) sera from patients with halothane hepatitis (Fig. 2A, *Hal hep*). Testing of six sera from patients who had received multiple halothane anesthesia without sustaining liver injury revealed that four were negative for CYP2E1, whereas two gave results that were very slightly above the normal range (Fig. 2A, *Hal C*). Negative results were also obtained with 16 of 18 sera from patients with various liver diseases unrelated to halothane (chronic autoimmune hepatitis, viral hepatitis, and alcoholic hepatitis), whereas two were found very weakly positive (Fig. 2A, *LDC*). A low anti-CYP2E1 reactivity could be detected in four of seven sera from patients with primary biliary cirrhosis (Fig. 2A, *PBC*). However, it is notable that the levels of antibody binding to CYP2E1 were markedly higher for 9 of the 20 sera from patients with halothane hepatitis than for any of the various control sera (Fig. 2A). Further ELISA studies, undertaken using 10 of the sera from patients with halothane hepatitis that contained elevated levels of antibodies to CYP2E1, revealed that the sera did not contain antibodies to purified rat CYP3A (Fig. 2B) or purified rat NADPH-dependent P450 reductase (data not shown).

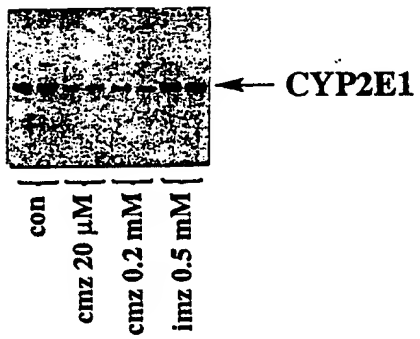

Fig. 3. Regulation of expression of CYP2E1 in FGC4 rat hepatoma cells. FGC4 cells were grown in the absence or presence of imidazole (*imz*) or chlormethiazole (*cmz*) for 2 days. Cells were harvested and microsomal CYP2E1 levels were analyzed by SDS-PAGE and immunoblotting with anti-CYP2E1 antiserum (loading 15 μg of microsomal protein/well). *con*, control.

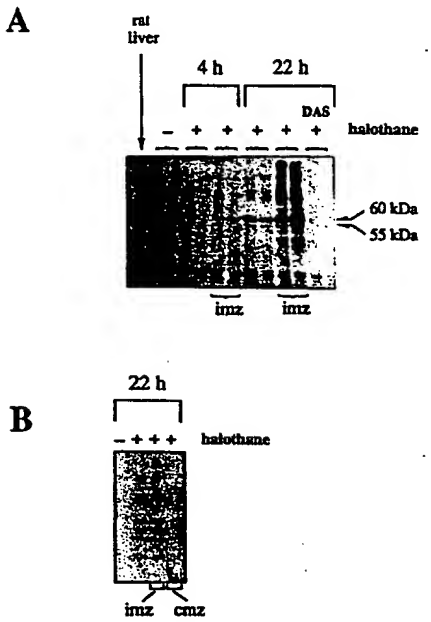

Fig. 4. Formation of microsomal CF_3CO adducts in FGC4 cells. A, Cell cultures were pretreated with or without imidazole, washed, and incubated with or without halothane. Some cells were preincubated for 1 hr with DAS (1 mM) before the addition of halothane. After 4 or 22 hr, cells were harvested in PBS, and formation of microsomal CF_3CO-protein adducts was detected by SDS-PAGE (10% gel, 40 μg of microsomal protein/well) and immunoblotting with anti-CF_3CO adduct antiserum. B, Formation of CF_3CO adducts in FGC4 cells pretreated with or without imidazole or chlormethiazole and then incubated with halothane for 22 hr. Microsomal proteins were resolved using an 8.5% gel and then developed as described above. The results were replicated two or three times.

Expression of CYP2E1 and CF_3CO adducts in FGC4 cells. The highly differentiated FGC4 rat hepatoma cell line (14) was used as a model system to study the expression of

CYP2E1 in relation to the intracellular formation of CF_3CO adducts. The basal level of CYP2E1 expression in FGC4 hepatoma cells was estimated, by immunoblotting, to be ~1-2 pmol/mg of microsomal protein. Treatment of cell cultures with the CYP2E1-stabilizer imidazole [0.5 mM, (17)] for 2 days caused a 3-fold increase in CYP2E1 expression (293 ± 126% of untreated control cells, three experiments). In contrast, the expression of CYP2E1 decreased to 25 ± 3% (three experiments) after 2 days in the presence of chlormethiazole (20 μM) (Fig. 3). As shown in Fig. 1A, CF_3CO-modified microsomal proteins were formed when FGC4 cells were pretreated with or without imidazole or chlormethiazole and thereafter incubated with halothane for 4 or 22 hr at 37°. Formation of the adducts was more rapid and extensive after pretreatment of the cells with imidazole. In these cells, only two distinct adducts (55 and 60 kDa) were detectable after 4 hr, whereas many other adducts had been formed after 22 hr (Fig. 4A). The addition of the CYP2E1-selective inhibitor DAS (18) (1 mM) to the cell cultures completely blocked adduct formation (Fig. 4A), as did pretreatment of cells with chlormethiazole (Fig. 4B).

The subcellular locations of CF_3CO adducts and CYP2E1 in FGC4 cells. Studies in which expression of CF_3CO adducts in halothane-treated FGC4 cells was investigated by indirect immunofluorescence, using the anti-CF_3CO adduct antiserum, revealed no significant expression of adducts after 4 hr (Fig. 5A), whereas intense immunofluorescence was evident after 22 hr (Fig. 5B). The fluorescence was distributed in a granular pattern throughout the cytoplasm in permeabilized cells, whereas no reactivity was seen in the area corresponding to the cell nuclei (Fig. 5, B and E), which was easily identified in phase-contrast microscopy (data not shown). A very similar picture was seen when specimens were probed for the expression of PDI, an abundant ER enzyme (Fig. 6D). However, studies of adduct expression in intact cells resulted in detection of a more diffuse immunofluorescence, which was concentrated at the edges of the cell (Fig. 5, C and F). This corresponds to the pattern expected for the plasma membrane (18a). Essentially no fluorescence was detected in cells incubated without halothane (Fig. 5D) or in cells developed using preimmune serum (data not shown).

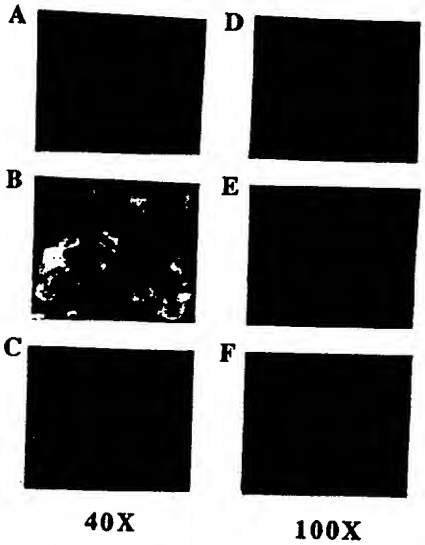

Fig. 5. Subcellular location of CF_3CO adducts in FGC4 cells. Cells were grown on Slide-Flasks and pretreated with imidazole for 2 days before washing and incubation with halothane. After 4 or 22 hr, cells were fixed in 5% formaldehyde, washed in PBS (C and F) or PBS/Triton X-100 (A, B, D, and E), and then blocked in 10% FBS and incubated with anti-CF_3CO adduct serum [1:400 in 1% (w/v) BSA/PBS] followed by anti-rabbit IgG/FITC (1:200 in 3% BSA/PBS) before analysis by immunofluorescence microscopy. A, Four hours with halothane (permeabilized cells), 40× magnification; B, 22 hr with halothane (permeabilized cells), 40×; C, 22 hr with halothane (nonpermeabilized cells), 40×; D, 22 hr without halothane (permeabilized cells), 100×; E, 22 hr with halothane (permeabilized cells), 100×; and F, 22 hr with halothane (nonpermeabilized cells), 100×.

Investigations of the cellular distribution of CYP2E1, which were undertaken using the anti-CYP2E1 antiserum, yielded a very similar pattern of results. In these studies, cells were visualized by conventional fluorescence microscopy (Fig. 6, A–C) and also by confocal microscopy (Fig. 6, D and E). In the permeabilized cells, immunofluorescence was distributed in a granular pattern all throughout the cytoplasm, whereas no fluorescence was detected in the cell nuclei (Fig. 6, B and D). Immunoreactivity was also detected to a minor extent on the surface of nonpermeabilized cells (Fig. 6, C and E). No significant fluorescence was detected in cell samples incubated without the anti-CYP2E1 antiserum (Fig. 6A).

The subcellular location of human CYP2E1 in transfected V79 cells. As a control for the specificity of the anti-CYP2E1 antibody reaction and to investigate whether human CYP2E1 is expressed on the cell surface, experiments were performed using V79 Chinese hamster fibroblast cells transfected with human CYP2E1-cDNA, which stably express human CYP2E1 (12). Immunofluorescence analysis of the transfected V79 cells after membrane permeabilization by detergent revealed that human CYP2E1 was distributed in a pattern corresponding to the ER (Fig. 7A). Immunofluorescence was also detected along the edges of cells without pretreatment with detergent (Fig. 7B). No signal was detected when nontransfected, parental V79 cells were permeabilized and incubated with the anti-CYP2E1 serum (Fig. 7C) or when immunofluorescence studies of either parental or transfected V79 cells were performed using nonimmune serum (data not shown).

Identification of intact CYP2E1 apoprotein on the surface of Fao cells. IP studies were undertaken to evaluate whether the anti-CYP2E1 reactivity evident on the surface of cultured cells corresponded to intact CYP2E1 or proteolytic fragments of the protein. Cultures of an FGC4-related cell line, Fao (15), which has a higher expression of CYP2E1 than FGC4 cells, were incubated with biotinylated anti-CYP2E1 IgG. Incubations were performed using intact cells and cells that had been permeabilized using digitonin. Subsequently, cells were washed extensively and lysed with detergent; then, the biotinylated IgG was precipitated using streptavidin-agarose beads. The precipitates were subjected to SDS-PAGE and immunoblotted using anti-CYP2E1 antiserum. This procedure showed that the CYP2E1 immunoprecipitated from the surface of nonpermeabilized cells exhibited an identical electrophoretic mobility to the intact CYP2E1 apoprotein immunoprecipitated from digitonin-permeabilized cells (Fig. 8). Furthermore, it was evident that only a very small fraction of the total cellular contents of CYP2E1 was expressed on the surface. Control experiments confirmed that no

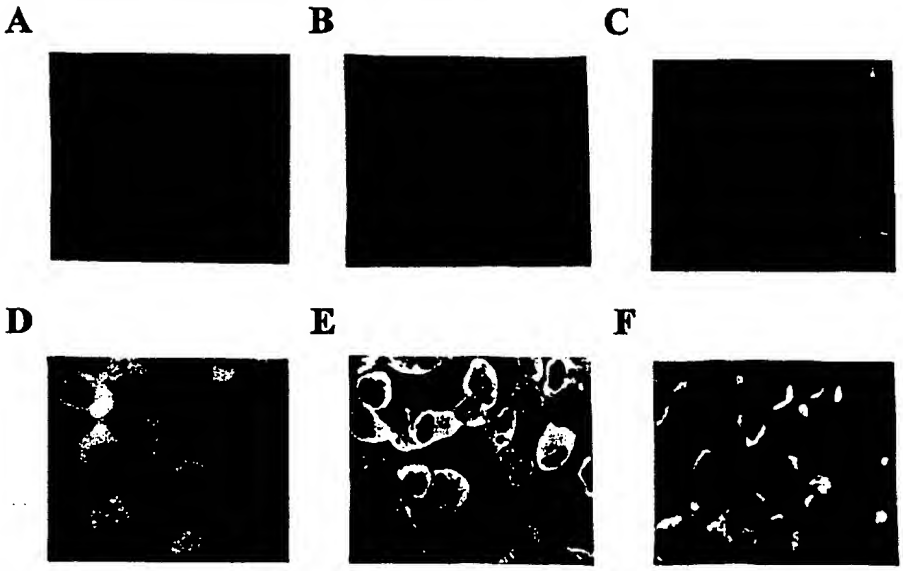

Fig. 6. Subcellular location of rat CYP2E1 in FGC4 cells. FGC4 cells were grown to 60–70% confluency in Slide-Flasks. Thereafter, cells were fixed in formaldehyde and either permeabilized by detergent or left intact, as described in Materials and Methods, and then incubated with anti-CYP2E1 antiserum (diluted 1:2000) or anti-PDI antiserum (1:2000) and, finally, FITC-coupled goat anti-rabbit IgG. The results on CYP2E1 distribution have been replicated at least five times, whereas the PDI control was performed twice. A, FITC-goat anti-rabbit IgG only (permeabilized cells), 100× magnification; B, anti-CYP2E1 antiserum (permeabilized cells), 100×; C, anti-CYP2E1 antiserum (nonpermeabilized cells), 100×; D, anti-PDI antiserum (permeabilized cells), 63×; E, confocal microscopy, anti-CYP2E1 (permeabilized cells), 40×; and F, confocal microscopy, anti-CYP2E1 (nonpermeabilized cells), 40×.

CYP2E1 was precipitated when solubilized rat liver microsomes were incubated with streptavidin-agarose in the absence of anti-CYP2E1 antibodies (data not shown).

Discussion

Identification of CF_3CO-modified CYP2E1. The IP studies of liver microsomes revealed that CF_3CO modification of CYP2E1 occurs relatively rapidly (within 3 hr) after intraperitoneal administration of a single dose of halothane to rats (Fig. 1C). The relatively rapid appearance of CF_3CO-CYP2E1, compared with other CF_3CO adducts, is consistent with the demonstration that CYP2E1 is a major catalyst of protein trifluroacetylation *in vitro* in rat and human liver microsomes[1] and *in vivo* in the rat (8). Furthermore, in agreement with previous studies (8), a 55-kDa adduct that most probably corresponds to CF_3CO-CYP2E1 was one of only two modified proteins detected at the 3-hr time point (Fig. 1A). It should also be noted that high levels of 55-kDa CF_3CO adducts have been detected after incubation of both rat and human liver microsomes with halothane *in vitro* (5, 6).[1]

It is unclear why significantly higher levels of CF_3CO-CYP2E1 were detected at 18 hr after administration of halothane than after 3 hr (Fig. 1C). One possible explanation is concentration-dependent inhibition of P450-dependent bioactivation of halothane at the early time point (16, 19).[1] Covalent modification of CYP2E1, either by cAMP-dependent phosphorylation (20) or by heme alkylation caused by reactive metabolites of carbon tetrachloride (21), has been shown to result in denaturation of the enzyme and subsequent rapid degradation. Presumably, this explains why in contrast to the many other CF_3CO adducts detectable after 18 hr, CF_3CO-modified CYP2E1 was not detectable at 42 hr (Fig. 1C).

CYP2E1 as an autoantigen in halothane hepatitis. Markedly elevated levels of antibodies that recognized rat liver CYP2E1 were detected in a high proportion (70%) of the sera from patients with halothane hepatitis, whereas only low levels of such antibodies were present in a range of control sera (Fig. 2). It is conceivable that a higher number of patient sera might recognize the human form of CYP2E1. By analogy, antibodies that recognized a purified rat liver microsomal carboxylesterase were detected by ELISA in only 2 of 10 sera from patients with halothane hepatitis (20%) (22), whereas the corresponding human enzyme, which exhibited 77% amino acid sequence identity, was recognized by 17 of 20 sera (85%) (23). Rat and human CYP2E1 are 78% homologues at the amino acid level (24), and the substrate specificities of the two forms are highly similar. However, a few minor structural differences do exist, mainly distributed on surface of the CYP2E1 molecule, as predicted by comparison with the known three-dimensional structure of bacterial CYP102 (24a). For example, it is possible that surface-located Asp92, Asp96, Pro259, and Pro262, all present only in the human enzyme, represent part of epitopes to which autoantibody binding could be reduced in ELISA assays with the rat CYP2E1 enzyme.

Sera from patients with halothane hepatitis have been shown to contain elevated levels of antibodies to numerous hepatic protein antigens other than CYP2E1 and microsomal carboxylesterase. These include protein disulfide isomerase (57 kDa), a 58-kDa protein of unknown function; calreticulin (63 kDa); ERp72 (80 kDa); and the stress proteins BiP/GRP78 (82 kDa) and endoplasmin/GRP94 (100 kDa) (reviewed in Refs. 1 and 22). Initially, immunoblotting studies revealed that the the antibodies of patients recognized unique CF_3CO-modified epitopes expressed on the adduct-modified forms of the proteins (5). However, ELISA studies undertaken using purified non-CF_3CO-modified forms of several of the proteins subsequently showed that the predominant antibody responses detectable in the sera of patients are directed against non-CF_3CO-modified epitopes, which presumably are conformational because they are not detectable by immunoblotting (1, 13, 22). It is probable that the antibody response to unmodified epitopes arises because CF_3CO adduct formation causes a specific loss of immunological tolerance and that a similar adduct-induced loss of immunological tolerance underlies the anti-CYP2E1 autoantibody response demonstrated in the present investigation. A

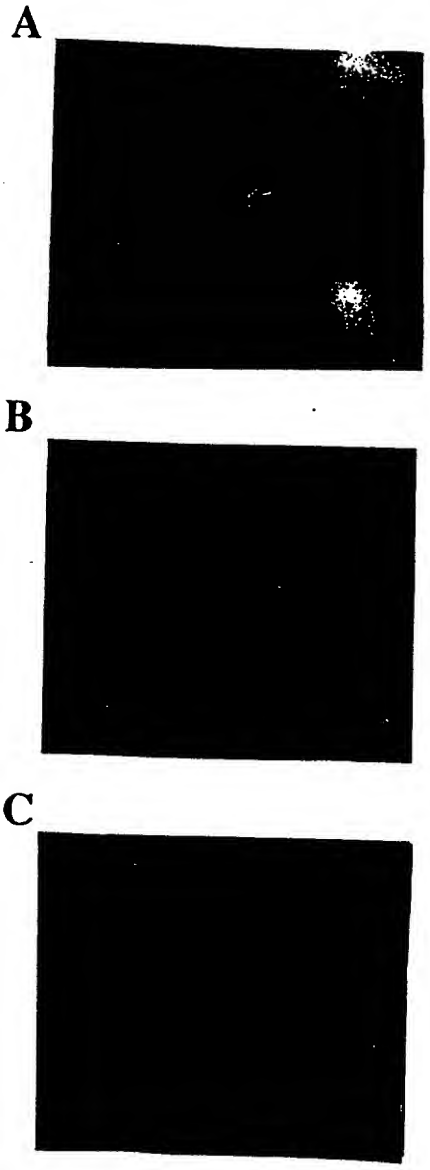

Fig. 7. Subcellular location of human CYP2E1 in V79 cells transfected with human CYP2E1-cDNA. V79 cells stably expressing human CYP2E1, or parental V79 cells, were grown to 40% confluency and fixed, washed in PBS (B) or PBS/Triton X-100 (A and C), blocked in FBS, incubated with anti-CYP2E1 antiserum and anti-rabbit IgG/FITC, and then analyzed by immunofluorescence microscopy. A, Human CYP2E1-cDNA-transfected V79 cells (permeabilized), 100× magnification; B, human CYP2E1-cDNA-transfected V79 cells (nonpermeabilized), 100×; and C, parental V79 cells (permeabilized), 100×.

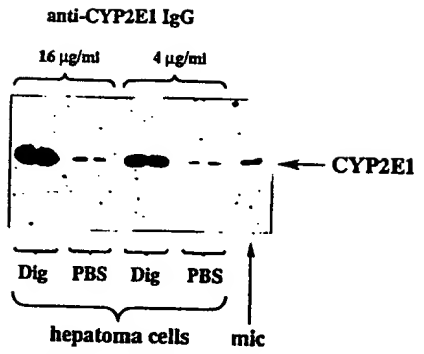

Fig. 8. IP of CYP2E1 from the surface of Fao hepatoma cells. Fao hepatoma cell cultures were permeabilized by digitonin (*Dig*) or left intact in PBS and then incubated at +5° with biotinylated anti-CYP2E1 IgG in the presence of bovine serum. Thereafter, cell cultures were washed extensively and lysed in a detergent-containing buffer including protease inhibitors. The lysate was incubated with streptavidin-agarose, which was precipitated by centrifugation and thoroughly washed in lysis buffer. Streptavidin-adsorbed proteins were eluted by boiling in SDS sample buffer, resolved by SDS-PAGE, and immunoblotted using anti-CYP2E1 antiserum. A reference sample of rat liver microsomes (*mic*; 2 μg) was also included in the electrophoresis. The results presented are duplicate precipitations from each culture. Similar results were obtained in two independent experiments.

nonspecific loss of immunological tolerance toward hepatic proteins seems unlikely because significant autoreactivity against another P450 (CYP3A) (Fig. 2) or against NADPH-dependent P450 reductase was not detected.

A specific loss of tolerance toward native CYP2E1, as a consequence of CF_3CO-CYP2E1 adduct formation, would be analogous with two other examples of drug-induced hepatitis, namely, hepatitis caused by tienilic acid and by dihydralazine. In both cases, P450 isozyme-specific metabolism of the causative agent to reactive metabolites that bind covalently to the same P450s was demonstrated, as was the presence in the sera of patients of autoantibodies that recognized the relevant P450s (CYP2C9 and CYP1A2) (25, 26). Furthermore, it was reported that anti-CYP3A antibodies are expressed in sera of patients who develop hypersensitivity reactions to carbamazepine, a CYP3A substrate (27). Overall, these findings prompted the speculation that autoimmune responses to P450s could be a common process underlying many allergic drug reactions. Clearly, the present findings are consistent with this hypothesis.

CYP2E1 is the first example of an integral membrane protein that has been shown to be recognized by antibodies from patients with halothane hepatitis. The other protein antigens identified to date are believed to be concentrated in the lumen of the endoplasmic reticulum and are either soluble or peripheral membrane proteins (6). A group of halothane-induced liver antigens was described recently that is recognized by antibodies from patients with halothane hepatitis in a conformation-dependent manner (7). It seems likely that a part of this group of microsomal neoantigens, shown to be integral membrane proteins (7), constitutes CF_3CO-CYP2E1 adducts.

Cell model systems for investigation of expression of CF_3CO adducts. Cultured FGC4 rat hepatoma cells provided a very useful model system for investigation of formation and trafficking of CF_3CO adducts. The FGC4 cell is highly differentiated and constitutively expresses liver-specific proteins, including albumin, phosphoenolpyruvate carboxykinase, alcohol dehydrogenase, and the P450 isozymes CYP2B (14) and CYP2E1 (28). Regulation of CYP2E1 expression in these cells shows several similarities with primary hepatocytes and with regulatory mechanisms operative *in vivo*. Thus, the cellular level of CYP2E1 is increased by imidazole (Fig. 3) and by ethanol (28), which is most probably explained by a specific ligand-dependent stabilization of the CYP2E1 holoenzyme (17). Chlormethiazole has been recog-

covalent binding of halothane *in vitro*: studies with [^{3}H] and [^{14}C] halothane. *J. Pharmacol. Exp. Ther.* 214:721-725 (1980).
4. Kenna, J. G., J. Neuberger, and R. Williams. Identification by immunoblotting of three halothane-induced liver microsomal polypeptide antigens recognized by antibodies in sera from patients with halothane hepatitis. *J. Pharmacol. Exp. Ther.* 242:733-740 (1987).
5. Kenna, J. G., H. Satoh, D. D. Christ, and L. R. Pohl. Metabolic basis for a drug hypersensitivity: antibodies in sera from patients with halothane hepatitis recognize liver neoantigens that contain the trifluoroacetyl group derived from halothane. *J. Pharmacol. Exp. Ther.* 245:1103-1109 (1988).
6. Kenna, J. G., J. L. Martin, and L. R. Pohl. The topography of trifluoroacetylated protein antigens in liver microsomal fractions from halothane treated rats. *Biochem. Pharmacol.* 44:621-629 (1992).
7. Knight, T. L., K. M. Scatchard, F. N. A. M. van Pelt, and J. G. Kenna. Sera from patients with halothane hepatitis contain antibodies to halothane-induced liver antigens which are not detectable by immunoblotting. *J. Pharmacol. Exp. Ther.* 270:1325-1333 (1994).
8. Kenna, J. G., J. L. Martin, H. Satoh, and L. R. Pohl. Factors affecting the expression of trifluoroacetylated liver microsomal protein neoantigens in rats treated with halothane. *Drug Metab. Dispos.* 18:788-793 (1990).
9. Johansson, I., G. Ekström, B. Scholte, D. Puzycki, H. Jörnvall, and M. Ingelman-Sundberg. Ethanol-, fasting-, and acetone-inducible cytochromes P-450 in rat liver: regulation and characteristics of enzymes belonging to the IIB and IIE gene subfamilies. *Biochemistry* 27 :1925-1934 (1988).
10. Halpert, J. R. Multiplicity of steroid-inducible cytochromes P-450 in rat liver microsomes. *Arch. Biochem. Biophys.* 263:59-68 (1988).
11. Satoh, H., Y. Fukida, D. K. Anderson, V. J. Ferrans, J. R. Gilette, and L. R. Pohl. Immunological studies on the mechanism of halothane-induced hepatotoxicity: immuno-histochemical evidence of trifluoroacetylated hepatocytes. *J. Pharmacol. Exp. Ther.* 233:857-862 (1985).
12. Schmalix, W. A., M. Barrenscheen, R. Landsiedel, C. Janzowski, G. Eisenbrand, F. J. Gonzalez, E. Eliasson, M. Ingelman-Sundberg, M. Perchermeier, F. Wiebel, H. Greim, and J. Doehmer. Stable expression of human cytochrome P450 2E1 in V79 Chinese hamster cells. *Eur. J. Pharmacol.* 293:123-131 (1995).
13. Martin, J. L., J. G. Kenna, B. M. Martin, D. Thomassen, G. F. Reed, and L. R. Pohl. Halothane hepatitis patients have serum antibodies that react with protein disulfide isomerase. *Hepatology* 18:858-863 (1993).
14. Angrand, P.-O., S. Kallenbach, M. C. Weiss, and J.-P. Rousset. An exogenous albumin promotor can become silent in dedifferentiated hepatoma variants as well as intertypic hybrids. *Cell Growth Diff.* 1:519-526 (1990).
15. de Waziers, I., J. Bouguet, P. H. Beaune, F. J. Gonzalez, B. Ketterer, and R. Barouki. Effects of ethanol, dexamethasone and RU 486 on expression of cytochromes P450 2B, 2E, 3A and glutathione transferase in a rat hepatoma cell line (Fao). *Pharmacogenetics* 2:12-18 (1992).
16. van Pelt, F. N. A. M., and J. G. Kenna. Formation of trifluoroacetylated protein antigens in cultured rat hepatocytes exposed to halothane *in vitro*. *Biochem. Pharmacol.* 48:461-471 (1994).
17. Eliasson, E., I. Johansson, and M. Ingelman-Sundberg. Ligand-dependent maintenance of ethanol-inducible cytochrome P-450 in primary rat hepatocyte cell cultures. *Biochem. Biophys. Res. Commun.* 150: 436-443 (1988).
18. Brady, J. F., D. Li, H. Ishizaki, and C. S. Yang. Effect of diallyl sulfide on rat liver microsomal nitrosamine metabolism and other monooxygenase activities. *Cancer Res.* 48:5937-5940 (1988).
18a. Loeper, J., V. Descatoire, M. Maurice, P. Beaune, J. Belghiti, D. Houssin, F. Ballet, G. Feldmann, F. P. Guengerich, and D. Pessayre. Cytochromes P-450 in human hepatocyte plasma membrane: recognition by several autoantibodies. *Gastroenterology* 104:203-216 (1993).
19. Lind, R. C., and A. J. Gandolfi. Concentration-dependent inhibition of halothane biotransformation in the guinea pig. *Drug Metab. Dispos.* 21:386-389 (1993).
20. Eliasson, E., I. Johansson, and M. Ingelman-Sundberg. Substrate-, hormone-, and cAMP-regulated cytochrome P450 degradation: *Proc. Natl. Acad. Sci. USA* 87:3225–3229 (1990).
21. Tierney, D. J., A. L. Haas, and D. R. Koop. Degradation of cytochrome P450 2E1: selective loss after labilization of the enzyme. *Arch. Biochem. Biophys.* 293:9-16 (1992).
22. Pohl, L. R., D. Thomassen, N. R. Pumford, L. E. Butler, H. Satoh, V. J. Ferrans, A. Perrone, B. M. Martin, and J. L. Martin. Hapten carrier conjugates associated with halothane hepatitis, in *Biological Reactive Intermediates IV* (C. Witmer, R. Snyder, and D. Jollow, eds.). Plenum Press, New York, 111–120 (1990).
23. Smith, G. C. M., J. G. Kenna, D. Harrison, D. Tew, and C. R. Wolf. Autoantibodies to hepatic carboxylesterase in halothane hepatitis. *Lancet* 342:963-964 (1993).
24. Song, B. J., H. V. Gelboin, S. S. Park, C. S. Yang, and F. J. Gonzalez. Complementary DNA, and protein sequences of ethanol-inducible rat and human cytochrome P-450s: transcriptional and post-transcriptional regulation of the rat enzyme. *J. Biol. Chem.* 261:16689-16697 (1986).
24a. Hasemann, C. A., R. G. Kurumbail, S. S. Boddupalli, J. A. Peterson, and J. Deisenhofer. Structure and function of cytochromes P450: a comparative analysis of three crystal structures. *Structure* 2:41–62 (1995).
25. Lecoeur, S., E. Bonierbale, D. Challine, J.-C. Gautier, P. Valadon, P. M. Dansette, R. Catinot, F. Ballet, D. Mansuy, and P. H. Beaune. Specificity of *in vitro* covalent binding of tienilic acid metabolites to human liver microsomes in relationship to the type of hepatotoxicity: comparison with two directly hepatotoxic drugs. *Chem. Res. Toxicol.* 7:434-442 (1994).
26. Leeder, J. S., A. Gaedigk, X. Lu, and V. A. Cook. Epitope mapping studies with human anti-cytochrome P450 3A antibodies. *Mol. Pharmacol.* 49: 234-243 (1996).
27. Bourdi, M., M. Tinel, P. H. Beaune, and D. Pessayre. Interactions of dihydralazine with cytochromes P450 1A: a possible explanation for the appearance of anti-P450 1A2 autoantibodies. *Mol. Pharmacol.* 45:1287-1295 (1994).
28. McGehee, R. E., Jr., M. J. J. Ronis, R. M. Cowherd, M. Ingelman-Sundberg, and T. M. Badger. Characterization of cytochrome 450 2E1 induction in a rat hepatoma FGC-4 cell model by ethanol. *Biochem. Pharmacol.* 48:1823-1833 (1994).
29. Hu, Y., V. Mishin, I. Johansson, C. von Bahr, A. Cross, M. J. J. Ronis, T. M. Badger, and M. Ingelman-Sundberg. Chlormethiazole as an efficient inhibitor of cytochrome P450 2E1 expression in rat liver. *J. Pharmacol. Exp. Ther.* 269:1286-1291 (1994).
30. Brands, R., M. D. Snider, Y. Hino, S. S. Park, H. V. Gelboin, and J. E. Rothman. Retention of membrane proteins by the endoplasmic reticulum. *J. Cell Biol.* 101:1724-1732 (1985).
31. Ilyin, G. P., M. Rissel, Y. Malledant, M. Tanguy, and A. Guillouzo. Human hepatocytes express trifluoroacetylated neoantigens after *in vitro* exposure to halothane. *Biochem. Pharmacol.* 48:561-567 (1994).
32. Deleted in proof.
33. Wu, D., and A. I. Cederbaum. Presence of functionally active cytochrome P-450IIE1 in the plasma membrane of rat hepatocytes. *Hepatology* 15: 515-524 (1992).
34. Robin, M.-A., M. Maratrat, J. Loeper, A.-M. Durand-Schneider, M. Tinel, F. Ballet, P. Beaune, G. Feldmann, and D. Pessayre. Cytochrome P4502B follows a vesicular route to the plasma membrane in cultured rat hepatocytes. *Gastroenterology* 108:1110-1123 (1995).
35. Heijink, E., F. De Matteis, A. H. Gibbs, A. Davies, and I. N. H. White. Metabolic activation of halothane to neoantigens in C57B1/10 mice: immunochemical studies. *Eur. J. Pharmacol.* 248:15-25 (1993).
36. Yamamoto, A. M., C. Mura, C. De Lemos-Chiarandini, R. Krishnamoorthy, and F. Alvarez. Cytochrome P450IID6 recognized by LKM1 antibody is not exposed on the surface of hepatocytes. *Clin. Exp. Immunol.* 92:381-390 (1993).
37. Black, S. D. Membrane topology of the mammalian P450 cytochromes. *FASEB J.* 6:680-685 (1992).
38. Terelius, Y., K. O. Lindros, E. Albano, and M. Ingelman-Sundberg. Isozyme-specificity of cytochrome P450-mediated hepatotoxicity, in *Frontiers of Biotransformation* (H. Rein and K. Ruckpaul, eds.). Vol 8. Akademic Verlag, Berlin, 187-232 (1992).

Send reprint requests to: Dr. Erik Eliasson, Division of Molecular Toxicology, Department of Environmental Medicine, Karolinska Institutet, S-171 77 Stockholm, Sweden. E-mail: erieli@ki.se

Identification of tryptophan hydroxylase as an intestinal autoantigen

Olov Ekwall, Håkan Hedstrand, Lars Grimelius, Jan Haavik, Jaakko Perheentupa, Jan Gustafsson, Eystein Husebye, Olle Kämpe, Fredrik Rorsman

Summary

Background Autoimmune polyendocrine syndrome type 1 (APS1) is an autosomal recessive disorder with both endocrine and non-endocrine features. Periodic gastrointestinal dysfunction occurs in 25–30% of APS1 patients. We aimed to identify an intestinal autoantigen.

Methods A human duodenal cDNA library was immunoscreened with serum samples from APS1 patients. A positive clone was identified and used for in-vitro transcription and translation, followed by immunoprecipitation with serum samples from 80 APS1 patients from Norway, Finland, and Sweden. Sections of normal and APS1-affected small intestine were immunostained with serum from APS1 patients and specific antibodies. An enzyme-inhibition assay was used to characterise the autoantibodies.

Findings We isolated a cDNA clone coding for tryptophan hydroxylase. 48% (38/80) of APS1 patients had antibodies to tryptophan hydroxylase, whereas no reactivity to this antigen was detected in patients with other autoimmune diseases (n=372) or healthy blood donors (n=70). 89% (17/19) of APS1 patients with gastrointestinal dysfunction were positive for antibodies to tryptophan hydroxylase, compared with 34% (21/61) of patients with no gastrointestinal dysfunction ($p<0.0001$). Serum from antibody-positive APS1 patients specifically immunostained tryptophan-hydroxylase-containing enterochromaffin cells in normal duodenal mucosa. No serotonin-containing cells were seen in duodenal biopsy samples from APS1 patients. Serum from antibody-positive APS1 patients almost completely inhibited activity of tryptophan hydroxylase.

Interpretation Tryptophan hydroxylase is an endogenous intestinal autoantigen in APS1, and there is an association between antibodies to the antigen and gastrointestinal dysfunction. Analysis of antibodies to tryptophan hydroxylase may be a valuable diagnostic tool to predict and monitor gastrointestinal dysfunction in APS1.

Lancet 1998; **352:** 279–83
See Commentary page 255

Departments of Internal Medicine (O Ekwall MD, H Hedstrand MD, O Kämpe MD, F Rorsman MD), **Pathology** (Prof L Grimelius MD), **and Pediatrics** (J Gustafsson MD), **University Hospital, Uppsala University, Uppsala, Sweden; Department of Biochemistry and Molecular Biology** (Prof J Haavik MD) **and Medical Department B** (E Husebye MD), **University of Bergen, Bergen, Norway; and Hospital for Children and Adolescents, University of Helsinki, Helsinki, Finland** (Prof J Perheentupa MD)

Correspondence to: Dr Olov Ekwall, Department of Internal Medicine, University Hospital, Uppsala University, S-751 85 Uppsala, Sweden

(e-mail: olov.ekwall@medicin.uu.se)

Introduction

Autoimmune polyendocrine syndrome type 1 (APS1; otherwise known as autoimmune polyendocrinopathy, candidosis, ectodermal dystrophy) is a monogenic, autosomal, recessively inherited disorder. The gene that causes this disorder, autoimmune regulator (*AIRE*), has been identified.[1,2] A diagnosis of APS1 requires two of the following features: mucocutaneous candidosis, adrenocortical insufficiency, and hypoparathyroidism.[3] Other common features are failure of gonad function, chronic active hepatitis, alopecia, vitiligo, insulin-dependent diabetes mellitus, and gastrointestinal dysfunction.[4] Autoantibodies to tissue-specific key enzymes are common in APS1.[5–10]

The intestinal dysfunction that affects 25–30% of APS1 patients is characterised by periodic, therapy-resistant steatorrhoea, watery diarrhoea, or constipation. These gastrointestinal disorders interfere with the pharmacological treatment of other elements of APS1. The links between the gastrointestinal symptoms and the other elements of APS1 are unclear, except that hypocalcaemia is known to exacerbate diarrhoea.[11] There is no consistent evidence that dysfunction of the exocrine pancreas[12] or intestinal lymphangiectasis[13] is the cause of the intestinal dysfunction. Organ-specific autoantibodies against many organs have been identified in APS1 patients. We aimed to identify an intestinal autoantigen that could be correlated with symptoms of gastrointestinal dysfunction in APS1 patients.

Patients and methods

Patients

Serum samples were taken from eight Swedish patients, nine Norwegian patients (table 1), and 63 Finnish patients with APS1; the clinical characteristics of the Swedish and Finnish patients have been described elsewhere.[4,10] We also tested serum samples from 224 patients with isolated insulin-dependent diabetes mellitus, 51 with Graves' disease, 31 with Hashimoto's thyroiditis, and 66 with Addison's disease. 70 healthy Swedish blood donors were used as controls. Duodenal biopsy samples from two Swedish APS1 patients with severe gastrointestinal dysfunction were used for immunostaining. The local ethics committee approved our methods, and all experiments were done in accordance with the Helsinki Declaration.

Methods

We used a commercial λGT11 cDNA library constructed from human duodenum (Clontec, Palo Alto, CA, USA) for immunoscreening (as described elsewhere[4]) of APS1 patients' (n=7) serum samples, diluted 1 in 3000. The positive cDNA clones were amplified by PCR with vector primers flanking the insert (KEBO, Solna, Sweden). The products were separated by agarose-gel electrophoresis, and purified with a Jetsorb purification kit (Genomed, Triangle Park, NC, USA). The DNA was quantified and then sequenced with internal primers (KEBO), a dye-terminator-sequencing kit (Perkin Elmer, Foster City, CA, USA), and a DNA sequencer (version 310 or 373A, Applied Biosystems, Foster City, CA, USA).

The cDNA clone that encoded tryptophan hydroxylase

Characteristic	Patient								
	1	2	3	4*	5*	6*	7	8	9
Sex	F	F	M	F	F	F	M	F	M
Year of birth	1957	1958	1948	1990	1986	1981	1990	1967	1962
Intestinal dysfunction	+	−	−	−	−	−	−	−	−
Insulin-dependent diabetes mellitus	−	−	−	−	−	−	−	−	−
Adrenal insufficiency	+	+	+	+	+	+	+	+	+
Hypoparathyroidism	+	+	+	+	−	−	+	+	+
Alopecia	−	−	+	−	−	−	−	+	−
Vitiligo	−	−	+	−	−	+	−	−	−
Pernicious anaemia	−	−	−	−	−	+	−	−	−
Gonad failure	+	+	−	−	−	−	−	+	−

*These patients are sisters.

Table 1: **Clinical characteristics of Norwegian APS1 patients**

(EC.1.14.16.4) was then subcloned into the pSP64-polyA vector (Promega, Madison, WI, USA) to allow optimum in-vitro translation and transcription. We used primers (KEBO) designed to amplify the 1335 bp coding portion of the cDNA and add a 23 bp upstream sequence (CGCAAGCTTGGATCCAATTCACC: A Falorni, personal communication), with the aim of improving transcription and introducing appropriate restriction enzyme sites. After ligation into the *Hind*III/*Xba*I site of the pSP64-polyA vector, the sequence was analysed to make sure it was correct.

The pSP64-polyA/tryptophan hydroxylase clone was transcribed and translated in vitro with a TNT-SP6 coupled reticulocyte-lysate system (Promega). The size of the radioactive product was measured by means of sodium dodecyl sulphate/polyacrylamide-gel electrophoresis (BioRad, Richmond, CA, USA). Immunoprecipitation was done,[14] and the results were expressed as:

$$\text{Tryptophan hydroxylase antibody index} = \frac{\text{cpm sample} - \text{cpm negative control}}{(\text{cpm positive control} - \text{cpm negative control})} \times 100$$

Each sample was tested three times. One APS1 patient known to have a high titre of antibodies to tryptophan hydroxylase was used as a positive control, and one of the blood donors was used as a negative control. The upper normal limit of the tryptophan hydroxylase antibody index was 14—the mean value for the blood donors plus four SD. Values above this cut-off were taken to indicate the presence of autoantibodies to tryptophan hydroxylase.

Tissue samples from normal human small intestine and duodenal biopsy samples from two APS1 patients were fixed in 10% buffered formalin and processed routinely to paraffin. 5 µm sections were immunostained by the avidin-biotin technique.[15] This method gives better results than immunofluorescence staining of unfixed tissue samples, presumably because of the large amounts of mucins and proteolytic enzymes in intestinal tissue. To assess colocalisation, consecutive intestinal sections made by the mirror technique were immunostained. Before immunostaining, the sections were stored in a citrate buffer at pH 6·0, heated in a microwave oven at 750 W for two periods of 5 min, then left in the buffer at room temperature for 15 min. The sections were then treated with 3% aqueous hydrogen peroxide in a phosphate buffer at pH 7·4 for 15 min so that endogenous peroxide activity was inhibited. We used serum samples from APS1 patients, a specific serotonin antibody (code number YC5/45, Medicorp, Montreal, Canada), and an antiserum to tryptophan hydroxylase (Chemicon, Temecula, CA, USA) as primary antibodies at a dilution of 1 in 100. Control stains omitted the primary antibody or replaced it with serum from a healthy blood donor at a dilution of one in ten.

Activity of tryptophan hydroxylase was measured by radioenzymatic assay,[16] which used 25 µmol/L tritium-labelled L-tryptophan and 0·5 µmol/L 6*R*-tetrahydrobiopterin as substrates. We used 4 µL reticulocyte lysate as the source of tryptophan hydroxylase. The final assay volume of 100 µL contained 0–10 µL patient's serum. The mixture was incubated at 30°C in pH 7·0 buffer for 10 min. A second assay, which used high-performance liquid chromatography with fluorimetric detection, gave similar results (data not shown). Gel chromatography on a Sephacryl-200 column (Pharmacia, Uppsala, Sweden) of tryptophan hydroxylase produced in vitro showed that a substantial fraction migrated as a tetramer complex (data not shown).

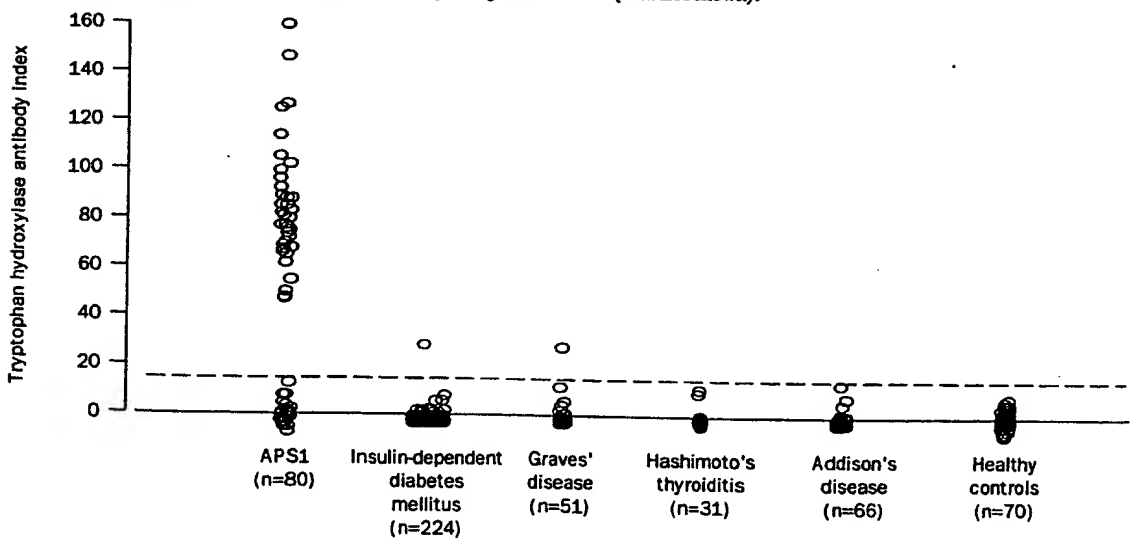

Figure 1: **Immunoreactivity to tryptophan hydroxylase of serum samples from 80 APS1 patients, controls, and patients with other autoimmune endocrine diseases**

Broken line indicates cut-off value for positive result, mean value of negative controls plus 4 SD.

Clinical disorder	Number with disorder/ total	Number with antibodies to tryptophan hydroxylase/total		p*
		With disorder	Without disorder	
Intestinal dysfunction	19/80 (24%)	17/19 (89%)	21/61 (34%)	<0·0001
Insulin-dependent diabetes mellitus	9/80 (11%)	4/9 (44%)	34/71 (48%)	>0·99
Adrenal insufficiency	66/80 (83%)	34/66 (52%)	4/14 (29%)	0·15
Hypoparathyroidism	65/80 (81%)	30/65 (46%)	8/15 (53%)	0·78
Alopecia	26/80 (32%)	11/26 (42%)	27/54 (50%)	0·63
Vitiligo	17/80 (21%)	12/17 (71%)	26/63 (41%)	0·054
Pernicious anaemia	16/80 (20%)	7/16 (44%)	31/64 (48%)	0·79
Gonad failure	27/80 (34%)	13/27 (48%)	25/53 (47%)	>0·99

*Calculated by use of Fisher's test.

Table 2: **Clinical disorders and tryptophan-hydroxylase antibodies in 80 patients with APS1**

Statistical analysis

Fisher's exact test was used to compare the frequencies of reactivity to tryptophan hydroxylase in the patients with and without intestinal and other symptoms.

Results

Immunoscreening of the cDNA library with serum samples from seven APS1 patients identified 13 positive clones, which were partly sequenced. When the clones were screened again with serum samples from nine APS1 patients, two clones showed immunoreactivity with eight of the nine serum samples. These two clones, identified as tryptophan hydroxylase and aromatic aminoacid decarboxylase, were roughly 1·5 kb and 1·4 kb in size. The clone encoding tryptophan hydroxylase was fully sequenced, and comparison with the published sequence[17] showed no variation or mutations.

After in-vitro transcription and translation of the tryptophan hydroxylase gene, we showed that 6–7% of sulphur-35-labelled methionine was incorporated into the protein. On denaturing polyacrylamide-gel electrophoresis a band with the expected size of about 58 kDa was seen.

38 (48%) of the 80 patients had a tryptophan hydroxylase antibody index of more than 14, indicating the presence of autoantibodies (figure 1). However, the frequency of reactivity varied between patients from different countries. All eight of the Swedish APS1 patients showed reactivity against tryptophan hydroxylase, compared with only 28 of the 63 Finnish patients and two of the nine Norwegian patients. There was no significant difference in frequency of reactivity between men (17 [46%] of 37) and women (21 [48%] of 43). 17 (89%) of 19 patients with intestinal symptoms showed reactivity, compared with 21 (34%) of 61 patients without intestinal symptoms ($p<0·0001$). No significant associations were shown between the presence of tryptophan hydroxylase autoantibodies and other components of the syndrome (table 2).

All eight of the serum samples from Swedish patients with autoantibodies to tryptophan hydroxylase also caused cytoplasmic staining of enterochromaffin cells. These cells were identified by staining of consecutive duodenal sections with a specific antibody against serotonin (figure 2). Some samples also stained secretory granules in Paneth cells (three) and goblet cells (three). Serum samples from blood donors and APS1 patients without

Figure 2: **Immunostaining of consecutive sections of normal human small intestine with serum from an APS1 patient (A) and a specific serotonin antibody (B)**
Reduced by 33% from ×281. Immunostains diluted 1 in 100. Cells stained by the patients' serum are the same as the enterochromaffin cells stained by the serotonin antibody (arrows).

Figure 3: **Immunostaining of normal duodenum (A) and duodenal biopsy sample from an APS1 patient with gastrointestinal dysfunction (B) with monoclonal antibody to serotonin**
Reduced by 50% from ×62·5. Immunostains diluted 1 in 100.

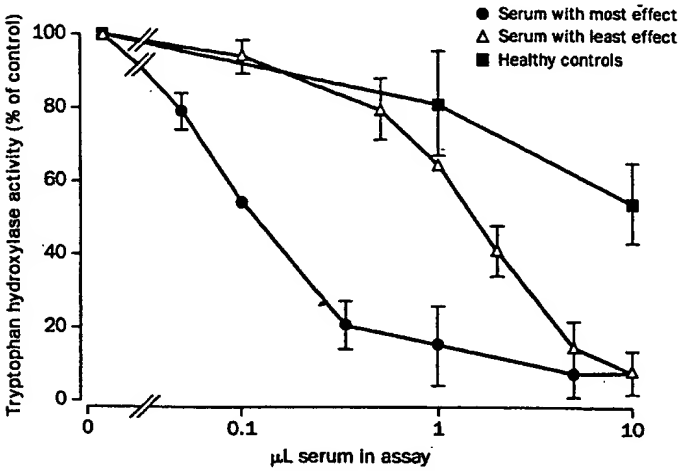

Figure 4: **Effect of serum from two APS1 patients and blood donors on activity of human tryptophan hydroxylase**

Activity without serum added 0·13 nmol min^{-1} mL^{-1}. Representative results for the patients with the greatest and the least effect are shown; values are mean of three or four separate assays (patients) or single assay (controls); error bars indicate SD.

antibodies to tryptophan hydroxylase did not cause any specific immunostaining. Immunostaining of duodenal biopsy samples from two APS1 patients showed no serotonin-containing enterochromaffin cells, unlike normal duodenum (figure 3).

To assess whether the presence of serum from APS1 patients affected the activity of tryptophan hydroxylase, we produced the enzyme by in-vitro translation and transcription, and assayed its activity in the presence of serum samples from 16 APS1 patients and 11 healthy blood donors. Addition of serum from blood donors at a final dilution of one in ten resulted in a non-specific decrease in activity to about 50–60% of that of control experiments without any serum (figure 4). The decrease was possibly due to high concentrations of protein and free aminoacids in the serum. By contrast, serum samples at a similar dilution from APS1 patients almost completely inhibited the enzyme activity; also there was partial inhibition of enzyme activity with patients' serum at a dilution at which the blood-donor serum samples had no significant effect (figure 4). At a final dilution of 1 in 100, addition of serum samples with reactivity to tryptophan hydroxylase caused 35–98% inhibition of the enzyme activity.

Discussion

Our findings suggest that tryptophan hydroxylase, the rate-limiting enzyme in the synthesis of serotonin,[18] is an important intestinal autoantigen in patients with APS1. Tryptophan hydroxylase is a 230 kDa tetramer made up of identical subunits each with a molecular mass of 58 kDa. It is expressed in serotonin-producing cells in the central nervous system and the intestine.[19] In the intestine, tryptophan hydroxylase and serotonin are present in enterochromaffin cells in the mucosa, and in neuronal cells in the submucosal and myenteric plexus. The specific staining of enterochromaffin cells in the mucosa of normal duodenum by serum from APS1 patients and the complete absence of enterochromaffin cells from duodenal biopsy samples from APS1 patients suggest that tryptophan hydroxylase is an antigen linked to intestinal dysfunction in APS1. The staining of Paneth and goblet cells suggests that there are additional intestinal autoantigens linked to APS1. These findings also support the hypothesis that autoimmune mechanisms, rather than mechanisms secondary to other components of APS1 such as candidosis or hypocalcaemia, may cause the intestinal symptoms.

Polyclonal and monoclonal antibodies to the pteridine-dependent aminoacid hydroxylases tryptophan hydroxylase, tyrosine hydroxylase, and phenylalanine hydroxylase have been generated experimentally.[20,21] Some of these antibodies are enzyme-specific, and others recognise all three enzymes. Although the mouse and rabbit antibodies can either stimulate or inhibit the enzymes, all the tryptophan hydroxylase antibodies that we found in APS1 patients are inhibitory. The inhibitory autoantibodies in APS1 patients were specific for tryptophan hydroxylase; there was no significant inhibition of human tyrosine hydroxylase (isoform 1) or human phenylalanine hydroxylase under similar experimental conditions (data not shown). Although the inhibition of tryptophan hydroxylase activity by APS1 serum in vitro shows that the autoantibody reaction is highly specific, we cannot assume that the same is true in vivo without further experimental evidence.[22]

Serotonin is generally believed to upregulate intestinal motility.[23] However, we cannot rule out the possibility that the complete loss of serotonin-producing enterochromaffin cells observed in our patients may affect other regulatory systems; this hypothesis would explain why both diarrhoea and constipation occur in APS1 patients. In our study, 17 (89%) of 19 APS1 patients with gastrointestinal problems were positive for antibodies to tryptophan hydroxylase, which suggests that these antibodies are a marker for gastrointestinal dysfunction in APS1. The absence of these antibodies from patients with other autoimmune diseases and healthy blood donors shows that these antibodies are highly specific. The finding that 34% (21 of 61) APS1 patients without gastrointestinal symptoms were positive for antibodies to tryptophan hydroxylase may be explained by under-reporting of gastrointestinal symptoms, subclinical disease, or the appearance of antibodies before the onset of clinical symptoms. The differences in frequency of autoantibodies in APS1 patients from Sweden, Finland, and Norway may perhaps be explained by the occurrence of different mutations of the *AIRE* gene in the three populations.

Our findings may lead to the identification of autoantigens in other autoimmune diseases.[24] Antibodies to tryptophan hydroxylase should be sought in people with other gastrointestinal diseases, such as Crohn's disease, ulcerative colitis, and irritable-bowel syndrome. Autoimmune enteropathy[25,26] and pseudo-obstruction in connection with small-cell carcinoma[27] are two disorders in which immunoreactivity against mucosal cells or submucosal neurons has been shown, but no autoantigen has yet been identified. Immunotherapy of malignant melanoma with tyrosinase has been proposed,[28] and tyrosinase has also been identified as an autoantigen in autoimmune vitiligo.[29] Immunisation with tryptophan hydroxylase, or with fragments of this protein, may be a suitable treatment for malignant gut carcinoids that

originate from serotonin-producing enterochromaffin cells.

The identification of tryptophan hydroxylase as an intestinal autoantigen raises the question of why many autoantigens, such as glutamic acid decarboxylase in insulin-dependent diabetes mellitus and aminoacid decarboxylase in APS1, are key enzymes in the synthetic pathways of neurotransmitters. These enzymes may share properties that make them potent triggers of the immune system. Alternatively, the presentation of these enzymes in the thymus may be incomplete, since they are expressed rather late during fetal development.

We identified tryptophan hydroxylase through immunoscreening of an intestinal cDNA library despite the fact that initial immunoblotting experiments did not show any consistent reactivity against whole intestinal tissue. In retrospect, this was probably because tryptophan hydroxylase is only present in a small fraction of intestinal cells and in concentrations below the detection level for immunoblotting. This may be of relevance when trying to identify other autoantigens in tissues containing different cell types. Further showing the specificity of the approach to immunoscreen cDNA libraries, a clone coding for aminoacid decarboxylase—a known autoantigen in APS1[8] with a much broader tissue-distribution—was identified by several serum samples.[30]

The identification of antibodies to tryptophan hydroxylase in APS1 may be a useful diagnostic marker to predict and monitor intestinal disorders associated with this autoimmune disease. It may also add to our understanding of the pathogenesis of these intestinal disorders in APS1, and lead to more effective treatment.

Contributors

Olov Ekwall was the main investigator, supervised by Fredrik Rorsman and Olle Kämpe. Håkan Hedstrand contributed to the cloning of tryptophan hydroxylase. Lars Grimelius did the immunostainings and interpreted the results. Jan Haavik designed and ran the assays for tryptophan hydroxylase. Jaakko Perheentupa in Finland, Jan Gustafsson in Sweden, and Eystein Husebye in Norway supplied serum samples from APS1 patients and information on their clinical characteristics. All investigators contributed to writing of the paper.

Acknowledgments

This study was supported by grants from the Swedish Medical Research Council, the Swedish Cancer Society, the Torsten and Ragnar Söderberg Fund, the Swedish Diabetes Association, the Swedish Society of Medicine, the Torsten Nilsson Fund, the Åke Wiberg Foundation, the Lennander Fund, and the Ernfors Family Fund. We thank Katrin Österlund and Majlis Book for technical assistance, Lars Berglund for help with statistical analysis, Mona Landin-Olsson for insulin-dependent diabetes mellitus serum samples, and Tiinamaija Tuomi for help with the Finnish APS1 serum samples.

References

1 The Finnish-German APECED Consortium. An autoimmune disease, APECED, caused by mutations in a novel gene featuring two PHD-type zinc-finger domains. *Nat Genet* 1997; 17: 399–403.

2 Nagamine K, Peterson P, Scott HS, et al. Positional cloning of the APECED gene. *Nat Genet* 1997; 17: 393–98.

3 Neufeld M, Maclaren N, Blizzard R. Autoimmune polyglandular syndromes. *Pediatr Ann* 1980; 9: 154–62.

4 Ahonen P, Myllarniemi S, Sipila I, Perheentupa J. Clinical variation of autoimmune polyendocrinopathy-candidiasis-ectodermal dystrophy (APECED) in a series of 68 patients. *N Engl J Med* 1990; 322: 1829–36.

5 Chen S, Sawicka J, Betterle C, et al. Autoantibodies to steroidogenic enzymes in autoimmune polyglandular syndrome, Addison's disease, and premature ovarian failure. *J Clin Endocrinol Metab* 1996; 81: 1871–76.

6 Peterson P, Uibo R, Peranen J, Krohn K. Immunoprecipitation of steroidogenic enzyme autoantigens with autoimmune polyglandular syndrome type I (APS I) sera; further evidence for independent humoral immunity to P450c17 and P450c21. *Clin Exp Immunol* 1997; 107: 335–40.

7 Winqvist O, Karlsson FA, Kämpe O. 21-Hydroxylase, a major autoantigen in idiopathic Addison's disease. *Lancet* 1992; 339: 1559–62.

8 Rorsman F, Husebye ES, Winqvist O, Björk E, Karlsson FA, Kämpe O. Aromatic-L-amino-acid decarboxylase, a pyridoxal phosphate-dependent enzyme, is a beta-cell autoantigen. *Proc Natl Acad Sci USA* 1995; 92: 8626–29.

9 Tuomi T, Björses P, Falorni A, et al. Antibodies to glutamic acid decarboxylase and insulin-dependent diabetes in patients with autoimmune polyendocrine syndrome type I. *J Clin Endocrinol Metab* 1996; 81: 1488–94.

10 Gebre-Medhin G, Husebye ES, Gustafsson J, et al. Cytochrome P450IA2 and aromatic L-amino acid decarboxylase are hepatic autoantigens in autoimmune polyendocrine syndrome type I. *FEBS Lett* 1997; 412: 439–45.

11 Heubi JE, Partin JC, Schubert WK. Hypocalcemia and steatorrhea—clues to etiology. *Dig Dis Sci* 1983; 28: 124–28.

12 Scire G, Magliocca FM, Cianfarani S, Scalamandre A, Petrozza V, Bonamico M. Autoimmune polyendocrine candidiasis syndrome with associated chronic diarrhea caused by intestinal infection and pancreas insufficiency. *J Pediatr Gastroenterol Nutr* 1991; 13: 224–27.

13 Bereket A, Lowenheim M, Blethen SL, Kane P, Wilson TA. Intestinal lymphangiectasia in a patient with autoimmune polyglandular disease type I and steatorrhea. *J Clin Endocrinol Metab* 1995; 80: 933–35.

14 Husebye ES, Gebre-Medhin G, Tuomi T, et al. Autoantibodies against aromatic L-amino acid decarboxylase in autoimmune polyendocrine syndrome type I. *J Clin Endocrinol Metab* 1997; 82: 147–50.

15 Portela-Gomes GM, Stridsberg M, Johansson H, Grimelius L. Complex co-localization of chromogranins and neurohormones in the human gastrointestinal tract. *J Histochem Cytochem* 1997; 45: 815–22.

16 Vrana SL, Dworkin SI, Vrana KE. Radioenzymatic assay for tryptophan hydroxylase: [^{3}H]H_2O release assessed by charcoal adsorption. *J Neurosci Methods* 1993; 48: 123–29.

17 Boularand S, Darmon MC, Ganem Y, Launay JM, Mallet J. Complete coding sequence of human tryptophan hydroxylase. *Nucleic Acids Res* 1990; 18: 4257.

18 Boadle-Biber MC. Regulation of serotonin synthesis. *Prog Biophys Mol Biol* 1993; 60: 1–15.

19 Hufton SE, Jennings IG, Cotton RG. Structure and function of the aromatic amino acid hydroxylases. *Biochem J* 1995; 311: 353–66.

20 Friedman PA, Lloyd T, Kaufman S. Production of antibodies to rat liver phenylalanine hydroxylase: cross-reactivity with other pterin-dependent hydroxylases. *Mol Pharmacol* 1972; 8: 501–10.

21 Haan EA, Jennings IG, Cuello AC, et al. Identification of serotonergic neurons in human brain by a monoclonal antibody binding to all three aromatic amino acid hydroxylases. *Brain Res* 1987; 426: 19–27.

22 Manns MP, Zanger U, Gerken G, et al. Patients with type II autoimmune hepatitis express functionally intact cytochrome P-450 db1 that is inhibited by LKM-1 autoantibodies in vitro but not in vivo. *Hepatology* 1990; 12: 127–32.

23 Kobayashi T, Hasegawa H, Kaneko E, Ichiyama A. Gastrointestinal serotonin: depletion due to tetrahydrobiopterin deficiency induced by 2,4-diamino-6-hydroxypyrimidine administration. *J Pharmacol Exp Ther* 1991; 256: 773–79.

24 Winqvist O, Gebre-Medhin G, Gustafsson J, et al. Identification of the main gonadal autoantigens in patients with adrenal insufficiency and associated ovarian failure. *J Clin Endocrinol Metab* 1995; 80: 1717–23.

25 Mirakian R, Richardson A, Milla PJ, et al. Protracted diarrhoea of infancy: evidence in support of an autoimmune variant. *BMJ* 1986; 293: 1132–36.

26 Corazza GR, Biagi F, Volta U, Andreani ML, De Franceschi L, Gasbarrini G. Autoimmune enteropathy and villous atrophy in adults. *Lancet* 1997; 350: 106–09.

27 Lennon VA, Sas DF, Busk MF, et al. Enteric neuronal autoantibodies in pseudo-obstruction with small-cell lung carcinoma. *Gastroenterology* 1991; 100: 137–42.

28 Yee C, Gilbert MJ, Riddell SR, et al. Isolation of tyrosinase-specific CD8+ and CD4+ T cell clones from the peripheral blood of melanoma patients following in vitro stimulation with recombinant vaccinia virus. *J Immunol* 1996; 157: 4079–86.

29 Song YH, Connor E, Li Y, Zorovich B, Balducci P, Maclaren N. The role of tyrosinase in autoimmune vitiligo. *Lancet* 1994; 344: 1049–52.

30 Rahman MK, Nagatsu T, Kato T. Aromatic L-amino acid decarboxylase activity in central and peripheral tissues and serum of rats with L-DOPA and L-5-hydroxytryptophan as substrates. *Biochem Pharmacol* 1981; 30: 645–49.

Identification of tissue transglutaminase as the autoantigen of celiac disease

WALBURGA DIETERICH[1], TOBIAS EHNIS[1], MICHAEL BAUER[1], PETER DONNER, UMBERTO VOLTA, ERNST OTTO RIECKEN[1] & DETLEF SCHUPPAN[1]

[1]*Department of Gastroenterology, Klinikum Benjamin Franklin, Free University of Berlin, Hindenburgdamm 30, 12200 Berlin, Germany*
[2]*Research Laboratories of Schering AG, 13342 Berlin, Germany*
[3]*Istituto di Clinical Medical generale e Terapia Medica, Policlinico S.Orsola, via Massarenti 9, 40138 Bologna, Italy*
Correspondence should be addressed to D.S.

Celiac disease is characterized by small intestinal damage with loss of absorptive villi and hyperplasia of the crypts, typically leading to malabsorption[1]. In addition to nutrient deficiencies, prolonged celiac disease is associated with an increased risk for malignancy, especially intestinal T-cell lymphoma[1-3]. Celiac disease is precipitated by ingestion of the protein gliadin, a component of wheat gluten, and usually resolves on its withdrawal. Gliadin initiates mucosal damage which involves an immunological process in individuals with a genetic predisposition. However, the mechanism responsible for the small intestinal damage characteristic of celiac disease is still under debate[4-6]. Small intestinal biopsy with the demonstration of a flat mucosa which is reversed on a gluten-free diet is considered the main approach for diagnosis of classical celiac disease[7]. In addition, IgA antibodies against gliadin and endomysium, a structure of the smooth muscle connective tissue, are valuable tools for the detection of patients with celiac disease and for therapy control[7-9]. Incidence rates of childhood celiac disease range from 1:300 in Western Ireland to 1:4700 in other European countries[10-12], and subclinical cases detected by serological screening revealed prevalences of 3.3 and 4 per 1000 in Italy and the USA, respectively[13,14]. IgA antibodies to endomysium are particularly specific indicators of celiac disease[8,15], suggesting that this structure contains one or more target autoantigens that play a role in the pathogenesis of the disease[16,17]. However, the identification of the endomysial autoantigen(s) has remained elusive. We identified tissue transglutaminase as the unknown endomysial autoantigen. Interestingly, gliadin is a preferred substrate for this enzyme, giving rise to novel antigenic epitopes.

Western blotting with serum samples from active celiac disease patients containing high-titer antiendomysial IgA antibodies did not allow us to identify specific protein bands in extracts from placenta, uterus, liver or gut, possibly because of loss of antigenicity of the partially denatured protein preparations. Therefore, we used immunoprecipitation from cell cultures, a method that can be used for target antigens susceptible to denaturation.

Cell cultures were screened by immunohistochemistry for the expression of the autoantigen with high-titer sera of patients with celiac disease and the alkaline phosphatase/monoclonal anti-alkaline phosphatase (APAAP) technique[18]. This method revealed that cytoplasmic vesicles of HT1080 (human fibrosarcoma) cells, WI38 (human embryonal fibroblasts) as well as Hep1 and HepG2 (human hepatocarcinoma) cells were specifically stained by the patients' IgA antibodies. We then immunoprecipitated both supernatant and cell lysate of HT1080 cells metabolically labeled with [^{35}S]methionine, using the IgA fraction from celiac disease sera bound to Sepharose. After separation by SDS–polyacrylamide gel electrophoresis (SDS–PAGE) and autoradiography, immunoprecipitation of the supernatant yielded varying amounts of a high-molecular-weight protein that was identified as fibronectin by western blotting and by the characteristic peptide pattern after protease V8 digest (data not shown). When the cell lysate was analyzed in a similar way, a single protein band with an apparent relative molecular weight (M_r) of 85,000 before and after disulfide reduction was immunoprecipitated exclusively with 25 celiac disease serum samples, but with none of 25 control serum samples (from healthy adults, patients with ulcerous colitis or Crohn's disease, or patients with Sjögren's syndrome, an autoimmune disease characterized by high-titer serum autoantibodies) (Fig. 1, *a* and *b*). As before, varying quantities of fibronectin could be precipitated in celiac disease, but also small amounts were precipitated in some control sera, suggesting that this large adhesive glycoprotein was not the primary target of the celiac disease autoimmune response. Instead, fibronectin may have precipitated nonspecifically or in association with the 85-kDa autoantigen (see below).

In order to further characterize the putative 85-kDa autoantigen, larger quantities of the protein were isolated by immunoprecipitation, SDS–PAGE and electrophoretic elution, followed by cleavage with endoproteinase Asp-N. The resultant fragments were separated in a 10% tricine gel (Fig. 2*a*) and transferred to a polyvinylidene-difluoride membrane. Three major cleavage products with M_r 10,000, 14,000 and 16,000 were excised and subjected to amino-terminal sequence analysis. All three peptides yielded sequences that could be clearly assigned to tissue transglutaminase (EC 2.3.2.13, tTG)[19] (Fig. 2*b*). An interaction of tTG with fibronectin has been described[20], which might explain the occasional coprecipitation of fibronectin with tTG in our immunoprecipitation experiments.

Tissue transglutaminase (synonymous with erythrocyte, cellular, endothelial, cytoplasmic, type II or liver TG)[21] belongs to a family of calcium-dependent enzymes that catalyze the crosslinking of proteins resulting in the formation of an ε-(γ-glutamyl)-lysine bond. Whereas several proteins can serve as acceptor substrates, only a limited number of donor substrates exists. The physiological role of the tTG has only been partly explored. Although the enzyme is normally localized in the cytoplasm, tTG can be released during wounding, where it associ-

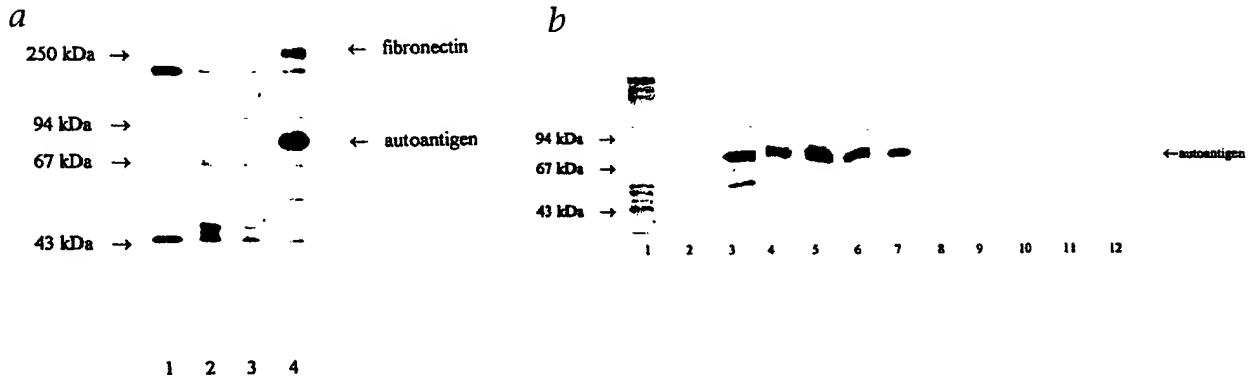

Fig. 1 IgA antibodies of celiac disease sera precipitate a characteristic protein species from cell cultures. Autoradiography of the immunoprecipitated cell lysate from HT1080 cells after separation by SDS–PAGE under reducing conditions. *a* (lane 1), Preadsorption on plain Sepharose CL-4B shows nonspecific binding of two major proteins; (lanes 2 and 3), immunoprecipitates with serum IgA from healthy controls and (lane 4), precipitation of the 85-kDa autoantigen by serum IgA from a patient with celiac disease. Note high-molecular-mass material that was identified as fibronectin, which coprecipitated from samples from patients with celiac disease as well as some with non-celiac disease. *b*, Immunoprecipitates with serum IgA from celiac disease patients and controls: (lane 1), material preadsorbed on plain Sepharose; (lane 2), healthy control; (lanes 3–7), patients with celiac disease; (lane 8), Crohn's disease; (lane 9), ulcerative colitis; (lanes 10–12), patients with Sjögren's syndrome.

ates with cell surfaces or certain extracellular matrix molecules[22]. tTG can crosslink fibronectin[20,23], osteonectin[24], collagen II[24], V and XI[25], procollagen III[26] and nidogen[27]. Thus, secreted tTG is thought to stabilize the provisional extracellular matrix in granulation tissue[22]. Furthermore, its expression is enhanced during apoptosis, leading to irreversible crosslinking of intracellular proteins, and may be deranged during growth of some tumors[28,29]. The commercially available enzyme from guinea pig liver shows a high-protein sequence identity with human tTG (>80%)[19], with a high probability of conserved antigenic epitopes, which allowed us to carry out further experiments with this preparation.

Gliadin, the dietary factor incriminated in the initial pathogenesis of celiac disease, contains numerous glutamines amounting to approximately 40% of its amino acids[4]. In order to test whether gliadin could serve as a substrate for tTG, we used an *in vitro* assay with radiolabeled putrescine as acceptor substrate[27]. Gliadin proved to be an excellent substrate and was quantitatively crosslinked by tTG, whereas the control proteins (chicken albumin, bovine serum albumin, α-lactalbumin, β-lactoglobulin) were essentially unaltered (data not shown). These results are in accord with previous reports that showed preferential incorporation of putrescine in gliadin by a transglutaminase extract from intestinal tissue[30] and also crosslinking of gliadin by a lysate of human red blood cells that contain tTG (ref. 31).

The celiac disease-specific IgA autoantibodies to endomysium are detected and semiquantified by performing indirect im-

b

tissue transglutaminase: 28′ Arg Glu Lys Leu Val Val Arg Arg Gly Gln Pro Phe Trp

10 kDa fragment: Arg Glu Lys Leu Val Val Arg Arg Gly Gln Pro Phe (Ser)

tissue transglutaminase: 581′ Asp Leu Tyr Leu Glu Asn Pro Glu Ile Lys Ile Arg Ile Leu Gly

14 kDa fragment: Asp Leu Tyr Leu Glu Asn Pro Glu Ile -X- Ile -X- Ile Leu Gly

tissue transglutaminase: 438′ Asp Ile Thr His Thr Tyr Lys Tyr Pro Glu

16 kDa fragment: Asp Ile Thr Leu Thr Tyr Gln Tyr Pro (Val)

Fig. 2 Purification and amino-terminal sequence analysis of the 85-kDa autoantigen. *a*, Separation of the unlabeled immunoprecipitated 85-kDa autoantigen by SDS–PAGE under reducing conditions; proteins revealed by silver staining. (lane 1), Molecular weight standard (as mass); (lane 2), immunoprecipitate of the 85-kDa autoantigen; additional major bands are fibronectin, and light and heavy immunoglobulin chains (25–30 kDa and 60–65 kDa, respectively); (lane 3), 85-kDa autoantigen purified by electrophoretic elution; (lane 4), fragments of the purified autoantigen after digestion with endoproteinase Asp-N; the three peptides subjected to N-terminal sequence analysis are marked. *b*, The N-terminal sequence data of the three fragments of the 85-kDa autoantigen generated by endoproteinase Asp-N were compared with the Swiss-Prot 31 data base (PC/GENE, IntelliGenetics) and found compatible with human tissue transglutaminase (EC 2.3.2.13). The identity of residue X is unknown, residues in parentheses are uncertain.

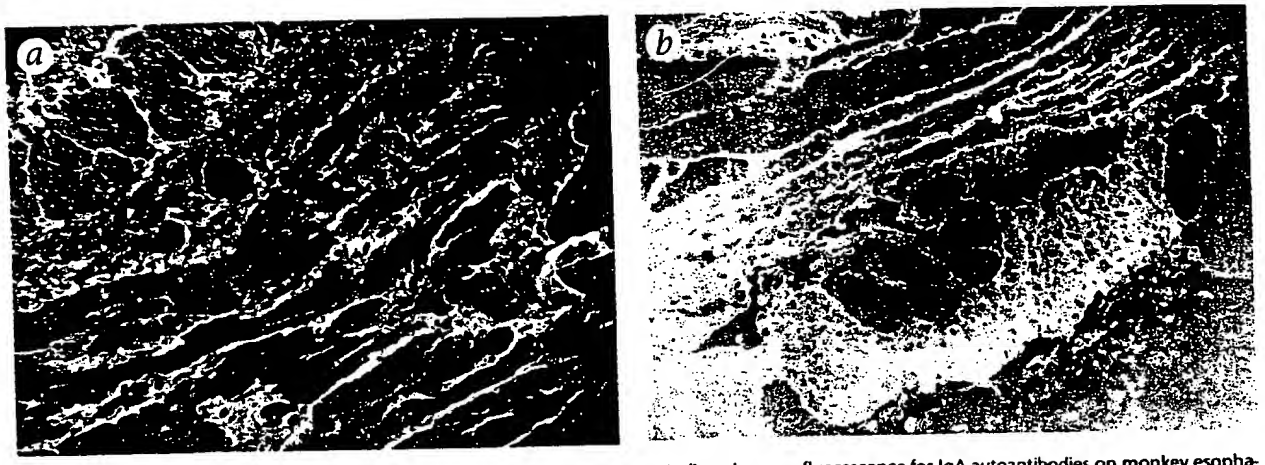

Fig. 3 Tissue transglutaminase as the prominent autoantigen of celiac disease. Indirect immunofluorescence for IgA autoantibodies on monkey esophagus (×62.5). *a*, The characteristic staining of endomysial structures by high-titer celiac disease serum (dilution 1:320). *b*, Loss of specific staining after preincubation of the same serum dilution with tTG, suggesting that the identified tTG is the prominent, if not sole, autoantigen in celiac disease.

munofluorescence on muscular sections of monkey esophagus or umbilical cord[9,15,42]. In order to further confirm tTG as the autoantigen in celiac disease, we performed indirect immunofluorescence with high-titer celiac disease serum samples on monkey esophagus with or without prior preincubation of the sera with tTG. Whereas untreated celiac disease serum samples showed the characteristic feature of endomysial labeling, pretreatment with tTG nearly completely abolished endomysial immunofluorescence (Fig. 3, *a* and *b*). This demonstrated that tTG represents the predominant, if not sole, endomysial autoantigen considered characteristic for celiac disease.

On the basis of these data, we established an enzyme-linked immunosorbent assay (ELISA) for the detection of IgA anti-tTG antibodies. Serum samples either from celiac disease patients with well-known anti-endomysium titers (as determined by immunofluorescence) or from controls were analyzed. In this ELISA only celiac disease patients displayed elevated levels of IgA anti-tTG, whereas none of the controls showed significant reactivity (Table 1). Furthermore, two of the high-titer sera were retested at higher dilutions. Even at 1:3200 these sera exhibited extinctions of $A = 1.02 \pm 0.09$ (celiac disease A) and 0.84 ± 0.12 (celiac disease C), thus demonstrating the high sensitivity of the ELISA test (data not shown). In addition, there was a good correlation between decreasing titers of anti-endomysium IgA and the IgA antibodies to tTG as measured by ELISA once patients were on a gluten-free diet (Table 2). We also measured IgG autoantibodies to tTG using the same ELISA system, in which the anti-IgA antibody was replaced by an anti-IgG antibody. Even though the high-titer celiac disease sera showed elevated anti-tTG IgG levels, this system was not comparable in sensitivity and specificity to the IgA-based ELISA (Table 2). In addition, some control sera, especially those of patients with chronic inflammatory disorders, showed raised titers of IgG anti-tTG (data not shown). The high sensitivity and specificity for celiac disease of IgA class autoantibodies to tTG is most plausibly explained by the prominent production of IgA by mucous membranes, especially those of the intestinal tract, with the IgA anti-tTG response thus reflecting the active phase of intestinal mucosal injury.

The identification of tTG as the autoantigen in celiac disease should fuel novel concepts about the insufficiently understood pathogenesis of celiac disease. The usually intracellular enzyme is released from cells during wounding[22]. One of its roles is the irreversible crosslinking of a small set of extracellular matrix and some cytoplasmic proteins, including cytoskeletal elements. This crosslinking might stabilize the wound area and protect the surrounding tissue from further damage. In addition, cytoskeletal crosslinking has been reported in apoptosis, leading to the noninflammatory elimination of potentially dangerous infected cells[28].

The finding that gliadin is a preferred substrate for the otherwise highly substrate-specific enzyme is of particular interest.

Table 1 Enzyme-linked immunosorbent assay (ELISA) based on tTG for the celiac disease (CD) autoantigen

Serum sample	EmA titer	Serum IgA anti-tTG dilution (1:400)
CD A	(1:640)	>3.500
CD B	(1:320)	>3.500
CD C	(1:320)	3.114 ± 0.024
CD D	(1:320)	1.257 ± 0.024
CD E	(1:320)	1.977 ± 0.018
CD F	(1:320)	1.525 ± 0.085
CD G	(1:160)	1.208 ± 0.019
CD H	(1:160)	0.747 ± 0.048
CD I	(1:160)	2.174 ± 0.291
CD K	(1:80)	0.667 ± 0.037
CD L	(1:80)	1.372 ± 0.093
CD M	(1:40)	0.286 ± 0.009
Ulcerative colitis	(ND)	0.119 ± 0.014
Indeterminate colitis	(ND)	0.092 ± 0.016
Crohn's disease	(ND)	0.090 ± 0.001
Sjögren's syndrome	(ND)	0.137 ± 0.004
Sjögren's syndrome	(ND)	0.082 ± 0.003
Alcoholic liver fibrosis	(ND)	0.059 ± 0.001
Healthy control	(ND)	0.070 ± 0.001

An ELISA for IgA antibodies against tTG was established. Shown are the optical densities of twelve different celiac disease serum samples with varying anti-endomysium antibody (EmA) titers as well as seven control sera. Sera were diluted 1:400 and listed according to their EmA titer (in parentheses). All celiac disease sera with high EmA-titers (>1:80) show high anti-tTG IgA titers, whereas the control sera display background levels. Celiac disease sera with low EmA-titer (<1:80) show only slightly raised ELISA titers, but are highly elevated above controls when diluted 1:100 (0.67 ± 0.02 versus 0.12 ± 0.01; celiac disease M, not shown). Values are means (±s.d.) of three parallel determinations. ND, not determined.

Table 2 IgA and IgG anti-tTG antibodies in celiac disease (CD) patients before and after a gluten-free diet

Serum sample	EmA titer	IgA anti-tTG dilution (1:400)	IgG anti-tTG dilution (1:100)
CD A	(1:640)	>3.500	1.267 ± 0.030
CD A gfd	(neg)	0.321 ± 0.013	1.055 ± 0.055
CD B	(1:320)	>3.500	3.116 ± 0.058
CD B gfd	(1:40)	0.286 ± 0.009	0.569 ± 0.009
CD C	(1:320)	3.114 ± 0.024	1.360 ± 0.009
CD C gfd	(neg.)	0.162 ± 0.002	0.959 ± 0.024
CD E	(1:320)	1.977 ± 0.018	0.827 ± 0.032
CD E gfd	(neg.)	0.186 ± 0.041	0.504 ± 0.045
CD F	(1:320)	1.525 ± 0.085	0.555 ± 0.016
CD F gfd	(1:80)	1.372 ± 0.093	3.186 ± 0.069
CD G	(1:160)	1.208 ± 0.019	1.154 ± 0.011
CD G gfd	(1:20)	0.066 ± 0.010	0.370 ± 0.008
CD H	(1:160)	0.747 ± 0.048	0.563 ± 0.014
CD H gfd	(1:80)	0.667 ± 0.037	1.632 ± 0.016

ELISA data for IgA (1:400) and IgG (1:100) class antibodies against tTG of seven different CD serum samples before and after a gluten-free diet (gfd). EmA-titers are given in parentheses. IgA anti-tTG antibodies decline in most patients kept on a gfd. Compared with IgA anti-tTG antibodies, IgG anti-tTG antibodies appear less sensitive markers for the active phase of CD; titers are means (±s.d.) of three parallel determinations.

Bruce *et al.*[30] already demonstrated that gliadin efficiently incorporates putrescine in the presence of intestinal extracts containing transglutaminase. However, these researchers did not differentiate the responsible enzyme nor implicate tTG as the endomysial autoantigen of celiac disease. Furthermore, localization of the intestinal TG within the lamina propria mucosae, with only 1% in the epithelial layer[30], is in agreement with the site of immunological damage in celiac disease.

We hypothesize that damage or hyperpermeability of the intestinal epithelium, either owing to toxic gluten fractions or to other (minor) irritants, triggers the abundant extracellular release of cytosolic tTG, mainly by lamina propria mononuclear or mesenchymal cells. Subsequent crosslinking of dietary gliadin results in gliadin–gliadin or gliadin–tTG complexes and thus creates antigenic neoepitopes. These neoepitopes could then initiate an immune response in genetically susceptible individuals, finally directed both to gliadin and tTG. In fact, a genetic predisposition has been found in celiac disease patients, who often bear the major histocompatibility complex antigens HLA-DQ(α1*0501,β1*0201)[4,31]. Further support comes from our preliminary data showing that a proportion of the IgA autoantibodies of celiac disease patients are directed to such neoepitopes (data not shown). Taken together, these data are well in line with the suggested importance of the celiac disease autoantigen in the pathogenesis of the disease as suggested by others[14,17]. Nevertheless, it must be borne in mind that celiac disease is not a classical autoimmune disease, since IgA antibodies to tTG disappear when gliadin is strictly removed from the diet, and the mucosal damage is reversed without residual fibrosis or scarring.

Our findings further suggest that the immunological detection of IgA autoantibodies to tTG, the newly discovered autoantigen of celiac disease, is a useful tool in the diagnosis and follow-up of the disease. Because of its simplicity, the ELISA for the identified autoantigen now allows an economical and rapid screening of large portions of the general population for the presence of latent or subclinical celiac disease. Therefore, the too-long intervals from early symptoms to diagnosis and finally treatment of celiac disease (median 5.4 years in Germany)[14] could be shortened decisively, leading to a decreased morbidity from this intestinal disease.

We cannot completely exclude IgA autoantibodies to tTG in diseases with mucosal lesions that are similar to celiac disease lesions, for example, tropical sprue, giardiasis, cow milk enteropathy or postenteritis syndrome. However, we think that it is quite unlikely to find these tTG autoantibodies in sera of these patients, because no IgA EmA were found in serum samples from patients with cow milk enteropathy, giardiasis or postenteritis syndrome[9]. Furthermore, no association of these diseases to the celiac disease-associated HLA-DQ genes is described.

By assuming a yet unproven potential of tTG, which is released during wound healing to serve as a further trigger for celiac disease, a novel treatment based on oral feeding of the autoantigen and induction of an oral tolerance may be envisaged[25]. tTG apparently elicits autoantibodies of the IgG class in various other chronic inflammatory conditions and might play a role in the initiation and perpetuation of certain autoimmune diseases.

Methods

Cell culture and immunoprecipitation. HT1080 cells were cultured in Dulbecco's modified Eagle's medium containing 10% fetal calf serum (Gibco, Eggenstein, Germany). For radioactive labeling 10^5 cells were incubated with 0.2 mCi [^{35}S]methionine (Expre^{35}S^{35}S, Du Pont-NEN, Bad Hamburg, Germany) and cultivated for further 16–20 h. For immunoprecipitation (IP) the cells were lysed in 3 ml 50 mM Tris-HCl, 150 mM NaCl, 1% nonionic detergent, protease inhibitors, pH 7.5, for 10 min at 4 °C. Cell fragments were removed by centrifugation. 1 ml lysate was incubated with 50 µl Sepharose CL-4B (Pharmacia, Freiburg, Germany) for 30 min at room temperature to remove nonspecifically binding proteins. The thus pretreated lysate was incubated with CNBr-activated Sepharose 4B (Pharmacia) preadsorbed with serum IgA either from celiac disease patients or from controls via an anti-human IgA bridging antibody from rabbit (2.4 mg antibody/ml Sepharose; Dianova, Hamburg, Germany) for 16 h at 4 °C. After several washes the precipitated proteins were dissolved in 50 µl SDS sample buffer under reducing conditions and separated by SDS–PAGE (ref. 36).

Isolation, cleavage and sequencing of the autoantigen. For isolation of the autoantigen by electrophoretic elution (Prep Cell 491, Bio-Rad, Krefeld, Germany) the discontinuous buffer system of Laemmli[36] was used. A 7.5% resolving gel (acrylamide, bisacrylamide 30:0.4, Pharmacia) was preceded by a 4% stacking gel. The immunoprecipitated sample was reduced and heated in sample buffer and then separated by a constant voltage of 225 V. Elution was performed in 25 mM Tris-HCl, 0.1 M glycin, 0.01% sodium laurylsulfate and fractions of 1.5 ml (0.8 ml/min) were collected. Fractions of interest were analyzed by tricine-SDS–PAGE (ref. 37) and further concentrated with Centriprep-50 (Amicon, Witten, Germany). Cleavage with endoproteinase Asp-N (Boehringer Mannheim, Germany) was performed in the elution buffer for 30 min at 37 °C, with an enzyme-to-substrate ratio of 1:100. Protein fragments were transferred to a polyvinylidene-difluoride membrane (Immobilon, Millipore, Eschborn, Germany) in a semi-dry-fast-blot apparatus (Fastblot B32/33 Biometra, Göttingen, Germany) and excised. Amino-terminal sequences were determined by Edman-degradation in an Applied Biosystems 477A sequencer (Foster City, CA).

Inhibition of endomysial staining. Preincubation of celiac disease sera (10 µl, diluted 1:320 in phosphate-buffered saline, pH 7.3, PBS) with 1 µg or 10 µg tTG from guinea pig liver (Sigma, Deisenhofer, Germany) or with 10 µg bovine serum albumin (Sigma) was performed for 1 h at room temperature. Monkey esophagus tissue slides (Euroimmun, Lübeck, Germany) were then incubated with the pretreated celiac disease sera, their untreated controls or non-celiac disease control sera in a humidified chamber for 1 h

at room temperature and washed 3× in PBS containing 0.2% bovine serum albumin. Bound IgA was detected with TRITC-labeled antihuman IgA from rabbit (1:50 in PBS; Dianova) for 30 min at room temperature.

Enzyme linked immunosorbent assay. For the ELISA 1 µg tTG (Sigma) in 100 µl PBS was coated per well on 96-well microtiter plates (Nunc, Wiesbaden, Germany) for 2 h at 37 °C, and unreacted sites were blocked with PBS containing 1% bovine serum albumin at 4 °C overnight. Patient and control sera were diluted in 100 µl PBS, 0.1% Tween-20 (Sigma), added to the wells and incubated for 1 h at room temperature. Three washes with PBS, 0.1% Tween-20 were followed by incubation with 100 µl peroxidase-conjugated antibody to human IgA (Dianova) diluted 1:1000 in PBS, 0.1% Tween-20, for 1 h at room temperature. Unbound antibodies were removed by three washes and color was developed by addition of 200 µl 0.1 M sodium citrate, 1 mg/ml o-phenylenediamine-hydrochloride, 0.06% H_2O_2, pH 4.2, for 30 min at room temperature. The absorbance was read on an ELISA reader (MRX, Dynatech Laboratories/Dynex Technologies, Denkendorf, Germany) at 450 nm.

Acknowledgments

We thank M. Becker, B. Gerling and S. Daum for making available some of the celiac disease sera, P.C. Fox for the kind gift of the Sjögren's syndrome sera, N. Otto for performing amino-terminal sequence analysis and J. Atkinson for valuable suggestions. The study was supported in part by project DFG Schu 646/10-1 and SFB366 CS. D.S. is the recipient of a Hermann and Lilly Schilling professorship.

RECEIVED 11 FEBRUARY; ACCEPTED 12 MAY 1997

1. Trier, J.S. Celiac sprue. *N. Engl. J. Med.* 325, 1709–1719 (1991).
2. Holmes, G.K.T., Prior, P., Lane, M.R., Pope, D. & Allan, R.N. Malignancy in coeliac disease — effect of a gluten-free diet. *Gut* 30, 333–338 (1989).
3. Logan, R.F.A., Rifkin, E.A., Turner, I.D. & Ferguson, A. Mortality in celiac disease. *Gastroenterology* 97, 265–271 (1989).
4. Marsh, M.N. Gluten, major histocompatibility complex, and the small intestine: A molecular and immunobiologic approach to the spectrum of gluten sensitivity ('celiac sprue'). *Gastroenterology* 102, 330–354 (1992).
5. Sturgess, R. *et al.* Wheat peptide challenge in coeliac disease. *Lancet* 343, 758–761 (1994).
6. Ferguson, A., Arranz, E. & Kingstone, K. Clinical and pathological spectrum of coeliac disease. in: *Malignancy and Chronic Inflammation in the Gastraintestinal Tract — New Concepts.* (eds. Riecken, E.O., Zeitz, M., Stallmach, A. & Heise, W.) 51–63 (Kluwer Acad. Press, Dordrecht, the Netherlands, 1995).
7. Walker-Smith, J.A., Guandalini, S., Schmitz, J., Shmerling, D.H. & Visakorpi, J.K. Revised criteria for diagnosis of coeliac disease. *Arch. Dis. Child.* 65, 909–911 (1990).
8. Bürgin-Wolff, A. *et al.* Antigliadin and antiendomysium antibody determination for coeliac disease. *Arch. Dis. Child.* 66, 941–947 (1991).
9. Volta, U., Molinaro, N., Fusconi, M., Cassani, F. & Bianchi, F.B. IgA antiendomysial antibody test: A step forward in celiac disease screening. *Dig. Dis. Sci.* 36, 752–756 (1991).
10. Mylotte, A., Egan-Mitchell, B., McCarthy, C.F. & McNicholl, B. Incidence of coeliac disease in the west of Ireland. *Br. Med. J.* 1, 703–705 (1973).
11. Greco, L., Mäki, M., Di Donato, F. & Visakorpi, J.K. Epidemiology of coeliac disease in Europe and the Mediterranean Area. in: *Common Food Intolerances*, Vol. I, *Epidemiology of Coeliac Disease.* (eds. Auricchio, S. & Visakorpi, J.K.) 25–44 (Karger, Basel, Switzerland, 1992).
12. Sandforth, F. *et al.* Inzidenz der einheimischen Sprue/Zöliakie in Berlin (West): Eine prospektive Untersuchung mit kurzer Falldiskussion. *Z. Gastroenterol.* 29, 327–332 (1991).
13. Catassi, C. *et al.* Coeliac disease in the year 2000: Exploring the iceberg. *Lancet* 343, 200–203 (1994).
14. Not, T. *et al.* Endomysium antibodies in blood donors predicts a high prevalence of celiac disease in the USA. *Gastroenterology* 110, A351 (1996).
15. Lerner, A., Kumar, V. & Iancu, T.C. Immunological diagnosis of childhood coeliac disease: comparison between antigliadin, antireticulin and antiendomysial antibodies. *Clin. Exp. Immunol.* 95, 78–82 (1994).
16. Picarelli, A. *et al.* Production of antiendomysial antibodies after in-vitro gliadin challenge of small intestine biopsy samples from patients with coeliac disease. *Lancet* 348, 1065–1067 (1996).
17. Mäki, M. Coeliac disease and autoimmunity due to unmasking of cryptic epitopes? *Lancet* 348, 1046–1047 (1996)
18. Cordell, J.L. *et al.* Immunoenzymatic labeling of monoclonal antibodies using immune complexes of alkaline phosphatase and monoclonal anti-alkaline phosphatase (APAAP) complexes. *J. Histochem. Cytochem.* 32, 219–229 (1984).
19. Gentile, V. J. *et al.* Isolation and characterization of cDNA clones to mouse macrophage and human endothelial cell tissue transglutaminases. *J. Biol. Chem.* 266, 478–483 (1991).
20. Barsigian, C., Stern, A.M. & Martinez, J. Tissue (type II) transglutaminase covalently incorporates itself, fibrinogen, or fibronectin into high molecular weight complexes on the extracellular surface of isolated hepatocytes. *J. Biol. Chem.* 266, 22501–22509 (1991).
21. Greenberg, C.S., Birckbichler, P.J. & Rice, R.H. Transglutaminases: Multifunctional cross-linking enzymes that stabilize tissues. *FASEB J.* 5, 3071–3077 (1991).
22. Upchurch, H.F., Conway, E., Patterson, M.K. & Maxwell, M.D. Localization of cellular transglutaminase on the extracellular matrix after wounding: Characteristics of the matrix bound enzyme. *J. Cell Physiol.* 149, 375–382 (1991).
23. Martinez, J., Chalupowicz, D.G., Roush, R.K., Sheth, A. & Barsigian, C. Transglutaminase-mediated processing of fibronectin by endothelial cell monolayers. *Biochemistry* 33, 2538–2545 (1994).
24. Aeschlimann, D., Kaupp, O. & Paulsson, M. Transglutaminase-catalyzed matrix cross-linking in differentiating cartilage: Identification of osteonectin as a major glutaminyl substrate. *J. Cell Biol.* 129, 881–892 (1995).
25. Kleman, J., Aeschlimann, D., Paulsson, M. & van der Rest, M. Transglutaminase-catalyzed cross-linking of fibrils of collagen V/XI in A204 rhabdomyosarcoma cells. *Biochemistry* 34, 13768–13775 (1995).
26. Bowness, J.M., Folk, J.E. & Timpl, R.J. Identification of a substrate site for liver transglutaminase on the aminopropeptide of type III collagen. *J. Biol. Chem.* 262, 1022–1024 (1987).
27. Aeschlimann, D. & Paulsson, M. Cross-linking of laminin-nidogen complexes by tissue transglutaminase. *J. Biol. Chem.* 266, 15308–15317 (1991).
28. Piacentini, M. Tissue transglutaminase: A candidate effector element of physiological cell death. *Curr. Top. Microbiol. Immunol.* 200, 163–175 (1995).
29. Knight, C.R.L., Rees, R.C. & Griffin, M. Apoptosis: A potential role for cytosolic transglutaminase and its importance in tumour progression. *Biochim. Biophys. Acta* 1096, 312–318 (1991).
30. Bruce, S.E., Bjarnason, I. & Peters, T.J. Human jejunal transglutaminase: Demonstration of activity, enzyme kinetics and substrate specificity with special relation to gliadin and coeliac disease. *Clin. Sci.* 68, 573–579 (1985).
31. Szabolcs, M., Sipka, S. & Csorba, S. In vitro cross-linking of gluten into high-molecular-weight polymers with transglutaminase. *Acta Paediatr. Hung.* 28, 215–227 (1987).
32. Ladinser, B., Rossipal, E. & Pittschieler, K. Endomysium antibodies in coeliac disease: An improved method. *Gut* 35, 776–778 (1994).
33. Lundin, K.E.A. *et al.* Gliadin-specific, HLA-DQ(α1*0501,β1*0201) restricted T cells isolated from the small intestinal mucosa of celiac disease patients. *J. Exp. Med.* 178, 187–196 (1993).
34. Lankisch, P.G. *et al.* Diagnostic intervals for recognizing celiac disease. *Z. Gastroenterol.* 34, 473–477 (1996).
35. Sosroseno, W. A review of the mechanisms of oral tolerance and immunotherapy. *J. R. Soc. Med.* 88, 14–17 (1995).
36. Lämmli, U.K. Cleavage of structural proteins during the assembly of the head of bacteriophage T4. *Nature* 227, 680–685 (1970).
37. Schägger, H. & von Jagow, G. Tricine-sodium dodecyl sulfate-polyacrylamide gel electrophoresis for the separation of proteins in the range from 1 to 10 kDa. *Anal. Biochem.* 166, 368–379 (1987).

Molecular Characterization of the Ro/SS-A Autoantigens

Daniel P. McCauliffe and Richard D. Sontheimer

Department of Dermatology (DPM), University of North Carolina, Chapel Hill, North Carolina; and Department of Dermatology and Internal Medicine (RDS), University of Texas Southwestern Medical Center, Dallas Texas, U.S.A.

Molecular techniques have recently revealed that there are several immunologically distinct Ro/SS-A antigens. Three genes encoding putative Ro/SS-A protein antigens with calculated masses of 46, 52, and 60 kD have been isolated. The encoded amino acid sequence of each is quite dissimilar. The 46-kD antigen is calreticulin (CR), a highly conserved calcium-binding protein that resides predominately in the endoplasmic reticulum where it may be involved in protein assembly. Although CR has recently been confirmed to be a new human rheumatic disease-associated autoantigen, its relationship to the other components of the Ro/SS-A ribonucleoprotein has become somewhat controversial owing predominately to the fact that recombinant forms of calreticulin have not displayed the same pattern of autoantibody reactivity possessed by the native form of this protein.

The 52-kD antigen most likely resides in the nucleus and may be involved in the regulation of gene expression. The cellular location and function of the 60-kD antigen is uncertain but studies indicate that it is a RNA-binding protein.

The 46- and 60-kD antigens share homology with foreign polypeptides, suggesting that an immune response initially directed against a foreign protein may give rise to the autoimmune response directed at cross-reacting self proteins.
J Invest Dermatol 100:73S–79S, 1993

In 1969 Clark *et al* first demonstrated a novel antigen in human tissue extracts that by immunodiffusion analysis reacted with sera from patients with systemic lupus erythematosus and Sjögren's syndrome [1]. This antigen and its reactive autoantibodies were called Ro (auto)antigen and Ro (auto)antibodies, respectively. In 1975 Alspaugh and Tan similarly demonstrated the presence of three different autoantibodies in sera from patients with Sjögren's syndrome that they designated SS-A, SS-B, and SS-C [2]. Later it was demonstrated that SS-A autoantibodies were immunologically equivalent to the Ro autoantibodies [3], and thus we now commonly preface these autoantibodies and their respective antigens with the term Ro/SS-A. SS-B autoantibodies were also shown to be identical to La autoantibodies, a specificity that frequently accompanies Ro/SS-A autoantibodies [3].

Reprint requests to: Dr. Daniel P. McCauliffe, Department of Dermatology, CB 7600, Room 137 North Carolina Memorial Hospital, Chapel Hill, 27514.

Abbreviations:
ANA: anti-nuclear antibody
cDNA: complementary DNA
CMV: cytomegalovirus
CR: calreticulin
ELISA: enzyme-linked immunosorbent assay
ER: endoplasmic reticulum
GRP: glucose-regulated protein
hY RNA: human cytoplasmic RNA
LE: lupus erythematosus
NLE: neonatal lupus erythematosus
PDI: protein disulfide isomerase
RNP: ribonucleoprotein
SCLE: subacute cutaneous lupus erythematosus
SDS-PAGE: sodium dodecyl sulfate polyacrylamide gel electrophoresis
UV: ultraviolet
VSV: vesicular stomatitis virus

CLINICAL SIGNIFICANCE OF THE Ro/SS-A ANTIGENS AND ANTIBODIES

The Ro/SS-A antigens are of clinical interest in that antibodies directed against them are found in the majority of patients with primary Sjögren's syndrome, subacute cutaneous lupus erythematosus (SCLE), neonatal lupus erythematosus (NLE), anti-nuclear antibody (ANA) negative lupus erythematosus (LE), and systemic LE-like disease secondary to homozygous C2 or C4 complement deficiency [4–9]. Substantial evidence indicates that they play a major role in the pathogenesis of disease [10,11]. The strongest evidence comes from observations in patients with NLE. Pregnant mothers with circulating Ro/SS-A autoantibodies can pass them across the placenta to their fetus. The fetus can develop congenital heart block, hepatic inflammation, and thrombocytopenia from tissue injury presumably caused by these antibodies [12,13]. Additionally, shortly after birth and perhaps triggered by ultraviolet (UV) light exposure, these infants can develop skin lesions clinically and histopathologically similar to those of SCLE [12]. In several months, as the maternally acquired antibodies are cleared from the infant's circulation, the skin lesions resolve [12].

Investigative work has provided additional evidence that Ro/SS-A antibodies may be pathogenic. Ro/SS-A antibodies administered intravenously to immunodeficient mice engrafted with human skin bind preferentially in and about the human basal keratinocytes [14]. This binding is augmented by UV light exposure. This pattern of immunoglobulin deposition is identical to that found in biopsies from NLE and SCLE skin lesions.

CHARACTERIZATION OF THE Ro/SS-A ANTIGENS

Since Clark *et al* first demonstrated the presence of Ro/SS-A autoantibodies by immunodiffusion studies in 1969[1], we have learned a great deal more about their target antigens.

In 1981 Lerner *et al* demonstrated that human Ro/SS-A autoimmune sera immunoprecipitated a novel class of small RNAs that they designated the human (h) cYtoplasmic (Y) RNAs or hY RNA

0022-202X/93/$06.00

[15]. In 1984 Wolin and Steitz showed that this hY RNA immunoprecipitation resulted from the binding of Ro/SS-A autoantibodies to a 60-kD protein to which the hY RNAs were apparently linked [16]. From 1984 until 1988 it was generally thought that Ro/SS-A autoantibodies were directed at a single 60-kD protein. However, in 1988 Ben-Chetrit *et al* demonstrated a novel 52-kD Ro/SS-A antigen by immunoblot analysis that was immunologically distinct from the 60-kD antigen [17]. In 1989 Rader *et al* demonstrated four immunologically distinct antigens that react with monospecific Ro/SS-A autoimmune sera [18]. Over the past four years genes encoding 60-, 46-, and 52-kD autoantigens have been isolated.

60-kD Ro/SS-A In 1988 Deutscher *et al* reported the cloning of a 60-kD Ro/SS-A antigen from a human placental complementary (cDNA) library [19]. In 1989 Ben-Chetrit *et al* [20] reported the cDNA sequence cloned from a human T-cell leukemia cDNA library that appeared to be a homologous gene or a differentially spliced version of the gene characterized by Deutscher *et al*. Deutscher's and Ben-Chetrit's sequences both encoded a 60-kD protein that was identical except for several amino acids at the carboxy-terminus. Both amino acid sequences contain a zinc finger motif and a sequence motif common to RNA binding proteins [19,20]. Zinc fingers are thought to serve as a site of nucleic acid binding or protein binding [21].

There is no extensive sequence homology between the 60-kD protein and other published protein sequences; however, six segments of this protein have limited homology to different portions of a vesicular stomatitis virus (VSV) nucleocapsid protein [22]. Five of these homologous regions have significant reactivity to human Ro/SS-A autoimmune sera by enzyme-linked immunosorbent assay (ELISA), which suggests that an immune response initially directed at the VSV protein or a similar viral protein might cross-react with the 60-kD Ro/SS-A protein by way of its cross-reacting epitopes. VSV is not known to be particularly pathogenic in humans, but the data suggest that this VSV protein or a similar viral protein might elicit the Ro/SS-A autoimmune response. This is an example of "molecular mimicry" where a microbial protein is thought to trigger an immune response that cross-reacts with a self-antigen [23].

46-kD Ro/SS-A Our group isolated a cDNA from an Epstein-Barr virus transformed human B-cell line that encodes a protein reactive with human Ro/SS-A autoimmune sera [24]. The encoded 46-kD protein migrates aberrantly at 60 kD by sodium dodecylsulfate–polyacrylamide gel electrophoresis (SDS-PAGE). The amino acid sequence of this 46-kD molecule reveals a hydrophobic leader sequence at its amino terminal typical of molecules transported into the endoplasmic reticulum (ER), and a KDEL carboxy terminal sequence that is classic for proteins that are retained in the ER [24,27]. This sequence is extremely homologous to murine and rabbit CR (94% and 92%, respectively) [28]. CR is a calcium-binding protein that resides in the endoplasmic and sarcoplasmic reticulum [29]. From this high degree of sequence homology and other data it has been concluded that the 46-kD molecule is human CR [28,30].

Recent evidence indicates that CR may be coordinately expressed with the glucose-regulated protein (GRP)78, GRP94, and protein disulfide isomerase (PDI) genes [31]. The protein products of all four of these genes are highly acidic, localize to the ER, and bind calcium [32]. GRP78 and GRP94 are highly homologous to heat-shock proteins [33,34]. Both of these proteins and PDI are thought to play a major role in protein assembly within the ER [33–35]. Thus, by implication, CR may also play a role in protein assembly.

It is also interesting to note that patients infected with *Onchocerca volvulus,* a filarial nematode that causes river blindness, sclerosing lymphadenitis, and dermatologic disease in humans residing in parts of Africa and Central America, have antibodies directed against the Ral-1 antigen, which is highly homologous to CR [28,36]. Although patients with this nematode are not at increased risk for developing Sjögren's syndrome or LE, this homology between CR and a filarial protein raises the possibility that a foreign Ro/SS-A protein equivalent might trigger the autoimmune Ro/SS-A antibody response seen in some patients with Sjögren's syndrome and several LE-related disorders. *Drosophila melanogaster* and the marine snail *Aplysia californica* have molecules similar to CR [28].

Work recently presented by other laboratories has now confirmed our initial suggestion that calreticulin is a rheumatic disease–associated autoantigen [37,38]. One group has found that an *Escherichia coli* recombinant form of human calreticulin reacted by ELISA with 40% of the serum samples from unselected SLE patients [37], whereas another group found 33% of their SLE sera to react with the same form of recombinant CR by Western blot [38]. Curiously, neither group found a significant correlation between anti-CR and anti-Ro/SS-A autoantibody levels in their SLE patient sera.

We have reason to believe that post-translational modification such as phosphorylation, perhaps through the augmentation of hY RNA binding, could also be relevant to the configuration of CR that is recognized by Ro/SS-A autoantibodies. Non-mammalian forms of recombinant CR are unlikely to possess the same pattern of RNA binding or phosphorylation that is displayed by the native configuration of CR present in mammalian cells. The concern that CR may not be a component of the Ro/SS-A RNP complex stems from the fact that *recombinant* forms of CR both in our laboratory (personal unpublished observation) and in others [37,38] do not display the same degree of reactivity with Ro/SS-A autoantibodies that has previously been demonstrated with *native* human CR purified from human Wil-2 cells. We now have evidence that the protein-RNA binding site present on a subpopulation of CR molecules that bind hY RNA contributes to the structure that is being recognized by human anti-Ro/SS-A autoantibodies [39].

52-kD Ro/SS-A Chan *et al* and Itoh *et al* independently isolated the same cDNA sequence from two different human T-cell cDNA libraries that encodes a 52-kD protein reactive with human Ro/SS-A autoimmune sera [40,41]. The amino acid sequence predicted by this cDNA contained leucine zipper and zinc finger binding motifs and also had significant homology with the human ret transforming protein and the murine T-cell regulatory protein rpt-1, which are thought to play a role in gene regulation[40,41]. These sequence motifs and homologies suggest that the 52-kD Ro/SS-A molecule may be involved in gene regulation and thus probably resides in the nucleus.

There are no significant sequence homologies between the 60-, 46-, or 52-kD antigens (Table I). Despite the knowledge gained from analyzing the encoded amino acid sequences of each Ro/SS-A cDNA, there still remain a number of unanswered questions that several investigators have started to address.

Are These Antigens Structurally Associated and What Are Their Relationships to the hY RNAs? Ro/SS-A autoimmune sera from patients with LE and Sjögren's syndrome immunoprecipitate four hY RNAs (hY1,3,4, and 5) from human cell extracts [15] (see Fig 1). Antisera specific for either a 52-kD or a 60-kD protein have been shown to immunoprecipitate the hY RNAs from cellular extracts. However, in one study whenever 52-kD specific antibodies (not reactive to the 60-kD antigen by immunoblot analysis) were used, the hY RNAs and 52-kD protein were precipitated along with a small amount of 60-kD protein [17]. Thus it is not certain whether 1) the 52-kD species binds the hY RNAs directly; 2) the 52-kD protein is indirectly associated with the hY RNA through a direct association with a 60-kD hY RNA binding protein; or 3) the antibodies that appeared specific for the 52-kD antigen by immunoblot may recognize a cross-reactive epitope on the native Ro/SS-A ribonucleoprotein (RNP) particle.

Deutscher *et al* have demonstrated that the 60-kD Ro/SS-A protein directly associates with hY RNAs in reconstitution studies [19]. There is some evidence that CR associates with the hY RNA as suggested by UV cross-linking studies [24], immunoprecipitation of hY RNA by affinity-purified CR antisera [24], and the fact that onchocerciasis patient sera with CR reactive antibodies can immunoprecipitate hY RNA [42]. Additionally, preliminary data indicate that rabbit antisera raised against two synthetic peptides corre-

Table I. Characteristics of Three Ro/SS-A cDNA-Encoded Products

Protein	Location	Function	Homology	Pathogenic Role
60 kD	Nuclear? Cytoplasmic?	RNA binding	VSV nucleocapsid protein	Molecular mimicry?
46 kD	Predominantly cytoplasmic ± nuclear	Ca^{++} binding Protein folding?	Calreticulin Ral-1	Translocation Parasite homology
52 kD	Predominantly nuclear ± cytoplasmic	Gene regulation?	rfp, rpt-1	?

sponding to different portions of the CR amino acid sequence can precipitate hYRNA [39]. However, the relationships that exist between CR and the other molecular constituents of the Ro/SS-A RNP particle continue to be debated [38,43,44].

Earlier data suggested that Ro/SS-A autoimmune sera precipitated a 60-kD protein along with the hY RNA and this immunoprecipitation was dependent on the presence of protein [15]. More recently Boire and Craft have identified Ro/SS-A antibodies that specifically immunoprecipitate hY5 RNA and a 60-kD protein, but not the other types of hY RNA [45]. They concluded that some Ro/SS-A autoimmune sera contain autoantibodies directed at a conformational epitope that is expressed only on Ro/SS-A-hY5 RNA particles but absent on hY1,2,3, and 4 containing particles.

The 60-kD protein immunoprecipitated in the above studies most probably represents the authentic 60-kD protein as its amino acid sequence contains a sequence motif typically found in RNA-binding proteins, although it is clear that proteins without the classic RNA-binding consensus sequence can also bind RNA molecules [46,47]. The hY RNAs and Ro/SS-A proteins might exist in a RNP multimeric complex similar to the U1 RNPs. One could hypothesize that the zinc finger motif in the 60-kD Ro/SS-A molecule might serve as a site for this protein to bind one or more of the other Ro/SS-A molecules, whereas the RNA binding motif would serve as a site of hY RNA binding.

Several different investigators have reported different masses for the Ro/SS-A RNP particle. Three groups have reported a mass of approximately 100–150 kD for the Ro/SS-A particle as determined by gel filtration [1,48,49]. Wolin and Steitz determined that the particle sediments in sucrose at approximately 7S [16]. This is equivalent to ~93 kD, which could be accounted for by the mass of one 60-kD protein and the average mass of one hY RNA molecule. Boire and Craft biochemically purified Ro/SS-A particles and found them to partition into three different groups by sucrose sedimentation gradients [50]. The particles in two of these groups have a mass of approximately 300–350 kD by gel filtration and the other has a mass of approximately 230 kD. These investigators concluded that Ro/SS-A RNP particles are heterogeneous and may exist as multimeric units consisting of hY RNA, a 60-kD protein, and perhaps other polypeptides including the La/SS-B protein [50] (see Fig 2).

Some investigators argue that if a particular protein reactive with Ro/SS-A autoantibodies is not part of the hY RNA-bearing RNP complex, then perhaps it should not be called a Ro/SS-A antigen. Although this is a matter of semantics, there is a clear need to

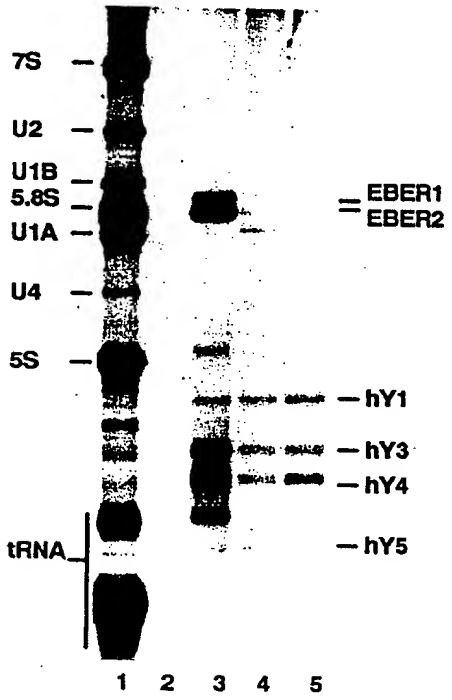

Figure 1. hY RNA immunoprecipitation. Wil-2 cells, an EBV transformed B-cell line, were radiolabeled with ^{32}P-orthophosphoric acid and sonicated. The resulting cell extract was incubated with sera and the immunoprecipitated material was harvested and subjected to gel electrophoresis according to previously established protocols [15]. *Lane 1* contains total radiolabeled RNA from the extract and serves to provide molecular weight standards as indicated to the left of this lane. *Lane 2* demonstrates that no RNA was immunoprecipitated with normal human serum. *Lane 3* is RNA immunoprecipitated with human autoimmune sera containing both Ro/SS-A and La/SS-B autoantibodies. *Lanes 4* and *5* are sera from two different patients with Ro/SS-A autoantibodies as defined by double immunodiffusion. All three sera with Ro/SS-A autoantibodies immunoprecipitated the four major types of hY RNA. The very faint unlabeled band in *lane 3* between hY1 and hY3 is hY2, a breakdown product of hY1. The Epstein-Barr virus encoded EBER 1 and 2 immunoprecipitate with La/SS-B antibodies as previously described [56].

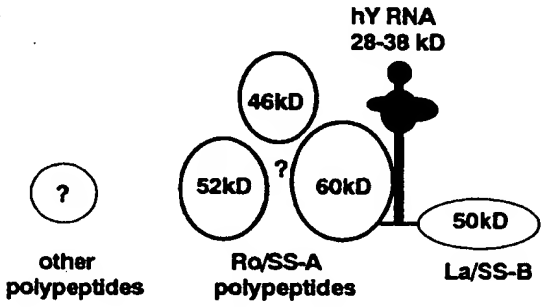

Figure 2. One model of the Ro/SS-A RNP particle. The proposed relationship between hY RNA and the Ro/SS-A and La/SS-B proteins is indicated. The hY RNA are RNA polymerase III transcripts and are thought to be at least transiently associated with the La/SS-B protein through binding of its uridine rich 3′ end. The 60-kD Ro/SS-A protein contains an RNA binding motif believed to be the site of hY RNA binding. It is uncertain if the 46- and/or 52-kD proteins reactive with Ro/SS-A autoimmune sera or other polypeptides are a part of this particle, although there is some evidence that the 46-kD protein is associated with hY RNA.

develop a more precise designation for each of these antigens. However, it should be remembered that Ro/SS-A antigens were initially defined by immunodiffusion assays, not by hY RNA association. It has not yet been determined which of the molecules reactive with Ro/SS-A autoimmune sera are responsible for the immunoprecipitate seen in immunodiffusion assays. Rader *et al*, however, observed that non-reducing SDS-PAGE of eluted precipitins from counter-immunoelectrophoresis showed the precipitins to be composed of a 60-kD protein [18].

What Is the Cellular Distribution of Each Ro/SS-A Molecule? Some investigators have reported predominantly intranuclear localization of the Ro/SS-A antigens by indirect immunofluorescence [51–54] whereas others have reported cytoplasmic [55–57] or both cytoplasmic and nuclear localization [58,59]. Whether this discrepancy in subcellular localization is related to the method of cell fixation, cell substrate, or the specificity of the Ro/SS-A autoimmune sera used has not been fully investigated.

Koch *et al* have demonstrated that conventional cell fixation for ANA testing does not allow full visualization of proteins, such as CR, that reside in the ER [60]. They demonstrated that ER proteins can be better visualized by immunofluorescence techniques with detergent permeabilization of fixed cells or of unfixed cells that have been equilibrated in 9% sucrose [60].

Isolation of antibodies specific for each Ro/SS-A antigenic polypeptide has allowed more precise cellular localization of the Ro/SS-A polypeptides and these results have helped explain the discrepancies encountered previously with immunofluorescence staining using whole Ro/SS-A patient sera.

Ben-Chetrit *et al* demonstrated strong punctate nuclear and slight cytoplasmic staining of cells with Ro/SS-A autoimmune serum immunoaffinity purified from a 52-kD protein and also with monospecific anti–52-kD serum (as determined by immunoblot analysis) [17]. They reported an indistinguishable pattern with Ro/SS-A autoimmune serum immunoaffinity purified from a 60-kD protein [17]. There is some evidence that there may be Ro/SS-A antibodies that react with an epitope on the native 60-kD RNP antigen that cross-react with an epitope on the 52-kD protein [61]. Thus one might speculate that the 60-kD protein resides primarily in the cytoplasm and that nuclear staining results from antibodies that recognize a cross-reactive epitope on the 52-kD protein. Preliminary ELISA data have revealed that all Ro/SS-A autoimmune sera with high-titer antibodies directed against a recombinant 52-kD Ro/SS-A protein have given a speckled nuclear ANA pattern of fluorescence (personal unpublished observation). The 52-kD Ro/SS-A amino acid sequence reveals motifs and homologies that indicate that it may be involved in gene regulation and thus would likely reside in the nucleus [40,41]. Antiserum specific for CR has revealed predominantly perinuclear cytoplasmic staining with lesser amounts of nuclear staining [62,63].

Kato *et al* have reported that the majority of the hY5 RNA is found in the cytoplasmic fraction of HeLa cells [64]. More recently Boire and Craft have demonstrated that more than 90% of the Ro/SS-A particles were recovered from the cytoplasmic fraction of HeLa cells [50]. One should recall that Ro/SS-A antigen was originally described as a saline-soluble, "cytoplasmic" autoantigen [1].

Is There Any Correlation Between the Type of Ro/SS-A Autoantibodies Patients Produce and Their Diagnosis, Disease Course, and/or Response to Therapy? Preliminary data suggest that patients with Ro/SS-A autoantibodies might be clinically categorized according to the Ro/SS-A proteins or epitopes their sera recognize. The specificity of the maternally acquired Ro/SS-A autoantibodies may determine which infants develop NLE. Buyon *et al* have shown that the predominant antibody response in the NLE patient group with acquired heart block was directed against the 52-kD Ro/SS-A protein, although some patients also had antibodies directed against a 60-kD protein [65]. Ben-Chetrit *et al* have demonstrated that of 51 SLE patients who were Ro/SS-A positive by immunodiffusion, 47% had antibodies that recognized both a 60-kD and a 52-kD protein, 18% had antibodies that recognized a 60-kD protein only, and 35% were nonreactive to both [66]. Similarly, they demonstrated that of 47 Ro/SS-A–positive Sjögren's syndrome patients, 47% had antibodies reactive to both a 60-kD and a 52-kD protein, 40% reacted only with a 52-kD protein only, and 13% were non-reactive. Unfortunately the results obtained by both Buyon *et al* and Ben-Chetrit *et al* were obtained by immunoblot analysis and might not detect conformational epitopes, including epitopes that might be present on a multimeric complex.

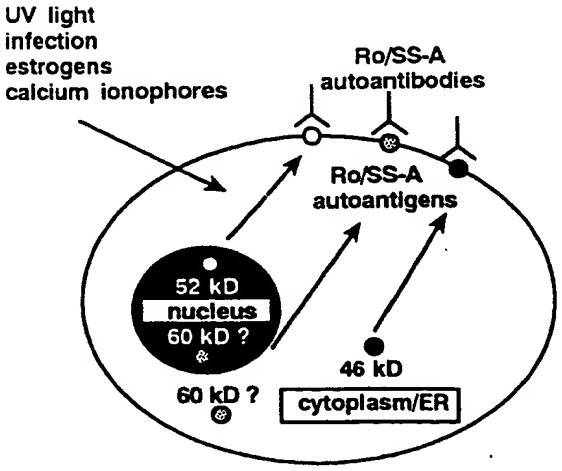

Figure 3. Ro/SS-A translocation. Agents that may translocate Ro/SS-A antigens to the cell surface where they are available to bind circulating Ro/SS-A autoantibodies are listed. The likely predominant location of the 46- and 52-kD antigens are indicated. The location of the 60-kD antigen is more uncertain.

Work is currently in progress in several laboratories, including our own, to determine those portions of each Ro/SS-A molecule to which Ro/SS-A autoantibodies bind and to define further the nature of conformational epitopes that may exist on an individual Ro/SS-A protein or as part of a multimeric structure. Epitope mapping should determine if subsets of Ro/SS-A autoantibody-associated disease can be based on antigenic site-recognition patterns. Such subclassification may have clinical use regarding the pathogenesis, diagnosis, and treatment of the Ro/SS-A autoantibody–associated diseases.

What Role Do the Ro/SS-A Autoantigens Play in the Pathogenesis of SCLE and NLE Skin Disease and How Might Their Cellular Expression Be Affected by Factors that May Influence These Two Skin Diseases? A number of agents have been shown to influence SCLE and NLE disease expression. Some of these agents have been shown to displace Ro/SS-A antigens to the surface of cells (Fig 3).

UV light SCLE and NLE skin diseases are frequently exacerbated by UV light exposure, primarily of the UVB type (290–320 nM) [67,68]. Investigators have demonstrated that UVB light can displace Ro/SS-A antigen from within keratinocytes to the cell surface [69,70]. Similar results have recently been reported for the La/SS-B antigen [71]. Such displacement would allow the autoantigen to have access to the Ro/SS-A autoantibody binding that could result in tissue injury through complement-mediated lysis or antibody-dependent cell-mediated cytotoxicity. At this time it is uncertain which of the various molecular components of the Ro/SS-A autoantigen complex are affected by UV light exposure. Recent preliminary studies have indicated that physiologically relevant doses of UVB induce both CR gene transcription [72] (personal observation) and translation [73]. However, similar doses of UVB did not increase cellular levels of the 60-kD Ro/SS-A protein [73]. No evidence has yet been presented regarding the displacement of the various Ro/SS-A proteins to the cell surface by UV light.

Estrogens The hormonal milieu may also play an important role in Ro/SS-A–associated disease, as approximately 75% of SCLE patients and infants with NLE skin disease are female. Estrogen treatment of cultured keratinocytes results in increased expression of Ro/SS-A antigens on the cell surface, but it is uncertain which of the Ro/SS-A molecules are so displaced [74].

Heat Some SCLE patients have noted that heat can exacerbate their skin disease [67]. The similarities that CR shares with the heat shock–like proteins GRP78 and GRP94 is of interest in this regard. There is recent evidence that heat shock–like proteins can be translocated to the cell surface, where they may participate in antigen presentation or may be a target for gamma/delta T-cell–directed cytotoxicity [75,76].

State of keratinocyte differentiation and proliferation Studies have shown that human keratinocytes grown in low-calcium–containing culture media have greater amounts of cytoplasmic Ro/SS-A antigen as detected by immunofluorescence staining with Ro/SS-A autoimmune sera [59]. It is uncertain which of the Ro/SS-A antigens are expressed in greater amounts, however. At lower calcium concentrations, cultured keratinocytes are in a less-differentiated, more rapidly proliferating state, more like the basal layer keratinocytes [77]. This might explain why the more rapidly proliferating basal keratinocytes appear to be preferentially targeted in SCLE and NLE [11,78]. Preliminary evidence indicates that CR is expressed at higher levels in rapidly proliferating cells (personal unpublished observation).

There is some evidence that CR can be transiently secreted from cells after treatment with calcium ionophores [79], although this has not been fully substantiated by others [80]. Recent studies in our laboratory employing calreticulin reporter gene constructs have indicated that calreticulin transcription is markedly augmented in A431 cells following treatment with the calcium ionophore ionomycin [72] (personal unpublished observation). Additionally, it has been suggested that calcium ionophore treatment of cultured human keratinocytes displaces Ro/SS-A antigen to the cell membrane, although it is uncertain which of the Ro/SS-A antigens is (are) so displaced [81].

Infection There is considerable evidence that viral infections can precipitate or exacerbate autoimmune disease [82]. Some work has suggested that virally infected cells in culture displace Ro/SS-A antigens to the cell surface, similar to the effects caused by UV light [83]. Jianhui and Newkirk have recently presented evidence that suggests that human cytomegalovirus (CMV) infection increases the expression of CR in MRC-5, a human embryonic lung fibroblast line [84]. These studies found that total cellular CR levels increased following CMV infection, but the greatest increase in CR antigenicity was associated with the plasma membrane. CMV infection also resulted in increased intracellular levels of the 60-kD Ro/SS-A antigen, but similar increases were not observed in the plasma membrane. Viral infection has also been shown to displace the La/SS-B antigen from the nucleus [85].

Polymorphism It is not known whether Ro/SS-A proteins are polymorphic. Preliminary studies have indicated, however, that the CR encoding gene is not highly polymorphic in normal individuals by restriction fragment length polymorphism analysis [24]. There is evidence of at least two forms of the 60-kD Ro/SS-A encoding gene [18–20]. Kutsch *et al* have recently reported variability in Ro/SS-A displacement to keratinocyte membranes after treatment with calcium ionophore or tumor necrosis factor alpha, which they suggest might arise from genetic differences in the keratinocyte donors [81]. It is possible that certain forms of a Ro/SS-A molecule may be more immunogenic, expressed at higher levels, or more easily displaced to the cell surface where it could participate in immune-mediated injury.

SUMMARY

With molecular techniques, we have recently learned that there are several immunologically distinct Ro/SS-A antigens. Three putative Ro/SS-A genes have been isolated and the encoded proteins from these three genes have been found to be quite dissimilar. CR, the 46-kD protein, appears to reside predominately in the endoplasmic reticulum/cytoplasm, whereas the 52-kD protein most likely resides in the nucleus. The structure of the 60-kD protein and at least one immunofluorescence study suggest that it may also reside predominantly in the nucleus, although if it is the authentic hY RNA binding protein, it should also reside in the cytoplasm. The Ro/SS-A RNP particles are heterogeneous multimeric complexes that may include more than one Ro/SS-A molecule, hY RNA, La/SS-B, and perhaps other currently undefined molecules.

Two of the putative Ro/SS-A proteins share significant homology with foreign proteins, suggesting that an immune response initially directed against a foreign protein, such as a viral protein, may give rise to the autoimmune response directed at cross-reacting self Ro/SS-A protein. This, plus the possibility that viral infection can alter the normal cellular distribution of Ro/SS-A antigens, presents the intriguing paradigm illustrated in Fig 4 where virus infection might have a dual impact on the Ro/SS-A autoimmune response.

Work is in progress to determine if there is an association between which Ro/SS-A molecules and/or epitopes are targeted by patient autoimmune sera and patient diagnosis, clinical course, and/or response to therapy. We are hopeful that efforts to characterize the structures and functions of the Ro/SS-A antigens will further elucidate the pathogenesis of the Ro/SS-A autoantibody-associated diseases and aid in the development of better diagnostic and therapeutic modalities for those afflicted.

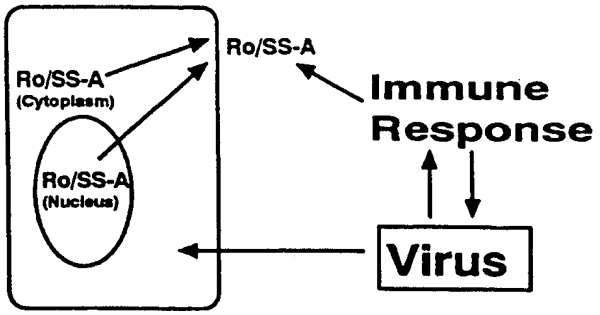

Figure 4. Model for a dual effect of virus infection on the Ro/SS-A autoimmune response. Infection with viruses that express molecules structurally associated with Ro/SS-A molecular subunits could result in translocation of Ro/SS-A antigens to the surface of cells. The immune response generated by the virus could then recognize the translocated Ro/SS-A antigens at the cell surface and mediate cellular damage through mechanisms such as complement-mediated lysis or antibody-dependent cell-mediated cytotoxicity.

Dr. McCauliffe is the recipient of a Dermatology Foundation Career Development Award sponsored by Sandoz Pharmaceuticals and Dr. Sontheimer is the recipient of an NIH Research Career Development Award (ARO1784). This work was supported by NIH grant AR19101.

REFERENCES

1. Clark G, Reichlin M, Tomasi TB: Characterization of a soluble cytoplasmic antigen reactive with sera from patients with systemic lupus erythematosus. J Immunol 102:117–122, 1969
2. Alspaugh MA, Tan EM: Antibodies to cellular antigens in Sjögren's syndrome. J Clin Invest 55:1067–1073, 1975
3. Alspaugh MA, Maddison P: Relation of the identity of certain antigen-antibody systems in systemic lupus erythematosus and Sjögren's syndrome: an interlaboratory collaboration. Arthritis Rheum 22:796–798, 1979
4. Martinez-Lavin M, Vaughan JH, Tan EM: Autoantibodies and the

spectrum of Sjögren's syndrome. Ann Intern Med 91:185–190, 1979

5. Sontheimer RD, Maddison PJ, Reichlin M, Jordon RE, Stastny P, Gilliam JN: Serologic and HLA associations in subacute cutaneous lupus erythematosus, a clinical subset of lupus erythematosus. Ann Intern Med 97:664–671, 1982
6. Maddison PJ, Provost TT, Reichlin M: ANA negative systemic lupus erythematosus: serological analysis. Medicine (Baltimore) 60:87–94, 1981
7. Kephart D, Hood AF, Provost TT: Neonatal lupus: serologic findings. J Invest Dermatol 77:331–333, 1981
8. Provost TT, Arnett FC, Reichlin M: Homozygous C2 deficiency, lupus erythematosus and anti-Ro(SSA) antibodies. Arthritis Rheum 26:1279–1282, 1983
9. Meyer O, Hauptmann G, Tuppeiner G, Ochs HD, Mascart-Lemone F: Genetic deficiency of C4, C2 or C1q and lupus syndromes: association with anti-Ro(SS-A) antibodies. Clin Exp Immunol 62:678–684, 1985
10. McCauliffe DP, Lux F, Lieu TS, Sanz I, Hanke J, Newkirk M, Siciliano MJ, Sontheimer RD, Capra JD: Ro/SS-A and the pathogenic significance of its antibodies. J Autoimmun 2:375–381, 1989
11. Sontheimer RD, McCauliffe DP: Pathogenesis of anti-Ro/SS-A autoantibody-associated cutaneous lupus erythematosus. Dermatol Clin 8:751–758, 1990
12. Lee LA, Weston WL: New findings in neonatal lupus syndrome. Am J Dis Child 138:233–236, 1984
13. Laxer RM, Roberts EA, Gross KR, Britton JR, Cutz E, Dimmick J, Petty RE, Silverman ED: Liver disease in neonatal lupus erythematosus. J Pediatr 116:238–242, 1990
14. Lee LA, Gaither KK, Coulter SN, Norris DA, Harley JB: Pattern of cutaneous immunoglobulin G deposition in subacute cutaneous lupus erythematosus is reproduced by infusing purified anti-Ro(SSA) autoantibodies into human skin-grafted mice. J Clin Invest 83:1556–1562, 1989
15. Lerner MR, Boyle J, Hardin JA, Steitz JA: Two novel classes of small ribonucleoproteins detected by antibodies associated with lupus erythematosus. Science 211:400–402, 1981
16. Wolin SL, Steitz JA: The Ro small cytoplasmic ribonucleoproteins: identification of the antigenic protein and its binding site on the Ro RNA's. Proc Natl Acad Sci USA 81:1996–2000, 1984
17. Ben-Chetrit E, Chan EK, Sullivan KF, Tan EM: A 52-kD protein is a novel component of the SS-A/Ro antigenic particle. J Exp Med 167:1560–1571, 1988
18. Rader MD, O'Brien C, Liu Y, Harley JB, Reichlin M: The heterogeneity of the Ro/SSA antigen: different molecular forms in lymphocytes and red blood cells. J Clin Invest 83:1293–1298, 1989
19. Deutscher SL, Harley JB, Keene JD: Molecular analysis of the 60-kDa human Ro ribonucleoprotein. Proc Natl Acad Sci USA 85:9479–9483, 1988
20. Ben-Chetrit E, Gandy BJ, Tan EM, Sullivan KF: Isolation and characterization of a cDNA clone encoding the 60-kD component of the human SS-A/Ro ribonucleo-protein autoantigen. J Clin Invest 83:1284–1292, 1989
21. Frankel AD, Pabo C: Fingering too many proteins. Cell 53:675, 1988
22. Scofield RH, Harley JB: Autoantigenicity of a Ro/SSA is related to a nucleocapsid protein of vesicular stomatitis virus. Proc Natl Acad Sci USA 88:3343–3347, 1991
23. Oldstone MBA: Molecular mimicry and autoimmune disease. Cell 50:819–820, 1987
24. McCauliffe DP, Lux FA, Lieu TS, Sanz I, Hanke J, Newkirk MM, Bachinski LL, Itoh Y, Siciliano MJ, Reichlin M, Sontheimer RD, Capra JD: Molecular cloning, expression, and chromosome 19 localization of a human Ro/SS-A autoantigen. J Clin Invest 85:1379–1391, 1990
25. Lingappa VR: Intracellular traffic of newly synthesized proteins. Current understanding and future prospects. J Clin Invest 83:739–751, 1989
26. Fliegel L, Burns K, Wlasichuk K, Michalak M: Peripheral membrane proteins of the sarcoplasmic and endoplasmic reticulum. Comparison of carboxy-terminal amino acid sequences. Biochem Cell Biol 67:696–702, 1989
27. Andres DA, Dickerson IM, Dixon JE: Variants of the carboxyl-terminal KDEL sequence direct intracellular retention. J Bio Chem 265:5952–5955, 1990
28. McCauliffe DP, Lieu T-S, Michalak M, Sontheimer RD, Capra JD: A human Ro/SS-A autoantigen is the homologue of calreticulin and is highly homologous with onchocercal Ral-1 antigen and an aplysia memory molecule. J Clin Invest 86:332–335, 1990
29. Smith MJ, Koch GL: Multiple zones in the sequence of calreticulin, a major calcium binding ER/SR protein. EMBO 8:3581–3586, 1989
30. Lieu T-S, McCauliffe DP, Volpe P, Alderson-Lang BH, Michalak M, Capra JD, Sontheimer RD: Structural and functional homology between a human Ro/SS-A autoantigen and the calcium-binding protein, calreticulin (abstr). Clin Res 38:408A, 1990
31. McCauliffe DP, Yang YS, Wilson J, Sontheimer RD, Capra JD: The 5′ flanking region of the human calreticulin gene is highly homologous with the human GRP78, GRP94 and protein disulfide isomerase promoters. J Biol Chem 267:2557–2562, 1992
32. Sambrook JF: The involvement of calcium in transport of secretory proteins from the endoplasmic reticulum. Cell 61:197–199, 1990
33. Munro S, Pelham HRB: An hsp70-like protein in the ER: identity with the 78 kD glucose-regulated protein and immunoglobulin heavy chain binding protein. Cell 46:291–300, 1986
34. Sorger PK, Pelham HRB: The glucose-regulated protein grp94 is related to heat shock protein hsp90. J Mol Biol 194:341–344, 1987
35. Freedman RB: Protein disulfide isomerase: multiple roles in the modification of nascent secretory proteins. Cell 57:1069–1072, 1989
36. Lux FA, McCauliffe DP, Buttner DW, Capra JD, Sontheimer RD, Lieu TS: Antibodies to *Onchocerca volvulus* cross-react with a human Ro/SS-A autoantigen (abstr). Clin Res 38:626A, 1990
37. Hunter FA, Barger BD, Schrohenloher R, Koopman WJ, Dohlman JG: Autoantibodies to calreticulin in the sera of systemic lupus erythematosus (abstr). Arthritis Rheumat 34 (suppl 9):S75, 1991
38. Rokeach LA, Haselby JA, Meilof JF, Smeenk RJT, Unnasch TR, Greene BM, Hoch SO: Characterization of the autoantigen calreticulin. J Immunol 147:3031–3039, 1991
39. Lieu TS, Capra JD, Sontheimer RD: Calreticulin is a component of the human Wil-2 cell Ro/SS-A autoantigen complex (abstr). Clin Res 40:508A, 1992
40. Edward K, Chan L, Harnel JC, Buyon JP, Jan EM: Molecular definition and sequence motifs of the 52-kD component of human SS-A/Ro autoantigen. J Clin Invest 87:68–76, 1991
41. Itoh K, Itoh Y, Frank MB: Protein heterogeneity in the human Ro/SSA ribonucleoproteins. The 52- and 60-kD Ro/SSA autoantigens are encoded by separate genes. J Clin Invest 87:117–186, 1991
42. Lux FA, McCauliffe DP, Buttner DW, Capra JD, Sontheimer RD, Lieu TS: Serologic cross-reactivity between a human Ro/SS-A autoantigen (calreticulin) and the Ral-1 antigen of *Onchocerca volvulus*. J Clin Invest 89:1945–1951, 1992
43. Lieu TS, McCauliffe DP, Volpe P, Alderson-Lang BH, Heilman C, Leberer E, Michalak M, Fliegel L, Capra JD, Sontheimer RD: Further evidence supporting the identity of a native human Wil-2 cell 46 kD Ro/SS-A autoantigen with the highly conserved calcium binding protein, calreticulin (submitted for publication)
44. Sontheimer RD, Lieu TS, McCauliffe DP: Molecular characterization of the Ro/SS-A autoimmune response. Semin Dermatol 10:199–205, 1991
45. Boire G, Craft J: Biochemical and immunological heterogeneity of the Ro ribonucleoprotein particles. Analysis with sera specific for the RohY5 particle. J Clin Invest 84:270–279, 1989
46. Swanson MS, Nakagawa TY, LeVan, Dreyfuss G: Primary structure of human nuclear ribonuclear particle C proteins: conservation of sequence and domain structures in heterogeneous nuclear RNA, mRNA and pre-rRNA-binding proteins. Mol Cell Biol 7:1731–1739, 1987
47. Rokeach LA, Haselby JA, Hoch SO: Molecular cloning of a cDNA encoding the human Sm-D autoantigen. Proc Natl Acad Sci USA 85:4832–4836, 1988
48. Yamagata H, Harley JB, Reichlin, M: Molecular properties of the Ro/SS-A antigen and enzyme-linked immunosorbent assay for quantitation of antibody. J Clin Invest 74:625–633, 1984
49. Scopelitis E, Biundo JJ, Alspaugh MA: Anti-SS-A antibody and other antinuclear antibodies in systemic lupus erythematosus. Arthritis Rheum 23:287–293, 1980
50. Boire G, Craft J: Human Ro ribonucleoprotein particles: characterization of native structure and stable association with the La polypeptide. J Clin Invest 85:1182–1190, 1990
51. Harmon CE, Deng JS, Peebles CL, Tan EM: The importance of tissue

substrate in the SS-A/Ro antigen-antibody system. Arthritis Rheum 27:166–173, 1984

52. Wermuth DJ, Geoghegan WD, Jordon RE: Anti-Ro/SS-A antibodies. Association with a particulate. (large, speckled-like thread) immunofluorescent nuclear staining pattern. Arch Dermatol 121:335–338, 1985
53. Elenitsas R, Bair LW, Medsger TA, Deng JS: Discordance of SS-A/Ro and SS-B/La cellular antigens in synchronized cells. J Invest Dermatol 87:504–509, 1986
54. Gaither KK, Fox OF, Yamagata H, Mamula MJ, Reichlin M, Harley JB: Implications of anti-Ro/Sjögren's syndrome A antigen autoantibody in normal sera for autoimmunity. J Clin Invest 79:841–846, 1987
55. Maddison PJ: ANA-negative SLE. Clin Rheum Dis 8:105–119, 1982
56. Hendrick JP, Wolin SL, Rinke J, Lerner MR, Steitz JA: Ro small cytoplasmic ribonucleoproteins are a subclass of La ribonucleoproteins: further characterization of the Ro and La small ribonucleoproteins from uninfected mammalian cells. Mol Cell Biol 12:1138–1149, 1981
57. Bachmann M, Mayet WJ, Schroder HC, Pfeifer K, Neyer Zum Buschenfelde KH, Muller WEG: Association of La and Ro antigens with intracellular structures in HEp-2 carcinoma cells. Proc Natl Acad Sci USA 83:7770–7774, 1986
58. Wollina U, Beensen H, Kittler L, Schaarschmidt H, Knopf B: PUVA treatment of human cultured fiberglass from sclerotic skin enhances the binding of antibodies to SS-A (Ro). Arch Dermatol Res 279:206–208, 1987
59. Miyagawa S, Okada N, Inagaki Y, Kitano Y, Ueki H, Sakamoto K, Steinberg ML: SSA/Ro antigen expression in simian virus 40-transformed human keratinocytes. J Invest Dermatol 90:342–345, 1988
60. Koch GLE, Macer DRJ, Smith MJ: Visualization of the intact endoplasmic reticulum by immunofluorescence with antibodies to the major ER glycoprotein, endoplasmin. J Cell Sci 87:535–542, 1987
61. Itoh Y, Reichlin M: Molecular conformation and autoantibodies to the Ro/SSA particle. Arthritis Rheum 34(suppl):S101, 1991
62. Sontheimer RD, McCauliffe DP, Michalak M, Capra JD, Lieu TS: Cytoplasmic localization of a calcium-binding 46 kD human Ro/SS-A antigen. Arthritis Rheum 33S:B15, 1990
63. Milner RE, Baksh S, Shemanko C, Carpenter MR, Smillie L, Vance JE, Opas M, Michalak M: Calreticulin, and not calsequestrin, is the major calcium binding protein of smooth muscle sarcoplasmic reticulum and liver endoplasmic reticulum. J Biol Chem 266:7155–7165, 1991
64. Kato N, Hoshimo H, Harada F: Nucleotide sequence of 4.5S RNA (C8 or hY5) from HeLa cells. Biochem Biophys Res Commun 108:363–370, 1982
65. Buyon JP, Ben-Chetrit E, Karp S, Roubey RAS, Pompeo L, Reeves WH, Tan EM, Winchester R: Acquired congenital heart block. Pattern of maternal antibody responses to biochemically defined antigens of the SSA/Ro-SSB/La system in neonatal lupus. J Clin Invest 84:627–634, 1989
66. Ben-Chetrit E, Fox RI, Tan EM: Dissociation of immune responses to the SS-A (Ro) 52-kD and 60-kD polypeptides in systemic lupus erythematosus and Sjögrens syndrome. Arthritis Rheum 33:349–355, 1990
67. Sontheimer RD: Subacute cutaneous lupus erythematosus. Clin Dermatol 3:58–68, 1985
68. Lee LA, David KM: Cutaneous Lupus erythematosus. Curr Probl Dermatol 1:161–200, 1989
69. LeFeber WP, Norris DA, Ryan SR, Huff JC, Lee LA, Kubo M, Boyce ST, Kotzin BL, Weston WL: Ultraviolet light induces binding of antibodies to selected nuclear antigens on cultured human keratinocytes. J Clin Invest 74:1545–1551, 1984
70. Furukawa F, Kashihara-Sawami M, Lyons MB, Norris DA: Binding of antibodies to ENA SS-A/Ro and SS-B/La is induced on the surface of human keratinocytes by UVL: implications for the pathogenesis of photosensitive cutaneous lupus. J Invest Dermatol 94:77–85, 1990
71. Bachmann M, Chang SH, Slor H, Kukulies J, Muller WEG: Shuttling of the autoantigen La between nucleus and cell surface after UV irradiation of human keratinocytes. Exp Cell Res 191:171–180, 1990
72. Sontheimer RD, McCauliffe DP, Wilson JL, Capra JD: Transcriptional regulation of human calreticulin. Clin Res 40:493A, 1992
73. Kawashima T, Lieu TS, Capra JD, Sontheimer RD: Ultraviolet irradiation preferentially upregulated expression of the 46 kD Ro/SS-A autoantigen (calreticulin) in transformed human epidermal keratinocytes (abstr). Clin Res 40:508A, 1992
74. Furukawa F, Lyons MB, Lee LA, Coulter SN, Norris DA: Estradiol enhances binding to cultured human keratinocytes of antibodies specific for SS-A/Ro and SS-B/La. J Immunol 141:1480–1488, 1988
75. Vanbruskirk A, Crump BL, Margoliash E, Pierce SK: A peptide binding protein having a role in antigen presentation is a member of the HSP70 heat shock family. J Exp Med 170:1799–1809, 1989
76. Fisch P, Malkovsky M, Kovats S, Strum E, Braakman E, Klein BS, Voss SD, Morrissey LW, DeMars R, Welch WJ, Bolhuis RLH, Sondel PM: Recognition by human Vgamma9/Vdelta2 T cells of a GroEL homolog on Daudi Burkitt's lymphoma cells. Science 250:1269–1273, 1990
77. Hennungs H, Michael D, Cheng C, Steinert P, Holbrook K, Yuspa SH: Calcium regulation of growth and differentiation of mouse epidermal cells in culture. Cell 19:245–254, 1980
78. Lee LA, Gaither KK, Coulter SN, Norris DA, Harley JB: Pattern of cutaneous immunoglobulin G deposition in subacute cutaneous lupus erythematosus is reproduced by infusing purified anti-Ro (SS-A) autoantibodies in human skin-grafted mice. J Clin Invest 83:1556–1562, 1989
79. Booth C, Koch GLE: Perturbation of cellular calcium induces secretion of luminal ER proteins. Cell 59:729–737, 1989
80. Lodish HF, Kong N: Perturbation of cellular calcium blocks exit of secretory proteins from rough endoplasmic reticulum. J Biol Chem 265:10893–10899, 1990
81. Kutsch CL, Norris DA, Middleton MH, Lee LA: Induction of anti-Ro/SS-A antibody binding to human keratinocytes stimulated by either calcium ionophore A23187 or by TNF-alpha (abstr). J Invest Dermatol 96:610, 478, 1991
82. Schattner A, Rager-Zisman B: Virus-induced autoimmunity. Rev Infect Dis 12:204–222, 1990
83. Tesar TT, Armstrong J: Expression of Ro/SSA and La/SSB on epithelial cell surface following *in vitro* adenovirus infection (abstr). Arthritis Rheum S74, C20, 1986
84. Jianhui Z, Newkirk MM: Viral induction of the human autoantigen calregulin Ro/SS-A (abstr). Arthritis Rheumat 34(suppl):S102, 1991
85. Bachmann M, Falke D, Shroder HC, Muller WEG: Intranuclear distribution of the La antigen in CV-1 cells after herpes simplex virus type I infection compared with the localization of U small nuclear ribonucleoprotein particles. J Gen Virol 70:881–891, 1989

Islet Cell Autoantigen 69 kD (ICA69)

Molecular Cloning and Characterization of a Novel Diabetes-associated Autoantigen

Massimo Pietropaolo,* Luis Castaño,* Sunanda Babu,* Roland Buelow,‡ Yu-Ling S. Kuo,‡ Stephan Martin,§ Andrea Martin,§ Alvin C. Powers,|| Michal Prochazka,¶ Jurgen Naggert,¶ Edward H. Leiter,¶ and George S. Eisenbarth*

Barbara Davis Center for Childhood Diabetes, University of Colorado Health Sciences Center, Denver, Colorado 80262; and Elliot P. Joslin Research Laboratory, Joslin Diabetes Center, Brigham and Women's Hospital, New England Deaconess Hospital, Harvard Medical School, Boston, Massachusetts 02215 ‡ImmuLogic Pharmaceutical Corporation, Palo Alto, California 94394; §Diabetes Forschungsinstitut, D-4000 Düsseldorf, Germany; ||Division of Endocrinology, Nashville Veterans Affairs Medical Center, Vanderbilt University, Nashville, Tennessee 37232; and ¶The Jackson Laboratory, Bar Harbor, Maine 04609

Abstract

We have identified a novel 69-kD peptide autoantigen (ICA69) associated with insulin-dependent diabetes mellitus (IDDM) by screening a human islet λgt11 cDNA expression library with cytoplasmic islet cell antibody positive sera from relatives of IDDM patients who progressed to the overt disease. The deduced open reading frame of the ICA69 cDNA predicts a 483–amino acid protein. ICA69 shows no nucleotide or amino acid sequence relation to any known sequence in GenBank, except for two short regions of similarity with BSA. The ICA69 cDNA probe hybridizes with a 2-kb mRNA in poly(A⁺) RNA from human pancreas, brain, heart, thyroid, and kidney, but not with skeletal muscle, placenta, spleen, or ovary. Expression of ICA69 was also detected in β cells and cell lines, as well as in tumoral tissue of islet cell origin. The native ICA69 molecule migrates to 69 kD in SDS-PAGE as detected with specific antibodies. Serum samples from relatives of IDDM patients specifically reacted with affinity-purified recombinant ICA69 on Western blotting. The structural gene for ICA69 was designated *ICA1*. A homologue in the mouse, designated *Ica-1* was mapped to the proximal end of chromosome 6 (within 6 cM of the Met protooncogene). ICA69 adds a novel autoantigen to the family of identified islet target molecules, and by the manner of its identification and characterization large amounts of antigen are available for development of quantitative, convenient predictive assays for autoantibodies and analysis of the role of this molecule in diabetes autoimmunity, as well as its physiologic function. (*J. Clin. Invest.* 1993. 92:359–371.) Key words: autoantigens • preclinical diabetes • molecular cloning • autoimmunity • ICA69

Introduction

There is evidence that insulin-dependent diabetes mellitus (IDDM)[1] is a chronic autoimmune disease in which the presence of autoantibodies, such as cytoplasmic islet cell antibodies or insulin autoantibodies, can be present years before the clinical onset of the disease (1). A common feature of type I diabetes and other autoimmune diseases is a humoral immune response characterized by the appearance of autoantibodies against cellular proteins, including islet peptides (2–4). Although all the target antigens in type I diabetes have not been identified, several autoantigens associated with the disease have been molecularly characterized using different experimental approaches, namely insulin (5), glutamic acid decarboxylase (GAD) (6), carboxypeptidase H (7), as well as the glycolipids GT3 (8) and GM2-1 (9). Recently, cDNA encoding for a fragment of carboxypeptidase H (7), a granule-associated enzyme, has been reported to react with sera from prediabetic patients and another peptide expressed in a λgt11 phage from a human islet library appears to be recognized by IDDM sera (10). Cellular proteins of unknown sequence whose molecular masses are 38 (11), 52 (12), and 69 kD (13), have also been reported to be recognized by a humoral and/or a cellular immune response. It is of interest that almost all patients with type I diabetes have elevated levels of IgG anti-BSA antibodies related to a 69,000-M_r islet peptide, which may represent a target antigen for cow milk–induced islet autoimmunity (14, 15).

The present study was undertaken to isolate clones that code for some of these or other unidentified autoantigens and characterize their molecular structure. Isolation of cDNA clones expressing antigenic determinants has been extensively used to identify clones coding for autoantigens in different autoimmune diseases (16). This approach offers the possibility of identifying and characterizing novel autoantigens that may be of restricted cellular distribution as well as low cellular expression (17). Such proteins may not be detected by routine screening tests such as immunofluorescence or immunoprecipitation.

We have used this approach to immunoscreen a human islet λgt11 expression library with a pool of sera from prediabetic relatives of IDDM patients, identify, sequence the clones, and characterize the expressed proteins. In this report, we describe the cloning of a cDNA that encodes a novel islet autoantigen, whose apparent migration is 69 kD on SDS-polyacrylamide gel chromatography.

Methods

Serum samples. Sera were obtained from first degree relatives of patients with type I diabetes. All of them were at high risk of developing IDDM, and some have already progressed to the overt disease on prospective follow-up. Clinical studies were performed with informed consent, as well as approval from the Joslin Clinic and University of Colorado institutional review boards. All the sera used for the screening of the human islet λgt11 library expressed high titer of islet cell antibodies (> 80 Juvenile Diabetes Foundation units). The sera were repeatedly absorbed with a protein lysate of a wild λgt11 phage–infected *Esche-*

Address correspondence and reprint requests to Dr. George S. Eisenbarth, The Barbara Davis Center for Childhood Diabetes, University of Colorado Health Sciences Center, 4200 East 9th Ave., Box B140, Denver, CO 80262.

Received for publication 6 October 1992 and in revised form 3 February 1993.

1. *Abbreviations used in this paper:* APAAP, alkaline phosphatase–antialkaline phosphatase; GAD, glutamic acid decarboxylase; ICA, islet cell antibodies; IDDM, insulin-dependent diabetes mellitus; IPTG, isopropyl-β-D-thiogalactopyranoside; LB, Luria-Bertani; PAP, peroxidase antiperoxidase; pfu, plaque-forming units; RFLV, restriction length fragment variation.

J. Clin. Invest.

0021-9738/93/07/359/13 $2.00
Volume 92, July 1993, 359–371

richia coli strain Y1090 (18) to remove anti–*E. coli* antibodies. Absorbed antibodies were stored at −20°C in the presence of 0.05% sodium azide until used for immunological screening. Originally, a pool of three sera was used to identify positive clones, and subsequently sera of three other relatives were studied for reactivity with the positive clone. 10 sera of normal individuals were also tested for reactivity with the positive clone. Sera from additional prediabetic relatives (subjects followed to diabetes onset) (n = 23), autoantibody positive but currently nondiabetic relatives (n = 31), and normal controls (n = 70) were tested for reactivity to the expressed molecule on Western blots.

λgt11 expression libraries. Two λgt11 libraries were used, a human islet library provided by Dr. Alan Permutt (Washington University, St. Louis, MO) and a human insulinoma library generated by Alvin C. Powers (Vanderbilt University, Nashville, TN). A human λgt11 islet library was constructed from human islet poly(A$^+$) mRNA by Clontech (Palo Alto, CA), with ~ 1×10^9 plaque-forming units (pfu)/ml and 85% being recombinants. A human insulinoma library was generated from insulinoma poly(A$^+$) mRNA and then cDNA was produced and packaged into the λgt11 phage (19), with ~ 1.3×10^9 pfu/ml and a recombinant rate of more than 80%.

Screening of λgt11 expression libraries with antibody and cDNA probes. A phage human islet λgt11 expression library was screened with a pool of sera from preclinical IDDM relatives (20). Isolated recombinant phages were plated on Luria-Bertani (LB) agar plates (150 mm diameter) with *E. coli* strain Y1090 at ~ $0.5–1 \times 10^4$ pfu/plate. After a 3-h incubation at 42°C, a nitrocellulose filter (Schleicher & Schuell, Keene, NH) saturated with 10 mM isopropyl-β-D-thiogalactopyranoside (IPTG) (BRL, Grand Island, NY) was overlaid on the agar overnight at 37°C to induce the expression of β-galactosidase fusion proteins. After that, the filters were blocked with 1% BSA (Sigma Immunochemicals, St Louis, MO) in Tris-buffered saline (TBS), incubated containing 0.05% Tween, incubated for 2 h at room temperature), and then incubated with 1/500 diluted sera overnight at 4°C. After several washes with TBS, the bound antibodies were detected by incubation with anti–human IgG alkaline phosphatase (Cappel Laboratories, Durham, NC) diluted 1/100 (2 h at room temperature). A phage human islet λgt11 expression library was initially screened with pooled sera from three prediabetics. The original positive plaque was replated and rescreened sequentially until all progeny of plaques were recognized by the sera. To determine whether prediabetic sera or controls reacted with the product of the clone and to reduce the possibilities of false positivity, plaque-purified recombinant bacteriophage was mixed ~ 1:1 with a wild-type λgt11 and plated with *E. coli* Y1090 as for screening. Pieces of nitrocellulose carrying plaque proteins were then incubated with individual sera. Reactions were considered positive if significant staining of ~ 50% of the plaques was observed. Intensity of staining was estimated to score reactivity of individual sera on a 0 (negative) to 4+ (strongest) scale. The cDNA insert of the original positive clone, termed PM1/1 (Fig. 1 *B*), was used as probe to further screen the human islet library and a human insulinoma library by plaque hybridization (21) to obtain several longer and overlapping cDNA clones. The probe was labeled with [α^{32}P]dCTP by random priming (21, 22) using Klenow fragment (Amersham Corp., Arlington Heights, IL) and used to rescreen the libraries.

Amplification of λgt11 cDNA insert and cloning. The λgt11 cDNA insert from the positive clones was amplified by PCR (23, 24) using λgt11 primers complementary to the β-galactosidase portion of the λgt11 template (primer 1218: 5′-GGTGGCGACGACTCCTGGAGCCCG-3′; primer 1222: 5′-TTGACACCAGACCAACTGGTAATG-3′, New England Biolabs, Beverly, MA). Reaction mixtures for PCR (0.1 ml) contained cDNA template, 100 pmol each of the primers, and 2.5 U of *Taq* I DNA polymerase (Perkin-Elmer Cetus Instruments, Norwalk, CT) in 10 mM Tris/HCl, pH 8.3, 50 mM KCl, 1.5 mM $MgCl_2$ containing dNTPs at 0.2 mM each and 0.01% gelatin. Reactions were carried out in a thermal cycler (Perkin-Elmer Cetus) for 30 cycles of denaturation (92°C, 1 min), annealing (60°C, 1.5 min), and elongation (72°C, 1 min). After *Eco* RI digestion and fractionation on 1% agarose gel stained with ethidium bromide to visualize the PCR products, the product of interest was excised, purified, and subcloned into the *Eco* RI site of pBluescript II vector. This vector was used to transform *E. Coli* strain XL1 Blue, and to sequence the PCR products across its polylinker arms (Stratagene, La Jolla, CA). cDNA samples for PCR were obtained from phage suspension.

DNA sequencing and computer analysis of nucleic acid and protein sequences. Nucleotide sequences were determined by using the dideoxynucleotide chain termination method of Sanger et al. (25), using T7 DNA polymerase (Sequenase; United States Biochemical Corp., Cleveland, OH). To avoid compression in G + C–rich sequences, additional sequencing reactions were performed with dITP alternating with dGTP (26).

Sequences were aligned and analyzed using the EUGENE, SAM, PIMA.SH, and PROSITE programs. The GenBank (DNA and Amino Acid Databank) was searched for similarities, and the PLSEARCH program analyzed for protein sequence patterns derived from the sequences of homologous protein families (Molecular Biology Computing Research Resource, Dana Farber Cancer Institute, and Harvard School of Public Health, Cambridge, MA). Hydropathy plots from the deduced amino acid sequence were prepared as described by Kyte and Doolittle (27, 28) and Klein et al. (29).

Cell lines. Cells were used at late log phase, when almost all were viable. RIN 1046-38, derived from a rat insulinoma (kindly provided by Christopher Newgard, Southwestern Medical Center, University of Texas, Dallas, TX), were cultured in DME supplemented with 10% FBS, and 5.6 mM glucose in a humidified atmosphere of 10% CO_2/90% air at 37°C (30). βTC-1 and αTC-1 were derived from progeny of transgenic mice expressing SV40 large T-antigen under control of the rat insulin II 5′-flanking region or rat preproglucagon 5′-flanking region respectively (31–33). The βTC-1 and αTC-6 cell lines were maintained in DME supplemented to a final concentration of 16.5 mM glucose and supplemented with Eagle's MEM, nonessential amino acids component, 44 mM sodium bicarbonate, 15 mM Hepes, 50 μg/liter gentamicin sulphate, and 10% heat-inactivated FBS in a humidified atmosphere of 5% CO_2/95% air. HIT cells, derived from a hamster insulin producing cell line (34), were grown in 5% CO_2/95% air in RPMI 1640 medium containing 10% FCS and 11.1 mM glucose. HeLa cells (ATCC CCL 2.2; American Type Culture Collection, Rockville, MD) (35), JEG cells (human choriocarcinoma; ATCC HTB 36) (36), and HepG2 cells (human hepatoma; ATCC HB 8065) (37) were maintained in RPMI 1640 supplemented with 10% FCS, 2 mM L-glutamine and 5 μg/ml gentamicine sulfate in 10% CO_2/90% air incubator. A human islet carcinoid cell line designated BON-1 (provided by Dr. Cortney Townsend, Department of Surgery, University of Texas Medical Branch, Galveston, TX) was maintained in DME with 10% heat-inactivated FCS and 5.6 mM glucose in a humidified atmosphere of 10% CO_2/90% air.

RNA isolation and Northern analysis. Total RNAs and poly(A$^+$) RNAs from various tissues and cell lines were prepared by the guanidinium isothiocyanate method, enriched for the polyadenylated (poly-A) fraction with an oligo(dT)-cellulose column and analyzed on Northern blots according to standard procedures (38). The hybridization was carried out for 18 h at 42°C in the prehybridization buffer (50% formamide, 5× SSPE [1× SSPE consists of 150 mM NaCl, 10 mM sodium phosphate, and 1 mM EDTA, pH 7.4]), 5× Denhardt's solution, 100 μg/ml denaturated salmon sperm DNA, and 0.1% SDS) (18) containing [α^{32}P]dCTP labeled cDNA purified probe. The probes consisted of either a 0.95-kb fragment from the original PM1/1 positive clone identified, or a 1.78-kb gt11 insert from an overlapping clone; 100 ng of each probe was labeled by the random priming method. 100 ng of a 2-kb human β-actin cDNA was used as control probe (39). The fresh hybridization solution contained the denatured radiolabeled DNA probes at a concentration of $2–4 \times 10^6$ cpm/ml with a specific activity ≥ 5×10^8 cpm/μg (18, 40). The nitrocellulose filters were washed in three changes of 2× SSC and 0.05% SDS at room temperature each time. The final three washes were carried out in 0.1× SSC and 0.1% SDS from room temperature to 65°C depending upon the stringency conditions required for each experiment. Filters were exposed to Kodak film at −80°C with intensifying screens. Ribosomal bands were used as size markers (41, 42).

Preparation of anti-ICA69 antibodies from synthetic peptides and from the purified molecule. Rabbit antibodies were produced using synthetic peptides from the deduced amino acid sequence as well as the ICA69 recombinant expressed molecule. Rabbits were immunized in order to generate antibodies against specific domains (28, 43). Two regions of the molecule, one corresponding to the COOH terminus, residues 471–483: GKTDKEHELLNA, and one to an internal polypeptide close to the COOH terminus, residues 458–470: ADLDPLSNPDAV, and the serum generated against the whole molecule, were used and found to yield antisera which reacted with the native ICA69 molecule on Western blots (44). The synthetic polypeptides were coupled to a carrier protein, keyhole limpet hemocyanin linked to bromoacetyl bromide. Five female New Zealand white rabbits were immunized with 1 mg of the keyhole limpet hemocyanin–peptide conjugate suspended in 1 ml of complete Freund's adjuvant. Rabbits were boosted three times with 1 mg of the specific polypeptide in incomplete Freund's adjuvant at 30-d intervals and serum samples were collected and stored in aliquots at −20°C. An ELISA was used to detect specific antipeptide antibodies.

Indirect ELISA. Indirect ELISA was performed for the detection of specific antibodies generated in rabbits against ICA69 polypeptides (45). 1 μg of specific polypeptide was used to coat each well of a microtiter plate (Immulon; Dymatech Laboratories, Inc., Chantilly, VA) (46), and after blocking residual binding of the plate with a PBS solution containing 1% BSA for 2 h, appropriate dilutions of rabbit pre- and postimmune sera were added to each well (1:100–1:32,000) and incubated overnight. All dilutions were tested in triplicate. After washing away unbound antibodies, a solution containing anti–rabbit IgG (whole molecule) peroxidase conjugate (Sigma Immunochemicals) as developing reagent was added to the wells. After 2 h incubation, unbound conjugate was washed away and a substrate solution (*o*-phenylenediamine dihydrochloride) (Sigma Immunochemicals), was added. A specific hyperimmune serum raised to another polypeptide (PEP-80, of the IRS-1 molecule kindly provided by Dr. M. White, Joslin Diabetes Center) (47) and preimmune sera from normal rabbits were used in each assay as positive and negative controls respectively. The optical density of the solutions in the wells was measured with a spectrophotometer through a 405-nm filter.

SDS-PAGE and immunoblotting. Cell line extracts and total homogenates of rat brain tissues were prepared as described by Laemmli (48). Cell line extracts and total-homogenate proteins were separated by SDS-PAGE using a constant voltage of 180 V for 4 h through stacking and the resolving gel. Bromophenol blue was included in the sample buffer to visualize buffer front. A mixture of individually colored and purified proteins were used as protein standards (Rainbow® Protein Molecular Weight Markers, Amersham Corp.): myosin, mol wt 200,000, blue; phosphorylase b, mol wt 97,400, brown; BSA, mol wt 69,000, red; ovalbumin, mol wt 46,000, yellow; carbonic anhydrase, mol wt 30,000, orange; trypsin inhibitor, mol wt 21,000, green; and lysozyme, mol wt 14,300, magenta. Homogenate protein concentrations were determined by Lowry's method (Pierce Chemical Co., Rockford, IL) and 4–50 μg of proteins per lane (depending on the size of the PAGE) were run on a 10% SDS-PAGE under reducing conditions. Proteins were then transferred onto nitrocellulose according to Towbin et al. (49) in transfer buffer (12.5 mM Tris, 96 mM glycine, 20% methanol) for 1 h on a semi-dry electrophoretic transfer cell at 15 V. The nitrocellulose was cut into strips, and incubated for 2 h at 37°C in 5% (wt/vol) nonfat dried milk diluted in PBS (Blotto buffer) to block the nonspecific binding sites. The nitrocellulose strips were then incubated with a 1:100 dilution of a rabbit anti-ICA69 antiserum and then washed in 5% (wt/vol) nonfat dried milk diluted in PBS adding Tween 20 to a final concentration of 0.01%. After incubation of the filters at room temperature for 2 h with ^{125}I-Protein A (Amersham Corp.) to detect the rabbit anti-ICA69 antibodies, unbound ^{125}I-Protein A was removed by washing as described above. Blots were exposed to Kodak film at −80°C with intensifying screens for 12–24 h.

Expression of the recombinant ICA69. PM1/3 clone cDNA was amplified by PCR. The PCR product was generated using a primer spanning the PM1/3 start codon and encoding the first eight amino acids (5′-TCAGGACACAAATGCAGTTATCCC-3′), and a primer containing the codon sequence for the last seven amino acids, a translational stop codon and a HindIII restriction site (5′-TTTAAGCTTTCATGCATTGAGCAATTCGTGTTC-3′). The pMAL-c vector (50, 51), which encodes for maltose binding protein as product of the *malE* gene, was cut with StuI and HindIII restriction enzymes and ligated with the PM1/3 PCR product. The constructs were then transfected into the appropriate *E. coli*, strain TB1 (52). Ampicillin-resistant colonies were grown overnight in 3 ml LB medium containing 100 μg/ml ampicillin. 100 μl of TB1 pMAL-c-PM1/3 transformants were diluted in 1 ml LB/ampicillin medium and grown 1 h at 37°C followed by induction with 1 mM IPTG for 2 h. Lysates were prepared by centrifugation of 200 μl bacterial cultures for 1 min and boiling the cell pellet with 50 μl SDS sample buffer with 5% mercaptoethanol. After SDS-PAGE of lysates (10 μl) with and without IPTG induction, gels were stained with Coomassie blue. One colony expressing a protein whose molecular mass migrated ~ 105 kD was identified, and the correct size of the insert was confirmed by restriction analysis.

Another vector system was used to express the purified recombinant ICA69 protein without maltose binding protein. The coding region of the PM1/3 cDNA clone, was amplified by PCR using the primers 5′-GAAGGATCCATGTCAGGACACAAATGCAG-3′ and 5′-GGTCTCGAGTCATGCATTGAGCAATTCGTG-3′ and cloned into the BamHI and XhoI sites of the expression vector pTrc99A (His_6). This vector was constructed by insertion of a synthetic DNA fragment encoding six histidines ($[CAC]_6$) into the polylinker of pTrc 99A (53). Recombinant proteins were tagged with six histidine residues at the NH_2 terminus. The plasmid construct was transformed into *E. coli*–Tg1 and protein expression was induced by the addition of IPTG to the culture medium. After 2 h at 37°C, bacteria were lysed in 100 mM Tris pH 8.0, 6 M GuHCl, and 10 mM DTT, and insoluble material was removed by centrifugation at 40,000 *g* for 30 min. Recombinant $(His)_6$-ICA69 was purified using Ni-NTA-agarose (Qiagen, Chatsworth, CA) in the presence of 6 M GuHCl, 1 mM DTT buffer. The correct size of the ICA69 cDNA in the vector was confirmed by sequencing.

Lysates containing ICA69 and maltose binding protein fusion protein, as well as the purified recombinant ICA69, have been used as source for performing Western blots with control sera such as rabbit anti-ICA69 sera (pre- and postimmune), human control sera, and prediabetic sera at a dilution 1:100. Optical density of the bands corresponding to the ICA69 fusion protein and the affinity-purified ICA69 has been evaluated to quantitate the reactivity of the serum samples to ICA69 using a video densitometer (Bio Rad Laboratories, Hercules, CA), and the results were expressed as relative densitometric units.

Immunohistochemistry. Immunohistochemistry has been performed in formalin fixed rat pancreas paraffin embedded sections (4 μm thickness). A double immunoenzymatic labeling of rat islet cellular constituents has been performed (54, 55) using as detection system horseradish peroxidase antiperoxidase (PAP) and alkaline phosphatase–antialkaline phosphatase (APAAP). The PAP immune complex served for the identification of ICA69, whereas the APAAP complex for the identification of insulin, glucagon and somatostatin. After removal of paraffin and rehydratation of tissue, the pancreas sections were first treated with an hydrogen peroxidase solution to suppress possible endogenous peroxidase activity. This was followed by an incubation with normal serum to quench nonspecific protein binding to certain tissue elements, and then the sections were incubated with a primary antibody mixture (rabbit anti-ICA69 antibody generated to the whole molecule, and a mouse mAb generated insulin [HPI-005] to glucagon [GLU 001], or anti-ICA69 and a mouse mAb generated to somatostatin [SOM 018] [Novo Nordisk, Denmark]) for 30 min at room temperature. Unbound antibodies were washed with TBS. Antibody to target antigens (primary antibody), antibody to the primary antibody (link antibody: swine anti–rabbit for ICA69, or goat anti–mouse for antiinsulin, antiglucagon or antisomatostatin mAbs), APAAP and PAP reagents (Dako Corp., Santa Barbara, CA) were applied sequentially for simultaneous double staining. The color development was stopped by washing the slides thoroughly in deionized water.

a

```
     CGGGCGGGGGATACCCCAGGAGATGGGGGTCGAGGAGAGACCCCGGGGAGTAGAGAGAGAGAAACTCACTCCCCGAGTCCCCGACCCTCCCCAAG -178
CAAGGTTATAATATAACTTATCCTCTCATGCTTTTTTCCTGCCCCTTCTCCCCAAATCATCAACAATAGAAGAAGAAGAAAAC ATG TCA GGA CAC   12
                                                                                        Met Ser Gly His    4

AAA TGC AGT TAT CCC TGG GAC TTA CAG GAT CGA TAT GCT CAA GAT AAG TCA GTT GTA AAT AAG ATG CAA CAG AGA   87
Lys Cys Ser Tyr Pro Trp Asp Leu Gln Asp Arg Tyr Ala Gln Asp Lys Ser Val Val Asn Lys Met Gln Gln Arg   29
                                          AMD                                          CK2
TAT TGG GAG ACG AAG CAG GCC TTT ATT AAA GCC ACA GGG AAG AAG GAA GAT GAA CAT GTT GTT GCC TCT GAC GCG  162
Tyr Trp Glu Thr Lys Gln Ala Phe Ile Lys Ala Thr Gly Lys Lys Glu Asp Glu His Val Val Ala Ser Asp Ala   54

GAC CTG GAT GCC AAG CTA GAG CTG TTT CAT TCA ATT CAG AGA ACC TGT CTG GAC TTA TCG AAA GCA ATT GTA CTC  237
Asp Leu Asp Ala Lys Leu Glu Leu Phe His Ser Ile Gln Arg Thr Cys Leu Asp Leu Ser Lys Ala Ile Val Leu   79
                                  CK2
TAT CAA AAG AGG ATA TGT TTC TTG TCT CAA GAA GAA AAC GAA CTG GGA AAA TTT CTT CGA TCC CAA GGT TTC CAA  312
Tyr Gln Lys Arg Ile Cys Phe Leu Ser Gln Glu Glu Asn Glu Leu Gly Lys Phe Leu Arg Ser Gln Gly Phe Gln  104
                                      PKC
GAT AAA ACC AGA GCA GGA AAG ATG ATG CAA GCG ACA GGA AAG GCC CTC TGC TTT TCT TCC CAG CAA AGG TTG GCC  387
Asp Lys Thr Arg Ala Gly Lys Met Met Gln Ala Thr Gly Lys Ala Leu Cys Phe Ser Ser Gln Gln Arg Leu Ala  129
                                          PKC
TTA CGA AAT CCT TTG TGT CGA TTT CAC CAA GAA GTG GAG ACT TTT CGG CAT CGG GCC ATC TCA GAT ACT TGG CTG  462
Leu Arg Asn Pro Leu Cys Arg Phe His Gln Glu Val Glu Thr Phe Arg His Arg Ala Ile Ser Asp Thr Trp Leu  154

ACG GTG AAC CGC ATG GAA CAG TGC AGG ACG GAA TAT AGA GGA GCA CTA TTA TGG ATG AAG GAC GTG TCT CAG GAG  537
Thr Val Asn Arg Met Glu Gln Cys Arg Thr Glu Tyr Arg Gly Ala Leu Leu Trp Met Lys Asp Val Ser Gln Glu  179

CTT GAT CCA GAC CTC TAC AAG CAA ATG GAG AAG TTC AGG AAG GTG CAA ACA CAA GTG CGC CTT GCA AAA AAA AAC  612
Leu Asp Pro Asp Leu Tyr Lys Gln Met Glu Lys Phe Arg Lys Val Gln Thr Gln Val Arg Leu Ala Lys Lys Asn  204

TTT GAC AAA TTG AAG ATG GAT GTG TGT CAA AAA GTG GAT CTT CTT GGA GCG AGC AGA TGC AAT CTC TTG TCT CAC  687
Phe Asp Lys Leu Lys Met Asp Val Cys Gln Lys Val Asp Leu Leu Gly Ala Ser Arg Cys Asn Leu Leu Ser His  229

ATG CTA GCA ACA TAC CAG ACC ACT CTG CTT CAT TTT TGG GAG AAA ACT TCT CAC ACT ATG GCA GCC ATC CAT GAG  762
Met Leu Ala Thr Tyr Gln Thr Thr Leu Leu His Phe Trp Glu Lys Thr Ser His Thr Met Ala Ala Ile His Glu  254
PKC                                       PKC      CK2
AGT TTC AAA GGT TAT CAA CCA TAT GAA TTT ACT ACT TTA AAG AGC TTA CAA GAC CCT ATG AAA AAA TTA GTT GAG  837
Ser Phe Lys Gly Tyr Gln Pro Tyr Glu Phe Thr Thr Leu Lys Ser Leu Gln Asp Pro Met Lys Lys Leu Val Glu  279
                                                                                            CK2
AAA GAA GAG AAG AAG AAA ATC AAC CAG CAG GAA AGT ACA GAT GCA GCC GTG CAG GAG CCG AGC CAA TTA ATT TCA  912
Lys Glu Glu Lys Lys Lys Ile Asn Gln Gln Glu Ser Thr Asp Ala Ala Val Gln Glu Pro Ser Gln Leu Ile Ser  304
                                  AMP      PKC                                        CK2
TTA GAG GAA GAA AAC CAG CGC AAG GAA TCC TCT AGT TTT AAG ACT GAA GAT GGA AAA AGT ATT TTA TCT GCC TTA  987
Leu Glu Glu Glu Asn Gln Arg Lys Glu Ser Ser Ser Phe Lys Thr Glu Asp Gly Lys Ser Ile Leu Ser Ala Leu  329

GAC AAA GGC TCT ACA CAT ACT GCA TGC TCA GGA CCC ATA GAT GAA CTA TTA GAC ATG AAA TCT GAG GAA GGT GCT 1062
Asp Lys Gly Ser Thr His Thr Ala Cys Ser Gly Pro Ile Asp Glu Leu Leu Asp Met Lys Ser Glu Glu Gly Ala  354

TGC CTG GGA CCA GTG GCA GGG ACC CCG GAA CCT GAA GGT GCT GAC AAA GAT GAC CTG CTG CTG TTG AGT GAG ATC 1137
Cys Leu Gly Pro Val Ala Gly Thr Pro Glu Pro Glu Gly Ala Asp Lys Asp Asp Leu Leu Leu Leu Ser Glu Ile  379
    *           CK2
TTC AAT GCT TCC TCC TTG GAA GAG GGC GAG TTC AGC AAA GAG TGG GCC GCT GTG TTT GGA GAC GGC CAA GTG AAG 1212
Phe Asn Ala Ser Ser Leu Glu Glu Gly Glu Phe Ser Lys Glu Trp Ala Ala Val Phe Gly Asp Gly Gln Val Lys  404

GAG CCA GTG CCC ACT ATG GCC CTG GGA GAG CCA GAC CCC AAG GCC CAG ACA GGC TCA GGT TTC CTT CCT TCG CAG 1287
Glu Pro Val Pro Thr Met Ala Leu Gly Glu Pro Asp Pro Lys Ala Gln Thr Gly Ser Gly Phe Leu Pro Ser Gln  429
                                          CK2
CTT TTA GAC CAA AAT ATG AAA GAC TTA CAG GCC TCG CTA CAA GAA CCT GCT AAG GCT GCC TCA GAC CTG ACT GCC 1362
Leu Leu Asp Gln Asn Met Lys Asp Leu Gln Ala Ser Leu Gln Glu Pro Ala Lys Ala Ala Ser Asp Leu Thr Ala  454
                                      CK2                                  PKC
TGG TTC AGC CTC TTC GCT GAC CTC GAC CCA CTC TCA AAT CCT GAT GCT GTT GGG AAA ACC GAT AAA GAA CAC GAA 1437
Trp Phe Ser Leu Phe Ala Asp Leu Asp Pro Leu Ser Asn Pro Asp Ala Val Gly Lys Thr Asp Lys Glu His Glu  479

TTG CTC AAT GCA TGA ATCTGTACCCTTCGGAGGGCACTCACATGCCGCCCCCAGCAGCTCCCCTGGGGGCTAGCAGAAGTATAAAGTGATCAGT 1531
Leu Leu Asn Ala END                                                                                 483

ATGCTGTTTTAATAATTATGTGCCATTTTAATAAAATGAAAGGGTCAACGGCCCTGTTAAAAAAAAAAAAAAAAAAA                    1607
```

b

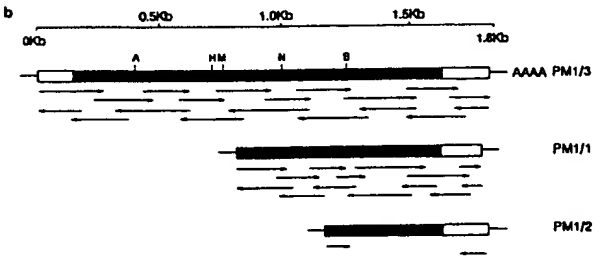

Figure 1. (*a*) Complete nucleotide and deduced amino acid sequence of the ICA69 molecule. Underlined are the first upstream in frame stop codon (*TAA*) at nucleotide −75 and the polyadenylation signal 29 bp upstream of the poly(A) tail. Homologous subunits with BSA are in boxes. A potential N-linked glycosylation site is indicated by an asterisk. Potential phosphorylation sites are as follows: PKC (protein kinase C), CK2 (casein kinase II), and AMP (cAMP/cGMP-dependent kinase). A potential amidation site is indicated as AMD. (*b*) Strategy for sequencing cDNA encoding ICA69 polypeptide and partial restriction map. Sequencing was performed with synthetic oligonucleotide primers, and the direction of sequencing is indicated by arrows. Restriction sites are: A, AccII; B, BglII; H, HgiAI; M, MaeII; and N, NdeI. The poly(A) tail (*AAAA*) was found in the PM1/3 clone. The coding region is indicated by solid bars and 5′ and 3′ untranslated regions are represented by empty bars. These sequence data are available from GenBank under accession number L01100.

The sections were then counterstained with Mayer's hematoxylin. Coverslips were mounted with an aqueous mounting medium without alcohol (Glicergel; Dako Corp.).

Mapping of the mouse homologue of Ica-1. Presence of a homologous locus in the mouse genome (*Ica-1*) was established by analysis of Southern blots of kidney DNA from the NOD (nonobese diabetic) mouse digested with a variety of restriction endonucleases and probed with the PM1/1 cDNA insert according to the procedure described in detail elsewhere (56). An XbaI restriction fragment length variation (RFLV) distinguishing the *Ica-1* locus in the diabetes-susceptible NOD/Lt (~ 8 kb fragment) from the related, but diabetes-resistant NON/Lt strain (~ 11 kb fragment), was used both to assign a chromosomal location and to assess whether a gene conferring susceptibility to IDDM was closely linked to the NOD/Lt allele of *Ica-1*. Segregation of this *Ica-1* RFLV was studied in a panel of kidney DNAs prepared from 19 first backcross diabetic mice from an NOD/Lt × NON/Lt outcross previously typed for other DNA markers (57), plus kidney DNAs from 40 diabetic F2 mice produced in an outcross between NOD/Lt and a diabetes-resistant NON/Lt stock congenic for the diabetogenic $H\text{-}2^{g7}$ haplotype of NOD (NON.NOD-H-2^{g7}) (58). A HindIII RFLV distinguished NOD/Lt (~ 8.5 kb fragment) from both NON/Lt and NON-NOD-H-2^{g7} (~ 7.8 kb fragment). Comparison of the *Ica-1* segregation pattern with previously typed markers indicated that this locus was linked to the *Met* protooncogene on proximal chromosome 6. To confirm this putative linkage, segregation of *D6Rck2*, *D6Mit1*, and *D6Mit16* was assessed by PCR using the oligonucleotide primer sequences described by Dietrich et al. (59). The recombination frequencies reported represent a weighted average using the information function (60).

Statistical analysis. Differences between groups of relatives and controls were analyzed by Wilcoxon rank sum test.

Results

Isolation of cDNA clones encoding the ICA69 molecule. A human islet λgt11 expression library was immunoscreened with a pool of sera from three prediabetic relatives of IDDM patients, which contained a high titer of cytoplasmic islet cell antibodies. Approximately 0.4×10^6 plaques were screened and a single, consistently positive 0.95 kb clone, designated PM1/1, was identified. Fusion protein from the purified clone induced by IPTG, reacted with three out of six ICA positive prediabetic subjects' sera (individually tested at 1:500 dilutions of the sera), whereas no reaction was obtained with 10 control individual sera. A labeled cDNA probe derived from the PM1/1 clone was used to screen both a human λgt11 islet library and a human insulinoma λgt11 library to obtain the full-length cDNA. Screening ~ 6.5×10^4 pfu, two additional hybridizing and overlapping clones were identified from the human islet λgt11 expression library, both of which retained specificity after secondary and tertiary screening to 100% purity. DNA sequence analysis (see below) confirmed that the clones contained fragments of the same gene.

DNA sequence. After PCR amplification and subcloning into pBluescript II vector, partial sequence indicates that the smallest overlapping clone (PM1/2), whose size is 0.6 kb, reveals sequence totally contained within the original sequenced PM1/1 insert (Fig. 1 *B*). The results of sequencing both cDNA strands of the longest clone (PM1/3), whose size is 1.78 kb, indicates complete identity in the region of the molecule overlapping with the two clones and sequence not contained within the previous clones.

Analysis of the nucleotide sequence 1,785 bp cDNA reveals a 1,449-bp open reading frame coding for 483 amino acids and ending in a poly(A) tail 29 bases downstream of the canonical polyadenylation signal (AATAAA). Translation of the ICA69 message putatively initiates from the first in frame ATG according to the criteria defined by Kozak (61). Upstream from the first ATG, there is an in frame stop codon (TAA) at −75 bp (Fig. 1 *A*). The predicted open reading frame from the deduced ATG start codon, codes for a protein with an estimated linear relative molecular mass of 54,600, which contains one potential N-linked glycosylation site.

Using computer programs to search databases of known nucleic acid or amino acid sequences, no significant similarities were found except for minimal homology with BSA, implying that our sequence was new and unique. Two short regions of bovine but not human serum albumin precursor appear to have similarities with the ICA69 molecule (Fig. 2).

A hydrophobicity plot generated from the ICA69 inferred amino acid sequence reveals a number of slightly hydrophobic regions, alternating with several very hydrophilic segments, which suggests that the molecule does not contain any membrane spanning domain, according to the criteria defined by both Kyte and Doolittle (27, 28) and Klein et al. (29). The segments of hydrophobicity appear not to be long enough to be potential transmembrane-spanning regions. The molecule is predominantly hydrophilic, with 27% of its amino acid residues positively or negatively charged.

Analysis of ICA69 transcripts in normal and tumor cells. The cDNA derived from two clones (PM1/1, PM1/3) was used to probe for transcripts in human and animal tissues and in several cell lines by Northern analysis (Figs. 3 and 4). Probes consisting of 0.95 kb (PM1/1) and 1.78 kb (PM1/3) hybridized with a 2-kb mRNA band in islet-derived cell lines, and in some tissues, with a 2.7-kb band. Fig. 3 shows a Northern blot of ICA69 transcripts in human tissues. A 2-kb poly(A^+) RNA band was detected in abundant amounts in both human pancreas and heart, and then in brain, and in small amounts in lung, liver and kidney, but not in placenta and skeletal muscle. In brain and heart, an additional 2.7-kb band is visible. A 2-kb poly(A^+) RNA band was also detected in human thyroid, but not in ovary and spleen (not shown). The β-actin control probe hybridized with a 2-kb band in all tissues with different intensity, and with a smaller band (1.6 kb) in both heart and

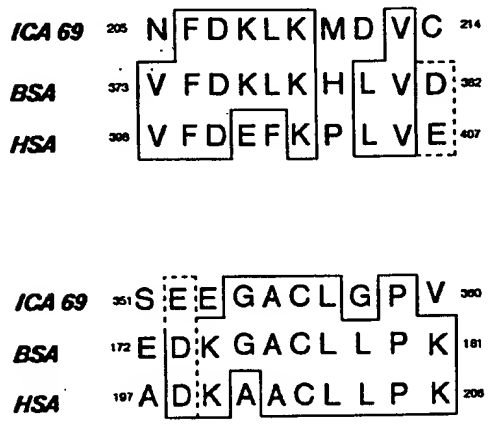

Figure 2. Regions of similarities between ICA69 molecule, BSA, and human serum albumin precursor (*HSA*). Solid line encloses identical amino acid residues. Dashed line encloses amino acid residues with similar charge. Numbers correspond to the amino acid residue numbers.

Figure 3. Northern blot analysis of poly(A$^+$) RNA from different human tissues hybridizing with the 0.95-kb cDNA insert of the PM 1/1 clone. The poly(A$^+$) RNA was obtained from Clontech. 2 μg of pure poly(A$^+$) RNA from each tissue was applied and resolved on denaturating gel as described under Methods. Lane *1*, human heart; lane *2*, human brain; lane *3*, human placenta; lane *4*, human liver; lane *5*, human lung; lane *6*, human skeletal muscle; lane *7*, human kidney; and lane *8*, human pancreas. The same blot was rehybridized with a human β-actin cDNA control probe to show that the mRNA was not degraded. Hybridization and washing were performed with identical conditions in the two different experiments. The blot was exposed for 4 h (β-actin cDNA probe) and 24 h (PM1/1 cDNA probe) at −80°C with intensifying screen.

skeletal muscle. This is because β-actin is not expressed in equal amount in all tissues and because there are two forms of β-actin mRNA in both heart and skeletal muscle (2 and 1.6 kb) (40). The labeled cDNA PM1/1 insert hybridizes with a 2-kb mRNA band in total RNA from rat pancreas, brain, and cerebellum and kidney (in the last three tissues, also with a 5-kb band). In contrast, no ICA69 transcripts were detectable in rat spleen, thymus, bowel, lymph nodes, and salivary gland (not shown). The heterogeneity of mRNA size among tissues may be caused by an alternative splicing of the *ICA1* gene. As shown in Fig. 4, the 2-kb *ICA1* transcript was detected in total RNA from human insulinoma and from a variety of endocrine cell lines, such as a human islet carcinoid cell line (BON-1), a hamster insulin-producing cell line (HIT), and three rodent islet cell lines, namely the rat RIN 1046-38 insulinoma cell line, the mouse βTC-1 (producing primarily insulin, but also some glucagon, and which shows a transcript after longer exposure than shown in Fig. 4), and the mouse αTC-6 (glucagon-producing clonal line). No *ICA1* transcripts were detected in total RNA from three human nonislet cell lines, namely HepG2-hepatoma, HeLa-cells, and JEG-choriocarcinoma (Fig. 4).

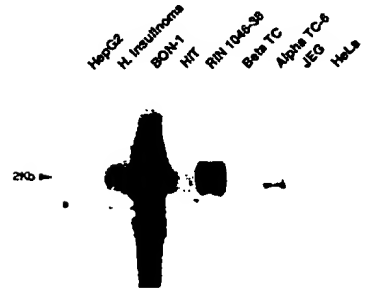

Figure 4. Northern blot analysis of ICA69 expression in human insulinoma, and rat, hamster, and mouse transformed cell lines. A 2-kb mRNA is detected in total RNA from human (*H*) insulinoma, a human islet carcinoid cell line (*BON-1*), a hamster insulin-producing cell line (*HIT*), RIN 1046-38, and the mouse islet lines βTC-1 (which is visible after longer exposure), and αTC-6 (a clonal line producing glucagon). No detectable mRNA was found in total RNA from three human nonislet cell lines: HepG2-hepatoma, HeLa-fibroblast, and JEG-choriocarcinoma. Autoradiograph exposure time was 2–7 d.

Immunoblotting. Western blots of cell line extracts (RIN 1046-38, BON-1) and brain tissue homogenate revealed a specific band of 69 kD after incubation with rabbit antibodies raised to the COOH terminus of ICA69 and an internal polypeptide. Fig. 5 illustrates that rabbit antiserum (rabbit number 1) raised against the COOH terminus of the molecule specifically reacted with a protein of 69 kD in RIN 1046-38 and BON-1 (visible after longer exposure than shown in Fig. 5) total cell homogenate, but not with HeLa cell line homogenate. The specific 69-kD band disappears after absorption with the polypeptide against which specific antibodies were produced. The control serum from the same rabbit before the polypeptide immunization does not show any 69-kD reactivity. The same specific 69-kD reactivity was also detectable in rat brain total homogenate (not shown), and also using hyperimmune sera generated to an internal polypeptide as well as antiserum produced against the whole ICA69 molecule (see Methods). Since the deduced amino acid sequence of ICA69 is 483 residues with an estimated relative molecular mass of 54,600, the difference between the Western blot size of the protein fractionated in the SDS-PAGE and the estimated size based on the deduced amino acid sequence is likely caused by an aberrant migration of the RIN and the brain tissue proteins in SDS-PAGE as a result of detergent solubilization, as previously observed for a brain protein of approximately the same sequence deduced molecular mass and a similarly discrepant migration on SDS-PAGE (62, 63).

Reactivity of recombinant ICA69 with serum of first degree relatives of IDDM patients on Western blotting. To determine whether sera from prediabetic subjects reacted with the recombinant ICA69 fusion protein, and then with the purified ICA69 recombinant molecule, further testing of Western blots was

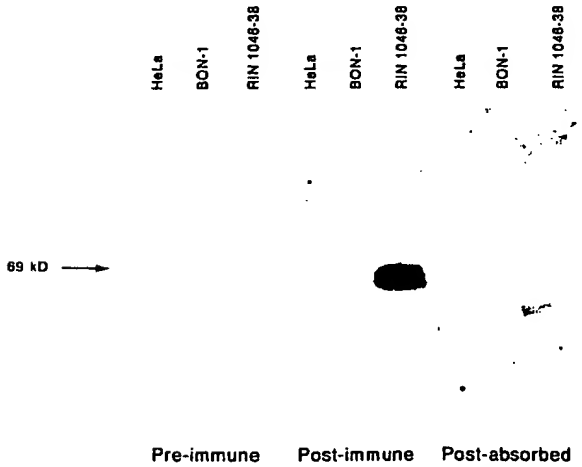

Figure 5. Rabbit antiserum raised against a COOH-terminal ICA69 peptide sequence specifically reacted with a protein of 69 kD in RIN 1046-38 and BON-1 (visible after longer exposure) cell total homogenate but not with homogenate from HeLa cells. The specific 69-kD band disappears after absorption with the polypeptide against which specific antibodies were produced. The serum from the same rabbit (rabbit number 1) before the polypeptide immunization does not react with the 69-kD band.

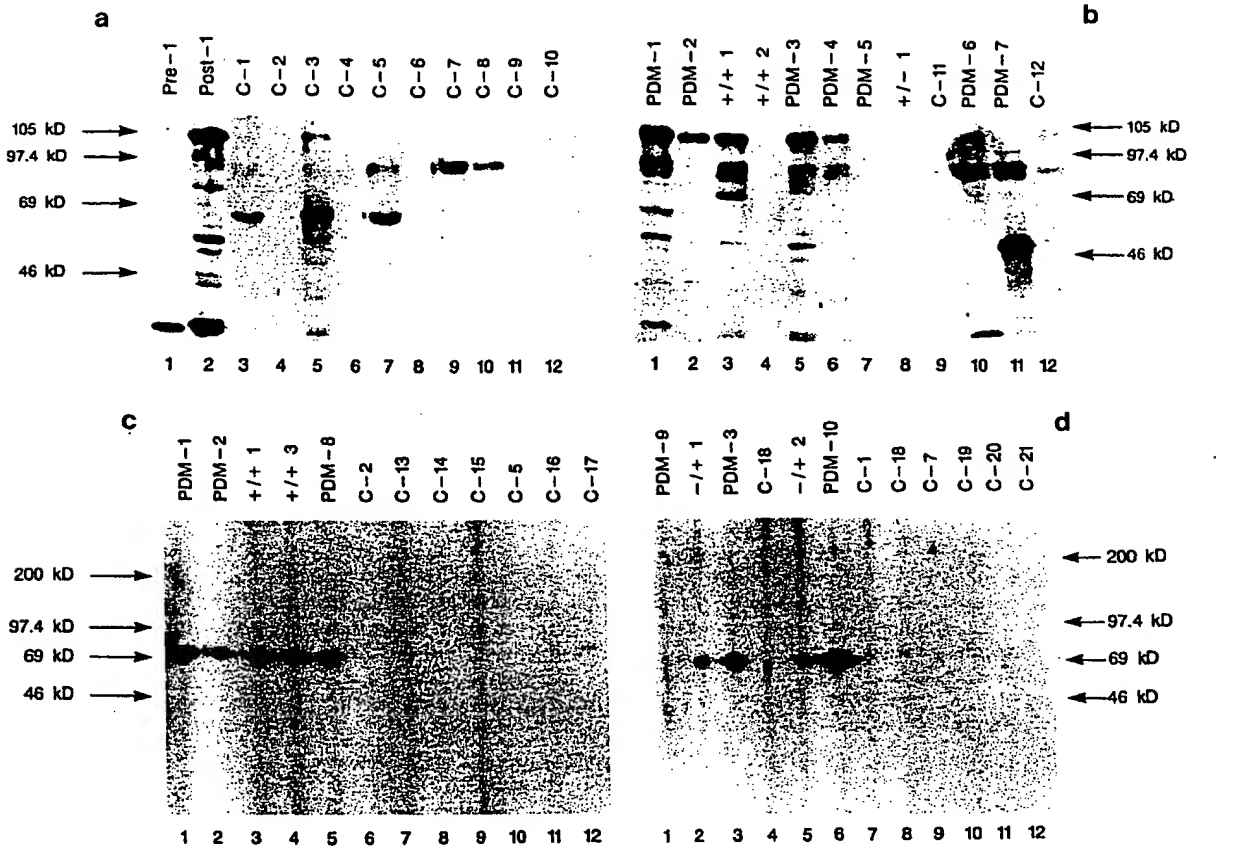

Figure 6. Anti-ICA69 sera from relatives of IDDM patients recognize a maltose binding protein-ICA69 fusion protein (*a* and *b*) and affinity-purified recombinant ICA69 without fusion protein (*c* and *d*) on Western blots. Fluorograms of 10% SDS-PAGE showing reactivity of normal control (C), prediabetic relatives' sera (PDM) from preclinical IDDM subjects (at dilution 1:100) and reactivity of serum samples from autoantibody positive relatives (citoplasmic islet cell antibody/insulin autoantibody +/+, +/−) who have not yet developed diabetes. Bands at ~ 105 kD (*arrows*) represent the PM1/3 clone fusion protein as indicated by reactivity with rabbit-anti ICA69 peptide antibody. The ~ 105 kD bands correspond to the SDS-PAGE migration of the whole fusion protein. Lanes *1–2* (*a*), samples from the same rabbit (rabbit number 1) before (*Pre-1*) and after (*Post-1*) the immunization with the deduced COOH terminus polypeptide of ICA69 (see Methods). Lanes *3–12*, serum samples from 10 healthy individuals. In *b*, sera from seven prediabetics (PDM-1 to 7), from two cytoplasmic islet cell antibody+/insulin autoantibody+ relatives who have not developed diabetes (+/+), from one cytoplasmic islet cell antibody+/insulin autoantibody negative (+/−) and two additional human control sera (C-11, C-12). Immunoblots showing reactivity of preclinical IDDM relatives cytoplasmic islet cell antibody–positive serum samples (PDM) with Ni-NTA-agarose purified recombinant $(His)_6$-ICA69 (*c* and *d*). The purified ICA69 was separated by a 10% SDS-PAGE, and probed with sera from relatives of IDDM patients, and from controls (at 1:100 dilution). Lanes *1*, *2*, and *5* (*c*) and lanes *3* and *6* (*d*) show reactivity of sera from relatives of IDDM patients followed to the overt disease (PDM) with the 69-kD band. Cytoplasmic islet cell antibody/insulin autoantibodies (+/+ and −/+), serum samples from relatives of IDDM patients that have not developed the disease, show also reactivity with ICA69. Note the absence of detectable reactivity with control sera (lanes *6–12* in *c*; lanes *4* and *7–12* in *d*). All the sera from both prediabetics and controls used in the preliminary MBP/PM1/3 clone fusion protein Western blot assay gave consistent results using the affinity-purified recombinant ICA69 as source of antigen for performing Western blots (some of the same serum samples, used in the immunoblots in *a* and *b*, are indicated with the same label in the two sets of immunoblots [Fig. 6, *a*, *b*, *c* and *d*]). Rabbit hyperimmune sera produced against the whole ICA69 and the COOH terminus of the molecule specifically reacted also with the Ni-NTA-agarose purified $(His)_6$-ICA69 (not shown). Positions of molecular mass markers ($M_r \times 10^{-3}$), and ~ 105 kD bands are indicated at right and left edges. The gels were exposed for 6–12 h.

performed. We first assessed whether antiserum raised against the COOH terminus and the whole ICA69 molecule, as well as the three sera from prediabetics previously reacting with the λgt11 IPTG-induced PM1/1 insert, could react on a Western blot with the PM1/3 clone expressed as a fusion protein with maltose binding protein. The rabbit hyperimmune serum and 6 out of 10 sera from relatives with IDDM specifically reacted with a ~ 105 kD band (Fig. 6, *a* and *b*) which corresponds to the SDS-PAGE migration of the whole fusion protein, whereas none of the 12 control sera reacted significantly (quantitating the sera reactivity to the ~ 105 kD band by scanning densitometry).

Sera from first degree relatives from patients with insulin-dependent diabetes mellitus demonstrated specific binding to the affinity purified recombinant ICA69 on Western blotting (Fig. 6, *c* and *d*, and Fig. 7). Serum samples from 23 relatives of IDDM patients who were initially found to be ICA positive and then followed to the clinical onset of the disease (*Pre-DM*; Fig. 7), 70 healthy volunteers, serum samples from 13 ICA+/IAA+ (cytoplasmic islet cell antibody+/insulin autoanti-

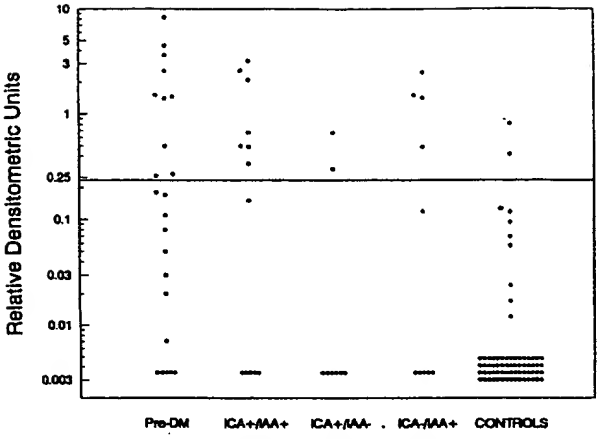

Figure 7. Quantitative comparison of serum binding to recombinant affinity-purified ICA69. Results of Western blots for individual serum samples (dilution 1:100) assayed against purified islet cell autoantigen 69 kD (ICA69) are shown. Levels of antibody to ICA69 in Pre-DM (preclinical IDDM relatives followed up to the overt disease [n = 23]); in relatives that have not developed diabetes, but with evidence of humoral antiislet autoimmunity, namely (cytoplasmic islet cell antibody/antiinsulin autoantibody) ICA+/IAA+ (n = 13), ICA+/IAA− (n = 8), and ICA−/IAA+ (n = 10); and in normal control subjects (n = 70). The horizontal line represents the value 2 SD above the pooled mean control values. Anti-ICA69 antibody levels are expressed as relative densitometric units.

body+), 8 ICA+/IAA−, and 10 ICA−/IAA+ who have not developed type I diabetes to date were assayed to determine their reactivity to highly purified ICA69. Most serum samples from the control group reacted minimally with the purified ICA69 in this assay format. When significant antigen binding was defined as an optical density of > 2 SD above the mean values for the control group (Fig. 7), serum from 10 of the 23 Pre-DM group, exceeded 2 SD of normal binding to ICA69 (43%), as well as serum samples from 7 of the 13 ICA+/IAA+ (54%), from 2 of the 8 ICA+/IAA− (25%), and from 4 of the 10 ICA−/IAA+ (40%). It is of interest that in the ICA+/IAA− group all the serum samples from relatives of IDDM patients that are considered negative, detected by our Western blot assay format, are restricted ICA, who rarely progress to the overt IDDM.

ICA69 islet immunohystochemistry. Staining of formalin-fixed sections of rat pancreas with antibodies raised to the human recombinant ICA69 revealed selective β cell reactivity (Fig. 8). In islets double immuno-enzymatically labeled with a polyclonal antibody to ICA69 and with mAbs to glucagon or somatostatin, antibodies to ICA69 reacted with the β cell core (Fig. 8 *a*) but not with either glucagon or somatostatin containing cells (Fig. 8, *b* and *c*).

Chromosome localization of Ica-1, the mouse homologue, to chromosome 6. Linkage data summarized in Fig. 9 indicate that *Ica-1* (*Ica-1* is the mouse gene symbol for the gene coding for ICA69; ICA1 is the human gene symbol for the gene coding for ICA69) is linked to the *Met* protooncogene (located 6 cM proximal on chromosome 6). Linkage to two other proximal *Met*-linked markers (*D6Mit1*, *D6Rck2*, 5 cM proximal) was demonstrated. The weighted average of the interval between *Met* and *Ica-1* was estimated to be 6.23±2.5 cM based on 1/17 recombinant in the backcross panel and 5/40 obligate recombinant in the F2 panel (total of 97 informative meioses). The proximal *D6Mit1* and *D6Rck2* markers were separable by the finding of three recombinations in 101 informative meioses between *Ica-1* and *D6Mit1* versus six recombinations in 94 informative meioses between *Ica-1* and *D6Rck2*. The weighted average of the interval between *Met* and *D6Mit1* was estimated to be 3.05±2.29 cM and the interval between *D6Mit1* and *Ica-1* to be 3.85±2.20 cM. The finding of 22 recombinations in 74 informative meiosis between *Ica-1* and the more distal marker *D6Mit16* confirms that *Ica-1* is proximal to *Met*. Collectively, these data would suggest a gene order of centromere-*Ica1-D6Mit1-D6Rck2-Met-D6Mit16* as indicated in Fig. 9. Though a polymorphism between NOD and NON exists for the *Ica-1* gene, and segregation of the NOD-derived *Ica-1* allele was not significantly associated with diabetes in either the backcross or the F2 generation ($P > 0.05$ by chi square analysis), indicating that it was not closely linked to a locus at the proximal end of chromosome 6 conferring susceptibility to insulin dependent diabetes (*Idd* gene) of NOD mice.

In the human, *MET* has been mapped to chromosome 7q21-7q31 (65). The localization of the mouse *Ica-1* gene within 6 cM of the *Met* protooncogene on chromosome 6, suggests that the human *ICA1* gene may be found close to the *MET* protooncogene protein-tyrosine kinase locus in a conserved region around 7q31.

Discussion

Recent findings have indicated that the range of autoantigens related to type I diabetes is more diverse than was originally thought. Sera from IDDM patients, as well as from stiff-man syndrome patients, appear to recognize one or both forms of the neuroendocrine-associated enzyme GAD (6, 66), namely GAD 65 (67), and GAD 67 (68), and one portion of the antibody response to islet cells, termed "restricted ICA," has been reported to recognize GAD (69, 70). In the present study, we have cloned, sequenced, and characterized a novel 69-kD diabetes-related autoantigen.

In an attempt to identify molecular targets for antiislet autoimmunity in IDDM, we have used sera from preclinical IDDM subjects as probe to isolate cDNA clones from a human islet λgt11 expression library. We have obtained a cDNA of a novel protein that codes for a full-length amino acid sequence 54.6 kD with an apparent mobility of 69 kD on SDS-PAGE. The detection of mRNA in neural tissues studied such as brain, the presence of ICA69 transcripts in islet-derived cell lines, namely, RIN 1046-38, BON-1, HIT, βTC-1, αTC-6, and in human insulinoma tissue, in contrast to nonneuroendocrine cell lines such as HeLa cells, JEG-choriocarcinoma, and HepG2-hepatoma likely reflect the sharing of many molecules between islets and neurons. A low level of ICA69 mRNA was also found in human lung, liver, and kidney. It is of interest that a high level of ICA69 mRNA is present in heart, whereas mRNA is undetectable in skeletal muscle and this could be related to the presence of selective cells expressing high levels of this molecule. Islets and neuronal cells both contain secretory granules and microvesicular bodies; for instance, GAD has been localized to microvesicular structures in both pancreatic β cells, as well as in synaptic nerve microvesicular structures (71). Many of the molecules of both of these shared structures appear to be prominent targets of the autoimmunity related to

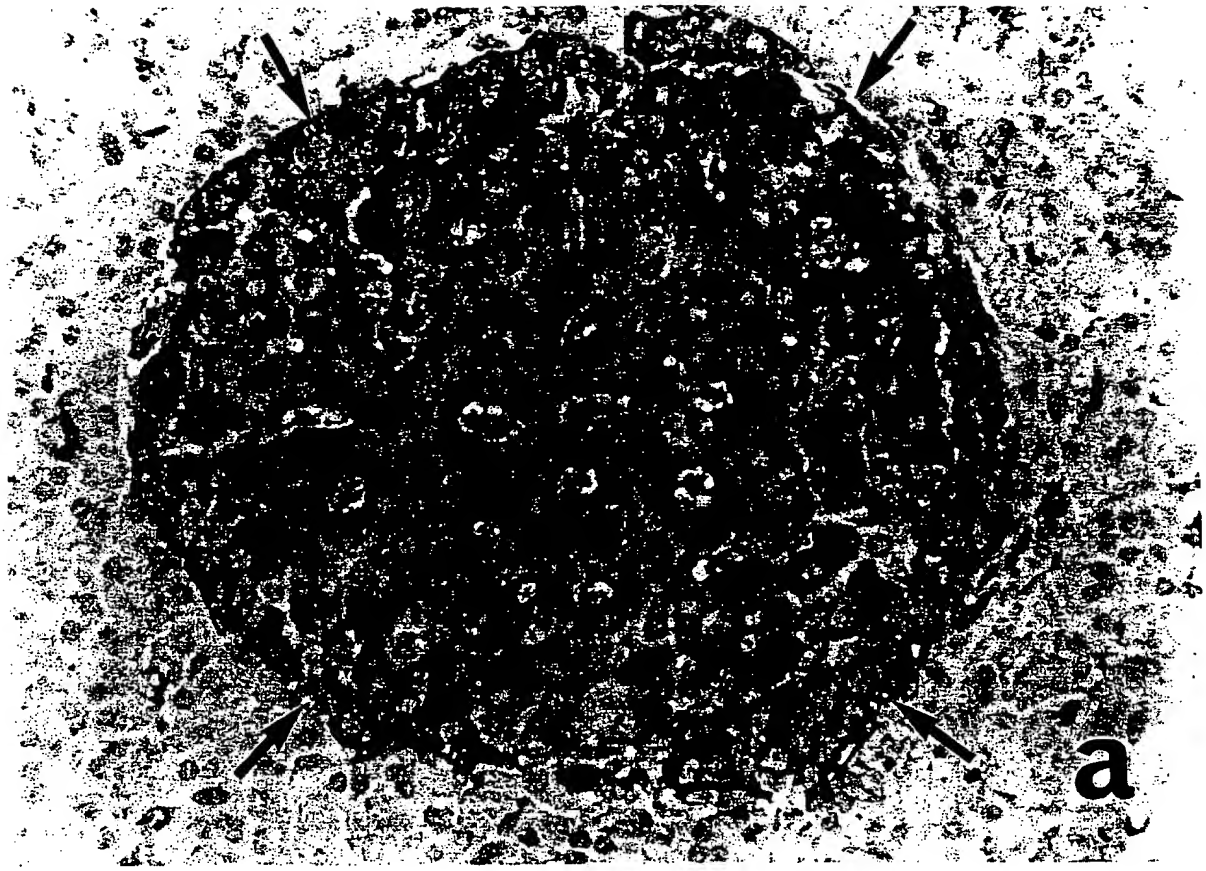

Figure 8. Microphotographs of peroxidase and alkaline phosphatase double immunoenzymatic rat islets labeling using anti-ICA69, antiinsulin, antiglucagon, and antisomatostatin antibodies. (*a*) The islet was double-labeled for ICA69 and glucagon. Anti-ICA69 antiserum reacted with the β cell core of the islet (*brown*), whereas the glucagon containing cells are stained with an antiglucagon mAb (*red, arrows*) and are not reactive with ICA69 (×350). (*b*) The islet was double-labeled for ICA69 and somatostatin. Anti-ICA69 antiserum (*brown*) reacted with the β cell core, whereas the somatostatin containing cells reacted with an antisomatostatin mAb (*red*); additional peripheral cells (*arrows*), negative for both ICA69 and somatostatin, are apparently non-β cells (×315). (*c*) An islet was double-labeled with mAb anti-insulin (*brown*) and antiglucagon (*red, arrows*), showing a pattern identical to that of (*a*) (anti-ICA69 and antiglucagon) (×350).

type I diabetes. The fact that ICA69 mRNA is detected mostly in endocrine cell lines of islet cell origin, and that ICA69 mRNA is also detected in brain, thyroid and heart, but not skeletal muscle, suggests that ICA69 may be in fact related to the neuroendocrine system. A 2-kb mRNA band is visible in total RNA a glucagon producing cell line, namely αTC-6, whereas no staining is visible on normal rat glucagon containing cells detecting by immunohystochemistry.

The putative polypeptide encoded by the longest open reading frame of ICA69 clones has a molecular mass of 54,600 D. On Western blots, immunoreactive ICA69 has a molecular mass of 69 kD suggesting aberrant migration on SDS-PAGE. A molecular mass discrepancy between that calculated from the deduced amino acid sequence and that measured by SDS-PAGE, has been reported in the cloning of a number of proteins (62, 63, 72–74). These proteins have highly charged regions that appear to be related to retarded SDS-PAGE gel migration, resulting thus in an overestimation of the true molecular mass. Our protein has several strongly charged regions, such as the segment of the molecule between residues 307 and 320. The fact that cDNA encoding the full length of the molecule produces a 69-kD protein when expressed in bacteria whose molecular mass is higher than the one inferred by the relative molecular mass of the deduced sequence (54.6 kD), supports aberrant gel migration as the likely cause of the relative molecular mass disparity.

Environmental factors are potential triggers of autoimmunity in type I diabetes (13). There is evidence in animal models of IDDM such as BB rats that the elimination of cow milk proteins from the diet significantly reduces the incidence of the clinical onset of diabetes in these animals (75). Sera from patients with type I diabetes as well as BB rats are reported to have high titer of IgG anti–BSA antibodies (but not of antibodies to other milk proteins) or IgG anti–ABBOS (a region of the BSA molecule extending from 152 to 158 amino acid residues) antibodies (13–15). It has been reported that antibodies raised to one short BSA unique peptide region (ABBOS) or serum from a newly diagnosed IDDM child react on a Western blot format

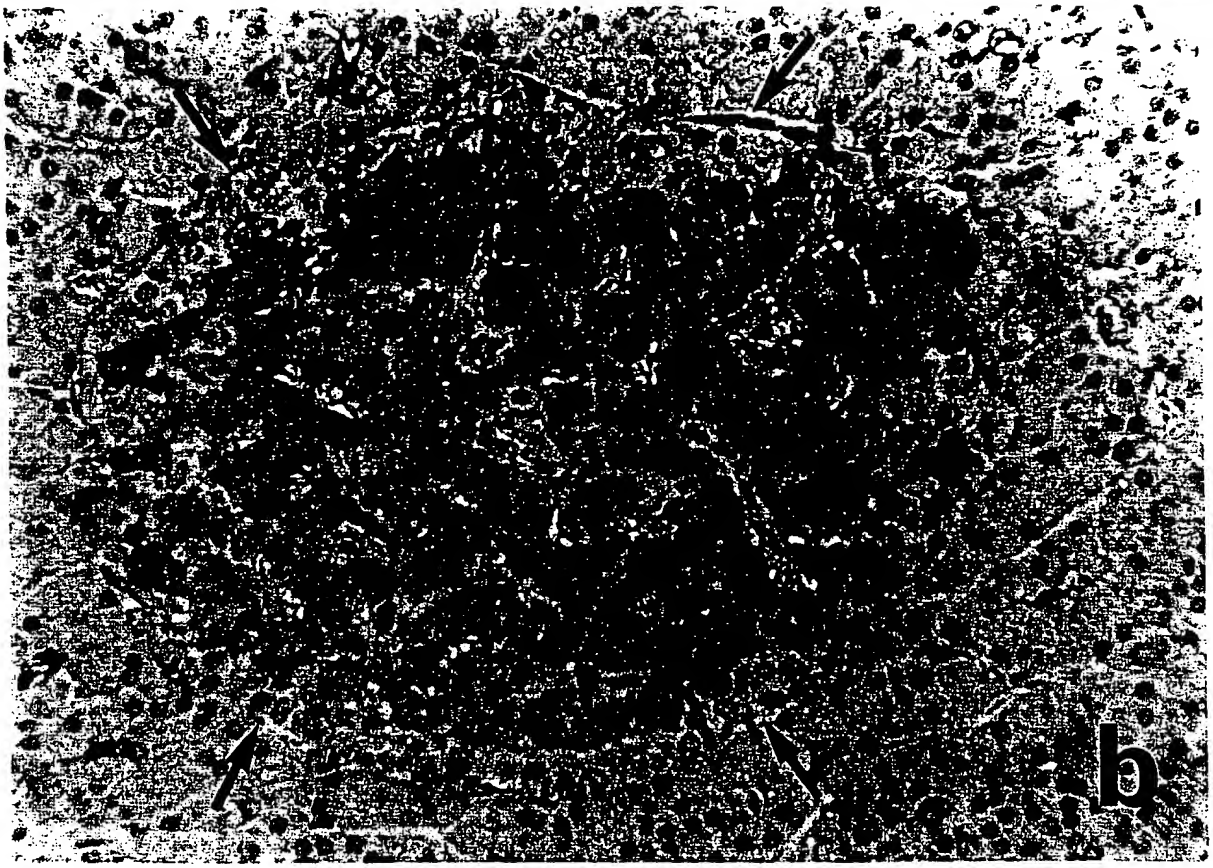

Figure 8 (Continued)

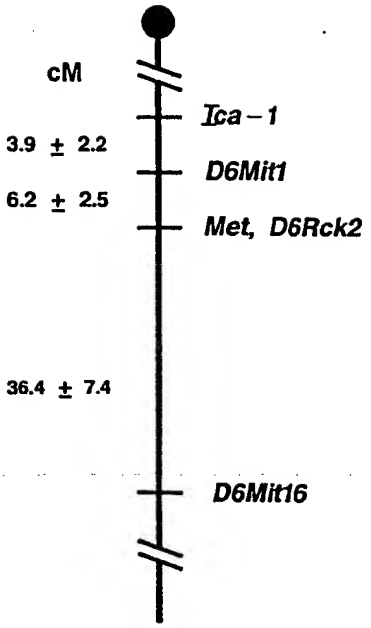

Figure 9. Localization of *Ica-1* on proximal chromosome 6 of the mouse. The recombination frequencies between linked loci are expressed in cM±SEM (shown at the left) and were estimated using a weighted average for backcross and F2 data. Multipoint linkage map constructed using MAPMAKER 1.9 (64) gave maximum likelihood estimates for the best three gene orders as follows: order 1, *Ica-1-D6Mit1-D6Rck2-Met* log likelihood −79.10; order 2, *D6Rck2-Met-Ica-1-D6Mit14* log likelihood −82.85; and order 3, *D6Rck2-Met-D6Mit1-Ica-1* log likelihood −86.88. *Recombination frequency estimated from F2 data only.

with γ-interferon–induced RIN 69-kD protein or with islet proteins with a similar mobility (60–70 kD), respectively (13).

It is of interest that our 69-kD molecule shares two short regions of similarity with bovine serum albumin (not with human serum albumin precursor). These two antigenic determinants perhaps could play a role in the induction of cow milk–induced autoimmunity based upon the hypothesis of pathogenesis related to molecular mimicry, or may be simply a cause of a cross-reactivity with anti-ICA69 antibodies and with anti-BSA antibodies. To prove one of these two hypotheses, further studies are required. We have just learned that a partial peptide sequence available from a p69 BSA-related molecule studied by Dosch and co-workers is identical to amino acids 262 to 325 of ICA69 (H.-M. Dosch, personal communication).

Our study shows that first degree relatives of patients with IDDM who developed the disease carry antibodies reacting with ICA69. Antibodies to ICA69 are detected also in relatives who have not yet developed the disease. Such antibodies are found in 43% of the serum samples from preclinical IDDM relatives assayed so far, and we believe that with the optimization of a more sensitive assay (such as a radioassay or an ELISA), the percentage of reactivity with ICA69 among IDDM relatives will increase.

Detecting by Western blotting, the percentage of anti-ICA69 reactivity among sera from relatives of IDDM patients that developed the disease and in from ICA+/IAA+ group appears to be higher than the ICA+/IAA− group (25%) (Fig. 7), seemingly because all the anti-ICA69 negative sera from ICA+/IAA− relatives assayed thus far, show a β cell–selective ICA pattern (termed "restricted"), that includes recognition of GAD, which is associated with the lack of progression to overt diabetes (69, 70). Therefore, the low percentage of anti-ICA69 positive sera in the ICA+/IAA− group as compared to the other groups appears to be related to the fact that most of the ICA+/IAA− IDDM serum samples from IDDM relatives assayed so far are restricted ICA and rarely progress to the overt IDDM. In light of these observations, we believe that with the combination of different assays for the detection of autoantibodies in IDDM, such as anti-IAA, anti-GAD, anti-ICA69, and in the future against other islet autoantigens, combinatorial algorithms for improving the prediction of type I diabetes will be designed.

The identification, the characterization of the molecular structure and the availability of the ICA69 molecule will help to add this autoantigen to a battery of markers for the prediction of diabetes risk, and will enhance our understanding of islet biochemistry. A family of islet antigen specific therapies are considered for the suppression of insulin-dependent diabetes; e.g., oral tolerance to insulin (76). ICA69 with its β cell expression and autoantigenicity becomes an additional candidate molecule for manipulation of β cell autoimmunity.

Acknowledgments

We are grateful to Dr. Mary Loeken for helpful technical suggestions on the cloning, Dr. Temple Smith for the computer-based sequence analysis, and in particular, Dr. Alan Permutt for provision of the human islet library, Dr. Christopher Newgard for providing the RIN 1046-38 cell line and for valuable discussions, and Dr. Cortney Townsend for providing the BON-1 cell line. Drs. Linda Wicker and Larry Peterson (Merck Research Laboratories, Rahway, NJ) are thanked for providing kidneys from diabetic F2 mice. Drs. Ben Taylor and Don Doolittle (The Jackson Laboratory, Bar Harbor, ME) are thanked for their assistance in establishing mouse genetic map distances. We thank Dr. Filippo Calcinaro and Dr. Francisco G. La Rosa for assisting with the microphotography, and David Stenger for careful review of the manuscript.

Dr. Pietropaolo was the recipient of a Juvenile Diabetes Foundation International postdoctoral fellowship and was supported by a postdoctoral fellowship from the Italian Ministero della Pubblica Istruzione. Dr. Prochazka was the recipient of a Juvenile Diabetes Foundation International postdoctoral fellowship.

Supported by grants from the Greenwall Foundation, the Blum-Kovler Foundation, the Juvenile Diabetes Foundation, the American Diabetes Association, ImmuLogic Pharmaceutical Corporation, the National Institutes of Health (DK 32083, DK 36175, and DK 27722), the Veterans Administration Research Service, and the Italian Ministero della Pubblica Istruzione.

References

1. Eisenbarth, G. S. 1986. Type I diabetes mellitus: a chronic autoimmune disease. *N. Engl. J. Med.* 314:1360–1368.

2. Bottazzo, G. F., S. Genovese, E. Bosi, B. M. Dean, M. R. Christie, and E. Bonifacio. 1991. Novel considerations on the antibody/autoantigen system in type I (insulin-dependent) diabetes mellitus. *Ann. Med.* 23:453–461.

3. Pietropaolo M., and G. S. Eisenbarth. 1992. Prediction of type I diabetes mellitus. *Diabetes Nutr. Metab.* 5(Suppl. 1):105–110.

4. Tan, E. M. 1991. Autoantibodies in pathology and cell biology. *Cell.* 67:841–842.

5. Palmer, J. P., C. M. Asplin, P. Clemons, K. Lyen, O. Tatpati, P. K. Raghu, and T. L. Paquette. 1983. Insulin antibodies in insulin-dependent diabetics before insulin treatment. *Science (Wash. DC).* 222:1337–1339.

6. Baekkeskov, S., H. Aanstoot, S. Christgau, A. Reetz, M. S. Solimena, M. Cascalho, F. Folli, H. Richter-Olsen, and P. De Camilli. 1990. Identification of the 64K autoantigen in insulin dependent diabetes as the GABA-synthesizing enzyme glutamic acid decarboxylase. *Nature (Lond.).* 347:151–156.

7. Castaño, L., E. Russo, L. Zhou, M. A. Lipes, and G. S. Eisenbarth. 1991. Identification and cloning of a granule autoantigen (carboxypeptidase H) associated with type I diabetes. *J. Clin. Endocrinol. & Metab.* 73:1197–1201.

8. Gillard, B. K., J. W. Thomas, L. J. Nell, and D. M. Marcus. 1989. Antibodies against ganglioside GT3 in the sera of patients with type I diabetes mellitus. *J. Immunol. Methods.* 142:3826–3832.

9. Dotta, F., P. G. Colman, D. Lombardi, D. W. Scharp, D. Andreani, G. M. Pontieri, U. Di Mario, L. Lenti, G. S. Eisenbarth, and R. C. Nayak. 1989. Ganglioside expression in human pancreatic islets. *Diabetes.* 38:1478–1483.

10. Rabin, D. U., S. Pleasic, R. Palmer-Crocker, and J. A. Shapiro. 1992. Cloning and expression of IDDM-specific human autoantigens. *Diabetes.* 41:183–186.

11. Roep, B. O., A. A. Kallan, W. L. W. Hazenbos, G. J. Bruining, E. M. Bailyes, S. Arden, J. C. Hutton, and R. R. P. DeVries. 1991. T-cell reactivity to 38 kD insulin-secretory-granule protein in patients with recent-onset type 1 diabetes. *Lancet.* 337:1439–1441.

12. Karounos, D. G., and J. W. Thomas. 1990. Recognition of common islet antigen by autoantibodies from NOD mice and humans with IDDM. *Diabetes.* 39:1085–1090.

13. Martin, J. M., B. Trink, D. Daneman, H.-M. Dosch, and B. Robinson. 1991. Milk proteins in the etiology of insulin-dependent diabetes mellitus (IDDM). *Ann. Med.* 23:447–452.

14. Karjalainen, J., J. M. Martin, M. Knip, J. Ilonen, B. H. Robinson, E. Savilahti, H. K. Akerblom, and H.-M. Dosch. 1992. A bovine albumin peptide as a possible trigger of insulin-dependent diabetes mellitus. *N. Engl. J. Med.* 327:302–307.

15. Karjalainen, J., T. Saukkonen, E. Savilahti, and H.-M. Dosch. 1992. Disease-associated anti-bovine serum albumin antibodies in type 1 (insulin-dependent) diabetes mellitus are detected by particle concentration fluoroimmunoassay and not by enzyme linked immunoassay. *Diabetologia.* 35:985–990.

16. Coppel, R. L., M. E. Gershwin, and A. D. Sturgess. 1989. Cloned autoantigens in the study and diagnosis of autoimmune diseases. *Mol. Biol. Med.* 6:27–34.

17. Dropcho, E. J., Y.-T. Chen, J. B. Posner, and L. J. Old. 1987. Cloning of a brain protein identified by autoantibodies from a patient with a paraneoplastic cerebellar degeneration. *Proc. Natl. Acad. Sci. USA.* 84:4552–4556.

18. Sambrook, J., E. F. Fritsch, and T. Maniatis. 1989. Molecular Cloning: A Laboratory Manual. Cold Spring Harbor Laboratory Press, Cold Spring Harbor, NY.

19. Huynh, T. V., R. A. Young, and R. W. Davis. 1985. *In* Constructing and Screening cDNA libraries λgt10 and λgt11. D. M. Glover, editor. JRL Press, Oxford. 49–78.

20. Young, R. A., and R. W. Davis. 1984. Yeast RNA polymerase II genes: isolation with antibody probes. *Science (Wash. DC).* 222:778–782.

21. Feinberg, A. P., and B. Vogelstein. 1983. A technique for radiolabeling DNA restriction endonuclease fragments to high specific activity. *Anal. Biochem.* 132:6–13.

22. Wallace, R. B., M. J. Johnson, T. Hirose, T. Miyake, E. H. Kawashima, and K. Itakura. 1981. The use of synthetic oligonucleotides as hybridization probes. Hybridization of oligonucleotides of mixed sequence to rabbit β-globin DNA. *Nucleic Acids Res.* 9:879–894.

23. Friedman, K. D., N. L. Rosen, P. J. Newman, and R. R. Montgomery. 1988. Enzymatic amplification of specific cDNA from λgt11 libraries. *Nucleic Acids Res.* 16:8718.

24. Innis, M., D. Gelfand, J. Sninsky, and T. White. 1990. PCR Protocols: a Guide to Methods and Applications. Academic Press, Inc., San Diego, CA 253–258.

25. Sanger, F., S. Nickel, and A. R. Consoln. 1977. DNA sequencing with chain terminating inhibitors. *Proc. Natl. Acad. Sci. USA.* 74:5463–5467.

26. Tabor, S., and C. C. Richardson. 1975. DNA sequence analysis with a modified bacteriophage T7 DNA polymerase. *Proc. Natl. Acad. Sci. USA.* 84:4767–4771.

27. Kyte, J., and R. F. Doolittle. 1982. A simple method for displaying hydrophobic character of a protein. *J. Mol. Biol.* 157:105–132.

28. Doolittle, R. F. 1987. Of URSF and ORFS. A Primer on How to Analyze Derived Amino Acid Sequences. University Sciences Books, Mill Valley, CA.

29. Klein, P., M. Kanehisa, and C. DeLisi. 1985. The detection and classification of membrane-spanning proteins. *Biochim. Biophys. Acta.* 815:468–476.

30. Clark, S. A., B. Burnham, and W. L. Chick. 1990. Modulation of glucose-induced insulin secretion from a rat clonal beta-cell line. *Endocrinology.* 127, 6:2779–2788.

31. Hamaguchi, K., and E. H. Leiter. 1990. Comparison of cytokine effects on mouse pancreatic alpha cell and beta cell lines. Viability, secretory function, and MHC antigen expression. *Diabetes.* 39:415–425.

32. Powers, A. C., S. Efrat, S. Mojsov, D. Spector, J. F. Habener, and D. Hanahan. 1990. Proglucagon processing similar to normal islets in pancreatic alpha-like cell line derived from transgenic mouse tumor. *Diabetes.* 39:406–414.

33. Breant, B., C. Lavergne, and G. Rosselin. 1990. Cell cycle and gene expression in the insulin producing pancreatic cell line βTC-1. *Diabetologia.* 33:586–592.

34. Purrello, F., M. Buscema, M. Vetri, C. Vinci, C. Gatta, F. Forte, A. M. Rabuazzo, and R. Vigneri. 1991. Glucose regulates both glucose transport and the glucose transporter gene expression in a hamster-derived pancreatic beta-cell line (HIT). *Diabetologia.* 21:366–369.

35. Contreras, G., D. F. Summers, J. Maizel, and E. Ehrenfeld. 1973. HeLa cell nucleolar RNA synthesis after poliovirus infection. *Virology.* 53:120–129.

36. Kohler, P. O., W. E. Bridson, J. M. Hammond, B. Weintraub, M. A. Kirschner, and D. M. Van Thiel. 1971. Clonal lines of human choriocarcinoma cells in culture. *Acta Endocrinol.* 153(Suppl.):137–150.

37. Broze, G. J., and J. P. Miletich. 1987. Isolation of the tissue factor inhibitor produced by HepG2 hepatoma cells. *Proc. Natl. Acad. Sci. USA.* 84:1886–1890.

38. Thomas, P. S. 1980. Hybridization of denatured RNA and small DNA fragments transferred to nitrocellulose. *Proc. Natl. Acad. Sci. USA.* 77:5201–5205.

39. Cleveland, D. W., M. A. Lopata, R. J. MacDonald, N. J. Cowan, W. J. Rutter, and M. W. Kirschner. 1980. Number and evolutionary conservation of alpha- and beta-tubulin and cytoplasmic beta- and gamma-actin genes using specific cloned cDNA probes. *Cell.* 20:95–105.

40. Pari, G., K. Jardine, and M. W. McBurney. 1991. Multiple CArG boxes in the human cardiac actine gene promoter required for expression in embryonic cardiac muscle cells developing in vitro from embryonal carcinoma cells. *Mol. Cell. Biol.* 11:4796–4803.

41. Hassouna, N., B. Michot, and J.-P. Bachellerie. 1984. The complete nucleotide sequence of mouse 28 S RNA gene. Implications for the process of size increase of the large subunit rRNA in higher eukaryotes. *Nucleic Acids Res.* 12:3563.

42. Raynal, F., B. Michot, and J.-P. Bachellerie. 1984. Complete nucleotide sequence of mouse 18 S rRNA gene: comparisons with other available homologs. *FEBS (Fed. Eur. Biochem. Soc.) Lett.* 167:263.

43. Van Regenmortel, M. H. V., J. P. Briand, S. Muller, and S. Plaue. 1988. Syntetic polypeptides antigens. *In* Laboratory Techniques in Biochemistry and Molecular Biology. R. H. Burdon and P. H. von Knippenberg, editors. Elsevier Science Publishing Co., Inc., New York.

44. Walter, G. 1986. Production and use of antibodies against synthetic peptides. *J. Immunol. Methods.* 88:149–161.

45. Kurstak, E. 1986. Enzyme Immunodiagnostic. Academic Press, San Diego, CA.

46. Jitsukawa, T., S. Nakajima, I. Sugawara, and H. Watanabe. 1989. Increased coating efficiency of antigens and preservation of original antigenic structure after coating in ELISA. *J. Immunol. Methods.* 116:251–257.

47. Sun, X. J., P. Rothenberg, C. R. Kahn, J. M. Backer, E. Araki, P. A. Wilden, D. A. Cahill, B. J. Goldstein, and M. F. White. 1991. Structure of the insulin receptor substrate IRS-1 defines a unique signal transduction protein. *Nature (Lond.).* 352:73–77.

48. Laemmli, U. K. 1970. Cleavage of structural proteins during the assembly of the head of bacteriophage T4. *Nature (Lond.).* 227:680–685.

49. Towbin, H., T. Staehelin, and J. Gordon. 1979. Electrophoretic transfer of proteins from polyacrylamide gels to nitrocellulose sheets: procedure and some applications. *Proc. Natl. Acad. Sci. USA.* 76:4350.

50. Maina, C. V., P. D. Riggs, A. G. Grandea III, B. E. Slatko, L. S. Moran, J. A. Tagliamonte, L. A. McReynolds, and C. di Guan. 1988. An *Escherichia coli* vector to express and purify foreign proteins by fusion to and separation from maltose-binding protein. *Gene (Amst.).* 74:365–373.

51. di Guan, C., P. Li, P. D. Riggs, and H. Inouye. 1988. Vectors that facilitate the expression and purification of foreign peptides in *Escherichia coli* by fusion to maltose-binding protein. *Gene (Amst.).* 67:21–20.

52. Johnston, T. C., R. B. Thompson, and T. O. Baldman. 1986. Nucleotide sequence of the luxB gene of vibrio harveyi and the complete amino acid sequence of the beta subunit of bacterial luciferase. *J. Biol. Chem.* 261:4805–4811.

53. Aman, E. B., B. Oclis, and K. J. Abel. 1988. Tightly regulated *tac* promoter useful for the expression of unfused and fused proteins in *Escherichia coli*. *Gene (Amst.).* 69:301–315.

54. Mason, D., and Y. R. Sammons. 1978. Alkaline phosphatase and peroxidase for double immunoenzimatic labelling of cellular constituents. *J. Clin. Pathol.* 31:454.

55. Mason, D. Y., B. F. Abdulaziz, and H. Stein. 1983. Double immunoenzimatic labelling. *In* Immunocytochemestry. Practical Application in Pathology and Biology. J. M. Polak and S. Van Noorden, editors. Wright PSG, Boston.

56. Prochazka, M., D. V. Serreze, S. M. Worthen, and E. H. Leiter. 1989. Genetic control of diabetogenesis in NOD/Lt mice: development and analysis of congenic stocks. *Diabetes.* 38:1446–1455.

57. Prochazka, M., E. H. Leiter, D. V. Serreze, and D. L. Coleman. 1987. Three recessive loci required for insulin-dependent diabetes in NOD mice. *Science (Wash. DC).* 237:286–289.

58. Leiter, E. H., and D. V. Serreze 1992. Antigen presenting cells and the immunogenetics of autoimmune diabetes in NOD mice. *Reg. Immunol.* 4:263–273.

59. Dietrich, W., H. Katz, S. Lincoln, H.-S. Shin, J. Friedman, N. Dracopoli, and E. S. Lander. 1992. A genetic map of the mouse suitable for typing intraspecific crosses. *Genetics.* 131:423–447.

60. Green, E. L. 1985. Tables and a computer program for analyzing linkage data. *Mouse News Let.* 73:20–21.

61. Kozak, M. 1987. An analysis of 5'-noncoding sequences from 699 vertebrate messenger RNAs. *Nucleic Acids Res.* 20:8125–8132.

62. Krumar, K. N., N. Tilakaratne, P. S. Johnson, A. E. Allen, and E. K.

Michaelis. 1991. Cloning of cDNA for the glutamate-binding subunit of the NMDA receptor complex. *Nature (Lond.)*. 354:70–73.

63. Krumar, K. N., K. T. Eggman, J. L. Adams, and E. K. Michaelis. 1991. Hydrodynamic proterties of the purified glutamate-binding protein subunit of the *N*-methyl-D-aspartate receptor. *J. Biol. Chem.* 23:14947–14952.

64. Lander, E. S., P. Green, J. Abrahamson, A. Barlow, M. J., Daly, S. E. Daly, and L. Newberg. 1987. MAPMAKER: an interactive computer package for constructing primary genetic linkage maps for experimental and natural populations. *Genomics*. 1:174–181.

65. Dean, M., M. Park, M. M. LeBeau, T. S. Robins, M. O. Diaz, J. D. Rowley, D. G. Blair, and G. F. Vande Woude. 1985. The human met oncogene is related to the tyrosine kinase oncogenes. *Nature (Lond.)*. 318:385–388.

66. Thivolet, C. H., M. Tappaz, A. Durand, J. Petersen, A. Stefanutti, P. Chaelain, B. Bialettes, W. Scherbaum, and J. Orgiazzi. 1992. Glutamic acid decarboxylase (GAD) autoantibodies are additional predictive markers of type 1 (insulin-dependent) diabetes mellitus in high risk individuals. *Diabetologia*. 35:570–576.

67. Hagopian W. A., B. Michelsen, A. E. Karlsen, F. Larsen, A. Moody, C. E. Grubin, R. Rowe, J. Petersen, R. McEvoy, and Å. Lernmark. 1993. Autoantibodies in IDDM primarily recognize the 65,000-M_r rather than 67,000-M_r isoform of glutamic acid decarboxylase. *Diabetes*. 42:631–636.

68. Kaufman, D. L., M. G. Erlander, M. Clare-Salzer, M. A. Atkinson, N. K. Maclaren, and A. J. Tobin. 1992. Autoimmunity to two forms of glutamate decarboxylase in insulin-dependent diabetes mellitus. *J. Clin. Invest.* 89:283–292.

69. Gianani, R., A. Pugliese, S. Bonner-Weir, A. J. Shiffrin, J. S. Soeldner, H. Erlich, Z. L. Awdeh, C., A. Alper, R., A. Jackson, and G. S. Eisenbarth. 1992. Prognostically significant heterogeneity of cytoplasmic islet cell antibodies in relatives of patients with type I diabetes. *Diabetes*. 41:347–353.

70. Genovese, S., E. Bonifacio, J. M. McNally, B. M. Dean, R. Wagner, E. Bosi, E. A. M. Gale, and G. F. Bottazzo. 1992. Distinct cytoplasmic islet cell antibodies with different risks for type I (insulin-dependent) diabetes mellitus. *Diabetologia*. 35:385–388.

71. Christgau, S., H. J. Aanstoot, H. Schierbeck, K. Begley, T. Tullin, K. Hejnaes, and S. Baekkeskov. 1992. Membrane anchoring of the autoantigen GAD65 to microvesicles in pancreatic beta-cells by palmitoylation in the NH_2-terminal domain. *J. Cell Biol.* 118(2):309–320.

72. McCauliffe, D. P., F. A. Lux, T.-S. Lieu, I. Sanz, J. Hanke, M. M. Newkirk, L. J. Bachinski, Y. Itoh, M. J. Siciliano, M. Reichlin, R. D. Sontheimer, and J. D. Capra. 1990. Molecular cloning, expression, and chromosome 19 localization of a human Ro/SS-A autoantigen. *J. Clin. Invest.* 85:1379–1391.

73. Benedum, U. M., D. S. Baeuerle, D. S. Konecki, R. Frank, J. Powell, J. Mallet, and W. B. Huttner. 1986. The primary structure of bovine chromogranin A: a representative of a class of acidic secretory proteins common to a variety of peptidergic cells. *EMBO (Eur. Mol. Biol. Organ.) J.* 5:1495–1502.

74. Spritz, R. A., K. Strunk, C. S. Surowy, S. O. Hoch, D. E. Barton, and U. Francke. 1987. The human U1-70K snRNP protein: cDNA cloning, chromosomal localization, expression, alternative splicing and RNA-binding. *Nucleic Acids Res.* 15:10373–10391.

75. Elliot, R. B., and J. M. Martin. Dietary protein: a trigger of insulin-dependent diabetes in rat? 1984. *Diabetologia*. 26:297–299.

76. Zhang, Z. J., L. Davidson, G. S. Eisenbarth, and H. L. Weiner. 1991. Suppression of diabetes in NOD mice by oral administration of porcine insulin. *Proc. Natl. Acad. Sci. USA*. 88:10252–10256.

Proc. Natl. Acad. Sci. USA
Vol. 93, pp. 6367–6370, June 1996
Medical Sciences

IA-2, a transmembrane protein of the protein tyrosine phosphatase family, is a major autoantigen in insulin-dependent diabetes mellitus

(autoantibodies)

MICHAEL S. LAN†‡, CLIVE WASSERFALL§, NOEL K. MACLAREN§, AND ABNER LOUIS NOTKINS†

†Laboratory of Oral Medicine, National Institute of Dental Research, National Institutes of Health, Bethesda, MD 20892-4322; and §Department of Pathology and Laboratory Medicine, University of Florida College of Medicine, Gainesville, FL 32610

Communicated by Hugh McDevitt, Stanford University School of Medicine, Stanford, CA, February 27, 1996 (received for review November 20, 1995)

ABSTRACT **IA-2 is a 105,847 Da transmembrane protein that belongs to the protein tyrosine phosphatase family. Immunoperoxidase staining with antibody raised against IA-2 showed that this protein is expressed in human pancreatic islet cells. In this study, we expressed the full-length cDNA clone of IA-2 in a rabbit reticulocyte transcription/translation system and used the recombinant radiolabeled IA-2 protein to detect autoantibodies by immunoprecipitation. Coded sera (100) were tested: 50 from patients with newly diagnosed insulin-dependent diabetes mellitus (IDDM) and 50 from age-matched normal controls. Sixty-six percent of the sera from patients, but none of the sera from controls, reacted with IA-2. The same diabetic sera tested for autoantibodies to islet cells (ICA) by indirect immunofluorescence and glutamic acid decarboxylase (GAD_{65}Ab) by depletion ELISA showed 68% and 52% positivity, respectively. Up to 86% of the IDDM patients had autoantibodies to IA-2 and/or GAD_{65}. Moreover, greater than 90% (14 of 15) of the ICA-positive but GAD_{65} Ab-negative sera had autoantibodies to IA-2. Absorption experiments showed that the immunofluorescence reactivity of ICA-positive sera was greatly reduced by prior incubation with recombinant IA-2 or GAD_{65} when the respective antibody was present. A little over one-half (9 of 16) of the IDDM sera that were negative for ICA were found to be positive for autoantibodies to IA-2 and/or GAD_{65}, arguing that the immunofluorescence test for ICA is less sensitive than the recombinant tests for autoantibodies to IA-2 and GAD_{65}. It is concluded that IA-2 is a major islet cell autoantigen in IDDM, and, together with GAD_{65}, is responsible for much of the reactivity of ICA with pancreatic islets. Tests for the detection of autoantibodies to recombinant IA-2 and GAD_{65} may eventually replace ICA immunofluorescence for IDDM population screening.**

Autoantibodies that react with pancreatic islets were first detected by immunofluorescent techniques over 20 years ago (1). It is now clear that these antibodies recognize several different antigens in the islets (2–7). In recent years, extensive efforts have been made to identify and characterize the antigens with which these islet cell autoantibodies (ICA) react. Autoantibodies to one of these antigens, now known to be the lower molecular weight isoform of glutamic acid decarboxylase (GAD_{65}), have been widely used as a marker for identifying individuals with insulin-dependent diabetes mellitus (IDDM) and in predicting the risk of developing IDDM in nondiabetic individuals (8–12). GAD_{65} is primarily an intracellular antigen. Recently, we described a new member of the protein tyrosine phosphatase family, IA-2, (13, 14). IA-2 cDNA predicts a transmembrane protein of 979 amino acids in length and has a molecular mass of 105,847 Da. The extracellular domain extends from amino acid 1 to 576, the transmembrane domain from amino acid 577 to 601, and the intracellular domain from amino acid 602 to 979. The gene is expressed in human, mouse, and rat insulinoma cells as well as enriched normal islets (13). It also is found in human brain and neuroendocrine cells.

In the present report, we describe the expression of the full-length of IA-2 in a eukaryotic reticulocyte transcription/translation system and a sensitive radioimmunoprecipitation assay for detecting autoantibodies to IA-2 in the sera of IDDM patients. For comparison, the same sera were tested for ICA and GAD_{65} antibody (GAD_{65}Ab). The relationship of IA-2 antibody (IA-2Ab) to GAD_{65}Ab and ICA also was assessed.

MATERIALS AND METHODS

Human Subjects. New-onset IDDM patients (50) who had been diagnosed within a week of their blood sampling and 50 age-matched controls with no history of autoimmune disease were studied (15). Blood samples were collected under informed consent as approved by the University of Florida Institutional Review Board. Some IDDM patients were selected for the study because they had ICA but not GAD_{65}Ab.

Radioimmunoprecipitation of *in Vitro* Translated Full-Length IA-2 Autoantigen. The full-length human IA-2 cDNA without the leader sequence (13) was cloned into a pCRII cloning vector (Invitrogen) with a perfect Kozak translational start sequence (GCCGCCACCATGG) (16). Plasmid DNA (1 μg) was added to TNT coupled rabbit reticulocyte lysate system (Promega) in the presence of [^{35}S]methionine (Amersham) at 30°C for 2 hr. Radiolabeled protein was determined by 10% trichloroacetic acid precipitation. Immunoprecipitation was performed as described (17). Briefly, translated reticulocyte lysate (approximately 50,000–75,000 cpm) and 5 μl of tested serum were mixed in 100 μl of immunoprecipitation buffer (20 mM Tris (pH 7.4), 150 mM NaCl, 1% Triton X-100). The reaction mixture was incubated at 4°C overnight and 50 μl of 50% (vol/vol) protein A-Agarose (Life Technologies) was added to the solution at 4°C for 1 hr. The immunoprecipitation mixture was washed four times with immunoprecipitation buffer, boiled in sample buffer, and applied to an 8% SDS/PAGE gel. The gels were fixed with acetic acid/methanol (12.5%:12.5%), then exposed to film overnight. The intensity of the IA-2 bands (≈106 kDa) was scored from 1+ to 4+ by two independent investigators and corresponded very

The publication costs of this article were defrayed in part by page charge payment. This article must therefore be hereby marked "*advertisement*" in accordance with 18 U.S.C. §1734 solely to indicate this fact.

Abbreviations: ICA, islet cell autoantibodies; IDDM, insulin-dependent diabetes mellitus; GAD_{65}, glutamic acid decarboxylase; GAD_{65}Ab, GAD_{65} antibody; IA-2Ab, IA-2 antibody; JDF, juvenile diabetes foundation.

‡To whom reprint requests should be addressed.

closely to counts in the immunoprecipitate as determined by liquid scintillation (unpublished data).

ICA and GAD_{65}Ab. ICA and GAD_{65}Ab were determined as described (15, 18). Recombinant baculovirus-expressed GAD_{65} was kindly supplied by Syra (Palo Alto, CA), and used in an antigen depletion ELISA (D-ELISA) assay (19, 20). The results obtained closely parallel those by our previously published radioimmunoassay (21).

ICA Absorption. Tests were performed to see if the reactivity of ICA with pancreatic islets could be removed by absorption with recombinant GAD_{65} and/or IA-2. Serum (200 μl) was incubated overnight with an equal volume of biotinylated GAD_{65} bound to streptavidin-Sepharose beads. The slurry then was centrifuged and the supernatants tested in the usual way for ICA reactivity. Similarly, the intracellular domain of IA-2, expressed as a fusion protein with glutathione *S*-transferase and bound to glutathione-sepharose beads, was used to absorb serum antibody to IA-2. Sepharose beads, bound to neither GAD_{65} nor IA-2, served as controls.

RESULTS

Radiolabeled IA-2 was immunoprecipitated with serum from IDDM patients and the immunoprecipitate was separated on an 8% SDS/PAGE gel. As seen in Fig. 1, seven representative sera from IDDM patients identified a band with a relative molecular mass of 106 kDa. The intensity of the bands ranged from 1+ to 4+. No bands were seen when control sera were used.

Coded sera (50) from diabetic patients and 50 sera from controls were tested by this assay for autoantibodies to IA-2. As seen in Fig. 2, 66% of the sera from IDDM patients, but none of the sera from controls, reacted with IA-2. The intensity of the bands varied from 1+ to 4+ with 21 of the 33 positive sera being in the strongly positive (3+ to 4+) range. Equivocal bands (±) were scored as negative.

The sera used in Fig. 2 also were tested by D-ELISA for antibodies that reacted with GAD_{65}. As seen in Figs. 3 and 4, 52% of the sera from IDDM patients, but none of the sera from controls, reacted with GAD_{65}. Up to 86% of the IDDM patients developed autoantibodies to IA-2 and/or GAD_{65}. Some of the patients (34%) developed antibodies to both antigens, 12% to only GAD_{65}, and 4% to only IA-2. The current data, together with data from other studies (15), suggest that the age of the onset of IDDM may influence the nature of the immune response. Of 60 patients diagnosed with IDDM before age 20, 68% had antibodies to IA-2 and 60% had antibodies to GAD_{65}. However, of 15 patients diagnosed with IDDM after age 20, only 46% had antibodies to IA-2, whereas 86% had antibodies to GAD_{65}.

Detection of autoantibodies to islet cells by indirect immunofluorescence on human blood group O pancreatic sections has been widely used as a marker for IDDM. One of the antigens recognized by the immunofluorescence assay is GAD_{65} (18). However, it is known that at least 20% of sera that

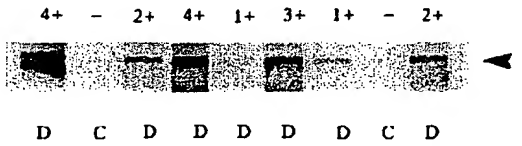

FIG. 1. Autoantibodies to IA-2 in patients with IDDM as measured by radioimmunoprecipitation. Sera were incubated with recombinant IA-2 expressed in a reticulocyte system. The dissociated precipitates were run on an 8% SDS/PAGE gel. Bands with a molecular mass of 106 kDa were scored on an intensity scale of 1+ to 4+. Representative sera with different band-intensities are illustrated. D, diabetic sera; C, control sera.

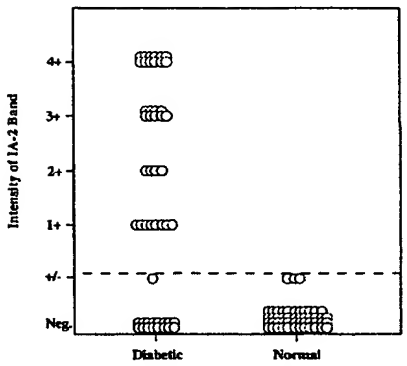

FIG. 2. Sera from 50 patients with clinically documented IDDM and 50 normal controls were tested for autoantibodies to IA-2 by radioimmunoprecipitation. The intensity of bands were scored as illustrated in Fig. 1. Equivocal bands (±) were considered negative for autoantibodies.

are positive for ICA by immunofluorescence do not react with GAD_{65}, indicating that the immunofluorescence assay is recognizing a still unidentified antigen(s). In the present study (Fig. 3), 68% of the sera were positive for ICA, but only 52% had autoantibodies to GAD_{65}. Remarkably, of the 15 ICA-positive sera that did not react with GAD_{65}, 14 reacted unambiguously with IA-2, arguing that IA-2 is one of the islet antigens that is routinely recognized by ICA in the immunofluorescence test. Moreover, of the 34 ICA-positive sera, 33 reacted with IA-2 and/or GAD_{65}.

Absorption experiments (Table 1) showed that the immunofluorescence reactivity of IA-2Ab-positive, but GAD_{65}Ab-negative, sera with islet cells was greatly reduced by absorption with IA-2, but not by absorption with GAD_{65}. Conversely, the immunofluorescence reactivity of IA-2Ab-negative but GAD_{65}Ab-positive sera with islet cells was greatly reduced by absorption with GAD_{65}, but not by absorption with IA-2. Taken together, our studies strongly argue that IA-2 and GAD_{65} are two of the major autoantigens recognized by ICA immunofluorescence. In one case (serum 4), however, islet cell reactivity was not substantially reduced by absorption with either IA-2 or GAD_{65}, suggesting that another still unidentified islet cell autoantigen(s) is being recognized by some ICA-positive sera. Preliminary experiments suggest that this autoantigen is closely related to IA-2.

DISCUSSION

In the present experiments, using full-length IA-2 cDNA and a eukaryotic expression system, we developed a radioimmunoassay for detecting autoantibodies to IA-2. Two-thirds of our IDDM patients had autoantibodies to IA-2 as compared with none of the controls. This radioimmunoassay is considerably more sensitive and specific than the ELISA used in our laboratory (unpublished data) or the one described by Rabin *et al.* (22), with a truncated form of IA-2 lacking the first 389 amino acids, designated ICA512. Moreover, the radioimmunoassay used here is a liquid phase assay and therefore is more likely to detect conformational epitopes than the solid phase ELISA.

Autoantibodies to GAD_{65} have been widely used as a marker for IDDM. At least 20% or more of newly diagnosed IDDM patients, however, are known to be negative for antibodies to GAD_{65} (23). In the present report, the patient population we studied was somewhat biased because a higher than expected percentage of patients were GAD_{65}Ab-negative (48%). However, of particular interest is the finding that of 15 ICA-positive

Sera	IA-2	GAD	ICA (JDF)
3	neg.	8	160
8	3+	8	320
9	neg.	neg.	neg.
10	4+	neg.	1280
13	2+	neg.	160
16	3+	6	1320
19	neg.	>16	neg.
20	4+	10	320
25	2+	neg.	neg.
27	neg.	2	320
28	3+	16	320
30	neg.	neg.	neg.
32	3+	neg.	160
34	1+	4+	neg.
35	3+	6	2560
38	4+	neg.	320
41	4+	>16	160
42	4+	neg.	320
43	4+	neg.	neg.
44	1+	neg.	160
47	2+	8	320
48	neg.	>16	neg.
50	neg.	neg.	20
52	neg.	neg.	neg.
53	5+	>16	1280
54	neg.	>16	neg.
57	neg.	>16	neg.
59	1+	>16	80
60	neg.	neg.	neg.
61	1+	neg.	20
62	neg.	>16	neg.
63	4+	neg.	640
65	6+	12	320
67	6+	4	1280
69	neg.	3	80
73	4+	>16	640
74	neg.	12	neg.
75	4+	>16	320
77	4+	neg.	640
78	neg.	neg.	neg.
79	4+	neg.	80
80	neg.	neg.	neg.
85	4+	>16	1280
87	1+	neg.	160
88	2+	>16	320
91	4+	neg.	320
92	3+	neg.	160
93	3+	>16	320
95	1+	neg.	40
97	neg.	neg.	neg.

FIG. 3. Sera from patients and controls were tested for: IA-2Ab by radioimmunoassay; GAD_{65}Ab by D-ELISA; and ICA by immunofluorescence. Numbers in the ICA column represent JDF units. Patients (coded numbers) are indicated in the serum column. Fifty normal controls (not shown) were negative in all three autoantibody tests.

patients who showed no reactivity to GAD_{65}, 14 had autoantibodies to IA-2, arguing that IA-2 is one of the major autoantigens recognized by ICA in the indirect immunofluorescence test using human pancreas as tissue substrate. Additional support for this contention comes from our absorption studies (Table 1), which showed that a major portion of the reactivity of ICA could be absorbed by IA-2 or GAD_{65} when the respective antibody was present.

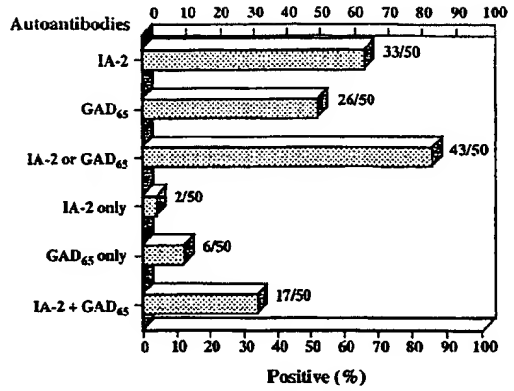

FIG. 4. Comparison of autoantibody response to IA-2 and GAD_{65} in 50 patients with IDDM.

The data further show that measurements of antibodies to both IA-2 and GAD_{65} detect a higher percentage of IDDM patients than measurement of either antibody alone. In the current study (Fig. 3), autoantibodies to IA-2 were identified in 66% (33/50) of the IDDM patients, whereas autoantibodies to GAD_{65} were detected in 52% (26/50) of the IDDM patients. Of the patients in this series, 34% (17/50) showed antibodies to both GAD_{65} and IA-2, with 65% (17/26) of the GAD_{65}Ab-positive patients also having antibodies to IA-2 and 52% (17/33) of the IA-2Ab-positive patients also having antibodies to GAD_{65}. However, up to 86% of the IDDM patients had antibodies to one or the other antigens or both. Thus, some IDDM patients will be missed if detection relies on only one autoantibody test. Of particular interest, 33 of the 34 ICA-positive patients showed autoantibodies to IA-2 and/or GAD_{65}. Moreover, of the 16 patients who were negative for ICA, nine were positive for autoantibodies to IA-2 and/or GAD_{65} demonstrating that, in some cases, these latter two assays detect autoantibodies when the ICA immunofluorescence assay is negative. Thus, the measurement of autoantibodies to both IA-2 and GAD_{65} seems to have advantages over the immunofluorescence assay for ICA in terms of sensitivity and specificity. The assays for IA-2 and GAD_{65} use molecularly expressed proteins and do not rely on the more subjective readings of tissue immunofluorescence and the inherent variations of human pancreatic sections. Prospective studies involving large number of subjects are ongoing in our laboratories and the preliminary data indicates that the positive predictive value of IA-2Ab, in identifying subjects likely to develop IDDM, is over 90% (unpublished data). Based on our present findings, IDDM patients diagnosed before age 20 are more likely to have IA-2Ab than patients diagnosed after age 20, but further studies are needed to settle whether IA-2Ab generally appears before or after GAD_{65}Ab in the natural history of the preclinical disease. Although autoantibodies to IA-2 and GAD_{65} seem to account for much and perhaps most of the immunofluorescence reactivity of ICA, the fact that some ICA reactivity remains after absorption with IA-2 or GAD_{65} argues for the existence of still another autoantigen. In this connection, we recently identified a novel cDNA from beta cells that encodes a protein, designated IA-2β, that is closely related to IA-2 (24). Moreover, these studies showed that IA-2β is the precursor of the 37-kDa tryptic fragment isolated from pancreatic islets, whereas IA-2 is the precursor of the 40-kDa tryptic fragment also isolated from pancreatic islets (24, 25).

Whether autoantibodies to IA-2 and GAD_{65} are a cause or a result of the immunologically mediated destruction of pan-

Table 1. Absorption of ICA-positive sera with IA-2 and GAD_{65}

	Reactivity of sera with			Absorption of ICA-positive sera with	
				IA-2	GAD_{65}
Patient serum	Islet cells	IA-2	GAD_{65}	Reactivity of absorbed sera with islet cells	
1	Pos	Pos	Neg	⇊	—
2	Pos	Pos	Neg	⇊	—
3	Pos	Pos	Neg	↓	—
4	Pos	Pos	Neg	↓	↓
5	Pos	Neg	Pos	—	⇊
6	Pos	Neg	Pos	—	⇊

Reactivity of ICA-positive sera with islet cells as measured by intensity of immunofluorescence: ⇊, greatly reduced; ↓, moderately reduced; ↓, slightly reduced; —, not reduced. Pos, positive; Neg, negative.

creatic beta cells underlying IDDM, is still not clear. However, what is clear is that these autoantibodies serve as markers of the underlying disease process, and thus have strong predictive power. In ongoing studies, we found that antibodies to GAD_{65} (26) and now IA-2 occur at highest frequencies among nondiabetic relatives who have the highest risk HLA phenotypes, especially DRB1*03/DQB1*0201; DRB1*04/DQB1*0302 heterozygotes. Why the host should make an immune response to two such seemingly unrelated antigens as GAD_{65} and IA-2 is unknown. While both are expressed in neuroendocrine cells (i.e., pancreatic islets and brain), IA-2 is particularly interesting because, in contrast to GAD_{65}, it has an extracellular domain. The possibility that the extracellular domain of IA-2 serves as a target for an autoimmune attack and/or is the site for deleterious transmembrane signaling is currently under investigation.

We thank Drs. Hersh Mehta and Barbara Vold for their assistance with the assay for autoantibodies to GAD_{65}. We gratefully acknowledge the editorial help of Janice Solomon. This study was supported by Grants R01 HD 19469, P01 DK39079, and GCRC MO1 RR00082 from the National Institutes of Health.

1. Bottazzo, G. F., Florin-Christensen, A. & Doniach, D. (1974) *Lancet* 2, 1279–1282.
2. Nayak, R. C., Omar, M. A., Rabizadeh, A., Srikanta, S. & Eisenbarth, G. S. (1985) *Diabetes* 34, 617–619.
3. Christie, M. R., Tun, R. Y., Lo, S. S., Cassidy, D., Brown, T. J., Hollands, J., Shattock, M., Bottazzo, G. F. & Leslie, D. G. (1992) *Diabetes* 41, 782–787.
4. Castano, L., Russo, E., Zhou, L., Lipes, M. H. & Eisenbarth, G. S. (1991) *J. Clin. Endocrinol. Metab.* 73, 1197–1201.
5. Atkinson, M. A. & Maclaren, N. K. (1994) *N. Engl. J. Med.* 331, 1428–1436.
6. Baekkeskov, S., Aanstoot, H. J., Christgau, S., Reetz, A., Solimena, M., Cascalho, M., Folli, F. & Richter-Oleson, H. (1990) *Nature (London)* 347, 151–156.
7. Inman, L. R., McAllister, C. T., Chen, L., Hughes, S., Newgard, C. B., Kettman, J. R., Unger, R. H. & Johnson, J. H. (1993) *Proc. Natl. Acad. Sci. USA* 90, 1281–1284.
8. Baekkeskov, S., Landin, M., Kristensen, J. K., Srikanta, S., Bruining, G. J., Mandrup-Poulsen, T., deBeaufort, C., Soeldner, J. S., Eisenbarth, G., Lindgren, F., Sundkvuist, G. & Lernmark, Å. (1987) *J. Clin. Invest.* 79, 926–934.
9. Christie, M., Landin-Olsson, M., Sundkvist, G., Dahlquist, G., Lernmark, Å. & Baekkeskov, S. (1988) *Diabetologia* 31, 597–602.
10. Atkinson, M. A., Maclaren, N. K., Scharp, D. W., Lacy, P. E. & Riley, W. J. (1990) *Lancet* 335, 1357–1360.
11. DeAizpurua, H. J., Wilson, Y. M. & Harrison, L. C. (1992) *Proc. Natl. Acad. Sci. USA* 89, 9841–9845.
12. Tuomilehto, J., Zimmet, P., Mackay, I. R., Koskela, P., Vidgren, G., Toivanen, L., Tuomilehto-Wolf, E., Kohtamäki, K., Stengård, J. & Rowley, M. J. (1994) *Lancet* 343, 1383–1385.
13. Lan, M. S., Lu, J., Goto, Y. & Notkins, A. L. (1994) *DNA Cell Biol.* 13, 505–514.
14. Lu, J., Notkins, A. L. & Lan, M. S. (1994) *Biochem. Biophys. Res. Commun.* 204, 930–936.
15. Riley, W. J., Maclaren, N. K., Krischer, J., Spillar, R. P., Silverstein, J. H., Schatz, D. A., Schwartz, S., Malone, J., Shah, S., Vadheim, C. & Rotter, J. I. (1990) *N. Engl. J. Med.* 323, 1167–1172.
16. Kozak, M. (1987) *Nucleic Acids Res.* 15, 8125–8148.
17. Grubin, C. E., Daniels, T., Toivola, B., Landin-Olsson, M., Hagopian, W. A., Karlsen, A. E., Boel, E., Michelsen, B. & Lernmark, Å. (1994) *Diabetologia* 37, 344–350.
18. Atkinson, M. A., Kaufman, D. L., Newman, D., Tobin, A. J. & Maclaren, N. K. (1993) *J. Clin. Invest.* 91, 350–356.
19. Wasserfall, C., Schatz, D., Mehta, H., Vold, B., Krischer, J., Atkinson, M. & Maclaren, N. (1995) *Diabetes* 44, Suppl. 77A (abstr. 287).
20. Mehta, H., Vold, B., Minkin, S., & Ullman, E. (1996) *Clin. Chem.* 42, 263–269.
21. Scott, M., Schatz, D., Atkinson, M., Krischer, J., Mehta, H., Vold, B. & Maclaren, N. (1994) *J. Autoimmun.* 7, 865–872.
22. Rabin, D. U., Pleasic, S. M., Shapiro, J. A., Yoo-Warren, H., Oles, J., Hicks, J. M., Goldstein, D. E. & Rae, P. M. M. (1994) *J. Immunol.* 152, 3183–3188.
23. Verge, C. F., Howard, N. J., Rowley, M. J., Mackay, I. R., Zimmet, P. Z., Egan, M., Hulinska, H., Hulinsky, I., Silvestrini, R. A., Kamath, S., Sharp, A., Arundel, T. & Silink, M. (1994) *Diabetologia* 37, 1113–1120.
24. Lu, J., Li, Q., Xie, H., Chen, Z. J., Borovitskaya, A. E., Maclaren, N. K., Notkins, A. L. & Lan, M. S. (1996) *Proc. Natl. Acad. Sci. USA* 93, 2307–2311.
25. Payton, M. A., Hawkes, C. J. & Christie, M. R. (1995) *J. Clin. Invest.* 96, 1506–1511.
26. Huang, W., She, J., Muir, A., Laskowska, D., Zorovich, B., Schatz, D. & Maclaren, N. (1994) *J. Autoimmun.* 7, 889–897.

Autoimmunity to Two Forms of Glutamate Decarboxylase in Insulin-dependent Diabetes Mellitus

Daniel L. Kaufman,* Mark G. Erlander,‡ Michael Clare-Salzler,§ Mark A. Atkinson,|| Noel K. Maclaren,|| and Allan J. Tobin¶**‡‡
*Department of Psychiatry and Behavioral Sciences; ‡Program for Neuroscience; §Department of Medicine; ¶Department of Biology; **Molecular Biology Institute; and ‡‡Brain Research Institute, University of California Los Angeles, Los Angeles, California 90024; and ||Department of Pathology and Laboratory Medicine, College of Medicine, University of Florida, Gainesville, Florida 32610

Abstract

Insulin-dependent diabetes mellitus (IDDM) is thought to result from the autoimmune destruction of the insulin-producing β cells of the pancreas. Years before IDDM symptoms appear, we can detect autoantibodies to one or both forms of glutamate decarboxylase (GAD_{65} and GAD_{67}), synthesized from their respective cDNAs in a bacterial expression system. Individual IDDM sera show distinctive profiles of epitope recognition, suggesting different humoral immune responses. Although the level of GAD autoantibodies generally decline after IDDM onset, patients with IDDM-associated neuropathies have high levels of antibodies to GAD, years after the appearance of clinical IDDM. We note a striking sequence similarity between the two GADs and Coxsackievirus, a virus that has been associated with IDDM both in humans and in experimental animals. This similarity suggests that molecular mimicry may play a role in the pathogenesis of IDDM. (*J. Clin. Invest.* 1992. 89:283–292.) Key words: insulin-dependent diabetes mellitus • glutamate decarboxylase • diabetic neuropathy

Introduction

Insulin-dependent diabetes (IDDM;[1] type I diabetes) is one of the most serious and common of metabolic disorders, affecting approximately 1 person in 300 in the U.S., while epidemiological studies in Europe suggest that its incidence is increasing (reviewed in 1–3). The disease is thought to result from the autoimmune destruction of the insulin-producing β cells of the pancreas and the subsequent metabolic derangements. Although insulin therapy allows most patients to lead active lives, this replacement is imperfect since it does not restore normal metabolic homeostasis. Metabolic abnormalities are thought to be important in the subsequent development of common complications, which include retinopathy, cataract formation, nephropathy, neuropathy, and heart disease.

While the initiating agent of IDDM autoimmunity is not known, it ultimately provokes a loss of immunological tolerance to self-antigens present in insulin-secreting β cells within the pancreatic islets (4–6). IDDM begins with an asymptomatic stage, characterized by a chronic inflammatory infiltrate of the islets (insulitis), which selectively destroys the β cells. Only after the destruction of the majority of the β cells, often occurring over several years, do hyperglycemia and ketosis appear.

The pathogenesis of IDDM involves both genetic and environmental factors. One or more susceptibility factors are encoded by the major histocompatibility complex on chromosome 6, probably by the DQ A1 and B1 loci (7, 8). Studies of monozygotic twins, however, show a concordance for IDDM of < 40%, suggesting that environmental factors play an important role (9). Long suspected environmental causes of IDDM include a number of viruses, such as rubella, encephalomyocarditis virus, and especially Coxsackie virus B_4 (reviewed in 10–12).

Autoantibodies to a 64,000 M_r islet cell protein are associated with IDDM and have been detected years before the onset of symptoms (13–15). Other IDDM-associated autoantibodies, such as those against insulin and cytoplasmic gangliosides of islet cells (ICA), appear later, possibly as a consequence of the release of these antigens (or their precursors) from the damaged islet cells (16, 17). Antibodies to the 64,000 M_r proteins are, however, the earliest and most reliable predictive marker of IDDM in humans and are also present in the two animal models for IDDM, the nonobese diabetic (NOD) mouse and the Biobreeding rat (14, 15, 18, 19).

Baekkeskov et al. (20) reported that the 64,000 M_r islet cell autoantigen is a form of glutamate decarboxylase (GAD; E.C. 4.1.1.15), the enzyme responsible for the synthesis of γ-aminobutyric acid (GABA) in brain, peripheral neurons, pancreas, and other organs (21). We have recently shown that the brain contains two forms of GAD, which are encoded by two separate genes (22). The two GADs (GAD_{65} and GAD_{67}) differ in molecular size (with M_rs = 65,000 and 67,000) and amino acid sequence (with ~ 30% sequence divergence), as well as in their intracellular distributions and interactions with the GAD cofactor pyridoxal phosphate (22–25). In brain neurons, GAD_{65} is preferentially associated with axon terminals, while GAD_{67} is present in both terminals and cell bodies (25).

Previous studies of the 64,000 M_r IDDM autoantigen have used pancreatic extracts enriched for membrane-associated

Dr. Erlander's present address is Department of Molecular Biology, Scripps Clinic, La Jolla, CA 92037. Address correspondence to Daniel L. Kaufman, Ph.D., Department of Psychiatry and Behavioral Sciences, UCLA, Los Angeles, CA 90024-1759, or to Allan J. Tobin, Ph.D., Department of Biology, UCLA, Los Angeles, CA 90024-1606.

Received for publication 22 March 1991 and in revised form 20 September 1991.

1. *Abbreviations used in this paper:* GAD, glutamate decarboxylase; ICA, islet cell antibodies; IDDM, insulin-dependent diabetes mellitus; JDF, Juvenile Diabetes Foundation; NIDDM, non-IDDM; NOD, nonobese diabetic; PAS, protein A-Sepharose; PCR, polymerase chain reaction.

J. Clin. Invest.

0021-9738/92/01/0283/10 $2.00
Volume 89, January 1992, 283–292

proteins. In view of our demonstration that the brain contains two GADs, we set out to determine the molecular identity of islet cell GAD by immunohistochemistry with monospecific antibodies. We then used GAD_{65} and GAD_{67} produced in genetically engineered bacteria from our GAD cDNAs to examine the specificity of IDDM autoantibodies for the two GADs and for restricted sets of GAD epitopes.

Our results lead to two new suggestions concerning the pathogenesis of IDDM and its complications: (*a*) GAD autoimmunity may play a role in the pathogenesis of IDDM-associated neuropathies; and (*b*) IDDM autoimmunity may result from molecular mimicry of GAD and a Coxsackievirus peptide.

Methods

Patient sera. IDDM patients and individuals at high risk for later developing IDDM were selected from a previous study at the University of Florida Diabetes Clinics (15, 26). IDDM patients with peripheral neuropathies were selected from the University of Florida Diabetes Clinics and the UCLA Diabetes Clinic.

Nondiabetic controls and the individuals studied before the documented clinical onset were ascertained through ongoing prospective screening for islet cell antibodies of more than 5,000 first-degree relatives of IDDM probands, and 8,200 individuals from the general population, of whom 4,813 were school children. These studies were approved by the University of Florida's Institutional Review Board. All participating individuals first gave their written informed consent. Individuals at high risk for the development of IDDM were identified by the presence of high titers of ICAs, assayed by indirect immunofluorescence on cryostat sections of blood group O human pancreas. All results were interpreted on coded samples, with control negative and positive sera in each batch. The ICA levels were estimated as Juvenile Diabetes Foundation units, according to the standardization guidelines established by the Immunology Diabetes Workshop (IDW), as previously described. M. Atkinson and N. Maclaren subscribe to the IDW's ICA proficiency testing program, which they currently supervise.

GAD assays. Patient sera were assayed blind for their ability to bind GAD enzymatic activity from a cleared homogenate of human cerebellar cortex in "GAD buffer," which contained 60 mM potassium phosphate, pH 7.1, 0.5% Triton X-100, 1 mM PMSF, 1 mM 2-aminoethylisothiouronium bromide, and 0.1 mM pyridoxal phosphate. IgG from each serum was bound to protein A-Sepharose (PAS) by adding 40 μl of serum to 80 μl of a 1:1 slurry of preswollen PAS in GAD buffer, incubating for 30 min at 4°C with gentle rocking, isolated by centrifugation, and then washing four times in the same buffer. 100 μl of brain extract was then added to each sample and incubated for 1 h at 4°C with gentle rocking, washed four times, resuspended in buffer, and assayed for GAD activity as previously described (25). Values shown are means of three determinations.

Immunohistochemistry. Immunochemical detection of the two forms of GAD was performed as previously described for rat cerebellum (25).

Antigen preparation and immunoadsorption. Rat GAD_{65} and GAD_{67} cDNAs were subcloned in the NcoI site of pET 8C and the Nhe I site of pET-5C respectively and transformed into *Escherichia coli* BL21 (DE3) (20, 27). Control and GAD-producing *E. coli* were grown and induced with isopropyl-thio-β-D-galactoside, harvested by centrifugation, resuspended in GAD buffer, sonicated, and cleared by centrifugation at 55,000 *g* for 15 min. For immunocompetition, 30 μl of each patient serum was incubated with 100 μl of extract from control bacteria or from bacteria that produced either GAD_{65} or GAD_{67} for 1 h at 4°C. Human pancreatic islets were labeled with ^{35}S-methionine as previously described (15). A detergent extract (300 μl) was first precleared with human control serum. The material that bound to the control IgG was removed with protein A-Sepharose. The precleared islet cell detergent extract was then split into three fractions and then incubated (2 h on ice) with serum that had been absorbed with each of the *E. coli* lysates. IgG-bound material was isolated with protein A-Sepharose as described above, and the bound material was analyzed by polyacrylamide gel electrophoresis in SDS (SDS-PAGE), followed by fluorography.

Detection of GAD autoantibodies. E. coli expressing rat GAD_{65} and GAD_{67} cDNAs were grown in minimal medium and induced with isopropyl-thio-β-D-galactoside in the presence of a mixture of ^{35}S-labeled amino acids (Tran-^{35}S; ICN Pharmaceuticals, Inc., Irvine, CA). The bacteria were harvested, sonicated in GAD buffer, and centrifuged to remove debris. Sera were preadsorbed with extracts of unlabeled host bacteria and then added to a mixture of ^{35}S-labeled extracts of GAD_{65}- and GAD_{67}-producing bacteria. IgG-bound polypeptides were isolated with PAS and analyzed by SDS-PAGE. Initial experiments analyzed sera for their ability to precipitate GAD_{65} and GAD_{67} separately (data not shown). Using a mixture of the two extracts simplified the assay. A number of *E. coli* polypeptides were also immunoadsorbed by some patient and some control sera. One such band, with M_r ~ 70,000, is apparent in many samples.

Epitope mapping. Portions of GAD_{65} cDNA were amplified by the polymerase chain reaction (PCR; 28) to produce DNA segments encoding three polypeptide segments: amino acid residues 1–224 (segment A); 224–398 (segment B); and 398–585 (segment C). Each construct also contained a T_7 promoter, a consensus sequence for the initiation of translation and an initiating methionine codon (29). Each PCR product was then transcribed in vitro with T_7 RNA polymerase and translated in vitro in a rabbit reticulocyte cell-free system in the presence of ^{35}S-methionine, using conditions recommended by the supplier (Amersham Corp., Arlington Heights, IL). Each test serum (30 μl) was incubated with the resulting ^{35}S-polypeptides. The bound peptides were isolated with PAS and analyzed by SDS-PAGE in 15% polyacrylamide and fluorography.

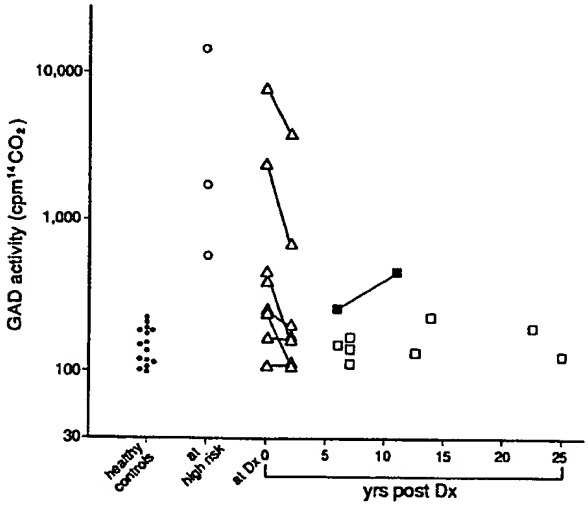

Figure 1. Immunoprecipitation of GAD activity by IDDM sera. GAD activity in brain extracts was immunoprecipitated with sera from healthy controls (●); individuals at high risk for IDDM (○); IDDM patients at diagnosis and two years later (△); and unrelated patients more than six years after diagnosis (□); one patient (■) developed a sensory neuropathy.

Results

IDDM patients have autoantibodies to GAD. We initially performed a blind trial to test for the presence of GAD autoantibodies in IDDM sera. We tested IDDM sera for the presence of GAD autoantibodies by assaying their ability to immunoprecipitate GAD activity from human brain homogenates (Fig. 1). We included sera from 35 individuals, which included 3 people judged to be at high risk for IDDM on the basis of their previously determined ICA titers, reduced responses to intravenous glucose, and their HLA DR/DQ haplotypes (15, 26), 8 IDDM patients studied at onset and 7 of these same patients two years later, 9 unrelated patients six or more years after IDDM onset, and 15 normal controls. Our results parallel those independently reported by Baekkeskov et al. (20).

The three high-risk individuals whose sera we examined had high anti-GAD titers, in one case comparable to those raised against purified brain GAD in experimental animals (data not shown). The levels of antibodies to GAD in five of eight newly diagnosed patients exceeded the mean + 1 SD of the control sera. Levels in these patients decreased by ~ 50% during the subsequent two years, with only two of seven sera having levels more than the mean + 1 SD of the control sera. In most patients ≥ 6 years after diagnosis, the concentrations of antibodies to GAD were indistinguishable from controls. In one patient in this series, however, anti-GAD levels actually rose between 6 and 11 years after onset, during which time the patient developed a sensory neuropathy.

Levels of anti-GAD antibodies in these patients generally parallel the previously determined titers of autoantibodies to the 64,000 M_r antigen. Our assays of immunoprecipitated GAD enzymatic activity easily identified individuals with high titers of autoantibodies to the 64,000 M_r antigen, but did not often distinguish individuals with low titers from controls.

This study established that autoantibodies to GAD are present at and before the clinical diagnosis of IDDM and decline within a few years after diagnosis. We next addressed the question of the molecular identity of the GAD autoantigen.

Islet cells contain both GAD_{65} and GAD_{67}. Immunohistochemical experiments with the GAD-6 monoclonal antibody, which recognizes only GAD_{65}, show the presence of GAD_{65} in pancreatic islets (Fig. 2; references 20, 25, 30). Using our recently described K-2 antiserum, which recognizes only GAD_{67}, we show that islet cells also contain GAD_{67} (Fig. 2; reference 25). Since both GAD_{65} and GAD_{67} are present in islets, either or both could be the autoantigen recognized by the IDDM sera surveyed in Fig. 1 and by Baekkeskov et al. (20).

The 64,000 M_r islet cell autoantigen is GAD_{65}. To define further the molecular identity of the IDDM autoantigen, we performed two sets of experiments. In the first experiment we used GAD-6 (the GAD_{65}-specific monoclonal antibody) to immunoadsorb GAD_{65} both from detergent extracts of ^{35}S-labeled islet cells and from soluble extracts of ^{35}S-labeled GAD-producing bacteria. GAD-6 specifically recognized a 65,000 M_r immunoreactive polypeptide in both islet cells and GAD_{65}-producing bacteria with identical electrophoretic mobilities, which were distinct from bacterially produced GAD_{67}. Prior immunoadsorption with an IDDM serum removes immunoreactive GAD_{65} (i.e., "64K") from both islet cell and bacterial extracts (data not shown).

In the second set of experiments, we examined the ability of bacterially produced GAD_{65} and GAD_{67} to compete with the immunoadsorption of islet cell autoantigens by IDDM sera. Sera taken from two patients (patient 052 and 496 which recognize both GADs; see Table I) specifically precipitate a polypeptide of M_r 64–65,000 from detergent-phase extracts of ^{35}S-labeled islets in the presence of extracts of host bacteria (i.e., bacteria not engineered to produce GAD), containing 400 μg of protein (Fig. 3, lanes *1* and *2*). When we added extracts (also containing 400 μg of total protein) of genetically engineered bacteria that produce either GAD_{65} or GAD_{67}, we found that an extract containing 100 μg of GAD_{67} partially blocked the binding of the islet cell antigen, as would be expected if GAD_{67} adsorbs some of the antibodies that recognize epitopes common to GAD_{65} and GAD_{67} (Fig. 3, lanes *5* and *6*). In contrast, an extract containing only 10 μg of GAD_{65} completely blocked immunoadsorption of the 64K autoantigen (Fig. 3, lanes *9* and *10*). These data show that the previously identified 64,000 M_r autoantigen is immunologically indistinguishable from GAD_{65}. A serum (patient 476) that predominantly recognizes GAD_{67} (which does not partition into the detergent phase of the islet cell extracts used in these studies) precipitated a very faint 64K band. The healthy control serum did not precipitate a 64K antigen.

IDDM sera differ in the recognition of GAD_{65} and GAD_{67}. Antisera raised in experimental animals against purified brain GAD vary in their recognition of GAD_{65} and GAD_{67}. With this in mind, we determined the specificity of individual IDDM sera for each species of GAD. We examined their ability to immunoprecipitate ^{35}S-labeled GAD_{65} and GAD_{67}, produced from GAD cDNAs in a bacterial expression system. We examined sera from 59 individuals (to whose IDDM status we were blind), including 8 people at high risk for IDDM, 12 people who later (3–64 months) developed IDDM, 3 newly diagnosed IDDM patients, 12 patients 2–22 years after onset who had no neurological symptoms, and 9 patients 10–48 years after onset who developed sensory or autonomic neuropathies (Table I; Fig. 4). None of the control sera from 15 healthy individuals had detectable ICA, antibodies to the 64,000 M_r pancreatic antigen, or antibodies to either form of GAD.

Levels of GAD autoantibodies were generally highest in the sera of individuals who were likely to have been in the process of developing the disease; those who were known to develop IDDM some time after their sera were drawn and those thought to be at high risk for IDDM on the basis of their previously determined ICA levels and autoantibodies to 64K. Levels were much lower in the sera of patients examined a few years after IDDM onset. None of the nine patients without neuropathies tested long after onset (≥ 5 years) had detectable antibodies to GAD. The intensity of the ^{35}S-labeled GAD_{65} immunoprecipitated by the IDDM sera generally paralleled the previously determined titers of autoantibodies to the 64,000 M_r islet cell polypeptide (15, 26), again supporting the latter's identification as GAD_{65}. There was no obvious correlation between ICA titers and the levels of autoantibodies to either GAD form.

Among IDDM sera, the ability to precipitate each of the two GADs varied among individuals. Of the 23 individuals tested whom we thought to be at early stages of IDDM (8 at high risk, 12 tested before subsequent onset, and 3 newly diagnosed), 15 recognized both GADs, 3 recognized only GAD_{65}, and 4 recognized only GAD_{67}. We found no obvious correlation between the time before or after diagnosis and the specific-

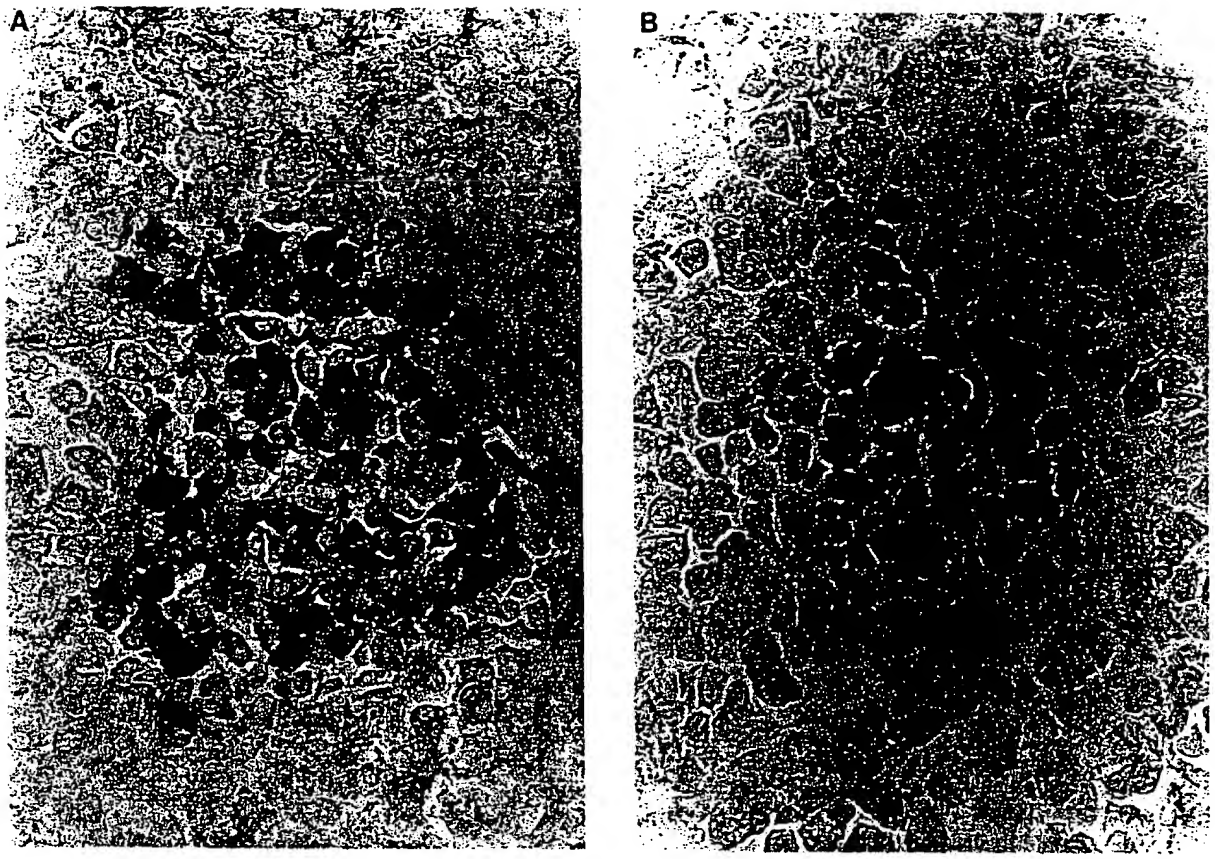

Figure 2. Pancreatic islets contain both GAD_{65} and GAD_{67}. (*A*) Immunohistochemistry with the GAD-6 monoclonal antibody specific for GAD_{65}, and (*B*) with the K-2 antiserum specific for GAD_{67}.

ity of autoantibodies for either form of GAD. A more sensitive assay (for example, one using human rather than rat GADs) might in fact reveal antibodies to both forms of GAD.

Altogether 78% (18/23) of sera from early stage IDDM individuals recognized GAD_{65}, a frequency similar to that reported in previous studies of 64,000 M_r autoantibodies (reviewed in 15, 20). When we tested for both GADs, however, we could detect autoantibodies to either or both in 96% (22/23) of the early stage individuals tested.

The sera of NOD mice also show immunoreactivity both to GAD_{65} and to GAD_{67} (Fig. 4, lane *22*). This finding further underscores the similarity of the disease processes in human IDDM and in NOD mice.

Individual sera vary in epitope recognition. To examine the individual variability in epitope recognition of IDDM autoantibodies, we determined the ability of sera from four individuals to recognize three polypeptide segments of GAD_{65} (Fig. 5). Each of these individuals was at a different stage in the progression of the disease: 052 (high risk), 723 (a patient who subsequently developed IDDM), 705 (at diagnosis), and UC2 (advanced neuropathy). We used PCR amplification followed by in vitro transcription and translation of the PCR products to produce ^{35}S-labeled polypeptides that represented the amino-terminal (A), middle (B), and carboxy-terminal (C) thirds of GAD_{65}. None of the four sera reacted with the segment A, two (052 and UC2) reacted with segments B and C, one (705) with the carboxy-terminal segment C only, and one (723) with none of the GAD_{65} segments. Our inability to immunoprecipitate polypeptides with serum 723 (which, as shown in Fig. 4, does precipitate both GAD_{65} and GAD_{67} as intact molecules) may have resulted from a lack of sensitivity of the assay or from the inability of any of the utilized peptides to fold into the recognized epitope. While the three peptides that we investigated are unlikely to have formed all their native epitopes, our epitope mapping data, like our studies of the differential recognition of GAD_{65} and GAD_{67}, suggest that each of the tested sera has a distinctive profile of anti-GAD antibodies. Although IDDM autoantibodies recognize different GAD epitopes, we do not know which epitopes are recognized by the self-reactive T lymphocytes, which contribute to both humoral and cellular autoimmunity.

Persistent autoimmunity to GAD is often associated with peripheral and autonomic neuropathy. The occurrence of antibodies to GAD (and to the previously determined 64,000 M_r antigen), is unusual in patients many years after onset (Fig. 1, Table I, and M. Atkinson, unpublished data). Autoantibodies to GAD were, however, present in 8 of 9 IDDM patients with sensory or autonomic neuropathies, long (10–41 years) after

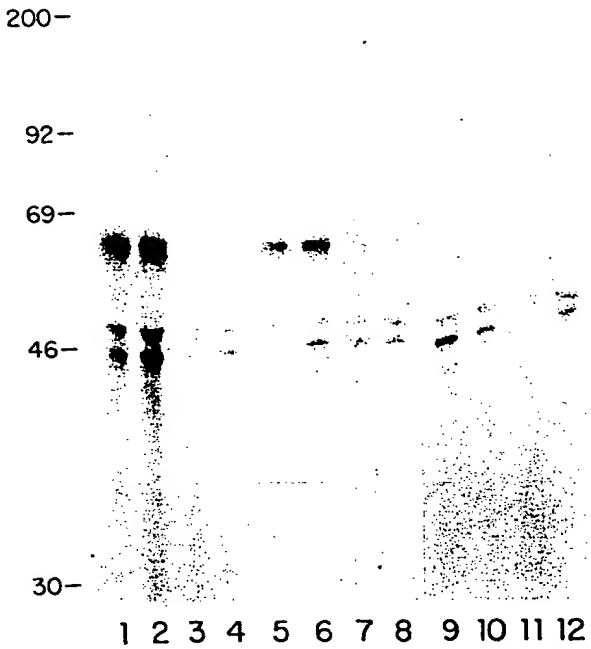

Figure 3. The 64,000 M_r autoantigen is GAD_{65}. The ability of sera which recognize both GADs (patients 052 and 496) to bind the previously described 64,000 M_r islet cell autoantigen was not blocked by preadsorption with an extract of wild-type BL21 (DE3) *E. coli*. Preadsorption with an extract of GAD_{67}-producing bacteria produced only partial blocking of these sera's ability to bind the pancreatic antigen. In contrast, preadsorption with extracts of GAD_{65}-producing bacteria, abolished the serum's ability to bind 64K antigen. Lanes *1–4* preadsorbed with 400 μg of a wild-type *E. coli* extract. Lanes *5–8* preadsorbed with a 400-μg extract containing 100 μg of GAD_{67}. Lanes *9–12* preadsorbed with a 400-μg extract containing 10 μg of GAD_{65}. Lanes *1, 5, 9;* patient 052. Lanes *2, 6, 10;* patient 496. Lanes *3, 7, 11;* healthy control. Lanes *4, 8, 12;* patient 476, whose serum predominantly recognizes GAD_{67} (Table I), does bind the 64K antigen very weakly which is not apparent in the photograph.

the onset of diabetic symptoms (Table I; Fig. 4, lanes *18–21*). Six of the sera examined had detectable levels of autoantibodies to both GAD_{65} and GAD_{67}, while two had detectable autoantibodies only to GAD_{67}. Two patients with rapidly progressing autonomic neuropathies (UC1 and UC2) had especially high levels of autoantibodies to GAD. In contrast, none of the nine patients who were free of IDDM-associated complications examined at or more than five years after onset had detectable antibodies to GAD. The GAD autoantibodies in neuropathy patients may result from the restimulation of the immune system by GAD released from damaged neurons, or they may be involved in the actual pathogenesis of this complication. In either case, GAD autoantibodies may serve as a useful marker of an ongoing degenerative process.

Sequence similarities between GAD and Coxsackievirus. Although we observe high levels of autoantibodies to GAD before IDDM onset, their presence may merely reflect an immune reaction to the exposure of previously sequestered antigens following β cell damage. Indeed, the initiating agent of the autoimmune response in IDDM is completely unknown, though the increasing incidence of IDDM and its frequent discordance in monozygotic twins has led to the suggestion that an environmental agent triggers autoimmunity (31, reviewed in 3, 12). In other autoimmune diseases, pathogenesis is thought to involve "molecular mimicry," in which a bacterial or viral antigen triggers an immune response that then reacts with a similar self antigen (reviewed 4, 32, 33).

Analysis of the deduced amino acid sequences of GAD_{65} and GAD_{67} shows an extensive and surprising sequence similarity to the P2-C protein of Coxsackievirus B_4. Coxsackievirus B_4 is a picornavirus with a worldwide distribution. It causes a mild upper respiratory infection and can also infect β cells (reviewed in 10–12). It has a small genome (7,395 bases), and its P2-C protein appears to contribute to the membrane-bound replication complex (34). A core polypeptide segment of six amino acid residues is identical in sequence between GAD_{65} and P2-C (Fig. 6; 22, 34). The immediately adjacent polypeptide segments also share a high level of similarity both in sequence and

Figure 4. Detection of autoantibodies against GAD_{65} and GAD_{67} in IDDM sera. Sera were incubated with a mixture of ^{35}S-labeled lysates of GAD_{65}- and GAD_{67}-producing *E. coli*, and IgG-bound polypeptides were analyzed by SDS-PAGE. The composite photo shows representative data from controls and from individuals at different stages of IDDM: three controls (lanes *1–3*), four people at high risk for IDDM (lanes *4–7*), four who later developed IDDM (lanes *8–11*), three patients at diagnosis (lanes *12–14*), three IDDM patients more than seven years after diagnosis (lanes *15–17*), four IDDM patients with neuropathies (lanes *18–21*), and NOD mice (lane *22*).

Table I. Analysis of Characterized Sera for GAD_{65} and GAD_{67} Immunoreactivity

Patient ID				ICA	Anti-64K	Anti-GAD_{65}	Anti-GAD_{67}
				JDF units			
Individuals at high risk for IDDM							
052				160	+++	+++	+++
825				20	+++	++	0
375				0	+++	++	+
143				40	++	0	++
692				ND	++	0	+++
356				160	+++	++	+++
112				80	ND	+++	+++
410				0	++	++	++
Individuals who later developed IDDM							
	Months before IDDM diagnosis						
624	12			20	++	0	++
UF1	4			ND	+	+	++
584	24			0	++	+	0
035	64			40	+	+	0
496	6			160	+++	+++	+++
171	3			40	+	0	+
470	13			0	+++	+	+
055	8			40	+	0	0
438	42			320	++	+	+
840	9			0	+	+	+
723	14			ND	+++	+++	+
476	11			ND	+	+	+++
At onset of clinical symptoms							
048				320	+++	+	++
705				160	+++	+++	++
291				0	+++	++	++
IDDM patients without neuropathies							
	Years after diagnosis						
147	2			ND	+	0	0
476	3			0	ND	0	+
604	3			0	ND	+	0
113	5			160	ND	0	0
238	6			0	ND	0	0
997	6			80	ND	0	0
867	7			ND	ND	0	0
382	7			0	ND	0	0
052	12			0	ND	0	0
571	13			0	ND	0	0
M31	15			0	ND	0	0
025	22			0	ND	0	0
IDDM patients with neuropathies							
	Years after diagnosis	Autonomic neuropathy	Peripheral neuropathy				
UC1	35	+	+	0	ND	0	++
UC2	10	+	+	0	ND	+++	+++
UC3	13	+	+	0	ND	+	+
082	11	+	−	0	+	+	+

Table I. (Continued)

Patient ID				ICA	Anti-64K	Anti-GAD_{65}	Anti-GAD_{67}
038	21	+	+	ND	ND	+++	+++
344	33	–	+	0	ND	0	+
194	41	–	+	0	ND	+	+
310	48	–	+	0	ND	0	0
64	29	–	+	-0	ND	+	++

Patient sera were obtained and assayed for ICA and autoantibodies to the 64,000 M_r protein as part of a previous study (15, 26) or from the UCLA Diabetes Clinic. Patients that are part of the University of Florida's database are identified by three digit numbers. Other patients are identified by sequential numbers, with UF numbers representing patients seen in Gainesville and UC patients seen in Los Angeles. ICA titers are expressed in JDF units. +++, high titers; ++, intermediate; +, detectable; ND, not determined. Patients UC1, UC2, and UC3 had rapidly progressing sympathetic neuropathies. None of the sera from 15 healthy controls had detectable ICA, antibodies to the 64,000 M_r protein, or antibodies to either form of GAD.

in the positions of charged residues. In the 24 residue segments of GAD_{65} and P2-C that are illustrated in Fig. 6, 19 residues are either identical or conservative differences. The three peptides shown in Fig. 6 have nearly identical hydrophobicity profiles (data not shown). The high charge density and the presence of a proline residue in the shared core suggest that the segments are highly antigenic. No other significant similarities were found between GAD and other viruses implicated in IDDM, such as rubella, mumps, encephalomyocarditis virus, and cytomegalovirus. A generally similar sequence similarity is also present in the P2-C region of other members of the Coxsackievirus family. If specific members of the Coxsackievirus family (such as B_4 and B_5) are indeed involved in the etiology of IDDM, their pathogenicity may involve factors such as their particular amino acid sequences, virulence, and cell trophism, as well as the host immune repertoire.

Discussion

In a blind clinical study, we tested IDDM sera for the presence of GAD autoantibodies by their ability to immunoprecipitate

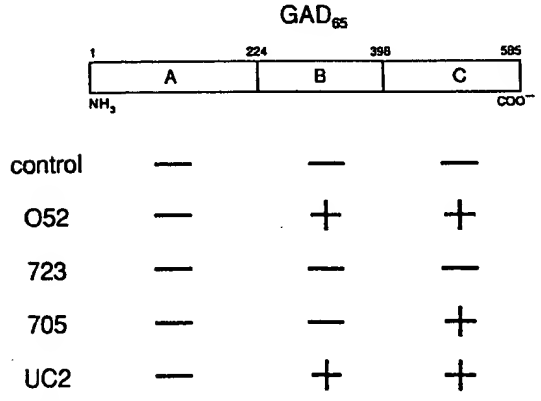

Figure 5. Epitope mapping of GAD_{65}. Three labeled segments containing the amino-terminal (*A*), middle (*B*), and carboxy-terminal (*C*) portions of GAD_{65} were immunoprecipitated with four IDDM sera that were initially characterized in the experiment shown in Fig. 4.

GAD enzymatic activity from brain homogenates. We found the highest levels of GAD autoantibodies in individuals at high risk for IDDM and in newly diagnosed IDDM patients. Levels of GAD autoantibodies decreased by ~ 50% within two years after diagnosis. Six years after IDDM onset, the patients whose sera we examined had GAD autoantibody levels indistinguishable from controls. One patient, however, displayed increased GAD antibodies years after onset, during which time the patient developed a sensory neuropathy.

Our studies of GADs in the brain have shown that neurons express two forms of GAD, which derive from separate genes (22). Pancreatic β cells also express GAD and use GABA to regulate glucagon secretion by α cells (35). Our immunohistochemical data, using antibodies monospecific for GAD_{65} and GAD_{67}, show that β cells, like most GABA neurons, contain both GAD_{65} and GAD_{67}. Although our enzymatic studies, and those of Baekkeskov et al. (20), demonstrated GAD autoimmunity in IDDM, they did not distinguish the two forms of GAD.

We used GAD_{65} and GAD_{67} cDNAs to express large amounts of each GAD in a bacterial expression system and tested the ability of each form to compete with the immunoadsorption of the 64,000 M_r autoantigen from ^{35}S-labeled islet cells. Only GAD_{65}-containing lysates effectively competed, suggesting that the 64,000 M_r autoantigen corresponds to GAD_{65}.

The islet cell homogenates previously used to characterize IDDM autoantigens were enriched for membrane-associated molecules and may preferentially have included GAD_{65}. In contrast, both our studies of the soluble fraction and those of Christie et al. (36) show a complex pattern of antigens recognized by IDDM autoantibodies (data not shown). Since islet cells contain both GAD_{65} and GAD_{67}, (Fig. 2) we sought to characterize the GAD autoantibodies by testing the ability of IDDM sera to recognize bacterially produced GAD_{65} and GAD_{67}.

We could detect autoantibodies to either GAD_{65} or GAD_{67} or both in almost all people who later developed IDDM, in some cases years before the onset of clinical symptoms. Of 23 early stage IDDM individuals tested, we found antibodies to both GADs in 15, to GAD_{65} alone in 3, and to GAD_{67} alone in 4. By testing for antibodies to both forms of GAD we were able to detect GAD antibodies in 96% of the individuals tested.

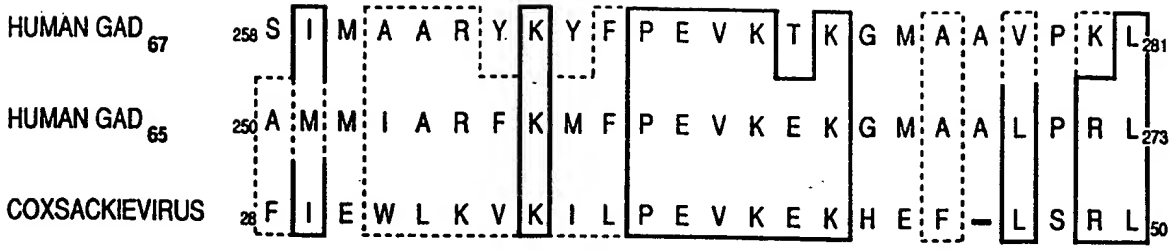

Figure 6. GAD and Coxsackievirus P2-C share common sequences. Solid line encloses identical amino acid residues. Dashed line encloses amino acid residues with similar charge, polarity, or hydrophobicity. Numbers refer to the amino acid residues in GAD_{65}, GAD_{67}, and Coxsackievirus protein P2-C. The human GAD amino acid sequences, which are almost identical to the rat GAD sequences, were determined by Bu Dingfang et al. (manuscript submitted for publication).

Levels of GAD autoantibodies were usually highest before IDDM onset and, in our patient sample, appeared as early as five years before onset of symptoms. GAD antibody levels declined after onset, presumably in parallel with the loss of GAD-containing β cells and the extinction of antigen-driven autoimmunity.

Patients showed varying immunoreactivity to GAD_{65} and GAD_{67}, which share ~ 70% amino acid similarity and are most divergent at their amino termini (22). They also varied in their ability to recognize individual polypeptide segments of GAD_{65}. These data suggest a diverse B lymphocyte response to different epitopes of GAD. While not all IDDM sera recognize the GAD_{65} polypeptide that contains the sequence shared with Coxsackievirus (segment B in Fig. 5), the antibodies may recognize GAD epitopes different from those that originally activated T lymphocytes.

Because our initial survey of IDDM patients detected increased levels of GAD autoantibodies in a patient who developed a sensory neuropathy long after the onset of diabetes itself, we further studied GAD autoimmunity in patients with IDDM-associated neuropathies. We found that 8/9 patients who had developed clinical IDDM symptoms 10–41 years earlier, showed significant levels of autoantibodies to GAD_{65}, GAD_{67}, or both. Of the eight patients in this group for whom we had ICA data, none had detectable ICA, and their low basal C-peptide did not respond to intravenous glucagon, suggesting that the continued high levels of anti-GAD autoantibodies did not result from the persistence of GAD-containing β cells.

The production of anti-GAD autoantibodies in patients with diabetic neuropathy may reflect continued stimulation of the immune system by GAD in the peripheral nervous system. Consistent with this hypothesis, Rabinowe et al. (37) have shown that, in some IDDM patients, autoantibodies to sympathetic ganglia are present at the diagnosis of IDDM, before the onset of clinical neuropathy. In addition, postmortem examination has revealed lymphocytic infiltration of sympathetic ganglia in IDDM patients with autonomic neuropathy (38). Our data suggest that autoimmunity to GAD, together with the metabolic effects of hyperglycemia, may play an important pathogenic role in diabetic neuropathy in IDDM.

The surprising similarity of the amino acid sequences of GAD_{65} and GAD_{67} to the P2-C protein of Coxsackievirus suggests that IDDM autoimmunity may arise by molecular mimicry, as a consequence of infection by Coxsackievirus. Epidemiological studies have shown that 39% of newly diagnosed IDDM patients have IgM responses to Coxsackievirus, compared to 6% of controls (39, 40). The molecular mimicry hypothesis suggests a mechanism to explain both the epidemiological association of Coxsackievirus B_4 with human IDDM and its ability (in contrast to other viruses epidemiologically associated with IDDM) to produce diabetes in mice and primates (31, 41–44). Direct association of Coxsackie B_4 infection and subsequent onset of human IDDM has been documented in a few cases (45, 46).

Coxsackievirus infection (perhaps of β cells themselves) may, in genetically susceptible individuals, initiate the characteristic autoimmune attack on pancreatic β cells. Viral peptides would then be presented to T lymphocytes, probably on the surface of antigen-presenting cells in the context of class II molecules. Although the sequences of both GADs suggest that they are cytosolic molecules, GAD polypeptides may be presented on the cell surface in the context of MHC molecules (as discussed in 47 and 48). Christie et al. (36), moreover, have demonstrated the association of the molecule we now know to be GAD_{65} with β cell membranes. GAD epitopes on the surface of β cells, in the context of either class I or class II molecules, could thus become the targets of immune responses initially directed against a Coxsackievirus epitope. The resultant destruction of β cells would then release more GAD_{65} and GAD_{67}, including GADs from the cytoplasm. The released GAD could then continue to stimulate lymphocytes already primed to the Coxsackievirus peptide, thus perpetuating the immune response long after the termination of the viral infection. This molecular mimicry would then lead to the continued autoimmune destruction of β cells and eventually to the development of clinical diabetes.

Assays for antibodies to recombinant GADs should allow a straightforward means of distinguishing IDDM from other forms of diabetes mellitus. This should be especially useful for evaluating adult patients presenting with the more common type II, non-insulin-dependent diabetes mellitus (NIDDM). Patients with true NIDDM do not have ICAs or autoantibodies to the 64,000 M_r protein or to insulin. Of adult onset patients initially diagnosed as having NIDDM, however, 10–15% are true type I (IDDM) diabetics and will eventually require insulin therapy.

Clinical trials are now under way to test the effectiveness of general immunosuppressive agents (such as cyclosporin and azathioprine) in delaying the onset of IDDM in individuals at high risk, that is, who already have islet cell autoantibodies

(49). Autoantibodies to GAD are the earliest indication of autoimmunity in IDDM and the two GADs are therefore excellent candidates for the initial targets for autoimmunity. Future experiments will determine whether the epitope shared by GAD and Coxsackievirus contributes to IDDM pathogenesis. If GAD is indeed involved in the etiology of IDDM, it may be possible to devise specific, rather than nonspecific, immunosuppressive strategies to block the function of specific MHC and T cell receptor molecules.

Acknowledgments

We thank the following people for helpful discussions and support: Bu Dingfang, Cheryl Craft, Chris Evans, Ken Pischel, Christian Ruppert, Richard Spielman, Niranjala Tillakaratne, Robert Weatherwax, Leslie Weiner, and Janis Young. We are especially grateful for the support and advice of Glen Evans.

This work was supported by grants from the National Institutes of Health to A. Tobin, M. Clare-Salzler, and N. Maclaren, and from the American Diabetes Association to N. Maclaren and M. Atkinson.

References

1. LaPorte, R., and K. Cruickshanks. 1988. Incidence and risk factors for insulin dependent diabetes mellitus. *In* Diabetes in America, National Diabetes Data Group. NIH Publication No. 85-1468. Chapter III, pp. 1–12.

2. Krolewski, A. S., J. H. Warram, L. I. Rand, and C. R. Kahn. 1987. Epidemiologic approach to the etiology of type I diabetes mellitus and its complications. *N. Engl. J. Med.* 317:1390–1398.

3. Castaño, L., and G. S. Eisenbarth. 1990. Type I-diabetes: a chronic autoimmune disease of human, mouse, and rat. *Annu. Rev. Immunol.* 8:647–679.

4. Sinha, A. A., M. T. Lopez, and H. O. McDevitt. 1990. Autoimmune diseases: the failure of self tolerance. *Science (Wash. DC).* 248:1380–1393.

5. Bottazzo, G. F., R. Pujol-Borrell, T. Hanafusa, and M. Feldman. 1983. Role of aberrant HLA-DR expression and antigen presentation in induction of endocrine autoimmunity. *Lancet.* ii:1115–1118.

6. Maclaren, N., D. Schatz, A. Drash, and G. Grave. 1989. The initial pathogenic events in insulin-dependent diabetes. *Diabetes.* 38:534–538.

7. Todd, J. A., H. Acha-Orbea, J. I. Bell, N. Chao, Z. Fronek, C. O. Jacob, M. McDermott, A. A. Sinha, L. Timmerman, L. Steinman, and H. O. McDevitt. 1988. A molecular basis for MHC class II autoimmunity. *Science (Wash. DC).* 240:1003–1009.

8. Todd, J. A. 1990. Genetic control of autoimmunity in type 1 diabetes. *Immunol. Today.* 11:122–129.

9. Olmos, P., R. A'Hern, D. A. Heaton, B. A. Millward, D. Risley, D. A. Pyke, and R. D. G. Leslie. 1988. The significance of the concordance rate for type 1 (insulin-dependent) diabetes in identical twins. *Diabetologia.* 31:747–750.

10. Gamble, D. R. 1980. The epidemiology of insulin dependent diabetes, with particular reference to the relationship of virus infection to its etiology. *Epidemiol. Rev.* 2:49–69.

11. Barrett-Connor, E. 1985. Is insulin-dependent diabetes mellitus caused by coxsackievirus B infection? a review of the epidemiologic evidence. *Rev. Infect. Dis.* 7:207–215.

12. Banatvala, J. E. 1987. Insulin-dependent (juvenile-onset, type 1) diabetes mellitus coxsackie B viruses revisited. *Prog. Med. Virol.* 34:33–54.

13. Baekkeskov, S., J. H. Nielsen, B. Marner, T. Bilde, J. Ludvigsson, and Å. Lernmark. 1982. Autoantibodies in newly diagnosed diabetic children immunoprecipitate human pancreatic islet cell proteins. *Nature (Lond.).* 298:167–169.

14. Baekkeskov, S., M. Landin, J. K. Kristensen, S. Srikanta, G. J. Bruining, T. Mandrup-Pousen, C. de Beaufort, J. S. Soeldner, G. Eisenbarth, F. Lindgren, et al. 1987. Antibodies to a 64,000 *M*, human islet cell antigen precede the clinical onset of insulin-dependent diabetes. *J. Clin. Invest.* 79:926–934.

15. Atkinson, M. A., N. K. Maclaren, D. W. Scharp, P. E. Lacy, and W. J. Riley. 1990. 64,000 *M*, autoantibodies as predictors of insulin-dependent diabetes. *Lancet.* 335:1357–1360.

16. Maclaren, N. K. 1988. How, when, and why to predict IDDM. *Diabetes.* 37:1591–1594.

17. Ziegler, A. G., R. D. Herskowitz, R. A. Jackson, J. S. Soeldner, and G. Eisenbarth. 1990. Predicting type I diabetes. *Diabetes Care.* 13:762–775.

18. Baekkeskov, S., T. Dyrberg, and Å. Lernmark. 1984. Autoantibodies to a 64-kilodalton islet cell protein precede the onset of spontaneous diabetes in the BB rat. *Science (Wash. DC).* 224:1348–1350.

19. Atkinson, M. A., and N. K. Maclaren. 1988. Autoantibodies in nonobese diabetic mice immunoprecipitate 64,000-*M*, islet antigen. *Diabetes.* 37:1587–1590.

20. Baekkeskov, S., H.-J. Aanstoot, S. Christgau, A. Reetz, M. Solimena, M. Cascalho, F. Folli, H. Richter-Olesen, and P. De Camilli. 1990. Identification of the 64K autoantigen in insulin-dependent diabetes as the GABA-synthesizing enzyme glutamic acid decarboxylase. *Nature (Lond.).* 347:151–156.

21. Erdö, S. L., and J. R. Wolff. 1990. γ-Aminobutyric acid outside the mammalian brain. *J. Neurochem.* 54:363–372.

22. Erlander, M. G., N. J. K. Tillakaratne, S. Feldblum, N. Patel, and A. J. Tobin. 1991. Two genes encode distinct glutamate decarboxylases with different responses to pyridoxal phosphate. *Neuron.* 7:91–100.

23. Kaufman, D. L., J. F. McGinnis, N. R. Krieger, and A. J. Tobin. 1986. Brain glutamate decarboxylase cloned in λ-gt-11: fusion protein produces γ-aminobutyric acid. *Science (Wash. DC).* 232:1138–1140.

24. Kobayashi, Y., D. L. Kaufman, and A. J. Tobin. 1987. Glutamic acid decarboxylase cDNA: nucleotide sequence encoding an enzymatically active fusion protein. *J. Neurosci.* 7:2768–2772.

25. Kaufman, D. L., C. R. Houser, and A. J. Tobin. 1991. Two forms of the γ-aminobutyric acid synthetic enzyme glutamate decarboxylase have distinct intraneuronal distributions and cofactor interactions. *J. Neurochem.* 56:720–723.

26. Riley, W. J., N. K. Maclaren, J. Krischer, R. P. Spillar, J. H. Silverstein, D. A. Schatz, S. Schwartz, J. Malone, S. Shah, C. Vadheim, and J. I. Rotter. 1990. A prospective study of the development of diabetes in relatives of patients with insulin-dependent diabetes. *N. Engl. J. Med.* 323:1167–1172.

27. Studier, F. W., and B. A. Moffatt. 1986. Use of bacteriophage T7 RNA polymerase to direct selective high-level expression of cloned genes. *J. Mol. Biol.* 189:113–130.

28. Saiki, R. K., D. H. Gelfand, S. Stoffel, S. J. Scharf, R. Higuchi, G. T. Horn, K. B. Mullis, and H. A. Erlich. 1988. Primer-directed enzymatic amplification of DNA with a thermostable DNA polymerase. *Science (Wash. DC).* 239:487–491.

29. Kozak, M. 1989. The scanning model for translation: an update. *J. Cell Biol.* 108:229–241.

30. Chang, Y. C., and D. I. Gottlieb. 1988. Characterization of the proteins purified with monoclonal antibodies to glutamic acid decarboxylase. *J. Neurosci.* 8:2123–2130.

31. Toniolo, A., T. Onodera, J.-W. Yoon, and A. L. Notkins. 1980. Induction of diabetes by cumulative environmental insults from viruses and chemicals. *Nature (Lond.).* 288:383–385.

32. Oldstone, M. B. A. 1987. Molecular mimicry and autoimmune disease. *Cell.* 50:819–820.

33. Oldstone, M. B. A. 1989. Molecular mimicry as a mechanism for the cause and as a probe uncovering etiologic agent(s) of autoimmune disease. *Curr. Top. Microbiol. Immunol.* 145:126–135.

34. Jenkins, O., J. D. Booth, P. D. Minor, and J. W. Almond. 1987. The complete nucleotide sequence of coxsackievirus B4 and its comparison to other members of the picornaviridae. *J. Gen. Virol.* 68:1835–1848.

35. Rorsman, P., P.-O. Berggren, K. Bokvist, H. Ericson, H. Möhler, C.-G. Östenson, and P. A. Smith. 1989. Glucose-inhibition of glucagon secretion involves activation of $GABA_A$-receptor chloride channels. *Nature (Lond.).* 341:233–236.

36. Christie, M. R., D. G. Pipeleers, Å. Lernmark, and S. Baekkeskov. 1990. Cellular and subcellular localization of an *M*, 64,000 protein autoantigen in insulin-dependent diabetes. *J. Biol. Chem.* 265:376–381.

37. Rabinowe, S. L., F. M. Brown, M. Watts, M. M. Kadrofske, and A. I. Vinik. 1989. Anti-sympathetic ganglia antibodies and postural blood pressure in IDDM subjects of varying duration and patients at high risk of developing IDDM. *Diabetes Care.* 12:1–6.

38. Duchen, L. W., N. A. Anjorin, P. J. Watkins, and J. D. Mackay. 1980. Pathology of autonomic neuropathy in diabetes mellitus. *Ann. Intern. Med.* 92:301–303.

39. King, M. L., A. Shaikh, D. Birdwell, A. Voller, and J. E. Banatvala. 1983. Coxsackie-B-virus-specific IgM responses in children with insulin-dependent (juvenile-onset; type 1) diabetes mellitus. *Lancet.* i:1397–1399.

40. Banatvala, J. E., G. Schernthaner, E. Schober, L. M. DeSilva, J. Byrant, M. Borkenstein, D. Brown, and M. A. Menser. 1985. Coxsackie B, mumps, rubella, and cytomegalovirus specific IgM responses in patients with juvenile-onset insulin-dependent diabetes mellitus in Britain, Austria and Australia. *Lancet.* i:1409–1412.

41. Toniolo, A., T. Onodera, G. Jordan, J.-W. Yoon, and A. L. Notkins. 1982. Glucose abnormalities produced in mice by the six members of the coxsackie B virus group. *Diabetes.* 31:496–499.

42. Yoon, J.-W., W. T. London, B. L. Curfman, R. L. Brown, and A. L. Notkins. 1986. Coxsackie Virus B_4 produces transient diabetes in nonhuman primates. *Diabetes.* 35:712–716.

43. Chatterjee, N. K., C. Nejman, and I. Gerling. 1988. Purification and characterization of a strain of coxsackievirus B4 of human origin that induces diabetes in mice. *J. Med. Virol.* 26:57–69.

44. Gerling, I., C. Nejman, and N. K. Chatterjee. 1988. Effect of Coxsackievirus B4 infection in mice on expression of 64,000-M_r autoantigen and glucose sensitivity of islets before development of hyperglycemia. *Diabetes.* 37:1419–1425.

45. Yoon, J.-W., M. Austin, T. Onodera, and A. L. Notkins. 1979. Virus induced diabetes mellitus. Isolation of a virus from the pancreas of a child with diabetic ketoacidosis. *N. Engl. J. Med.* 300:1173–1179.

46. Gladish, R., W. Hofmann, and R. Waldherr. 1976. Myokarditis und insulinitis nach coxsackie virus infect. *Z. Kardiol.* 65:835–849.

47. Germain, R. N. 1986. The ins and outs of antigen processing and presentation. *Nature (Lond.).* 322:687–689.

48. Nuchtern, J. G., J. S. Bonifacino, W. E. Biddision, and R. D. Klausner. 1989. Befeldin A implicates egress from endoplasmic reticulum in class I restricted antigen presentation. *Nature (Lond.).* 339:223–226.

49. Skyler, J. S., O. B. Crofford, J. Dupre, G. S. Eisenbarth, G. C. Sathman, E. A. M. Gale, D. Goldstein, J. T. Harmon, M. W. Haymond, R. A. Jackson, et al. 1990. Prevention of type I diabetes mellitus. *Diabetes.* 39:1151–1152.

Human Desmocollin 1 (Dsc1) Is an Autoantigen for the Subcorneal Pustular Dermatosis Type of IgA Pemphigus

Takashi Hashimoto,* Chie Kiyokawa,* Osamu Mori,* Minoru Miyasato,* Martyn A. J. Chidgey,† David R. Garrod,† Yasushi Kobayashi,‡ Koji Komori,‡ Ken Ishii,‡ Masayuki Amagai,‡ and Takeji Nishikawa‡

*Department of Dermatology, Kurume University School of Medicine, Fukuoka, Japan, †Epithelial Morphogenesis Research Group, University of Manchester, Manchester, U.K.; and ‡Department of Dermatology, Keio University School of Medicine, Tokyo, Japan

IgA pemphigus showing IgA anti-keratinocyte cell surface autoantibodies is divided into subcorneal pustular dermatosis (SPD) and intraepidermal neutrophilic IgA dermatosis (IEN) types. We previously showed by immunoblotting that IgA from some IgA pemphigus patients reacted with bovine desmocollins (Dsc), but not human Dsc. To determine the antigen for IgA pemphigus, we focused on conformation-dependent epitopes of Dsc, because sera of patients with classical pemphigus recognize conformation-sensitive epitopes of desmogleins. We constructed mammalian expression vectors containing the entire coding sequences of human Dsc1, Dsc2, and Dsc3 and transiently transfected them into COS7 cells by lipofection. Immunofluorescence of COS7 cells transfected with single human Dscs showed that IgA antibodies of all six SPD-type IgA pemphigus cases reacted with the surface of cells expressing Dsc1, but not with cells expressing Dsc2 or Dsc3. In contrast, none of seven IEN-type IgA pemphigus cases reacted with cells transfected with any Dscs. These results convincingly indicate that human Dsc1 is an autoantigen for SPD-type IgA pemphigus, suggesting the possibility of an important role for Dsc1 in the pathogenesis of this disease. This study shows that a Dsc can be an autoimmune target in human skin disease. ***Key words: autoimmune bullous disease/desmosome/keratinocyte/mammalian cell transfection. J Invest Dermatol 109:127–131, 1997***

Desmosomal cadherins are of two types, desmoglein (Dsg) and desmocollin (Dsc), both of which occur as three isoforms, Dsg1, 2, and 3 and Dsc1, 2, and 3, derived from different genes (Buxton *et al*, 1993; Amagai *et al*, 1995). Each Dsc gene produces two alternatively spliced products, the longer "a" form and the shorter "b" form, i.e., Dsc1a and Dsc1b.

Classical pemphigus, characterized by the presence of IgG anti-keratinocyte cell surface autoantibodies in the sera, consists of two major subtypes, pemphigus vulgaris (PV) and pemphigus foliaceus (PF). Brazilian PF is endemic in South America and shows features similar to PF. Extensive studies of these diseases have revealed that the autoantigen for PF and Brazilian PF is Dsg1 (Stanley *et al*, 1986; Hashimoto *et al*, 1990; Koch *et al*, 1990; Amagai *et al*, 1995) and for PV is Dsg3 (Hashimoto *et al*, 1990, Stanley *et al*, 1982; Amagai *et al*, 1991). Recently, a number of cases with anti-cell surface antibodies of the IgA class and showing distinct clinical features have been reported (Ebihara *et al*, 1991; Iwatsuki *et al*, 1991). Although various terms have been used for these conditions, we will use the most simple term, IgA pemphigus, throughout this report. IgA pemphigus is divided into two subtypes, intraepidermal neutrophilic IgA dermatosis (IEN) type, showing pustule formation through the entire depth of the epidermis (Huff *et al*, 1985; Teraki *et al*, 1991), and subcorneal pustular dermatosis (SPD) type, showing pustules in the upper epidermis (Tagami *et al*, 1983, Hashimoto *et al*, 1987).

We have sought the target antigens for the IgA anti-keratinocyte cell surface autoantibodies of IgA pemphigus and found that certain IgA pemphigus sera recognized bovine Dsc (Ebihara *et al*, 1991; Iwatsuki *et al*, 1991). The significance of this finding, however, was unclear, because no IgA pemphigus sera reacted human Dsc by immunoblotting. We speculated that the cause of this failure may be that the IgA pemphigus sera react with conformation-dependent epitopes on Dsc because most pathogenic autoantibodies recognize conformation-sensitive epitopes of desmogleins in PV and PF (Amagai *et al*, 1994, 1995; Emery *et al*, 1995). The widely used technique of immunoprecipitation is able to detect such conformation-dependent epitopes on IgG antibodies. A technique for immunoprecipitation with IgA antibodies, however, has not been established.

In the current study, to detect antibodies to native Dsc molecules, we constructed mammalian expression vectors containing the entire coding sequence of human Dsc1, Dsc2, or Dsc3 and transfected them into COS7 cells by lipofection. We found that IgA in the sera of SPD type, but not IEN type, reacted with Dsc1. This study shows that human Dsc can be a target autoantigen in human

Manuscript received February 26, 1997; revised May 14, 1997; accepted for publication May 22, 1997.

Reprint requests to: Dr. Takashi Hashimoto, Department of Dermatology, Kurume University School of Medicine, 67 Asahimachi, Kurume, Fukuoka 830, Japan.

Abbreviations: Dsg, desmoglein; Dsc, desmocollin; PV, pemphigus vulgaris; PF, pemphigus foliaceus; IEN, intraepidermal neutrophilic IgA dermatosis; SPD, subcorneal pustular dermatosis; mAb, monoclonal antibody; pAb, polyclonal antibody

0022-202X/97/$10.50

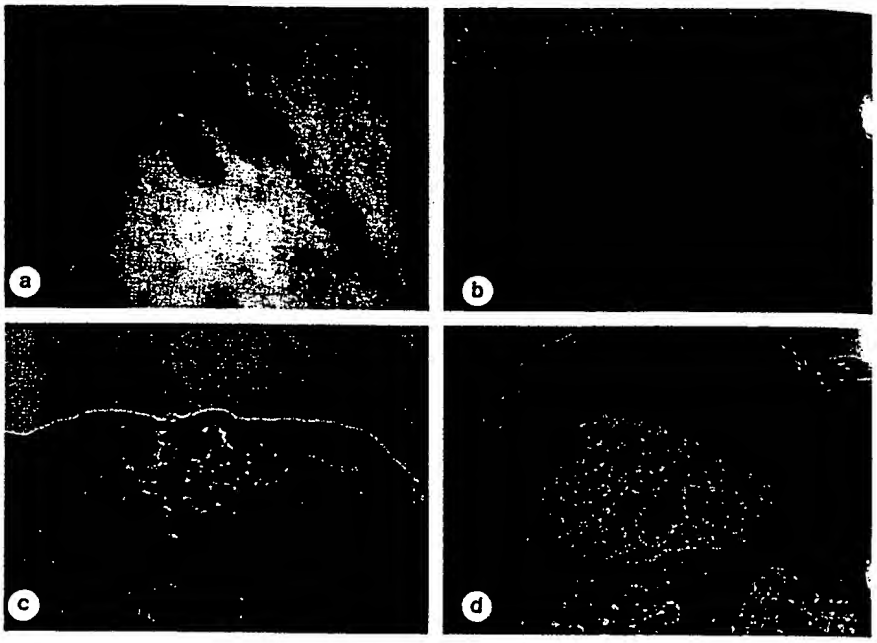

Figure 1. Clinical and histopathologic features are distinct between SPD and IEN types of IgA pemphigus. A patient of SPD type IgA pemphigus clinically showed superficial pustules *(a)*. A patient of IEN type showed different cutaneous lesions with deeper pustules *(b)*. A patient of SPD type histopathologically showed subcorneal pustule formation *(c)*. A patient of IEN type showed pustule formation in the entire epidermis *(d)*. *Scale bar*, 30 μm.

skin disease and also suggests an important insight into the pathogenesis of IgA pemphigus.

MATERIALS AND METHODS

Sera We selected 13 typical cases with IgA pemphigus (six SPD type and seven IEN type). All the patients of SPD type showed SPD-like clinical features of superficial pustules (**Fig 1*a***) and histopathologically subcorneal pustule formation in the upper epidermis (**Fig 1*c***). In contrast, all the patients of IEN type showed deeper vesiculo-pustular skin lesions, occasionally characterized by sunflower-like arrangement (**Fig 1*b***), and pustule formation in the entire epidermis (**Fig 1*d***).

Sera obtained from three patients each with PV and PF as well as from five normal volunteers were used as controls. All sera were stored at −30°C or −80°C as aliquots and used immediately after thawing because IgA may be less stable than IgG.

Antibodies Anti-Dsg monoclonal antibody (mAb) 32–2B (Vilela *et al*, 1987) and anti-Dsc mAb 52–3D (Collins *et al*, 1991) were characterized previously. Polyclonal antibody (pAb) JCMC was obtained by immunizing a rabbit with a recombinant bovine Dsc1-specific peptide (North *et al*, 1996). pAbs D1K2 and C+DGII were obtained by immunizing rabbits with peptides specific to human Dsc1 and Dsc2, respectively (Suzuki *et al*, manuscript in preparation).

Kawamura *et al* (1994) have recently isolated a novel human Dsc cDNA, which was tentatively designated human Dsc4. By comparison of human Dsc sequences with bovine Dsc sequences that are taken as standards (Collins *et al*, 1991; Parker *et al*, 1992; King *et al*, 1993; Theis *et al*, 1993; Troyanovsky *et al*, 1993; Kawamura *et al*, 1994; Legan *et al*, 1994; Yue *et al*, 1995), this is now re-designated human Dsc3. pAb LNCF3 was obtained by immunizing a rabbit with a human Dsc3-specific peptide (Suzuki *et al*, manuscript in preparation). The pAbs D1K2, C+DGII, and LNCF3 were generous gifts from Tadaaki Suzuki, Kazuo Kawamura, and Susumu Tsurufuji (Institute of Cytosignal Research, Inc.).

Preparation of Mammalian Cell Expression Constructs of Human Dsc1, 2, and 3 and Transfection into COS7 Cells To prepare a construct of human Dsc1, we used cDNA clones K24 (King *et al*, 1993) and K55 (King, 1994) (generous gifts from Dr. R.S. Buxton and Dr. I.A. King, Laboratory of Eukaryotic Molecular Genetics, National Institute for Medical Research, Mill Hill, London, U.K.). K24 contains almost the entire coding sequence except for the N-terminal end, and K55 contains the N-terminal region including the ATG initiation codon. To obtain cDNA covering the entire coding sequence, we utilized the *Acc*I sites at nucleotide 1494 in human Dsc1 and within the multiple cloning site of pBluescript II SK . The 3.0-kbp fragment excised from K24 by *Acc*I digestion, which contains the C-terminal region of Dsc1, was subcloned into *Acc*I-digested K55, and a clone with the proper orientation, designated K24/K55, was selected. The *Bam*HI/*Xba*I-digested fragment of K24/K55 containing the entire coding sequence of human Dsc1 was subcloned into the eukaryotic expression vector pcDNAI/Amp (Invitrogen Corp., San Diego, CA) previously digested with *Bam*HI/*Xba*I. A clone designated pcDNAI-hDsc1 was selected and propagated.

To prepare a construct of human Dsc2, the entire coding sequence was obtain by *Eco*RI digestion from pPB192 (a generous gift from Dr. R.S. Buxton and Dr. I.A. King), which is a pBluescript vector carrying the L5 clone (Parker *et al*, 1992). This cDNA fragment was subcloned into *Eco*RI-digested pcDNAI/Amp, and a clone with the proper orientation, designated pcDNAI-hDsc2, was selected.

pcDNAI-hDsc1 and pcDNAI-hDsc2 allow the expression of full-length cDNA inserts of human Dsc1 and Dsc2 under the control of the cytomegalovirus promoter.

Preparation of human Dsc3 cDNA (a generous gift from Tadaaki Suzuki, Kazuo Kawamura, and Susumu Tsurufuji) subcloned into the eukaryotic expression vector, pcDL-SRa296, was previously described (Kawamura *et al*, 1994). This clone allows the expression of a full-length human Dsc3 cDNA insert under the control of the simian virus early promoter, SRa (Kawamura *et al*, 1994; Takabe *et al*, 1988). All three clones produced "a" form (longer form) of each Dsc species.

Transient transfection of COS7 cells using lipofectAMIN reagent (Life Technologies, Gaithersburg, MD) was carried out according to the manufacturer's recommendations.

Immunofluorescence Immunofluorescence of normal human skin sections was performed by a standard method (Beutner *et al*, 1968) using fluorescein-conjugated anti-human IgG (specific to γ-chains), anti-human IgA (specific to α-chains), anti-mouse Igs, and anti-rabbit Igs antisera (DAKO, Glostrup, Denmark) as secondary antibodies.

Immunofluorescence of unfixed COS7 cells transiently transfected with Dsc1, 2, or 3 cDNAs was performed by the method of Stanley *et al* (1982). The cells cultured on coverglasses were first incubated at 4°C for 30 min in phosphate-buffered saline containing 1% bovine serum albumin and 0.1% NaN_3 to reduce background and membrane fluidity, respectively. The cells were incubated for 1 h at 4°C with patients' sera or specific antibodies diluted in the same buffer and subsequently with second antibodies conjugated with either FITC or rhodamine. For double labeling, the cells were incubated with a mixture of diluted sera and rabbit anti-Dsc pAb and subsequently with mixture of fluorescein-conjugated anti-human IgA antiserum and rhodamine-conjugated anti-rabbit Ig antiserum (DAKO). In some experiments, the cells were fixed and permeabilized by treatment with 100% methanol for 20 min at −20°C before immunostaining.

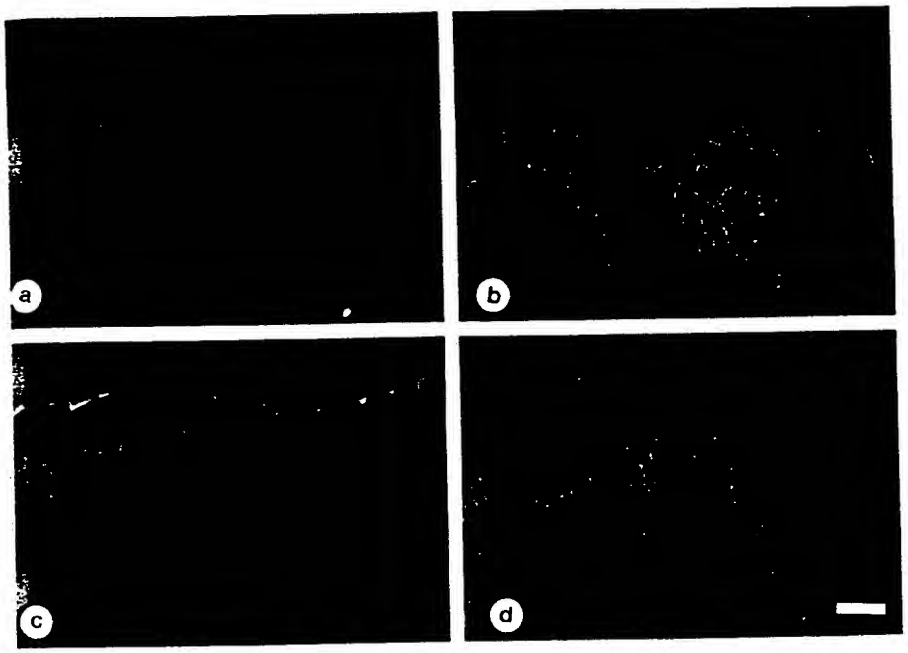

Figure 2. Immunofluorescence of normal human skin sections for anti-Dsc pAbs and IgA pemphigus sera suggested that SPD and IEN types may react with Dsc1 and Dsc3, respectively. Anti-Dsc1 peptide pAb JCMC stained keratinocyte cell surfaces in the upper epidermis *(a)*, whereas anti-Dsc3 peptide pAb LNCF3 stained cell surfaces in the entire epidermis *(b)*. A SPD type IgA pemphigus serum stained the uppermost epidermis *(c)*, and an IEN type IgA pemphigus serum stained the entire epidermis *(d)*. *Scale bar*, 30 μm.

Immunoblot Analysis of Normal Human Epidermal Extracts, Bovine Desmosome Preparations, and Extracts of COS7 Cells Transfected with Dsc1, 2, and 3 Preparation of extracts of normal human epidermis separated by dispase treatment, partial purification of desmosomes from bovine snout epidermis, and procedures for electrophoresis and immunoblotting were described previously (Hashimoto *et al*, 1990; Ebihara *et al*, 1991). All peroxidase-conjugated anti-human IgG (specific to γ-chains), anti-human IgA (specific to α-chains), anti-mouse Igs, and anti-rabbit Ig antisera used as secondary antibodies were obtained from DAKO.

COS7 cells transiently expressing Dsc1, 2, and 3 were lysed with Laemmli's sample buffer (Laemmli, 1970) and subjected to electrophoresis. Immunoblotting was performed by the same method as for epidermal extracts or desmosome preparations.

RESULTS

Immunofluorescence of Normal Human Skin Sections Suggested that SPD and IEN Types of IgA Pemphigus May React with Dsc1 and Dsc3, Respectively With immunofluorescence of normal human skin sections, anti-Dsc1 peptide pAbs (JCMC and D1K2) stained keratinocyte cell surfaces in the upper epidermis but not the keratinized layer (**Fig 2*a***). By contrast, pAb against Dsc3 peptides (LNCF3) stained cell surfaces at all levels in the epidermis except the keratinized layer (**Fig 2*b***). The reactivity of the anti-Dsc2 pAb C+DGII was very weak and stained cell surfaces of the spinous layer nearly down to the basal layer in normal skin, staining in the upper layers being much stronger. All

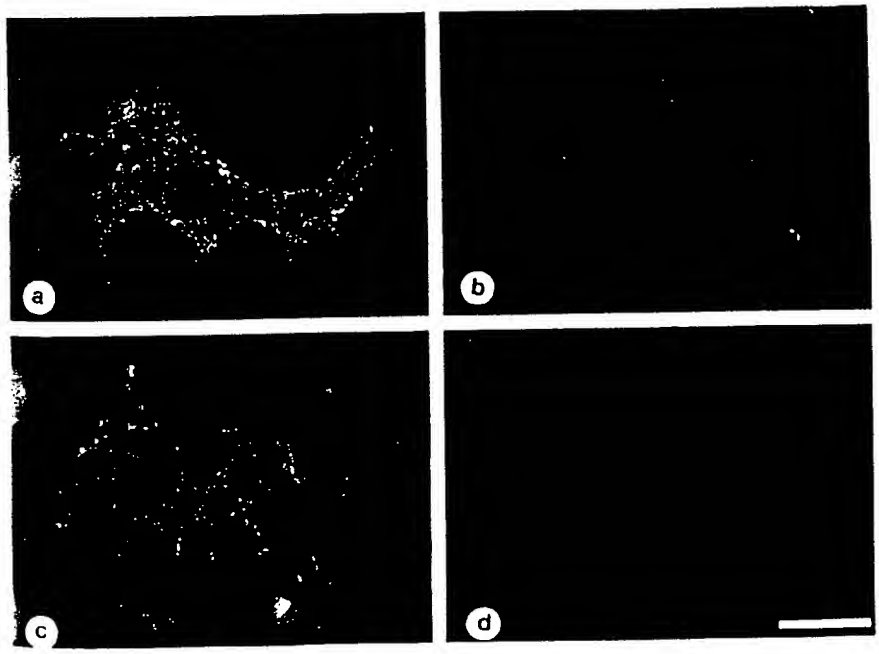

Figure 3. Immunofluorescence of COS7 cells transfected with human Dsc1, 2, or 3 indicated that the autoantigen for SPD type IgA pemphigus is Dsc1. A SPD type IgA pemphigus serum clearly stained cell surface of COS7 cells transfected with Dsc1 in a granular pattern *(a)*, whereas an IEN type IgA pemphigus serum showed no reactivity *(b)*. With double immunostaining, IgA antibodies in a SPD type of IgA pemphigus serum *(c)* and anti-Dsc1 pAb JCMC *(d)* showed exactly the same staining pattern. *Scale bar*, 30 μm.

Table I. Immunofluorescence of Various Antibodies and Sera with Normal Epidermal Sections and Dsc1-3-Transfected COS7 cells

Antibodies and Sera	(No.)	Section of Epidermis	COS7 Cells with Dsc1	Dsc2	Dsc3
mAB 52-3D		(+) all layers	+	+	+
pAb JCMC		(+) upper layers	+	−	−
pAb D1K2		(+) upper layers	+	−	−
pAb C+DGII		(+) upper-mid layers	−	+	−
pAb LNCF3		(+) all layers	−	−	+
SPD type IgA pemphigus	(6)	(+) upper layers	6	0	0
IEN type IgA pemphigus	(7)	(+) all layers	0	0	0
PV	(3)	(+) lower layers	0	0	0
PF	(3)	(+) all layers	0	0	0
Normal	(5)	(−)	0	0	0

the sera of patients with SPD-type IgA pemphigus stained the upper epidermis (Fig 2*c*), resembling the pattern for Dsc1, whereas all the sera from patients with IEN-type IgA pemphigus stained the entire epidermis (Fig 2*d*), resembling staining for Dsc3. All the IgA pemphigus sera contained autoantibodies of IgA class, but not IgG class. All the results are summarized in Table I.

Immunoblotting of Epidermal Extracts and Desmosome Preparations Showed Controversial Results We first examined the reactivity of anti-Dsc autoantibodies of the IgA class by immunoblot analyses using both normal human epidermal extracts and bovine snout desmosome preparations and then compared their reactivities with those of anti-Dsc mAb or pAbs.

With immunoblotting of bovine desmosome preparations, the anti-Dsc mAb, 52–3D, and the rabbit pAbs against Dsc1, 2, and 3 peptides reacted with two protein bands of approximately 115 kDa and 105 kDa (data not shown, but see Ebihara *et al*, 1991). The IgA antibodies in the sera of three cases with SPD type and two cases with IEN type also reacted with a doublet of proteins showing similar mobilities to those recognized by the anti-Dsc antibodies. With immunoblotting of normal human epidermal extracts, none of the IgA pemphigus sera showed specific reactivity, whereas PV and PF sera reacted with the 130-kDa Dsg3 and the 160-kDa Dsg1 polypeptides, respectively, both of which were also recognized by the 32–2B anti-Dsg mAb. The 110-kDa and 100-kDa human Dscs were recognized by the 52–3D mAb (data not shown). The normal control sera showed no specific reactivity with immunoblotting of either antigen source.

Immunofluorescence of COS7 Cells Transfected with Human Dsc1, 2, or 3 Indicated That the Autoantigen for SPD-type IgA Pemphigus Is Dsc1 When COS7 cells transiently transfected with human Dsc1, 2, and 3 cDNAs were stained without fixation, the transfected cells reacted with pAbs specific to each Dsc: i.e., Dsc1 with JCMC and D1K2 pAbs, Dsc2 with C+DGII, and Dsc3 with LNCF3. No cross-reactivity was observed (data not shown). The positive cells, approximately 10% of the population, showed clear granular staining on the cell surface. Because 52–3D mAb reacts with the cytoplasmic domain of Dscs, the cells were permeabilized by treatment with 100% methanol. This mAb reacted with COS7 cells transfected with each of the three Dscs.

The IgA antibodies in all six sera of SPD-type IgA pemphigus reacted with COS7 cells expressing Dsc1 (Fig 3*a*), but none of the seven sera of the IEN type showed this reactivity (Fig 3*b*). The IgA antibodies in both types of IgA pemphigus did not react with either Dsc2 or Dsc3. IgG antibodies in three serum samples of SPD-type IgA pemphigus were examined, but no staining was observed in the Dsc-transfected cells. Neither IgG nor IgA in any control PV, PF, or normal sera showed reactivity. All the results are summarized in Table I.

When the COS7 cells were stained simultaneously with SPD-type IgA pemphigus serum and anti-Dsc1 pAb JCMC, the cell stained with the patient's IgA were also stained with the pAb (Fig 3*c,d*). The staining intensity of both the IgA pemphigus sera and anti-Dsc1 pAb, however, was considerably reduced, suggesting that the patient's IgA reacts with a region similar to that recognized by the pAb and interferes with the reactivity of the pAb by steric hindrance.

To examine the possibility that IgA of IEN-type IgA pemphigus may react with intracytoplasmic domain of Dsc3, the cells permeabilized by 100% methanol treatment were also examined. None of the seven IEN-type IgA pemphigus sera, however, stained cell surfaces of Dsc3-transfected COS7 cells, although considerable background staining made the staining a little obscure (data not shown).

Immunoblotting of Lysates of COS7 Cells Transfected with Human Dsc1, 2, or 3 Confirmed That All the Dsc1–3 cDNA Clones Expressed Each Molecule with a Proper Size With immunoblotting of the lysate of COS7 cells transfected with human Dsc1, 2, or 3 cDNAs, proteins of approximately 100 kDa were detected by pAb specific for each Dsc. In Fig 4, *lane 1* is for standard molecular weight markers. *Lane 2* shows the lysate of Dsc1-transfected cells stained with anti-Dsc1 pAb JCMC; *lane 3* shows the lysate of Dsc2-transfected cells stained with pAb C+DGII, and *lane 4* shows the lysate of Dsc3-transfected cells stained with mAb 52–3D. The pAb LNCF3 reacted with the same protein band in the Dsc3-transfected cell lysate. No Dsc protein was detected by pAb specific to other isoforms of Dsc, confirming the specificity of each pAb. Whereas a single protein band was recognized in Dsc2- and Dsc3-transfected COS7 cells, however, a doublet of protein bands as well as lower protein bands was detected in Dsc1-transfected cells *(lane 2)*. The reason for this reactivity is not known. These protein bands could be accounted for by unprocessed precursor or breakdown product. It is not likely that these bands represent "a" and "b" forms of Dsc, because the cells were transfected with cDNA. The same proteins were also recognized by the 52–3D mAb (data not shown). The Dscs expressed in COS7 cells, however, were not detected by IgA antibodies in any IgA pemphigus sera (data not shown).

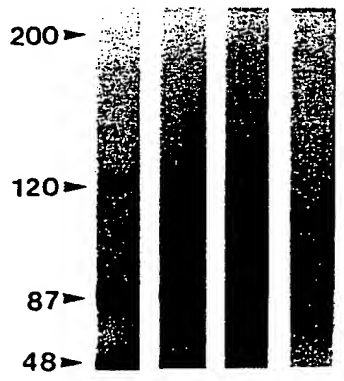

Figure 4. Immunoblotting of lysates of COS7 cells transiently transfected with human Dsc1, 2, or 3 confirmed that all the Dsc1–3 cDNA clones expressed each molecule with correct size. *Lane 1* is for standard molecular mass markers, indicating the positions of 200 kDa, 120 kDa, 87 kDa, and 48 kDa from top to bottom. *Lane 2* shows the lysate of Dsc1-transfected cells stained with anti-Dsc1 pAb JCMC; *lane 3* shows the lysate of a Dsc2-transfected cells stained with pAb C+DGII; and *lane 4* shows the lysate of a Dsc3-transfected cells stained with mAb 52–3D.

DISCUSSION

Immunofluorescence of normal human skin sections showed that IgA antibodies in sera of IEN-type IgA pemphigus bind to the keratinocyte cell surfaces at all levels in the epidermis, whereas IgA in sera of SPD-type IgA pemphigus bind only to the upper epidermis. The staining pattern of the SPD-type sera was very similar or identical to that shown by anti-Dsc1 pAbs. This suggested that sera of SPD-type IgA pemphigus might contain autoantibodies against Dsc1.

We have shown, with immunofluorescence of non-fixed COS7 cells expressing human Dsc1, 2, or 3, that all the sera of SPD-type IgA pemphigus reacted with Dsc1, but none of the sera of IEN type showed this reactivity. IgA antibodies in both types of IgA pemphigus reacted with neither Dsc2 nor Dsc3. The most likely reason, therefore, for the failure to detect human Dsc with immunoblotting of human epidermal extracts is that these epitopes on Dsc molecules may be altered by extraction, isolation, and immunoblotting procedures.

These results convincingly show that human Dsc1 is an autoantigen for SPD-type IgA pemphigus, which may therefore play an important role in the pathogenesis of this disease. This study also shows that a human Dsc can be a target antigen for an autoimmune blistering skin disease.

We initiated this study because we found that some IgA pemphigus sera react with bovine Dsc molecules in immunoblotting. It is still not clear, however, why some IgA pemphigus sera reacted with bovine, but not human, Dsc under these conditions. It may be that greater amounts of Dsc proteins were obtained in the bovine desmosome preparations than in extracts of human epidermis. Alternatively, it may be that bovine desmosomal glycoproteins retain more of their normal conformation on immunoblots because of some undefined species difference. The autoantibodies would then react with epitopes in the bovine desmosomes while similar epitopes disrupted in blotted human glycoproteins.

We anticipated that sera of IEN-type IgA pemphigus might react with Dsc3, because the staining pattern in human epidermis was similar to that of anti-Dsc3 pAb. This study does not indicate, however, that the target antigen for IEN-type IgA pemphigus is Dsc. Our previous immuno-electron microscopic study also indicated that the antigen for IEN type is not present in desmosomes (Akiyama *et al*, 1992). Therefore, it is plausible that the antigen for the IEN type is not a desmosomal protein. The results of this study reinforce the view that distinct antigen profiles are responsible for the clinico-pathologic differences between the IEN and SPD types of IgA pemphigus.

Although the target antigen of these IgA autoantibodies has been identified, their pathogenic role has not been directly confirmed. This question should now be resolved using the mouse model, as has been done for pemphigus autoantibodies. This study also shows that immunofluorescence using cells transfected with cDNA encoding possible antigen proteins is a useful method for defining antigens whose epitopes are conformation-dependent and so cannot be detected with conventional immunoblotting.

We are grateful to Dr. Roger S. Buxton and Dr. Ian A. King, Laboratory of Eukaryotic Molecular Genetics, National Institute for Medical Research, Mill Hill, London, U.K., for providing the cDNA clones of human Dsc1 and Dsc2. We also thank Tadaaki Suzuki, Kazuo Kawamura, and Susumu Tsurufuji, Institute of Cytosignal Research, Inc., Tokyo, Japan, for the cDNA clone for human Dsc3 and polyclonal antibodies to human Dsc1–3. This work was supported by Grant-in-Aid for Scientific Research from the Ministry of Education, Science and Culture of Japan (04454289), a grant from the Ministry of Health and Welfare of Japan, and a Collaboration Research Project of the British Council, Tokyo, Japan.

REFERENCES

Akiyama M, Hashimoto T, Sugiura M, Nishikawa T: Ultrastructural localization of autoantigens of intercellular IgA vesiculopustular dermatosis in cultured human squamous cell carcinoma cells. *Arch Dermatol Res* 284:371–3, 1992

Amagai M, Klaus-Kovtun V, Stanley JR: Autoantibodies against a novel epithelial cadherin in pemphigus vulgaris, a disease of cell adhesion. *Cell* 67:869–877, 1991

Amagai M, Hashimoto T, Shimizu T, Nishikawa T: Absorption of pathogenic autoantibodies by the extracellular domain of pemphigus vulgaris antigen (Dsg3) produced by baculovirus. *J Clin Invest* 94:59–67, 1994

Amagai M, Hashimoto T, Green K, Shimizu N, Nishikawa T: Antigen-specific immunoadsorption of pathogenic autoantibodies in pemphigus foliaceus. *J Invest Dermatol* 104:895–901, 1995

Amagai M: Adhesion molecules. I: Keratinocyte-keratinocyte interactions; Cadherins and pemphigus. *J Invest Dermatol* 104:146–152, 1995

Beutner EH, Jordon RE, Chorzelski TP: The immunopathology of pemphigus and bullous pemphigoid. *J Invest Dermatol* 51:63–80, 1968

Buxton RS, Cowin P, Franke WW, Garrod DR, Green KJ, King IA, Koch PJ, Magee AI, Rees DA, Stanley JR, Steinberg MS: Nomenclature of the desmosomal cadherins. *J Cell Biol* 121:481–483, 1993

Collins JE, Legan PK, Kenny TP, MacGarvie J, Holton JL, Garrod DR: Cloning and sequence analysis of desmosomal glycoproteins 2 and 3 (desmocollins): cadherin-like desmosomal adhesion molecules with heterogenous cytoplasmic domains. *J Cell Biol* 113:381–391, 1991

Ebihara T, Hashimoto T, Iwatsuki K, Takigawa M, Ando M, Ohkawara A, Nishikawa T: Autoantigens for IgA anti-intercellular antibodies of intercellular IgA vesiculopustular dermatosis. *J Invest Dermatol* 97:742–745, 1991

Emery DJ, Diaz LA, Fairley JA, Lopez A, Taylor AF, Giudice GJ: Pemphigus foliaceus and pemphigus vulgaris autoantibodies react with the extracellular domain of desmoglein-1. *J Invest Dermatol* 104:323–328, 1995

Hashimoto T, Inamoto N, Nakamura K, Nishikawa T: Intercellular IgA dermatosis with clinical features of subcorneal pustular dermatosis. *Arch Dermatol* 123:1062, 1987

Hashimoto T, Ogawa MM, Konohana A, Nishikawa T: Detection of pemphigus vulgaris and pemphigus foliaceus antigens by immunoblot analysis using different antigen sources. *J Invest Dermatol* 94:327–331, 1990

Huff JC, Golitz LE, Kunke KS: Intraepidermal neutrophilic IgA dermatosis. *N Engl J Med* 313:1643, 1985

Iwatsuki K, Hashimoto T, Ebihara T, Teraki Y, Nishikawa T, Kaneko F:Intercellular IgA vesiculo-pustular dermatosis and related disorders: diversity of IgA anti-intercellular autoantibodies. *Eur J Dermatol* 3:7–11, 1991

Kawamura K, Watanabe K, Suzuki T, Yamakawa T, Kamiyama T, Nakagawa H, Tsurufuji S: cDNA cloning and expression of novel human desmocollin. *J Biol Chem* 269:26295–26302, 1994

King IA, Arnemann J, Spurr NK, Buxton RS: Cloning of the cDNA (DSC1) coding for human type 1 desmocollin and its assignment to chromosome 18. *Genomics* 18:185–194, 1993

King IA: Identification of the ATG initiation codon in human type 1 desmocollin. *J Invest Dermatol* 102:822, 1994

Koch PJ, Walsh MJ, Schmelz M, Goldschmidt MD, Zimbelmann R, Franke WW: Identification of desmoglein, a constitutive desmosomal glycoprotein, as a member of the cadherin family of cell adhesion molecules. *Eur J Cell Biol* 53:1–12, 1990

Kowalczyk AP, Anderson JE, Borgwardt JE, Hashimoto T, Stanley JR, Green K.J: Pemphigus sera recognize conformationally sensitive epitopes in the amino-terminal region of desmoglein-1 (Dsg1). *J Invest Dermatol* 105:147–152, 1995

Laemmli UK: Cleavage of structural proteins during the assembly of the head of bacteriophage T4. *Nature* 227:680–685, 1970

Legan PK, Yue KKM, Chidgey MAJ, Holton JL, Wilkinson RW, Garrod DR: The bovine desmocollin family: a new gene and expression patterns reflecting cell proliferation and differentiation. *J Cell Biol* 126:507–518, 1994

North AJ, Chidgey MAJ, Clarke JP, Bardsley WG, Garrod DR: Distinct desmocollin isoforms occur in the same desmosomes and show reciprocally graded distributions in bovine nasal epidermis. *Proc Natl Acad Sci USA* 93:7701–7705, 1996

Parker AE, Wheeler GN, Arnemann J, Pidsley SC, Ataliotis P, Thomas CL, Rees DA, Magee AI, Buxton RS: Desmosomal glycoproteins II and III: cadherin-like junctional molecules generated by alternative splicing. *J Biol Chem* 266:10438–10445, 1992

Stanley JR, Yaar M, Hawley-Nelson P, Katz SI: Pemphigus antibodies identify a cell surface glycoprotein synthesized by human and mouse keratinocytes. *J Clin Invest* 70:281–288, 1982

Stanley JR, Koulu L, Klaus-Kovtun V, Teinberg MS: A monoclonal antibody to the desmosomal glycoprotein desmoglein I binds the same polypeptide as human autoantibodies in pemphigus foliaceus. *J Immunol* 136:1227–1230, 1986

Tagami H, Iwatsuki K, Iwase Y, Yamada M: Subcorneal pustular dermatosis with vesiculo-bullous eruption: demonstration of subcorneal IgA deposits and a leukocyte chemotactic factor. *Br J Dermatol* 109:581–587, 1983

Takabe Y, Seiki M, Fujisawa J, Hoy P, Yokota K, Arai K, Yoshida M, Arai N: SRa promoter: an efficient and versatile mammalian cDNA expression system composed of the simian virus 40 early promoter and the R-U5 segment of human T-cell leukemia virus type 1 long terminal repeat. *Mol Cell Biol* 8:466–472, 1988

Teraki Y, Amagai M, Hashimoto T, Kusunoki T, Nishikawa T: Intercellular IgA dermatosis of childhood. selective deposition of monomer IgA1 in the intercellular space of the epidermis. *Arch Dermatol* 127:221–224, 1991

Theis DG, Koch PJ, Franke WW: Differential synthesis of type 1 and type 2 desmocollin mRNA in human stratified epithelia. *Int J Dev Biol* 37:101–110, 1993

Troyanovsky SM, Eshkind LG, Troyanovsky RB, Leube RE, Franke WW: Contributions of cytoplasmic domains of desmosomal cadherins to desmosome assembly and intermediate filament anchorage. *Cell* 72:561–574, 1993

Vilela MJ, Parrish EP, Wright DH, Garrod DR: Monoclonal antibody to desmosomal glycoprotein 1—A new epithelial marker for diagnostic pathology. *J Pathol* 153:365–375, 1987

Yue KKM, Holton JL, Clarke JP, Hyam JLM, Hashimoto T, Chidgey MAJ, Garrod DR: Characterization of a desmocollin isoform (bovine Dsc3) exclusively expressed in lower layers of stratified epithelia. *J Cell Sci* 108:2163–2173, 1995

Brief Definitive Report

The Synaptic Vesicle-associated Protein Amphiphysin Is the 128-kD Autoantigen of Stiff-Man Syndrome with Breast Cancer

By Pietro De Camilli,*‡ Annette Thomas,*‡ Roxanne Cofiell,*‡ Franco Folli,* Beate Lichte,§ Giovanni Piccolo,‖ Hans-Michael Meinck,¶ Mario Austoni,** Giuliano Fassetta,‡‡ Gianfranco Bottazzo,§§ David Bates,‖‖ Niall Cartlidge,‖‖ Michele Solimena,*‡ and Manfred W. Kilimann§

*From the *Department of Cell Biology and ‡Howard Hughes Medical Institute, Yale University School of Medicine, New Haven, Connecticut 06510; the §Institüt für Physiologische Chemie, D-W-4630 Bochum 1, Germany; the **Istituto Neurologico Mondino, Universita' di Pavia, 27100 Pavia, Italy; the ¶Neurologische Klinik, University of Heidelberg, D44780 Heidelberg, Germany; the **Istituto di Semeiotica Medica, University of Padova, 35100 Padova, Italy; the ‡‡Divisione Neurologica, Ospedale di Belluno, 32100 Belluno, Italy; the §§Department of Immunology, London Hospital Medical College, London E1, 2AD, United Kingdom; and the ‖‖Department of Neurology, Royal Victoria Infirmary, Newcastle upon Tyne NE1, 4LP, United Kingdom*

Summary

Stiff-Man syndrome (SMS) is a rare disease of the central nervous system (CNS) characterized by progressive rigidity of the body musculature with superimposed painful spasms. An autoimmune origin of the disease has been proposed. In a caseload of more than 100 SMS patients, 60% were found positive for autoantibodies directed against the GABA-synthesizing enzyme glutamic acid decarboxylase (GAD). Few patients, all women affected by breast cancer, were negative for GAD autoantibodies but positive for autoantibodies directed against a 128-kD synaptic protein. We report here that this antigen is amphiphysin. GAD and amphiphysin are nonintrinsic membrane proteins that are concentrated in nerve terminals, where a pool of both proteins is associated with the cytoplasmic surface of synaptic vesicles. GAD and amphiphysin are the only two known targets of CNS autoimmunity with this distribution. This finding suggests a possible link between autoimmunity directed against cytoplasmic proteins associated with synaptic vesicles and SMS.

Stiff-Man syndrome (SMS) is a rare human central nervous system (CNS) disease, characterized by chronic rigidity of the body musculature with superimposed painful spasms (1). It is thought to result from an impairment of inhibitory pathways that control motor neuron activity (2–4). It was previously suggested that SMS may have an autoimmune pathogenesis. 60% of the patients affected by this condition are positive in their serum and cerebrospinal fluid (CSF) for autoantibodies directed against the GABA-synthesizing enzyme glutamic acid decarboxylase (GAD) (5–8). In our current caseload of 119 patients referred to us with a clinical diagnosis of SMS, 72 were found positive for these autoantibodies (Guarnaccia, J., M. Solimena, K. Marek, and P. De Camilli, unpublished observations). In the SMS patient subpopulation positive for GAD autoantibodies, a frequent occurrence of insulin-dependent diabetes mellitus and of other organ-specific autoimmune diseases is observed (6, 7).

We have recently described three female patients with SMS and breast cancer and no signs of organ-specific autoimmune diseases. These three patients (referred to henceforth as patients BC-SMS 1, 2, and 3, respectively) were negative for GAD autoantibodies but were positive for autoantibodies directed against a 128-kD neuronal antigen concentrated at synapses (9). We have now identified a fourth patient with both breast cancer and SMS syndrome. This patient (BC-SMS 4), as well, was positive for autoantibodies to the 128-kD protein (this study). The characterization of this autoantigen is crucial to the elucidation of pathogenetic mechanisms in SMS with breast cancer.

Recently, a novel synaptic vesicle-associated protein, amphiphysin, was described (10). This protein was identified by screening a chicken brain λgt11 library with antibodies raised against chicken brain synaptic proteins. Amphiphysin, an acidic protein present in chicken as well as in mammalian nervous tissue, was shown by immunocytochemistry to be concentrated in nerve terminals. A large fraction of am-

J. Exp. Med. © The Rockefeller University Press • 0022-1007/93/12/2219/05 $2.00
Volume 178 December 1993 2219–2223

phiphysin is present in cytosolic fractions of brain homogenates but a pool of the protein is recovered in a tightly bound form in highly purified synaptic vesicles, although the protein is not enriched on these organelles (10). Some of the properties of amphiphysin were reminiscent of the properties of the 128-kD antigen (10). Therefore, a detailed comparison of the characteristics of the two proteins was performed. We report here that the 128-kD antigen is amphiphysin.

Materials and Methods

Materials. Three sera of SMS patients affected by breast cancer were previously described (9). These sera, defined BC-SMS 1, 2, and 3, correspond to sera of patients 1, 2, and 3, respectively, of reference 9. Serum BC-SMS 4 is from a new patient with both conditions. A GAD autoantibody-positive human serum is from our caseload of SMS sera (6, 8). Rabbit polyclonal antibodies directed against a β-galactosidase chicken amphiphysin fusion protein were previously described (10). These antibodies were shown to recognize rat amphiphysin (10). Rabbit sera directed against synaptophysin (11) and GAD (serum no. 6799 (12)) were the kind gift of Dr. R. Jahn (Yale University, New Haven, CT), and Drs. Z. Katarova and G. Szabo (Hungarian Academy of Sciences, Szeged, Hungary), respectively. Small-scale lysates of bacteria expressing β-galactosidase fusion proteins were prepared according to reference 13. βTC3 and αTC9 cell lines were the kind gift of Drs. D. Hanahan (University of California, San Francisco, CA), S. Efrat (Albert Einstein College of Medicine, New York, New York), and E. Leiter (Jackson Laboratories, Bar Harbor, ME), and PC12 cells were the gift of Dr. L. Greene (Columbia University, New York).

Western Blotting of One- and Two-dimensional Gels. Total rat brain homogenate was prepared as described (6, 14). Postnuclear supernatants of rat tissues and of cell lines were prepared by homogenization in 10 vol of ice-cold 10 mM Hepes buffer, pH 7.4, containing freshly added protease inhibitors (0.1 mM PMSF, 1 μg/ml each of antipain, leupeptin, aprotinin, and pepstatin A) followed by centrifugation at 1,000 *g* for 10 min at 4°C. For two-dimensional gels, this supernatant (S1) was centrifuged at 170,000 *g* for 2 h at 4°C and the resulting supernatant was analyzed by the procedure described by O'Farrell et al. (15) and modified by Ames and Nikaico (16). Western blotting was performed as described (6, 14) using ^{125}I–protein A. Patient sera were used at the dilution of 1:250.

Cell Fractionation and Triton X-114 Phase Separation. A postnuclear supernatant of rat brain (S1) was prepared as described above. S1 was centrifuged at 36,000 *g* for 30 min at 4°C. The resulting supernatant (S2) was separated into particulate (P3) and cytosolic (S3) fractions by centrifugation at 170,000 *g* for 2 h at 4°C. P3 and S3 were extracted in 2% Triton X-114, and insoluble material was removed by centrifugation at 20,000 *g* for 30 min at 4°C. The soluble material was separated into detergent (D) and aqueous (A) phases as described (17). Volumes loaded in each lane were normalized so that corresponding aliquots of supernatants and pellets (or detergent and aqueous phases) were loaded for each pair of fractions.

Immunoprecipitation. A soluble fraction of rat brain (S3) prepared as described above was extracted in ice-cold 2% Triton X-100, 150 mM NaCl, 10 mM Hepes, pH 7.4, for 2 h. Insoluble material was removed by centrifugation at 20,000 *g* for 30 min at 4°C. The resulting supernatant was diluted with an equal volume of 150 mM NaCl, 10 mM Hepes, pH 7.4 (buffer A), to a final protein concentration of 1 mg/ml. 900-μl aliquots of extract were precleared as described (5) and used for each immunoprecipitation. For immunoprecipitation, the following additions were made in sequential order: (*a*) 25 μl human sera (16 h); (*b*) 20 μl rabbit anti-human IgGs (1.5 h); and (*c*) 125 μl 50% protein A–Sepharose in buffer A (1.5 h). All incubations were performed at 4°C with rotation. Immunoprecipitated material was recovered and analyzed by Western blotting as described (14).

Results and Discussion

Fig. 1 shows Western blots of total rat brain homogenate demonstrating that the 128-kD antigen, i.e., the protein recognized by the sera of BC-SMS patient (lanes *1–3*), has the same electrophoretic mobility in SDS-PAGE as the protein recognized by rabbit serum (lane *4*) and affinity-purified antibodies (lane *5*) raised against a chicken amphiphysin fusion protein. Chicken amphiphysin was calculated to have a molecular mass of 75,204 daltons, but in SDS-PAGE runs, it had an apparent molecular mass of 115–125 kD (10). This molecular mass is very similar to the one of 128 kD estimated here for the rat protein. Fig. 2 shows that the 128-kD antigen and amphiphysin have an identical isoelectric point of 4.7 in two-dimensional gels. This isoelectric point is similar to the predicted isoelectric point of 4.4, calculated on the basis of the amino acid composition of chicken amphiphysin (10).

The distribution of the 128-kD antigen and of amphiphysin were compared in the course of subcellular fractionation of brain homogenates. As shown in Fig. 3, *a* and *b*, both the autoantigen and amphiphysin were present in roughly equal amounts in a cytosolic fraction (S3) and in a particulate fraction (P3) obtained from rat brain. Synaptophysin, an intrinsic membrane protein of synaptic vesicles, was present exclusively in the particulate fraction (P3) (Fig. 3 *c*), demonstrating that the centrifugation conditions used were sufficient to sediment all membranes. Membrane-bound amphiphysin was previously shown to be recovered in the aqueous phase after Triton X-114 extraction and phase separation (10). As shown in Fig. 3, *a* and *b*, both the 128-kD antigen and amphiphysin were completely solubilized by Triton X-114 and were recovered exclusively in the aqueous phase irrespectively of whether the extraction was performed on P3 or S3 (Fig. 3, *a* and *b*). The effectiveness of phase separation conditions was confirmed by the presence of the bulk of synaptophysin (a protein with

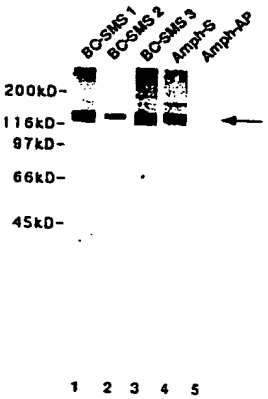

Figure 1. The 128-kD antigen and amphiphysin have identical electrophoretic mobilities in SDS gels. Western blots of total rat brain homogenate probed with sera of three BC-SMS patients and rabbit antiamphiphysin antibodies (lane *4*, crude serum [*Amph-S*]; lane *5*, affinity-purified antibodies [*Amph-AP*]). The 128-kD antigen is indicated by an arrow. The single band of amphiphysin and of the 128-kD antigen visible in this gel can be resolved in a doublet of two closely spaced bands under different electrophoresis conditions (9, 10).

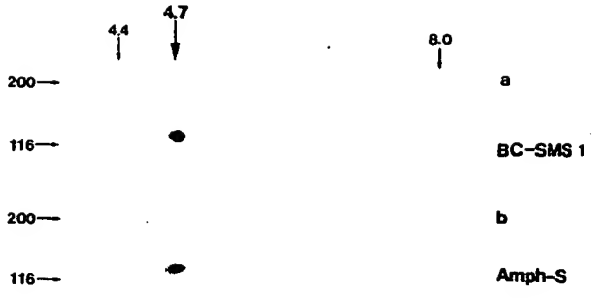

Figure 2. The 128-kD antigen and amphiphysin have identical electrophoretic mobilities in two-dimensional gels. Western blot of two-dimensional gels of a soluble rat brain fraction probed with BC-SMS 1 serum (*a*) and rabbit antiamphiphysin serum (*b*). Numbers at the top indicate isoelectric points, numbers at the left indicate molecular mass markers (in kD).

four transmembrane regions (18)) in the detergent phase obtained from P3 (Fig. 3 *c*).

The 128-kD antigen and amphiphysin were found to be immunologically cross-reactive. To prove that antiamphiphysin antibodies recognize the 128-kD antigen, BC-SMS patient sera were used to immunoprecipitate the 128-kD antigen from soluble extracts of rat brain. The presence of amphiphysin in the immunoprecipitate was then analyzed by Western blotting using antiamphiphysin serum. An immunoreactive band with electrophoretic mobility of 128 kD was detected (Fig. 4 *a*, lanes *1–3*) while no GAD was recovered in the same immunoprecipitates (Fig. 4 *b*, lanes *1–3*) confirming previous

Figure 3. The 128-kD antigen and amphiphysin partition similarly in differential centrifugation and Triton X-114 phase separation. Particulate (P_3) and cytosolic (S_3) fractions of rat brain were extracted in Triton X-114 and centrifuged to obtain a soluble (*sol*) and an insoluble (*ins*) fraction. The Triton X-114–soluble material (lanes *3* and *8*) was separated into detergent (*D*; lanes *4* and *9*) and aqueous (*A*; lanes *5* and *10*) phases. The fractions were probed by immunoblotting with antiamphiphysin affinity-purified antibodies (*Amph-AP*), with BC-SMS 1 serum (*BC-SMS 1*), and with antisynaptophysin serum (*Synapt-S*). The 128-kD antigen and amphiphysin were recovered in both the cytosolic (S3) and in the particulate (P3) fractions, and exclusively in the Triton X-114 aqueous phase derived from these fractions. Synaptophysin, which is an integral membrane protein with four transmembrane spanning domains, is recovered only in P3 and primarily in the detergent phase derived from the Triton X-114–soluble material obtained from P3.

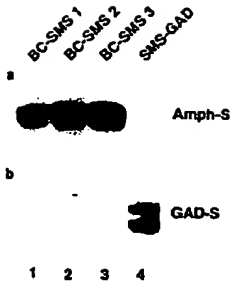

Figure 4. BC-SMS patient sera immunoprecipitate amphiphysin from rat brain extracts. Immunoprecipitates obtained with the sera of three BC-SMS patients (lanes *1–3*) and with the serum of a SMS patient positive for GAD autoantibodies (*SMS-GAD*) (lane *4*) were separated by SDS-PAGE. (*a*) Immunoblotted with rabbit antiamphiphysin serum (*Amph-S*); and (*b*) immunoblotted with the rabbit anti-GAD serum no. 6799 (*GAD-S*) (12).

results (9). As a control, immunoprecipitation was performed with a SMS patient serum that contained high-titer anti-GAD antibodies (6, 8), but no antibodies against the 128-kD autoantigen. This immunoprecipitate was positive for GAD (Fig. 4 *b*, lane *4*), but not for amphiphysin (Fig. 4 *a*, lane *4*). Conversely, a protein of 128 kD was detected when an immunoprecipitate obtained with antiamphiphysin serum was immunoblotted with BC-SMS patient sera (not shown). To

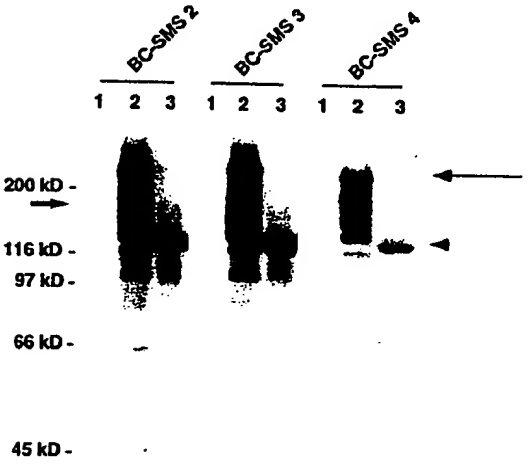

Figure 5. BC-SMS patient sera recognize recombinant amphiphysin. Western blots of three identical gel triplets reacted with sera BC-SMS 2, 3, and 4, as indicated. Lanes *1*, bacterial lysate expressing a 165-kD fusion protein of β-galactosidase with a yet unidentified synaptic protein (clone 10.12.1; B. Lichte, and M.W. Kilimann, unpublished observation). Lanes *2*, bacterial lysate expressing a β-galactosidase–chicken amphiphysin fusion protein (clone amphy-11.3; fusion protein size ~230 kD) (10). Lanes *3*, chicken brain total homogenate. Identical results were obtained with serum BC-SMS 1 (not shown). Long and short arrows indicate the mobilities of the chicken amphiphysin fusion protein and of the control fusion protein, respectively. Bands below the major immunopositive bands of lanes *2* most likely represent proteolytic fragments of the fusion protein. An arrowhead points to chicken brain amphiphysin.

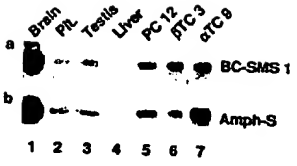

Figure 6. The 128-kD antigen and amphiphysin have the same tissue distribution. Western blot of postnuclear supernatants of rat tissues (brain, pituitary, testis, liver) and endocrine cell lines (PC12 cells [rat chromaffin cell line]; βTC3 cells [mouse insulinoma]; αTC9 [mouse glucagonoma]) probed with either BC-SMS patient serum (*BC-SMS 1*) or antiamphiphysin serum (*Amph-S*).

conclusively demonstrate that BC-SMS sera recognize amphiphysin, they were tested against bacterial lysates containing recombinant amphiphysin as shown in Fig. 5. BC-SMS sera labeled a β-galactosidase–chicken amphiphysin fusion protein (Fig. 5, lanes *2*) and chicken brain amphiphysin (Fig. 5, lanes *3*), but not a control fusion protein (Fig. 5, lanes *1*).

Amphiphysin was previously shown to have a restricted tissue distribution (10). Amphiphysin mRNA was detected at high levels in brain and at lower levels in adrenal gland. By immunoblotting amphiphysin was detected in the anterior and posterior pituitary as well (10). The expression of amphiphysin was compared with that of the 128-kD antigen in a variety of tissues and cell lines using Western blotting. Fig. 6 shows that the serum of a BC-SMS patient and the rabbit serum directed against amphiphysin label a similar protein in brain, pituitary, and cell lines derived from adrenal chromaffin cells (PC12 cells) and from pancreatic α and β cells (αTC9, βTC3) (19, 20) but not in liver. Presence of amphiphysin in all cells of pancreatic islets was confirmed by immunocytochemistry (not shown). Endocrine cells of the anterior pituitary, adrenal medulla, and pancreatic islets have many biochemical and functional similarities to neurons and contain organelles closely related to neuronal synaptic vesicles (21, 22). In addition, both amphiphysin and the 128-kD antigen were detected in the testis (Fig. 6). By immunocytochemistry with BC-SMS sera, amphiphysin immunoreactivity in the testis was found to be confined to germ cells. All germ cells expressed amphiphysin irrespective of their stage of differentiation (from spermatogonia to mature spermatozoa) (not shown). Previously, amphiphysin mRNA could not be detected in chicken testis (10), but this was probably so because the RNA had been purified from immature testis of 7-d-old animals. It should be noted that GAD as well is expressed in male germ cells (23).

These data convincingly demonstrate that the 128-kD antigen is amphiphysin. Amphiphysin contains in its sequence a hydrophobic 21–amino acid region that would be competent to form a transmembrane helix (10). However, the recovery of amphiphysin both in soluble and membrane fractions (10) as well as the presence of a pool of the protein detectable by immunocytochemistry throughout the neuronal cytoplasm (9) indicate that amphiphysin is not an intrinsic membrane protein. Like amphiphysin, GAD, the other major autoantigen of SMS, is concentrated in nerve terminals where it interacts with synaptic vesicles but is not an intrinsic membrane protein (14, 24–26). While GAD is expressed only by GABA-secreting neurons, amphiphysin is not restricted to these neurons (9, 10).

The similar subcellular localization of GAD and amphiphysin is intriguing if one considers that they are the only two known targets of CNS autoimmunity with this distribution. This observation raises the possibility that pathogenetic mechanisms in SMS may be linked to CNS autoimmunity directed against presynaptic components that interact with synaptic vesicles. Autoantibodies directed against GAD and amphiphysin are not likely to be directly pathogenetic because antibodies are not thought to have access to the cytoplasmic compartment. They may represent the dominant autoantibody species in the context of an autoimmune response directed against multiple antigens (27), including proteins exposed at the cell surface that may be the pathogenetic targets of the autoimmune response. Alternatively, these autoantibodies may reflect an autoimmune reaction in which T cells are the primary players. GAD and amphiphysin autoantibodies segregate with two SMS patient subpopulations, each characterized by different associated diseases. GAD autoantibody–positive SMS is often associated with organ-specific autoimmune diseases and primarily insulin-dependent diabetes mellitus (3–7). Amphiphysin autoantibody–positive SMS occurs only in association with cancer (9) and has the characteristics of an autoimmune paraneoplastic syndrome (28, 29). Therefore, the two patterns of autoimmunity are likely to be related to these different associated conditions. Further studies of antiamphiphysin autoimmunity and of the function of amphiphysin or amphiphysin-related molecules not only may shed some light on pathogenetic mechanisms in SMS, but may also help in the elucidation of the biology of at least some types of cancer. Although amphiphysin was not detected in breast cancer tissue (9), it will be of interest to determine whether amphiphysin-related proteins are expressed in breast cancer.

We thank Drs. J. Guarnaccia and K. Marek (New Haven, CT) for reviewing our case load of SMS patients; Drs. D. Hanahan (San Francisco, CA), S. Efrat (New York, NY), E. Leiter (Bar Harbor, ME), L. Greene (New York, NY), Z. Katarova, and G. Szabo (Szeged, Hungary) for the gift of cell lines and antibodies; and Dr. C. David (New Haven, CT) for critical reading of the manuscript.

This work was supported by grants from the National Institutes of Health and by a McKnight Research Project Award (P. De Camilli) and by the Fonds der Chemischen Industrie (M. W. Kilimann). F. Folli was supported by a Dottorato di Ricerca (University of Milano), M. Solimena by the Sydney Blackmer

Muscular Dystrophy Association fellowship and by a fellowship from the Juvenile Diabetes Foundation, and A. Thomas by a predoctoral National Institute for Mental Health fellowship. M. W. Kilimann is a Heisenberg Fellow of the Deutsche Forschungsgemeinschaft.

Address correspondence to Pietro De Camilli, Howard Hughes Medical Istitute, Department of Cell Biology, Boyer Center for Molecular Medicine, 295 Congress Avenue, New Haven, CT 06536-0812. F. Folli's permanent address is the Department of Medicine, Istituto Scientifico S. Raffaele, Via Olgettina 60, 20100 Milano, Italy, and his present address is the Joslin Diabetes Center, Harvard Medical School, 1 Joslin Place, Boston, MA 02215. B. Lichte's present address is the Institut für Biologie III, Universitat Freiburg, D-W-7800, Freiburg, Germany.

Received for publication 8 June 1993 and in revised form 4 August 1993.

References

1. Moersch, F.P., and H.W. Woltman. 1956. Progressive fluctuating muscular rigidity and spasm ("stiff-man" syndrome): report of a case and some observations in 13 other cases. *Mayo Clin. Proc.* 31:421.
2. Gordon, E.E., D.M. Januszko, and L. Kaufman. 1967. A critical survey of Stiff-man syndrome. *Am. J. Med.* 42:582.
3. McEvoy, K.M. Stiff-man syndrome. 1991. *Mayo Clin. Proc.* 66:300.
4. Blum, P., and J. Jankovic. 1991. Stiff-person syndrome: an autoimmune disease. *Movement Dis.* 6:12.
5. Solimena, M., F. Folli, S. Denis-Donini, G.C. Comi, G. Pozza, P. De Camilli, and A.M. Vicari. 1988. Autoantibodies to glutamic acid decarboxylase in a patient with Stiff-man syndrome, epilepsy, and type I diabetes mellitus. *N. Engl. J. Med.* 318:1012.
6. Solimena, M., F. Folli, R. Aparisi, G. Pozza, and P. De Camilli. 1990. Autoantibodies to GABA-ergic neurons and pancreatic beta-cells in Stiff-man syndrome. *N. Engl. J. Med.* 322:1555.
7. Solimena, M., and P. De Camilli. 1991. Autoimmunity to glutamic acid decarboxylase (GAD) in stiff-man syndrome and insulin-dependent diabetes mellitus. *Trends Neurosci.* 14:452.
8. Butler, M., M. Solimena, R. Dirkx, A. Hayday, and P. De Camilli. 1993. Identification of a dominant epitope of glutamic acid decarboxylase (GAD-65) recognized by autoantibodies in Stiff-Man syndrome. *J. Exp. Med.* 178:2097.
9. Folli, F., M. Solimena, R. Cofiell, M. Austoni, G. Tallini, G. Fassetta, D. Bates, N. Cartlidge, G.F. Bottazzo, G. Piccolo, and P. De Camilli. 1993. Autoantibodies to a 128kD synaptic protein in three women with the Stiff-man syndrome and breast cancer. *N. Engl. J. Med.* 328:546.
10. Lichte, B., R.W. Veh, H.E. Meyer, and M.W. Kilimann. 1992. Amphiphysin, a novel protein associated with synaptic vesicles. *EMBO (Eur. Mol. Biol. Organ.) J.* 11:2521.
11. Navone, F., R. Jahn, G. Di Gioia, H. Stukenbrok, P. Greengard, and P. De Camilli. 1986. Protein p38: an integral membrane protein specific for small vesicles of neurons and neuroendocrine cells. *J. Cell Biol.* 103:2511.
12. Katarova, Z., G. Szabo, E. Mugnaini, and R.J. Greenspan. 1989. Molecular identification of the 62 kD form of glutamic acid decarboxylase from the mouse. *Eur. J. Neurosci.* 2:190.
13. Carroll, S.B., and A. Laughon. 1987. DNA Cloning. Vol. III. D.M. Glover, editor. IRL Press Ltd., Eynsham, UK. 89–111.
14. Reetz, A., M. Solimena, M. Matteoli, F. Folli, K. Takei, and P. De Camilli. 1991. GABA and pancreatic β-cells: colocalization of glutamic acid decarboxylase (GAD) and GABA with synaptic-like microvesicles suggests their role in GABA storage and secretion. *EMBO (Eur. Mol. Biol. Organ.) J.* 10:1275.
15. O'Farrell, P.A., H. Goodman, and P.H. O'Farrell. 1977. Resolution of two dimensional electrophoresis of basic, as well as, acidic proteins. *Cell.* 12:1133.
16. Ames, B.F., and K. Nikaico. 1976. Two-dimensional gel electrophoresis of membrane proteins. *Biochemistry.* 15:616.
17. Bordier, C. 1981. Phase separation of integral membrane proteins in Triton X-114 solution. *J. Biol. Chem.* 256:1604.
18. Sudhof, T.C., F. Lottspeich, P. Greengard, E. Mehl, and R. Jahn. 1987. A synaptic vesicle protein with a novel cytoplasm domain and four transmembrane regions. *Science (Wash. DC).* 238:1142.
19. Efrat, S., S. Linde, H. Kofod, D. Spector, M. Delannoy, S. Grant, D. Hanahan, and S. Baekkeskov. 1988. Beta-cells derived from transgenic mice expressing a hybrid insulin gene-oncogene. *Proc. Natl. Acad. Sci. USA.* 85:9037.
20. Hamaguchi, K., and E.H. Leiter. 1990. Comparison of cytokine effects on mouse alpha-cell and beta-cell lines. *Diabetes.* 39:415.
21. De Camilli, P., and R. Jahn. 1990. Pathways to regulated exocytosis in neurons. *Annu. Rev. Physiol.* 52:625.
22. De Camilli, P. 1991. Co-secretion of multiple signal molecules from endocrine cells via distinct exocytotic pathways. *Trends Pharmacol. Sci.* 12:446.
23. Persson, H., M. Pelto-Huikko, and M. Metsis. 1990. Expression of the neurotransmitter synthesizing enzyme glutamic acid decarboxylase in male germ cells. *Mol. Cell. Biol.* 10:4701.
24. Erlander, M.G., N.J.K. Tillakaratne, S. Feldblum, N. Patel, and A.J. Tobin. 1991. Two genes encode distinct glutamate decarboxylases. *Neuron.* 7:91.
25. Christgau, S., H.-J. Aanstoot, H. Schierbeck, K. Begley, S. Tulin, K. Hejnaes, and S. Baekkeskov. 1992. Membrane anchoring of the autoantigen GAD 65 to microvesicles in pancreatic beta-cells by palmitoylation in the NH_2-terminal domain. *J. Cell Biol.* 118:309.
26. Solimena, M., D. Aggujaro, C. Muntzel, R. Dirkx, M. Butler, P. De Camilli, and A. Hayday. 1993. Association of GAD-65, but not of GAD-67, with the Golgi complex of transfected Chinese hamster ovary cells mediated by the N-terminal region. *Proc. Natl. Acad. Sci. USA.* 90:3073.
27. Tan, E. M. 1991. Autoantibodies in pathology and cell biology. *Cell.* 67:841.
28. Posner, J.B., and H.M. Furneaux. 1990. Paraneoplastic syndromes. *In* Immunologic Mechanisms in Neurologic and Psychiatric Disease. Research Publications: Association for Research in Nervous and Mental Disease. Vol. 68. B.H. Waksman, editor. Raven Press, Ltd., New York. 187–219.
29. Hetzel, D.J., C.R. Stanhope, O'Neill, and V.A. Lennon. 1990. Gynecologic cancer in patients with subacute cerebellar degeneration predicted by anti-Purkinje cell antibodies and limited in metastatic volume. *Mayo Clin. Proc.* 65:1558.

Autoantibodies to Glutamate Receptor GluR3 in Rasmussen's Encephalitis

Scott W. Rogers,* P. Ian Andrews, Lorise C. Gahring, Teri Whisenand, Keith Cauley, Barbara Crain, Thomas E. Hughes, Stephen F. Heinemann, James O. McNamara

Rasmussen's encephalitis is a progressive childhood disease of unknown cause characterized by severe epilepsy, hemiplegia, dementia, and inflammation of the brain. During efforts to raise antibodies to recombinant glutamate receptors (GluRs), behaviors typical of seizures and histopathologic features mimicking Rasmussen's encephalitis were found in two rabbits immunized with GluR3 protein. A correlation was found between the presence of Rasmussen's encephalitis and serum antibodies to GluR3 detected by protein immunoblot analysis and by immunoreactivity to transfected cells expressing GluR3. Repeated plasma exchanges in one seriously ill child transiently reduced serum titers of GluR3 antibodies, decreased seizure frequency, and improved neurologic function. Thus, GluR3 is an autoantigen in Rasmussen's encephalitis, and an autoimmune process may underlie this disease.

Rasmussen's encephalitis is a rare, progressive, catastrophic disease of unknown pathogenesis that begins in the first decade of life, affecting previously normal children (*1*). The disease affects the cortex of a single cerebral hemisphere, resulting in intractable seizures, hemiparesis, and dementia. The diagnosis is established by these typical clinical features, together with hemispheric atrophy and a characteristic inflammatory histopathology (*1*, *2*). Treatment of the incapacitating seizures with conventional anticonvulsants is of limited benefit. Surgical removal of the affected hemisphere is the standard therapy. Glutamate and related amino acids are the predominant excitatory neurotransmitters in the mammalian central nervous system (CNS) (*3*) and have been implicated in neurodegenerative diseases and epilepsy. To generate subtype-specific antibodies to recombinant GluR proteins, we immunized rabbits with bacterially expressed *trpE* gene fusion proteins that included a portion of the putative extracellular domain of GluR1, 2, 3, 5, or 6 or the putative cytoplasmic domain of subunits (β4) of the neuronal nicotinic acetylcholine receptor (nAChR) family (*4*).

After four immunizations with GluR3 fusion protein, two rabbits developed high titers of GluR3 antibodies, anorexia, and behaviors characteristic of seizures, consisting of brief periods of immobilization, unresponsiveness, and repetitive clonic movements. One rabbit had severely lacerated its tongue, suggestive of tongue biting during a seizure. By contrast, no behavioral abnormalities were seen in another rabbit immunized with GluR3 fusion protein or in any of more than 50 rabbits injected with fusion proteins containing GluR1, 2, 5, or 6 or neuronal nAChR subunits, although high titers of the appropriate antibodies were observed (*4*). Gross examination of the brains of the symptomatic, GluR3-immunized rabbits disclosed no abnormality. However, microscopic examination disclosed inflammatory changes consisting of microglial nodules and perivascular lymphocytic infiltration mainly, but not exclusively, in the cerebral cortex, together with lymphocytic infiltration of the meninges (Fig. 1). Microscopic examination of the brain of the asymptomatic rabbit immunized with GluR3 fusion protein disclosed no abnormality. We reasoned that the rabbits' symptoms and inflammatory CNS histopathology probably represented an autoimmune process directed against GluR3, on the basis of the immunization history, the occurrence of symptoms only in GluR3-immunized rabbits, and the similar distribution of inflammatory pathology in these animals and GluR3 mRNA in normal animals (*5*). The occurrence of disease in some, but not all, GluR3-immunized rabbits is similar to the incidence of autoimmune myasthenia gravis in mice immunized with nAChR (*6*).

These symptomatic rabbits resembled individuals with Rasmussen's encephalitis. Common features include (i) recurrent seizures (*1*); (ii) inflammatory histopathology, characterized by meningeal and perivascular lymphocytic infiltrates and microglial nodules (Fig. 1) (*2*); and (iii) predominant

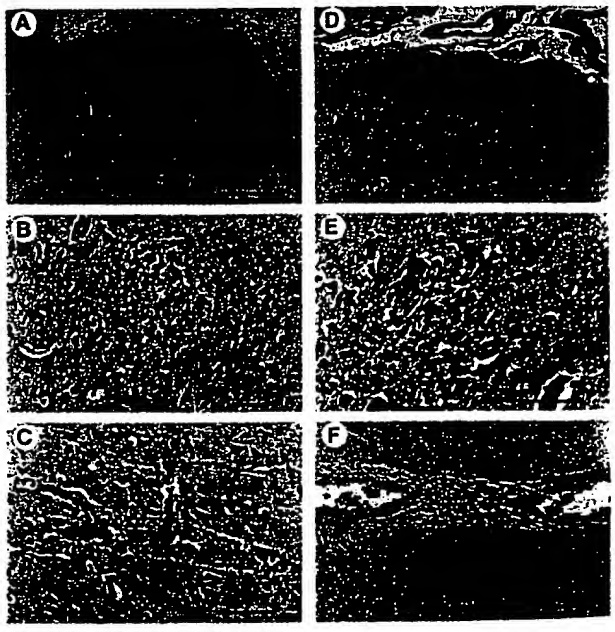

Fig. 1. Characteristic histopathology of neocortex of one symptomatic rabbit immunized with GluR3 (**A** through **C**) and comparable sections from resected temporal lobe of individual AI (**D** through **F**). (A) and (D) Neocortex with meningeal lymphocytic infiltrate (arrow) and a microglial nodule (double arrow). Bars are 200 μm. (B) and (E) Microglial nodules from (A) and (D). Bars are 50 μm. (C) and (F) Perivascular lymphocytic cuffing from entorhinal cortex in the rabbit and amygdala in individual AI. Bars are 100 μm.

S. W. Rogers, Salt Lake City Geriatric Research, Education, and Clinical Center, Veterans Affairs Medical Center; Human Molecular Biology and Genetics Program; and Department of Neurobiology and Anatomy; University of Utah, Salt Lake City, UT 84112, USA.
P. I. Andrews, Departments of Pediatrics and Medicine (Neurology), Duke University Medical Center, Durham, NC 27710, USA.
L. C. Gahring, Salt Lake City Geriatric Research, Education, and Clinical Center, Veterans Affairs Medical Center; Human Molecular Biology and Genetics Program; and Division of Human Development and Aging; University of Utah, Salt Lake City, UT 84112, USA.
K. Cauley and S. F. Heinemann, Salk Institute, La Jolla, CA 92307, USA.
B. Crain, Departments of Neurobiology and Medicine (Neurology), Duke University Medical Center, Durham, NC 27710, USA.
T. E. Hughes, Department of Ophthalmology, Yale University, New Haven, CT 06510, USA.
J. O. McNamara, Departments of Neurobiology, Medicine (Neurology), and Pharmacology, Duke University Medical Center, Durham, NC 27710, USA, and Department of Medicine (Neurology), Veterans Affairs Medical Center, Durham, NC 27705, USA.
*To whom correspondence should be addressed.

localization of this inflammatory process in the cerebral cortex with relative sparing of the basal ganglia, thalamus, deep white matter, brainstem, and cerebellum (2). We therefore hypothesized that Rasmussen's encephalitis is due to an autoimmune process directed at GluR3 protein.

To test this idea, we measured immunoreactivity toward GluR3 and other neural receptors in sera from four individuals with pathologically confirmed Rasmussen's encephalitis, four age- and sex-matched epileptic children, four age- and sex-matched children without CNS disease, five children with active CNS inflammation, four other epileptic children, and four other normal children. Protein immunoblot analysis was performed with *trpE* fusion proteins containing corresponding regions of the putative extracellular domains of GluR1, 2, 3, and 5 (Fig. 2 and Table 1) and a portion of the putative intracellular domain of nAChR subunit β4 (4, 7, 8); blots were interpreted by observers unaware of the sources of the sera. Immunoreactivity to GluR3 fusion protein was detected in multiple sera samples from two individuals with Rasmussen's encephalitis [CK in (9); AI in Fig. 2]. CK also exhibited weak immunoreactivity to GluR2 fusion protein. Serum from a third individual with Rasmussen's encephalitis (EM) exhibited weak immunoreactivity to GluR2 fusion protein but not to other antigens (9). The fourth individual with Rasmussen's encephalitis (GO) did not exhibit serum immunoreactivity to any tested antigen. Sera from 20 of 21 control individuals showed no immunoreactivity, and one control serum showed immunoreactivity to GluR3 (10) that was different from the serum GluR immunoreactivity exhibited by individuals with Rasmussen's encephalitis ($P = 0.006$; Fisher's exact test).

To obtain independent validation of GluR immunoreactivity in these sera, we examined immunoreactivity toward full-length GluR3 protein in its three-dimensional conformation. Human embryonic

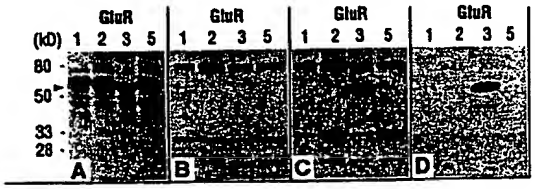

Fig. 2. Prominent serum reactivity toward GluR3-*trpE* fusion protein in an individual with active Rasmussen's encephalitis. Protein extracts enriched in fusion proteins were loaded on the designated lanes (GluR1, 2, 3, and 5) and visualized (4, 8). The site at which GluR fusion proteins reside is denoted by the arrowhead in (A). **(A)** Serum immunoreactivity of a rabbit immunized with *trpE* protein devoid of GluR protein. Because each GluR fusion protein contains *trpE* protein, each GluR fusion protein exhibits immunoreactivity. The bands not marked by the arrowhead represent irrelevant immunoreactivity, principally to bacterial proteins or to fragments of GluR fusion protein. **(B)** No immunoreactivity to any GluR fusion protein is evident in serum from the individual (GO) without active disease. This blot was typical for sera of 20 of 21 controls. **(C)** Serum from individual AI shows immunoreactivity to GluR3, but not to any other GluR. **(D)** We first adsorbed serum from individual AI with lysate from *trpE*-expressing *E. coli* to remove immunoreactivity to bacterial antigens (4, 8). The main GluR3 immunoreactivity is shown, with smaller faint bands presumably representing GluR3 fusion protein degradation products. Of the individuals tested, this serum exhibited the most prominent immunoreactivity to GluR3. Molecular size standards are shown at left (in kilodaltons).

Table 1. Summary of serum immunoreactivity to GluR in individuals with Rasmussen's encephalitis. Initials of all individuals were changed to protect their identity. Sz, seizures; GM Sz, generalized, tonic clonic seizures; R1, GluR1; and R6, GluR6 transiently expressed in transfected cells.

Diagnoses	Immunoreactivity	
	Immunoblot	In cells
	Rasmussen patients	
AI, progressive	GluR3	GluR3 (not R1 or R6)
CK, progressive	GluR3; weak GluR2	GluR3 (not R1 or R6)
EM, hemiparesis, Sz	Weak GluR2	GluR3 (not R1 or R6)
GO, stable, no Sz	None	None
	Age- and sex-matched epileptic controls	
Absence + GM Sz	None	None
Simple, partial Sz	None	None
Complex, partial Sz	None	None
Posttraumatic Sz	None	None
	Children with active CNS inflammation	
CNS lupus erythematosus	None	None
CNS lupus erythematosus	None	None
Multiple sclerosis	None	None
Varicella encephalitis	None	None
Tuberculous meningitis	None	None
	Age- and sex-matched normal controls	
Cardiac surgery	GluR3	None
Trauma	None	None
Trauma	None	None
Obesity	None	None
	Epileptic children	
Four children	None	None
	Normal children	
Four children	None	None

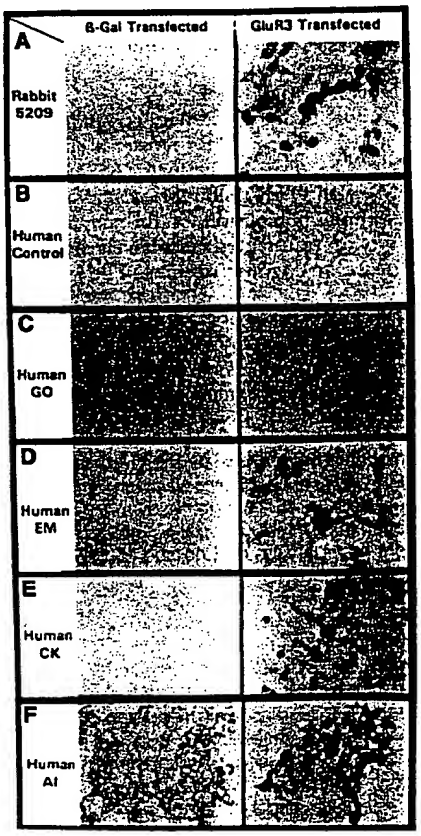

Fig. 3. Serum immunoreactivity toward transfected HEK 293 cells expressing either GluR3 or β-galactosidase (11). **(A)** Serum from one symptomatic, GluR3-immunized rabbit reacts with cells expressing GluR3. **(B)** Sera from control individuals exhibit no immunoreactivity. Immunoreactivity to transfected cells expressing GluR3 is present in sera of those individuals with active Rasmussen's encephalitis: EM **(D)**, CK **(E)**, and AI **(F)** but not in individual GO **(C)**, who exhibits no active disease.

kidney (HEK) 293 cells were transiently transfected with expression plasmids containing the complementary DNA (cDNA) for GluR3 or β-galactosidase (*11*). Sera from the three individuals with Rasmussen's encephalitis that exhibited immunoreactivity to GluR3 or GluR2 on protein immunoblots also reacted with transfected cells expressing GluR3 (Fig. 3 and Table 1). Serum from the fourth individual with Rasmussen's encephalitis, which was negative by protein immunoblot analysis, did not react with transfected cells. None of the control sera reacted with transfected cells, including the single control serum that was positive on the protein immunoblot (*10*). The correlation between serum immunoreactivity to GluR3 and Rasmussen's encephalitis was significant ($P = 0.002$; Fisher's exact test). Sera from individuals with Rasmussen's encephalitis did not react with transfected cells expressing the closely related GluRs GluR1 or GluR6, demonstrating the specificity of the GluR3 immunoreactivity. All measurable immunoreactivity in these individuals was of the immunoglobulin G (IgG) class.

GluR immunoreactivity correlated with clinical findings of Rasmussen's encephalitis. The three individuals (AI, CK, and EM) with GluR immunoreactivity on protein immunoblot and GluR3 immunoreactivity on transfected cells have progressive disease or ongoing seizures. The only individual (GO) with Rasmussen's encephalitis without immunoreactivity to any GluR proteins by protein immunoblot or transfected cell analyses underwent hemispherectomy 2 years before data collection and has since remained clinically stable and seizure-free.

The correlation between GluR3 immunoreactivity and disease activity suggested that GluR3 antibodies could be pathogenic in Rasmussen's encephalitis. We therefore hypothesized that removal of GluR3 antibodies by recurrent plasma exchange (PEX) would be beneficial. CK, now 9 years old, was well until a minor, left forehead injury in 1990, following which she experienced increasingly frequent generalized and right body seizures with progressive cognitive decline, speech disability, right hemiparesis, and left cerebral atrophy. No remissions occurred. Pathologic examination of a left temporal cortex biopsy confirmed the diagnosis of Rasmussen's encephalitis. GluR3 immunoreactivity, monitored with an enzyme-linked immunosorbent assay (ELISA) (*4*, *12*), was high. She was treated with recurrent, single-volume PEX and exhibited a beneficial response (Fig. 4). During the first 7 weeks of PEX, seizure frequency decreased by 80%. Cognition, speech, and hemiparesis improved, correlating in time with diminished GluR3 immunoreactivity. Over the ensuing 4 weeks, however, seizure frequency increased, and cognition, speech, and motor skills deteriorated in parallel with increased GluR3 immunoreactivity.

Molecular mimicry between self and foreign antigens expressed in microbes is one mechanism that has been proposed for the pathogenesis of autoimmune diseases (*13*). Structural similarities have been identified between the ligand-binding domains of multiple classes of GluRs and bacterial periplasmic amino acid–binding proteins (*14*). Infection with such microbes may induce an immune response that also targets GluRs.

The transient improvement after PEX in one seriously ill child suggests that circulating antibodies contribute to disease pathogenesis. The circulating autoantibodies would have to gain access to GluR3 in the brain, which is normally protected by the blood-brain-barrier (BBB). Focal disruption of the BBB can occur transiently with focal seizures (*15*) or as a consequence of head injury (*16*), an event that occasionally precedes Rasmussen's encephalitis (*2*, *17*). After disruption of the BBB, we hypothesize that the ensuing immune-mediated neural injury could trigger focal seizures. Thus, a cycle could be set in motion whereby focal seizures disrupt the BBB and facilitate the local access of pathogenic antibodies to brain antigens; the subsequent immune response could cause more seizures; and a progressive disorder results. This cycle could also explain the localized cortical onset of disease and the gradual expansion throughout one hemisphere. The contralateral hemisphere would be spared because it would not be a source of focal seizures, and the BBB would be relatively preserved.

Our data establish a link between circulating antibodies to a ligand-gated ion channel receptor of the CNS and a progressive encephalopathy with epileptic seizures. A related process may be operative in other forms of epilepsy, because histopathology similar to that of Rasmussen's encephalitis has been identified in 5 to 10% of individuals undergoing temporal lobectomy for refractory epilepsy (*18*). Related processes may also contribute to other CNS disorders with inflammatory histopathology.

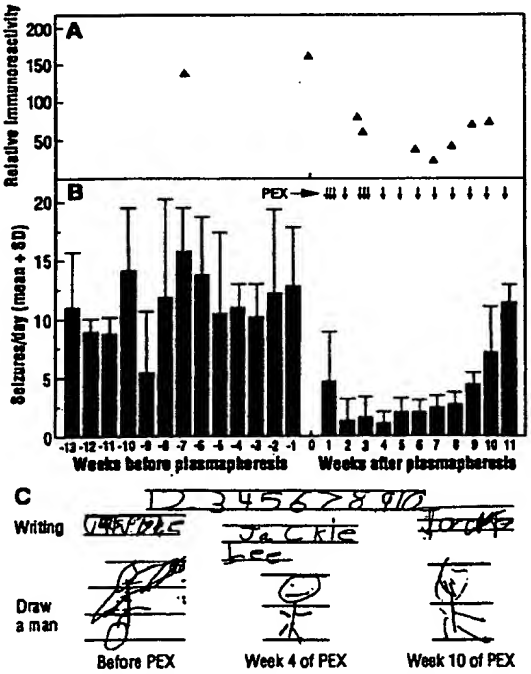

Fig. 4. Correlation of seizure frequency (**B**), neurologic function (**C**), and GluR3 immunoreactivity (**A**) in individual CK before and during 11 weeks of repeated PEX [indicated by arrows in (B)]. Before PEX, GluR3 antibody titer was high. She had 10 to 12 right body or generalized seizures daily, mild right hemiparesis, and no spontaneous speech. She was unable to read or solve simple math problems, and her writing and drawing were primitive. During the first 7 weeks of PEX, GluR3 antibody titer measured immediately before each PEX decreased, in temporal association with reduced seizure frequency. She spoke spontaneously in phrases and short sentences; her understanding, right hemiparesis, calculations, drawing, and writing improved. For the first time in 2 years, she resumed playing with dolls, riding a bicycle, and participating in household activities. During the last 4 weeks of PEX, GluR3 antibody titers gradually increased, seizure frequency increased, and cognitive skills declined. Numbers in (C) were written by the individual during week 4 of PEX. We omitted the individual's last name from her writing during week 4 of PEX to protect her identity. During PEX, other therapies were unchanged.

REFERENCES AND NOTES

1. T. Rasmussen, J. Olszewski, D. Lloyd-Smith, *Neurology* 8, 435 (1958); H. Oguni, F. Andermann, T. B. Rasmussen, in *Chronic Encephalitis and Epilepsy: Rasmussen's Syndrome*, F. Andermann, Ed. (Butterworth-Heinemann, Boston, 1991), pp. 7–36.
2. Y. Robitaille, in *Chronic Encephalitis and Epilepsy: Rasmussen's Syndrome*, F. Andermann, Ed. (Butterworth-Heinemann, Boston, 1991), pp. 79–110.
3. C. W. Cotman *et al.*, *Trends Neurosci.* 10, 273 (1987); C. Stevens, *Nature* 342, 620 (1989).

S. W. Rogers *et al.*, *J. Neurosci.* 11, 2713 (1991); *ibid.* 12, 4611 (1992).
J. Boulter *et al.*, *Science* 249, 1033 (1990); K. Keinanen *et al.*, *ibid.*, p. 556.
P. W. Berman *et al.*, *Ann. N.Y. Acad. Sci.* 377, 237 (1981).
G. W. Huntley *et al.*, *J. Neurosci.* 13, 2965 (1993).
Sera were numbered and frozen. GluR and β4-nAChR *trpE* fusion protein constructs were produced and analyzed as described (*4*, *7*), except we used 2% dry milk (Blotto) to block blots. Blots were incubated overnight at 4°C in primary serum diluted 1:1000 in Blotto, then in goat antibody to human IgG conjugated to alkaline phosphatase diluted at 1:750 in Blotto for 1 hour at 25°C, and then developed (*4*). We removed *Escherichia coli* background by incubating a suspension of lysed, *trpE*-expressing bacteria in the serum sample for 2 hours at 25°C and then centrifuging it. In another examination, each protein immunoblot was photographed, coded, and interpreted blindly by three investigators; interpretations were congruent in 73 of 76 samples (*9*).
S. W. Rogers *et al.*, unpublished data.
The single control individual whose serum exhibited immunoreactivity to GluR3 fusion protein by protein immunoblot analysis was sampled 1 week after open heart surgery. Cardiac bypass under hypothermic anesthesia may be a nonspecific activator of the immune system [J. R. Utley, *J. Cardiac Surg.* 5, 177 (1990)]. Her serum was not immunoreactive with GluR3 expressed in transfected cells, suggesting that the immunoreactivity detected by protein immunoblot analysis may not be to native GluR3.
HEK 293 cells were transfected with expression plasmids containing the cDNA for either GluR1, 3, or 6 or the bacterial protein β-galactosidase (*4*, *7*). The serum from individual AT exhibited nuclear immunoreactivity that we removed by adsorbing the serum samples with HEK 293 cells transfected with the parent expression plasmid without an insert (*4*). Sera were coded and tested in two laboratories independently (T.E.H. and S.W.R.). Sera from immunized rabbits served as the positive controls.
ELISA assays used either GluR3 or β4-nAChR fusion proteins that were solubilized and adsorbed to microtiter plates (Immulon) (*4*, *7*). Wells were blocked with Blotto for 2 hours at 25°C before we added sera at various dilutions for 1 hour at 25°C. We observed immunoreactivity using goat antibody to human IgG, conjugated with peroxidase, and 2,2′-azino-di-(3-ethylbenzthiazoline-6-sulfonic acid) (1 mg/ml) in McIlvain's buffer (pH 4.6) and 0.0005% hydrogen peroxide. Duplicate samples were scanned at 405 nM with an ELISA reader (Teritek). We determined GluR3-specific immunoreactivity by subtracting β4-nAChR reactivity from GluR3 reactivity.
R. T. Damian, *Am. Nat.* 98, 129 (1964); M. B. A. Oldstone, *Cell* 50, 819 (1987).
P. J. O'Hara *et al.*, *Neuron* 11, 41 (1993).
A. V. Lorenzo *et al.*, *Am. J. Physiol.* 223, 268 (1972); C. Nitsch and H. Hubauer, *Neurosci. Lett.* 64, 53 (1986).
J. C. Lee, in *Histology and Histopathology of the Nervous System*, W. Haymaker and R. D. Adams, Eds. (Thomas, Springfield, IL, 1982), pp. 798–870.
J. Peyser, J. Trevino, T. Resnick, *Int. Pediatr.* 7, 272 (1992).
K. D. Laxer, in *Chronic Encephalitis and Epilepsy: Rasmussen's Syndrome*, F. Andermann, Ed. (Butterworth-Heinemann, Boston, 1991), pp. 135–140.
We thank D. V. Lewis and G. R. DeLong for access to their patients and I. Verma for use of his cell culture laboratory. Supported by the National Institute of Neurological Disease and Stroke NS30990R29 (to S.W.R.), NS28709 (to S.F.H.), NS17771 and NS24448 (to J.O.M.), Research to Prevent Blindness and the National Eye Institute EY08362 (to T.E.H.), and the NIH General Clinical Research Centers Program to Duke University (MO1-RR-30).

28 December 1993; accepted 7 June 1994

Variable Gearing During Locomotion in the Human Musculoskeletal System

David R. Carrier,* Norman C. Heglund, Kathleen D. Earls

Human feet and toes provide a mechanism for changing the gear ratio of the ankle extensor muscles during a running step. A variable gear ratio could enhance muscle performance during constant-speed running by applying a more effective prestretch during landing, while maintaining the muscles near the high-efficiency or high-power portion of the force-velocity curve during takeoff. Furthermore, during acceleration, variable gearing may allow muscle contractile properties to remain optimized despite rapid changes in running speed. Force-plate and kinematic analyses of running steps show low gear ratios at touchdown that increase throughout the contact phase.

Toes were present in the earliest tetrapods (*1*) and occur in all modern tetrapods except those that are highly specialized for limbless or aquatic locomotion. Feet and toes form an adaptable interface between the animal and its environment. They provide traction and a means for grasping the substrate, function as various tools and weapons (*2*), and help to maintain balance (*3*). In this report, we suggest that feet and toes improve locomotor performance by varying the gear ratio (that is, the velocity ratio) between the ankle extensor muscles and the point of application of the force on the ground (the center of force) during the course of the contact phase of a running step.

The proposed mechanism is easily visualized during running at a steady speed (Fig. 1). The foot is analyzed as a simple Type 1 lever of zero mass with the fulcrum at the ankle by means of the equation $R \times F_r = r \times F_m$, where R is the ground force moment arm, F_r is the ground reaction force, r is the muscle force moment arm, and F_m is the muscle force. During the contact period of a step, the point at which force is applied to the ground (the center of force) moves from under the heel or middle portion of the foot at touchdown to the tips of the toes at takeoff. This forward translation could increase the length of the moment arm between the ankle and the force exerted on the ground (R) and, therefore, increase the gear ratio (R/r) of the ankle extensor muscles and tendons.

Variable gearing would be advantageous in running, as it is in the automobile, because in both cases the motors (cross-bridges in muscle and pistons in engines) have a limited speed range over which they operate at peak power or efficiency (*4*). In order to maintain a narrow range of optimal engine speeds despite varying drive speeds, the ratio of engine speed to drive speed must be changed by a variable gear ratio. Furthermore, muscles have unique properties that can benefit from variable gearing within the contact phase of a running step. Active muscles that are forcibly stretched just before shortening are able to do more work during the shortening. This nonelastic enhancement of the contractile properties of the muscle increases, within limits, with increasing stretch length (*5*) but is effective over relatively small shortening distances. If a runner were to land at a low gear ratio and take off at a higher gear ratio, both the prestretch and the subsequent shortening of the muscles could be optimized. Thus, variable gearing could reduce the need for locomotor specialization, allowing individuals to move about more efficiently, accelerate more quickly, run faster, and jump higher.

To test this hypothesis, five people (3 males and 2 females) ran over a Kistler 9281B force plate. Four of these people also accelerated maximally over the force plate, starting just off the plate so that the first step landed on the plate. A lateral view of limb position was recorded with a Peak high-speed video camera at 120 images per second (Fig. 1). Recordings of forces on the ground allowed calculation of the magnitude and orientation of the ground reaction force and the position of the center of force under the foot. For each video image taken during foot support (at 8.33-ms intervals), the ground force moment arm (R) was calculated by dividing the moment at the ankle by the resultant of the horizontal and vertical ground forces. Similarly, the mus-

D. R. Carrier and K. D. Earls, Department of Ecology and Evolutionary Biology, Brown University, Providence, RI 02912, USA.
N. C. Heglund, Pharos Systems, Inc., South Chelmsford, MA 01824, USA.
*To whom correspondence should be addressed.

Proc. Natl. Acad. Sci. USA
Vol. 93. pp. 1671–1676. February 1996
Genetics

Cyp1a2(−/−) null mutant mice develop normally but show deficient drug metabolism

(cytochrome P450/embryonic stem cells/arylamine carcinogenesis)

H.-C. LEONARD LIANG*, HUNG LI†, ROSS A. MCKINNON*, JOHN J. DUFFY‡, S. STEVEN POTTER†, ALVARO PUGA*, AND DANIEL W. NEBERT*§

*Department of Environmental Health, University of Cincinnati Medical Center, P.O. Box 670056, Cincinnati, OH 45267-0056; †Division of Basic Science Research, Children's Hospital Medical Center, University of Cincinnati, Cincinnati, OH 45229-2899; and ‡Department of Molecular Genetics, Biochemistry, and Microbiology, University of Cincinnati Medical Center, P.O. Box 650524, Cincinnati, OH 45267-0524

Communicated by I. C. Gunsalus, Gulf Breeze, FL, November 3, 1995

ABSTRACT **Cytochrome P450 1A2 (CYP1A2) is a predominantly hepatic enzyme known to be important in the metabolism of numerous foreign chemicals of pharmacologic, toxicologic, and carcinogenic significance. CYP1A2 substrates include aflatoxin B_1, acetaminophen, and a variety of environmental arylamines. To define better the developmental and metabolic functions of this enzyme, we developed a CYP1A2-deficient mouse line by homologous recombination in embryonic stem cells. Mice homozygous for the targeted *Cyp1a2* gene, designated *Cyp1a2*(−/−), are completely viable and fertile; histologic examination of 15-day embryos, newborn pups, and 3-week-old mice revealed no abnormalities. No CYP1A2 mRNA was detected by Northern blot analysis. Moreover, mRNA levels of *Cyp1a1*, the other gene in the same subfamily, appear unaffected by loss of the *Cyp1a2* gene. Because the muscle relaxant zoxazolamine is a known substrate for CYP1A2, we studied the *Cyp1a2*(−/−) genotype by using the zoxazolamine paralysis test: the *Cyp1a2*(−/−) mice exhibited dramatically lengthened paralysis times relative to the *Cyp1a2*(+/+) wild-type animals, and the *Cyp1a2*(+/−) heterozygotes showed an intermediate effect. Availability of a viable and fertile CYP1A2-deficient mouse line will provide a valuable tool for researchers wishing to define the precise role of CYP1A2 in numerous metabolic and pharmacokinetic processes.**

Cytochromes P450 represent the major class of phase I drug-metabolizing enzymes (1). Members of this enzyme superfamily are responsible for the metabolism of innumerable foreign chemicals. In addition, because of the metabolism of many endogenous compounds such as steroids, vitamin D_3, fatty acids, prostaglandins, and biogenic amines, cytochromes P450 are believed to be essential for such critical life functions as cell division, differentiation, apoptosis, homeostasis, and neuroendocrine functions (2–4).

As of October 1995, the P450 gene superfamily was composed of more than 480 genes classified into 74 families, 14 of which exist in all mammals (5). Both the murine and human *CYP1A* subfamilies comprise two genes, designated *Cyp1a1* and *Cyp1a2* in mouse, and *CYP1A1* and *CYP1A2* in humans (5, 6). In mice, the *Cyp1a* genes appear to be located within a 100-kb region on chromosome 9 (1, 7). The CYP1A enzymes are of particular interest due to their capacity for metabolizing numerous compounds relevant to the fields of pharmacology, toxicology, and carcinogenesis. In addition, both enzymes are induced by many foreign chemicals, including polycyclic aromatic hydrocarbons (e.g., benzo[*a*]pyrene) and 2,3,7,8-tetrachlorodibenzo-*p*-dioxin (1, 4). The induction process is regulated by the aromatic hydrocarbon receptor (AHR) (8, 9); the murine *Ahr* gene has been cloned (10, 11) and an *Ahr*(−/−) mouse line has recently been produced (12).

CYP1A2 is highly expressed in liver and is involved in the metabolism of many toxicologically significant compounds, including aflatoxin B_1, acetaminophen, and the food-derived heterocyclic amines (reviewed in ref. 13). In addition, most carcinogenic arylamines are known to be substrates for the human CYP1A2 enzyme (6, 14). To date, no endogenous substrate has been identified for the CYP1A2 enzyme, and there is little evidence for any physiologic role other than protection from chemical insult. On the basis of caffeine metabolism, two laboratories have suggested the presence of a human CYP1A2 genetic polymorphism, having a trimodal distribution of metabolizer phenotype (consistent with high/high, high/low, and low/low genotypes) in several populations (15, 16).

To define more clearly the involvement of the CYP1A2 enzyme in toxicity and carcinogenesis elicited by a variety of environmental chemicals, we have generated an embryonic stem (ES) cell-derived mouse line lacking a functional CYP1A2 enzyme. These null mutant mice exhibit normal development, viability, and fertility. The availability of this healthy *Cyp1a2*-deficient mouse line should provide an invaluable resource for researchers wishing to define the precise role of CYP1A2 in the metabolism of foreign, and perhaps endogenous, chemicals.¶

MATERIALS AND METHODS

Cloning of 129/SV *Cyp1a2* Genomic DNA. Using the mouse 1.5-kb 3′ *Cyp1a2*-specific cDNA probe (17), we isolated a 129/SV mouse genomic DNA clone isogenic to the ES cells used for recombination. DNA cloning and purification were performed as described (18). From the isolated clone, spanning 19 kb, we subcloned an 11-kb *Eco*RI fragment of the *Cyp1a2* gene into pBluescript II SK(+) (Stratagene). The wild-type *Eco*RI fragment includes exons 2–7 and the 3′ end of the *Cyp1a2* gene (Fig. 1 *Upper*).

Construction of *Cyp1a2* Gene-Targeting Vectors. The hypoxanthine phosphoribosyltransferase (*hprt*) gene-based vectors used for targeting the *Cyp1a2* gene were derived from the parent vector, pHPRT KO; this vector is derived from pBluescript II SK(+), contains a 2-kb *Kpn* I blunt-ended herpes simplex virus (HSV) thymidine kinase (*tk*) gene cassette, and features a 2.9-kb *Not* I–*Eco*RI blunt-ended *hprt* minigene cassette subcloned into the *Hin*dIII site (19). To generate the two vectors used for targeting, we subcloned a 0.4-kb *Hin*dIII–

The publication costs of this article were defrayed in part by page charge payment. This article must therefore be hereby marked "*advertisement*" in accordance with 18 U.S.C. §1734 solely to indicate this fact.

Abbreviations: ES cell, embryonic stem cell; GAPDH, glyceraldehyde-3-phosphate dehydrogenase.

§To whom reprint requests should be addressed.

¶This work was presented in abstract form at the Annual Meeting of the Society of Toxicology, March 5–9, 1995, Baltimore (43).

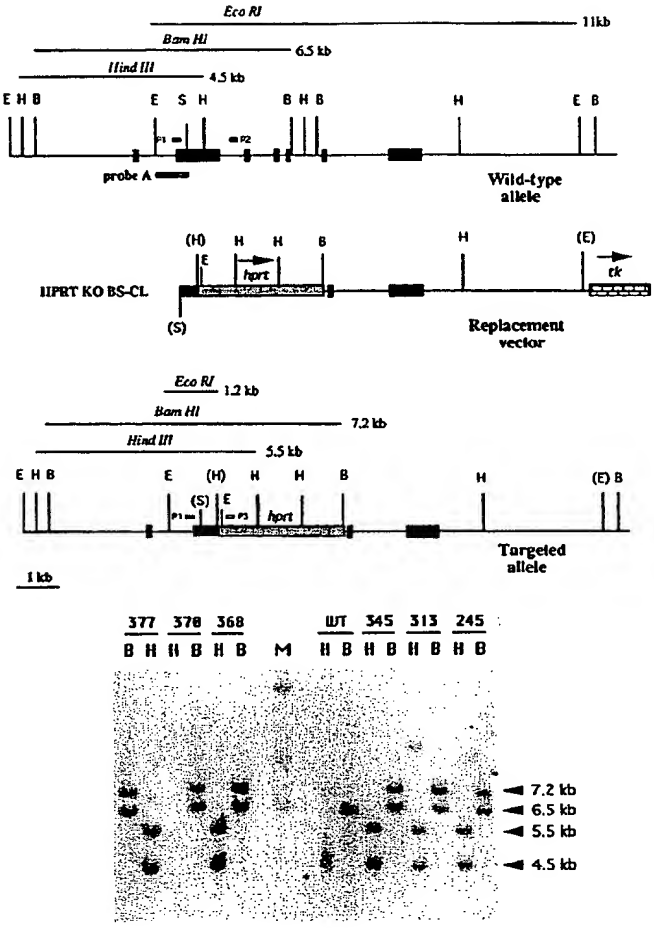

FIG. 1. Targeted modifications of the murine *Cyp1a2* gene. (*Upper*) The wild-type allele with all seven exons (solid boxes) and the targeted allele (containing the *hprt* gene) are shown. Probe A was used for genomic DNA analysis. E, *Eco*RI; H, *Hin*dIII; B, *Bam*HI; S, *Stu* I; sites in parentheses were lost during cloning/ligation. The predicted wild-type, and targeted allele, restriction fragment sizes for *Bam*HI and *Hin*dIII are shown. P1, P2, and P3 represent primers used for PCR analysis. (*Lower*) Diagnostic Southern blots for DNA from wild-type (WT) untargeted ES cells, plus DNA from six targeted ES cell lines designated 377, 370, 368, 345, 313, and 245. *Bam*HI (B) and *Hin*dIII (H) digests were hybridized with the flanking probe A. Heterozygote targeted lines contain the 7.2-kb *Bam*HI and the 5.5-kb *Hin*dIII fragments. M, molecular size markers.

Stu I fragment from exon 2 of the *Cyp1a2* gene into either the *Bam*HI site or the *Cla* I site of the pHPRT KO plasmid, generating products designated pHPRT KO BS and pHPRT KO CS, respectively. Subsequently, the *Cla* I site of the pHPRT KO BS plasmid and the *Bam*HI site of the pHPRT KO CS plasmid were used to subclone a 6.6-kb *Bam*HI–*Eco*RI fragment of the *Cyp1a2* gene. The resultant plasmids were designated pHPRT KO BS-CL and pHPRT KO CS-BL, respectively (Fig. 2*A*).

The targeting vector used in our earlier experiments was constructed from the multipurpose knockout vector pMJK KO, also derived from pBluescript II SK(+). pMJK KO possesses features similar to pHPRT KO, except that the *Hin*dIII site of pBluescript II SK(+) was used for subcloning a 1.6-kb *Xho* I–*Hin*dIII phophoglycerate kinase promoter–neomycin-resistance gene cassette instead of the *hprt* minigene cassette (20). The 0.4-kb *Hin*dIII–*Stu* I fragment of exon 2 of *Cyp1a2* (Fig. 1 *Upper*) was subcloned into the *Xho* I site of the pMJK KO plasmid. The *Bam*HI site of the pMJK KO plasmid was then used to subclone the 6.6-kb fragment. The resulting construct, designated pMJK KO XS-BL (Fig. 2*A Top*), contains 7.0 kb of target homology and produces a 2.2-kb deletion in the targeted locus. All three resulting plasmids were purified by the CsCl banding technique, linearized at the unique *Not* I site in the pBluescript II SK(+) backbone, and used for electroporation.

ES Cell Cultures. D3 ES cells (21) and E14tg2a ES cells, which are *hprt*$^-$ (22), were maintained at 37°C in a 5% CO_2 atmosphere on feeder layers of murine mitomycin C-treated embryonic fibroblasts in Dulbecco's modified Eagle's medium containing 15% heat-inactivated fetal bovine serum, 0.1 mM 2-mercaptoethanol, 1 mM sodium pyruvate, penicillin at 50 units/ml, streptomycin at 50 μg/ml, and leukemia inhibitory factor (LIF; GIBCO) at 1000 units/ml. The fibroblast feeder layer was prepared from 13- to 14-day-old mouse embryos and was grown in Dulbecco's modified Eagle's medium containing glucose at 4.5 mg/ml, penicillin at 50 units/ml, streptomycin at 50 μg/ml, and 1 mM L-glutamine, supplemented with 10% heat-inactivated fetal bovine serum. Confluent fibroblast monolayers were treated with mitomycin C at 10 μg/ml for 90 min at 37°C. The monolayers were then washed four times with phosphate-buffered saline prior to freezing or immediate use

A

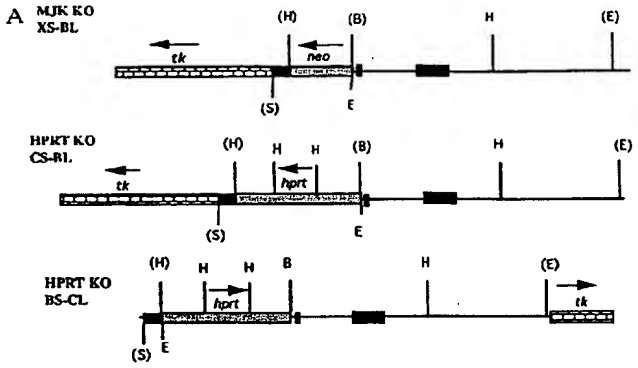

B

Construct	MJK KO XS-BL	HPRT KO CS-BL	HPRT KO BS-CL
ES cells	D3	E14	E14
Screened colonies	>800	200	380
Targeted lines	1	0	11
Chimera generated	13 males 9 females		12 males 1 females
Germline transmission	0		6

FIG. 2. Comparison of the three *Cyp1a2* gene-targeting constructs used in these experiments. (*A*) Diagram of the three constructs. The pMJK KO XS-BL vector carries the neomycin-resistance (*neo*) gene and the *Cyp1a2* gene fragment in opposite orientations. The pHPRT KO BS-CL vector carries the *hprt* gene in the same orientation as the *Cyp1a2* gene fragment, whereas the pHPRT KO CS-BL vector carries the *hprt* gene and the *Cyp1a2* gene fragment in opposite orientations. (*B*) Results of successfully targeted lines, generation of chimeric mice, and germline transmission.

as feeder layers (23). For electroporation, two confluent 100-mm dishes of ES cells were treated with trypsin and resuspended in 3 ml of phosphate-buffered saline (Ca^{2+}- and Mg^{2+}-free) containing *Not* I-digested targeting vector DNA at 20 μg/ml. Three 1-ml aliquots were electroporated at 900 V and 14 μF in a 0.4-cm-wide cuvette (Gene Zapper; IBI). The cells were then distributed onto 15-mm × 100-mm dishes containing mitomycin C-treated mouse embryo fibroblast feeder cells. Selection in hypoxanthine/aminopterin/thymidine (HAT) supplement (GIBCO/BRL) for E14 cells, or in G418 (150 μg/ml) for D3 cells, was initiated 24 h later. Further selection with 2 μM ganciclovir (Syntex, Palo Alto, CA) was begun at 48 hr following electroporation. Resistant ES colonies were selected 7 days after electroporation, treated with trypsin, and transferred to 24-well plates. After 2 or 3 days in culture, half the cells from each well were frozen, and the other half were transferred to gelatin-coated six-well plates. DNA was then prepared from each colony for PCR and/or Southern blot analysis, in order to identify putative homologous recombination events.

Selection of the Recombinant ES Cells. ES cells were lysed at 65°C for 10 min in 0.5 ml of buffer containing 0.2 M NaCl, 5 mM EDTA, 50 mM Tris·HCl (pH 7.5), 0.2% SDS, and proteinase K at 20 μg/ml. Genomic DNA was precipitated with potassium acetate and ethanol. The DNA was rinsed with 70% ethanol, then rinsed with 95% ethanol, air-dried, and resuspended in H_2O. Mouse tail DNA was prepared similarly, except that lysis buffer containing proteinase K at 15 μg/ml was used, and samples were incubated overnight at 65°C.

For Southern blotting, we digested DNA to completion with an excess of the restriction endonuclease *Eco*RI, *Bam*HI, or *Hin*dIII under reaction conditions recommended by the supplier (GIBCO/BRL). The digested DNA was fractionated through 0.8% agarose gels and transferred to Nytran Plus (Schleicher & Schuell) for further hybridization. Conditions for prehybridization and hybridization were as described (24). A 0.8-kb *Eco*RI–*Stu* I fragment was used as probe A (Fig. 1). Autoradiography was performed with Kodak XAR film and DuPont Lighting Plus intensifying screens.

For PCR screening of the HAT-resistant ES cell colonies, genomic DNA was added to a 20-μl PCR mixture containing 4 μl of 5× reaction buffer, 0.125 μg of each oligonucleotide primer (*Cyp1a2*-5′, CAGCCTGGGATGGAAATCAAGACA; *Cyp1a2*-3′, CGCTGCACACGGCACTCTGAGTAC; and *hprt* 3′, AGCGCCTCCCCTACCCGGTAGAAT), 2.5 units of *Taq* DNA polymerase (GIBCO/BRL), and a mixture of dATP, dCTP, dGTP and dTTP nucleotides at a final concentration of 500 μM for each nucleotide. The 5× reaction buffer contained 250 μM NaCl, 750 μM $MgCl_2$, 100 mM Tris·HCl (pH 8.4), 7.5 mM $MgCl_2$, 0.05% gelatin, and 0.5% Triton X-100. Samples were overlaid with one drop of mineral oil. PCR was performed for 35 cycles of 94°C for 1 min, 62°C for 2 min, and 72°C for 3 min in a thermal cycler (Perkin–Elmer/Cetus). The generated PCR products were 1.2 and 0.9 kb for *Cyp1a2*(+) wild-type and *Cyp1a2*(−) mutant alleles, respectively (Fig. 1). For screening of G418-resistant colonies, the above conditions were used with the following primers: *neo*-3′, ATGGCCGCTTTTCTGGATTCATCGACTTG; *Cyp1a2*-5′, GCGTTCTCCCAGTACATCTCCTTAGCCCCA; and *Cyp1a2*-3′, CTCACCTTGTTGAAGTCTTGGTAGTGCTCC.

Generation of the *Cyp1a2*(−/−) Mouse Line. Chimeric mice were generated by microinjection of targeted ES cells into embryos as described (24). Briefly, 10–15 targeted ES cells derived from the 129/Ola (slate, gray) mouse line were microinjected into the blastocoele cavity of C57BL/6J em-

bryos (nonagouti, black). Surviving blastocysts were transferred to pseudopregnant CD-1 females (albino, nonagouti) by uterine implantation. Identification of chimeric pups was determined by the presence of agouti or slate coat color at 10 days of age, depending on the origin of the ES cells. Chimeric males were bred to CF-1 females (nonagouti, white) or Swiss Black females (nonagouti, black). Germline transmission was determined by the presence of chinchilla-agouti and agouti coat colors in the offspring of the CF-1 and the Swiss Black females, respectively. Germline transmission was confirmed by both PCR and Southern blot analyses, as detailed above.

Northern Hybridization Analysis. Total RNA was isolated from the livers of 7- to 9-week-old mice by the acid guanidinium isothiocyanate extraction method (25). RNA was isolated 36 hr after treatment with a single intraperitoneal dose of either corn oil alone (25 ml/kg of body weight) or β-naphthoflavone (200 mg/kg) in corn oil. Total RNA (30 μg) was loaded onto 1% agarose/formaldehyde gels, transferred to nylon membranes (Nytran Plus; Schleicher & Schuell), and UV-crosslinked. Prehybridization and hybridization were performed in 10% dextran sulfate/1% SDS/6× standard saline citrate. Membranes were probed with a 1.5-kb 3′ fragment of CYP1A2 cDNA or a 1.2-kb 3′ fragment of CYP1A1 cDNA (17). The probe of a 780-bp *Pst* I–*Xba* I fragment of the glyceraldehyde-3-phosphate dehydrogenase (GAPDH) cDNA was used as an RNA-loading control. Hybridization was performed at 60°C, and the blots were washed at 60°C prior to autoradiography.

Zoxazolamine Paralysis Test. Four- to 6-week-old mice were given a single intraperitoneal dose of either β-naphthoflavone (200 mg/kg) in corn oil or corn oil alone. All animals received intraperitoneal zoxazolamine (300 mg/kg) in corn oil 36 hr later. Mice were then placed on their backs, and that time was recorded as time zero. The paralysis time was measured as that period of time until the animal had regained enough consciousness to right itself repeatedly (26).

Histology. Histologic specimens were prepared from 15-day embryos, newborn pups, and 3-week-old mice for analysis of any pathologic changes associated with the *Cyp1a2*-deficient genotype. The 15-day embryos and newborn pups were fixed whole in Bouin's fixative, whereas virtually all organs were dissected from 3-week-old mice and fixed in 10% formaldehyde. Paraffin-embedded sections (5 μm) were visualized by staining with hematoxylin and eosin.

RESULTS

Gene Targeting. Targeted disruption of the *Cyp1a2* gene was successfully achieved by insertion of the *hprt* gene in place of part of exon 2 and all of exons 3–5 (Fig. 1). Our design of the three gene-targeting vectors (Fig. 2*A*) was based on important structural features in the murine *Cyp1a2* gene, including a highly conserved cysteine-containing peptide in the N-terminus of the protein encoded by exon 2 and the so-called cytochrome P450 "conserved tridecapeptide" (27), encoded by exon 5 in the case of both of the *CYP1A* genes. Based on these structural details, homologous recombination constructs were designed in which the regions encoding the N-terminal cysteine-containing fragment and the conserved tridecapeptide would be replaced with either the *neo* or *hprt* positive selection markers. Targeted deletion of these essential gene components would be predicted to generate a null mutation.

Interestingly, pHPRT KO BS-CL (having the *hprt* promoter in the same orientation as the *Cyp1a2* gene) was the only successful construct of three used in our experiments (Fig. 2*B*). Whereas a high targeting frequency was achieved with pHPRT KO BS-CL in E14 ES cells, no homologous recombinant clones were generated from pHPRT KO CS-BL. In our earlier work using the *neo* gene in D3 ES cells, it is noteworthy that only a single homologous recombinant clone (of 800 screened) was obtained with the pMJK KO XS-BL construct, from which 13 chimeric males were produced, yet none of these was able to achieve germline transmission (Fig. 2*B*). The most widely accepted reason for the transmission of coat color but not the targeted gene is that a locus has been lost which allows colonization of the ES cells in the germline; this comes about through continued passage of ES cells both before and after targeting.

Homologous recombinant clones generated with the pHPRT KO BS-CL construct were confirmed by both genomic blotting and PCR analysis. Genomic blot analysis demonstrated that heterozygote clones were obtained, as indicated by the presence of extra 5.5-kb and 7.2-kb fragments upon digestion with *Hin*dIII and *Bam*HI, respectively (Fig. 1 *Lower*). PCR analysis of heterozygote clones showed the presence of a 0.9-kb band, corresponding to the mutant allele, in addition to the wild-type 1.2-kb band (Fig. 3). Two homologous recombinant clones generated with the pHPRT KO BS-CL construct were injected into the blastocoele cavity of C57BL/6J embryos; we subsequently generated 12 male chimeras, of which 6 gave germline transmission. Germline mice were derived from two independent ES clones, lines 368 and 377.

Viability and Fertility. The heterozygous *Cyp1a2*(+/−) mice displayed normal viability and fertility and were then used to generate homozygous mutants. Breeding of the heterozygotes produced offspring in the expected Mendelian distribution of one *Cyp1a2*(+/+) to two *Cyp1a2*(+/−) to one *Cyp1a2*(−/−), indicating no *in utero* lethality due to loss of both functional alleles of the *Cyp1a2* gene.

Homozygous *Cyp1a2*(−/−) null mutants were identified by the presence of only the 0.9-kb band upon PCR analysis (Fig. 3). Genotype was confirmed by Southern blotting. We found the homozygous *Cyp1a2*(−/−) mouse to be completely viable, fertile, and indistinguishable from its *Cyp1a2*(+/+) or *Cyp1a2*(+/−) littermates by appearance, mortality rate, reproductive capacity, and histologic examination of many organs and tissues; this has remained true—currently beyond 15 months of age. The organs and tissues examined histologically included: liver, lung, kidney, stomach, duodenum, small and large intestine, spleen, thymus, lymph nodes, heart, and brain.

CYP1A2 mRNA Analysis. The absence of CYP1A2 mRNA in *Cyp1a2*(−/−) mice was confirmed by Northern blot analysis of liver RNA from both control and β-naphthoflavone-treated animals. Fig. 4 *Left* shows a gene-dose effect: constitutive CYP1A2 mRNA levels in the heterozygote were intermediate between the null mutant, in which no mRNA was detectable even with 21-day exposures of the filter to x-ray film, and the wild type, which showed abundant mRNA. Induction by β-naphthoflavone treatment was found to increase the

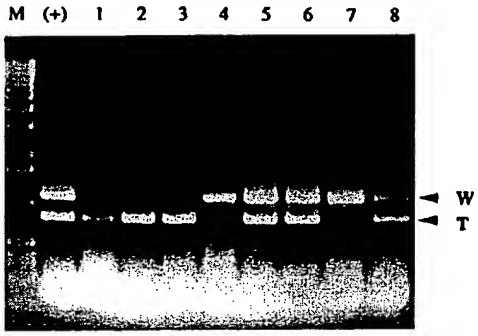

FIG. 3. PCR analysis of tail DNA from eight pups in the same litter generated from a *Cyp1a2*(+/−) × *Cyp1a2*(+/−) intercross. PCR products are 1.2 and 0.9 kb for the wild-type (W) and targeted (T) alleles, respectively. M, 1-kb nucleic acid markers. (+), targeted ES cell DNA.

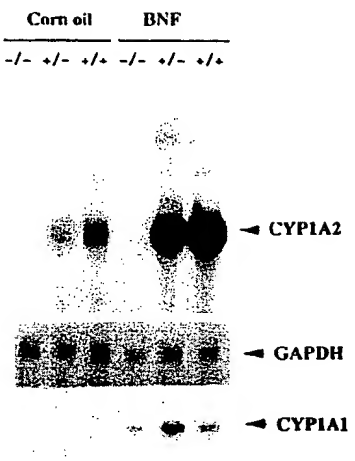

FIG. 4. Northern hybridization analysis of liver RNA from *Cyp1a2*(−/−), *Cyp1a2*(+/−), and *Cyp1a2*(+/+) mice. Probes include the CYP1A2-specific cDNA, the CYP1A1-specific cDNA as a positive control, and GAPDH cDNA to assess RNA loading in each lane. Sizes of the CYP1A2 and CYP1A1 mRNAs are 2.1 and 2.8 kb, respectively (17). Animals were treated with corn oil alone (controls) or β-naphthoflavone (BNF) 36 hr prior to sacrifice. When standardized for GAPDH, CYP1A1 mRNA levels are not significantly different in the three BNF lanes.

CYP1A2 mRNA 4- to 6-fold in the heterozygote and wild-type mouse (Fig. 4 *Right*), whereas no CYP1A2 mRNA was detected in the β-naphthoflavone-treated *Cyp1a2*(−/−) mouse.

CYP1A1 mRNA levels, detectable in liver only after β-naphthoflavone induction, were virtually identical in the *Cyp1a2*(+/+), *Cyp1a2*(+/−), and *Cyp1a2*(−/−) mice (Fig. 4 *Bottom*). These data indicate that expression of this other member of the mouse *Cyp1a* subfamily does not appear to compensate, or to be altered, by absence of the *Cyp1a2* gene.

Zoxazolamine Paralysis Test. The muscle relaxant zoxazolamine is a known CYP1A2 substrate, as well as a CYP2E1 substrate (28), and has been used for more than two decades to phenotype individual recombinant inbred or congenic mice having had CYP1A2 induced by β-naphthoflavone, benzo[*a*]pyrene, or 2,3,7,8-tetrachloro-*p*-dioxin (26, 29). It was expected that mice lacking any CYP1A2 enzyme would metabolize zoxazolamine more slowly and therefore remain paralyzed for a longer period of time and that β-naphthoflavone treatment—while inducing CYP1A2 in *Cyp1a2*(+/+) and *Cyp1a2*(+/−) mice—would have no effect on the *Cyp1a2*(−/−) mouse. The results of the zoxazolamine paralysis test (Table 1) show these expectations to be correct. Interestingly, the data are also correlated with the gene-dose mRNA data of Fig. 4 in that *Cyp1a2*(+/−) animals exhibited an intermediate paralysis time, when compared with the *Cyp1a2*(+/+) wild type and the *Cyp1a2*(−/−) null mutant. The CYP1A2-deficient mouse was paralyzed at least 9 times longer than the wild-type mouse. These results clearly illustrate the major role of CYP1A2 in zoxazolamine metabolism.

Table 1. Results of the zoxazolamine paralysis test in mice of the three genotypes

Genotype	Time paralyzed, min	
	Control	β-Naphthoflavone pretreatment
Cyp1a2(−/−)	>960	>960
Cyp1a2(+/−)	534 ± 225	309 ± 69
Cyp1a2(+/+)	498 ± 121	103 ± 59

The zoxazolamine paralysis test was performed as described (26). Zoxazolamine (chlorzoxazone) was given to all mice 36 hr after a single intraperitoneal dose of β-naphthoflavone (in corn oil); controls received corn oil alone. Paralysis times were assessed as the time taken for mice to right themselves three times. Values (mean ± SEM) are for four mice for each condition.

DISCUSSION

Evolutionary Considerations. We had anticipated that homozygous *Cyp1a2*(−/−) mutant mice would be viable and healthy, yet phenotypically different from wild-type *Cyp1a2*(+/+) and heterozygous *Cyp1a2*(+/−) mice toward CYP1A2-specific substrates such as zoxazolamine, based on several criteria. (*i*) Whereas constitutive expression of the *Cyp1a1* gene and its induction by polycyclic aromatic compounds occur very early during embryogenesis, increases in expression of the *Cyp1a2* gene are not detectable until the neonatal period (1, 30–32). These observations suggest that the *Cyp1a2* gene might not be critical for mouse embryogenesis but more likely is involved in metabolism of dietary and other foreign chemicals encountered after birth. (*ii*) Mammalian *CYP1A2* genes are extinguished in virtually all established and transformed cell lines examined, indicating that absence of CYP1A2 does not affect viability of cells in culture (1, 33, 34). (*iii*) Evolutionary analysis of the *CYP1A* family in trout and mammalian species (5) suggests that, while *CYP1A1* most likely encodes an enzyme critical to life, the *CYP1A2* gene is likely to be the result of a relatively recent gene duplication event in response to dietary selective pressures (35). Whereas trout appears to have only the *CYP1A1* gene, birds and mammals possess both *CYP1A1* and *CYP1A2*. It was therefore proposed that the *CYP1A2* gene originated ~350 million years ago via a gene duplication event—after the divergence of land animals from sea animals, and before divergence of land animals from birds (5, 35, 36). This duplication event may have been driven by evolutionary pressures caused by animal–plant interactions (35). Thus, it appears more likely that CYP1A2 might play an important role in protecting newborns from the insults of foreign (particularly dietary) chemicals during and after the neonatal period. We therefore had expected that the *Cyp1a2*-deficient mouse would develop normally, be viable, and display normal fertility, and this is what the present study shows.

Comparison of Two CYP1A2-Deficient Mouse Lines. The normal phenotype of the *Cyp1a2*(−/−) mouse line described in our study contrasts sharply with the phenotype of respiratory distress and neonatal lethality observed in another *Cyp1a2*(−/−) mouse line recently described (37). One possibility to explain the differences in phenotype would be differences in genetic background. This is not without precedent: for example, in studies of the insulin-like growth factor (*Igf1*) gene, differences in the phenotype of knockout mouse lines were found to be caused by differences in genetic background (38). In the present study, chimeric males in this laboratory were bred to CF-1 females or Swiss Black females, whereas chimeric males in the other laboratory were bred to C57BL/6J females (37).

Another possible explanation for differences in the phenotype of CYP1A2-deficient mice between the present study and a recent study (37) is a combination of genetic and nongenetic factors—i.e., presence of viral or other respiratory pathogens in a genetically susceptible host. In support of this possibility is that 19 of their 599 *Cyp1a2*(−/−) null mutants did survive to adulthood and are fertile (37).

An additional possible explanation has to do with the gene construct electroporated into the ES cells. It is not without precedent that different genomic approaches to knockouts of the same gene can lead to different phenotypes. For example, several laboratories engineered mutations that created null alleles with no residual expression of the cystic fibrosis transmembrane conductance regulator (*Cftr*) gene (39–41).

whereas a different laboratory created a "leaky" insertional mutation in exon 10 leading to an only mildly affected phenotype (42). It is exciting that both the mild and severe phenotypes of the *Cfir* gene knockout are proving to be valuable experimental model systems. Pineau *et al.* (37) disrupted the *Cyp1a2* gene by inserting the *neo* selection marker into exon 2, whereas we removed much of exon 2 and all of exons 3–5.

Conclusions. We have produced a *Cyp1a2*(−/−) null mutant mouse that develops normally, and is completely viable and fertile, yet exhibits altered drug metabolism. The generation of the *Cyp1a2*(−/−) mouse line described herein will provide an invaluable tool for researchers seeking to define the precise role of the CYP1A2 enzyme in numerous metabolic processes. Such a model will be particularly useful for further investigation of the CYP1A2 enzyme in terms of drug metabolism and toxicity, as well as cancer caused by environmental arylamines. Extrapolation of studies in this mouse line to human populations should also enable more educated predictions of the risk assessment associated with toxic exposures to chemicals via diet, life style, and occupation.

This project was supported by National Institutes of Health Grants RO1-ES06321 (D.W.N.) and P30 ES06096 (J.J.D., D.W.N., and S.S.P.).

1. Nebert, D. W. & Gonzalez, F. J. (1987) *Annu. Rev. Biochem.* **56**, 945–993.
2. Nebert, D. W. (1990) *Nature (London)* **347**, 709–710.
3. Nebert, D. W. (1991) *Mol. Endocrinol.* **5**, 1203–1214.
4. Nebert, D. W. (1994) *Biochem. Pharmacol.* **47**, 25–37.
5. Nelson, D. R., Koymans, L., Kamataki, T., Stegeman, J. J., Feyereisen, R., Waxman, D. J., Waterman, M. R., Gotoh, O., Coon, M. J., Estabrook, R. W., Gunsalus, I. C. & Nebert, D. W. (1996) *Pharmacogenetics* **6**, in press.
6. Nebert, D. W. & McKinnon, R. A. (1994) *Prog. Liver Dis.* **14**, 63–97.
7. Hildebrand, C. E., Gonzalez, F. J., Kozak, C. A. & Nebert, D. W. (1985) *Biochem. Biophys. Res. Commun.* **130**, 396–406.
8. Cobb, R. R., Stoming, T. A. & Whitney, J. B., III (1987) *Biochem. Genet.* **25**, 401–412.
9. Poland, A. P., Glover, E. & Taylor, B. A. (1988) *Mol. Pharmacol.* **32**, 471–478.
10. Burbach, K. M., Poland, A. & Bradfield, C. A. (1992) *Proc. Natl. Acad. Sci. USA* **89**, 8185–8189.
11. Ema, M., Sogawa, K., Watanabe, N., Chujoh, Y., Matsushita, N., Gotoh, O., Funae, Y. & Fujii-Kuriyama, Y. (1992) *Biochem. Biophys. Res. Commun.* **184**, 246–253.
12. Fernandez-Salguero, P., Pineau, T., Hilbert, D. M., McPhail, T., Lee, S. S. T., Kimura, S., Nebert, D. W., Rudikoff, S., Ward, J. M. & Gonzalez, F. J. (1995) *Science* **268**, 722–726.
13. Schweikl, H., Taylor, J. A., Kitareewan, S., Linko, P., Nagorney, D. & Goldstein, J. A. (1993) *Pharmacogenetics* **3**, 239–249.
14. Guengerich, F. P., Shimada, T., Raney, K. D., Yun, C.-H., Meyer, D. J., Ketterer, B., Harris, T. M., Groopman, J. D. & Kadlubar, F. F. (1992) *Environ. Health Perspect.* **98**, 75–80.
15. Butler, M. A., Lang, N. P., Young, J. F., Caporaso, N. E., Vineis, P., Hayes, R. B., Teitel, C. H., Massengill, J. P., Lawsen, M. F. & Kadlubar, F. F. (1992) *Pharmacogenetics* **2**, 116–127.
16. Tang, B. K., Zhou, Y. & Kalow, W. (1994) *Pharmacogenetics* **4**, 117–124.
17. Kimura, S., Gonzalez, F. J. & Nebert, D. W. (1984) *J. Biol. Chem.* **259**, 10705–10713.
18. Ausubel, F. M., Brent, R., Kingston, R. E., Moore, D. D., Smith, J. A., Seidman, J. G. & Struhl, K. (1991) *Current Protocols in Molecular Biology* (Greene/Wiley-Interscience, New York).
19. Li, H., Zeitler, P. S., Valerius, M. T., Small, K. & Potter, S. S. (1996) *EMBO J.*, in press.
20. Small, K. M. & Potter, S. S. (1993) *Genes Dev.* **7**, 2318–2328.
21. Doetschman, T., Eistetter, H., Katz, M., Schmidt, W. & Kemler, R. (1985) *J. Embryol. Exp. Morphol.* **87**, 27–45.
22. Hooper, M., Handy, K., Handyside, A., Hunter, S. & Monk, M. (1987) *Nature (London)* **326**, 292–295.
23. Doetschman, T. (1994) in *Transgenic Animal Technology: A Laboratory Handbook*, ed. Pinkert, C. (Academic, New York), pp. 115–146.
24. Li, H., Witte, D. P., Brandford, W. W., Aronow, B. J., Weinstein, M., Kaur, S., Wert, S., Singh, G., Schreiner, C. M., Whitsett, J. A., Scott, W. J. & Potter, S. S. (1994) *EMBO J.* **13**, 2876–2885.
25. Chomczynski, O. & Sacchi, N. (1987) *Anal. Biochem.* **162**, 156–159.
26. Robinson, J. R. & Nebert, D. W. (1974) *Mol. Pharmacol.* **10**, 484–493.
27. Ozols, J., Heinemann, F. S. & Johnson, E. F. (1981) *J. Biol. Chem.* **256**, 11405–11408.
28. Ono, S., Hatanaka, T., Hotta, H., Tsutsui, M., Satoh, T. & Gonzalez, F. J. (1995) *Pharmacogenetics* **5**, 143–150.
29. Nebert, D. W. (1980) *J. Natl. Cancer Inst.* **64**, 1279–1290.
30. Tuteja, N., Gonzalez, F. J. & Nebert, D. W. (1985) *Dev. Biol.* **112**, 177–184.
31. Kimura, S., Donovan, J. C. & Nebert, D. W. (1987) *J. Exp. Pathol.* **3**, 61–74.
32. Dey, A., Westphal, H. & Nebert, D. W. (1989) *Proc. Natl. Acad. Sci. USA* **86**, 7446–7450.
33. Pasco, D. S., Boyum, K. W., Merchant, S. N., Chalberg, S. C. & Fagan, J. B. (1988) *J. Biol. Chem.* **263**, 8671–8676.
34. Silver, G. J. & Krauter, K. S. (1988) *J. Biol. Chem.* **263**, 11802–11807.
35. Gonzalez, F. J. & Nebert, D. W. (1990) *Trends Genet.* **6**, 182–186.
36. Heilmann, L. J., Sheen, Y. Y., Bigelow, S. W. & Nebert, D. W. (1988) *DNA* **7**, 379–387.
37. Pineau, T., Fernandez-Salguero, P., Lee, S. T. T., McPhail, T., Ward, J. M. & Gonzalez, F. J. (1995) *Proc. Natl. Acad. Sci. USA* **92**, 5134–5138.
38. Liu, J. P., Baker, J., Perkins, A. S., Robertson, E. J. & Efstratiadis, A. (1993) *Cell* **75**, 59–72.
39. Ratcliff, R., Evans, M. J., Cuthbert, A. W., MacVinish, L. J., Foster, D., Anderson, J. R. & Colledge, W. H. (1993) *Nat. Genet.* **4**, 35–41.
40. O'Neal, W. K., Hasty, P., McCray, Jr., J. B., Casey, B., Rivera-Perez, J., Welsh, P. J., Beaudet, A. L. & Bradley, A. (1993) *Hum. Mol. Genet.* **2**, 1561–1569.
41. Hyde, S. C., Gill, D. R., Higgins, C. F., Trezise, A. E., MacVinish, L. J., Cuthbert, A. W., Ratcliff, R., Evans, M. J. & Colledge, W. H. (1993) *Nature (London)* **362**, 250–255.
42. Dorin, J. R., Dickinson, P., Alton, E. W., Smith, S. N., Geddes, D. M., Stevenson, B. J., Kimber, W. L., Fleming, S., Clark, A. R., Hooper, M. L., Anderson, L., Beddington, R. S. P. & Porteous, D. J. (1993) *Nature (London)* **359**, 211–215.
43. Liang, H. C., Li, H., Potter, S. S., Duffy, J. J., Puga, A., McKinnon, R. A. & Nebert, D. W. (1995) *Toxicologist* **15**, 59 (abstr.).

THE JOURNAL OF BIOLOGICAL CHEMISTRY

Vol. 271, No. 20, Issue of May 17, pp. 12063–12067, 1996
Printed in U.S.A.

Role of CYP2E1 in the Hepatotoxicity of Acetaminophen*

(Received for publication, January 29, 1996)

Susanna S. T. Lee‡, Jeroen T. M. Buters, Thierry Pineau§, Pedro Fernandez-Salguero, and Frank J. Gonzalez¶

From the Laboratory of Molecular Carcinogenesis, NCI, National Institutes of Health, Bethesda, Maryland 20892

CYP2E1, a cytochrome P-450 that is well conserved across mammalian species, metabolizes ethanol and many low molecular weight toxins and cancer suspect agents. The *cyp2e1* gene was isolated, and a mouse line that lacks expression of CYP2E1 was generated by homologous recombination in embryonic stem cells. Animals deficient in expression of the enzyme were fertile, developed normally, and exhibited no obvious phenotypic abnormalities, thus indicating that CYP2E1 has no critical role in mammalian development and physiology in the absence of external stimuli. When *cyp2e1* knockout mice were challenged with the common analgesic acetaminophen, they were found to be considerably less sensitive to its hepatotoxic effects than wild-type animals, indicating that this P-450 is the principal enzyme responsible for the metabolic conversion of the drug to its active hepatotoxic metabolite.

Cytochromes P-450 (P-450)[1] are a superfamily of hemoproteins that carry out oxidative metabolism of many endogenous and foreign chemicals (1). In mammals, P-450s can be functionally segregated into two groups, those that participate in biochemical pathways leading to the synthesis of steroid hormones and those that primarily metabolize foreign chemicals or xenobiotics such as drugs. The latter enzymes are included in the CYP1, CYP2, CYP3, and CYP4 families (2). Many of the hepatic xenobiotic-metabolizing P-450s also metabolize endogenous compounds, but the significance of these reactions is questionable. A clue to the lack of a critical role for many of the P-450s, particularly those in family 2, in development, reproduction, and longevity, is the marked species differences in their expression and catalytic activities (3). However, some of the xenobiotic-metabolizing P-450s are well conserved, including those in the CYP1 family and CYP2E1, suggesting that they may perform an important physiological function.

CYP2E1 is the principal P-450 responsible for the metabolism of ethanol and is considered as a major component of the microsomal ethanol-oxidizing system (4, 5). Among xenobiotics metabolized by CYP2E1 are acetaldehyde, acetaminophen, acrylamide, aniline, benzene, butanol, carbon tetrachloride, diethylether, dimethyl sulfoxide, ethyl carbamate, ethylene chloride, halothane, glycerol, ethylene glycol, *N*-nitrosodimethylamine, 4-nitrophenol, pyrazole, pyridine, and vinyl chloride (6). Many of these chemicals are known toxins, established chemical carcinogens, or suspected carcinogens. CYP2E1-mediated oxidation of a variety of substrates is also believed to liberate a substantial amount of reactive oxygen that can lead to membrane lipid peroxidation and cell toxicity (7).

CYP2E1 is also capable of metabolizing endogenous chemicals including acetone and acetol, which are key metabolites in the methylglyoxal and propanediol pathways of gluconeogenesis (8, 9). CYP2E1 can also carry out the metabolism of arachidonic acid, resulting in the production of several hydroxyeicosatetraenoic acids (10), some of which may have physiological and pharmacological properties (11).

CYP2E1 is inducible by ethanol and other low molecular weight substrates (5, 12). This induction is primarily due to a postranscriptional mechanism where presence of the substrate stabilizes the enzyme from degradation (13). However, transcriptional mechanisms have not been ruled out (14). This enzyme is also induced by starvation and in uncontrolled diabetes (15, 16).

P-450s have been implicated in the hepatotoxicity of acetaminophen (also called paracetamol), an over-the-counter analgesic and antipyretic that is commonly used worldwide as a substitute for acetylsalicylic acid (aspirin®) due to its lack of gastric ulceration and general low toxicity when used within the recommended dose range (17–19). Acetaminophen causes hepatotoxicity at a low frequency. It is metabolized to *N*-acetyl-*p*-benzoquinoneimine, a metabolite that is capable of reacting with cellular nucleophiles. The bulk of this metabolite is either reduced back to acetaminophen or conjugated with glutathione. It was postulated that toxicity results from low cellular glutathione leaving an excess of active metabolite that can cause cell toxicity (19–22).

The P-450s responsible for acetaminophen activation have been investigated. Ethanol was reported to increase the toxicity of acetaminophen in mice (20, 23), thus suggesting the involvement of CYP2E1 *in vivo*. *In vitro* studies have also implicated human CYP1A2 in addition to CYP2E1 in acetaminophen metabolism, although the latter P-450 had a lower K_m than CYP1A2 (24, 25).

The conservation across species in expression and catalytic activities of CYP2E1 and its ability to metabolize and be induced by chemicals that are generated endogenously, such as acetone and ethanol, suggests that it has an important physiological role in mammals. To investigate this possibility and to determine if this P-450 is involved in the hepatotoxicities and carcinogenesis potential of many of its substrates, mice lacking CYP2E1 expression were produced and characterized.

MATERIALS AND METHODS

Construction of the Targeting Vector—Genomic clones corresponding to *cyp2e1* were obtained by screening a 129/SV genomic library (Stratagene) with a rat CYP2E1 cDNA (26). A clone spanning 14.2 kb and containing all nine exons of the gene was subcloned as a *Sal*I fragment. To disrupt the gene, a 1.9-kb *Hin*dIII fragment containing exon 2 and

* The costs of publication of this article were defrayed in part by the payment of page charges. This article must therefore be hereby marked "*advertisement*" in accordance with 18 U.S.C. Section 1734 solely to indicate this fact.

‡ Present address: Dept. of Biochemistry, The Chinese University of Hong Kong, Shatin, New Territories, Hong Kong.

§ Present address: Laboratory of Pharmacology and Toxicology, INRA, BP3 31931 Toulouse Cedex, France.

¶ To whom correspondence should be addressed: Bldg. 37, Rm. 3E-24, NIH, Bethesda, MD 20892. Tel.: 301-496-9067; Fax: 301-496-8419; E-mail: fjgonz@helix.nih.gov.

[1] The abbreviations used are: P-450, cytochrome P-450; kb, kilobase pair(s); PGK, phosphoglycerate kinase-1; ES, embryonic stem.

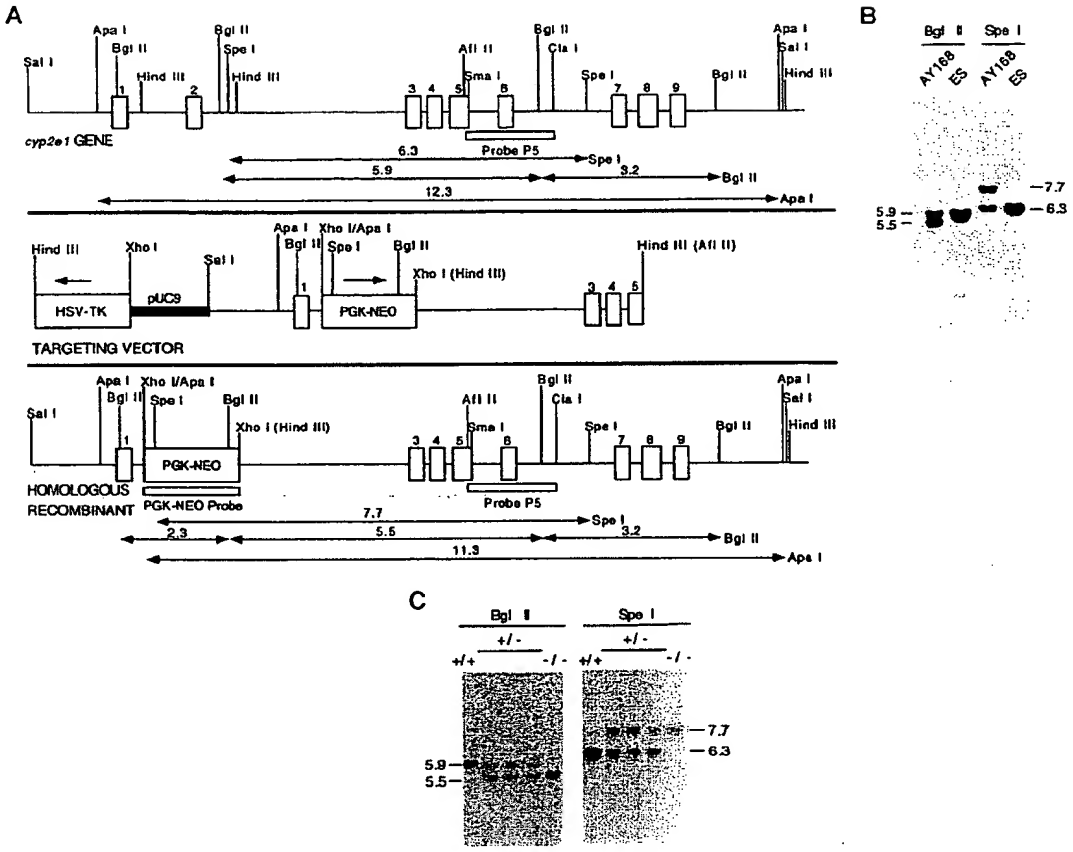

FIG. 1. *Panel A* displays the restriction map of the *cyp2e1* gene, the targeting vector, and the predicted homologous recombinant locus. The *numbers over* the *horizontal double arrows* are the predicted sizes of restriction fragments in kb. *Panel B* shows a Southern blot of the specific ES clone and wild-type ES cells, and *panel C* displays a Southern blot of a typical screen of tail clipping DNA from mice with different genotypes. The sizes of the fragments are in kb.

spanning from intron 1 to intron 2 was deleted and replaced with the bacterial phosphoribosyltransferase II gene, under control of the phosphoglycerate kinase-1 promoter (PGK-NEO), that confers resistance to the neomycin derivative G418 (Life Sciences Inc.). This gene was derived from the plasmid pPNT (27). The PGK-NEO cassette was inserted in the same transcriptional orientation as the *cyp2e1* gene. The herpes simplex virus thymidine kinase gene was inserted at the 3′ end of the *cyp2e1* gene as a negative selection against random integration of the construct (28). The construct used for targeting (see Fig. 1*A*), contained 2.3 kb of 5′ and 3.6 kb of 3′ genomic DNA flanking the PGK-NEO cassette.

The construct was made in six cloning steps (see Fig. 1A). 1) The *Hin*dIII site in the polylinker region of pGEM-3Z (Promega) was destroyed by *Hin*dIII digestion, Klenow polymerase treatment, and religation. 2) An 8-kb *Sal*I-*Sma*I *cyp2e1* genomic fragment was subcloned into the same sites in the modified pGEM-3Z. 3) The plasmid made in step 2 was digested with *Hin*dIII, treated with Klenow polymerase, and ligated with *Xho*I linkers in order to remove the 1.8-kb fragment containing exon 2 and add a restriction site compatible with the PGK-NEO cassette. This 1.9-kb cassette was previously modified by changing the *Bam*HI site at its 3′ end to an *Xho*I site by use of Klenow polymerase and *Xho*I linkers. 4) The *Xho*I fragment containing the PGK-NEO cassette was subcloned into the *cyp2e1* gene at the *Xho*I site. 5) The *cyp2e1* construct, containing the PGK-NEO cassette was digested with *Aff*II, treated with Klenow polymerase, and ligated with *Hin*dIII linkers. 6) The *cyp2e1* gene was released from this construct by digestion with *Sal*I and *Hin*dIII and inserted into the corresponding sites of pMC1TK plasmid (29) containing the herpes simplex virus thymidine kinase gene. The resulting plasmid was used as a targeting vector.

Production of Chimeric Mice—The plasmid DNA used for targeting was purified by banding twice on cesium chloride. After linearization with *Hin*dIII, 40 μg was electroporated into J1 embryonic stem (ES) cells (30) using conditions described previously (31). ES cell clones resistant to both G418 and ganciclovir (gift of Syntex) were selected and screened for homologous recombination, and clones having the expected Southern blot pattern for a homologous recombinant (see below) were regrown and injected into C57BL/6N blastocysts. The blastocysts were transferred into the uterus of a pseudopregnant recipient NIH Swiss mouse in order to produce an animal exhibiting chimerism (32). Male chimeras presenting greater than 95% 129/SV contribution, as determined by coat color, were bred with C57BL/6N females to determine if the trait was transmitted to the germ line. Southern blot genotyping performed on DNA extracted from tail clips, was used to score for the presence of the mutated *cyp2e1* gene in the progeny. Homozygotes were produced by crossing the F1 generation.

Genotyping of ES Cells and Mice—DNA was isolated from ES cells and mouse tail clips as described previously (33) and digested with either *Bgl*I or *Spe*I. The digested DNAs were subjected to electrophoresis in 0.6% agarose gels and transferred to GeneScreen Plus nylon membranes (DuPont) using 0.4 N NaOH. The conditions for hybridization and washing were described previously (31). A 3′-flanking probe derived from a *Aff*II-*Cla*I genomic fragment (see probe P5, Fig. 1*A*) was labeled with [^{32}P]dCTP using random primers. This probe hybridizes with 5.9- and 3.2-kb *Bgl*I fragments and with a 6.3-kb *Spe*I diagnostic fragment for the wild-type *cyp2e1* allele. The homologous recombinant allele generated fragments of 5.5 and 7.7 kb corresponding to digestions with *Bgl*I and *Spe*I, respectively (see Fig. 1, *A–C*). Mice homozygous for the disrupted *cyp2e1* allele were designated cyp2e1$^{-/-}$.

Analysis of CYP2E1 Expression—Mice were killed by carbon monoxide asphyxiation, and 400 mg of liver tissue was disrupted using a

Teflon-glass homogenizer in 3 ml of a buffer containing 20 mM Tris-HCl, pH 7.5, 1 mM EDTA, 25 mM KCl, 1 mM phenylmethylsulfonyl fluoride, 1 mM dithiothreitol, and 10% (v/v) glycerol. The homogenate was centrifuged for 20 min at 10,000 × *g*, and the supernatant was centrifuged for 12 min at 500,000 × *g* in a Beckman Optima TL tabletop ultracentrifuge to recover microsomes. All operations were performed at 4 °C. The microsome pellets were resuspended by homogenization in 0.1 M sodium potassium phosphate buffer, pH 7.4, containing 20% (v/v) glycerol and stored at −80 °C until use. Protein concentrations were determined with the bichinchoninic acid reagent (Pierce) using bovine serum albumin as a standard. SDS-polyacrylamide gel electrophoresis was carried out according to Laemmli (34) using 10 μg of microsomal protein. Proteins were electroblotted to nitrocellulose membranes by semi-dry transfer. Immunoblotting was performed according to Towbin *et al.* (35). Rabbit antibodies against CYP1A2 (36), CYP2A1 (37), CYP2B1 (38), and CYP3A1 (39) were produced as described earlier. Rabbit antisera against CYP2C6 was produced by Dr. Kiyoshi Nagata (Tohoku University, Sendai Japan). Antibody to CYP2E1, produced in goat, was obtained from the Gentest Corp. The secondary antibodies, labeled with horseradish peroxidase, were from Amersham Corp.

Messenger RNA was analyzed by Northern blots using liver RNA and the rat CYP2E1 cDNA as a probe. Total RNA was isolated from liver tissue using guanidinium thiocyanate extraction (40) and cesium trifluoroacetic acid centrifugation as described previously (31). Ten μg of total RNA was subjected to electrophoresis on 1% agarose gels containing 2.2 M formaldehyde (41) and blotted to GeneScreen Plus (DuPont) nylon membranes using 3 M NaCl and 0.15 M sodium citrate, pH 7.0. The CYP2E1 cDNA was labeled using random primers and [^{32}P]dCTP. The conditions for prehybridization, hybridization, and

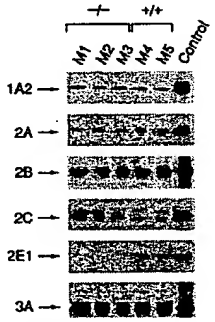

FIG. 2. **Western immunoblots of different P-450s in cyp2e1$^{-/-}$ mice. Each lane was loaded with 10 μg of microsomal protein from a single mouse.**

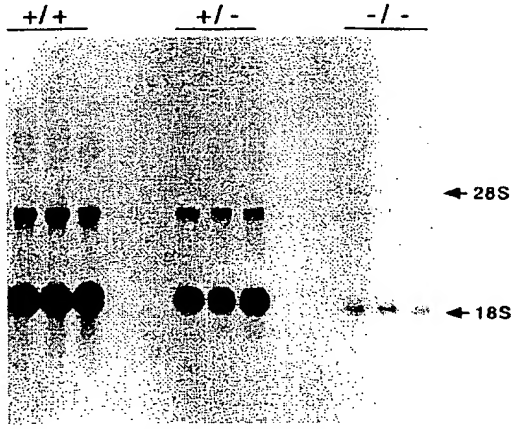

FIG. 3. **Analysis of RNA in livers of cyp2e1$^{-/-}$ mice. Each lane was loaded with 10 μg of total liver RNA from a single mouse. The blot was exposed for 24 h with aid of an intensifying screen.**

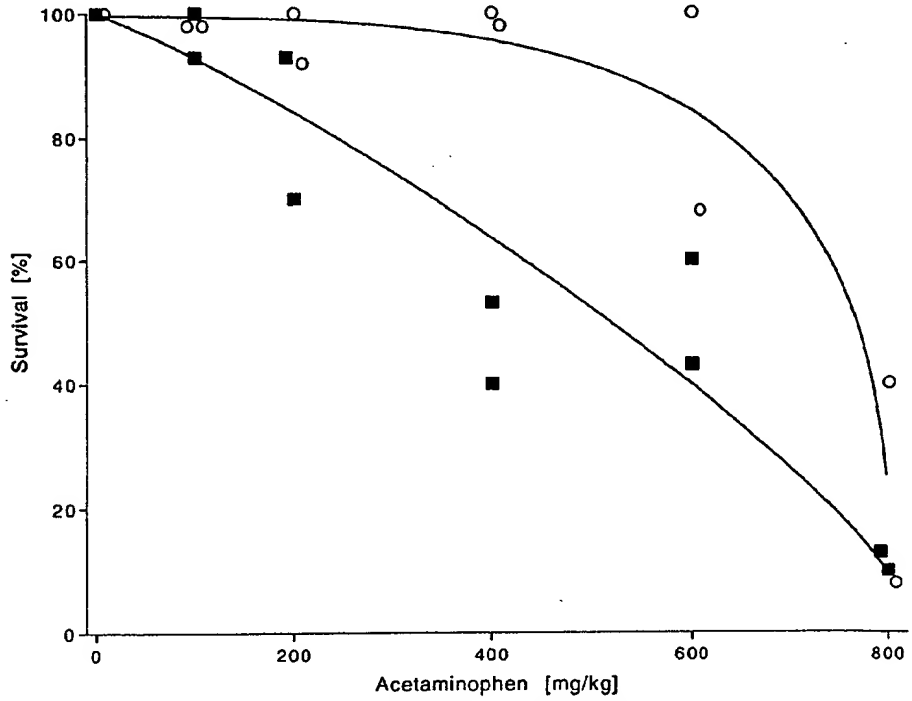

FIG. 4. **Survival rate of cyp2e1−/− (○) and wild-type (■) mice as a function of the dose of acetaminophen administered. Groups of 10 mice were injected intraperitoneally with acetaminophen in alkaline saline and survival scored after 48 h. Two complete and independent experiments were performed. The curves were manually fit to the data points.**

washing were described previously (31).

Acetaminophen Toxicity—The protocol for dosing mice with acetaminophen was approved by the National Cancer Institute's Animal Care and Use Committee (Protocol LMCE-023). Male cyp2e1$^{-/-}$ and wild-type strains, from 2 to 4 months of age, were administered acetaminophen by intraperitoneal injection at doses ranging from 0 to 800 mg/kg in alkaline saline solution. Each dose group consisted of 10 mice. To score toxicities, the number of surviving animals at 48 h were quantified. Two complete and independent experiments were conducted over the same dose range. From the remaining mice, blood was collected and serum was used to determine the levels of bilirubin, creatinine, alkaline phosphatase, aspartate aminotransferase, and alanine aminotransferase. These measurements were performed by the Diagnostic Services and Clinical Pathology Laboratory of the Uniformed Services University of the Health Sciences Clinical Chemistry Department using a Kodac Ektachem 250 automated plasma analyzer.

RESULTS AND DISCUSSION

Production and Characterization of the cyp2e1$^{-/-}$ Mice—The *cyp2e1* gene was isolated from a 129/SV mouse genomic library. The genomic clone spanned 14.2 kb and contained the complete coding region (Fig. 1*A*). The gene was disrupted by the replacement of exon 2 with the PGK-NEO cassette. A diagnostic probe, designated probe P5 and shown in Fig. 1*A*, was generated that detects homologous integrations of the targeting construct into the gene. Mice having the wild-type allele are expected to yield a 5.9-kb *Bgl*II and a 6.3-kb *Spe*I fragments. A typical autoradiography of a Southern blot of DNA from the ES cell clone AY168 and control ES cells hybridized with the probe P5 is shown in Fig. 1*B*. Upon longer exposure of the blot, an expected 3.2-kb *Bgl*II fragment was also detected. Specific recombinants had diagnostic 5.5- and 7.7-kb fragments from *Bgl*II and *Spe*I, respectively. Screening of mice generated by breeding for heterozygotes for the disrupted *cyp2e1* allele is shown in Fig. 1*C*. Heterozygous mice have the diagnostic fragments corresponding to the wild-type and disrupted alleles, whereas mice that have two copies of the disrupted allele yielded the 5.5- and 7.7-kb fragments after digestion with *Bgl*II and *Spe*I, respectively. Hybridization with the PGK-NEO gene as a probe revealed only a single hybridizing fragments of 2.3, 7.7, and 11.3 kb for the *Bgl*II-, *Spe*I-, and *Apa*I-digested DNA (data not shown), demonstrating that this clone did not contain any additional random integration of the targeting construct.

Mice homozygous for the disrupted allele, designated cyp2e1$^{-/-}$, were born normally and appeared indistinguishable from their wild-type counterparts. No differences were found between litter size and growth rates for the cyp2e1$^{-/-}$ animals as compared with wild-type littermate controls. The expression of CYP2E1 was determined by immunoblotting with anti-rat CYP2E1 antibody. As expected, a complete absence of protein expression was found in the livers of cyp2e1$^{-/-}$ mice (Fig. 2). The liver is the primary site of expression of this P-450 (16). P-450s in the CYP1A, CYP2A, CYP2B, CYP2C, and CYP3A subfamilies were expressed in the cyp2e1$^{-/-}$ mice at similar levels to those found in control animals, thus indicating that the loss of CYP2E1 was not compensated by an increase in expression of other P-450s, although it remains a possibility that a P-450 not detected with our anti-rat P-450 antibodies is overexpressed.

The expression of CYP2E1 mRNA was also analyzed in the cyp2e1$^{-/-}$ mice. Two transcripts were detected in the liver of normal mice and mice heterozygous for the disrupted allele (Fig. 3). In the cyp2e1$^{-/-}$ mice, neither of these two RNA transcripts were found. Instead, two lower abundance RNAs slightly smaller than the transcripts present in wild-type animals were detected. These may be transcripts from the disrupted allele that should be smaller than a transcript from the normal allele since exon 2 is deleted in the disrupted allele. The lower abundance of these RNAs, as compared with those from the wild-type allele, is not surprising since mRNAs that do not encode a normal protein are usually not stable. In any case, the protein and RNA establish with certainty that the *cyp2e1* gene is not expressed in the knockout animals. The change in size and abundance of the high molecular weight transcript annealing with the CYP2E1 cDNA in the cyp2e1$^{-/-}$ mice suggest that it is not due to a cross-hybridizing mRNA derived from another gene but is most likely a read-through transcript of the *cyp2e1* gene with an alternate polyadenylation signal.

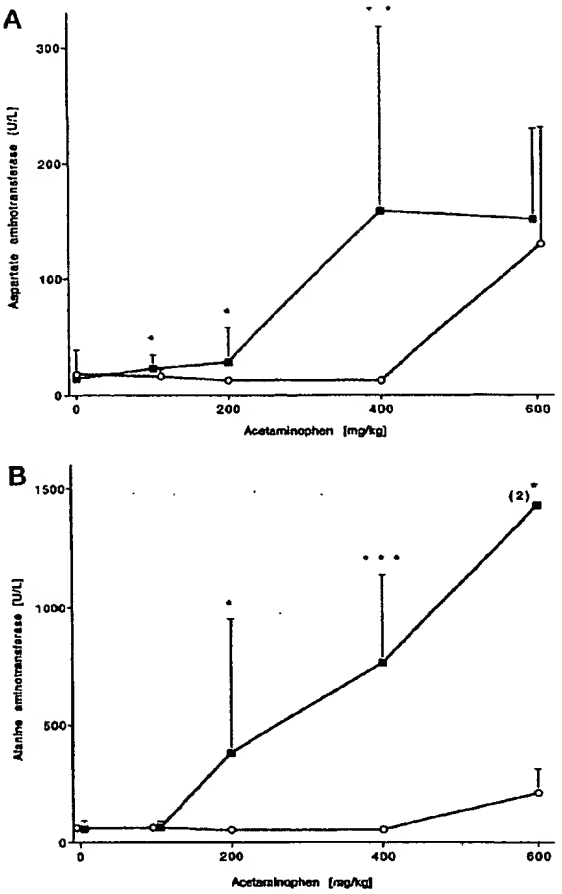

FIG. 5. **Determinations of aspartate aminotransferase (*panel A*) and alanine aminotransferase (*panel B*) activities in serum of cyp2e1$^{-/-}$ (○) and wild-type (■) mice as a function of the dose of acetaminophen administered.** The mean + standard deviations are shown with $n = 3$ (* $p < 0.05$, ** $p < 0.01$, *** $p < 0.001$). At the 600 mg/kg dose group for the wild-type mice in *panel B*, two animals were analyzed.

Acetaminophen Toxicity—P-450s have been implicated in the hepatotoxicity of acetaminophen. To determine whether CYP2E1 influences the toxicity of this compound in mice, the cyp2e1$^{-/-}$ animals were administered the drug and compared with wild-type mice. Survival curves indicated that the cyp2e1$^{-/-}$ mice were more resistant to acetaminophen toxicity than wild-type animals (Fig. 4). Levels of 400 mg of acetaminophen/kg producing toxicity in wild-type mice in this study were similar to those that produced toxicity in other studies (20, 23). Cyp2e1$^{-/-}$ mice survived at doses up to 400 mg/kg, whereas over 50% of wild-type animals died at these doses.

To determine the mechanism of toxicity, levels of enzymes and other serum components, some of which are diagnostic for liver and kidney injury, were measured in serum of treated mice that survived in the experiments described above. At all doses, levels of creatinine, bilirubin, and alkaline phosphatase were within the normal range for mice and were not significantly different between the cyp2e1$^{-/-}$ and wild-type mice. In contrast, liver enzymes aspartate aminotransferase and alanine aminotransferase were elevated at high doses of acetaminophen (Fig. 5). Elevation of these liver enzymes, which are considered a measure of liver cell death, were detected at doses of 200 and 400 mg/kg in wild-type animals but were unchanged at these doses in the cyp2e1$^{-/-}$ mice. These data indicate that liver damage is involved in mediating the toxicity of acetaminophen. This was confirmed by analysis of liver histology of acetaminophen-treated mice (data not shown). At doses higher than 600 mg/kg, a significant level of toxicity was also found in the cyp2e1$^{-/-}$ mice. These data suggest that CYP2E1 mediates the hepatotoxicity of acetaminophen. Other P-450s such as CYP1A2 having a higher K_m for acetaminophen may be responsible for the toxicity in cyp2e1$^{-/-}$ mice at high doses of the drug.

The present study using mice lacking expression of CYP2E1 establish that although this P-450 is highly conserved in mammals, it does not appear to play a significant role in development, reproductive vitality, and physiology. Under conditions of exposure to certain chemicals, CYP2E1 accentuates toxicity. Efforts are underway to use this animal model to determine whether this enzyme is responsible for the carcinogenicity of a number of its chemical substrates including *N*-nitrosodimethylamine and phenacetin.

CYP2E1 may also exert a role in alcoholic liver disease. Lipid peroxidation was found to be associated with alcoholic liver injury in humans and experiment animals (42). This could be the result, in part, of increased oxygen radical production by ethanol-induced CYP2E1 (7). The cyp2e1$^{-/-}$ mice could be used to test this possibility.

During fasting and diabetic ketosis, serum acetone, acetol, and 1,2-propanediol are elevated. CYP2E1 is concommitantly induced due to protein stabilization by acetone (16). Acetone is primarily oxidized to acetol by CYP2E1. Acetol is further metabolized to 1,2-propanediol by the same P-450 in a pathway of gluconeogenesis, suggesting a physiological role for this P-450 during pathophysiological and dietary stress (8). The cyp2e1$^{-/-}$ mice should be of use to determine if CYP2E1 plays an essential role in survival under conditions of starvation.

REFERENCES

1. Gonzalez, F. J. (1988) *Pharmacol. Rev.* **40**, 243–248
2. Nelson, D. R., Koymans, L., Kamataki, T., Stegeman, J. J., Feyereisen, R., Waxman, D. J., Waterman, M. R., Gotoh, O., Coon, M. J., Estabrook, R. W., Gunsalus, I. C., and Nebert, D. W. (1996) *Pharmacogenetics* **6**, 1–41
3. Gonzalez, F. J., and Nebert, D. W. (1989) *Trends Genet.* **6**, 182–187
4. Lieber, C. S., and DeCarli, L. M. (1970) *J. Biol. Chem.* **245**, 2505–2512
5. Koop, D. R., Morgan, E. T., Tarr, G. E., and Coon, M. J. (1982) *J. Biol. Chem.* **257**, 8472–8480
6. Guengerich, F. P., Kim, D. H., and Iwasaki, M. (1991) *Chem. Res. Toxicol.* **4**, 168–179
7. Coon, M. J., Roberts, E. S., and Vaz, A. D. N. (1991) in *Oxidative Damage and Repair: Chemical, Biological and Medical Aspects* (Davies, K. J. A., ed) Pergamon, New York, pp. 726–731
8. Casazza, J. P., Felver, M. E., and Veech, R. L. (1984) *J. Biol. Chem.* **259**, 231–236
9. Koop, D. R., and Casazza, J. P. (1985) *J. Biol. Chem.* **260**, 13607–13612
10. Laethem, R. M., Balazy, M., Falck, J. R., Laethem, C. L., and Koop, D. R. (1993) *J. Biol. Chem.* **268**, 12912–12918
11. Fitzpatrick, F. A., and Murphy, R. C. (1988) *Pharmacol. Rev.* **40**, 229–241
12. Koop, D. R., and Coon, M. J. (1984) *Mol. Pharmacol.* **25**, 494–501
13. Song, B. J., Matsunaga, T., Hardwick, J. P., Veech, R. L., Yang, C. S., Gelboin, H. V., and Gonzalez, F. J. (1987) *Mol. Endocrinol.* **1**, 542–547
14. Song, B. J. (1995) in *Drug and Alcohol Abuse Reviews, Vol. 6: Alcohol and Hormones* (Watson, R. R., ed) pp. 277–192, Human Press Inc., Totowa, NJ
15. Hong, J., Pan, J., Gonzalez, F. J., Gelboin, H. V., and Yang, C. S. (1987) *Biochem. Biophys. Res. Commun.* **142**, 1077–1083
16. Song, B. J., Gelboin, H. V., Park, S. S., Yang, C. S., and Gonzalez, F. J. (1986) *J. Biol. Chem.* **261**, 16689–16697
17. Jollow, D. J., Mitchell, J. R., Potter, W. Z., Davis, D. C., Gillette, J. R., and Brodie, B. B. (1973) *J. Pharmacol. Exp. Ther.* **187**, 195–202
18. Mitchell, J. R., Jollow, D. J., Potter, W. Z., Davis, D. C., Gillette, J. R., and Brodie, B. B. (1973) *J. Pharmacol. Exp. Ther.* **187**, 211–217
19. Potter, W. Z., Davis, D. C., Mitchell, J. R., Jollow, D. J., Gillette, J. R., and Brodie, B. B. (1973) *J. Pharmacol. Exp. Ther.* **187**, 203–210
20. Peterson, F. J., Holloway, D. E., Erickson, R. R., Duquette, P. H., McCain, C. J., and Holtzman, J. L. (1980) *Life Sci.* **27**, 1705–1711
21. Dahlin, D. C., Miwa, G. T., Lu, A. Y. H., and Nelson, S. D. (1984) *Proc. Natl. Acad. Sci. U. S. A.* **81**, 1327–1331
22. Prasad, J. S., Chen, N. Q., Liu, Y. X., Coon, D. J. W., and Holtzman, J. L. (1990) *Biochem. Pharamacol.* **40**, 1989–1995
23. Snawder, J. E., Roe, A. L., Benson, R. W., and Roberts, D. W. (1994) *Biochem. Biophys. Res. Commun.* **203**, 532–539
24. Raucy, J. L., Lasker, J. M., Lieber, C. S., and Black, M. (1989) *Arch. Biochem. Biophys.* **271**, 270–283
25. Snawder, J. E., Roe, A. L., Benson, R. W., Casciano., D. A., and Roberts, D. W. (1994) *Pharmacogenetics* **4**, 43–46
26. Song, B. J., Veech, R. L., Park, S. S., Gelboin, H. V., and Gonzalez, F. J. (1989) *J. Biol. Chem.* **264**, 3568–3572
27. Tybulewicz, V. L. J., Crawford, C. E., Jackson, P. K., Bronson, R. T., and Mulligan, R. C. (1991) *Cell* **65**, 1153–1163
28. Bradley, A. (1987) in *Teratocarcinoma and Embryonic Stem Cells: A Practical Approach* (Robertson, E. J., ed) pp. 133–151, IRL Press, Oxford
29. Mansour, S. L., Thomas, K. R., and Capecchi, M. R. (1988) *Nature* **336**, 348–352
30. Li, E., Bestor, T. H., and Jaenisch, R. (1992) *Cell* **69**, 915–926
31. Lee, S. S. T., Pineau, T., Drago, J., Lee, E. J., Owens, J. W., Kroetz, D. L., Fernandez-Salguero, P., Wesphal, H., and Gonzalez, F. J. (1995) *Mol. Cell. Biol.* **15**, 3012–3022
32. Hogan, B., Costantini, F., and Lacy, E. (eds) (1986) *Manipulating the Mouse Embryo: A Laboratory Manual*, Cold Spring Harbor Laboratory, Cold Spring Harbor, NY
33. Laird, P. W., Zijderveld, A., Linders, K., Rudnicki, M. A., Jaenisch, R., and Berns, A. (1991) *Nucleic Acids Res.* **19**, 4293
34. Laemmli, U. K. (1970) *Nature* **227**, 680–685
35. Towbin, H., Staehelin, T., and Gordon, J. (1979) *Proc. Natl. Acad. Sci. U. S. A.* **76**, 4350–4354
36. Aoyama, T., Gonzalez, F. J., and Gelboin, H. V. (1989) *Mol. Carcinogen.* **1**, 253–259
37. Nagata, K., Matsunaga, T., Gillette, J., Gelboin, H. V., and Gonzalez, F. J. (1987) *J. Biol. Chem.* **262**, 2787–2793
38. Yamano, S., Nhamburo, P. T., Aoyama, T., Meyer, U. A., Inaba, T., Kalow, W., Gelboin, H. V., McBride, O. W., and Gonzalez, F. J. (1989) *Biochemistry* **28**, 7340–7348
39. Gonzalez, F. J., Song, B. J., and Hardwick, J. P. (1986) *Mol. Cell. Biol.* **6**, 2969–2976
40. Chirgwin, J. M., Przybyla, A. E., MacDonald, R. J., and Rutter, W. J. (1979) *Biochemistry* **18**, 5294–5299
41. Lehrach, H., Diamond, D., Wozney, J. M., and Boedtker, H. (1977) *Biochemistry* **16**, 4743–4751
42. Shaw, S., Rubin, K. P., and Lelber, C. S. (1983) *Dig. Dis. Sci.* **28**, 585–589

BREVIA

NEUROSCIENCE

Synthesis of Serotonin by a Second Tryptophan Hydroxylase Isoform

Diego J. Walther,[1]* Jens-Uwe Peter,[1] Saleh Bashammakh,[1] Heide Hörtnagl,[2] Mechthild Voits,[2] Heidrun Fink,[3] Michael Bader[1]*

The neurotransmitter serotonin [5-hydroxytryptamine (5-HT)] is causally involved in multiple central nervous facets of mood control and in regulating sleep, anxiety, alcoholism, drug abuse, food intake, and sexual behavior (*1*). In peripheral tissues, 5-HT regulates vascular tone, gut motility, primary hemostasis, and cell-mediated immune responses (*1*). 5-HT is synthesized in two steps, with tryptophan hydroxylase (TPH) as the rate-limiting enzyme (*2*). TPH belongs to a superfamily of aromatic amino acid hydroxylases, together with phenylalanine (PAH) and tyrosine hydroxylases (TH), and has been detected mainly in the brain stem and gut enterochromaffin cells (*2*).

To study the physiological impact of the loss of 5-HT synthesis, we generated mice genetically deficient for TPH (*Tph*−/−). Like wild-type (*Tph*+/+) siblings and the mouse strains from which the *Tph*−/− animals were derived, *Tph*−/− mice still expressed normal amounts of 5-HT in classical serotonergic brain regions. However, *Tph*−/− mice lacked 5HT in the periphery except for in the duodenum (Fig. 1A), which contained about 4% of normal 5-HT levels, probably because of the serotonergic neurons in this tissue (*3*). Concordantly, *Tph*−/− mice exhibited no significant behavioral differences in elevated plus maze and hole board tests (table S1), which are indicative for 5-HT–related behavior.

Despite suggestions of a possible second TPH isoform (*4*), molecular verification has been lacking. Therefore, we screened the High Throughput Genomic Sequences database of GenBank with short translated sequences of *Tph* and obtained a human genomic clone on chromosome 12, with an open reading frame similar to *Tph* exon 4, but different from *Pah*, which is located on the same chromosome. On the basis of this sequence, we performed 5′- and 3′-RACE experiments with brain RNA of *Tph*−/− mice and obtained the full-length cDNA (referred to as *Tph2*; GenBank: AY090565; fig. S1), which was different from the known Tph (referred to here now as *Tph1*), *Pah*, and *Th* of the mouse.

We detected *Tph1* mRNA in the duodenum, but not in the brain, by ribonuclease (RNase) protection assays (RPAs) specific for each *Tph* isoform (Fig. 1B). In contrast, *Tph2* was detected exclusively in the brain (Fig. 1B). Brain stem total RNA samples from wild-type mice revealed about 150 times more *Tph2* than *Tph1* mRNA by RPAs (*5*).

Transfected COS7 cells expressing TPH2 acquired tryptophan-hydroxylating activity, confirming the identity of this enzyme (Fig. 1C). Moreover, commercially available antibodies against TPH1 also detected TPH2 in transfected cells (*5*), thus explaining previous detection of TPH in the brain.

We also cloned and sequenced the rat and human TPH2 homologs (GenBank: AY098915 and AY098914; fig. S1) and detected TPH2 expression in rat brain (*5*). By searching GenBank, we found one homologous expressed sequence tag from chicken and several from zebrafish brain, in addition to a sequence from zebrafish ovary with high homology to the mammalian TPH1 (*6*).

The discovered duality of the serotonin system in vertebrates may open up new avenues for specific therapeutic approaches exclusively affecting central or peripheral 5-HT actions. This is particularly important, because of efforts to find diagnostically useful correlations between peripheral levels of 5-HT and its metabolites and 5-HT function in the central nervous system of human patients suffering from psychiatric disorders (*7*). Also, numerous attempts linking polymorphisms in the *Tph1* gene with such diseases (*1*) have to be reconsidered now that it is known that this gene is hardly expressed in the brain.

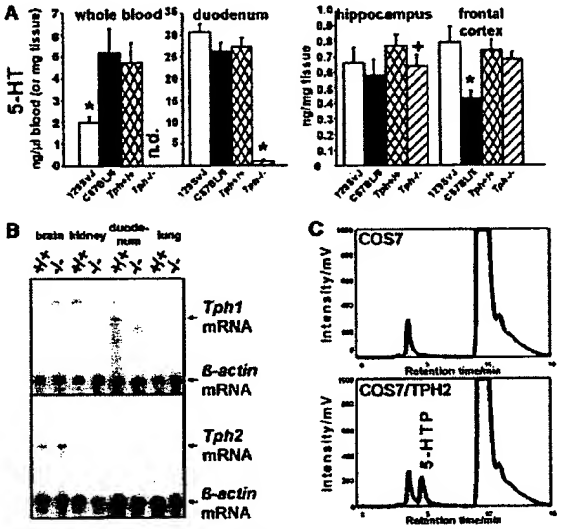

Fig. 1. (A) 5-HT in whole blood, duodenum, hippocampus, and frontal cortex of 129SvJ, C57BL/6, *Tph*+/+, and *Tph*−/− mice. n.d., below the detection limit of the assay (<5 pg/µl). *, statistically significant ($P < 0.05$), as compared with all other investigated mouse lines. +, statistically significant ($P < 0.05$), as compared with *Tph*+/+ mice, but not with other laboratory mouse lines. (B) RNase protection assays with probes specific for the two isoforms reveal the presence of *Tph1* mRNA in duodenum of wild-type animals, but not in *Tph*−/− mice. *Tph2* mRNA is present exclusively in brain, irrespective of the genotype. (C) Reversed-phase HPLC-FD chromatograms of TPH activity assays. (Top) Untransfected COS7 cells. (Bottom) COS7 cells transiently transfected with a eukaryotic expression vector containing the mouse *Tph2* cDNA. 5-Hydroxylated tryptophan (5-HTP) elutes with a retention time of 5 min.

References and Notes

1. J. Veenstra-VanderWeele, G. M. Anderson, E. H. Cook Jr., *Eur. J. Pharmacol.* **410**, 165 (2000).
2. P. F. Fitzpatrick, *Annu. Rev. Biochem.* **68**, 355 (1999).
3. J. J. Chen *et al. J. Neurosci.* **21**, 6348 (2001).
4. D. M. Kuhn, M. A. Meyer, W. Lovenberg, *Arch. Biochem. Biophys.* **199**, 355 (1980).
5. D. J. Walther *et al.*, data not shown.
6. Accession numbers of vertebrate *Tph* sequences are provided in the supplementary material available on *Science* Online.
7. M. Humble, S. Bejerot, P. B. F. Bergqvist, F. Bengtsson, *Biol. Psychiatry* **49**, 360 (2001).

Supporting Online Material
www.sciencemag.org/cgi/content/full/299/5603/76/DC1
Materials and Methods
Fig. S1
Table S1

[1]Max Delbrück Center for Molecular Medicine (MDC), Robert-Rössle-Strasse 10, D-13092 Berlin-Buch, Germany. [2]Institute of Pharmacology and Toxicology of the Medical Faculty, Charité, Humboldt University Berlin, Dorotheenstrasse 94, D-10117 Berlin, Germany. [3]Institute of Pharmacology and Toxicology of the School of Veterinary Medicine, Free University Berlin, Koserstrasse 20, D-14195 Berlin, Germany.

*To whom correspondence and requests for materials should be addressed. E-mail: dwalther@mdc-berlin.de or mbader@mdc-berlin.de

MOLECULAR AND CELLULAR BIOLOGY, Jan. 2001, p. 148–155 Vol. 21, No. 1
0270-7306/01/$04.00+0 DOI: 10.1128/MCB.21.1.148–155.2001

Gene Disruption of Tissue Transglutaminase

VINCENZO DE LAURENZI AND GERRY MELINO*

IDI-IRCCS Biochemistry Lab, Department of Experimental Medicine, University Tor Vergata, Rome, Italy

Received 20 July 2000/Returned for modification 12 September 2000/Accepted 28 September 2000

Transglutaminase 2 (TGase 2), or tissue transglutaminase, catalyzes either ε-(γ-glutamyl)lysine or N^1,N^8-(γ-glutamyl)spermidine isopeptide bonds. TGase 2 expression has been associated with apoptosis, and it has been proposed that its activation should lead to the irreversible assembly of a cross-linked protein scaffold in dead cells. Thus, TGase 2-catalyzed protein polymerization contributes to the ultrastructural changes typical of dying apoptotic cells; it stabilizes the integrity of the apoptotic cells, preventing the release of harmful intracellular components into the extracellular space and, consequently, inflammation and scar formation. In order to perform a targeted disruption of the enzyme, we prepared a construct deleting part of exons 5 and 6, containing the active site, and intron 5. Complete absence of TGase 2 was demonstrated by reverse transcription-PCR and Western blot analysis. TGase activity measured on liver and thymus extracts showed, however, a minimal residual activity in TGase $2^{-/-}$ mice. PCR analysis of mRNA extracted from the same tissues demonstrated that at least TGase 1 (normally present in the skin) is also expressed in these tissues and contributes to this residual activity. TGase $2^{-/-}$ mice showed no major developmental abnormalities, and histological examination of the major organs appeared normal. Induction of apoptosis ex vivo in TGase $2^{-/-}$ thymocytes (by CD95, dexamethasone, etoposide, and H_2O_2) and in vitro on TGase $2^{-/-}$ mouse embryonal fibroblasts (by retinoids, UV, and H_2O_2) showed no significant differences. A reduction in cross-linked apoptotic bodies with a modestly increased release of lactate dehydrogenase has been detected in some cases. Together our results show that TGase 2 is not a crucial component of the main pathway of the apoptotic program. It is possible that the residual enzymatic activity, due to TGase 1 or redundancy of other still-unidentified TGases, can compensate for the lack of TGase 2.

Transglutaminase 2 (TGase 2; also called tissue transglutaminase or TG C) belongs to the transglutaminase (EC 2.3.2.13) family, which includes intracellular and extracellular enzymes catalyzing Ca^{2+}-dependent reactions resulting in the formation of ε-(γ-glutamyl)lysine cross-links and/or in the covalent incorporation of di- and polyamines and histamine (25, 26). The establishment of these covalent cross-links leads to the posttranslational modification and, in many instances, the oligomerization of substrate proteins. The resulting protein polymers are resistant to breakage and chemical attack and can release polypeptides only through the proteolytic degradation of protein chains. At least seven distinct types of TGases in mammals have been characterized: TGase 1 (or TG K), TGase 2, TGase 3 (or TG E), TGase X, coagulation factor XIII, band 4.2, and prostate TGase. At least four transglutaminases (TGases 1, 2, 3, and X) are expressed and synthesized during terminal differentiation and death of human epidermal keratinocytes (44, 45), where they contribute to the formation of the cornified envelope.

The TGase 2 gene is constitutively expressed both during development (29, 48) and in adult tissues (for a review, see reference 36). In both cases a tight correlation between TGase 2 expression and occurrence of apoptosis has been found. This includes, for example, interdigital web formation (29), implantation of the embryo in utero (35), and mammary gland regression (31, 46). In addition, the presence and activity of the enzyme have been shown to increase in cells undergoing apoptosis in several models (2, 9, 10, 21, 23–25, 32–34, 37, 40). Indeed, during apoptosis de novo transcription of the TGase 2 gene is induced by several factors (e.g., retinoic acid [RA], prostaglandin E2, interleukin 6, and tumor growth factor β). Moreover, in addition to transcriptional regulation (24, 28, 41), TGase 2 can also be modulated posttranscriptionally (1, 23, 50) during apoptosis. TGase 2 activation leads to the assembly of intracellular cross-linked protein polymers, which irreversibly modifies cell organization, contributing to the wide ultrastructural changes occurring in cells undergoing apoptosis (9, 10, 39). This extensive TGase 2-dependent protein polymerization stabilizes apoptotic cells before their clearance by phagocytosis, thus contributing to the prevention of inflammation in the surrounding tissues (39).

In addition to its cross-linking activity, TGase 2 acts as the Gαh subunit, associated with the 50-kDa β subunit (Gβh), of the GTP-binding protein (Gh) in a ternary complex associated with the rat liver α1-adrenergic receptor (30). Thus, TGase 2-Gαh is a multifunctional protein, which by binding GTP in a Gαh-GTP complex can modulate receptor-stimulated phospholipase C activation.

In order to clarify the role of TGase 2 in apoptosis we have generated mice lacking TGase 2 by homologous recombination techniques. Our results, however, show that the disruption of TGase 2 does not produce a major phenotype and that apoptosis still occurs normally in the absence of TGase 2.

* Corresponding author. Mailing address: IDI-IRCCS, Biochemistry Lab, c/o Dep. Experimental Medicine, D26/F153, University of Rome Tor Vergata, Via Tor Vergata 135, 00133 Rome, Italy. Phone: 39 6 20427299. Fax: 39 6 20427290. E-mail: gerry.melino@uniroma2.it.

MATERIALS AND METHODS

Reagents. Ham's F-12 and minimal essential media were from Gibco (Berlin, Germany), and fetal calf serum was from HyClone (Oud-Beijerland, The Neth-

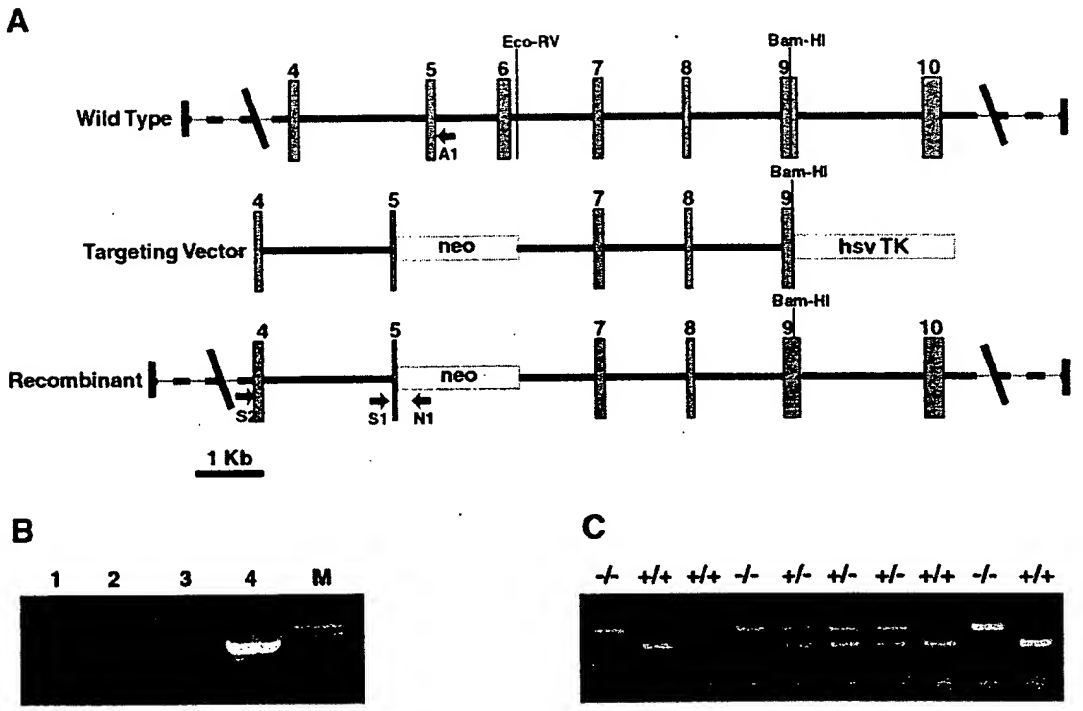

FIG. 1. (A) Schematic representation of the targeting construct used to generate TGase 2 knockout mice. An *Eco*RV/*Bam*HI genomic fragment (from intron 6 to exon 9) was cloned at the 5′ end of the neomycin resistance gene into the pPNT vector (49). Subsequently, a PCR fragment from exon 4 to exon 5 was cloned into this vector at the 5′ end of the neomycin resistance gene, using an *Xho*I site. As a result, part of exon 5 and the totality of exon 6 (containing the active site) and intron 5 were deleted. The arrows show the positions of the primers used for the screening of the recombinant clones (N1 and S2) and the genotyping of the mice (A1, N1, and S1). Intron positions were obtained by direct sequencing or PCR analysis with primers located in the flanking exons. The position of exon 7 was not determined, and therefore its position in the scheme is arbitrary. hsv TK, herpes simplex virus thymidine kinase. (B) PCR screening for the recombinant clone using a primer in the neomycin resistance gene (N1) and a primer on the TGase sequence (S2) in a region upstream of the fragment used to generate the targeting vector. Lanes 1 to 3 contain wild-type clones, and lane 4 contains the recombinant clone used to generate chimeras. (C) PCR screening for the genotyping of the mice. Three different primers (see Materials and Methods) were used at the same time: an antisense primer on the neomycin resistance gene (N1), an antisense primer in intron 5 (A1) deleted in the targeted alleles, and a sense primer in intron 4 (S1) present in both wild-type and targeted alleles.

erlands). HEPES, bovine serum albumin (BSA), RNase A, propidium iodide (PI), Triton X-100, RA, *N,N′*-dimethylcasein, and putrescine were obtained from Sigma Chemical (St. Louis, Mo.). The mouse monoclonal anti-TGase 2 antibodies (clone CUB 7402 and clone CUB 7402+TG100) were purchased from Neo-Markers (Union City, Calif.). All electrophoresis reagents and secondary antibodies were from Bio-Rad (Richmond, Calif.) [^{3}H]putrescine was obtained from Amersham (Arlington Heights, Ill.).

Generation of TGase 2-deficient mice. A genomic clone containing the genomic sequence 3′ of exon 5 was isolated by screening a 129/SvJ mouse genomic library (Stratagene, La Jolla, Calif.). The targeting vector (Fig. 1A) was constructed by cloning an ~4-kb *Eco*RV/*Bam*HI fragment of this clone, containing the sequence from intron 6 to exon 9, into the pPNT vector (49) 3′ of the neomycin resistance gene between the *Xba*I and *Bam*HI unique sites. An ~2-kb fragment containing intron 3 was generated by PCR using primers designed on the basis of the sequence of exons 4 and 5. This fragment was cloned into the *Xho*I site of the pPNT vector 5′ of the neomycin resistance gene. This construct deletes 1.2 kb containing part of exon 5, intron 5, exon 6, and a small piece of intron 6 up to the *Eco*RV site.

The targeting vector was linearized by *Not*I and electroporated into embryonic stem cells. Cells were selected with G418 and ganciclovir. Surviving clones were screened by PCR using the following primers: S2 (5′AGCCGATGATGTGTA CCTAGAC3′) and N1 (5′ACGAGACTAGTGAGACGTGC3′) (Fig. 1B). The following PCR program was used: 95°C for 5 min, followed by 40 cycles of 94°C for 1 min, 58°C for 1 min, and 72°C for 1 min. PCR products were resolved on a 0.8% agarose gel and stained with ethidium bromide. The positive clone was then confirmed by Southern blotting.

Cells from the positive clone were microinjected into C57BL/6 blastocysts and transferred into pseudopregnant recipients by Genome Systems, St. Louis, Mo. The six chimeric animals obtained were bred with C57BL/6 mice. The genotype of the subsequent offspring was determined by PCR using the following primers: S1 (5′TACTCCAGCTTCCTGTTCTG3′), A1 (5′TCCTGACCTGAGTCCTCG TC3′), and N1 (Fig. 1). The following PCR program was used: 95°C for 5 min, followed by 30 cycles of 94°C for 1 min, 56°C for 45 s, and 72°C for 1 min. PCR products were resolved on a 1% agarose gel and stained with ethidium bromide. Each mouse was individually genotyped before every experiment.

Cell cultures. Mouse embryonic fibroblasts (MEFs) and thymocytes were grown in a 1:1 mixture of minimal essential medium and Ham's F-12 medium supplemented with 10% heat-inactivated fetal calf serum, 1.2 g of sodium bicarbonate per liter, and 15 mM HEPES at 37°C with 5% CO_2 in a humidified atmosphere.

Western blotting. Livers were homogenized in 3 ml of cold lysis buffer containing 100 mM Tris-HCl (pH 7.4), 10 mM KCl, 2 mM $MgCl_2$, 0.1% Triton X-100, 1 mM EDTA, and 1 mM phenylmethylsulfonyl fluoride. They were then centrifuged, and the protein content of the supernatants was determined using the Bradford method (Bio-Rad). Proteins were normalized to 30 μg/lane, separated on sodium dodecyl sulfate (SDS)–12% polyacrylamide gels, and blotted onto nitrocellulose sheets. Filters were washed twice with phosphate-buffered saline (PBS) containing 0.1% Tween 20 before blocking nonspecific binding

overnight with 10% nonfat milk and 5% BSA dissolved in PBS–0.1% Tween 20. The TGase 2 antigen was detected by incubation for 2 h with a 1:1 mixture of mouse monoclonal anti-TGase 2 antibodies (1:300 in PBS–0.1% Tween 20). Nitrocellulose filters were washed five times, and detection was performed by horseradish peroxidase-conjugated goat anti-mouse monoclonal antibody (1:2,500 in PBS–0.1% Tween 20 with 10% milk and 5% BSA) for 1 h at room temperature, using the ECL method (Amersham).

Enzyme assay. TGase activity was determined by measuring the incorporation of [^{3}H]putrescine into *N,N'*-dimethylcasein (22, 26). The reaction mixture contained 150 mM Tris-HCl buffer (pH 8.3), 90 mM NaCl, 10 mM dithiothreitol, 15 mM $CaCl_2$, 12.5 mg of *N,N'*-dimethylcasein/ml, and 0.2 mM putrescine containing 1 μCi of [^{3}H]putrescine. Proteins from different tissue and cellular extracts (0.1 to 0.3 mg) were incubated with the reaction mixture in a final volume of 150 μl at 37°C. After 20 min of incubation, the reaction was stopped by spotting 100-μl quadruplicate aliquots onto Whatman 3MM filter paper. Unbound [^{3}H]putrescine was removed by washing with large volumes of 15, 10, and 5% trichloroacetic acid and absolute ethanol. Filters were then air dried and the radioactivity was measured by liquid scintillation counting.

PCR analysis of TGases 2 and 1. Total RNA was extracted from mouse livers, using the RNeasy minikit from Qiagen (Crawley, United Kingdom). Reverse transcription (RT)-PCRs were performed with the RT-PCR One Step System (Life Technologies, Paisley, United Kingdom), using 100 ng of total RNA, according to the manufacturer's instructions. The primers used for the amplification of TGase 2 were TG30 (5'GACAACAACTATGGGGATGGT3') and TG9B (5'ATCATCTCGCTCTTGTTCGTC3'). The primers used for the amplification of TGase 1 were MTG1F (5'ACCACCACAGTGCTCCGATG3') and MTG1R (CCACACGTGGAAGTTCCAAAC3'). The following PCR program was used in all cases: 42°C for 30 min and 94°C for 2 min, followed by 35 cycles of 94°C for 30 s, 57°C for 30 s, and 70°C for 30 s. PCR products were resolved on a 1.6% agarose gel and stained with ethidium bromide.

Determination of cell death. To estimate DNA fragmentation, a mixture of floating cells and cells mechanically recovered from flasks, which had been subjected to different treatments, were collected at 800 × *g* for 10 min and fixed with a 1:1 solution of PBS and methanol-acetone (4:1, vol/vol) at −20°C. The cell cycle was evaluated by flow cytometry using PI staining (40 mg/ml) (22) in the presence of 13 kU of RNase A per ml (20 min of incubation at 37°C) on a FACS-Calibur flow cytometer (Becton Dickinson, San Jose, Calif.). Cells were excited at 488 nm using a 15-mW argon laser, and the fluorescence was monitored at 578 nm at a rate of 150 to 300 events/s. Ten thousand events were evaluated using the Cell Quest program (Becton Dickinson). Electronic gating (FSC-a/vs/FSC-h) was used, when appropriate, to eliminate cell aggregates.

LDH release. For measurement of lactate dehydrogenase (LDH) levels, a kit was used according to the manufacturer's instructions (Sigma Chemical). Briefly, the cell culture supernatant was incubated with pyruvate and NADH, and the LDH activity was determined photometrically at 340 nm.

Quantification of cross-linked apoptotic bodies. Cross-linked apoptotic bodies were estimated on cells cultured in 175-cm^2 flasks, as previously described (26). Cells floating in the culture medium were collected by centrifugation at 800 × *g* for 10 min and pooled with the cells mechanically recovered from flasks. After being washed in PBS, cells were suspended in 1 ml of lysis buffer (10 mM KCl, 2 mM $MgCl_2$, and 0.5% Triton X-100 in 10 mM Tris-HCl, pH 7.4) containing 1 mM phenylmethylsulfonyl fluoride and 2 mM iodoacetamide. After centrifugation the pellet was washed in lysis buffer, suspended in a 2% sodium dodecyl sulfate solution containing 5% β-mercaptoethanol, and boiled, and the number of detergent-insoluble apoptotic bodies was scored using a phase-contrast microscope (Diaphot; Nikon) and normalized to milligrams of protein.

RESULTS

Generation of TGase 2-deficient mice. The TGase 2 gene was disrupted by homologous recombination. The targeting vector deletes 1,200 bp of the TGase gene from exon 5 to intron 6. This deletion includes exon 6, which contains the active site. The loss of the catalytic site abolishes the protein cross-linking activity of TGase 2, consequently removing its presumed role in the formation of the apoptotic body. Figure 1 shows the targeting vector and the screening strategy.

TGase $2^{-/-}$ mice show no clear phenotypic abnormality (macroscopic or microscopic); they develop normally and are capable of reproducing at the expected frequency.

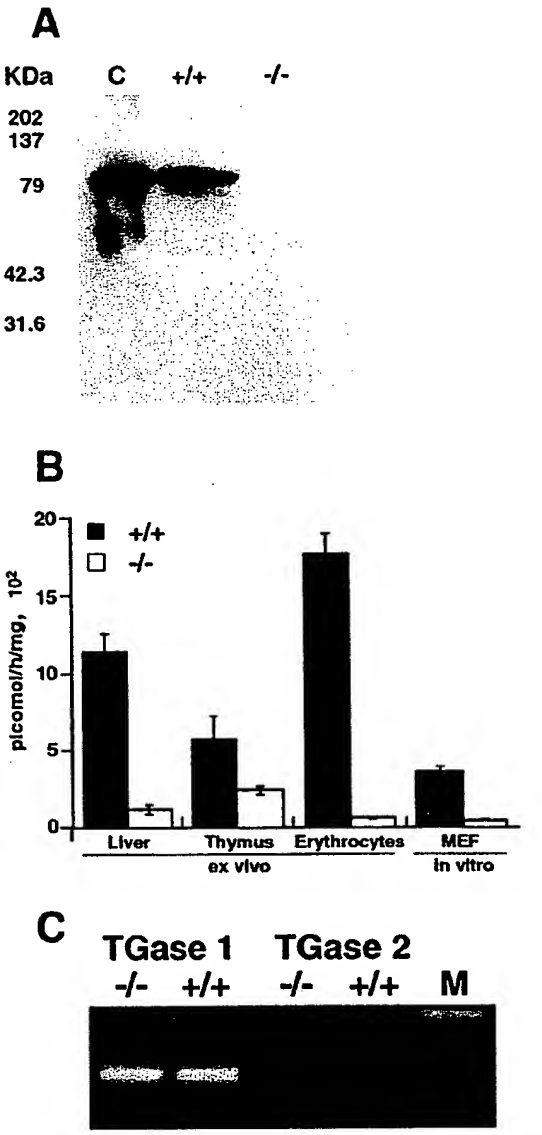

FIG. 2. (A) Western blotting performed on liver extracts from wild-type and TGase-knockout mice with anti-TGase 2 antibody. Thirty micrograms of total protein was loaded in each lane. Recombinant guinea pig TGase 2 (0.1 μg) was used as a positive control (C). This blot is representative of experiments performed on different tissues from four different animals per group. (B) TGase enzymatic activity measured in extracts from different mouse tissues and cultured MEFs in both wild-type and TGase-knockout mice. Activity was measured as incorporation of [^{3}H]putrescine into casein. Standard deviations for 10 different evaluations are shown. (C) RT-PCR performed on RNA extracted from thymus tissues of wild-type and TGase-knockout mice using primers for TGase 2 and TGase 1.

In order to confirm that no TGase 2 protein is produced in TGase 2-deficient mice, we performed Western blot analysis on liver, thymus, brain, and erythrocyte extracts from wild-type animals (TGase $2^{+/+}$) and from TGase $2^{-/-}$ mice. Our results

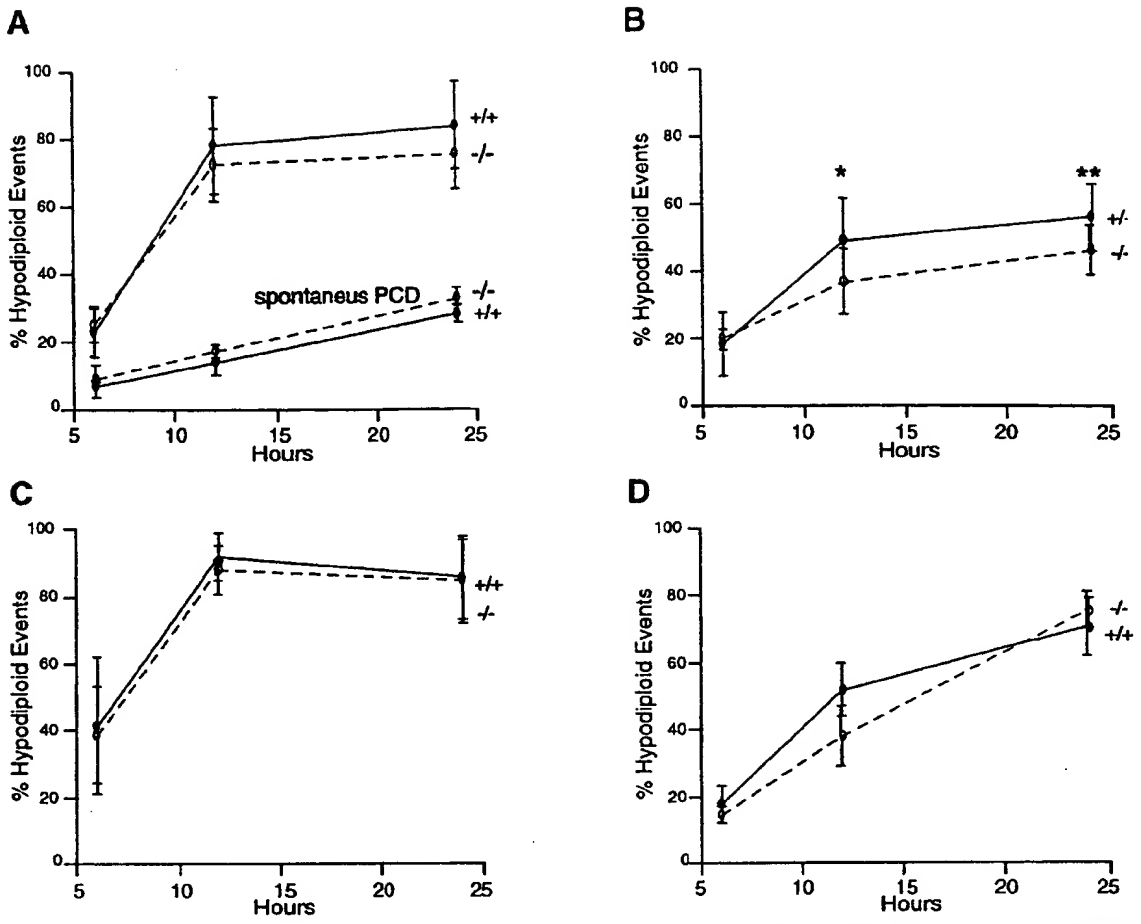

FIG. 3. Hypodiploid events in wild-type and knockout mouse thymocytes, either left untreated (spontaneous programmed cell death [PCD]) (bottom curves in panel A) or treated with etoposide (25 μM) (top curves in panel A), anti-CD95 agonist antibody (1 μg/ml) (B), dexamethasone (10 μM) (C), and H_2O_2 (30 μM) (D). Cells were treated for 6, 12, and 24 h, then fixed with a 1:1 solution of PBS and methanol-acetone (4:1, vol/vol) at −20°C and stained with PI. The number of events (10,000 collected) with hypodiploid DNA was measured by flow cytometry. The data reported are averages of four independent experiments performed on different mice. *, $P = 0.0352$ for +/+ versus −/− mice; **, $P = 0.0451$ for +/+ versus −/− mice (according to the Student t test). Differences not indicated are not statistically significant.

show the absence of TGase 2 protein in the −/− animals (Fig. 2A shows liver extracts). However, measurement of TGase activity (Fig. 2B) in different tissues extracted from TGase $2^{-/-}$ animals showed that some residual TGase enzyme activity was still present. Indeed, while erythrocytes showed a reduction in activity close to 100%, thymocytes showed the highest level of residual TGase activity, which is quite significant compared with the activity of TGase $2^{+/+}$ animals. RT-PCR of RNA extracted from thymus tissues of both +/+ and −/− animals showed that no transcript for TGase 2 was present in −/− animals (Fig. 2C).

In order to detect and identify TGases different from type 2, we performed RT-PCRs using both specific and degenerate primers for the catalytic site region of TGases. Figure 2C shows that similar amounts of TGase 1 were expressed in −/− and +/+ animals. This should account for the residual TGase enzymatic activity.

TGase $2^{-/-}$ thymocytes and MEFs show normal induction of apoptosis. Since a large number of reports suggest a role for TGase 2 in apoptosis, including in vivo in the thymus (47), we studied apoptosis induced ex vivo in mouse thymocytes and in vitro in MEFs.

Apoptosis was induced with different stimuli, namely, etoposide (Fig. 3A), CD95 ligation (Fig. 3B), dexamethasone (Fig. 3C), and H_2O_2 (Fig. 3D). Figure 3A shows also the spontaneous level of apoptosis of thymocytes ex vivo. No relevant difference in the number of cells undergoing apoptosis was observed between +/+ and −/− animals with any of the treatments.

The evaluation of apoptosis ex vivo was performed on cells presenting a significant TGase enzymatic activity (Fig. 2B), at least in part due to TGase 1. We therefore performed similar experiments on cultured MEFs, which show the lowest residual enzymatic activity (Fig. 2B).

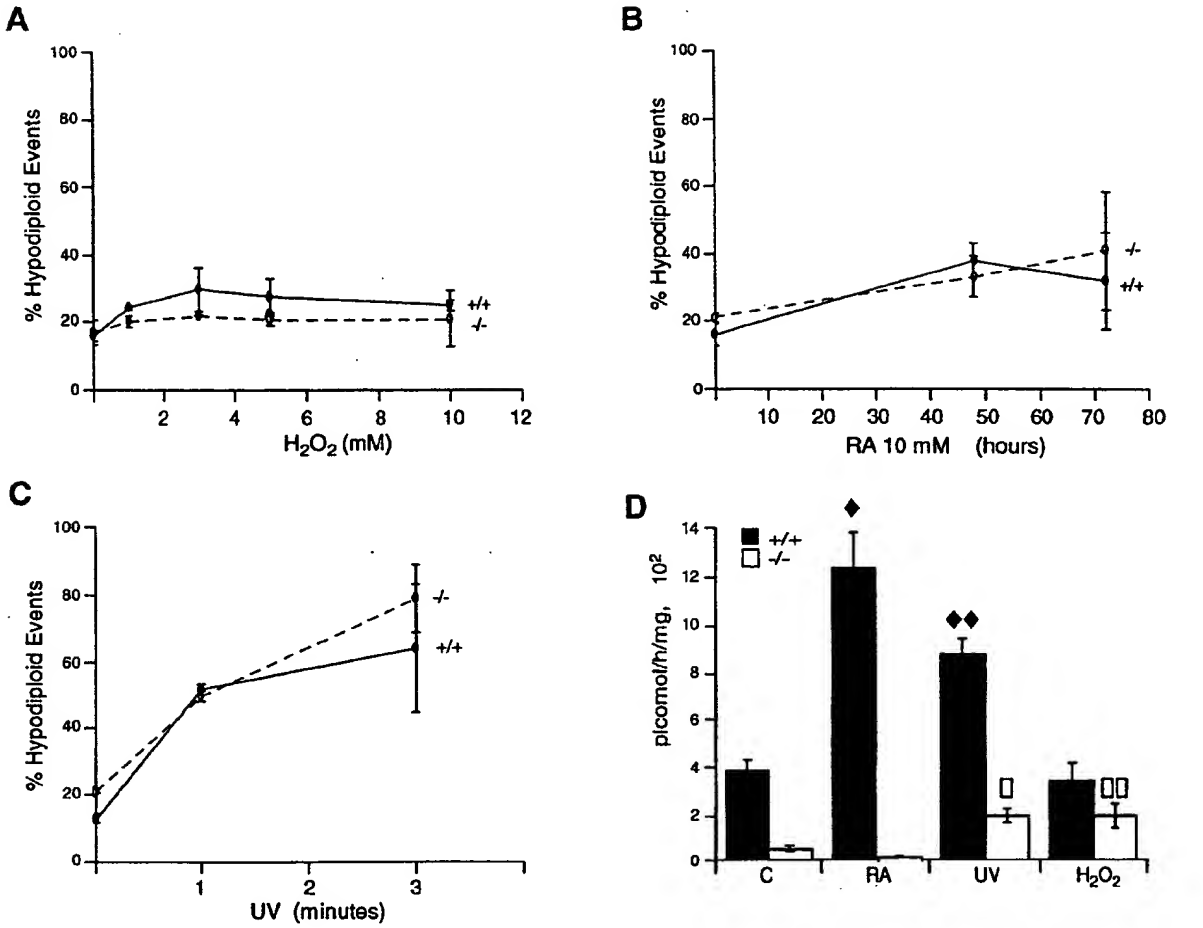

FIG. 4. Hypodiploid events in wild-type and knockout MEFs treated with 1, 3, 5, and 10 mM H_2O_2 for 15 min in PBS, washed, and then cultured in medium for 24 h (A); treated with 10 μM RA for 48 and 72 h (B); or treated with UV irradiation for 1 or 3 min in PBS and then cultured in medium for 24 h (C). Cells were fixed with a 1:1 solution of PBS and methanol-acetone (4:1, vol/vol) at −20°C and stained with PI. The number of events with hypodiploid DNA was measured by flow cytometry (see Materials and Methods). The data reported are averages of four independent experiments. (D) Corresponding transglutaminase activity in wild-type and knockout MEFs, untreated (C) or treated with 10 μM RA for 48 h, UV irradiation for 3 min followed by 24 h of culture, and 5 mM H_2O_2 followed by 24 h of culture. The data reported are averages of four independent experiments. Statistical differences between treated cells and the corresponding controls were evaluated. In detail, differences were statistically significant as follows: ◆, $P = 0.0189$ for control and RA-treated +/+ cells; ◆◆, $P = 0.0013$ for control and UV-treated +/+ cells; □, $P = 0.0294$ for control and UV-treated −/− cells; and □□, $P = 0.0475$ for control and H_2O_2-treated −/− cells. Differences not indicated were not statistically significant. All differences between +/+ and −/− cells are statistically significant.

As in the ex vivo studies, no difference was observed when +/+ and −/− MEFs were treated in vitro with H_2O_2 (Fig. 4A), RA (Fig. 4B), or UV (Fig. 4C). Treatment of +/+ MEFs with RA and UV resulted in an increase in TGase activity; −/− MEFs had a much lower basal activity that increased with UV and H_2O_2 treatment, while RA treatment resulted in a decrease of TGase activity (Fig. 4D). Since TGase 1 is negatively regulated by retinoids, while TGase 2 is upregulated (50), these results are in keeping with the evidence that the minimal residual activity observed in MEFs is due to TGase 1 (Fig. 4D). Indeed, as for thymocytes, mRNA for TGase 1 was also detected in MEFs by RT-PCR (data not shown).

Cross-linked apoptotic body formation is present in TGase $2^{-/-}$ mice. It has been consistently suggested that TGase 2 induction during apoptosis results in the formation of cross-linked insoluble apoptotic bodies. In order to investigate the possibility that the formation of cross-linked apoptotic bodies is impaired in TGase $2^{-/-}$ mice, we measured the number of insoluble apoptotic bodies in control or RA-, UV-, and H_2O_2-treated MEFs. Figure 5A shows that apoptotic bodies also formed in TGase $2^{-/-}$ cells, even though the number of cross-linked apoptotic bodies was significantly reduced in UV- and H_2O_2-treated −/− MEFs.

The reduction of cross-linked apoptotic bodies could be

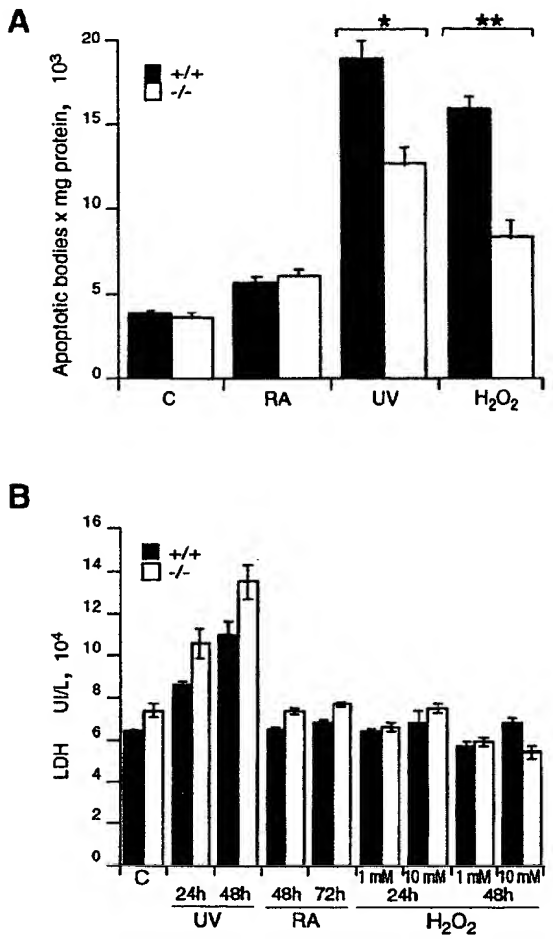

FIG. 5. (A) Cross-linked apoptotic body formation in wild-type and knockout MEFs. Cells were treated with 10 μM RA for 48 h, UV irradiation for 3 min followed by culture for 24 h, or 3 mM H_2O_2 for 15 min followed by culture for 24 h. See Materials and Methods for details. (B) LDH release in wild-type and knockout MEFs. Cells were left untreated (C) or treated with UV irradiation for 3 min followed by culture for 24 and 48 h, 10 μM RA for 48 and 72 h, or 1 and 10 mM H_2O_2 for 15 min followed by culture for 24 and 48 h. The data reported are averages of four independent experiments. Statistical analysis was performed according to the Student *t* test to compare +/+ and −/− cells: *, $P = 0.0014$; **, $P = 0.0003$. Differences not indicated are not statistically significant.

accompanied by an increased release of cytoplasmic material from cells undergoing apoptosis. In order to evaluate this aspect, we measured the release of LDH from +/+ and −/− MEFs after induction of apoptosis with UV, RA, and H_2O_2. Figure 5B shows that LDH release was only moderately increased (not statistically significant) in +/+ versus −/− MEFs. Treatment with UV, with which some necrosis was expected, showed a significant increase in LDH release in both +/+ and −/− cells. Therefore, our results are consistent with an essentially normal induction of apoptosis.

DISCUSSION

We have generated TGase 2-deficient mice through homologous recombination techniques. No TGase 2 was detectable in these mice by RT-PCR or Western blotting. The mice were viable and fertile and showed no developmental abnormalities. Apoptosis induced with different agents in both fibroblasts and thymocytes is normal. The reduction in enzymatic activity in −/− mice showed only a minor effect on both cross-linked apoptotic body formation (Fig. 5A) and LDH release (Fig. 5B), with no major consequences for the mice. Although we cannot exclude the possibility that TGase 2 deficiency may play a role in pathological situations (11, 38), aged mice (up to 20 months of age) do not show abnormalities such as cancer development and generation of autoimmunity (data not shown). It might be necessary to cross the mice into a more permissive genetic background in order to reveal an overt phenotype.

Deletion of various genes involved in apoptosis does not always produce an evident phenotype. Mice with deleted caspases 1, 2, 6, and 11 do not show evident developmental abnormalities (51), while in other cases a very specific or minimal phenotype is observed. Disruptions of other genes produce a phenotype only when animals are stressed with specific inducers requiring that protein, namely, radiation on $p53^{-/-}$ (8) or liposaccharides on caspase $1^{-/-}$ (16, 18) cells. Even though the accredited model for apoptosis indicates the requirement for the apoptosome and in particular for apaf-1 and caspases 3 and 9 (for a review, see references 6 and 17), the knockout of the genes for these proteins shows that thymocytes are still able to undergo apoptosis (for a review, see references 5 and 51). This has elicited various explanations, including the existence of additional unknown pathways or compensation mechanisms.

Similarly, there are different possible interpretations for the lack of phenotype in TGase 2 animals: (i) TGase 2 is not involved in apoptosis; (ii) it is not involved in the central, essential apoptotic machinery, but it is part of a regulatory or side pathway elicited only by specific inducers or only in specific tissues; or (iii) there is redundancy in the system.

The lack of effect on apoptosis of targeted disruption of the TGase 2 gene is in apparent contrast to previous evidence in favor of a role for TGase 2 in the apoptotic program. Indeed, it has been shown previously that transfection of an antisense TGase 2 construct into cell lines confers resistance to apoptosis induction, while sense transfectants show enhanced spontaneous apoptosis (22). There are several reasons for this disparity. First, not all models of apoptosis require TGase 2. For example, CD95 ligation elicits apoptosis independently of the steady-state levels of TGase 2 protein (3); correspondingly, there is no change in TGase enzymatic activity during CD95-induced apoptosis (3). Second, other TGases may assume the protein cross-linking role of TGase 2. Indeed, the TGase $2^{-/-}$ mice showed different degrees of TGase enzymatic activity in different tissues. Our data show the presence of TGase 1 in both +/+ and −/− mice. Recently, TGase 1 has been shown to exist in tissues different from the skin, namely, in the central nervous system (15). Furthermore, the TGase activity levels in −/− thymocytes is inhibited by GTP, a property of TGase X (E. Candi, G. Melino, et al., unpublished observation), sug-

gesting its expression in lymphoid tissue. Therefore, the possibility that other TGases, and particularly TGase 1, can compensate for TGase 2 loss cannot be excluded. TGases show very different biochemical properties, such as k_{cat}/K_m ratio, residue preference, and yield (26). Therefore, it is unlikely that there is a perfect compensation among distinct TGases. In fact, TGase 1 knockout animals show a lethal phenotype, despite the presence of four distinct TGases in the skin (20). However, point mutations for TGase 1 in humans, with complete loss of TGase enzymatic activity (4), are compatible with life but cause a skin disease known as lamellar ichthyosis (12, 42), suggesting a different degree of compensation in humans.

Despite the large body of data suggesting an involvement of TGase 2 in apoptosis, its precise role in this process is not evident from the present gene disruption study. While the TGase $2^{-/-}$ animals could be used to study other functions of the enzyme, particularly by further crossbreeding to evaluate its contribution in pathologies such as celiac (7, 27) and Huntington (13, 14, 19, 43) diseases, clarification of the importance of TGase 2 in apoptosis may well require the generation of animals deficient in multiple TGases.

ACKNOWLEDGMENTS

We thank Mauro Piacentini, Gennaro Ciliberto, and Richard A. Knight for generous support, critical discussions, and helpful suggestions. This work could not have been completed without the generous help of Francesca Bernassola, Eleonora Candi, Marco Corazzari, Daniela Barcaroli, and Marco Ranalli. We thank Giuseppe Bertini, Giancarlo Cortese, and Pierino Piccoli (S.S.D. SAFU, Instituto Fisioterapici Ospedalieri, Rome, Italy) for technical assistance and mouse husbandry.

The work was partially supported by grants from MURST, MinSan, Associazione Neuroblastoma, AIRC, Telethon (E 872 and E 1257), and EU (QLG1-1999-00739).

REFERENCES

1. **Achyuthan, K. E., and C. S. Greenberg.** 1987. Identification of a guanosine triphosphate-binding site on guinea pig liver transglutaminase. Role of GTP and calcium ions in modulating activity. J. Biol. Chem. 262:1901–1906.
2. **Amendola, A., M. L. Gougeon, F. Poccia, A. Bondurand, L. Fesus, and M. Piacentini.** 1996. Induction of "tissue" transglutaminase in HIV-pathogenesis: evidence for high rate of apoptosis of CD4+ T lymphocytes and accessory cells in lymphoid tissues. Proc. Natl. Acad. Sci. USA 93:11057–11062.
3. **Bernassola, F., C. Scheurpflug, I. Herr, P. H. Krammer, K. M. Debatin, and G. Melino.** 1999. Induction of apoptosis by IFNgamma in human neuroblastoma cell lines through the CD95/CD95L autocrine circuit. Cell Death Differ. 6:652–660.
4. **Candi, E., G. Melino, A. Lahm, R. Ceci, A. Rossi, I.-G. Kim, B. Ciani, and P. M. Steinert.** 1998. Transglutaminase 1 mutations in lamellar ichthyosis. J. Biol. Chem. 273:13693–13702.
5. **Cecconi, F.** 1999. Apaf1 and the apoptotic machinery. Cell Death Differ. 6: 1087–1098.
6. **De Laurenzi, V., and G. Melino.** 2000. Apoptosis. The little devil of death. Nature 406:135–136.
7. **Dieterich, W., T. Ehnis, M. Bauer, P. Donner, U. Volta, E. O. Riecken, and D. Schuppan.** 1997. Identification of tissue transglutaminase as the autoantigen of celiac disease. Nat. Med. 3:797–801.
8. **Donehower, L. A., M. Harvey, B. L. Slagle, M. J. McArthur, C. A. Montgomery, Jr., J. S. Butel, and A. Bradley.** 1992. Mice deficient for p53 are developmentally normal but susceptible to spontaneous tumours. Nature 356:215–221.
9. **Fesus, L., V. Thomazy, F. Autuori, M. P. Ceru', E. Tarcsa, and M. Piacentini.** 1989. Apoptotic hepatocytes become insoluble in detergents and chaotropic agents as a result of transglutaminase action. FEBS Lett. 245:150–154.
10. **Fesus, L., P. J. A. Davies, and M. Piacentini.** 1991. Apoptosis: molecular mechanisms in programmed cell death. Eur. J. Cell Biol. 56:170–177.
11. **Hettasch, J. M., N. Bandarenko, J. L. Burchette, T. S. Lai, J. R. Marks, Z. A. Haroon, K. Peters, M. W. Dewhirst, J. D. Iglehart, and C. S. Greenberg.** 1996. Tissue transglutaminase expression in human breast cancer. Lab. Investig. 75:637–645.
12. **Huber, M., I. Rettler, K. Bernasconi, E. Frenk, S. P. Lavrijsen, M. Ponec, A. Bon, S. Lautenschlager, D. F. Schorderet, and D. Hohl.** 1995. Mutations of keratinocyte transglutaminase in lamellar ichthyosis. Science 267:525–528.
13. **Igarashi, S., R. Koide, T. Shimohata, M. Yamada, Y. Hayashi, H. Takano, H. Date, M. Oyake, T. Sato, A. Sato, S. Egawa, T. Ikeuchi, H. Tanaka, R. Nakano, K. Tanaka, I. Hozumi, T. Inuzuka, H. Takahashi, and S. Tsuji.** 1998. Suppression of aggregate formation and apoptosis by transglutaminase inhibitors in cells expressing truncated DRPLA protein with an expanded polyglutamine stretch. Nat. Genet. 18:111–117.
14. **Kahlem, P., H. Green, and P. Djian.** 1998. Transglutaminase action imitates Huntington's disease: selective polymerization of Huntingtin containing expanded polyglutamine. Mol. Cell 1:595–601.
15. **Kim, S. Y., P. Grant, J. H. Lee, H. C. Pant, and P. M. Steinert.** 1999. Differential expression of multiple transglutaminases in human brain. Increased expression and cross-linking by transglutaminases 1 and 2 in Alzheimer's disease. J. Biol. Chem. 274:30715–30721.
16. **Kuida, K., J. A. Lippke, G. Ku, M. W. Harding, D. J. Livingstone, M. S.-S. Su, and R. A. Flavell.** 1995. Altered cytokine export and apoptosis in mice deficient in interleukin-1 beta converting enzyme. Science 281:2000–2002.
17. **Kumar, S.** 1999. Mechanisms mediating caspase activation in cell death. Cell Death Differ. 6:1060–1066.
18. **Li, P., H. Allen, S. Banerjee, S. Franklin, L. Herzog, C. Johnstone, J. McDowell, M. Paskind, L. Rodman, J. Salfeld, E. Townes, D. Tracey, S. Wardwell, F.-Y. Wei, W. W. Wong, R. Kamen, and T. Seshadri.** 1995. Mice deficient in IL-1 beta-converting enzyme are defective in production of mature IL beta and resistant to endotoxic shock. Cell 80:401–411.
19. **Lorand, L.** 1998. DRPLA aggregation and transglutaminase, revisited. Nat. Genet. 20:231.
20. **Matsuki, M., F. Yamashita, A. Ishida-Yamamoto, K. Yamada, C. Kinoshita, S. Fushiki, E. Ueda, Y. Morishima, K. Tabata, H. Yasuno, M. Hashida, H. Inouka, M. Ikawa, M. Okabe, G. Kondoh, T. Kinoshita, J. Takeda, and K. Yamanishi.** 1998. Defective stratum corneum and early neonatal death in mice lacking the gene for transglutaminase 1 (keratinocyte transglutaminase). Proc. Natl. Acad. Sci. USA 95:1044–1049.
21. **Melino, G., M. G. Farrace, M. P. Ceru', and M. Piacentini.** 1988. Correlation between transglutaminase activity and polyamine levels in human neuroblastoma cells. Effect of retinoic acid and alpha-difluoromethylornithine. Exp. Cell Res. 179:429–445.
22. **Melino, G., M. Annicchiarico-Petruzzelli, L. Piredda, E. Candi, V. Gentile, P. J. A. Davies, and M. Piacentini.** 1994. Tissue transglutaminase and apoptosis: sense and antisense transfection studies with human neuroblastoma cells. Mol. Cell. Biol. 14:6584–6596.
23. **Melino, G., F. Bernassola, M. T. Corasaniti, R. A. Knight, G. Nistico, and A. Finazzi-Agro.** 1997. S-nitrosylation regulates apoptosis. Nature 388:432–433.
24. **Melino, G., M. Draoui, M. Piacentini, L. Bellincampi, F. Bernassola, U. Reichert, and P. Cohen.** 1997. Retinoic acid receptors a and g mediate tissue-transglutaminase induction in human neuroblastoma cells undergoing apoptosis. Exp. Cell Res. 255:55–61.
25. **Melino, G., and M. Piacentini.** 1998. Tissue transglutaminase in apoptosis: a downstream or a multifunctional upstream effector? FEBS Lett. 430:59–63.
26. **Melino, G., E. Candi, and P. M. Steinert.** 2000. Assay for transglutaminases in cell death. Methods Enzymol 322:433–472.
27. **Molberg, O., S. N. Mcadam, R. Korner, H. Quarsten, C. Kristiansen, L. Madsen, L. Fugger, H. Scott, O. Noren, P. Roepstorff, K. E. Lundin, H. Sjostrom, and L. M. Sollid.** 1998. Tissue transglutaminase selectively modifies gliadin peptides that are recognized by gut-derived T cells in celiac disease. Nat. Med. 4:713–717.
28. **Nagy, L., M. Saydak, N. Shipley, S. Lu, J. P. Basilion, Z. H. Yan, P. Syka, R. Chandraratna, R. Heyman, and P. J. A. Davies.** 1996. Identification and characterization of a versatile retinoid response element (RARE/RXRE) in the promoter of the mouse tissue transglutaminase gene. J. Biol. Chem. 271: 4355–4365.
29. **Nagy, L., V. A. Thomazy, M. M. Saydak, J. P. Stein, and P. J. A. Davies.** 1997. The promoter of mouse tissue transglutaminase gene directs tissue-specific, retinoid-regulated and apoptosis-linked expression. Cell Death Differ. 4: 534–547.
30. **Nakaoka, H., D. M. Perez, K. J. Baek, T. Das, A. Husain, K. Misono, M. Im, and R. M. Graham.** 1994. Gh: a GTP-binding protein with transglutaminase activity and receptor signaling function. Science 264:1593–1596.
31. **Nemes, Z., Jr., R. R. Friis, D. Aeschlimann, S. Saurer, M. Paulsson, and L. Fesus.** 1996. Expression and activation of tissue transglutaminase in apoptotic cells of involuting rodent mammary tissue. Eur. J. Cell Biol. 70:125–133.
32. **Piacentini, M., L. Fesus, M. G. Farrace, L. Ghibelli, L. Piredda, and G. Melino.** 1991. The expression of "tissue" transglutaminase in two human cancer cell lines is related with the programmed cell death (apoptosis). Eur. J. Cell Biol. 54:246–254.
33. **Piacentini, M., M. Annicchiarico-Petruzzelli, S. Oliverio, L. Piredda, J. L. Biedler, and G. Melino.** 1992. Phenotype-specific "tissue" transglutaminase regulation in human neuroblastoma cells in response to retinoic acid: correlation with cell death by apoptosis. Int. J. Cancer 52:271–278.
34. **Piacentini, M., L. Fesus, and G. Melino.** 1993. Multiple cell cycle access to the apoptotic death programme in human neuroblastoma cells. FEBS Lett. 320:150–154.

35. **Piacentini, M., and F. Autuori.** 1994. Immunohistochemical localization of tissue transglutaminase and Bcl-2 in rat uterine tissues during embryo implantation and post-partum involution. Differentiation 57:51–61.
36. **Piacentini, M.** 1995. Tissue transglutaminase: a candidate effector element of physiological cell death. Curr. Top. Microbiol. Immunol. 200:163–176.
37. **Piacentini, M., L. Piredda, D. Starace, M. Annicchiarico-Petruzzelli, M. Mattei, S. Oliverio, M. G. Farrace, and G. Melino.** 1996. Differential growth properties of S- and N-type human neuroblastoma cell variants transplanted into SCID mice: correlation with apoptosis and effect of ethanol. J. Pathol. 180:415–422.
38. **Piacentini, M., and V. Colizzi.** 1999. Tissue transglutaminase: apoptosis versus autoimmunity. Immunol. Today 20:130–134.
39. **Piredda, L., A. Amendola, V. Colizzi, P. J. A. Davies, M. G. Farrace, M. Fraziano, V. Gentile, L. Uray, M. Piacentini, and L. Fesus.** 1997. Lack of "tissue" transglutaminase protein cross-linking leads to leakage of macromolecules from dying cells: relationship to development of autoimmunity in MRLlpr/lpr mice. Cell Death Differ. 4:463–472.
40. **Piredda, L., M. G. Farrace, M. Lo Bello, W. Malorni, G. Melino, R. Petruzzelli, and M. Piacentini.** 1999. Identification of 'tissue' transglutaminase binding proteins in neural cells committed to apoptosis. FASEB J. 13:355–364.
41. **Ritter, S. J., and P. J. Davies.** 1998. Identification of a transforming growth factor-beta1/bone morphogenetic protein 4 (TGF-beta1/BMP4) response element within the mouse tissue transglutaminase gene promoter. J. Biol. Chem. 273:12798–12806.
42. **Russell, L. J., J. J. DiGiovanna, G. R. Rogers, P. M. Steinert, N. Hashem, J. G. Compton, and S. J. Bale.** 1995. Mutations in the gene for transglutaminase 1 in autosomal recessive lamellar ichthyosis. Nat. Genet. 9:279–283.
43. **Saudou, F., S. Finkbeiner, D. Devys, and M. E. Greenberg.** 1998. Huntingtin acts in the nucleus to induce apoptosis but death does not correlate with the formation of intranuclear inclusions. Cell 95:55–66.
44. **Steinert, P. M.** 1995. A model for the hierarchical structure of the human epidermal cornified cell envelope. Cell Death Differ. 2:33–40.
45. **Steinert, P. M., E. Candi, E. Taresa, L. N. Marekov, M. Sette, M. Paci, B. Ciani, P. Guerrieri, and G. Melino.** 1999. Transglutaminase crosslinking and structural studies of the human small proline rich 3 protein. Cell Death Differ. 6:916–930.
46. **Strange, R., F. Li, S. Saurer, A. Bukhard, and R. R. Friis.** 1992. Apoptotic cell death and tissue remodelling during mouse mammary gland involution. Development 115:49–58.
47. **Szondy, Z., P. Molnar, Z. Nemes, M. Boyiardzis, N. Kedei, R. Toth, and L. Fesus.** 1997. Differential expression of transglutaminase during in vivo apoptosis of thymocytes induced via distinct signalling pathways. FEBS Lett. 404:307–313.
48. **Thomazy, V. A., and P. J. Davies.** 1999. Expression of tissue transglutaminase in the developing chicken limb is associated both with apoptosis and endochondral ossification. Cell Death Differ. 6:146–154.
49. **Tybulewicz, V. L., C. E. Crawford, P. K. Jackson, R. T. Bronson, and R. C. Mulligan.** 1991. Neonatal lethality and lymphopenia in mice with a homozygous disruption of the c-abl proto-oncogene. Cell 65:1153–1163.
50. **Zhang, L. X., K. J. Mills, M. I. Dawson, S. J. Collins, and A. M. Jetten.** 1995. Evidence for the involvement of retinoic acid receptor RAR alpha-dependent signaling pathway in the induction of tissue transglutaminase and apoptosis by retinoids. J. Biol. Chem. 270:6022–6029.
51. **Zheng, T. S., S. Hunot, K. Kuida, and R. A. Flavell.** 1999. Caspase knockouts: matters of life and death. Cell Death Differ. 6:1043–1053.

A lupus-like syndrome develops in mice lacking the Ro 60-kDa protein, a major lupus autoantigen

Dahai Xue*, Hong Shi*, James D. Smith*, Xinguo Chen*, Dennis A. Noe*, Tommy Cedervall*, Derek D. Yang†, Elizabeth Eynon†, Douglas E. Brash‡, Michael Kashgarian§, Richard A. Flavell†, and Sandra L. Wolin*¶

*Department of Cell Biology and Howard Hughes Medical Institute, Yale University School of Medicine, New Haven, CT 06536; †Section of Immunobiology and Howard Hughes Medical Institute and §Department of Pathology, Yale University School of Medicine, New Haven, CT 06510; and ‡Departments of Therapeutic Radiology and Genetics, Yale University School of Medicine, New Haven, CT 06520

Communicated by Joan A. Steitz, Yale University, New Haven, CT, April 23, 2003 (received for review March 3, 2003)

Antibodies against a conserved RNA-binding protein, the Ro 60-kDa autoantigen, occur in 24–60% of all patients with systemic lupus erythematosus. Anti-Ro antibodies are correlated with photosensitivity and cutaneous lesions in these patients and with neonatal lupus, a syndrome in which mothers with anti-Ro antibodies give birth to children with complete congenital heart block and photosensitive skin lesions. In higher eukaryotes, the Ro protein binds small RNAs of unknown function known as Y RNAs. Because the Ro protein also binds misfolded 5S rRNA precursors, it is proposed to function in a quality-control pathway for ribosome biogenesis. Consistent with a role in the recognition or repair of intracellular damage, an orthologue of Ro in the radiation-resistant eubacterium *Deinococcus radiodurans* contributes to survival of this bacterium after UV irradiation. Here, we show that mice lacking the Ro protein develop an autoimmune syndrome characterized by anti-ribosome antibodies, anti-chromatin antibodies, and glomerulonephritis. Moreover, in one strain background, $Ro^{-/-}$ mice display increased sensitivity to irradiation with UV light. Thus, one function of this major human autoantigen may be to protect against autoantibody development, possibly by sequestering defective ribonucleoproteins from immune surveillance. Furthermore, the finding that mice lacking the Ro protein are photosensitive suggests that loss of Ro function could contribute to the photosensitivity associated with anti-Ro antibodies in humans.

Patients suffering from systemic rheumatic diseases such as scleroderma, systemic lupus erythematosus, and polymyositis often produce antibodies against highly conserved RNA–protein complexes. A fascinating but poorly understood facet of these diseases is that specific autoantibodies are associated with distinct rheumatic disease syndromes. For example, antibodies against tRNAs and tRNA–synthetase complexes are commonly found in polymyositis, whereas antibodies against nucleolar components are associated with scleroderma (1). This association of particular autoantibodies with specific syndromes has been useful for establishing diagnoses and for predicting sequelae that may accompany the particular rheumatic disorder.

In two rheumatic diseases, systemic lupus erythematosus and Sjögren's syndrome, a major target of the immune response is an RNA-binding protein known as the Ro 60-kDa autoantigen. In lupus patients, anti-Ro antibodies are highly associated with photosensitivity and photosensitive skin lesions, particularly those of subacute cutaneous lupus erythematosus (1, 2). In addition, anti-Ro antibodies are associated with neonatal lupus, a syndrome in which maternal autoantibodies cross the placenta, resulting in infants with photosensitive skin lesions and a cardiac conduction defect, complete congenital heart block (3).

Studies of the Ro 60-kDa protein have revealed that it is present in both the nucleoplasm and cytoplasm of vertebrate cells (4–6). In the cytoplasm, the Ro protein is complexed with one of several small RNAs known as Y RNAs. These Y RNAs are ≈100 nt long, transcribed by RNA polymerase III, and bound almost entirely by the Ro protein (7). The Ro protein/Y RNA complex is conserved evolutionarily, because orthologues have been described in mammals, the frog *Xenopus laevis*, and the nematode *Caenorhabditis elegans*, as well as the radiation-resistant eubacterium *Deinococcus radiodurans* (8–12). Although the function of the Y RNAs remains unknown, genetic depletions of the Ro protein from *C. elegans* and *D. radiodurans* have revealed that Ro protein binding stabilizes Y RNAs from degradation (12, 13). Both mammalian cells and *Xenopus* oocytes contain a nuclear pool of Ro protein, which is not complexed with Y RNAs (4–6).

Experiments in *X. laevis* and *C. elegans* have led to the proposal that the Ro 60-kDa protein functions in a quality-control pathway for ribosome biogenesis (6, 13). In *Xenopus* oocyte nuclei, the Ro protein associates with a large class of variant 5S rRNA precursors. To synthesize the large numbers of ribosomes needed for early development, *X. laevis* contains ≈20,000 genes encoding the oocyte 5S rRNA, many of which diverge from the consensus 5S rRNA sequence (14). The 5S rRNA variants bound by the Ro protein contain additional gene-encoded nucleotides at their 3′ ends, suggesting that they are generated by read-through of the first termination signal for RNA polymerase III. The variants also contain one or more changes from the consensus 5S rRNA sequence that cause the RNAs to misfold into a structure recognized by the Ro protein (15). Because these variant pre-5S rRNAs are processed inefficiently to mature 5S rRNA and eventually degraded, the Ro protein is proposed to function in a quality-control pathway for 5S rRNA biogenesis (6, 15). Consistent with a role in ribosomal quality control, nematodes lacking the Ro protein have increased numbers of variant 5S rRNAs (13).

Genetic analyses in *C. elegans* and *D. radiodurans* have implicated the Ro 60-kDa protein in the resistance to environmental stress. *C. elegans* lacking the Ro protein are defective in the formation of dauer larvae, a stress-resistant stage formed when environmental conditions are unfavorable for growth (16). *D. radiodurans* lacking the Ro protein exhibit decreased survival after UV irradiation. Moreover, both the *D. radiodurans* Ro protein and a Y RNA orthologue are up-regulated after UV irradiation, suggesting a role for the Ro ribonucleoproteins (RNPs) in the recognition and/or repair of intracellular damage (12).

To examine the role of Ro RNPs in a mammalian organism, we created mice lacking the Ro 60-kDa protein. We report that mice lacking the Ro autoantigen develop an autoimmune syndrome that shares several features with the human disease systemic lupus erythematosus. Similar to lupus patients, $Ro^{-/-}$ mice exhibit anti-ribosome and anti-chromatin antibodies, glomerulonephritis, and sensitivity to sunlight. Thus, one normal

BIOCHEMISTRY

Abbreviation: RNP, ribonucleoprotein.

¶To whom correspondence should be addressed at: Department of Cell Biology and Howard Hughes Medical Institute, Boyer Center for Molecular Medicine, Yale University School of Medicine, 295 Congress Avenue, New Haven, CT 06536. E-mail: sandra.wolin@yale.edu.

function of this major lupus autoantigen may be to protect against the development of autoimmune disease.

Materials and Methods

Generation and Characterization of $Ro^{-/-}$ Mice. DNAs corresponding to the first 10 kb of the mouse *Ro* gene (17) were isolated from a λFIXII mouse genomic library (129/Sv strain; Stratagene) by using human cDNA (18) as a hybridization probe. To construct the targeting vector shown in Fig. 1*A*, we used plasmids (19) in which the PGKneo cassette (pBS-neo) and herpes simplex virus thymidine kinase genes (pBS-TK) were cloned into pBluescript SK (Stratagene). First, a 2.3-kb *Pst*I fragment containing intronic sequences between the second and third coding exons was inserted into the pBS-neo vector at the *Eco*RI site. Next, a 3-kb *Not*I/*Eco*RI fragment containing the 1.6-kb PGKneo cassette and 1.4 kb of Ro sequences was excised from the plasmid and inserted into the corresponding sites of pBS-TK. Last, a 4.7-kb *Not*I/*Xba*I fragment derived from the 5′ end of the Ro genomic clone was ligated into the corresponding sites of the TK/PGKneo/Ro-containing plasmid. The resulting plasmid was linearized with *Not*I and electroporated into W9.5 embryonic stem cells. Genomic DNA from transformants resistant to G418 (200 μg/ml) and ganciclovir (2 μM) was digested with *Pst*I and subjected to Southern blot analysis. Clones containing the targeted mutation were injected into C57BL/6 blastocysts, followed by implantation into pseudopregnant foster mothers. Male chimeric mice were mated with C57BL/6 female mice, and germ-line-transmitted progeny were obtained. Light and electron microscopic examination of kidneys was performed as described (20).

For Northern blot analyses to detect Y RNAs, total brain tissue was lysed in TRIzol (Invitrogen), and RNA was isolated as described by the supplier. After fractionation in 5% polyacrylamide/8 M urea gels, the RNA was transferred to Zeta-probe GT nylon membranes (Bio-Rad) in 0.5× TBE (1× TBE = 89 mM Tris/89 mM boric acid/2.0 mM EDTA, pH 8.3) at 150 mA for 16 h. Oligonucleotides used to detect mY1 and mY3 RNA were 5′-AAGGGGGGAAAGTGTAGAACAGGA-3′ and 5′-GAGCGGAGAAGGAACAAAGAAATCTG-3′, respectively.

For Western blot analyses, brain extracts were fractionated in SDS/polyacrylamide gels, transferred to nitrocellulose as described (21), and probed with a monoclonal anti-mouse Ro antibody. To prepare the antibody, oligonucleotides 5′-GGCGCGGGATCCGAAGGATCTGCAAACCAGTTGC-3′ and 5′-GCCGCGGAGCTCTTAAATGACATCCAATGTGAAATTCCG-3′ were used to amplify the mouse Ro protein-coding sequence. The DNA was digested with *Bam*HI and *Sac*I and inserted into pTrcHisA (Invitrogen). Because the recombinant protein was insoluble, it was solubilized in guanidine·HCl, purified from *Escherichia coli* lysates, and renatured as described (12). After renaturation, the protein was used to immunize $Ro^{-/-}$ mice. Spleen cells were fused to Ag8.653 cells by using standard methods. Antiserum against human Uch-L5 was a generous gift of R. Cohen (University of Iowa, Iowa City).

Analysis of T and B Cell Function. Thymus, spleen, lymph nodes, and bone marrow were isolated from $Ro^{-/-}$ and wild-type mice, stained with the appropriate antibodies [CD4, CD8, T cell receptor, CD69, CD44, CD25, CD45R, CD43, IgM, and IgD antibodies (Pharmingen)] and analyzed by using a FACSCalibur analysis instrument (Becton Dickinson). Adult $Ro^{-/-}$, $Ro^{+/-}$, and wild-type mice were immunized s.c. with keyhole limpet hemocyanin (Calbiochem) that was emulsified in complete Freund's adjuvant. After 10 days, mice were killed and lymph node cells were assayed for proliferation by [^{3}H]thymidine incorporation (New England Nuclear) and cytokine production by ELISA (Pharmingen). Blood was collected at this time, and anti-keyhole limpet hemocyanin antibodies were measured by ELISA (Southern Biotechnology Associates). Ig levels were measured by ELISA in unimmunized mice and in age-matched $Ro^{-/-}$, $Ro^{+/-}$, and wild-type mice.

Characterization of Autoantibodies. Mouse NIH 3T3 cells were fixed in 3% formaldehyde/120 mM sodium phosphate, pH 7.4, and subjected to immunofluorescence analysis. Sera were used at dilutions between 1:125 and 1:1,000. Antibodies against RNA-containing antigens were detected by performing immunoprecipitations from mouse L1210 cells as described (8, 22). RNAs contained within immunoprecipitates were labeled with [^{32}P]pCp and T4 RNA ligase (23) and fractionated in 5% polyacrylamide/8 M urea gels. Reference sera were anti-Sm and anti-ribosome mouse monoclonal antibodies (24) and human anti-P antibodies (a gift of K. Elkon, University of Washington, Seattle). Antibodies against histones were detected by Western blotting extracts of mouse L1210 cells as described (21) by using sera diluted to 1:500 and 1:1,000. Antibodies against double-stranded and single-stranded DNA (Euroimmun, Lübeck, Germany) and nucleosomes (Medizym, Medipan Diagnostics, Selchow, Germany) were detected by ELISA using precoated plates. For ELISAs, the mean reactivity for 18 wild-type antinuclear antibody (ANA)-negative mice was determined. Values higher than three standard deviations above the mean were considered positive.

To identify the ≈30-kDa doublet recognized by many sera, L1210 cells were sonicated in 40 mM Tris·HCl, pH 7.5/150 mM NaCl/2 mM $MgCl_2$ by using a Branson sonifier (twice for 20 sec at setting 3). After sedimentation at 10,000 × *g* for 10 min, the 30-kDa doublet was found in the pellet. The pellet was subjected to sequential salt extraction using 300 and 600 mM NaCl. The doublet corresponded to two bands in the 600 mM NaCl supernatant, which were microsequenced at the Yale Keck Facility. For the ≈15-kDa band, embryonic stem cells were lysed in a Dounce homogenizer in 40 mM Tris·HCl, pH 7.5/150 mM NaCl/2 mM $MgCl_2$/0.1% Nonidet P-40/10 mM DTT, and nuclei were sedimented at 10,000 × *g* for 10 min. After resuspension in the same buffer, nuclei were disrupted by sonication and the lysate was sedimented at 10,000 × *g* for 10 min. After washing the pellet with 300 mM NaCl in the above buffer, the pellet was incubated in 0.2 M HCl for 30 min on ice to extract histones, followed by sedimentation at 10,000 × *g* for 10 min. The supernatant was applied to a PD-10 column (Amersham Biosciences) equilibrated in 50 mM sodium phosphate, pH 8.5. The column eluate was applied to an SP Sepharose column equilibrated in the same buffer. Histones were eluted with 1 M NaCl.

UV Sensitivity. Mice (6–8 weeks old) were shaved on the back and irradiated 24 h later by using UVB lamps (FS20T12/UVB, National Biological, Twinsburg, OH; ref. 25). After 24 h, animals were killed and the exposed skin was excised, fixed, and examined for sunburn cells as described (25).

Results

Generation of Mice Lacking the Ro 60-kDa Autoantigen. Ro-deficient mice were generated through homologous recombination in embryonic stem cells. The targeting vector replaced the first coding exon of the Ro gene and parts of the adjacent introns with a *neo* gene cassette (Fig. 1 *A* and *B*). Targeted embryonic stem cells were injected into C57BL/6 blastocysts, and the resulting chimeric males were bred with C57BL/6 females to generate F_1 hybrid (129/Sv × C57BL/6) heterozygotes. The F_1 hybrid mice were inbred to generate F_2 and F_3 hybrid progeny. In addition, $Ro^{-/-}$ F_3 hybrid progeny were backcrossed three generations to C57BL/6 mice and then inbred to generate F_1 progeny. $Ro^{-/-}$ mice from both backgrounds were viable and fertile. Western

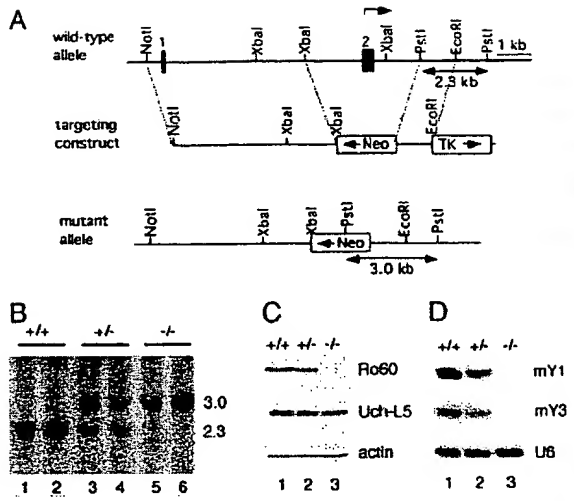

Fig. 1. Disruption of the *Ro* gene. (*A*) Diagram showing the *Ro* gene locus, the targeting construct, and the recombined mutant allele. The first two exons are indicated by filled boxes, and the translation initiation site is indicated (arrow). (*B*) Southern analysis of *Pst*I-digested DNA from wild-type (lanes 1 and 2), $Ro^{+/-}$ (lanes 3 and 4), and $Ro^{-/-}$ (lanes 5 and 6) mice. (*C*) Western blots of brain extracts with a rabbit anti-Ro serum. The blot was reprobed to detect Uch-L5, which runs as a doublet (*Middle*), and actin (*Bottom*). (*D*) Northern blot analyses of brain RNA reveal that Y RNAs are reduced in $Ro^{+/-}$ and $Ro^{-/-}$ mutant mice.

blotting of brain extracts confirmed that Ro protein levels were reduced in $Ro^{+/-}$ mice and undetectable in $Ro^{-/-}$ mice (Fig. 1*C*). Reprobing of the blot revealed that expression of the neighboring Uch-L5 gene, whose transcription start site is 2.9 kb from the *neo* insertion, was unaffected (Fig. 1*C*). Northern analyses revealed that the levels of the two mouse Y RNAs, mY1 and mY3 (26, 27), were reduced in $Ro^{+/-}$ mice and undetectable in $Ro^{-/-}$ mice (Fig. 1*D*), consistent with previous reports that Ro protein binding is required for stable accumulation of these RNAs (12, 13).

Mice Lacking the Ro Protein Develop Membranoproliferative Glomerulonephritis. Although histologic examination of 6-week-old $Ro^{-/-}$ mice revealed no significant abnormalities, ≈10% of the original F_2 and F_3 hybrid $Ro^{-/-}$ mice (8 of 74), but none of the wild-type mice (0 of 55), were dead within 6 months. By 12 months, this mortality had increased to 28% (21 of 74) of the $Ro^{-/-}$ mice, compared with 4% (2 of 55) of the wild-type mice. Mice showing signs of distress, such as fur ruffling and lethargy, were killed and subjected to histologic examination. All had evidence of membranoproliferative glomerulonephritis (Fig. 2). Examination of asymptomatic mice revealed that most (8 of 9) $Ro^{-/-}$ mice between 6 and 8 months of age showed changes characteristic of membranoproliferative glomerulonephritis. Inspection of other organs revealed no apparent differences compared with wild-type littermates. After three backcrosses to C57BL/6 mice, the $Ro^{-/-}$ mice no longer exhibited increased mortality compared with their wild-type counterparts. Nevertheless, examination of kidneys revealed that all $Ro^{-/-}$ mice >6 months of age exhibited histologic changes. The glomeruli were hypercellular with leukocytes in the capillary lumens (Fig. 2*B*), and immunofluorescence microscopy demonstrated the presence of IgG in a granular pattern (data not shown). Electron microscopy confirmed the presence of electron-dense deposits consistent with immune

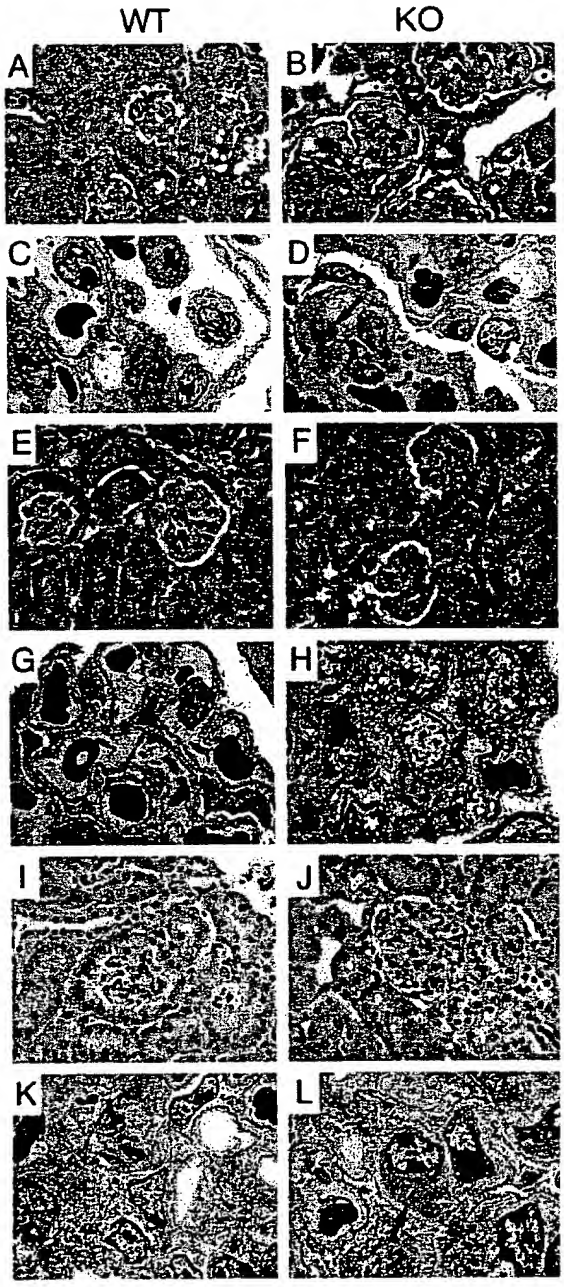

Fig. 2. Glomerulonephritis in $Ro^{-/-}$ mice. Light (*A*, *B*, *E*, *F*, *I*, and *J*; ×200) and electron (*C*, *D*, *G*, *H*, *K*, and *L*; ×5,000) microscopy of kidneys from $Ro^{-/-}$ mice and age-matched controls. $Ro^{-/-}$ and wild-type mice from the original hybrid strain (*A–D*) were examined at 16.5 months, and backcrossed mice were examined at 7 (*E–H*) and 12.5 (*I–L*) months. Age-matched controls show essentially normal histology. The hybrid $Ro^{-/-}$ mice show glomerular hypercellularity with large eosinophilic capillary deposits (*B*, arrow), which correspond to subendothelial immune complexes (*D*, arrow). Lesions in the backcrossed mice are less severe, with mesangial immune complexes at 7 months (*H*, arrow) and larger subendothelial complexes at 12.5 months (*L*, arrow).

Table 1. Autoantibodies in $Ro^{-/-}$, $Ro^{+/-}$, and wild-type mice

Age, months	No. of mice with autoantibodies		
	$Ro^{-/-}$	$Ro^{+/-}$	Wild type
129/Sv × C57BL/6 hybrid mice (ANA ≥1:1,000)			
6–7	5/6 (83%)	ND	ND
12–14	18/22 (82%)	ND	1/17 (6%)
After three backcrosses to C57BL/6 (ANA ≥1:125)			
9	17/25 (68%)	10/26 (38%)	2/24 (8%)

ANA, anti-nuclear antibody; ND, not done.

complexes (Fig. 2*D*). Deposits initially were seen predominantly in the glomerular mesangium (Fig. 2*H*) but, with increasing age, became larger and extended into the subendothelial region (Fig. 2*L*). These lesions were not as severe in the backcrossed mice as they were in the original, mixed background $Ro^{-/-}$ mice, suggesting the presence of modifier loci in the C57BL/6 background. Heterozygotes showed essentially normal histology by light microscopy, but those mice that developed antibodies (see below) demonstrated mild lesions characterized by the presence of small, electron-dense deposits by electron microscopy.

Anti-Chromatin and Anti-Ribosome Antibodies in $Ro^{-/-}$ Mice and Heterozygotes. To confirm the presence of autoantibodies, sera from the mice were analyzed by performing indirect immunofluorescence on NIH 3T3 cells. Autoantibodies (antinuclear and/or anticytoplasmic) with titers of at least 1:1,000 were detectable by 6 months of age in five of six (83%) $Ro^{-/-}$ mice from the original hybrid strain (Table 1; also see Fig. 3 *A–D*). After three backcrosses to C57/BL6 mice, antibodies remained detectable in the majority of $Ro^{-/-}$ mice (68%; 17 of 25). Autoantibodies also were detected in 10 of 26 (38%) $Ro^{+/-}$ heterozygotes but only 2 of 24 (8%) wild-type mice (Table 1). Although these antibodies tended to be of lower titer, between 1:125 and 1:500, high-titer antibodies (≥1:1,000) were detected in 7 of 25 (28%) backcrossed $Ro^{-/-}$ mice and 5 of 26 (19%) $Ro^{+/-}$ heterozygotes but were not detected in wild-type mice. Western blotting of mouse whole-cell extracts revealed that many sera detected a prominent doublet of 30 kDa and a second band of ≈16 kDa (Fig. 3*E*, lanes 3–6). Purification of these antigens, followed by protein microsequencing, revealed that they were histones H1 and H2b. Consistent with a prominent anti-chromatin response, characterization of the sera by ELISA revealed that many sera contained antibodies against nucleosomes, single-stranded DNA, and double-stranded DNA (Table 2).

To characterize further the targeted antigens, sera were used to immunoprecipitate from mouse whole-cell extracts, and the RNAs within the immunoprecipitates were labeled at the 3′ end. This assay detects many RNA-containing lupus antigens, including Sm, Ro, La, tRNA/synthetase complexes, and ribosomes (22). Although none of the mice contained detectable anti-Sm, anti-Ro, anti-La, or anti-tRNA/synthetase antibodies, a large fraction of the $Ro^{-/-}$ mice contained anti-ribosome antibodies, because both 5S and 5.8S rRNAs were contained within the immunoprecipitates (Fig. 3*F*, lanes 13–15). In addition, one mouse had antibodies directed against the U1 small nuclear RNP (snRNP; Fig. 3*F*, lane 9, asterisk), a common lupus antigen (1). For the original hybrid strain, anti-ribosome antibodies were detected in 50% of $Ro^{-/-}$ mice older than 6 months (Table 2). This was also a major specificity in sera from the backcrossed mice, as 43% of $Ro^{-/-}$ mice possessed these antibodies (Table 2). The majority of sera positive for anti-ribosome antibodies detected a doublet migrating below the histone H1 band (Fig. 3*E*, lane 3, asterisk).

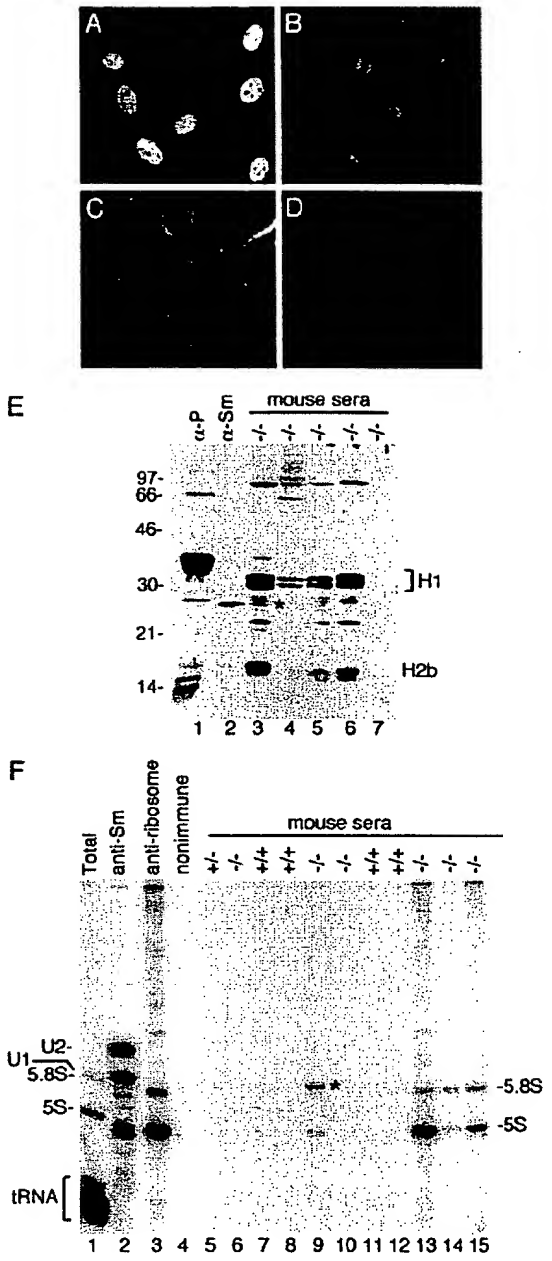

Fig. 3. Autoantibodies in Ro mutant mice. NIH 3T3 cells were stained with sera (diluted 1:1,000) from 6- to 7-month-old $Ro^{-/-}$ mice (*A–C*) and a 12-month-old wild-type mouse (*D*). (*E*) Reference sera (lanes 1 and 2) and sera from $Ro^{-/-}$ mice were used to probe Western blots of L1210 cell extracts. •, Doublet detected by most sera containing anti-ribosomal antibodies. (*F*) Reference sera (lanes 2–4) and sera from 129/Sv × C57BL/6 hybrid mice were used to immunoprecipitate from L1210 cell extracts. RNAs in immunoprecipitates were labeled with [^{32}P]pCp. *, Band identified as U1 RNA by cDNA sequencing.

Fractionation of cell extracts revealed that the doublet was found in the pellet after sedimentation at 100,000 × *g* for 1 h, consistent with a ribosomal protein (data not shown). None

Table 2. Subclassification of autoantibodies in $Ro^{-/-}$ and wild-type mice

	No. of mice with autoantibodies				
	(129/Sv × C57BL/6)		C57BL/6 backcross		
Antigen	Wild type (n = 18)	$Ro^{-/-}$ (n = 18)	Wild type (n = 19)	$Ro^{+/-}$ (n = 23)	$Ro^{-/-}$ (n = 23)
Histones	0	10	0	1	9
Ribosomes	1	9	0	3	10
Sm	0	0	0	0	0
U1 snRNP	0	1	0	0	0
Ro	0	0	0	0	0
La	0	0	0	0	0
dsDNA	2	9	0	3	6
ssDNA	2	6	1	3	5
Nucleosomes	2	10	1	8	6

snRNP, small nuclear RNP; dsDNA, double-stranded DNA; ssDNA, single-stranded DNA.

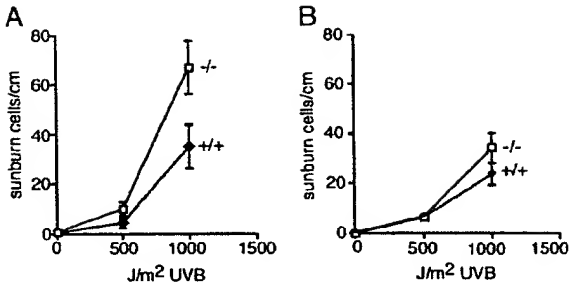

Fig. 4. $Ro^{-/-}$ mice are more sensitive to UVB irradiation. (*A*) After six backcrosses to C57BL/6 mice, the backs of wild-type (n = 8) and $Ro^{-/-}$ (n = 6) mice were shaved and exposed to the indicated doses of UVB. After 24 h, apoptotic keratinocytes (sunburn cells) were counted. (*B*) The backs of mice from the original hybrid 129/Sv × C57BL/6 strain were shaved and exposed to UVB, and apoptotic keratinocytes were counted. For the 1,000-J/m^2 dose, 14 wild-type and 13 $Ro^{-/-}$ mice were examined.

of the anti-ribosome antibodies recognized the ribosomal P proteins, which are common autoantigens in lupus patients (Fig. 3*E*, lane 1; ref. 1).

Evaluation of T and B Cell Populations and Function. T and B cell surface markers were evaluated in $Ro^{-/-}$ and wild-type mice by flow cytometric analysis. No obvious changes were found in mature T cell markers (CD4/CD8 ratios) or in the most immature (T cell antigen receptor-negative CD25/CD44 populations) cells in the thymus. Likewise in the bone marrow, B cell development appeared normal (using CD43/CD45R and IgM markers). Lymph node and spleen populations did not reveal differences in T and B cell activation status (using CD69 and CD25 markers). To determine whether $Ro^{-/-}$ mice respond abnormally to challenge with protein antigens, animals were immunized with the T cell-dependent antigen keyhole limpet hemocyanin. No significant differences in T cell proliferation, cytokine production, or anti-keyhole limpet hemocyanin antibody production were detected. However, total Ig levels in unimmunized 8-week-old $Ro^{-/-}$ mice were elevated slightly (1.4-fold). Among the Ig isotypes, increases were found in IgM (1.5-fold in the $Ro^{-/-}$ mice) and IgG2a (3-fold in $Ro^{+/-}$ mice and 3- to 29-fold in $Ro^{-/-}$ mice) (data not shown).

Sensitivity of $Ro^{-/-}$ Mice to UV Irradiation. Because a prokaryotic orthologue of the Ro protein is important for survival of the eubacterium *D. radiodurans* after UV irradiation (12), we examined the sensitivity of $Ro^{-/-}$ mice to UV light. The backs of wild-type and $Ro^{-/-}$ mice were shaved and the dorsal skin was exposed to UVB light at the physiologically relevant doses of 500 and 1,000 J/m^2. Twenty-four hours later, histological sections were prepared. For mice that had been backcrossed six times to C57BL/6 mice, the number of apoptotic keratinocytes (sunburn cells) in the $Ro^{-/-}$ mice after 1,000 J/m^2 UVB light was twice that of wild-type littermates (P = 0.02; Fig. 4*A*). Examination of mice from the original (129/Sv × C57BL/6) hybrid strain revealed that both wild-type and $Ro^{-/-}$ mice were less sensitive to irradiation than the backcrossed mice (Fig. 4*B*). However, although $Ro^{-/-}$ mice from the original hybrid strain also had higher numbers of apoptotic keratinocytes than did wild-type controls (Fig. 4*B*), the difference was not statistically significant (P = 0.08). Nonetheless, in at least one genetic background, the absence of the Ro protein results in significant photosensitivity, although modifier loci also may contribute.

Discussion

Although small RNA–protein complexes are major autoantigens in patients suffering from systemic lupus erythematosus, there have been few links between the RNP antigens and the disease pathology. We have shown that mice lacking the Ro 60-kDa autoantigen develop a lupus-like syndrome consisting of anti-ribosome and anti-chromatin antibodies, glomerulonephritis with subendothelial immune deposits, and photosensitivity. Thus, the Ro autoantigen may not be simply a passive target in the lupus immune response but, instead, may be important for the prevention of autoimmune disease.

Although a number of gene disruptions result in at least some degree of autoimmunity (28), our work is unique in several ways. First, we report that disruption of an RNA-binding protein can result in autoimmunity. Second, although photosensitivity occurs in a significant fraction of lupus patients, our backcrossed mice are unusual in displaying both autoimmune disease and sensitivity to sunlight. Although the observed difference is only 2-fold, similar changes in cell survival after UV are seen in cells from patients with the XP-E, XP-F, and XP-V forms of xeroderma pigmentosum, hereditary syndromes in which patients are predisposed to sunlight-induced skin cancers (29, 30). Last, our finding that mice lacking a major lupus autoantigen develop autoimmune disease raises the possibility that the anti-Ro antibodies seen in patients may not be an epiphenomenon but, instead, may contribute to the development or perpetuation of the autoimmune response and/or the observed photosensitivity.

How might the absence of an intracellular RNA-binding protein result in autoimmunity? Because the Ro protein binds misfolded, defective pre-5S rRNAs in *X. laevis* oocytes, it has been proposed to function in a quality-control pathway for ribosome biogenesis (6, 13, 15). Thus, one possibility is that the release of intracellular contents from $Ro^{-/-}$ cells that occurs normally during cell turnover triggers the autoimmune response. In this model, the presence of a small fraction of ribosomes containing subtle structural alterations resulting from the presence of misfolded 5S rRNAs causes a breach of tolerance by exposing normally cryptic determinants to the immune system. In support of this hypothesis, it often has been proposed that autoimmunity can be triggered by presentation of cryptic epitopes (31, 32). Such a mechanism would be reminiscent of the lupus-like syndromes that develop in mice lacking components of pathways involved in clearing extracellular debris, in that failure to remove cellular detritus triggers an autoimmune response (33–36). Alternatively, it remains possible that the absence of the Ro protein results in a subtle defect in immune system function that we have not yet uncovered.

In lupus patients, photosensitivity occurs in up to 90% of patients with anti-Ro autoantibodies (2). Moreover, maternal

BIOCHEMISTRY

anti-Ro antibodies that cross the placenta are highly associated with photosensitive skin lesions in infants. Because the disappearance of the skin lesions coincides with the loss of maternal antibodies from the circulation, it has been assumed that the antibodies play a direct role in the pathogenic process (37, 38). Our result that the absence of the Ro protein in one genetic background is associated with photosensitivity suggests that the photosensitivity long observed in patients could be related to a loss of Ro protein function in keratinocytes. However, although there are many reports that antibodies can enter cells (39–44), it is unlikely that they access the cytosol in quantities sufficient to ablate function of abundant target molecules (45). Nonetheless, inefficient entry of anti-Ro antibodies into a small fraction of patient keratinocytes potentially could enhance the sensitivity of these cells to sunlight, resulting in increased apoptotic cell death.

In summary, our genetic experiments have uncovered a new and surprising way in which the lack of an RNA-binding protein leads to an immune response to specific components of the subcellular machinery. Moreover, our experiments reveal that the Ro 60-kDa protein plays a critical role in the prevention of autoimmunity, possibly by removing defective RNPs from cells, allowing them to escape immune surveillance. In this regard, it is interesting that the human Ro protein maps to chromosome 1q31 (46), which has been linked to lupus (47–49).

We thank C. Delvecchio for technical assistance; R. Cohen, K. Elkon, and J. Steitz for providing antibodies; and J. Craft, R. Lifton, and M. Shlomchik for comments on the manuscript. Parts of this work were supported by grants from the National Institutes of Health (to M.K. and D.E.B.). R.A.F. is an Investigator and S.L.W. is an Associate Investigator of the Howard Hughes Medical Institute.

1. von Muhlen, C. A. & Tan, E. M. (1995) *Semin. Arthritis Rheum.* **24**, 323–358.
2. Provost, T. T., Watson, R. & Simmons-O'Brien, E. (1996) *J. Am. Acad. Dermatol.* **35**, 147–169.
3. Silverman, E. D. & Laxer, R. M. (1997) *Rheum. Dis. Clin. North Am.* **23**, 599–618.
4. Peek, R., Pruijn, G. J. M., van der Kemp, A. & van Venrooij, W. J. (1993) *J. Cell Sci.* **106**, 929–935.
5. Simons, F. H. M., Pruijn, G. J. M. & van Venrooij, W. J. (1994) *J. Cell Biol.* **125**, 981–988.
6. O'Brien, C. A. & Wolin, S. L. (1994) *Genes Dev.* **8**, 2891–2903.
7. Wolin, S. L. & Steitz, J. A. (1983) *Cell* **32**, 735–744.
8. Wolin, S. L. & Steitz, J. A. (1984) *Proc. Natl. Acad. Sci. USA* **81**, 1996–2000.
9. O'Brien, C. A., Margelot, K. & Wolin, S. L. (1993) *Proc. Natl. Acad. Sci. USA* **90**, 7250–7254.
10. Farris, A. D., O'Brien, C. A. & Harley, J. B. (1995) *Gene* **154**, 193–198.
11. Van Horn, D. J., Eisenberg, D., O'Brien, C. A. & Wolin, S. L. (1995) *RNA* **1**, 293–303.
12. Chen, X., Quinn, A. M. & Wolin, S. L. (2000) *Genes Dev.* **14**, 777–782.
13. Labbe, J. C., Hekimi, S. & Rokeach, L. A. (1999) *Genetics* **151**, 143–150.
14. Peterson, R. C., Doering, J. L. & Brown, D. D. (1980) *Cell* **20**, 131–141.
15. Shi, H., O'Brien, C. A., Van Horn, D. J. & Wolin, S. L. (1996) *RNA* **2**, 769–784.
16. Labbe, J. C., Burgess, J., Rokeach, L. A. & Hekimi, S. (2000) *Proc. Natl. Acad. Sci. USA* **97**, 13233–13238.
17. Kaufman, K. M., Farris, A. D., Gross, J. K., Kirby, M. Y. & Harley, J. B. (2000) *Genes Immunol.* **1**, 265–270.
18. Deutscher, S. L., Harley, J. B. & Keene, J. D. (1988) *Proc. Natl. Acad. Sci. USA* **85**, 9479–9483.
19. Yang, D., Tournier, C., Wysk, M., Lu, H. T., Xu, J., Davis, R. J. & Flavell, R. A. (1997) *Proc. Natl. Acad. Sci. USA* **94**, 3004–3009.
20. Liang, B., Gee, R. J., Kashgarian, M. J., Sharpe, A. H. & Mamula, M. J. (1999) *J. Immunol.* **163**, 2322–2329.
21. Yoo, C. J. & Wolin, S. L. (1994) *Mol. Cell. Biol.* **14**, 5412–5424.
22. Hardin, J. A., Rahn, D. R., Shen, C., Lerner, M. R., Wolin, S. L., Rosa, M. D. & Steitz, J. A. (1982) *J. Clin. Invest.* **70**, 141–147.
23. England, T. E., Bruce, A. G. & Uhlenbeck, O. C. (1980) *Methods Enzymol.* **65**, 65–74.
24. Lerner, E. A., Lerner, M. R., Janeway, C. A. & Steitz, J. A. (1981) *Proc. Natl. Acad. Sci. USA* **78**, 2737–2741.
25. Ziegler, A., Jonason, A. S., Leffell, D. J., Simon, J. A., Sharma, H. W., Kimmelman, J., Remington, L., Jacks, T. & Brash, D. E. (1994) *Nature* **372**, 773–776.
26. Hendrick, J. P., Wolin, S. L., Rinke, J., Lerner, M. R. & Steitz, J. A. (1981) *Mol. Cell. Biol.* **1**, 1138–1149.
27. Farris, A. D., Gross, J. K., Hanas, J. S. & Harley, J. B. (1996) *Gene* **174**, 35–42.
28. Wakeland, E. K., Liu, K., Graham, R. R. & Behrens, T. W. (2001) *Immunity* **15**, 397–408.
29. Andrews, A. D., Barrett, S. F. & Robbins, J. H. (1978) *Proc. Natl. Acad. Sci. USA* **75**, 1984–1988.
30. Bootsma, D., Kraemer, K. H., Cleaver, J. E. & Hoeijmakers, J. H. J. (2001) in *The Metabolic and Molecular Bases of Inherited Disease*, eds. Scriver, C. R., Beaudet, A. L., Sly, W. S. & Valle, D. (McGraw-Hill, New York), Vol. 1, pp. 677–703.
31. Lanzavecchia, A. (1995) *J. Exp. Med.* **181**, 1945–1948.
32. Andrade, F., Casciola-Rosen, L. & Rosen, A. (2000) *Rheum. Dis. Clin. North Am.* **26**, 215–227.
33. Botto, M., Dell'Agnola, C., Bygrave, A. E., Thompson, E. M., Cook, H. T., Petry, F., Loos, M., Pandolfi, P. P. & Walport, M. J. (1998) *Nat. Genet.* **19**, 56–59.
34. Bickerstaff, M. C., Botto, M., Hutchinson, W. L., Herbert, J., Tennent, G. A., Bybee, A., Mitchell, D. A., Cook, H. T., Butler, P. J., Walport, M. J., *et al.* (1999) *Nat. Med.* **5**, 694–697.
35. Napirei, M., Karsunky, H., Zevnik, B., Stephan, H., Mannherz, H. G. & Moroy, T. (2000) *Nat. Genet.* **25**, 177–181.
36. Scott, R. S., McMahon, E. J., Pop, S. M., Reap, E. A., Caricchio, R., Cohen, P. L., Earp, H. S. & Matsushima, G. K. (2001) *Nature* **411**, 207–211.
37. Lee, L. A. (2001) *Curr. Rheumatol. Rep.* **3**, 391–395.
38. Patel, P. & Werth, V. (2002) *Dermatol. Clin.* **20**, 373–385.
39. Alarcon-Segovia, D., Ruiz-Arguelles, A. & Fishbein, E. (1978) *Nature* **271**, 67–69.
40. Ma, J., Chapman, G. V., Chen, S. L., Melick, G., Penny, R. & Breit, S. N. (1991) *Clin. Exp. Immunol.* **84**, 83–91.
41. Yanase, K., Smith, R. M., Cizman, B., Foster, M. H., Peachey, L. D., Jarett, L. & Madaio, M. P. (1994) *Lab. Invest.* **71**, 52–60.
42. Zack, D. J., Stempniak, M., Wong, A. L., Taylor, C. & Weisbart, R. H. (1996) *J. Immunol.* **157**, 2082–2088.
43. Koscec, M., Koren, E., Wolfson-Reichlin, M., Fugate, R. D., Trieu, E., Targoff, I. N. & Reichlin, M. (1997) *J. Immunol.* **159**, 2033–2041.
44. Deng, S. X., Hanson, E. & Sanz, I. (2000) *Int. Immunol.* **12**, 415–423.
45. Musunuru, K. & Darnell, R. B. (2001) *Annu. Rev. Neurosci.* **24**, 239–262.
46. Chan, E. K., Tan, E. M., Ward, D. C. & Matera, A. G. (1994) *Genomics* **23**, 298–300.
47. Moser, K. L., Neas, B. R., Salmon, J. E., Yu, H., Gray-McGuire, C., Asundi, N., Bruner, G. R., Fox, J., Kelly, J., Henshall, S., *et al.* (1998) *Proc. Natl. Acad. Sci. USA* **95**, 14869–14874.
48. Lindqvist, A. K., Steinsson, K., Johanneson, B., Kristjansdottir, H., Arnasson, A., Grondal, G., Jonasson, I., Magnusson, V., Sturfelt, G., Truedsson, L., *et al.* (2000) *J. Autoimmun.* **14**, 169–178.
49. Johanneson, B., Lima, G., Von Salome, J., Alarcon-Segovia, D. & Alarcon-Riquelme, M. E. (2002) *Am. J. Hum. Genet.* **71**, 1060–1071.

ICA69^{null} Nonobese Diabetic Mice Develop Diabetes, but Resist Disease Acceleration by Cyclophosphamide[1]

Shawn Winer,[2]* Igor Astsaturov,[2]* Roger Gaedigk,[2]* Denise Hammond-McKibben,* Marc Pilon,* Aihua Song,* Violetta Kubiak,* Wolfram Karges,* Enrico Arpaia,* Colin McKerlie,† Peter Zucker,‡ Bhagirath Singh,‡ and H.-Michael Dosch[3]*

ICA69 (islet cell Ag 69 kDa) is a diabetes-associated autoantigen with high expression levels in β cells and brain. Its function is unknown, but knockout of its *Caenorhabditis elegans* homologue, *ric-19,* compromised neurotransmission. We disrupted the murine gene, *ica-1,* in 129-strain mice. These animals aged normally, but speed-congenic ICA69^{null} nonobese diabetic (NOD) mice developed mid-life lethality, reminiscent of NOD-specific, late lethal seizures in glutamic acid decarboxylase 65-deficient mice. In contrast to wild-type and heterozygous animals, ICA69^{null} NOD congenics fail to generate, even after immunization, cross-reactive T cells that recognize the dominant Tep69 epitope in ICA69, and its environmental mimicry Ag, the ABBOS epitope in BSA. This antigenic mimicry is thus driven by the endogenous self Ag, and not initiated by the environmental mimic. Insulitis, spontaneous, and adoptively transferred diabetes develop normally in ICA69^{null} NOD congenics. Like glutamic acid decarboxylase 65, ICA69 is not an obligate autoantigen in diabetes. Unexpectedly, ICA69^{null} NOD mice were resistant to cyclophosphamide (CY)-accelerated diabetes. Transplantation experiments with hemopoietic and islet tissue linked CY resistance to ICA69 deficiency in islets. CY-accelerated diabetes involves not only ablation of lymphoid cells, but ICA69-dependent drug toxicity in β cells that boosts autoreactivity in the regenerating lymphoid system. ***The Journal of Immunology,*** **2002, 168: 475–482.**

Type I diabetes (T1D)[4] is the consequence of chronic progressive autoimmunity that targets pancreatic islets of Langerhans, selectively eliminating insulin-producing β cells. Causes that underlie the development of diabetic autoimmunity remain obscure. Products of some 20^{+} predisposing genes interact with critical environmental accelerators and decelerators to generate the autoimmune phenotype (1).

Clinical insulin deficiency and its attendant metabolic abnormalities are the end result of a drawn-out prediabetes phase, in which autoreactive T cell pools accumulate in the islet. Prediabetes proceeds in a stepwise fashion (2, 3), from benign periinsulitis to islet invasion and progressively rising rates of β cell death, as signaled by the generation of autoantibodies (4, 5). Because of the difficulty of tissue access in humans, much of the current view of autoimmune diabetes derives from the excellent rodent models for the disease, BB rats and nonobese diabetic (NOD) mice (6, 7). However, many years of prediabetes are a reality of the human disease, in which B and T cell autoimmunity arise many years before and can persist for decades after onset of overt disease (see Refs. 8–10).

A similar set of autoantigens is targeted by self-reactive T cells in human and murine diabetes, including insulin/proinsulin, glutamic acid decarboxylase 65 (GAD65), GAD67, ICA69 (islet cell Ag 69 kDa), and IA-2/phogrin (1, 7). Of these, only insulin is (nearly) β cell specific, while others follow generally neuroendocrine gene expression profiles. In NOD mice, immunotherapies with any one of these autoantigens can halt, and in some circumstances accelerate development of overt diabetes, depending on the choice of epitopes and the timing of interventions early or later in prediabetes (11–17).

While there may be a hierarchy among autoimmune targets, in particular early on (18), established prediabetes involves multiple T cell pools that home to the islet, targeting more self epitopes with increasing effectiveness (19–21). The progression of prediabetes is complex and passes through checkpoints that halt progression for some periods of time (2). A single dose of cyclophosphamide (CY), an alkylating cancer pro-drug (22), overcomes these checkpoints and allows rapid diabetes development in a process that is dominated by the local activation of myeloid APCs and their cytokine products (3). In this commonly used diabetes model, CY was suggested to remove regulatory hemopoietic cells (23, 24), in a host whose lymphoid cell lineages are relatively resistant to the drug and able to mount a dramatic recovery of lymphoid mass quickly after drug exposure (25). Data presented in this work suggest that the drug's role in diabetes development is more complex and critically depends on direct islet cell toxicity in a process that appears to require the function of ICA69.

To explore the role of self Ag in prediabetes and its progression to overt disease, we disrupted the genomic locus of the autoantigen, ICA69 (14, 26, 27), and backcrossed the defect onto NOD, using a speed-congenic strategy (28). The conserved ICA69 gene, *ica-1,* maps to human chromosome 7p22 and a synthenic location

*The Hospital For Sick Children, Research Institute, University of Toronto, Toronto, Ontario, Canada; †Departments of Pediatrics and Immunology, Sunnybrook and Women's College Health Sciences Center, and ‡University of Western Ontario, Department of Immunology, John P. Robarts Research Institute, London, Ontario, Canada

Received for publication August 16, 2001. Accepted for publication October 25, 2001.

The costs of publication of this article were defrayed in part by the payment of page charges. This article must therefore be hereby marked *advertisement* in accordance with 18 U.S.C. Section 1734 solely to indicate this fact.

[1] This work was supported by grants from the Canadian Institutes of Health Research and the Juvenile Diabetes Research Foundation.

[2] S.W., I.A., and R.G. contributed equally.

[3] Address correspondence and reprint requests to Dr. H.-Michael Dosch, IIIR Program, The Hospital For Sick Children, 555 University Avenue, Toronto, Ontario, Canada, M5G 1X8. E-mail address: hmdosch@sickkids.ca

[4] Abbreviations used in this paper: T1D, type 1 diabetes; CY, cyclophosphamide; GAD, glutamic acid decarboxylase; ICA69, islet cell Ag 69 kDa; NOD, nonobese diabetic; Tep69, major NOD mouse T cell epitope in ICA69; tet07, artificial promoter tetoperon (×7) + TATA box; tTA, tetracycline transactivator.

0022-1767/02/$02.00

on mouse chromosome 6A1, 2, neither location mapping near known diabetes risk loci (27, 29). The molecule has a neuroendocrine expression pattern with peak levels in brain and β cell lines (30). Its function is unknown, but we found that *Caenorhabditis elegans* deficient for the well-conserved ICA69 homologue, *ric-19*, develops a neurotransmission defect (31).

The protein includes a single, dominant T cell epitope, Tep69 (major T cell epitope in ICA69), targeted by autoreactive T cells in both human and NOD mouse T1D (26). There is well-established antigenic mimicry between this epitope and the ABBOS epitope in the commonly encountered, dietary Ag, BSA (14). Because ABBOS is a highly dominant BSA epitope in NOD mice, it appeared possible that ICA69 autoimmunity might be triggered through mimicry with BSA/ABBOS (10, 14, 32), encountered through exposure to dietary cow milk protein, a risk factor for diabetes development (33–36). Observations in ICA69^{null} NOD congenics now indicate that the routinely generated Tep69/ABBOS mimicry T cell pools require and are driven by the endogenous self Ag, which also dictates the apparent dominance for ABBOS in BSA immune responses of wild-type NOD mice.

The 129SvJ mice with ICA69 deficiency had no obvious phenotype and aged normally. However, speed-congenic ICA69^{null} NOD mice develop sudden lethality beginning in early middle age, reminiscent of GAD65 deficiency that produces mid-life lethal seizures only on the NOD background (37). ICA69^{null} NOD female congenics develop diabetes at essentially wild-type NOD incidence. Like GAD65 (38), ICA69 emerges as a facultative, but not obligate element in diabetes progression. Surprisingly, and challenging current views, ICA69^{null} mice were highly resistant to CY-accelerated diabetes due to a previously unrecognized drug effect on islets, which appears to require the function of ICA69.

Materials and Methods

Animals

NOD/Li (H-2^{g7}) mice were bred in our rodent facility according to approved facility guidelines and protocols. Experiments were performed in our conventional unit, which presently has an 83–86% diabetes incidence in 36-wk-old female mice.

Adoptive transfer

Spleen cells from three to five recently diabetic NOD females were pooled, and 10^7 cells were transferred i.v. to 6- to 8-wk-old, irradiated NOD male (650 rad) or NOD.*scid* (200 rad) recipients. In all experiments, glucosuria (TesTape, Lilly, Toronto) was used for daily diabetes screens. Diabetes was confirmed through blood glucose measurements on 2 consecutive days (13.8 mM/L, SureStep; Life Technologies, Burnaby, British Columbia, Canada).

CY-accelerated diabetes

To induce accelerated diabetes development, 8- to 10-wk-old wild-type, heterozygous or homozygous ICA69 knockout females received one i.p. injection of 250 mg/kg CY (Sigma, St. Louis, MO). In some experiments, 14-wk-old animals were used, or a second injection was given 3 wk later.

Pancreatic islet transplantation

Islets were isolated from pancreata of 4- to 5-wk-old wild-type NODs by standard digestion and manual picking procedures (39). The grafts were placed under the kidney capsule of anesthetized, 8-wk-old ICA69^{null} NOD females. Sixteen days later, the recipients were treated with 250 mg/kg CY, and diabetes development was monitored for at least 4 wk. Sham-operated and nontransplanted wild-type NOD and ICA69^{null} mice provided controls.

Generation of ICA69^{null} mice

The ICA69 locus occupies approximately 100 kb on mouse chromosome 6 (27, 29). A murine 129SvJ genomic library (gift of T. Mak, Toronto, Canada) was screened with a full-length ICA69-α cDNA probe (26). A 2.7-kb clone containing exon 2 was excised with *Bgl*II and subcloned into pBluescript II-SK upstream of a *herpes simplex* thymidine kinase expression cassette. The aminoglycoside phosphotransferase (neo) gene was excised from the pPNT vector and ligated into a *Stu*I site at position 107 of exon 2, thus disrupting the coding region of the Tep69 epitope in ICA69 (27).

The tetracycline transactivator (tTA) coding region (40, 41) (gift of H. Bujard, Heidelberg, Germany) was moved in-frame into an *Age*I restriction site at position 38 of exon 2 in ICA69 (see below, Fig. 1). This was thought to allow future experiments, such as possible rescue of knockout phenotypes through doxycycline-regulatable expression of a tet07-ICA69 transgene (42). The function of the targeting vector, including the tTA knock-in, was confirmed in NIT-1 β cells (43) with one allele replaced by the vector. Transient transfection of these cells with low copy numbers of a tet07-luciferase expression plasmid (40) (gift of H. Bujard) resulted in excellent luciferase expression that was over 98% suppressed in the presence of 1 μM doxycycline (Hammond-McKibben et al., manuscript in preparation).

Targeting vector DNA was linearized with *Not*I and transfected into the R1 ES cell line, and multiple clones were selected in the presence of G418 and gancyclovir (44). Double-resistant embryonic stem cell clones (19 of 482 screened) were expanded for use in morula aggregations with fertilized NOD eggs (44), and chimeric male offspring were bred with NOD females. Transmission was analyzed by standard Southern blots (27). Offspring with germline transmission of the ICA69^{null} allele were backcrossed to NOD in a speed-congenic strategy (28). One founder repeatedly generated offspring with germline transmission of the null allele, and one of these ICA69$^{+/-}$ heterozygous offspring was homozygous for NOD variants of *D6 Mit52* and *D6 Mit339* on chromosome 6, suggesting a crossover event that replaced a considerable stretch of 129SvJ strain chromosome 6 with NOD genomic DNA. This male was mated to wild-type NOD females (backcross generation 2). Several offspring from backcross 5 were homozygous NOD for all 17 *Idd* loci, according to microsatellite markers (28). The ICA69-deficient mice analyzed in the present study were derived from backcross 7.

Subcellular fractionation of mouse brain

Mouse brain tissue was fractionated as described (31). Briefly, brains were homogenized in ice-cold, supplemented HBSS buffer. Nuclei and cell debris were removed, and supernatant (S1) was centrifuged at 13,000 × *g* for 13 min. Supernatant was collected and spun at 100,000 × *g* for 30 min to yield S3 (the cytosol) and P3 (the microsomal pellet). The synaptosome fraction was washed with HBSS buffer and centrifuged at 13,000 × *g* for 13 min. The pellet was lysed, buffered (10 mM HBSS, pH 7.4), and centrifuged at 45,000 × *g* for 20 min. The pellet (LP1) was resuspended in HKA buffer (10 mM HEPES-KOH, pH 7.4, 140 mM KoAC, 1 mM $MgCl_2$, 0.1 mM EGTA, 0.3 mM PMSF), while the crude synaptic vesicles were pelleted by further centrifugation of the supernatant at 150,000 × *g* for 1 h, then resuspended in HKA buffer. All procedures were performed on ice.

Western blots

Rabbit anti-ICA69 (gift from M. Pietropaolo, Pittsburgh, PA) was used at a final dilution of 1/7500 (30). Each subcellular fraction (40 μg) was separated on SDS polyacrylamide gels and transferred to nitrocellulose. Peroxidase-conjugated goat anti-rabbit Ab (The Jackson Laboratory, Bangor, ME; 1/15,000) was used to detect bound primary Ab. Rabbit anti-VAMP-2 provided a marker of synaptic vesicles (gift from W. Trimble, The Hospital For Sick Children).

Histology

Tissues for histological sections were fixed in 10% neutral buffered Formalin and stained with H&E. The degree of insulitis was scored blindly by two observers, using the following scale: 0, normal islet; 1, periinsulitis; 2, invasive infiltration of 25%–50% of islet surface area; 3, invasive infiltration of greater than 50% of islet surface area or a small retracted islet. Immunohistochemistry for insulin was performed on Formalin-fixed, paraffin-embedded tissue sections using guinea pig anti-insulin Ab and rabbit HRP-conjugated secondary Ab (Dako Diagnostics, Mississauga, Ontario, Canada). Reactions were visualized using diaminobenzidine peroxidase substrate, and sections were counterstained with hematoxylin.

Proliferative T cell responses

In vitro T cell proliferation was measured as described recently for immunized and nonimmunized NOD mice (16). Immunizations employed s.c. injection of a given Ag, 100 μg emulsified in CFA. Regional lymph nodes were removed 9–10 days after immunization, and 4 × 10^5 cells/well were cultured in serum-free AIM V medium (Life Technologies) to measure recall responses to 0.01–100 μM Ag. After 60 h, cultures were pulsed overnight with 1 μCi [^{3}H]thymidine and subjected to scintillation counting. Spontaneous T cell proliferation in spleen cells from unimmunized naive or adoptively transferred mice was similarly measured, except for the addition of 10 U human rIL-2 (45). Synthetic peptides were highly purified and confirmed by mass spectroscopy: Tep69, AFIKATGKKEDE, ABBOS,

FKADEKKFWGKYLYE. Grade V BSA and OVA were purchased from Sigma. Purified, mouse rICA69-β was prepared as described (26); rGAD65 was purchased (Diamyd Diagnostics, Stockholm, Sweden).

Statistics

Numeric values were compared by Mann-Whitney or Welsh tests; significance was set at 5%; and all tests were two tailed. Tables were used to compare diabetes incidence in different groups of animals (Fisher's exact test); odds ratios were calculated with Woolf's approximation.

Results

Generation of ICA69^{null} mice

The targeting construct (Fig. 1*A*) introduces a neomycin resistance cassette to disrupt the Tep69 epitope in exon 2 of ICA69, and inserts the tTA coding region in-frame after the leading 9 ICA69 aa residues, followed by poly(A) and stop sites. Homologous recombination of this vector in its genomic target locale introduces an additional *Xba*I site that produces a 3.2-kb *Xba*I restriction fragment, while the corresponding wild-type fragment is 3.6 kb in length (Fig. 1*A*). Homologous recombination of the targeting construct was confirmed in genomic DNA of progeny from several chimeric founders, using a 5′-end probe and *Xba*I restriction (Fig. 1*B*) and a neo probe and *Hin*dIII restriction (not shown). Several litters of this generation of *129SvJ x NOD* offspring were monitored for up to 26 mo, including 17 ICA69^{null} animals derived from brother-sister matings. No spontaneous deaths or obvious abnormalities were observed.

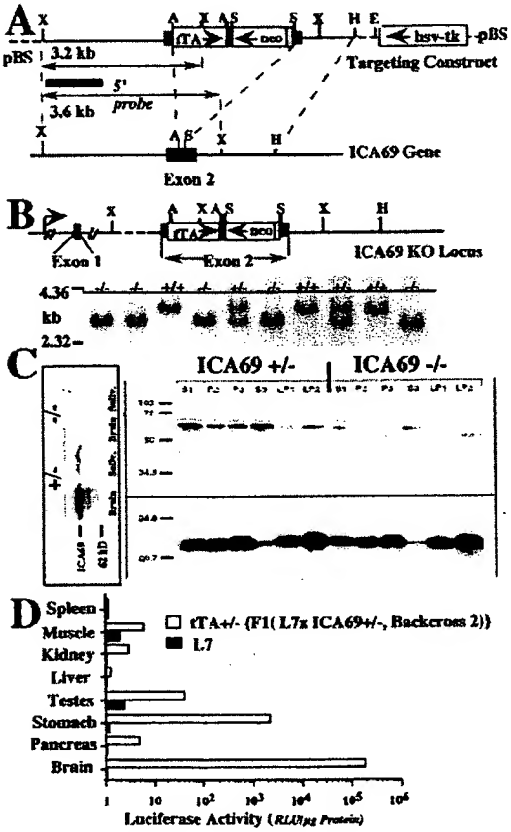

FIGURE 1. Development of ICA69^{null} mice. *A*, The ICA69 locus was genetically disrupted by insertion of tTA and neo genes into exon 2 of the ICA69 gene. The *top diagram* shows the targeting construct that targeted the ICA69 gene (*bottom*) and generated the knockout allele shown at the *top* of *B*. *B*, Southern blot of *Xba*I-restricted genomic DNA from *129vJ x NOD* mice backcross 2. The knockout allele generates a shortened 3.2-kb exon 2 fragment. *C*, Western blots of brain and salivary gland tissue extracts (backcross 11 mice, *left panel*) and fractionated brain protein from wild- type and homozygous ICA69 knockout mice (backcross 7) were probed with anti-ICA69 polyclonal Ab. A 23-kDa synaptic vesicle marker, VAMP2, is shown *below*. S1, postnuclear supernatant; P2, synaptosomes; S3, cytosol; P3, microsomes; LP1, plasma membrane; LP2, synaptic vesicles. *D*, Luciferase activity (relative light units/μg protein) in different tissues from L7 (tet07-luciferase transgenic) mice carrying a single ICA69 knockout/tTA-knock-in allele from backcross 2 mice (open bars). Expression patterns follow the tissue expression of ICA69. L7 mice without the tTA transgene express only background activities (filled bars, note the logarithmic scale).

ICA69 is expressed at low to very low levels in a variety of tissues, with its major expression locale in the brain, and highest levels found in β cell lines (30). Almost certainly reflecting post-translational modifications, Western blots resolve ICA69 as a doublet band of approximately 69 kDa, despite its calculated mass of 55 kDa (30, 46). There was no detectable ICA69 in Western blots of brain and salivary gland extracts from backcross 7 (not shown) or backcross 11 mice (Fig. 1*C*, *left panel*), but there were occasional ghost bands in brain subcellular fractions (*right panel*). These bands were not consistent, and could be detected only with one rabbit Ab raised against a C-terminal peptide (46) (Fig. 1*C*), but not with another rabbit Ab raised against a large, truncated ICA69 fragment (not shown). We were unable to obtain sufficient material for mass spectrography and sequencing studies of these ghost bands. As described below, the distinct phenotypes of these mice, results of extensive RT-PCR, Southern blot, and genomic PCR studies of the disrupted gene locus, and in particular the silencing of the natural ICA69 promoter (see below) make a hypomorphic phenotype with remnant gene expression of gene fragments from this locus unlikely.

Heterozygous (ICA69$^{+/-}$) progeny from backcross 2 were mated with the L7 transgenic mouse that carries a tet07-luciferase transgene (40). Offspring carrying the L7 transgene as well as one ICA69^{null}/tTA^{+} allele demonstrated high luciferase activity in brain (note the logarithmic scale), low levels in stomach and testes, and borderline levels in pancreas, in which β cells contribute 0.1% of total pancreas tissue (Fig. 1*D*). The latter observation is consistent with the fact that ICA69 expression in exocrine pancreas is at best minuscule (47). In mice receiving doxycycline ad libitum in drinking water (0.1 mg/ml), luciferase activity was suppressed to background levels (not shown). These observations provided an excellent readout of ICA69 promoter activity.

However, similar experiments with mice from backcross 3 showed a >10-fold reduction in luciferase activity, and no activity at all could be detected in offspring from L7 matings with knockout animals from backcross 5 and 7. While Southern blots and genomic PCR gave expected results, transcripts of tTA could be demonstrated by RT-PCR of brain RNA in backcross 2-derived, but not in animals from these latter experiments, indicating loss of ICA69 promoter activity. Transcriptional silencing is not rare among neuronal genes (48), and has been described for GAD65 (49).

Autoantigen skews the specificity of autoreactive T cells

Autoreactive T cells in wild-type NOD mice (like patients with T1D) recognize the dominant ICA69 epitope Tep69 (10, 26). These T cells show antigenic mimicry with the ABBOS epitope in BSA, and T cell hybridoma as well as alanine replacement studies indicated that these mimicry T cells represent the bulk of ICA69-specific NOD repertoires (16). ICA69^{null} NOD congenics allowed

us to determine the role of endogenous self Ag in the development of these self-reactive T cell pools. Immunization with BSA had divergent consequences in heterozygous and homozygous ICA69 knockout mice (Fig. 2*A*). Both lines of mice generated good and similar proliferative recall responses after a single BSA immunization in complete adjuvant. However, only heterozygous (+/−) animals generated the coordinate ABBOS and Tep69 mimicry responses typical for wild-type NODs (14, 16). In homozygous ICA69^{null} NOD congenics, ABBOS was no longer a prominent epitope, despite the fact that it binds to NOD I-A^{g7} with high affinity (16). Only some low affinity ABBOS responses were observed at a very high peptide dose. No mimicry responses to Tep69 were seen in BSA-immunized ICA69^{null} animals. Thus, the endogenous self Ag is required for the recruitment of precursor T cell pools that recognize both Tep69 and ABBOS, and the presence of these T cell pools is responsible for the strong immunodominance (14) of the ABBOS epitope in BSA.

Endogenous self Ag (and not dietary ABBOS) was also critical for the maintenance of these autoreactive mimicry T cell pools. Thus, when knockout mice were adoptively transferred with splenocytes from diabetic wild-type NODs, Tep69/ABBOS-specific T lymphocytes were specifically lost (Fig. 2*B*, filled bars), while other islet-reactive T cells, such as GAD65-specific pools, were maintained. Consistent with this critical role of the endogenous self Ag, Tep69/ABBOS-specific T cells were maintained in heterozygous ICA69$^{+/-}$ mice adoptively transferred with the same wild-type splenocyte grafts (Fig. 2*B*, open bars).

ICA69^{null} NOD mice develop diabetes

Autoimmunity to ICA69 is a routine element of prediabetes and of diabetes in wild-type NOD mice and humans (10, 14, 16). Spontaneously diabetic knockout females were observed beginning by wk 20, ~4 wk later than in wild-type or heterozygous animals (Fig. 3*A*). This difference was not quite significant ($p = 0.058$). The consecutive disease development in knockout mice paralleled that in heterozygous and wild-type NOD females ($p > 0.3$). There was a tendency for slightly less or slower development of invasive insulitis (Fig. 3*B*), but this again failed to reach significance. Thus, ICA69 appears to be a facultative, but not obligate element in NOD diabetes development.

This conclusion is somewhat tempered by the unexpected observation of spontaneous lethality in middle-aged NOD female congenics at 4–5 mo of age (Fig. 3*C*). A subset of these animals died suddenly without prodromal symptoms. These animals had no significant histopathology, except for insulitis commensurate with prediabetes progression and a severed tongue in one animal. This phenotype is reminiscent of GAD65 deficiency, which leads to lethal mid-life seizures on the NOD background (37). Neuropharmacological studies have to date failed to unmask a consistent abnormality in the CNS electrophysiology of ICA69^{null} mice. In our assessment of the spontaneous diabetes incidence in ICA69^{null} mice, we removed the prematurely dead animals from calculation. The implicit assumption that these animals would have developed diabetes at the same rate as survivors is based on the presence of invasive insulitis.

Adoptive transfer of diabetes

Accelerated models of diabetes such as adoptive transfer of diabetic spleen cells circumvent natural checkpoints in prediabetes progression (50). We asked whether the slight delay in spontaneous diabetes development would be amplified or eliminated following adoptive transfer of wild-type diabetic spleen cells into irradiated knockout recipients. The latter was observed: transferred animals developed disease at the same rate and incidence as heterozygous littermates or wild-type controls (Fig. 3*D*), unhindered by the fact that the knockout mice lost ICA69-specific T cells during disease development (see above, Fig. 2*B*), and lacked this target autoantigen.

Acceleration of diabetes with CY

In striking contrast to wild-type and heterozygous animals, injection of CY (250 mg/kg) failed to induce accelerated diabetes in ICA69^{null} mice (Fig. 4). Heterozygous littermates began to develop overt disease by 10–11 days post-CY, reaching a high disease incidence by 3 wk ($p < 0.0001$, odds ratio 27.4 vs knockout (Fig. 4*A*), $p > 0.3$ vs wild-type mice, not shown). ICA69 protein is not expressed in hemopoietic cells (30) (see Fig. 1*D* for splenocytes). Consistently, there was no detectable effect of ICA69 deficiency in this tissue, with homozygous, heterozygous NOD as well as 129 mice showing the same acute drug-induced fall in spleen weight and cellularity. CY metabolism with generation of, and response to the major toxic intermediates (22) was thus similar in these animals ($p > 0.3$, data not shown).

Curiously, there was only a slight, nonsignificant difference in insulitis severity of CY-treated homozygous and heterozygous animals (Fig. 4*B*, $p = 0.2$), suggesting that effector functions in the islet infiltrate of knockout mice lacked the competence to mediate β cell death. This incompetence was not due to a general delay of prediabetes, since ICA69^{null} NOD mice 14 wk of age, and thus close to the time of overt spontaneous diabetes development, were still protected from CY-induced disease (Fig. 4*C*). These older animals ultimately did develop diabetes, beginning in wk 20 with the incidence rising at wild-type rates (see Fig. 3*A*). The resistance to CY-accelerated diabetes in knockout mice was not absolute, since a second CY injection caused diabetes in nearly half of the

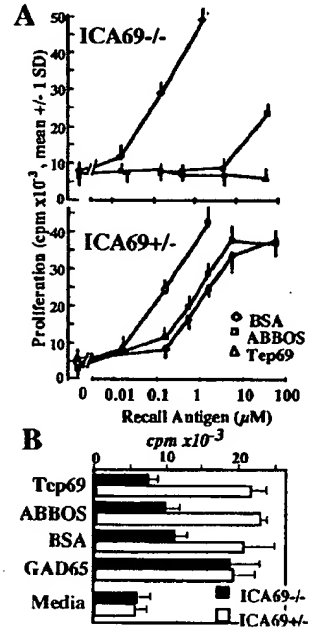

FIGURE 2. In vitro proliferative recall responses. *A*, Homo- and heterozygous knockout NOD congenics were immunized s.c. once with BSA emulsified in CFA, and in vitro lymph node responses to BSA, ABBOS, and Tep69 were elicited 10 days later. *B*, In vitro proliferative response of wild-type, diabetic spleen cells 14 days after transfer to irradiated ICA69$^{-/-}$ (filled columns) or ICA69$^{+/-}$ recipients (open columns).

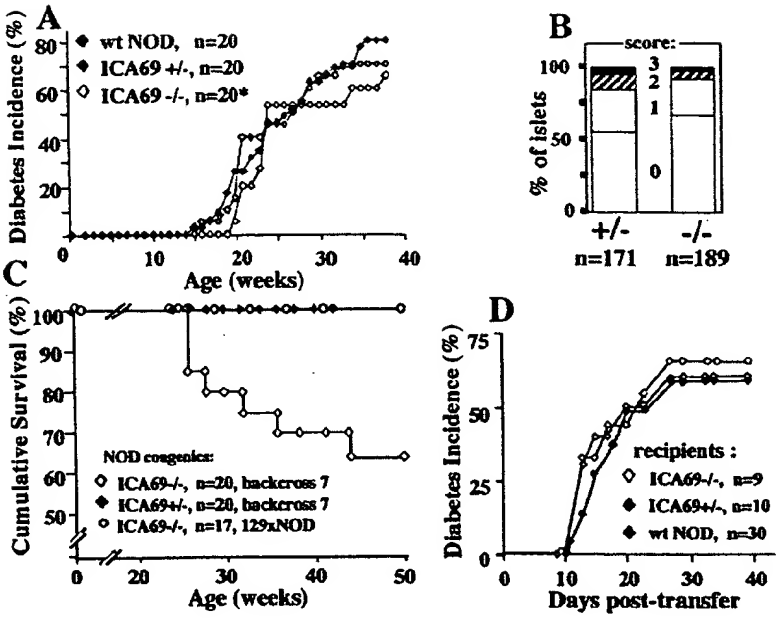

FIGURE 3. Diabetes development and survival of ICA69^{null} NOD mice. *A*, Spontaneous diabetes development: *, a proportion of ICA69^{null} mice died prematurely (see *C*) and were removed from the calculation of disease incidence. *B*, Insulitis in untreated ICA69$^{+/-}$ or ICA69$^{-/-}$ female congenics (seven animals/group) at 10 wk of age. *C*, Mid-life lethality of ICA69^{null} NOD females without prodromal disease symptoms or diagnostic histopathology. *D*, Wild-type diabetes development in irradiated ICA69$^{-/-}$, ICA69$^{+/-}$, or wild-type NOD mice adoptively transferred with spleen cells from diabetic wild-type donors.

homozygous mice (5 of 11), compared with 12 of 13 heterozygous animals (Fig. 4*D*, $p = 0.02$).

CY-accelerated diabetes has been associated with the selective elimination of regulatory T cells and/or with the induction of a massive wave of T cell regeneration that would coexpand diabetogenic pools (23, 24, 51). We more closely examined the CY responses of knockout hemopoietic cells. NOD.*scid* mice were pretreated with CY 2 days before adoptive transfer of spleen cells from 12-wk-old nondiabetic wild-type mice; diabetes did not develop within the observation period (Fig. 4*E*, *CY→Tx*). This confirmed the critical role of acute, drug-induced toxicity in lymphoid cells.

However, when NOD.*scid* mice were reconstituted with 10^7 spleen cells from 8-wk-old homozygous knockout mice, from heterozygous littermates, or wild-type NOD controls, 1 mo before CY treatment (Fig. 4*E*, *Tx→CY*), these transplanted NOD.*scid* animals developed CY-accelerated diabetes at the same rates and incidence ($p > 0.5$). This observation demonstrated that hemopoietic cells were not involved in the CY resistance of knockout mice. Collectively, these two observations delineated two drug targets prerequisite for diabetes development, one in hemopoietic and one in nonhemopoietic tissue.

Since the islet is one target tissue of CY toxicity (52), we asked whether the nonhemopoietic tissue required for disease acceleration by CY might be the islet itself. We therefore provided ICA69^{null} mice with a source of wild-type islets in small, subrenal islet grafts. Sixteen days later, the engrafted mice were injected with CY as before (Fig. 5*A*). The presence of wild-type islets reversed the resistance to CY-accelerated diabetes in ICA69^{null} mice, and allowed diabetes development in engrafted knockout

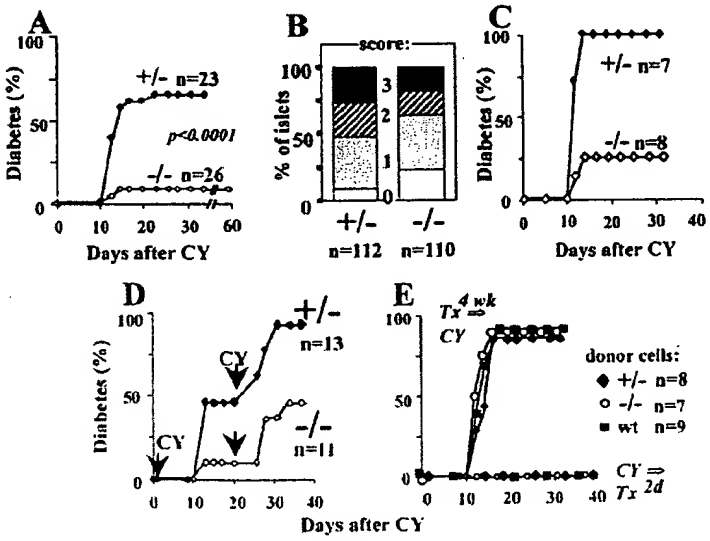

FIGURE 4. ICA69$^{-/-}$ NOD mice resist CY-accelerated diabetes. *A*, Diabetes incidence in CY-treated hetero- and homozygous knockout mice aged 8–10 wk. *B*, Insulitis score in CY-treated, nondiabetic ICA69$^{+/-}$ ($n = 5$) and ICA69$^{-/-}$ mice ($n = 8$) 35 days after drug treatment. The number of nonadjacent islets counted (n) is indicated at the *bottom*. See *Materials and Methods* for scoring scale. About one-half of heterozygote islets and only slightly fewer homozygote islets ($p = 0.2$) had severe, grade 2 and 3 insulitis. *C*, Diabetes incidence in CY-treated hetero- and homozygous knockout mice aged 14 wk. *D*, Dual injections of CY on day 0 and 20 in ICA69$^{-/-}$ and ICA69$^{+/-}$ animals. *E*, Diabetes development in NOD.*scid* mice reconstituted with 10^7 ICA69$^{-/-}$, ICA69$^{+/-}$, or wild-type spleen cells 1 mo before (*Tx→CY*) or 2 days after (*CY→Tx*) CY treatment.

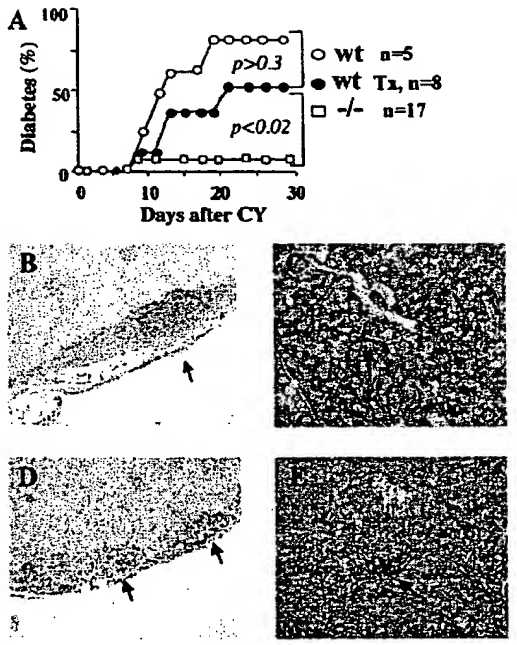

FIGURE 5. Transplantation of wild-type islets reverses CY resistance in ICA69^{null} mice. *A*, Incidence of CY-accelerated diabetes in sham-operated, wild-type mice (O); sham- or nontransplanted ICA69$^{-/-}$ NOD females (□); or ICA69^{null} females with wild-type islet grafts (Tx) under the kidney capsule, transplanted 16 days before CY (●). *B–E*, Immunohistochemical analysis of transplanted or pancreatic islets (×100, insulin stained in brown, counterstained with hematoxylin). *B*, Wild-type islet graft under the kidney capsule with massive inflammatory infiltrate (arrow) and absent insulin staining. *C*, Destroyed pancreatic islet of the same diabetic animal. *D*, Infiltration, but survival of insulin-producing cells in renal wild-type islet grafts (arrows) from a CY-treated, nondiabetic ICA69^{null} mouse. *E*, Infiltration, but survival of insulin-producing cells (arrow) in a pancreatic islet from the same animal.

animals ($p > 0.3$, knockout-operated vs sham-operated wild-type NOD; $p = 0.016$, islet-engrafted vs sham-operated or nontransplanted ICA69^{null} mice). These observations confirm and extend previous, indirect evidence for a duality of CY effects that accelerate diabetes development (53).

Histological examination of transplanted, CY-induced diabetic ICA69^{null} mice showed massive infiltration and complete disappearance of insulin-producing cells in the subrenal, wild-type islet grafts (Fig. 5*B*). Endogenous (pancreatic) islets in these knockout mice were similarly infiltrated and depleted of insulin-producing β cells (Fig. 5*C*). Destruction of wild-type islet grafts was a prerequisite for the destruction of endogenous (knockout) islets in the pancreas: those ICA69^{null} mice that escaped CY-accelerated diabetes showed less infiltration and intact insulin-producing cells in the wild-type islet grafts (Fig. 5*D*). The endogenous islets in these mice were heavily infiltrated, but retained a prominent compartment of insulin-producing β cells (Fig. 5*E*), suggesting that this infiltrate was incompetent to mediate β cell destruction.

These observations suggest that the resistance of ICA69^{null} mice to CY-accelerated diabetes reflects a relative resistance to CY toxicity in β cells, which require ICA69 for an apoptotic drug response (52). Consistently, CY resistance can be bypassed if a source of drug-sensitive islets is present somewhere in the body, suggesting a systemic effect that boosts T cell pools with pathogenic potential during the rapid recovery and expansion of lymphoid cells after CY treatment.

Discussion

Deficiency of ICA69 generated several distinct phenotypes in NOD mice. It answered several core questions about the role of endogenous self Ag in disease-associated antigenic mimicry and the ability of the diabetic autoimmune process to shape disease-relevant T cell pools. The unexpected resistance to CY-accelerated diabetes allowed a reevaluation of its mechanistic basis in vivo. There is previous evidence for acute, CY-mediated islet toxicity that peaks within a day of drug injection and removes a substantial proportion of β cells (52). We have only begun mechanistic studies of how ICA69 might be involved in this process.

The function of ICA69 remains unclear. The neurotransmission defect generated by knockout of its neuron-specific *C. elegans* homologue, *ric-19* (31), requires further study, as does the mid-life lethality of ICA69^{null} NOD mice. Current experiments suggest that possible abnormalities in neurotransmission of ICA69^{null} mice will be subtle. However, we recently observed that NOD mice undergoing the spontaneous NOD autoimmune encephalitis develop seizures with considerable incidence (45), and Kash et al. (37) provided evidence for a rather strong modifier gene that predisposes NOD to seizures. Neurological similarities in GAD65 and ICA69 knockout mice may place ICA69 into the GABAergic pathway of neurotransmission, consistent with its pre- and postsynaptic localization (e.g., see Fig. 1*C*).

We were fortunate to identify a crossover event early in the backcrossing process, which replaced about two-thirds of the 129-derived chromosome 6 with NOD DNA. Nevertheless, a substantial stretch of 129-derived chromosome 6 remains. We had planned rescue experiments with a tet07-controlled ICA69 transgene, driven by the knock-in tTA transactivator. The silencing of the ICA69 promoter and consequent lack of tTA expression precluded this experiment, meant to rule out specific contributions of 129 genes to the knockout phenotype. However, comparing the CY toxicity in 129 and NOD mice failed to delineate differences in acute drug toxicity in spleen as well as testes, a tissue targeted by the drug (54). Although theoretically possible, it is therefore unlikely that the observed CY resistance of knockout mice reflects an unidentified 129 gene near the *ica-1* locus. Nevertheless, whether CY resistance maps to ICA69 (likely) or a 129 gene (unlikely) is immaterial for the major conclusion of these experiments, i.e., that CY-accelerated diabetes involves direct drug toxicity to the islet.

Several and similar T cell autoreactivities appear to participate in murine and human diabetogenesis (7, 10). Immunotherapy of NOD prediabetes with single autoantigens such as GAD65, GAD67, insulin, ICA69, IA-2, and others can each dramatically modify the disease course, provided that they are applied early in life, generally before the islet is breached (7). The exact mechanisms of effective immunotherapy are still elusive (for a discussion, see Ref. 16), but these consistent observations assign important potential, but not necessarily obligate roles to each target Ag. Removal of one player through gene targeting, e.g., ICA69 or GAD65 (37, 38), is the most accurate way to measure the role of an individual autoantigen, and the data available support a model of many facultative, but not obligate autoantigens in the progression to diabetes.

An unresolved question in autoimmunity is whether autoantigens drive autoimmunity, or whether they are more passive elements, perhaps victims of mimicry with exogenous proteins (55, 56). At least in the case of ICA69, the former appears to be correct. There is well-established mimicry between the major T cell epitopes in ICA69 (Tep69) and the commonly encountered BSA

(ABBOS) (10, 14, 16, 26, 32). T cell responses of wild-type NOD mice to BSA are extremely biased toward ABBOS reactivity. The same cells recognize Tep69 in NOD mice (16), and the same appears to apply to diabetes-prone humans (10). We expected that this polarization solely reflected properties of MHC alleles, with a very high ABBOS-binding affinity for diabetes risk-associated human and NOD MHC class II (16). This turned out to be incorrect: ICA69^{null} mice have entirely different BSA responses, in which ABBOS is at best a minor epitope, recognized by low affinity T cells that do not show mimicry with Tep69. Demonstrating antigenic mimicry, therefore, does not per se imply a primary mechanism for loss of tolerance. However, wild-type NOD mice reared on a diet free of BSA also fail to generate mimicry T cell pools (57). The functional outcome of mimicry is thus affected by both endogenous and exogenous Ag.

The resistance of ICA69^{null} mice to CY-induced diabetes was unexpected and has since been reproduced in backcross 11 mice with ICA69 deficiency. This resistance did not reflect a generalized resistance to β cell death or autoimmune attack, since ICA69^{null} mice develop diabetes spontaneously with wild-type incidence, and since alloxan treatment eliminates β cells just as in wild-type mice (unpublished observation). These observations, and the normal, accelerated diabetes development in NOD.*scid* mice reconstituted with spleen cells from either heterozygous or homozygous knockout donors suggested: 1) that CY-induced diabetes had to require effects in a second target tissue, and 2) that the resistance to diabetes acceleration in ICA69^{null} animals could not be attributed solely to the hemopoietic cell compartment. Islet transplant experiments strongly suggest that the second drug target is islet β cells themselves.

If this is substantially correct, then the islet toxicity of CY is dependent on the presence of ICA69. We propose that direct islet toxicity provides a boost to pathogenic T cell pools, providing islet Ags during the rapid, post-CY regeneration. Injury to β cells has also been implicated as a requirement for virus-accelerated diabetes (58, 59). The earliest, CY-induced change previously reported is the rapid accumulation of monokines IL-12, TNF-α, and IL-18 in the pancreas ~2 days after drug treatment (3), 1 day after the peak of drug-induced β cell death (52). While it may ultimately not be trivial to separate cause and effect, the most obvious scenario would be that CY-induced β cell death attracts and activates professional APCs, which then engender pathogenic competence in preexisting T cell pools with islet autoreactivity. Our data demonstrate that without this event, T cells still home to the islet, but are incompetent to mediate β cell death.

Overall, this process would then be analogous to the induction of NOD autoimmune thyroiditis following induction of thyroid cell death by high dose iodide treatment (60). It would differ from the effects of drugs such as streptozotocin, which kill β cells and cause diabetes in any strain, while CY-accelerated diabetes requires the NOD host with established autoimmune T cell repertoires. Consistently, the provision of wild-type islet grafts under the kidney capsule was sufficient to reverse CY resistance in knockout mice, with rapid elimination of endogenous β cells in the pancreas and consequent diabetes. This outcome confirms that islets drive pathogenic, diabetic autoimmunity, as has been suggested for natural disease development (61).

The exact function of ICA69 remains unclear, but knockout mice will provide excellent tools for further study. Collectively, ICA69 knockout mice generated new insights into the role of a typical autoantigen targeted in autoimmune diabetes. The observations make it unlikely that the exogenous ICA69 mimicry Ag, BSA, has a primary triggering role in the loss of tolerance to ICA69. Instead, the highly biased T cell repertoire of NOD mice immunized with BSA now emerges as a function of autoreactive mimicry T cells driven by the endogenous self Ag. The combination of several autoantigen knockout mice should eventually allow a more complete dissection of diabetic autoimmunity. The long, drawn-out character of prediabetes remains a puzzle. The CY resistance in ICA69^{null} mice sheds new light on this process, with a critical role for drug-induced β cell death, probably coupled to autoimmunity through the activation of local APCs. The heavy islet infiltration in CY-treated ICA69^{null} mice vividly illustrates that the endowment of pathogenicity in infiltrating T cells is a critical progression event, which normally does not occur until very late in prediabetes. These observations favor the view that prediabetes progression is not a linear process of gradual β cell destruction (62), but rather a process that culminates late with massive β cell destruction near disease onset (63). If correct and applicable to the human disease, immunotherapy of prediabetes may be effective even late in prediabetes if it avoids precipitation of diabetes in an immune system precariously balanced between pathogenicity and nonpathogenicity.

Acknowledgments

We thank Dr. Xiao Rong Peng (Toronto, Ontario, Canada) for her excellent suggestions and support throughout this project, Dr. H. Bujard (Heidelberg, Germany), Dr. M. Pietropaolo (Pittsburgh, PA), Dr. J. Elliott (Edmonton, Alberta), and Dr. W. Trimble and Dr. Tak Mak (Toronto, Ontario, Canada) for providing valuable reagents.

References

1. Karges, W., J. Ilonen, B. H. Robinson, and H.-M. Dosch. 1995. Self and non-self antigen in diabetic autoimmunity: molecules and mechanisms. *Mol. Aspects Med. 16:79.*
2. Andre, I., A. Gonzalez, B. Wang, J. Katz, C. Benoist, and D. Mathis. 1996. Checkpoints in the progression of autoimmune disease: lessons from diabetes models. *Proc. Natl. Acad. Sci. USA 93:2260.*
3. Andre-Schmutz, I., C. Hindelang, C. Benoist, and D. Mathis. 1999. Cellular and molecular changes accompanying the progression from insulitis to diabetes. *Eur. J. Immunol. 29:245.*
4. Reddy, S., N. Bibby, and R. B. Elliott. 1990. Longitudinal study of islet cell antibodies and insulin autoantibodies and development of diabetes in non-obese diabetic (NOD) mice. *Clin. Exp. Immunol. 81:400.*
5. Yu, L., D. T. Robles, N. Abiru, P. Kaur, M. Rewers, K. Kelemen, and G. S. Eisenbarth. 2000. Early expression of antiinsulin autoantibodies of humans and the NOD mouse: evidence for early determination of subsequent diabetes. *Proc. Natl. Acad. Sci. USA 97:1701.*
6. Schranz, D. B., and A. Lernmark. 1998. Immunology in diabetes: an update. *Diabetes Metab. Rev. 14:3.*
7. Atkinson, M. A., and E. H. Leiter. 1999. The NOD mouse model of type 1 diabetes: as good as it gets? *Nat. Med. 5:601.*
8. Lipton, R. B., M. Kocova, R. E. LaPorte, J. S. Dorman, T. J. Orchard, W. J. Riley, A. L. Drash, D. J. Becker, and M. Trucco. 1992. Autoimmunity and genetics contribute to the risk of insulin-dependent diabetes mellitus in families: islet cell antibodies and HLA DQ heterodimers. *Am. J. Epidemiol. 136:503.*
9. Verge, C. F., D. Stenger, E. Bonifacio, P. G. Colman, C. Pilcher, P. J. Bingley, and G. S. Eisenbarth. 1998. Combined use of autoantibodies (IA-2 autoantibody, GAD autoantibody, insulin autoantibody, cytoplasmic islet cell antibodies) in type 1 diabetes: Combinatorial Islet Autoantibody Workshop. *Diabetes 47:1857.*
10. Dosch, H.-M., R. K. Cheung, W. Karges, M. Pietropaolo, and D. J. Becker. 1999. Persistent T cell anergy in human type 1 diabetes. *J. Immunol. 163:6933.*
11. Kaufman, D. L., M. Clare-Salzler, J. Tian, T. Fortshuber, G. S. P. Ting, P. Robinson, M. A. Atkinson, E. Sercarz, A. J. Tobin, and P. V. Lehman. 1993. Spontaneous loss of T cell tolerance to glutamic acid decarboxylase in murine insulin dependent diabetes. *Nature 366:69.*
12. Daniel, D., and D. R. Wegmann. 1996. Protection of nonobese diabetic mice from diabetes by intranasal or subcutaneous administration of insulin peptide B-(9-23). *Proc. Natl. Acad. Sci. USA 93:956.*
13. Elliott, J. F., H. Y. Qin, S. Bhatti, R. Singh, D. K. Smith, J. Lauzon, and B. Singh. 1994. Immunization with the large isoform of mouse glutamic acid decarboxylase (GAD67) prevents autoimmune diabetes in NOD mice. *Diabetes 43:1494.*
14. Karges, W., D. Hammond-McKibben, R. Gaedigk, N. Shibuya, R. Cheung, and H.-M. Dosch. 1997. Loss of self-tolerance to ICA69 in non-obese diabetic mice. *Diabetes 46:1548.*
15. Tisch, R., B. Wang, and D. V. Serreze. 1999. Induction of glutamic acid decarboxylase 65-specific Th2 cells and suppression of autoimmune diabetes at late stages of disease is epitope dependent. *J. Immunol. 163:1178.*
16. Winer, S., L. Gunaratnam, I. Astsaturov, R. K. Cheung, V. Kubiak, W. Karges, D. Hammond-McKibben, R. Gaedigk, D. Graziano, M. Trucco, et al. 2000. Peptide dose, MHC-affinity and target self-antigen expression are critical for effective immunotherapy of NOD mouse prediabetes. *J. Immunol. 165:4086.*

17. Trembleau, S., G. Penna, S. Gregori, G. Magistrelli, A. Isacchi, and L. Adorini. 2000. Early Th1 response in unprimed nonobese diabetic mice to the tyrosine phosphatase-like insulinoma-associated protein 2, an autoantigen in type 1 diabetes. *J. Immunol. 165:6748.*
18. Wong, F. S., J. Karttunen, C. Dumont, L. Wen, I. Visintin, I. M. Pilip, N. Shastri, E. G. Pamer, and C. A. Janeway, Jr. 1999. Identification of an MHC class I-restricted autoantigen in type 1 diabetes by screening an organ-specific cDNA library. *Nat. Med. 5:1026.*
19. Sercarz, E. E., P. V. Lehmann, A. Ametani, G. Benichou, A. Miller, and K. Moudgil. 1993. Dominance and crypticity of T cell antigenic determinants. In *Annu. Rev. Immunol.*, Vol. 11. W. E. Paul, C. G. Fathman, and H. Metzger, eds. Annual Rev., Palo Alto. p. 729.
20. Bonifacio, E., V. Lampasona, L. Bernasconi, and A. G. Ziegler. 2000. Maturation of the humoral autoimmune response to epitopes of GAD in preclinical childhood type 1 diabetes. *Diabetes 49:202.*
21. Amrani, A., J. Verdaguer, P. Serra, S. Tafuro, R. Tan, and P. Santamaria. 2000. Progression of autoimmune diabetes driven by avidity maturation of a T-cell population. *Nature 406:739.*
22. Ludeman, S. M. 1999. The chemistry of the metabolites of cyclophosphamide. *Curr. Pharm. Des. 5:627.*
23. Yasunami, R., and J. F. Bach. 1988. Anti-suppressor effect of cyclophosphamide on the development of spontaneous diabetes in NOD mice. *Eur. J. Immunol. 18:481.*
24. Charleton, B., A. Bacelj, R. M. Slattery, and T. E. Mandel. 1989. Cyclophosphamide-induced diabetes in NOD/Wehi mice: evidence for suppression in spontaneous autoimmune diabetes mellitus. *Diabetes 38:441.*
25. Colucci, F., C. M. Cilio, K. Lejon, C. P. Goncalves, M. L. Bergman, and D. Holmberg. 1996. Programmed cell death in the pathogenesis of murine IDDM: resistance to apoptosis induced in lymphocytes by cyclophosphamide. *J. Autoimmun. 9:271.*
26. Karges, W., R. Gaedigk, M. F. Hui, R. K. Cheung, and H.-M. Dosch. 1997. Molecular cloning of murine ICA69: diabetes-prone mice recognize the human autoimmune-epitope, Tep69, conserved in splice variants from both species. *Biochim. Biophys. Acta 1360:97.*
27. Gaedigk, R., W. Karges, M. F. Hui, and H.-M. Dosch. 1996. Genomic organization of human and mouse ICAp69, a target antigen in in diabetic autoimmunity. *Genomics 38:382.*
28. Serreze, D. V., H. D. Chapman, D. S. Varnum, M. S. Hanson, P. C. Reifsnyder, S. D. Richard, S. A. Fleming, E. H. Leiter, and L. D. Shultz. 1996. B lymphocytes are essential for the initiation of T cell-mediated autoimmune diabetes: analysis of a new "speed congenic" stock of NOD.Ig μ null mice. *J. Exp. Med. 184:2049.*
29. Gaedigk, R., A. M. V. Duncan, I. Miyazaki, B. H. Robinson, and H.-M. Dosch. 1994. ICA1 encoding p69, a protein linked to the development of type 1 diabetes mellitus, maps to chromosome 7p22. *Cytogenet. Cell Genet. 66:274.*
30. Karges, W., M. Pietropaolo, C. Ackerley, and H.-M. Dosch. 1996. Gene expression of islet cell antigen p69 (ICAp69) in man, mouse and rat. *Diabetes 45:513.*
31. Pilon, M., X.-R. Peng, A. M. Spence, R. H. A. Plasterk, and H.-M. Dosch. 2000. ICA69 and its *C. elegans* homolog, ric-19, are novel regulators of neuroendocrine secretion. *Mol. Biol. Cell 11:3277.*
32. Miyazaki, I., R. K. Cheung, R. Gaedigk, M. F. Hui, J. Van der Meulen, R. V. Rajotte, and H.-M. Dosch. 1995. T cell activation and anergy to islet cell antigen in type 1 diabetes. *J. Immunol. 154:1461.*
33. Perez-Bravo, F., E. Carrasco, M. D. Gutierrez-Lopez, M. T. Martinez, G. Lopez, and, M. Garcia de los Rios. 1996. Genetic predisposition and environmental factors leading to the development of insulin-dependent diabetes mellitus in Chilean children. *J. Mol. Med. 74:105.*
34. Karges, W., and H.-M. Dosch. 1996. Environmental factors: cow milk and others. In *Diabetes Prediction, Prevention and Genetic Counselling in IDDM.* J. P. Palmer, ed. John Wiley & Sons, Chichester, p. 167.
35. Verge, C. F., N. J. Howard, L. Irwig, J. M. Simpson, D. Mackerras, and M. Silink. 1994. Environmental factors in childhood IDDM. *Diabetes Care 17:1381.*
36. Hypponen, E., M. G. Kenward, S. M. Virtanen, A. Piitulainen, P. Virta-Autio, J. Tuomilehto, M. Knip, and H. K. Akerblom. 1999. Infant feeding, early weight gain, and risk of type 1 diabetes: Childhood Diabetes in Finland (DiMe) Study Group. *Diabetes Care 22:1961.*
37. Kash, S. F., R. S. Johnson, L. H. Tecott, J. L. Noebels, R. D. Mayfield, D. Hanahan, and S. Baekkeskov. 1997. Epilepsy in mice deficient in the 65-kDa isoform of glutamic acid decarboxylase. *Proc. Natl. Acad. Sci. USA 94:14060.*
38. Kash, S. F., B. G. Condie, and S. Baekkeskov. 1999. Glutamate decarboxylase and GABA in pancreatic islets: lessons from knock-out mice. *Horm. Metab. Res. 31:340.*
39. Ballinger, W. F., and P. E. Lacy. 1972. Transplantation of intact pancreatic islets in rats. *Surgery 72:175.*
40. Furth, P. A., L. St Onge, H. Boger, P. Gruss, M. Gossen, A. Kistner, H. Bujard, and L. Hennighausen. 1994. Temporal control of gene expression in transgenic mice by a tetracycline-responsive promoter. *Proc. Natl. Acad. Sci. USA 91:9302.*
41. Gossen, M., A. L. Bonin, and H. Bujard. 1993. Control of gene activity in higher eukaryotic cells by prokaryotic regulatory elements. *Trends Biochem. Sci. 18:471.*
42. Kistner, A., M. Gossen, F. Zimmermann, J. Jerecic, C. Ullmer, H. Lubbert, and H. Bujard. 1996. Doxycycline-mediated quantitative and tissue-specific control of gene expression in transgenic mice. *Proc. Natl. Acad. Sci. USA 93:10933.*
43. Hamaguchi, K., H. R. Gaskins, and E. H. Leiter. 1991. NIT-1, a pancreatic β-cell line established from a transgenic NOD/Lt mouse. *Diabetes 40:842.*
44. Nagy, A., J. Rossant, R. Nagy, N. W. Abramow, and J. C. Roder. 1993. Derivation of completely cell culture-derived mice from early-passage embryonic stem cells. *Proc. Natl. Acad. Sci. USA 90:8424.*
45. Winer, S., I. Astsaturov, R. K. Cheung, L. Gunaratnam, V. Kubiak, M. A. Moscarello, P. O'Connor, C. McKerlie, D. J. Becker, and H.-M. Dosch. 2001. Type I diabetes and MS patients target islet plus CNS-autoantigens, non-immunized NOD mice can develop autoimmune encephalitis. *J. Immunol. 166:2832.*
46. Pietropaolo, M., L. Castano, S. Babu, R. Buelow, Y.-L. Kuo, S. S. Martin, A. Martin, A. C. Powers, M. Prochazka, J. Naggert, et al. 1993. Islet cell autoantigen 69 kD (ICA69): molecular cloning and characterization of a novel diabetes-associated autoantigen. *J. Clin. Invest. 92:359.*
47. Stassi, G., N. Schloot, and M. Pietropaolo. 1997. Islet cell autoantigen 69 kDa (ICA69) is preferentially expressed in the human islets of Langerhans rather than exocrine pancreas. *Diabetologia 40:120.*
48. Naruse, Y., T. Aoki, T. Kojima, and N. Mori. 1999. Neural restrictive silencer factor recruits mSin3 and histone deacetylase complex to repress neuron-specific target genes. *Proc. Natl. Acad. Sci. USA 96:13691.*
49. Pinal, C. S., V. Cortessis, and A. J. Tobin. 1997. Multiple elements regulate GAD65 transcription. *Dev. Neurosci. 19:465.*
50. Wicker, L. S., B. J. Miller, and Y. Mullen. 1986. Transfer of autoimmune diabetes mellitus with splenocytes from nonobese diabetic (NOD) mice. *Diabetes 35:855.*
51. Colucci, F., M. L. Bergman, C. Penha-Goncalves, C. M. Cilio, and D. Holmberg. 1997. Apoptosis resistance of nonobese diabetic peripheral lymphocytes linked to the Idd5 diabetes susceptibility region. *Proc. Natl. Acad. Sci. USA 94:8670.*
52. O'Brien, B. A., B. V. Harmon, D. P. Cameron, and D. J. Allan. 2000. Nicotinamide prevents the development of diabetes in the cyclophosphamide-induced NOD mouse model by reducing β-cell apoptosis. *J. Pathol. 191:86.*
53. Casteels, K., M. Waer, R. Bouillon, J. Depovere, D. Valckx, J. Laureys, and C. Mathieu. 1998. 1,25-Dihydroxyvitamin D3 restores sensitivity to cyclophosphamide-induced apoptosis in non-obese diabetic (NOD) mice and protects against diabetes. *Clin. Exp. Immunol. 112:181.*
54. Cai, L., B. F. Hales, and B. Robaire. 1997. Induction of apoptosis in the germ cells of adult male rats after exposure to cyclophosphamide. *Biol. Reprod. 56:1490.*
55. Wucherpfennig, K. W., and J. L. Strominger. 1995. Molecular mimicry in T cell-mediated autoimmunity: viral peptides activate human T cell clones specific for myelin basic protein. *Cell 80:695.*
56. Von Herrath, M. G., A. Holz, D. Homann, and M. B. Oldstone. 1998. Role of viruses in type 1 diabetes. *Semin. Immunol. 10:87.*
57. Karges, W., D. Hammond-McKibben, R. K. Cheung, M. Visconti, N. Shibuya, D. Kemp, and H. M. Dosch. 1997. Immunological aspects of nutritional diabetes prevention in NOD mice: a pilot study for the cow's milk-based IDDM prevention trial. *Diabetes 46:557.*
58. Horwitz, M. S., L. M. Bradley, J. Harbertson, T. Krahl, J. Lee, and N. Sarvetnick. 1998. Diabetes induced by coxsackie virus: initiation by bystander damage and not mimicry. *Nat. Med. 4:781.*
59. Horwitz, M. S., C. Fine, A. Ilic, and N. Sarvetnick. 2001. Requirements for viral-mediated autoimmune diabetes: β-cell damage and immune infiltration. *J. Autoimmun. 16:211.*
60. Many, M. C., S. Maniratunga, I. Varis, M. Dardenne, H. A. Drexhage, and J. F. Denef. 1995. Two-step development of Hashimoto-like thyroiditis in genetically autoimmune prone non-obese diabetic mice: effects of iodine-induced cell necrosis. *J. Endocrinol. 147:311.*
61. Larger, E., C. Becourt, J. F. Bach, and C. Boitard. 1995. Pancreatic islet β cells drive T cell-immune responses in the nonobese diabetic mouse model. *J. Exp. Med. 181:1635.*
62. Augstein, P., A. G. Elefanty, J. Allison, and L. C. Harrison. 1998. Apoptosis and β-cell destruction in pancreatic islets of NOD mice with spontaneous and cyclophosphamide-accelerated diabetes. *Diabetologia 41:1381.*
63. Shimada, A., B. Charlton, E. C. Taylor, and C. G. Fathman. 1996. β-Cell destruction may be a late consequence of the autoimmune process in nonobese diabetic mice. *Diabetes 45:1063.*

Targeted Disruption of the Protein Tyrosine Phosphatase-Like Molecule IA-2 Results in Alterations in Glucose Tolerance Tests and Insulin Secretion

Keiichi Saeki,[1] Min Zhu,[2] Atsutaka Kubosaki,[1] Jingping Xie,[1] Michael S. Lan,[2] and Abner Louis Notkins[1]

IA-2 is a major autoantigen in type 1 diabetes. Autoantibodies to IA-2 appear years before the development of clinical disease and are being widely used as predictive markers to identify individuals at risk for developing type 1 diabetes. IA-2 is an enzymatically inactive member of the transmembrane protein tyrosine phosphatase family and is an integral component of secretory granules in neuroendocrine cells. To study its function, we generated IA-2–deficient mice. Northern and Western blot analysis showed that neither IA-2 mRNA nor protein was expressed. Physical examination of the IA-2$^{-/-}$ animals and histological examination of tissues failed to reveal any abnormalities. Nonfasting blood glucose levels, measured over 6 months, were slightly elevated in male IA-2$^{-/-}$ as compared to IA-2$^{+/+}$ littermates, but remained within the nondiabetic range. Glucose tolerance tests, however, revealed statistically significant elevation of glucose in both male and female IA-2$^{-/-}$ mice and depressed insulin release. In vitro glucose stimulation of isolated islets showed that male and female mice carrying the disrupted gene released 48% ($P < 0.001$) and 42% ($P < 0.01$) less insulin, respectively, than mice carrying the wild-type gene. We concluded that IA-2 is involved in glucose-stimulated insulin secretion. *Diabetes* **51:1842–1850, 2002**

IA-2 is a major autoantigen in type 1 diabetes (1,2). At the time of diagnosis, ~70% of newly diagnosed patients have autoantibodies to IA-2. Because these autoantibodies appear months and years before the onset of clinical symptoms, they have become useful markers for identifying individuals who are at high risk for developing type 1 diabetes (3–7). Individuals with no clinical symptoms, but who have autoantibodies to IA-2 and GAD, have an ~50% risk of developing type 1 diabetes within 5 years and an even higher risk within 7–10 years. For these reasons, the measurement of autoantibodies to recombinant IA-2 and GAD is being widely used to predict risk for type 1 diabetes (8,9).

IA-2 is a 979–amino acid transmembrane protein. It has an extracellular, transmembrane, and intracellular domain consisting of 576, 24, and 379 amino acids, respectively (1). Autoantibodies to IA-2 are directed exclusively to the intracellular domain, primarily to the COOH-terminus and, to a somewhat lesser extent, to the juxtamembrane region (10–12). The gene encoding IA-2 is located on human chromosome 2q35. The coding region extends over ~20 kb and consists of 23 exons (13). Exons 1–12 encode the extracellular domain; exon 13, the transmembrane domain; and exons 14 through 23, the intracellular domain. A region extending ~200 bp 5′-upstream from the translation start site and a region encompassing exon 1 and intron 1 have been shown to have strong promoter activity (R. Alam and A.L.N., unpublished data; 13).

The function of IA-2 is not known. Based on sequence analysis, IA-2 belongs to a subgroup of the transmembrane protein tyrosine phosphatase (PTP) family. Homologs have been found in cows, rats, mice, macaca, zebrafish, *Drosophilia*, and *Caenorhabditis elegans* and show 99, 98, 97, 73, 82, 58, and 46% identity, respectively, to human IA-2 (14). IA-2 differs from other PTPs in that it is enzymatically inactive because of substitution of amino acids (Ala 911→Asp and Asp 877→Ala) at conserved sites known to be critical for enzymatic activity (15). Electron microscopic studies and immunohistochemical studies have localized the IA-2 protein (also known as ICA512) to the secretory vesicles of neuroendocrine cells (16).

The present study was initiated to determine the function of IA-2 by targeted disruption of the mouse IA-2 gene. Mouse IA-2 is very similar to human IA-2. It is 981 amino acids in length, consists of 23 exons, and is located on mouse chromosome 1 (17). A targeting construct, in which the 5′-upstream promoter region, exons 1–3 and introns 1, 2, and most of 3, were replaced with a neomycin cassette, was used to transfect embryonic stem (ES) cells by homologous recombination. ES cells in which the IA-2 construct had become integrated were injected into blastocysts, and the resulting chimeric animals and their offspring were bred and tested for evidence of homologous recombination and germ-line transmission. Here we describe the successful targeted disruption of the IA-2 gene in mice and provide a description of the resulting phenotype.

From the [1]Experimental Medicine Section, Oral Infection and Immunity Branch, National Institute of Dental and Craniofacial Research, National Institutes of Health, Bethesda, Maryland; and the [2]Research Institute for Children, Children's Hospital, and Departments of Pediatrics and Genetics, Louisiana State University Health Sciences Center, New Orleans, Louisiana.

Address correspondence and reprint requests to Abner L. Notkins, National Institutes of Health, Building 30/Room 121, 30 Convent Dr., MSC 4322, Bethesda, MD 20892-4322. E-mail: anotkins@dir.nidcr.nih.gov.

Received for publication 30 November 2001 and accepted in revised form 11 February 2002.

K.S., M.Z., and A.K. contributed equally to the work.

ELISA, enzyme-linked immunosorbent assay; ES, embryonic stem; KRBB, Krebs-Ringer bicarbonate buffer; PTP, protein tyrosine phosphatase.

RESEARCH DESIGN AND METHODS

Generation of IA-2–deficient mice. A 129SvJ mouse genomic library (Stratagene, Cedar Creek, TX) was screened with a mouse IA-2 cDNA probe. A 17-kb fragment of mouse IA-2 containing the coding sequence of exons 1–13 was used to construct a targeting vector. A 3.5-kb *Sall-Eco*RI fragment upstream of the first exon was subcloned into pBluescript SK+ (Stratagene). From this plasmid, the 5′-segment was subcloned as a 3.5-kb *Kpn*I-*Bam*HI fragment into pPNT vector (18), resulting in pPNT-5′IA-2. Subsequently, a 3.3-kb *Xho*I-*Xho*I fragment containing exons 4–6 was subcloned into pPNT-5′IA-2 vector, resulting in pPNT-IA-2. Homologous recombination resulted in the replacement of IA-2 exons 1–3 and introns 1, 2, and most of 3 with the neo-resistant gene cassette from the pPNT-IA-2 vector into the *Eco*RI-*Xho*I site of the targeted locus. The targeting plasmid was linearized using the unique *Not*I site before electroporation. The HSV-tk cassette was used for negative selection.

JI ES cells (19) were transfected with the linearized targeting vector (50 μg/1.5 × 10^7 cells) using a BioRad Gene Pulser and grown under double-selection conditions (350 μg/ml G418, 2 μmol/l ganciclovir). After 7–10 days, G418-ganciclovir–resistant ES cell clones were picked and expanded (20).

Genomic DNA from individual ES cell clones was extracted and analyzed by Southern blot hybridization. A 1.1-kb *Xho*I-*Hin*dIII fragment (outside probe) containing exons 7 and 8 just downstream of the *Xho*I-*Xho*I segment was used for screening. Homologous recombinant clones selected by the outside probe were also analyzed with a 1.9-kb neo cassette probe to check for multiple integrations. Five ES cell clones were injected into C57BL/6 mice blastocysts to generate chimeras. Overt chimeras were backcrossed with C57BL/6 mice to produce germline transmission of the targeted allele. Tail DNA of agouti offspring and subsequent pups was screened for the presence of the mutant IA-2 allele by Southern blot analysis and PCR. All protocols were approved by our institutional animal care and use committees.

Genotyping. Tail DNA-PCR using four primers was designed to discriminate between wild-type (IA-$2^{+/+}$), heterozygous (IA-$2^{+/-}$), and homozygous (IA-$2^{-/-}$) mice. The wild-type allele was detected as a 1.3-kb product using an exon 3 sense primer (5′-TACAAGGTGTGCTCCGGCAACTCATGT-3′) and an exon 4 antisense primer (5′-GGTCCATCTCCTGGGAGATCACATGCT-3′). The recombinant allele was detected as a 3.5-kb product using the PGK-1 primer (5′-GGTGCTGTCCATCTGCACGAGACTAGT-3′) in the promoter of the neo cassette and an exon 7 antisense primer (5′-CAGCAGTCAATCTCTGCA GACTCAATT-3′). PCR was performed with the TaqPlus Precision PCR System (Stratagene) at 35 cycles of 94°C for 0.5 min, 60°C for 1 min, and 72°C for 3 min in a GeneAmp PCR System 9700 (Applied Biosystems, Forest City, CA). Each PCR product was separated on 1% agarose gels containing ethidium bromide and visualized under ultraviolet light.

RNA analysis. Total RNA from brain (10-week-old male IA-$2^{+/+}$, IA-$2^{+/-}$, and IA-$2^{-/-}$ mice) was isolated using TRIZOL reagent (Life Technology, Rockville, MD). For Northern blot analysis, 20 μg of each sample were separated on a 1% (wt/vol) agarose/2.2 mol/l formaldehyde gel and transferred to a Hybond-XL membrane (Amersham Pharmacia Biotech, Piscataway, NJ). The blot was subsequently hybridized with ^{32}P-radiolabeled mouse IA-2 cDNA intracellular and extracellular probes and an IA-2β cDNA 3′ noncoding region probe.

Western blot analysis. Brain samples from IA-$2^{+/+}$ or IA-$2^{-/-}$ mice were homogenized with PBS. After centrifugation at 10,000*g* for 5 min, cell debris was sonicated in lysis buffer (50 mmol/l Tris-HCl [pH 7.4], 150 mmol/l NaCl, 1 mmol/l EDTA, 1% sodium deoxycholate, 1% NP-40, 0.4% SDS, and 1 mmol/l phenylmethylsulfonyl fluoride). Equivalent amounts of protein dissolved in SDS-PAGE sample buffer were subjected to SDS-PAGE on an 8% polyacrylamide gel. Separated proteins were transferred onto polyvinylidine difluoride membranes by electrotransfer. Blots were processed as recommended by the manufacturer (enhanced chemiluminescence detection; Amersham Pharmacia Biotech). Rabbit anti–IA-2 serum made from the intracellular domain of recombinant mouse IA-2 and absorbed with brain lysate from IA-$2^{-/-}$ mice was used as the primary antibody (1:2,000 dilution) followed by anti-rabbit Ig antibody conjugated to horseradish peroxidase (Amersham Pharmacia Biotech).

Histological and immunohistochemical analysis. All the major organs and tissues were collected in 10% neutral-buffer formalin or 4% paraformaldehyde and processed for paraffin embedding. Sections were stained with hematoxylin and eosin. Pancreatic sections were incubated with antibodies to insulin, glucagon, or somatostatin (DAKO, Carpinteria, CA) followed by biotin-conjugated second antibody and streptavidin-horseradish peroxidase.

Intraperitoneal glucose tolerance test and insulin release. Mice aged 10–23 weeks were fasted for 16 h, followed by glucose injection (2 g/kg body wt i.p.). Venous blood was drawn from the tail vein at 0, 15, 30, 60, and 120 min after the injection. Blood glucose was measured using a portable glucometer (Bayer, Elkhart, IN). For acute insulin release, glucose (3 g/kg body wt) was injected intraperitoneally into male and female mice aged 10–23 weeks. Venous blood was collected at 0, 3, 9, and 15 min in heparinized tubes. After centrifugation, plasma was stored in −20°C. Insulin levels were measured with an enzyme-linked immunosorbent assay (ELISA) kit using a mouse insulin standard (ALPCO, Windham, NH).

Isolation of pancreatic islets. IA-$2^{-/-}$ or IA-$2^{+/+}$ mice were anesthetized with ketamine and xylazine. Pancreases were perfused with 3 ml of collagenase IV (2 mg/ml in Hank's solution; Life Technologies) and further digested in a water bath at 37°C for 25 min. The digested pancreases were washed with Hank's solution three times and passed through mesh to remove undigested tissues. The islet preparation was further subjected to percoll density gradient separation (density 1.089–1.062) and handpicked under a stereomicroscope (21). The purity of islets reached >95% and was verified by dithizone staining (22). The purified islets were cultured overnight in RPMI-1640 medium supplemented with 5.5 mmol/l glucose, 100 units/ml benzypenicillin, 100 μg/ml streptomycin, and 10% fetal bovine serum before insulin secretion tests.

Glucose-stimulated insulin secretion of pancreatic islets. Insulin secretion was measured by placing 10 islets in each of five wells (New Transwell Clear; Costar Scientific, Cambridge, MA). Experiments were repeated at least three times. The islets were preincubated in 1 ml oxygenated Krebs-Ringer bicarbonate buffer (KRBB) containing 143.5 mmol/l Na^+, 5.8 mmol/l K^+, 2.5 mmol/l Ca^{2+}, 25 mmol/l HCO_3, 0.3% BSA (Fraction V; ICN, Lisle, IL), and 3.3 mmol/l glucose at 37°C for 30 min. After preincubation, the islets were incubated in 1.0 ml of KRBB supplemented with 3.3 mmol/l glucose for 1 h. Subsequently, the islets were transferred to media containing 27.7 mmol/l glucose and incubated for 1 h. Aliquots were removed and stored at −20°C for quantitation of insulin by ELISA.

Statistical analysis. Statistical analysis was performed using the Student's *t* test for unpaired comparisons. Data are presented as means + SE. $P < 0.05$ was considered significant.

RESULTS

ES cells were transfected with the IA-2 targeting vector pPNT-IA-2 (Fig. 1). By homologous recombination of the targeting vector with the IA-2 wild-type locus, the 5′-upstream promoter region, exons 1–3 and introns 1, 2, and most 3 of the wild-type IA-2 locus were replaced with a neomycin cassette. Successful homologous recombination in ES cells was detected by Southern blot analysis of neomycin-resistant colonies with a 1.1-kb *Xho*I-*Hin*dIII fragment (outside probe) and a 1.9-kb neo probe (data not shown). Three IA-$2^{+/-}$ ES cells clones were injected into blastocysts to make chimeric mice that transmitted the modified IA-2 allele to their offspring. Wild-type (IA-$2^{+/+}$), heterozygous (IA-$2^{+/-}$), and homozygous (IA-$2^{-/-}$) mice were identified by tail DNA PCR with appropriate primers. As seen in Fig. 2*A*, wild-type IA-$2^{+/+}$ mice were identified by a 1.3-kb PCR product; homozygous IA-$2^{-/-}$ mice, by a 3.5-kb PCR product; and heterozygous IA-$2^{+/-}$ mice, by both 1.3- and 3.5-kb PCR products. The identification of these mice was confirmed by Southern blot analysis. As seen in Fig. 2*B*, tail DNA digested with *Kpn*I and hybridized with the 1.1-kb *Xho*I-*Hin*dIII outside probe produced a 6.9-kb band with IA-$2^{+/+}$ DNA, a 10.7-kb band with IA-$2^{-/-}$ DNA, and both a 6.9- and 10.7-kb band with IA-$2^{+/-}$ DNA.

Further evidence that the homologous recombination was successful and disrupted the IA-2 gene was obtained from Northern blot analysis. As seen in Fig. 2*C*, hybridization of total brain RNA with a probe corresponding to the extracellular domain of IA-2 (nt 485–1,708) resulted in a strong 3.8-kb band with IA-$2^{+/+}$ RNA, a marked reduction in the band with IA-$2^{+/-}$ RNA, and no band with IA-$2^{-/-}$ RNA. A probe corresponding to the intracellular domain of IA-2 (nt 1992–3036) yielded similar results (Fig. 2*D*). In contrast, a probe generated from the 3′ noncoding region (nt 3,040–3,193) of the closely related protein IA-2β (23,24) showed that IA-2β mRNA was not affected by the

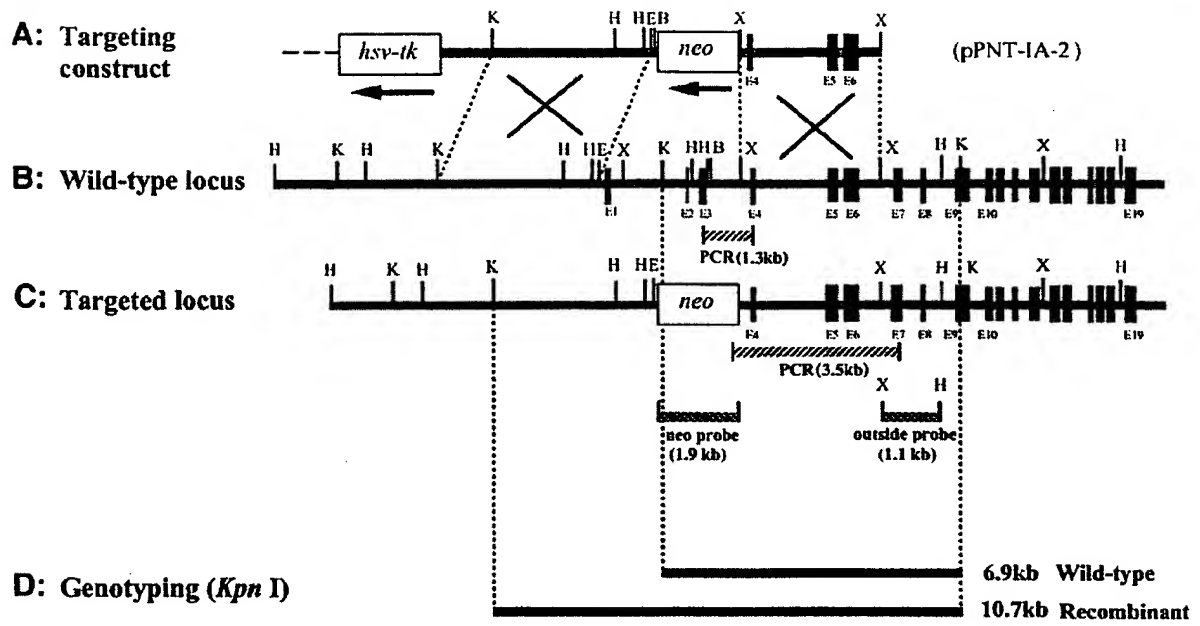

FIG. 1. Targeted disruption of the IA-2 gene. Vertical bars represent exons E1 through E19. Restriction enzyme sites shown are *Kpn*I (K), *Hin*dIII (H), *Eco*RI (E), *Xho*I (X), and *Bam*HI (B). *A*: Targeting construct shows that a portion of the 5′-upstream promoter, exons 1, 2, and 3 and introns 1, 2, and most of 3, are replaced by the neomycin cassette. *B*: Wild-type locus. Dashed lines with large "X" show areas where homologous recombination takes place. *C*: Targeted locus shows integration of targeting construct, containing the neomycin cassette, into the wild-type locus. *D*: Size of restriction fragments when wild-type locus and targeted locus are cleaved with *Kpn*I and hybridized with the 1.1-kb outside probe. Location of PCR products and probes was with PCR (1.3 kb), PCR (3.5 kb), neo probe (1.9 kb), and outside probe (1.1 kb).

IA-2 knockout and was expressed equally in IA-$2^{+/+}$ and IA-$2^{-/-}$ mice (Fig. 2*E*). Western blot analysis, using rabbit anti–IA-2 sera to measure protein expression in mouse brain extract, showed no expression of IA-2 protein in IA-$2^{-/-}$ mice as compared to IA-$2^{+/+}$ mice (Fig. 2*F*).

Physical examination of the IA-$2^{-/-}$ mice revealed no gross abnormalities. Litter size (data not shown) and body weight did not differ from the IA-$2^{+/+}$ mice (Fig. 3*A*). Histological studies failed to reveal any abnormality in the neuroendocrine cells of the IA-$2^{-/-}$ mice, including pancreatic islets (Fig. 4*A*) and brain (Fig. 4*E* and *F*), nor were abnormalities found in any of the other organs or cell types examined. Immunohistochemical studies on the IA-$2^{-/-}$ mice also revealed normal-appearing pancreatic islets, with no difference in the morphology or staining pattern of the insulin-, glucagon-, or somatostatin-producing cells (Fig. 4*B–D*) as compared to the IA-$2^{+/+}$ controls (not shown).

Nonfasting blood glucose levels of the IA-$2^{-/-}$ male mice, measured over a 22-week period, were slightly elevated as compared to IA-$2^{+/+}$ mice, but they did not fall within the diabetic range (Fig. 3*B*). Glucose tolerance tests, however, showed that glucose was significantly elevated at 15 and 30 min in both male and female IA-$2^{-/-}$ mice (Fig. 5*A*). Moreover, after glucose injection, acute insulin release was depressed in both male and female IA-$2^{-/-}$ mice, with statistically significant differences in the female mice and near significance ($P = 0.055$ at 15 min) in the male mice (Fig. 5B). In glucose-stimulated insulin secretion assays, pancreatic islets isolated from IA-$2^{-/-}$ mice also responded less vigorously to glucose stimulation. As seen in Fig. 6, male and female IA-$2^{-/-}$ mice released 48 and 42% less insulin, respectively, than IA-$2^{+/+}$ mice when switched from basal (3.3 mmol/l) to high (27.7 mmol/l) glucose.

DISCUSSION

Insulin is located in the dense-core secretory granules of pancreatic β-cells. Dense-core granules are complex structures, but a number of their constituents are now known (25). IA-2, a transmembrane glycoprotein, is an integral component of dense-core granules (16). The intracellular domain of IA-2 is thought to protrude into the cytoplasm of the cell, whereas at least a portion of the extracellular (luminal) domain resides within dense-core granules. There are two potential dibasic (KK) cleavage sites located at amino acid positions 386–387 and 448–449 of the extracellular domain. Transfection and pulse chase experiments have shown that IA-2 is expressed as a 120-kDa glycosylated protein that is then processed into a predominant 64-kDa fragment and several smaller fragments (26). Whether these fragments from the extracellular domain remain within the cytoplasm or are retained within the secretory granules is still not clear, nor is their function known. Similar posttranslational modifications have been observed in bovine pituitary cells (27). Except for these studies and a reported correlation between secretagogue stimulation of β-cells and upregulation of IA-2 mRNA (28,29), very little is known about the cell biology of IA-2.

In the present study, we succeeded in deleting the IA-2 gene by targeted gene disruption. Northern and Western

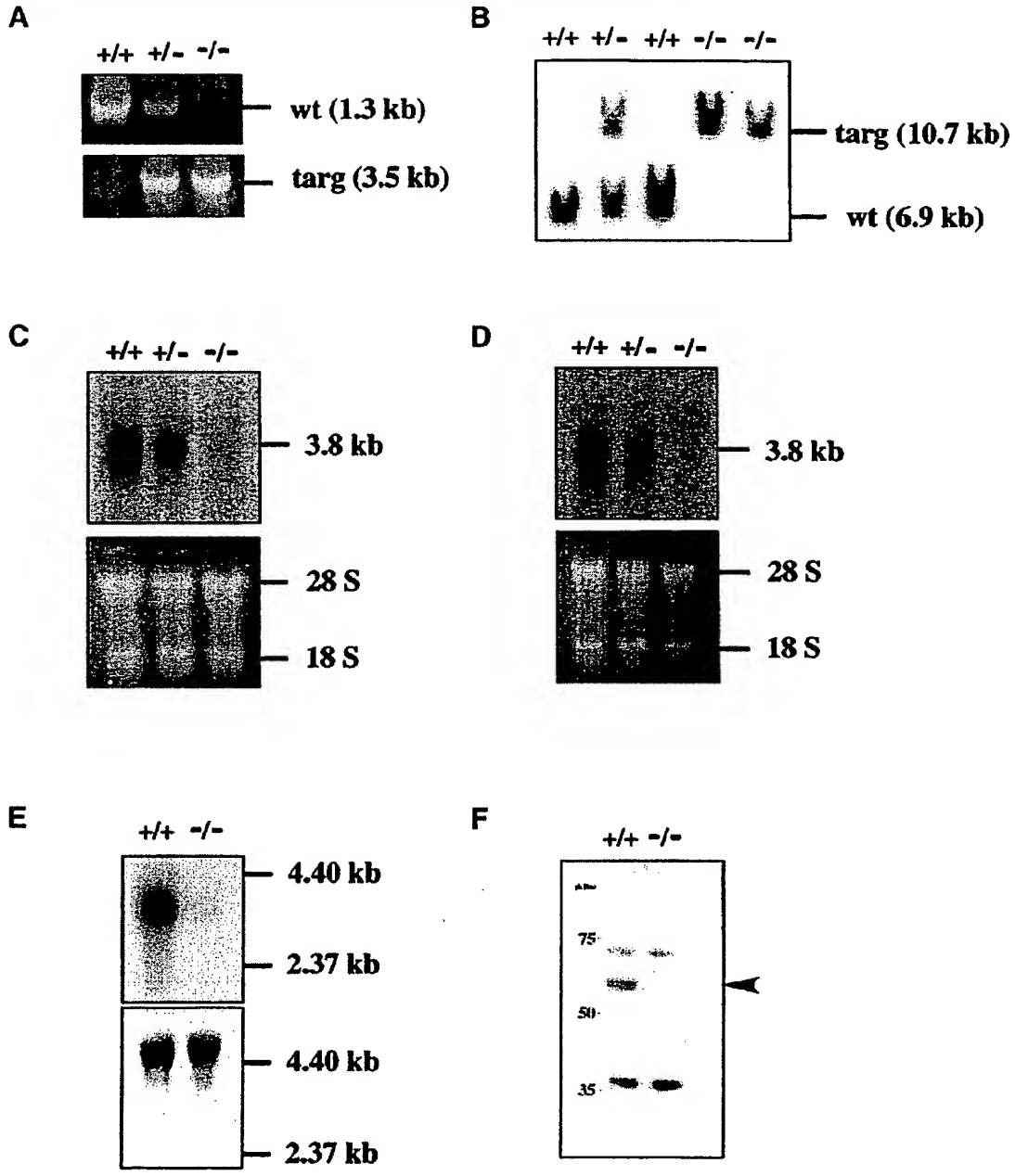

FIG. 2. Evidence for IA-2 gene disruption. *A*: PCR analysis. Primer pairs designed to produce a 1.3-kb product with cDNA from IA-$2^{+/+}$ mice, but a 3.5-kb product from IA-$2^{-/-}$ mice (see Fig. 1), showed that homologous recombination took place and that wild-type IA-2 had been eliminated. *B*: Southern blot analysis. DNA from IA-$2^{+/+}$, IA-$2^{+/-}$, and IA-$2^{-/-}$ mice were digested with *Kpn*I and hybridized with the 1.1-kb outside probe. DNA from the IA-$2^{+/+}$ mice yielded the expected 6.9-kb band, whereas DNA from the IA-$2^{-/-}$ mice gave a 10.7-kb band. IA-$2^{+/-}$ mice showed both bands. *C* and *D*: Northern analysis. Probes generated from either the extracellular (*C*) or intracellular (*D*) domains of IA-2 showed a strong 3.8-kb band with IA-$2^{+/+}$ mice, a weaker band with IA-$2^{+/-}$ mice, and no band with the IA-$2^{-/-}$ mice. *E*: IA-2β mRNA expression in IA-$2^{+/+}$ and IA-$2^{-/-}$ brain tissue. Probe generated from the intracellular domain of IA-2 showed a strong 3.8-kb band with IA-$2^{+/+}$, but no band with IA-$2^{-/-}$ mice (top). In contrast, a probe generated from the 3′ noncoding region of IA-2β showed a strong band (~5.5 kb) with both IA-$2^{+/+}$ and IA-$2^{-/-}$ mice (bottom). *F*: Western blot analysis. Antibody to IA-2 recognizes the IA-2 protein (arrow) in brain tissue from the IA-$2^{+/+}$ mice, but not from the IA-$2^{-/-}$ mice.

blot analysis showed that neither IA-2 mRNA nor protein was expressed. Although nonfasting blood glucose levels remained in the normal range, glucose tolerance tests revealed statistically significant elevated blood glucose levels in both male and female IA-$2^{-/-}$ mice. Glucose-stimulated insulin secretion showed statistically depressed insulin release in female IA-$2^{-/-}$ mice, with a similar trend, just missing statistical significance, in male

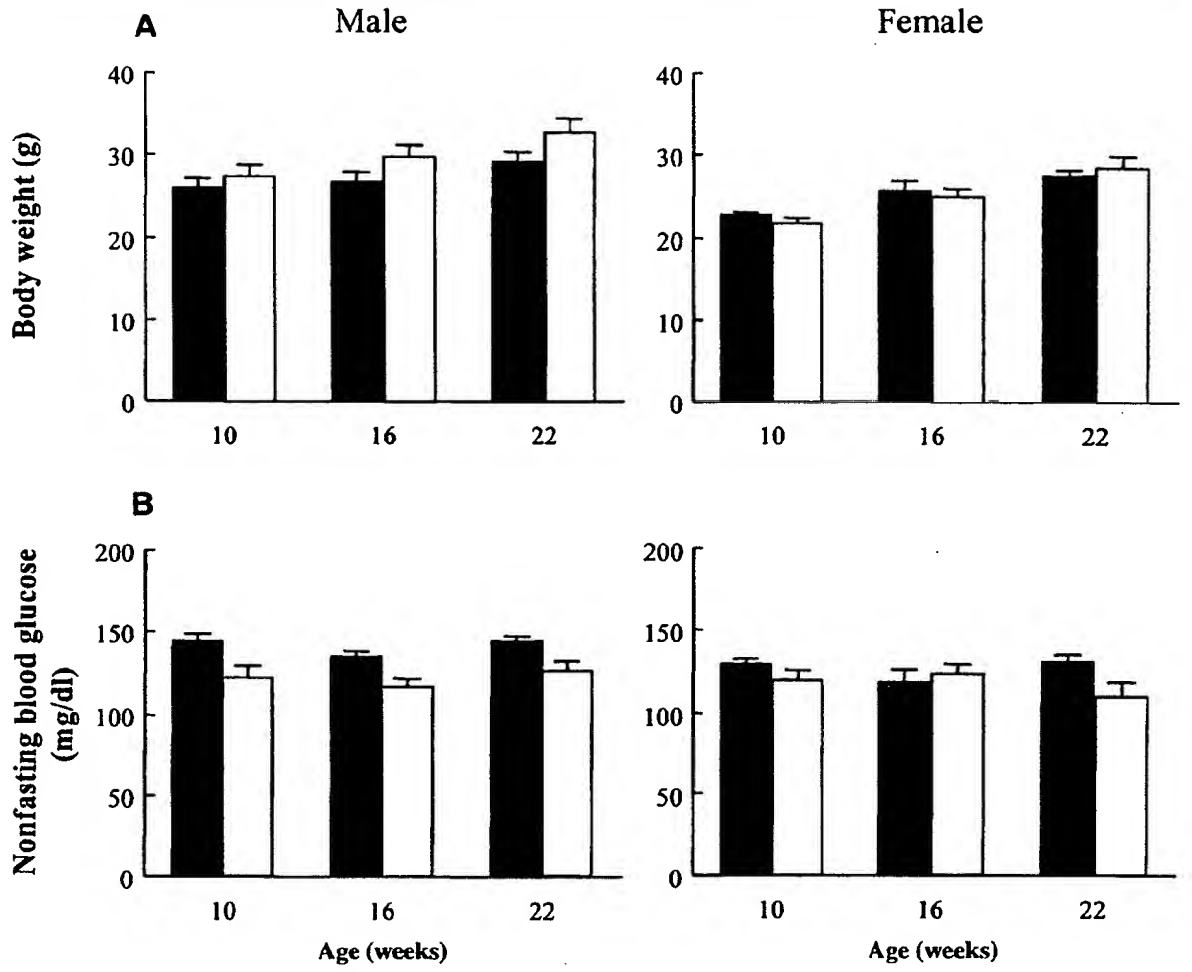

FIG. 3. Body weight and nonfasting blood glucose levels. Body weight (*A*) and nonfasting blood glucose levels (*B*) in male ($n = 6$) and female ($n = 6$) IA-$2^{-/-}$ (■) and male ($n = 6$) and female ($n = 6$) IA-$2^{+/+}$ (□) mice measured over 22 weeks. Data are means ± SE

IA-$2^{-/-}$ mice. Islets from both male and female IA-$2^{-/-}$ mice also showed significantly lower insulin release than islets from IA-$2^{+/+}$ mice when the cultures were switched from basal (3.3 mmol/l) to high (27.7 mmol/l) glucose levels. These findings, taken together with the known location of IA-2 in dense-core secretory granules, argue that IA-2 plays a role in insulin secretion. Although the alterations in glucose tolerance tests and insulin release are statistically significant, they are mild, and this may explain why IA-$2^{-/-}$ mice do not develop elevated nonfasting blood glucose levels and overt diabetes.

The findings with IA-$2^{-/-}$ mice raise questions about the contribution of IA-2β, also known as phogrin, to the secretory process. IA-2β is structurally similar to IA-2, showing 74% identity within the intracellular domain. This protein also is an integral component of dense-core granules and is phosphorylated in a Ca^{2+}-sensitive manner in response to secretagogue stimulation of β-cells (30). It is therefore possible that IA-2 and IA-2β work together or that one serves in a compensatory capacity for the other. However, at least at the mRNA level, IA-2 knockout does not result in a compensatory increase in IA-2β mRNA (Fig. 2*E*). Recently we succeeded in deleting the IA-2β gene (A.K. and A.L.N., unpublished data), and experiments are now underway to determine whether this protein also is involved in insulin secretion.

In terms of the pathogenesis of type 1 diabetes, it is of interest to ask whether there is any relationship between the autoimmune response to IA-2 and the functional role of IA-2 in secretion. It is known that autoantibodies to IA-2 are directed exclusively to the intracellular domain of the molecule that protrudes into the cytoplasm. Because there is no evidence that these autoantibodies are internalized and act within the cytoplasm, it seems unlikely that the autoimmune response to IA-2 would have any effect on the secretory function of the IA-2 molecule. Depressed insulin secretion, however, is one of the features of type 2 diabetes. Although

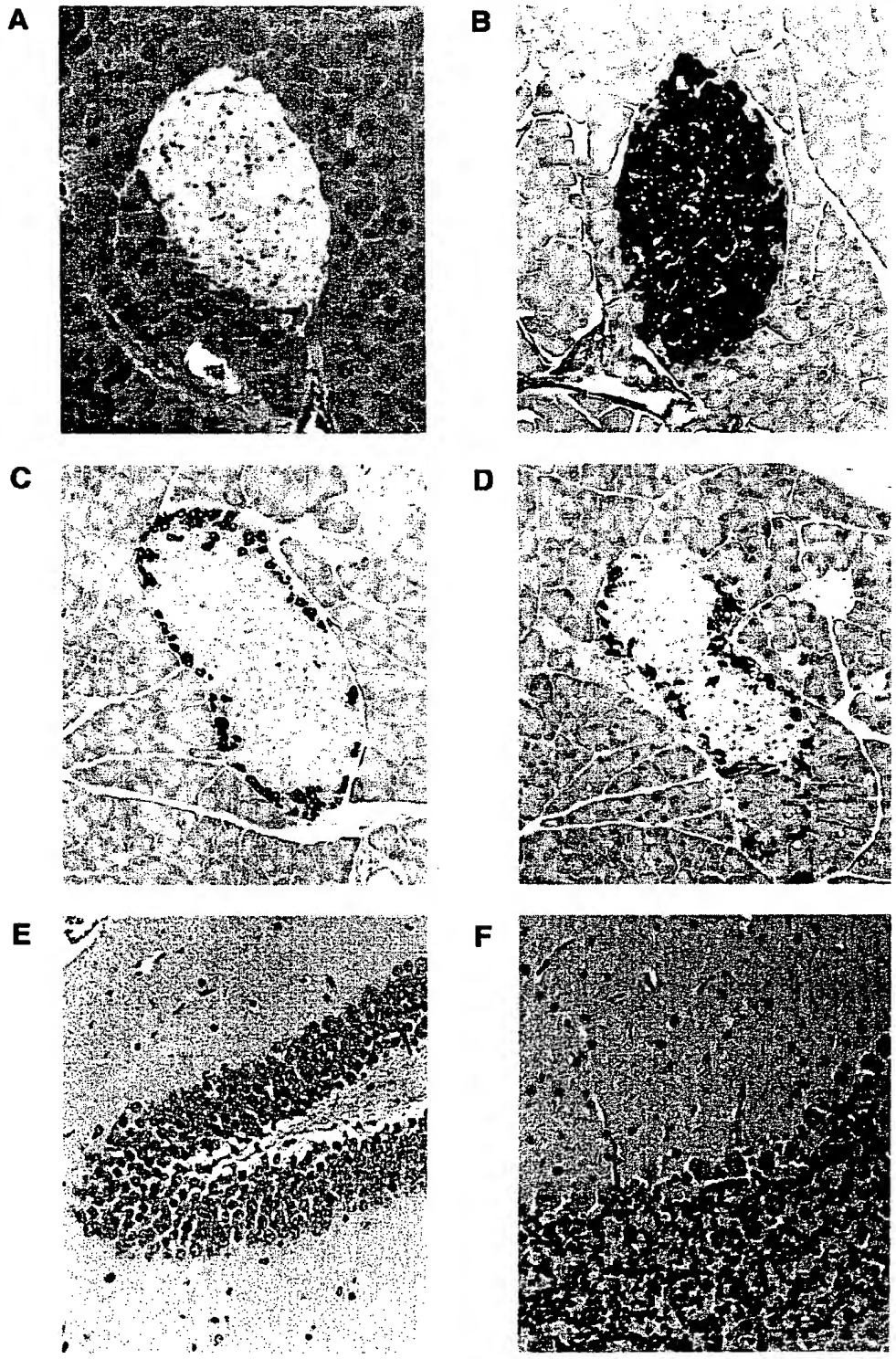

FIG. 4. Histological appearance and immunostaining of pancreases and brain from IA-2$^{-/-}$ mice. Sections of pancreases were fixed and stained with hematoxylin and eosin (*A*) or incubated with anti-insulin antibody (*B*), anti-glucagon antibody (*C*), or anti-somatostatin antibody (*D*) followed by biotin-conjugated second antibody and streptavidin horseradish peroxidase. Sections of brain (hippocampus [*E*] and cerebellum [*F*]) were fixed and stained with hematoxylin and eosin (magnification ×200 [*A*–*E*] and ×300 [*F*]).

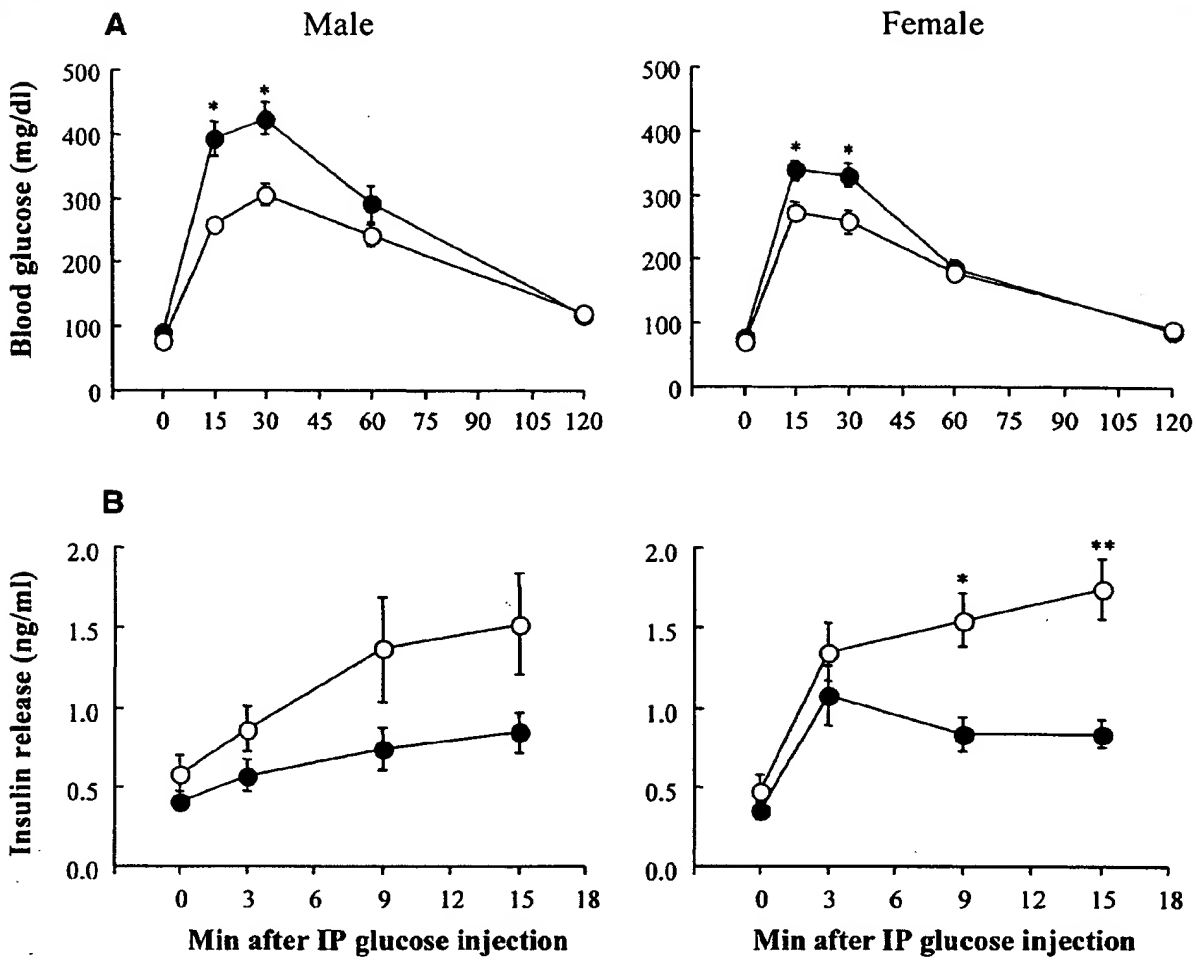

FIG. 5. Glucose tolerance and insulin secretion tests. *A*: Intraperitoneal (IP) glucose tolerance tests in male (n = 20) and female (n = 22) IA-2$^{+/+}$ (○) and male (n = 15) and female (n = 19) IA-2$^{-/-}$ (●) mice. After overnight fasting, D-glucose (2 g/kg body wt) was injected intraperitoneally, and blood glucose levels were measured at different time points. *B*: Acute insulin secretion in response to intraperitoneal glucose in male (n = 17) and female (n = 17) IA-2$^{+/+}$ (○) and male (n = 17) and female (n = 14) IA-2$^{-/-}$ (●) mice. Blood samples were drawn from the tail vein using heparinized capillary tubes before and after glucose injection (3 g/kg body wt). The results represent the average of three independent experiments. Data are means ± SE. *P < 0.01; **P < 0.001.

no association between IA-2 and type 2 diabetes has been recognized thus far, any gene that is involved in insulin secretion becomes a possible candidate gene for type 2 diabetes.

The process of secretion is complex and encompasses a number of different signals and pathways (25). Secretory vesicles are transported from the Golgi to the plasma membrane, where docking, priming, and fusion take place. Insulin is then secreted by exocytosis, a process that involves Ca^{2+} influx through voltage-dependent channels and regulation of exocytosis by a variety of phosphorylation events (31). Where in this multistep process IA-2 plays a role is not known. Recently, by use of the yeast two-hybrid system and co-immunoprecipitation, several proteins have been identified that bind to IA-2. This includes βIV spectrin and the PDZ domains of β2-syntrophin and neuronal nitric oxide synthase. Solimena and colleagues (32,33) have postulated that IA-2 may link the secretory granules with the actin cystoskeleton through its association with βIV spectrin or β2-syntrophin, and that this might affect granule traffic and exocytosis. Alternatively, because nitric oxide regulates the release of certain hormones, it is possible that the association of IA-2 with nitric oxide synthase may modulate insulin secretion.

The demonstration in the present study that deletion of IA-2 affects insulin secretion and the identification in other studies of IA-2 binding proteins (32,33) begin to provide insight into the function and possible mechanism of action of IA-2. The fact that IA-2 is present in the secretory granules of many different neuroendocrine cells raises the possibility that IA-2 may be involved not only in the secretion of insulin from β-cells, but also in the secretion of hormones from a broad range of neuroendocrine cells.

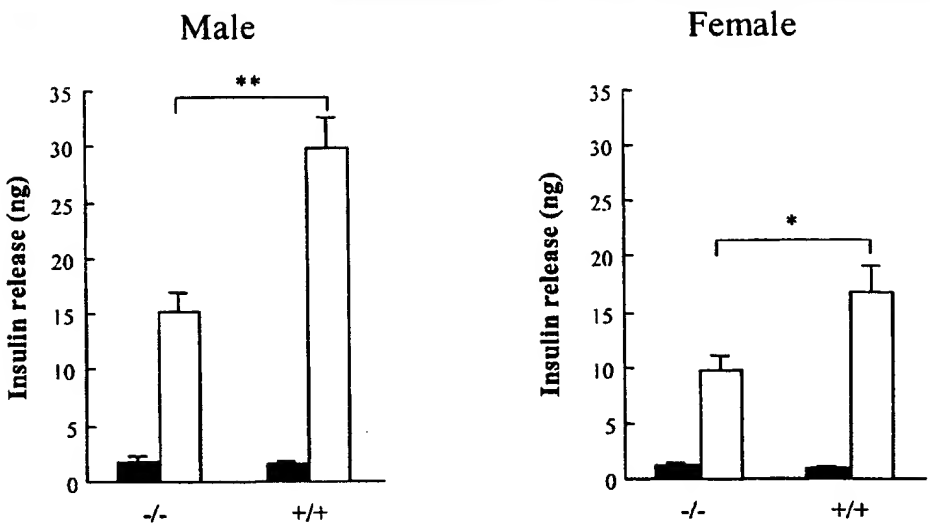

FIG. 6. Glucose-stimulated insulin release in vitro. Pancreatic islets isolated from IA-2$^{+/+}$ and IA-2$^{-/-}$ mice were placed in five wells, each containing 10 islets, in KRBB with 3.3 mmol/l glucose (■). At the end of 1 h, insulin levels in the supernatants were measured. The cells were then transferred to KRBB containing 27.7 mmol/l glucose (□), and at the end of 1 h insulin levels were again measured. The results represent the average of three independent experiments. Data are means ± SE. *$P < 0.01$; **$P < 0.001$.

ACKNOWLEDGMENTS

The authors thank Dr. Ashok Kulkarni for his advice and Glenn Longenecker for his help in preparing the IA-2 knockout mice.

REFERENCES

1. Lan MS, Lu J, Goto Y, Notkins AL: Molecular cloning and identification of a receptor-type protein tyrosine phosphatase, IA-2, from human insulinoma. *DNA Cell Biol* 13:505–514, 1994
2. Lan MS, Wasserfall C, Maclaren NK, Notkins AL: IA-2, a transmembrane protein of the protein tyrosine phosphatase family, is a major autoantigen in insulin-dependent diabetes mellitus. *Proc Natl Acad Sci U S A* 93:6367–6370, 1996
3. Gorus FK: Diabetes registries and early biological markers of insulin-dependent diabetes mellitus: Belgian Diabetes Registry. *Diabetes Metab Rev* 13:247–274, 1997
4. Verge CF, Gianani R, Kawasaki E, Yu L, Pietropaolo M, Jackson RA, Chase HP, Eisenbarth GS: Prediction of type I diabetes in first-degree relatives using a combination of insulin, GAD, and ICA512bdc/IA-2 autoantibodies. *Diabetes* 45:926–933, 1996
5. Hawa M, Rowe R, Lan MS, Notkins AL, Pozzilli P, Christie MR, Leslie RD: Value of antibodies to islet protein tyrosine phosphatase-like molecule in predicting type 1 diabetes. *Diabetes* 46:1270–1275, 1997
6. Bingley PJ, Bonifacio E, Williams AJ, Genovese S, Bottazzo GF, Gale EA: Prediction of IDDM in the general population: strategies based on combinations of autoantibody markers. *Diabetes* 46:1701–1710, 1997
7. Kulmala P, Savola K, Petersen JS, Vahasalo P, Karjalainen J, Lopponen T, Dyrberg T, Akerblom HK, Knip M: Prediction of insulin-dependent diabetes mellitus in siblings of children with diabetes: a population-based study: the Childhood Diabetes in Finland Study Group. *J Clin Invest* 101:327–336, 1998
8. Leslie RD, Atkinson MA, Notkins AL: Autoantigens IA-2 and GAD in type I (insulin-dependent) diabetes. *Diabetologia* 42:3–14, 1999
9. Notkins AL, Lernmark A: Autoimmune type I diabetes: resolved and unresolved issues. *J Clin Invest* 108:1247–1252, 2001
10. Lampasona V, Bearzatto M, Genovese S, Bosi E, Ferrari M, Bonifacio E: Autoantibodies in insulin-dependent diabetes recognize distinct cytoplasmic domains of the protein tyrosine phosphatase-like IA-2 autoantigen. *J Immunol* 157:2707–2711, 1996
11. Zhang B, Lan MS, Notkins AL: Autoantibodies to IA-2 in IDDM: location of major antigenic determinants. *Diabetes* 46:40–43, 1997
12. Xie H, Zhang B, Matsumoto Y, Li Q, Notkins AL, Lan MS: Autoantibodies to IA-2 and IA-2 beta in insulin-dependent diabetes mellitus recognize conformational epitopes: location of the 37- and 40-kDa fragments determined. *J Immunol* 159:3662–3667, 1997
13. Xie J, Zhang B, Lan MS, Notkins AL: Genomic structure and promoter sequence of the insulin-dependent diabetes mellitus autoantigen, IA-2 (PTPRN). *Genomics* 54:338–343, 1998
14. Cai T, Krause MW, Odenwald WF, Toyama R, Notkins AL: The IA-2 gene family: homologs in *Caenorhabditis elegans*, *Drosophila* and zebrafish. *Diabetologia* 44:81–88, 2001
15. Magistrelli G, Toma S, Isacchi A: Substitution of two variant residues in the protein tyrosine phosphatase-like PTP35/IA-2 sequence reconstitutes catalytic activity. *Biochem Biophys Res Commun* 227:581–588, 1996
16. Solimena M, Dirkx R Jr, Hermel JM, Pleasic-Williams S, Shapiro JA, Caron L, Rabin DU: ICA 512, an autoantigen of type I diabetes, is an intrinsic membrane protein of neurosecretory granules. *Embo J* 15: 2102–2114, 1996
17. Saeki K, Xie J, Notkins AL: Genomic structure of mouse IA-2: comparison with its human homologue. *Diabetologia* 43:1429–1434, 2000
18. Tybolewicz VL, Crawford CE, Jackson PK, Bronson RT, Mulligan RC: Neonatal lethality and lymphopenia in mice with a homozygous disruption of the c-abl proto-oncogene. *Cell* 65:1153–1163, 1991
19. Li E, Bestor TH, Jaenisch R: Targeted mutation of the DNA methyltransferase gene results in embryonic lethality. *Cell* 69:915–926, 1992
20. Geiser AG, Letterio JJ, Kulkarni AB, Karlsson S, Roberts AB, Sporn MB: Transforming growth factor beta 1 (TGF-beta 1) controls expression of major histocompatibility genes in the postnatal mouse: aberrant histocompatibility antigen expression in the pathogenesis of the TGF-beta 1 null mouse phenotype. *Proc Natl Acad Sci U S A* 90:9944–9948, 1993
21. Brunstedt J, Nielsen JH, Lernmark A, Hagedorn Study Group: Isolation of islets from mice and rats. In *Methods in Diabetes Research*. New York, John Wiley & Sons, 1985, p. 245–259
22. Latif ZA, Noel J, Alejandro R: A simple method of staining fresh and cultured islets. *Transplantation* 45:827–830, 1988
23. Lu J, Li Q, Xie H, Chen ZJ, Borovitskaya AE, Maclaren NK, Notkins AL, Lan MS: Identification of a second transmembrane protein tyrosine phosphatase, IA-2beta, as an autoantigen in insulin-dependent diabetes mellitus: precursor of the 37-kDa tryptic fragment. *Proc Natl Acad Sci U S A* 93:2307–2311, 1996
24. Wasmeier C, Hutton JC: Molecular cloning of phogrin, a protein-tyrosine phosphatase homologue localized to insulin secretory granule membranes. *J Biol Chem* 271:18161–18170, 1996
25. Lang J: Molecular mechanisms and regulation of insulin exocytosis as a paradigm of endocrine secretion. *Eur J Biochem* 259:3–17, 1999
26. Xie H, Deng YJ, Notkins AL, Lan MS: Expression, characterization,

processing and immunogenicity of an insulin-dependent diabetes mellitus autoantigen, IA-2, in Sf-9 cells. *Clin Exp Immunol* 113:367–372, 1998
27. Hermel JM, Dirkx R Jr, Solimena M: Post-translational modifications of ICA512, a receptor tyrosine phosphatase-like protein of secretory granules. *Eur J Neurosci* 11:2609–2620, 1999
28. Lee MS, Dirkx R Jr, Solimena M, Dannies PS: Stabilization of the receptor protein tyrosine phosphatase-like protein ICA512 in GH4C1 cells upon treatment with estriadol, insulin, and epidermal growth factor. *Endocrinology* 139:2727–2733, 1998
29. Seissler J, Nguyen TB, Aust G, Steinbrenner H, Scherbaum WA: Regulation of the diabetes-associated autoantigen IA-2 in INS-1 pancreatic beta-cells. *Diabetes* 49:1137–1141, 2000
30. Wasmeier C, Hutton JC: Secretatogue-dependent phosphorylation of the insulin granule membrane protein phogrin is mediated by cAMP-dependent protein kinase. *J Biol Chem* 276:31919–31928, 2001
31. Jones PM, Persaud SJ: Protein kinases, protein phosphorylation, and the regulation of insulin secretion from pancreatic beta-cells. *Endocr Rev* 19:429–461, 1998
32. Ort T, Maksimova E, Dirkx R, Kachinsky AM, Berghs S, Froehner SC, Solimena M: The receptor tyrosine phosphatase-like protein ICA512 binds the PDZ domains of beta2-syntrophin and nNOS in pancreatic beta-cells. *Eur J Cell Biol* 79:621–630, 2000
33. Berghs S, Aggujaro D, Dirkx R Jr, Maksimova E, Stabach P, Hermel JM, Zhang JP, Philbrick W, Slepnev V, Ort T, Solimena M: BetaIV spectrin, a new spectrin localized at axon initial segments and nodes of ranvier in the central and peripheral nervous system. *J Cell Biol* 151:985–1002, 2000

BIOCHEMICAL AND BIOPHYSICAL RESEARCH COMMUNICATIONS 229, 891–895 (1996)
ARTICLE NO. 1898

Mice Lacking the 65 kDa Isoform of Glutamic Acid Decarboxylase (GAD65) Maintain Normal Levels of GAD67 and GABA in Their Brains but Are Susceptible to Seizures

Hideo Asada, Yuuki Kawamura, Kei Maruyama, Hideaki Kume, Ri-gao Ding, Feng Yun Ji, Nobuko Kanbara, Hiroko Kuzume, Makoto Sanbo,* Takeshi Yagi,* and Kunihiko Obata[1]

*Laboratory of Neurochemistry and *Laboratory of Neurobiology and Behavioral Genetics, National Institute for Physiological Sciences, Myodaiji, Okazaki, Aichi 444 Japan*

Received November 13, 1996

The gene encoding of the 65 kDa isoform of the γ-aminobutyric acid (GABA)-synthesizing enzyme, glutamic acid decarboxylase (GAD), GAD65, was targeted in mice by homologous recombination. Viable GAD65 −/− mice were obtained with the expected mendelian frequency and displayed no gross morphological defects. Despite the complete loss of GAD65 mRNA and protein in a homozygous mutant, there was no difference in GABA content in the brains of GAD65 +/+, +/−, and −/− mice. As for the other 67 kDa isoform (GAD67), the levels of mRNA and protein were largely unchanged by the GAD65 mutation. General behavior, including locomotor activity and performance in the Morris water maze task, appeared normal, but seizures were more easily induced by picrotoxin and pentylenetetrazol: the latencies to seizures induced by picrotoxin were shorter and the dose of pentylenetetrazol required for induction of seizures was lower.

γ-Aminobutyric acid (GABA) is a principal inhibitory neurotransmitter in the mammalian central nervous system (1) and is synthesized from glutamic acid by glutamic acid decarboxylase (GAD) in a specific population of nerve cells (GABAergic neurons). GAD has two isoforms, GAD65 and GAD67, named for their molecular mass of 65 and 67 kDa, respectively, which are encoded by two independent genes (2, 3). It has been suggested that GAD65 is rather membrane-associated, whereas GAD67 is a soluble cytosolic protein (3, 4). Although GAD65 and GAD67 appear to be coexpressed in GABAergic neurons, there are some differences in the subcellular distribution in nerve terminals and cell bodies (3-5). Furthermore, GABA and GAD are transiently expressed in embryonic nervous tissue and affect proliferation, migration and neurite extension of neurons, and synapse formation (6-9), indicating that there are some developmental or trophic functions of GABA, in addition to the conventional neurotransmitter role. Several truncated forms of GAD67 are also expressed transiently during development (10). After seizure in the adult rat, GAD67 and GABA appear in the granule cells of the hippocampus, which are non-GABAergic excitatory neurons (11 and K. Obata, unpublished observation). These findings suggest that GABA itself may be present in different intracellular compartments of not only well-differentiated, GABAergic neurons, but also in undifferentiated or non-GABAergic cells, and may serve diverse functions in the nervous system. Gene targeting of GAD in mice will be useful for elucidating the specific roles of GAD65 and GAD67.

In the present investigation GAD65 gene was disrupted by targeted mutation in mice, and chemical and histological analyses on GAD expression and behavioral studies were performed.

[1] Corresponding author. Fax: +81-564-55-7825. E-mail: obata@nips.ac.jp.
Abbreviations: GAD, glutamic acid decarboxylase; GABA, γ-aminobutyric acid.

0006-291X/96 $18.00

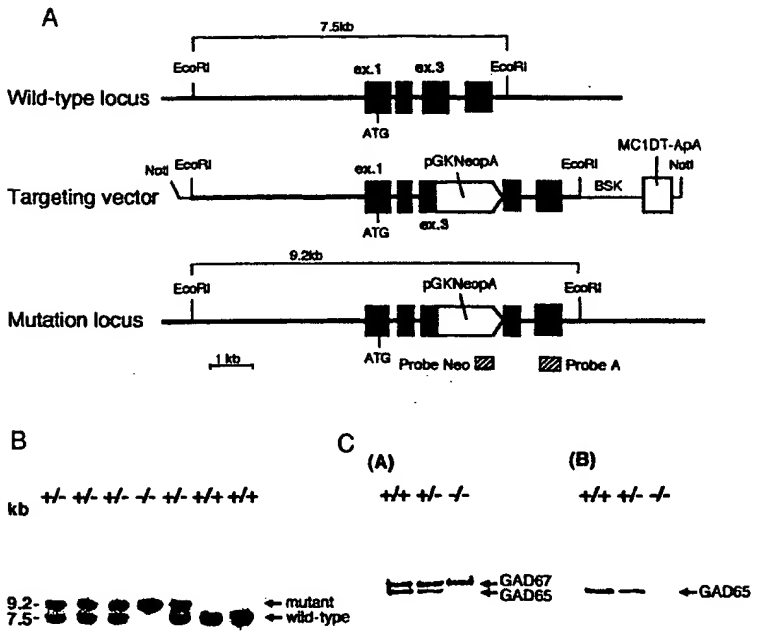

FIG. 1. Targeted disruption of the mouse GAD65 gene. (A) Schematic representation of GAD65 genomic DNA, targeting vector, and the disrupted gene. The targeting vector contains the diphtheria toxin A fragment gene (pMC1DT-ApA) for negative selection. Exon 1 contains the translation initiation codon ATG, and a neomycin-resistant cassette (PGKNeopA, Ref. 15) was inserted into exon 3. Probes Neo and A were used for Southern blot analysis. (B) Southern blot analysis using probe A was performed on EcoRI-digested tail DNA isolated from 21-day-old mice. (C) Western blot analysis of GAD65 and GAD65 expression in wild-type(+/+) and GAD65 mutant (+/− and −/−) brain. The GAD proteins were detected with anti-GAD65/67 (A) and anti-GAD65 (B) antisera.

GAD65 −/− mice maintained normal GAD67 and GABA levels in the brain. General behavior was not impaired but seizure was more easily induced by picrotoxin and pentylenetetrazol.

MATERIALS AND METHODS

Production of the GAD65 mutant mice. A genomic library of TT2 cell (12) was screened using the 5′ portion of GAD65 cDNA. The whole sequence of mouse GAD65 cDNA was registered at accesssion number D42051 in GenBank (13) as a probe (14). The structure of the targeting vector is shown in Fig 1A. The 0.6 kb Xho I-Sal I fragment of pMC1DT-A (15) and the 3.7 kb Sal I-Sma I fragment of pGKPuro (16) were ligate to yield pMC1DT-ApA. TT2 embryonic stem cells (15) were transfected with the targeting vector and then introduced into 8-cell embryos from ICR mice. The mutant mice were obtained by mating chimeric mice with C57BL/6 mice, as reported (15).

Biochemical analysis of the mutant mice. Southern blot analysis was performed according to the general procedure (14, 17). Rabbit antisera, anti-GAD65/67, against C-terminal portion of GAD (DIDFLIEEIERLGQDL) and anti-GAD65, against N-terminal portion of GAD65 (ASPGSGFWSFGSEDGS), were obtained by the injection of synthetic peptides, respectively. Western blot was performed as previously described (17). Anti-GAD65/67 recognized both GAD 65 and GAD67 and anti-GAD65 selectively detected GAD65 in Western blots. Enzymatic activity of GAD was assayed by convertion of ^{14}C-glutamate to $^{14}CO_2$ in the presence and absence of pyridoxal 5′-phosphate (PLP) as in (18), with a slight modification. GABA in the tissue homogenates was measured by high performance liquid chromatography (BAS, Japan).

Behavioral analysis of mutant mice. Locomotor activity and water maze learning were studied with an open field (diameter: 60 cm) and a water maze (diameter: 120 cm) (Neuroscience, Inc.). Motor coordination was observed on a Rota-Rod treadmill (UGO Basile). Passive avoidance learning was tested using a step-through type apparatus (O'Hara).

Induction of convulsion by picrotoxin and pentylenetetrazol. Five mg/kg picrotoxin was injected intraperitoneally and the times of onset of sedation and seizure were recorded. Immediately after a generalized convulsion was induced, diazepam (5 mg/kg) was intraperitoneally administered to suppress the convulsion. Effective doses of pentylenetetrazol were determined by the time of onset of twitch, clonic convulsion and limb extension leading to death after starting intravenous injection with a 1% solution at a constant rate (100 μl/min.) (19).

RESULTS

Southern blot analysis of 21-day-old mice tail DNA (Fig. 1B) showed that wild-type, heterozygous and homozygous mutant mice were obtained from heterozygous GAD65+/− parents with the expected mendelian frequency (+/+, number of mice n=19; +/−, n=33; −/−, n=13). Homozygous GAD65 −/− mice appeared healthy, were of similar size and weight to wild-type and heterozygous GAD65 +/− littermates, and had no gross defects. No morphological abnormalities were observed in brain sections (data not shown).

Northern blot analysis showed that GAD65 mRNA was absent in GAD65 −/− brain and was reduced to one-half of wild-type brain levels in GAD65 +/− brain (data not shown). Levels of GAD67 mRNA in homozygous and heterozygous brain tissue were similar to those in wild-type brain. These results were confirmed by *in situ* hybridization histochemistry of mice brain (not illustrated): homozygous mice had no GAD65 mRNA-positive neurons, and in heterozygous mice the number of GAD65 mRNA-positive neurons was normal, but the intensity of staining was about one-half that of wild-type neurons. No change was found in the number and staining intensity of GAD67 mRNA-positive neurons. Western blot analysis also demonstrated that GAD65 protein was absent in GAD65 −/− brain and was reduced to about one-half the level in GAD65 +/− brain (Fig. 1C). Close examination did not reveal any bands which might be derived from the partial translation of exons 1 and 2 of GAD65 gene remaining after mutation. Levels of GAD67 protein were almost the same. Immunohistochemistry of GAD65 −/− mice brain also demonstrated that no cell was GAD65-positive and the expected population of neurons were GAD67-positive (not illustrated).

GAD activities in the cerebral cortex in the presence of PLP were (cpm/30min/μg protein: mean ± SEM, n=3): 8.22±0.96 for wild-type mice, 5.97±0.35 for GAD65 +/− mutants and 3.63±0.54 for null mutants. The decrease for the null mutants was statistically significant ($p<0.05$) and was largely due to decrease in PLP-dependent activity. It is known that a large part of GAD65 exists as apoenzyme and requires exogenous PLP (2). The similar changes in GAD activities of the mutants were also observed in the striatum, hippocampus and cerebellum. GABA contents were (nmol/mg protein: n=15): 2.39±0.19 for the cerebral cortex, 3.45±0.27 for the striatum, 3.22±0.27 for the hippocampus and 2.61±0.25 for the cerebellum. No significant difference was observed among three groups of mice. Immunohistochemistry of GABA also demonstrated normal number and distribution of GABA-positive neurons in GAD65 −/− brain sections (not illustrated).

Locomotor activity in novel environments and its accommodation with time were studied in an open field. Distances (cm) which mice passed during 2 min. immediately after introduction into the apparatus and after 10 min. of stay in the same apparatus were: 1,423±107 and 894±77 for wild-type littermates (number of mice, n=9), 1,314±60 and 682±62 for GAD65 +/− mice (n=18) and 1,377±193 and 938±119 for GAD65 −/− mice (n=4), respectively. These values did not differ statistically among groups. No ataxic behavior was observed in free movement in an open field and during stay on a rotating rod (Rota-Rod test). No difference was observed in passive avoidance test. For training, electrical shock was delivered to mice from the grids on the floor when they moved from a lighted compartment to a dark compartment. When the mice were introduced to the same dark compartment 24 hours after the training, most mice including all GAD65−/− mice did not step through to the dark room during 3 min. of observation. Spatial learning was evaluated by escape latency to a hidden platform in the Morris water maze and did not reveal any differences among three groups.

TABLE 1
Sensitivity of *GAD65* Mutant Mice to Seizure Induced with Picrotoxin or Pentylenetetrazol

	Latency of picrotoxin effects (sec)		Dose for pentylenetetrazol convulsion (mg/kg)	
Genotype	Sedation	Seizure	Seizure	Tonic extension
+/+	249.1±16.0(7)	849.2±52.3 (7)	62.1±2.1 (4)	86.7±8.8 (4)
+/−	250.3±15.3(12)	831.9±56.9 (12)	52.9±1.5[a](4)	78.5±14.7 (3)
−/−	215.0±32.2(6)	515.7±68.8[a,b](8)	41.1±6.8[a](4)	54.6±7.9[a] (4)

Note. Picrotoxin (5mg/kg) was injected intraperitoneally, and pentylenetetrazol was infused into the tail vein at a constant rate of 0.0167 mg/sec. Values represent mean±SEM (numbers of mice).
[a] Statistically different from wild-type group using Student t-test. ($p<0.05$).
[b] Statistically different from heterozygous group using Student t-test. ($p<0.05$).

Escape latencies (sec) in the first session (mean value of five trials in each session) were: 85.7±2.8 for wild-type mice (n=6), 82.8±4.7 for GAD65 +/− mice (n=8) and 81.2±8.8 for GAD65 −/− mice (n=4). On the 6th day (session 6), escape latencies of the same mice were 12.4±2.7 for wild-type, 12.0±1.5 for GAD65 +/− and 13.0±2.2 for GAD65 −/− animals. On the 7th day, the mice were forced to learn to locate a visible platform with a flag in the same water maze. All mice escaped to the platform within 10 sec after 3-4 trials.

Sensitivity of mutant mice to convulsants was assessed in two ways. Intraperitoneal administration of picrotoxin (5 mg/kg) induced sedation in most mice after 3-5 min.: sedation was characterized by lying motionless on their stomach with lightly extended limbs. After 10-15 min. of sedation the animals again assumed crouching posture and walked around. This was followed by a generalized convulsive fit. Latency to seizure was significantly shorter for GAD65 −/− mice (Table 1). Six GAD65 −/− mice had a similar latency to sedation but in the remaining 2 homozygotes a convulsion developed without sedation, probably representing a higher seizure susceptibility. Continuous infusion of pentylenetetrazol induced twitch, clonic convulsion and tonic extension, sequentially. Doses required for induction of clonic and tonic convulsion were significantly lower for homozygous mutants than for wild-type mice (Table 1). Seizure threshold for heterozygous mutants was between those for wild-type and −/− mice.

DISCUSSION

Targeted disruption of the GAD65 gene at exon 3 might allow expression of a small N-terminal peptide, but will certainly eliminate GAD65 enzyme activity (2). Absence of GAD65 in homozygotes was confirmed by Western blot analysis and immunohistochemistry. Compensatory up-regulation of GAD67 was not the observed. In GAD65 −/− mice, GABA should be synthesized exclusively by GAD67. There were no significant changes in GABA levels in four brain regions in GAD65 −/− and +/− mice, in which GAD65 expression was reduced, indicating the presence of homeostatic regulation of GABA synthesis. Although the PLP dependent GAD activity was reduced in the mutant mice, the remaining GAD67 activity might be enough to keep the level of GABA.

Although locomotor activity and several types of behavior were not affected, GAD65 −/− mice showed an increased susceptibility to picrotoxin and pentylenetetrazol. Picrotoxin blocks the GABA receptor complex (1) and one of the targets of pentylenetetrazol is also the GABA receptor (20). Therefore, higher sensitivity of GAD65 −/− mice to these convulsants may reflect reduced GABAergic transmission. A possible mechanism could be the reduction of

GABA in GABAergic nerve terminals of GAD65 −/− mice, since GAD65 is considered to be concentrated in the nerve terminals (3,5). Electrophysiological investigation of GABAergic synapses will be required to determine if there is any change in GABA release from GABAergic nerve terminals and/or a change in the sensitivity of GABA receptors in postsynaptic neurons. Changes in GABA release will also be evaluated by brain microdialysis.

Gross anatomy and brain histology revealed no marked abnormality in GAD65 −/− mice. It has been suggested that GABA regulates proliferation, migration and process extension of neurons (5-8) and that GABA derived from GAD67 might play the important role in the early neurogenesis.

The present findings on GAD65 −/− mice will provide the basis for further investigation on the diverse functions of GABA and GAD. Multilateral analyses of GAD65 −/−, GAD67 −/− and double knockout mice should allow the elucidation of specific or cooperative roles of GAD65 and GAD67 in histogenesis, synaptic transmission and other trophic/regulatory mechanism of the nervous system.

ACKNOWLEDGMENT

This work was supported by Grants-in-Aid from the Ministry of Education, Science, Sports and Culture (Japan).

REFERENCES

1. Obata, K. (1977) *in* Handbook of Physiology: The Nervous System (Kandel, E. R., Ed.), Vol. 1, Part 1, pp.625–650, American Physiological Society, Bethesda, MD.
2. Erlander, M. G., Tillakaratne, N. J. K., Feldblum, S., Patel, N., and Tobin, A. J. (1991) *Neuron* **7**, 91–100.
3. Erlander, M. G., and Tobin, A. J. (1991). *Neurochem. Res.* **16**, 215–226.
4. Dirkx, R., Jr., Thomas, A., Li, L., Lernmark, Å., Sherwin, R. S., De Camilli, P., and Solimena, M. (1995) *J. Biol. Chem.* **270**, 2241–2246.
5. Esclapez, M., Tillakaratne, N. J. K., Kaufman, D. L., Tobin, A. J., and Houser, C. R. (1994) *J. Neurosci.* **14**, 1834–1855.
6. Barbin, G., Pollard, H., Gaïarsa, J. L., and Ben-Ari, Y. (1993) *Neursci. Lett.* **152**, 150–154.
7. Behar, T. N., Schaffner, A. E., Colton, C. A., Somogyi, R., Olah, Z., Lehel, C., and Barker, J. L. (1994) *J. Neurosci.* **14**, 29–38.
8. LoTurco, J. J., Owens, D. F., Heath, M. J. S., Davis, M. B. E., and Kriegstein, A. R. (1995) *Neuron* **15**, 1287–1298.
9. Schousboe, A., and Redburn, D. A. (1995) *J. Neursci. Res.* **41**, 1–7.
10. Szabo, G., Katarova, Z., and Greenspan, R. (1994) *Mol. Cell. Biol.* **14**, 7535–7545.
11. Schwarzer, C., and Sperk, G. (1995) *Neuroscience* **69**, 705–709.
12. Yagi, T., Tokunaga, T., Furuta, Y., Nada, S., Yoshida, M., Tsukada, T., Saga, Y., Takeda, N., Ikawa, Y., and Aizawa, S. (1993) *Anal. Biochem.* **214**, 70–76.
13. Asada, H., Maruyama, K., Kawamura, Y., and Obata, K. (1995) *Soc. Neurosci. Abstr.* **21**, 2198.
14. Sambrooke, J., Fritsch, E. F., and Maniatis, T. (1989) Molecular Cloning: A Laboratory Mannual, 2nd ed., Cold Spring Harbor Laboratory Press, Cold Spring Harbor, NY.
15. Yagi, T., Aizawa, S., Tokunaga, T., Shigetani, Y., Takeda, N., and Ikawa, Y. (1993) *Nature* **366**, 742–745.
16. Watanabe, S., Kai, N., Yasuda, M., Kohmura, N., Sanbo, M., Mishina, M., and Yagi, T. (1995) *Biochem. Biophys. Res. Commun.* **213**, 130–137.
17. Kume, H., Maruyama, K., Tomita, T., Iwatsubo, T., Saido, T. C., and Obata, K. (1996) *Biochem. Biophys. Res. Commun.* **219**, 526–530.
18. Moskal, J. R., and Basu, S. (1975) *Anal. Biochem.* **65**, 449–457.
19. Tecott, L. H., Sun, L. M., Akana, S. F., Strack, A. M., Lowenstein, D. H., Dallman, M. F., and Julius, D. (1995) *Nature* **374**, 542–546.
20. Stringer, J. L. (1994) *Brain Res.* **636**, 221–226.

Article

Mice lacking desmocollin 1 show epidermal fragility accompanied by barrier defects and abnormal differentiation

Martyn Chidgey,[1,2] Cord Brakebusch,[3] Erika Gustafsson,[3] Alan Cruchley,[4] Chris Hail,[2] Sarah Kirk,[1] Anita Merritt[1], Alison North,[1] Chris Tselepis,[2] Jane Hewitt,[1] Carolyn Byrne,[1] Reinhard Fassler,[5] and David Garrod[1]

[1]School of Biological Sciences, University of Manchester, Manchester M13 9PT, UK
[2]Division of Medical Sciences, University of Birmingham, Birmingham B15 2TH, UK
[3]Department of Experimental Pathology, Lund University, S-221 85 Lund, Sweden
[4]Clinical and Diagnostic Oral Sciences, Barts and The London, Queen Mary's School of Medicine and Dentistry, London E1 2AT, UK
[5]Department of Molecular Medicine, Max Plank Institute for Biochemistry, D-82152 Martinsried, Germany

The desmosomal cadherin desmocollin (Dsc)1 is expressed in upper epidermis where strong adhesion is required. To investigate its role in vivo, we have genetically engineered mice with a targeted disruption in the *Dsc1* gene. Soon after birth, null mice exhibit flaky skin and a striking punctate epidermal barrier defect. The epidermis is fragile, and acantholysis in the granular layer generates localized lesions, compromising skin barrier function. Neutrophils accumulate in the lesions and further degrade the tissue, causing sloughing (flaking) of lesional epidermis, but rapid wound healing prevents the formation of overt lesions. Null epidermis is hyperproliferative and overexpresses keratins 6 and 16, indicating abnormal differentiation. From 6 wk, null mice develop ulcerating lesions resembling chronic dermatitis. We speculate that ulceration occurs after acantholysis in the fragile epidermis because environmental insults are more stringent and wound healing is less rapid than in neonatal mice. This dermatitis is accompanied by localized hair loss associated with formation of utriculi and dermal cysts, denoting hair follicle degeneration. Possible resemblance of the lesions to human blistering diseases is discussed. These results show that Dsc1 is required for strong adhesion and barrier maintenance in epidermis and contributes to epidermal differentiation.

Introduction

The desmosomal cadherins, desmocollin (Dsc)* and desmoglein (Dsg), mediate adhesion in desmosomes, one of the principal types of intercellular junction in epithelia and cardiac muscle (Chitaev and Troyanovsky, 1997; Marcozzi et al., 1998; Tselepis et al., 1998). Each constitutes a cadherin subfamily that comprises three genetic isoforms (Dsc1, 2, and 3 and Dsg1, 2, and 3) (Buxton et al., 1993). Dscs and Dsgs show tissue-specific expression: Dsc2 and Dsg2 are ubiquitous in desmosome-containing tissues, whereas Dscs 1 and 3 and Dsgs 1 and 3 are restricted to stratified epithelia. In stratified epithelia such as epidermis, the desmosomal cadherins also show differential expression with the "1" isoforms expressed in suprabasal differentiated layers and the "2" and "3" isoforms in more basal layers (Garrod et al., 1996). Dsg1 and 3 and Dsc1 and 3 expression in epidermis is graded reciprocally; the "3" isoforms decrease exponentially from the basal layer as the "1" isoforms increase (Shimizu et al., 1995; North et al., 1996). This implies that their expression patterns may be linked, a possibility also

Address correspondence to David R. Garrod, School of Biological Sciences, 3.239 Stopford Bldg., University of Manchester, Oxford Rd., Manchester M13 9PT, UK. Tel.: 44-161-275-5243. Fax: 44-161-275-3915. E-mail: david.garrod@man.ac.uk

J. Hewitt's present address is Queen's Medical Centre, Genetics Division, Nottingham University, Nottingham NG7 2UH, UK.

A. North's present address is The Rockefeller University, 1230 York Ave., New York, NY 10021.

*Abbreviations used in this paper: DP, desmoplakin; Dsc, desmocollin; Dsg, desmoglein; ES, embryonic stem; K, keratin; PF, pemphigus foliaceus; PG, plakoglobin; RT, reverse transcriptase; TEWL, transepidermal water loss.

Key words: desmosome; desmocollin; epidermis; epidermal barrier; null mutation

suggested by the adjacent chromosomal locations of desmosomal cadherin genes (Hunt et al., 1999). Where they occur together, Dsc1 and Dsc3 are mixed in the same desmosomes. Thus, the Dsc1:Dsc3 ratio increases with stratification, indicating turnover during epidermal differentiation and showing that adhesion at different levels in the epidermis involves different combinations of desmosomal cadherins (North et al., 1996).

Desmosomal adhesion plays an important role in the maintenance of tissue architecture as indicated by the study of human disease and null mutations in mice (Hashimoto et al., 1997; Amagai, 1999; Mahoney et al., 1999; Green and Gaudry, 2000). The loss of expression of desmosomal components in some human carcinomas and the ability of desmosomal expression to block cellular invasion suggests that desmosomes may also have a tumor suppressor function (Garrod, 1995; Shinohara et al., 1998; Tselepis et al., 1998).

A pressing question is whether the differential expression of desmosomal cadherins indicates specific functions for the distinct isoforms. Their graded expression in stratified epithelia implies a possible role in epithelial differentiation. Stratification itself is clearly not dependent on the presence of multiple desmosomal cadherin isoforms, since cornea possesses only Dsc2 and Dsg2 (Messent et al., 2000). In other epithelia, Dsc3 and Dsg3 are associated positionally with cell proliferation and the early stages of differentiation, whereas Dsc1 and Dsg1 are associated with terminal differentiation and keratinization. Thus, the "1" isoforms may provide strong adhesion to resist abrasion in keratinized epithelia, and the "3" isoforms may provide weaker adhesion required for cell proliferation and motility (Legan et al., 1994). Desmosomal cadherins also may be involved in differentiative signaling. Desmosomes participate in both inside-out and outside-in signal transduction (Osada et al., 1997; Wallis et al., 2000). Furthermore, the Dsc and Dsg cytoplasmic domains bind the armadillo proteins plakoglobin (PG) and plakophilin, and PG signaling in the epidermis has been demonstrated, since overexpression affects hair growth (Charpentier et al., 2000). The nuclear location of plakophilins suggests a possible gene regulation role (Hatzfeld, 1999). Thus, either a structural/morphogenetic role and/or a direct or indirect differentiative signaling role for desmosomal cadherins may be envisaged. Mice expressing dominant negative Dsg3 exhibit abnormalities of epidermal proliferation and differentiation (Allen et al., 1996), although $Dsg3^{-/-}$ mice show no obvious abnormalities of epidermal differentiation (Koch et al., 1997).

To approach the question of the function of Dsc isoforms, we have performed targeted ablation of the mouse *Dsc1* gene. This results in a complex phenotype, showing epidermal fragility together with defects of epidermal barrier and differentiation. The epidermis of neonatal mice shows lesions, which resemble those found in IgA pemphigus, and older mice develop chronic dermatitis. These results demonstrate that Dsc1 contributes substantially to epidermal adhesion and function.

Results

Characterization of the *Dsc1* gene

Two λ clones (λC1 and λC4) and a PAC clone (364c17) containing Dsc1 sequence were obtained from library screens. From these, the mouse *Dsc1* gene was characterized in detail. The gene spans ~32 kb and consists of 17 exons (Fig. 1). Exon 10 is the largest (260 bp) and exon 16, which is alternatively

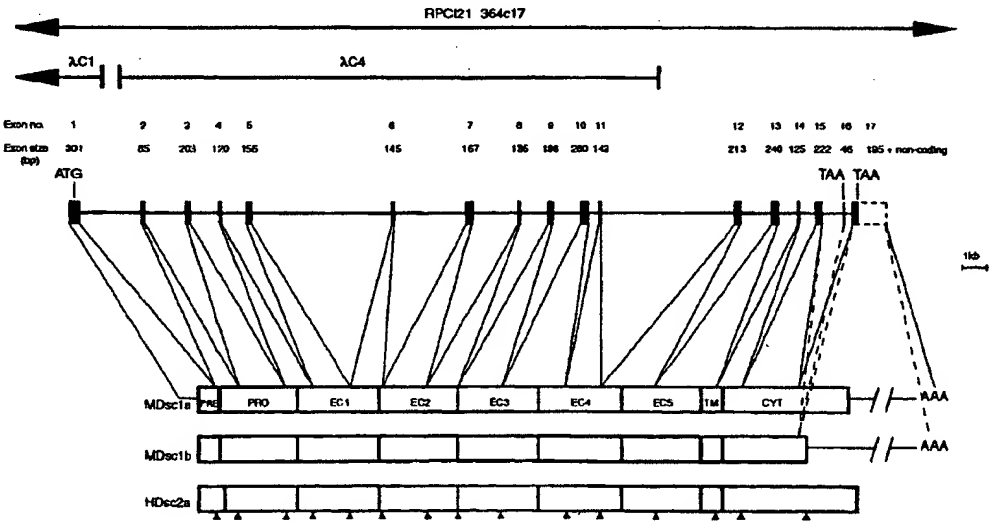

Figure 1. **Exon-intron organization of the murine *Dsc1* gene.** The analysis was conducted using a PAC clone (RPCI21 346c17) and two λ clones (λC1 and λC4). The location of each exon is shown relative to the *Dsc1* gene and a schematic representation of the mouse (M) Dsc1a and Dsc1b proteins. Results from RNase protection assay (unpublished data) suggest that there are no additional 5′ exons. Alternative splicing of RNA can occur; the shorter "b" form of the protein is produced if RNA encoded by exon 16 (which contains an in-frame stop codon) is included in the final message. PRE, signal peptide; PRO, propeptide; EC1-EC5, extracellular homologous repeat domains 1–5; TM, transmembrane domain; CYT, cytoplasmic domain. The locations of introns in human (H) *DSC2* (Greenwood et al., 1997) are shown for comparison and indicated by arrowheads.

Table I. Exon-intron boundaries of the mouse *Dsc1* gene

Exon	Exon size	5′ donor	Intron size	3′ acceptor
	bp		*kb*	
1	NC + 63	TTTCTCCTGgtgagt	2.6	ttgagGTTCTGGTA
2	85	TAGGCAAAGgtgagc	1.7	ctgtagTGAATCTGG
3	203	GAAAAAAAGgtaaag	1.1	atatagGTTTTTAGG
4	120	ATTCAGCAGgtctgt	1.1	ttatagATCCAATCT
5	156	CAATTTTTGgtaaga	5.8	ttccagGTATATGGA
6	145	GCCGATCTGgtgagt	3.0	gaacagGAACTTCAG
7	167	GACAGAGAGgtaatg	1.9	ttacagAAATGTGAC
8	135	CAAACTTCTgtgagt	1.2	cctcagTATACTACA
9	186	AGGCTTAAGgtaatg	1.1	aaacagCCACTGAAC
10	260	AGGCTTAAGgtaatg	0.4	acctagGTATGAGAT
11	143	CAGATACAGgtgagt	5.5	tcctagCTGGCCGAT
12	213	CACAGGATGgtaagt	1.3	cttcagGTAAACGTG
13	240	TGCTACTGTgtaagt	0.8	ctgtagGCATTTTGT
14	125	GAAGTGACGgtaaat	0.7	ctttagGAAGCCAAT
15	222	CTTGGTGAAgtaagt	0.9	atacagAAGGTGTAT
16	46	CTTGGTGAAgtaagt	0.3	atgtagGAATCCATT
17	195 + NC			

Consensus ag/gt splice sequences are shown in bold. Intron sizes were determined by PCR using primers positioned on flanking exons. NC, noncoding.

spliced to generate the "a" and "b" forms of the protein (Collins et al., 1991), is the smallest (46 bp). Single exons do not correspond to known structural elements such as the extracellular domain internal repeats or the transmembrane or cytoplasmic domains (Fig. 1). All intron-exon borders conform to 5′ and 3′ splice site consensus sequences (Table I). The organization of mouse *Dsc1* shows a striking resemblance to that of other Dsc and classical cadherin genes (Greenwood et al., 1997; Whittock et al., 2000) with exon boundaries highly conserved (Fig. 1).

Generation of *Dsc1*-null mice by homologous recombination

The *Dsc1* gene was disrupted in embryonic stem (ES) cells using the targeting vector shown in Fig. 2 A. On homologous recombination, the vector replaces the translation initiation codon (ATG) and the coding sequence from exon 1 with a neo-cassette. 98 bp at the 3′ end of exon 1 (including 63 bp encoding the start of the Dsc1 signal peptide) and 2.2 kb of intron 1 are replaced by vector DNA.

Four ES cell clones containing a disrupted *Dsc1* allele were identified, and one was used to generate chimeric mice that transmitted the mutated allele to their progeny. Mice heterozygous for the targeted mutation were identified by Southern blotting; wild-type and mutant alleles produced fragments of 20- and 6-kb, respectively (Fig. 2 B). Additional Southern blotting with a probe located 3′ to the homologous sequences in the targeting vector confirmed the presence of the mutated allele in heterozygous mice, and a

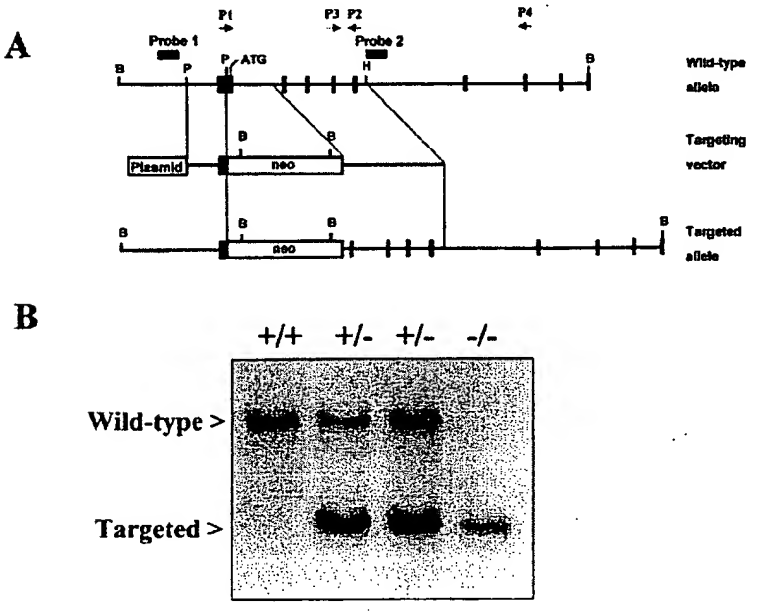

Figure 2. **Targeted disruption of the mouse *Dsc1* gene.** (A) Targeting strategy. The targeting vector consisted of pUC DNA, a neomycin (neo) resistance cassette, and portions of the *Dsc1* gene including 2.1 kb of homology (5′ arm) and 5.2 kb of homology (3′ arm). Filled vertical boxes represent exons. B, BamHI; P, PvuII; H, HindIII. (B) Southern blot analysis of genomic DNA from wild-type (+/+), heterozygous (+/−), and homozygous (−/−) mice. DNA was digested with BamHI, subjected to agarose gel electrophoresis, and transferred to nitocellulose. Wild-type (20 kb) and mutant (6 kb) alleles were detected with probe 1, which hybridized to DNA just outside of the 5′ region of homology. Similarly, probe 2, which hybridized to DNA just outside the 3′ region of homology, detected wild-type (20 kb) and mutant (14 kb) bands (unpublished data).

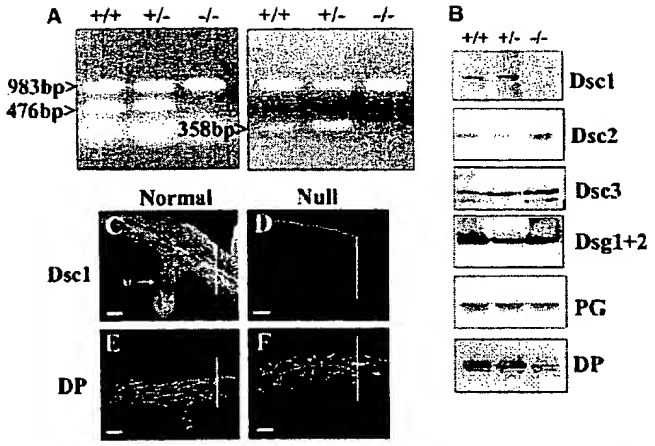

Figure 3. **Expression of desmosomal constituents in Dsc1 mutant mice.** (A) RT-PCR showing absence of Dsc1 message in $Dsc1^{-/-}$ mice. Amplification of Dsc1 mRNA was performed using primer pairs P1 and P2 and P3 and P4 (Fig. 2 A) to give 476- and 358-bp products, respectively, in wild-type and heterozygous mice only. Control amplifications using glyceraldehyde-3-phosphate dehydrogenase primers (983-bp product) were performed. (B) Western blot analysis of epidermal extracts using antibodies specific for Dsc1, Dsc2, Dsc3, Dsg1+2, PG, and DP. Equal protein loadings were determined by prior staining with Coomassie brilliant blue. (C–F) Immunofluoresoence of epidermis from 2-d-old normal and null mice. Dsc1 is expressed in the epidermis and hair follicles of normal mice (C) but is absent from the skin of null animals (D). DP distribution is unaffected apparently by the absence of Dsc1 and is similar in normal (E) and null mice (F). Vertical bars indicate position of epidermis. Skin samples were taken from the backs of mice. hf, hair follicle. Bars, 25 μm.

neo-derived probe was used to show the presence of only one copy of the neo gene (unpublished data). Heterozygous mice, which could not be distinguished from their wild-type littermates, were crossed and their progeny genotyped. Litter sizes were normal. Of the pups, 26% were wild-type (+/+), 56% were heterozygous (+/−), and 18% were homozygous for the disrupted allele (−/−) ($n = 308$). Thus, the number of homozygous-null offspring was slightly lower than expected. Dsc1 is first expressed at embryonic day (E)13.5 in the outer layers of epidermis (King et al., 1996; Chidgey et al., 1997). To determine whether absence of Dsc1 results in some embryonic mortality, we genotyped E17 embryos from heterozygous crosses. Of these, 28% were wild-type, 43% were heterozygous, and 29% were −/− ($n = 65$). This is a normal Mendelian ratio. These data suggest that some of the $Dsc1^{-/-}$ neonates are eaten by the mothers at birth, although no direct evidence for this was found. $Dsc1^{-/-}$ mice were fertile: pups from $Dsc1^{-/-} \times Dsc1^{-/-}$ crosses were reared and weaned successfully.

Mice lacking Dsc1 show a neonatal phenotype involving skin, hair, eyes, and growth

Using primers P1 and P2 specific for exons 1 and 5, respectively (Fig. 2 A), full-length Dsc1 mRNA was absent from the epidermis of $Dsc1^{-/-}$ mice by reverse transcriptase (RT)-PCR (Fig. 3 A). To confirm the absence of a 5′-truncated message, RT-PCR was performed using primers P3 and P4 specific for exons 4 and 7, respectively (Fig. 2 A). No evidence for a truncated message was found (Fig. 3 A). Primer P3 hybridizes to DNA downstream of that encoding the beginning of the mature protein. Hence, it is extremely unlikely that a truncated message smaller than that which would be detected by primer pair P3-P4 would produce a functional protein. Western blotting with a polyclonal antibody raised against a substantial portion of the extracellular domain of Dsc1 (North et al., 1996) showed absence of the protein from $Dsc1^{-/-}$ epidermis (Fig. 3 B). No evidence for the production of a truncated protein was found. Western blotting also showed no clear differences in expression of other desmosomal components (Dsc2, Dsc3, Dsg1+2, PG, desmoplakin [DP]) (Fig. 3 B). Immunofluorescence demonstrated absence of Dsc1 from $Dsc1^{-/-}$

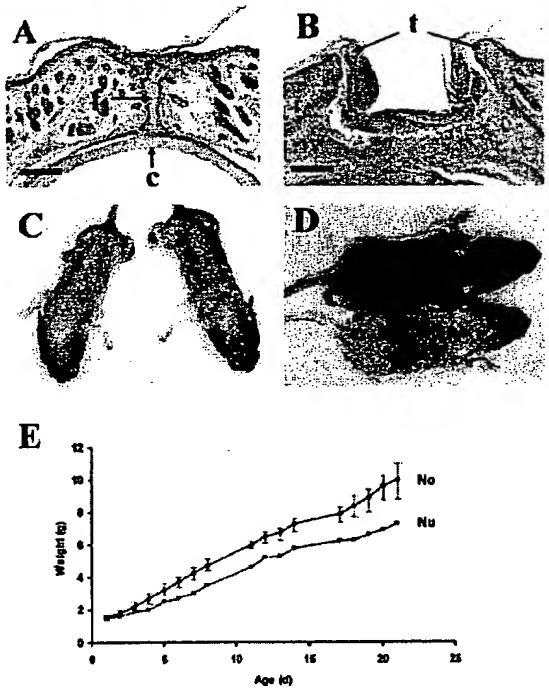

Figure 4. **Eye, skin, and growth abnormalities in Dsc1-null mice.** (A) Eyelids from a 2-d-old normal mouse. f, fused eyelid epidermis; c, cornea. (B) Eyelids from a $Dsc1^{-/-}$ littermate showing a failure of eyelid fusion, inflammation, and corneal damage. t, eyelid tips which have failed to fuse. (C) Flaky skin in two null mice at 2-d-old. At this age, null mice were indistinguishable in size from their normal littermates. (D) Flaky skin and characteristic runted appearance in an 8-d-old null mouse (bottom animal) when compared with a normal littermate (top animal). (E) Delayed weight gain in Dsc1-null mice. Results from a typical litter consisting of nine pups in which a null (Nu) mouse and its normal (No) littermates were born with equal weights, but at weaning (21 d) the null mouse weighed 30% less than the average of the others. Bars represent range of weights of normal littermates. 10 litters were examined with similar results. Bars, 150 μm.

epidermis and the inner root sheaths of hair follicles (Fig. 3, C and D). Other desmosomal components were unchanged (DP shown) (Fig. 3, E and F).

At birth, homozygous mice were generally indistinguishable from their littermates, but 10% were born with one or both eyes open (Fig. 4, A and B). Failure of eyelid fusion led to corneal damage and inflammation and corneal opacity or micropthalmia later in life. From day 2, null mice could be distinguished from their normal (i.e., $Dsc1^{+/+}$ and $Dsc1^{+/-}$) littermates because null skin was covered in white flakes or scales (Fig. 4, C and D).

Although born at the same size, null mice usually grew less rapidly (Fig. 4 D), and by weaning (21 d) they were ~30% smaller than littermates (Fig. 4 E; see Fig. 9 A). Slower growth was not due to an obvious feeding defect. The guts of null mice had milk in their stomachs and a normal appearance throughout their length, indicating that the food was processed normally. Dsc1 is expressed in mouse tongue, hard palate, esophagus, and forestomach (King et al., 1996, 1997), but histological examination of these tissues from null mice revealed no abnormalities of the epithelia. Inspection of the oral cavities of null pups revealed no blistering of epithelia. Thus, $Dsc1^{-/-}$ mice did not show the type of oral blistering defects responsible for feeding defects and small size in $Dsg3^{-/-}$ mice (Koch et al., 1997). Of null animals, 10% remained runted, but others caught up after weaning so that by 3 mo there was no significant difference in weight between them and normal mice. Thus, although growth was slower adult size was not generally affected.

Dsc1 is expressed in the Hassal bodies of human thymus (Nuber et al., 1996). To test for an effect on thymus, we examined it histologically and counted numbers of peripheral blood T cells labeled with antibodies to CD4 and CD8 by flow cytometry. No differences were found.

Mice lacking Dsc1 show abnormal epidermal proliferation and differentiation

Histology showed that the epidermis of $Dsc1^{-/-}$ mice was considerably thicker than that of littermates. Normal epidermis consisted of two to three cell layers below the cornified layer, but that of null mice had one, two, or three additional layers, and thickening was found at all body sites. At 2 d, thickening was principally in the spinous layer (Fig. 3, E and F, and Fig. 5, A and B), although localized hyperkeratosis and parakeratosis were also seen (Fig. 5 C). The epidermal cells often but not always appeared larger in the thickened null epidermis (Fig. 5, A and B, compared with Fig. 3, E and F). To determine whether epidermal thickening was due to increased cell proliferation, we examined the skin from null and normal mice using an antibody against Ki67. Proliferating cells were infrequent (3% of all epidermal nuclei) in normal mouse skin and found exclusively in the basal cell layer (Fig. 5 D). By contrast, in null mouse epidermis keratinocytes with nuclear Ki67 were extremely abundant (33% of all epidermal nuclei) and observed frequently in suprabasal layers (Fig. 5 E).

To investigate the effects of the null mutation on epidermal differentiation, we examined the expression of differentiation markers by immunofluorescence. No differences between normal and null epidermis from 2-d-old animals were observed in the distributions of the basal markers P-cadherin (Fig. 6, A and B), β_4-integrin (Fig. 6, D and E), and keratin 5 (unpublished data). Early markers of terminal differentiation (keratin [K]1, involucrin) and a marker for late epidermal differentiation (filaggrin) were normal in 2-d-old null mice (unpublished data). However, a striking difference in the hyperproliferation markers keratins 6 and 16 was found. In normal 2-d epidermis, expression of K6 was restricted mostly to hair follicles (Fig. 6 G), although localized interfollicular epidermal staining was found occasionally. In null epidermis, K6 was present in both hair follicles and interfollicular epidermis (Fig. 6 H). Such K6 expression was observed at all body sites but was patchy locally: in some places expression was present throughout interfollicular epidermis but was absent from others. In normal epidermis, K16 was expressed in hair follicles, and superficial staining was present in suprabasal interfollicular epidermis (Fig. 6 J). In null animals, expression of the protein was upregulated and detected in all cell layers of interfollicular epidermis (Fig. 6 K).

In later life, null mice were susceptible to skin ulceration (see below). In lesioned epidermis from adult null mice,

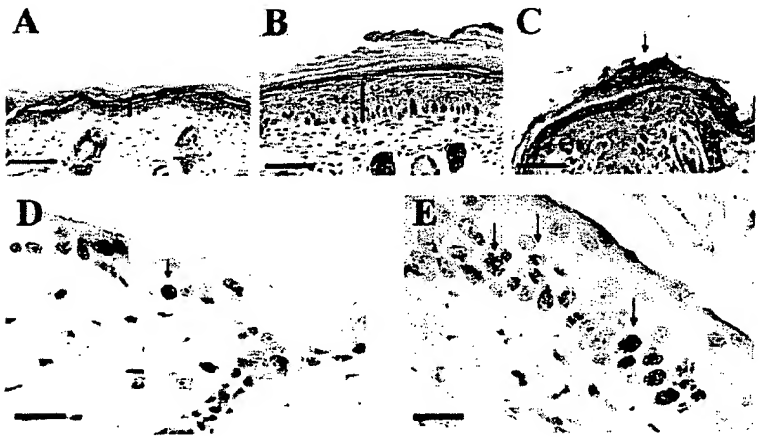

Figure 5. **Hyperplasia and increased cell proliferation in Dsc1-deficient epidermis.** (A) Epidermis from a 2-d-old normal mouse. (B) Epidermis from a $Dsc1^{-/-}$ littermate showing hyperplasia. Bars (e) indicate thickness of living layers of epidermis. (C) Epidermis from a Dsc1-null mouse showing localized hyperkeratosis and parakeratosis (retention of nuclei in the cornified layer) (arrow). (D) Expression of Ki67 in the epidermis in a normal mouse. (E) Ki67 staining in the epidermis of a $Dsc1^{-/-}$ mouse. Only one proliferating cell located in the basal layer is present in D (arrow), whereas in E almost all of the cells in the basal layer and numerous suprabasal cells (arrows) are undergoing cell division. A–C show head skin; D and E show back skin. Bars: (A–C) 100 μm; (D and E) 50 μm.

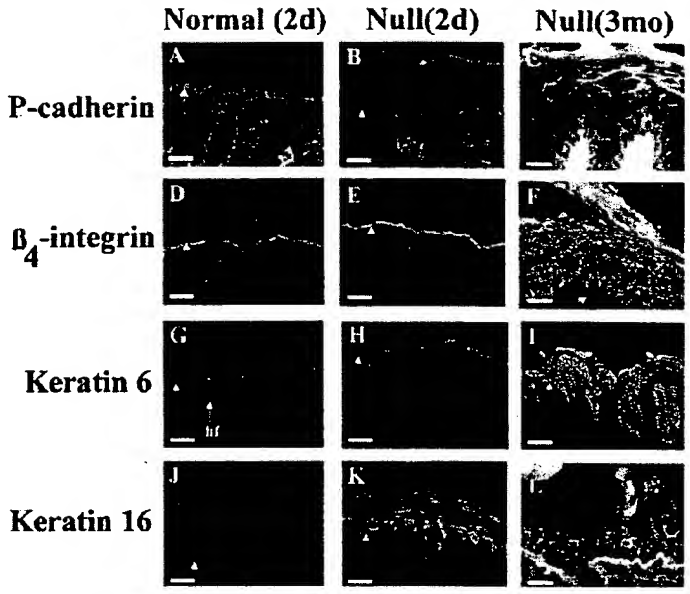

Figure 6. **Immunofluorescence of differentiation markers in Dsc1-null mice.** Distribution of P-cadherin in normal (A) and null (B) 2-d-old animals. In both cases, expression is confined to the basal cell layer and hair follicles. However, dramatic upregulation of P-cadherin is found in lesioned epidermis from adult (~3-mo-old) null animals (C). Similarly, distribution of β_4-integrin expression is similar in normal (D) and null (E) 2-d epidermis but is increased dramatically in all cell layers of lesioned epidermis from older null mice (F). Keratin 6 is expressed in hair follicles of normal mice (G), whereas in unlesioned epidermis from 2-d-old null animals it is found both in hair follicles and interfollicular epidermis (H). Dramatic upregulation of keratin 6 is found in lesioned epidermis from adult null animals (I). In normal animals, superficial keratin 16 staining is detected in suprabasal layers (J), whereas in null mice it is expressed strongly throughout the epidermis including the basal cell layer in both nonlesioned (K) and lesioned epidermis (L). Arrowheads indicate the basement membrane. All micrographs show back skin. Bars: (A–F and J–L) 25 μm; (G–I) 150 μm.

basal layer markers were expressed in all cell layers (Fig. 6, C and F). There were no differences in the distributions of K1 and filaggrin. Both K6 (Fig. 6 I) and K16 (Fig. 6 L) were found throughout lesioned epidermis.

Cornified envelope formation is an important aspect of epidermal terminal differentiation. Because a Dsc, Dsc3, has been reported as a component of cornified envelopes (Robinson et al., 1997) and because *Dsc1*$^{-/-}$ mice showed abnormal epidermal differentiation, we compared cornified envelopes from the epidermis of null and wild-type mice. No difference in appearance was detectable.

Dsc1 deficiency produces epidermal fragility with localized loss of barrier activity

Two observations from neonatal mice suggested that the epidermis of *Dsc1*$^{-/-}$ mice is more fragile than that of littermates. First, histology revealed splits in the epidermis. Such acantholysis, which was absent from normal epidermis, occurred within the granular layer between the granular and spinous layers (Fig. 7 A) or between the cornified and granular layers. Second, when we attempted to isolate the epidermis from 2-d-old mice we found that null epidermis could only be removed in small pieces, whereas normal epidermis remained in sheets (Fig. 7, B and C).

We determined the effects of eliminating Dsc1 on desmosome ultrastructure in the epidermis. No abnormalities in the structure or number of desmosomes were found, including those at the level of the upper spinous and granular layers where Dsc1 expression is strongest (Fig. 7, D and E). Similarly no changes in desmosomes in the inner root sheaths of hair follicles were apparent (unpublished data). By EM, epidermal splits showed an absence of cell lysis and desmosomes, indicating that splitting occurred because of weakened adhesion (Fig. 7 F).

We speculated that flaky skin and epidermal fragility could lead to defects in the skin barrier. To examine this, barrier activity was tested by dye penetration assays (Hardman et al., 1998; Marshall et al., 2000). E17 embryos showed no staining so the barrier was complete before birth. Also, 2-d-old normal mice stayed uniformly white, indicating complete barrier formation (unpublished data; Hardman et al., 1998). However, 2-d-old null mice showed numerous dark spots, indicating localized loss of barrier function (Fig. 8 A). These lesions were not left-right symmetric, indicating that environmental factors contributed to their formation.

Histology of stained spots showed that formation and repair of the lesions could be viewed as sequential events. Early lesions appear in the subcorneal region of epidermis as localized accumulations of neutrophils (Fig. 8, B and C). Such lesions bear a striking resemblance to those found in the subcorneal pustular dermatosis form of IgA pemphigus (Fig. 8 B compared with Fig. 1 c in Hashimoto et al., 1997). Next, the epidermis is degraded by inflammatory cells and partially detaches from the underlying matrix (Fig. 8, D and E), allowing penetration of dye (Fig. 8 A). Concurrently, epithelial cell migration into the wound site is initiated (Fig. 8 E). Finally, when wound healing is complete the damaged epidermis detaches from the underlying tissue, leaving behind an intact newly formed barrier (Fig. 8 F).

To quantify loss of barrier function, body skin from 2-d-old animals was used for determination of permeability constants (Kp) to water and mannitol, a marker for paracellular permeability (Fig. 8 G). Values for Kp were significantly higher ($p < 0.05$) for null animals. The null skin Kp for mannitol was twice that for normal skin, and permeability to water was increased 1.6-fold (Fig. 8 G). These results indicate that absence of Dsc1 causes a defect in the skin barrier.

To examine transepidermal water loss (TEWL), measurements were performed on 25 wild-type and 29 null pups. These gave values of 5.2 mg/h and 6.3 mg/h, respectively.

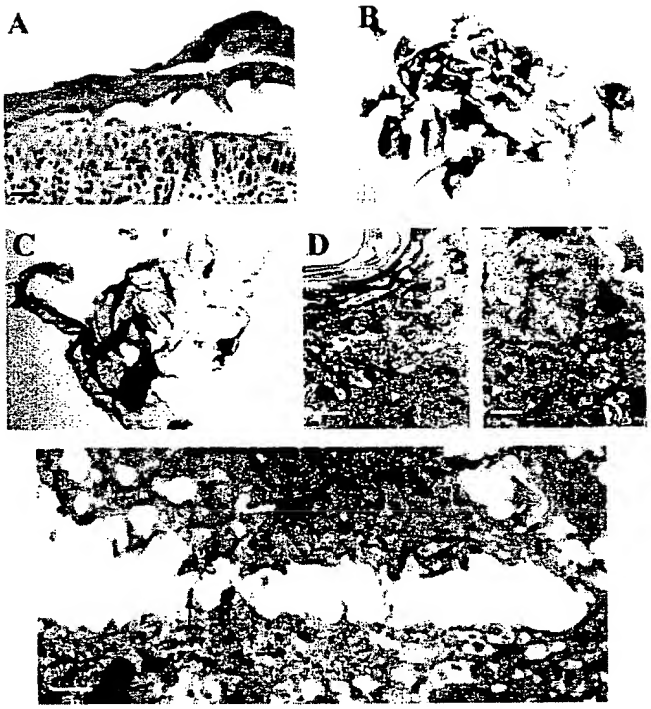

Figure 7. **Absence of Dsc1 weakens adhesion in upper epidermis despite the presence of ultrastructurally normal desmosomes.** (A) Epidermis from a 2-d-old null mouse showing hyperplasia and acantholysis. The granular layer appears to be separating from the upper spinous layer. (B) Epidermis isolated from a 2-d-old *Dsc1*$^{-/-}$-null mouse after treatment with EDTA showing that the tissue fragments allow only small pieces of epidermis to be separated from the dermis. (C) Epidermis isolated using the same technique from a normal littermate. (D) Ultrastructure of outer layers of epidermis from a normal mouse showing desmosomes (arrows). (E) Ultrastructure of outer layers of epidermis from a Dsc1-null mouse with desmosomes (arrows) of a normal appearance. (F) Ultrastructure of lesional epithelium in a Dsc1-null mouse showing splitting between cells and an absence of cell lysis. Arrows indicate possible remains of split desmosomes. All samples were from back skin. Bars: (A) 20 μm; (D and E) 1 μm; (F) 2 μm.

Thus, TEWL for null mice was ~1.2-fold greater than for wild-type controls ($p = 0.02$).

Dsc1-null mice develop alopecia and chronic dermatitis

The coats of adult null mice had a slightly untidy ruffled appearance (Fig. 9 A). Their pelage hairs were indistinguishable from those of normal littermates with similar distributions of awls, auchenes, zig-zags, and guard hairs, and whiskers appeared normal. In later life (usually manifesting at between 1 and 2 mo), >90% of null mice suffered hair loss and skin ulceration (Fig. 9, B and C). Hair loss was most common ventrally (Fig. 9 B), but some individuals had bald patches on the back, and two mice showed more general hair loss. Ulceration was most common around the muzzle (Fig. 9 C) but was also found elsewhere on the head, ventrally, or on the back. Muzzle lesions appeared between 6 wk and 6 mo, and affected mice were killed. Mice that were caged alone developed the same phenotype.

To investigate the mechanism of hair loss, we examined hair follicles at various stages of the hair cycle. No striking abnormalities were found at 5 (first anagen), 18 (catagen), 21 (telogen), and 28 d (second anagen). Tape stripping of the coats detached no more hairs from null than from normal mice, indicating that hairs were firmly anchored in null follicles.

In older animals, severe epidermal and follicular hyperplasia was observed in ulcerated areas of skin (Fig. 9 C) and occasionally in uninvolved skin. In hyperplastic epidermis, substantial thickening of the stratum corneum (hyperkeratosis) was observed (Fig. 9, D and E). Normally differentiated hair follicles were absent and replaced by large comedo-like malformations (utriculi) and cysts (Fig. 9, D and F). Such structures characteristically result from disintegration of hair follicles, suggesting that the observed alopecia is a result of hyperplasia and loss of normal hair follicle morphology. In some ulcerated regions, the epidermis was lost completely (Fig. 9 E). Severe inflammation and tissue necrosis were also observed. The most striking examples of focal overgrowth of keratinocytes were found in both apparently normal and ulcerated whisker pads, which showed a marked papillomatous nature (Fig. 9, G compared with H) with hyperkeratosis and parakeratosis. No evidence of malignant conversion was found. *Dsc1*-null mice were diagnosed as suffering from chronic dermatitis.

Discussion

Deletion of *Dsc1* has two consequences for epidermis. First, weakened adhesion gives rise to epidermal fragility and acantholysis. In early life, this produces a striking localized loss of barrier function and skin flaking. In older mice, substantial ulceration occurs. Second, epidermal differentiation is abnormal, manifested as epidermal hyperproliferation and thickening, an upregulation of keratin 6 and 16 expression, and localized hyperkeratosis and parakeratosis.

Absence of Dsc1 did not result in any alteration in the structure of desmosomes in the upper epidermis, but acantholysis indicates that they are more weakly adhesive than in normal mice, presumably relying on other Dscs for their structure and adhesion. However, there was also no apparent alteration in the expression of other desmosomal components, a result similar to that found in *Dsg3*$^{-/-}$ mice (Koch et al., 1997). Thus, although the expression of the glycopro-

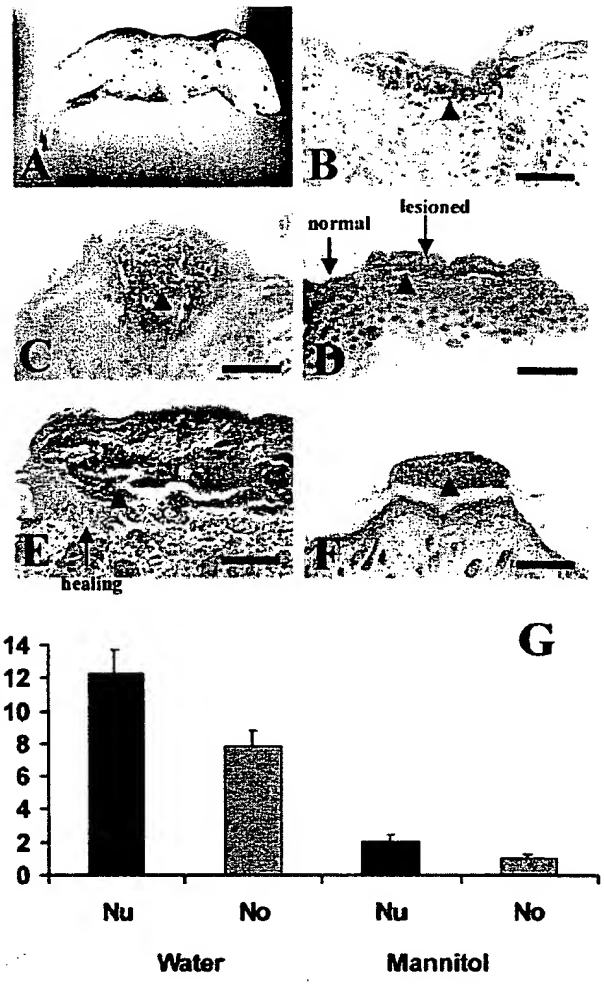

Figure 8. **Dsc1-null mice have skin barrier defects.** (A) Localized breaches in the skin barrier allow penetration of dye into the epidermis of a null mouse but not its normal littermate, which was completely white, that is, unstained (unpublished data). (B and C) Early lesions in the skin of 2-d-old null mice showing infiltration of epidermis with polymorphonuclear cells (neutrophils). (D) More developed lesion in 2-d epidermis showing epidermal degradation and detachment from the underlying dermis. (E) Higher magnification showing epithelial cell migration from intact tissue into wound site. (F) Healed lesion in the epidermis of a 2-d-old null mouse. The damaged epidermis has completely detached from the underlying healed tissue. Arrowheads indicate polymorphonuclear cells. (G) Measurement of permeability coefficients (Kp) for water and mannitol under passive conditions show that skin from 2-d-old null mice is more permeable to both water and solutes ($p < 0.05$ in both cases) than that of a normal littermate. Nu, null; No, normal. Bars: (B, C, and E) 25 μm; (D and F) 100 μm.

tein genes has been postulated to be linked (North et al., 1996; King et al., 1997) two examples of gene deletion have not resulted in compensatory upregulation of other family members.

The acantholysis in the upper epidermis in *Dsc1*$^{-/-}$ resembles that seen in the human autoimmune blistering disease pemphigus foliceus (PF) (Mahoney et al., 1999), reflecting the similar epidermal expression patterns of Dsc1 and the PF antigen Dsg1. In PF, acantholysis results from binding of IgG autoantibody to the extracellular domain of Dsg1. There is no evidence for the involvement of antibodies to Dsc1 in PF. Subsequently, the localized acantholytic lesions in *Dsc1*$^{-/-}$ mice become infiltrated with polymorphonuclear cells (neutrophils). The lesions are reminiscent of those seen in the human subcorneal form of IgA pemphigus in which IgA autoantibodies to Dsc1 bind to the peripheries of epidermal keratinocytes (Hashimoto et al., 1997). No evidence for the pathogenicity of these antibodies has yet emerged. Whether the resemblance between the lesions is coincidental or has significance for the etiology of IgA pemphigus awaits clarification.

Although the acantholytic lesions appear similar, those in young *Dsc1*$^{-/-}$ mice do not progress. In the human diseases, red encrusted lesions are characteristic of PF and red pustular blisters are characteristic of IgA pemphigus, yet the epidermis of the mice remain unblemished apart from the appearance of white flakes. We suggest that skin lesions in young mice are triggered by local acantholysis but do not progress because wound healing is rapid. Reepithelialization of wounds takes ~50% longer in 6–8-wk-old mice than in neonatal mice (Whitby and Ferguson, 1991). This difference in the rate of wound healing can account for the difference in severity between the lesions of neonatal mice and older mice. The environmental insults experienced by older animals are more severe than in young mice during suckling. Repeated insults, especially scratching, give rise to lesions in the epidermis that cannot be healed as rapidly as in neonatal animals. Exacerbation of lesions leads to ulceration and chronic dermatitis, which in this case is a proliferative response of the epidermis to damage. Similar lesions have been found in *Dsg3*$^{-/-}$ mice (Amagai et al., 2000).

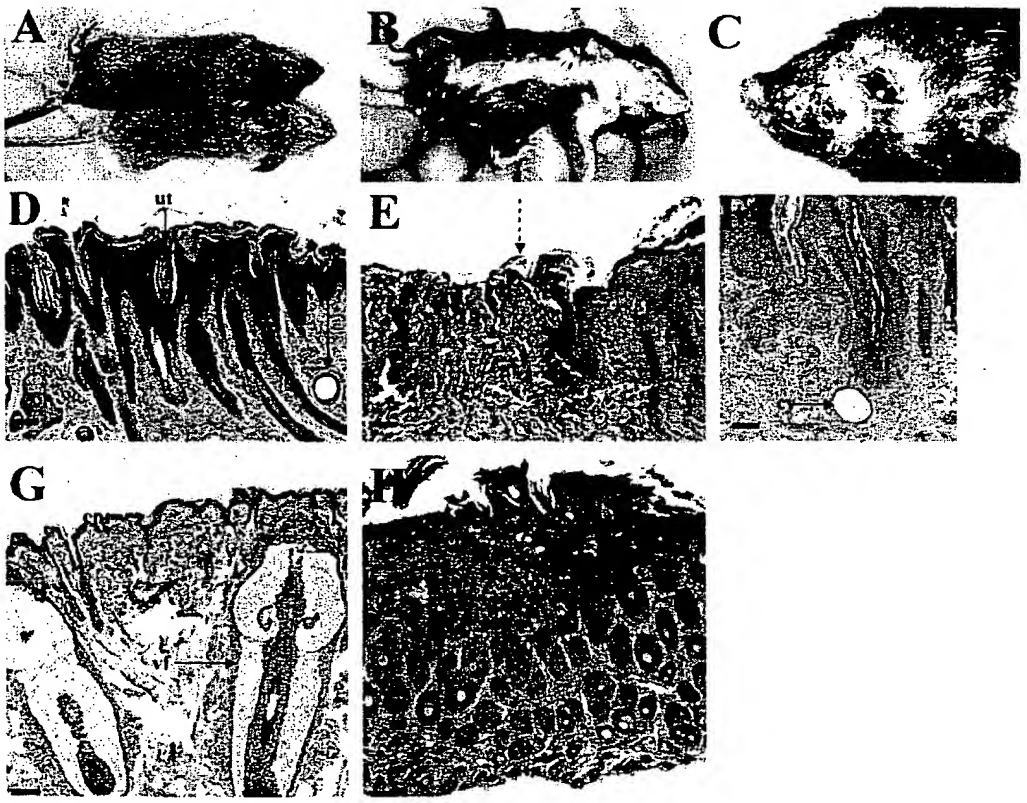

Figure 9. **Phenotype of Dsc1-null mice increases in severity with age.** (A) Scruffy and untidy coat appearance in an adult null mouse (bottom) compared with a normal littermate (top). Mice shown are 21-d-old (day of weaning). Note that the null mouse is smaller. (B) Alopecia in an adult null mouse showing the most typical pattern observed. Some ulceration on the ventral surface of the head and neck is visible also. (C) Snout ulceration in an adult null mouse showing a moderately severe example of the pattern found in all null animals and commencing after 1 mo of age. (D) Hyperplastic epidermis from the ventral surface of an adult null mouse showing acanthosis, hyperkeratosis with utriculi (ut), and cysts (cy). (E) Ulcerated skin from the abdomen of an adult Dsc1$^{-/-}$ mouse showing complete loss of epidermis from the site of the ulcer and severe inflammation. The right hand margin of the ulcer is indicated by an arrow. At this low magnification, the presence of inflammatory cells is indicated by the dermal basophilia of this region. (F) Higher magnification of a utricule (ut) and a cyst (cy). (G) Whisker pad of an adult normal mouse. vf, vibrissa follicle. (H) Whisker pad of an adult null mouse. Severe hyperplasia is present in the null as indicated by the increased number of epidermal cell layers. Approximate thickness of epidermis indicated by bars (ep) in G and H. Bars: (D, E, and G) 150 μm; (F) 25 μm.

Epidermal barrier function is compromised in neonatal *Dsc1*$^{-/-}$ mice. The defect appears to arise as a consequence of localized acantholysis and thus does not imply a direct role for Dsc1 in barrier formation, although we cannot completely exclude the possibility of a slight, more generalized defect. The effect is clearly mild and not life threatening. However, the slight reduction in epidermal barrier function and increase in water loss may cause stress to null mice and result in growth retardation. Area measurements of water and mannitol permeability and TEWL indicate a decrease in barrier function of less than twofold. A fourfold increase in TEWL is not lethal in mice transgenic for COOH-terminally truncated loricrin (Suga et al., 2000). By contrast, a targeted mutation in the keratin 10 gene results in an eightfold increase in TEWL and neonatal death (Jensen et al., 2000). Mice deficient in the cornified envelope proteins involucrin and loricrin exhibit no neonatal barrier defect, although the latter show delayed barrier formation before birth (Dijan et al., 2000; Koch et al., 2000). Therefore, these mice are affected less severely than *Dsc1*$^{-/-}$ mice.

Clear evidence for hyperproliferation and epidermal thickening was found in *Dsc1*$^{-/-}$ mice. Hyperproliferation may be a response to damage to the skin barrier. Underlying cells can sense defects in cells above and respond by proliferating in several experimental situations. Disruption of the barrier elicits DNA synthesis and epidermal hyperplasia (Proksch et al., 1991; Denda et al., 1998), and expression of the *whn* gene and NH_2-terminally truncated Dsg3 in suprabasal layers of transgenic mouse epidermis leads to both hyperproliferation and an immune response (Allen et al., 1996; Prowse et al., 1999). However, the major barrier defect in *Dsc1*$^{-/-}$ mice is localized, whereas the hyperproliferation and epidermal thickening is not. Thus, it seems likely that alterations in the program of keratinocyte terminal differentiation occur in the absence of Dsc1. Two pieces of evidence support this view. First, proliferating keratinocytes were

found in suprabasal layers of null epidermis, and second, parakeratosis was found, suggesting that the later stages of differentiation are delayed. Furthermore, there is evidence to suggest that expression of K6 and K16 in interfollicular epidermis is associated with alterations in differentiation rather than hyperproliferation (Schermer et al., 1989; Sellhayer et al., 1993; Porter et al., 1998b). However, the whole question of whether the effects we observe are a primary consequence of loss of Dsc1 or a secondary consequence of acantholysis and wound healing is a complex one that will form the subject of further investigation.

Epidermal hyperproliferation may suggest a resemblance to the common human skin disease psoriasis. However, the changes in differentiation and skin inflammation are less severe than in psoriasis, and other features, such as loss of the granular layer, formation of deep rete pegs, and dilation of dermal blood vessels, are absent.

Hair loss in *Dsc1*$^{-/-}$ mice differs from that in Dsg3-null animals. In the latter, hair loss occurs in wave-like patterns as the result of defective cell adhesion in the telogen phase of the hair cycle (Koch et al., 1998). Dsc1 is expressed in inner cell layers of the hair follicle (Chidgey et al., 1997; King et al., 1997), but despite extensive examination we found no abnormalities in timing of the hair cycle or in structure of hair follicles in *Dsc1*$^{-/-}$ mice of up to 4 wk of age. Hair loss occurred generally in older animals and was often associated with loss of normal hair follicle morphology and the presence of comedo-like structures (utriculi) and dermal cysts. Such structures characteristically result from hair follicle degeneration (Montagna et al., 1952; Mann, 1971; Panteleyev et al., 1998). Further work will be required to determine whether hair follicle degeneration is an indirect consequence of the hyperproliferative and inflammatory environment or whether Dsc1 has a role in the maintenance of normal follicle morphology.

In conclusion, the phenotype of *Dsc1*$^{-/-}$ mice demonstrates a role for this desmosomal glycoprotein in keratinocyte adhesion in the upper epidermis and in the normal function of the skin. Furthermore, our data suggest that Dsc1 contributes to the regulation of epidermal differentiation, and *Dsc1*$^{-/-}$ mice may prove useful in determining the role of desmosomes in skin disease.

Materials and methods

Isolation and characterization of the mouse *Dsc1* gene

Mouse 129SVJ λFixII (Stratagene) and PAC (RPCI21; UK HGMP Resource Centre) genomic libraries were screened with overlapping fragments of the mouse Dsc1 cDNA. Two unique nonoverlapping λ clones (λC1 and λC4) and one PAC clone (364c17) were characterized in detail. Intron sizes were determined by generating PCR products using synthetic oligonucleotide primers based on flanking exon sequences derived from the Dsc1 cDNA sequence (King et al., 1996). Exon-intron boundaries were determined by DNA sequencing and comparison with cDNA sequence.

Construction of a targeting vector and generation of Dsc1-null mice

To construct a targeting vector, a PvuII fragment from λC1, comprising 2.1 kb of DNA 5′ of the *Dsc1* initiation codon, was cloned upstream of a neomycin resistance gene under the control of a phosphoglycerate kinase promoter (Fig. 2 A). A 5.2-kb NotI (from the λFixII vector) to HindIII fragment from λC4, containing exons 2–5 of *Dsc1*, was cloned downstream of the neo gene. Vector DNA was linearized and electroporated into ES cells. Neomycin-resistant clones were isolated and screened by Southern blot analysis using BamHI-digested genomic DNA and a probe (1 kb), which hybridized to DNA 5′ to the homologous sequences used in the targeting vector (Fig. 2 A). One recombinant ES cell clone was injected into C57Bl/6J blastocysts, and the resulting chimeric male offspring were mated with female C57Bl/6J mice. Tail DNA from agouti offspring was tested for the presence of the mutated allele by Southern blot hybridization. Heterozygous mice were intercrossed to obtain mice, which were homozygous for the *Dsc1*-null allele.

RT-PCR

Newborn (2-d-old) mice were killed, and their skin was removed and immersed in 5 mM EDTA in PBS for 3 min at 50°C. The epidermis was peeled from the dermis, homogenized in Trizol reagent, and total RNA was prepared according to the manufacturer's instructions (Life Technologies). First strand cDNA synthesis was performed from RNA using a kit (Roche) and random primers. An aliquot (1 μl) of the first strand cDNA reaction was amplified using primers P1 (AGGGAGCACCTTCTCTAAGCAG) and P2 (AAGGCTCTTTGTCTACTCCTGG), specific for exons 1 and 5, respectively, and P3 (GGTCCATTTCCACAACACATT) and P4 (TGTACTTCAGACGAGTGTGTA), specific for exons 4 and 7, respectively. Glyceraldehyde-3-phosphate dehydrogenase primers (CLONTECH Laboratories, Inc.) were added to PCR reactions as a positive control.

Western blotting

Epidermis was isolated from 2-d-old mice as above and dissolved in sample buffer. Proteins were separated by SDS-polyacrylamide gel electrophoresis and transferred to polyvinylidene difluoride membrane (Amersham Pharmacia Biotech). Primary antibodies were JCMC (1:10,000) against Dsc1 (North et al., 1996), JB1 (1:500) against Dsc2 (Hyam, J.L.M., personal communication), rabbit anti-mouse Dsc3 (1:100; unpublished data; Liu, K., and D. Marshall, personal communication), DG3.10 (1:100) against Dsg1+2 (Progen), mouse anti-human PG (1:5,000; Transduction Laboratories), and 11–5F (1:40) against DP (Parrish et al., 1987). Primary antibodies were detected using appropriate peroxidase-conjugated secondary antibodies and the ECL detection system (Amersham Pharmacia Biotech).

Histological and immunochemical analysis

For histological analysis, tissues were fixed routinely in formol saline, embedded in paraffin, and stained with hematoxylin and eosin. Cell proliferation was examined in paraffin sections by staining for Ki67 (Gerdes et al., 1984). Expression of desmosomal constituents and differentiation markers were examined in frozen sections. Tissue was embedded in cryoprotectant (OCT; Miles), frozen in liquid nitrogen, and cryosections fixed in ice-cold methanol (5 min). Primary antibodies were JCMC (1:500), PAT-C (1:10) against Dsc2 (Messent et al., 2000), DG3.10 (1:50), PG-11E4 (1:100) against PG (Zymed Laboratories), 11–5F (1:25), MK1 (1:2,500) against keratin 1 (Covance), MK6 (1:2,500) against keratin 6 (Covance), MK14 (1:20,000) against keratin 14 (Covance), RPmK16 (1:500) against keratin 16 (Porter et al., 1998a), rat anti–mouse β_4 integrin (10 μg/ml; Pharmingen), PCD-1 (10 μg/ml) against P-cadherin (R & D Systems), rabbit antiinvolucrin (1:100; Covance), and rabbit antifilaggrin (1:1,000; Covance). Primary antibodies were detected with the appropriate FITC-conjugated secondary antibodies. Sections were examined using an Olympus BX49 microscope.

EM

Fresh skin was dissected into small pieces (~1 × 1 × 0.5 mm) and fixed by immersion in 2% formaldehyde (freshly made from paraformaldehyde powder) plus 2% glutaraldehyde in 0.1 M sodium cacodylate buffer (pH 7.3). Tissues were fixed for 2 h at room temperature and then washed four times with cacodylate buffer. They were then post-fixed with 1% osmium tetroxide for 2 h, dehydrated through an ethanol series, and embedded in Spurr's resin. Ultrathin sections were contrasted with uranyl acetate and lead citrate and examined on a Philips 400 electron microscope.

Analysis of skin barrier function

Dye penetration assays. These were performed as described by Hardman et al. (1998) and Marshall et al. (2000).

Passive diffusion of solutes. Samples of mouse back skin were clamped in continuous flow-through perfusion chambers. ^3H_2O (5 μCi/ml) and [^{14}C]mannitol (0.1 μCi/ml) were added to the donor compartment, and PBS (4 ml/h) was passed across the connective tissue side and collected hourly for up to 18 h. Samples were counted in a Beckman LS 6000 liquid scintillation counter, and a steady-state permeability constant (Kp) was determined in units of cm/min (Healy et al., 2000; Selvaratnam et al., 2001). Experiments were performed at 32°C.

TEWL. This was determined using a Tewameter (Courage and Khazaka). After decapitation or halothane anesthesia, a probe (1 cm diameter) was applied to the back of 2-d-old animals, and measurements of 1-min duration were taken.

Cornified envelope preparation

Epidermis from 2-d-old mice (see above) was heated to 95°C for 10 min in extraction buffer (0.1 M Tris-HCl, pH 8.5, 2% SDS, 20 mM dithiothreitol, and 5 mM EDTA), and the cornified envelopes were collected by centrifugation at 5,000 *g* for 15 min. The extraction was repeated once, and the envelopes were resuspended and stored in extraction buffer.

We are grateful to Dr. S. Andrew, Dr. E. Bell, Professor C.M. Griffiths, Dr. M. Hardman, Professor T. Hashimoto, Mr. D. Marshall, Mr. G. Morrissey, Mrs. J. Morrissey, and Miss Anjana Patel for help and advice.

The work was supported by the Wellcome Trust, Medical Research Council, and Royal Society.

Submitted: 1 May 2001
Revised: 22 August 2001
Accepted: 15 October 2001

References

Allen, E., Q.-C. Yu, and E. Fuchs. 1996. Mice expressing a mutant desmosomal cadherin exhibit abnormalities in desmosomes, proliferation, and epidermal differentiation. *J. Cell Biol.* 133:1367–1382.

Amagai, M. 1999. Autoimmunity against desmosomal cadherins in pemphigus. *J. Dermatol. Sci.* 20:92–102.

Amagai, M., K. Tsunoda, H. Suzuki, K. Nishifuji, S. Koyasu, and T. Nishikawa. 2000. Use of autoantigen-knockout mice in developing an active autoimmune disease model for pemphigus. *J. Clin. Invest.* 105:625–631.

Buxton, R.S., P. Cowin, W.W. Franke, D.R. Garrod, K.J. Green, I.A. King, P.J. Koch, A.I. Magee, D.A. Rees, J.R. Stanley, et al. 1993. Nomenclature of the desmosomal cadherins. *J. Cell Biol.* 121:481–483.

Charpentier, E., R.M. Lavker, E. Acquista, and P. Cowin. 2000. Plakoglobin suppresses epithelial proliferation and hair growth in vivo. *J. Cell Biol.* 149:503–519.

Chidgey, M.A.J., K.K.M. Yue, S. Gould, C. Byrne, and D.R. Garrod. 1997. Changing pattern of desmocollin 3 expression accompanies epidermal organisation during skin development. *Dev. Dyn.* 210:315–327.

Chitaev, N.A., and S.M. Troyanovsky. 1997. Direct Ca^{2+}-dependent heterophilic interaction between desmosomal cadherins, desmoglein and desmocollin, contributes to cell–cell adhesion. *J. Cell Biol.* 138:193–201.

Collins, J.E., P.K. Legan, T.P. Kenny, J. MacGarvie, J.L. Holton, and D.R. Garrod. 1991. Cloning and sequence analysis of desmosomal glycoproteins 2 and 3 (desmocollins): cadherin-like desmosomal adhesion molecules with heterogeneous cytoplasmic domains. *J. Cell Biol.* 113:381–391.

Denda, M., J. Sato, T. Tsuchiya, P.M. Elias, and K.R. Feingold. 1998. Low humidity stimulates epidermal DNA synthesis and amplifies the hyperproliferative response to barrier disruption: implication for seasonal exacerbations of inflammatory dermatoses. *J. Invest. Dermatol.* 111:873–878.

Dijan, P., K. Easley, and H. Green. 2000. Targeted ablation of the murine involucrin gene. *J. Cell Biol.* 151:381–387.

Garrod, D.R. 1995. Desmosomes and cancer. *In* Cancer Surveys. Vol. 24. Cell adhesion and cancer. I. Hart and N. Hogg, editors. Cold Spring Harbor Laboratory Press, New York. 97–111.

Garrod, D., M. Chidgey, and A. North. 1996. Desmosomes: differentiation, development, dynamics and disease. *Curr. Opin. Cell Biol.* 8:670–678.

Gerdes, J., H. Lemke, H. Baisch, H.H. Wacker, U. Schwab, and H. Stein. 1984. Cell cycle analysis of a cell proliferation-associated human nuclear antigen defined by the monoclonal antibody Ki-67. *J. Immunol.* 133:1710–1715.

Green, K.J., and C.A. Gaudry. 2000. Are desmosomes more than tethers for intermediate filaments? *Nat. Rev. Mol. Cell Biol.* 1:208–216.

Greenwood, M.D., M.D. Marsden, C.M.E. Cowley, V.K. Sahota, and R.S. Buxton. 1997. Exon-intron organisation of the human type 2 desmocollin gene (DSC2): desmocollin gene structure is closer to "classical" cadherins than to desmogleins. *Genomics.* 44:330–335.

Hardman, M.J., P. Sisi, D.N. Banbury, and C. Byrne. 1998. Patterned acquisition of skin barrier function during development. *Development.* 125:1541–1552.

Hashimoto, T., C. Kiyokawa, O. Mori, M. Miyasato, M.A.J. Chidgey, D.R. Garrod, Y. Kobayashi, K. Komori, K. Ishii, M. Amagai, et al. 1997. Human desmocollin 1 (Dsc1) is an autoantigen for the subcorneal pustular dermatosis type of IgA pemphigus. *J. Invest. Dermatol.* 109:127–131.

Hatzfeld, M. 1999. The armadillo family of structural proteins. *Int. Rev. Cytol.* 186:179–224.

Healy, C.M., A.T. Cruchley, M.H. Thornhill, and D.M. Williams. 2000. The effect of sodium lauryl sulphate, triclosan and zinc on the permeability of normal oral mucosa. *Oral Diseases.* 6:118–123.

Hunt, D.M., V.K. Sahota, K. Taylor, D. Simrak, N. Hornigold, J. Arnemann, J. Wolfe, and R.S. Buxton. 1999. Clustered cadherin genes: a sequence-ready contig for the desmosomal cadherin locus on human chromosome 18. *Genomics.* 62:445–455.

Jensen, J.-M., S. Schütze, C. Neumann, and E. Proksch. 2000. Impaired cutaneous permeability barrier function, skin hydration, and sphingomyelinase activity in keratin 10 deficient mice. *J. Invest. Dermatol.* 115:708–713.

King, I.A., T.J. O'Brien, and R.S. Buxton. 1996. Expression of the "skin-type" desmosomal cadherin DSC1 is closely linked to the keratinization of epithelial tissues during mouse development. *J. Invest. Dermatol.* 107:531–538.

King, I.A., B.D. Angst, D.M. Hunt, M. Kruger, J. Arnemann, and R.S. Buxton. 1997. Hierarchical expression of desmosomal cadherins during stratified epithelial morphogenesis in the mouse. *Differentiation.* 62:83–96.

Koch, P.J., M.G. Mahoney, H. Ishikawa, L. Pulkkinen, J. Uitto, L. Shultz, G.F. Murphy, D. Whitaker-Menezes, and J.R. Stanley. 1997. Targeted disruption of the pemphigus vulgaris antigen (desmoglein 3) gene in mice causes loss of keratinocyte cell adhesion with a phenotype similar to pemphigus vulgaris. *J. Cell Biol.* 137:1091–1102.

Koch, P.J., M.G. Mahoney, G. Cotsarelis, K. Rothenberger, R.M. Lavker, and J.R. Stanley. 1998. Desmoglein 3 anchors telogen hair in the follicle. *J. Cell Sci.* 111:2529–2537.

Koch, P.J., P.A. de Viragh, E. Scharer, D. Bundman, M.A. Longley, J. Bickenbach, Y. Kawachi, Y. Suga, Z. Zhou, M. Huber, et al. 2000. Lessons from loricrin-deficient mice: compensatory mechanisms maintaining skin barrier function in the absence of a major cornified envelope protein. *J. Cell Biol.* 151:389–400.

Legan, P.K., K.K.M. Yue, M.A.J. Chidgey, J.L. Holton, R.W. Wilkinson, and D.R. Garrod. 1994. The bovine desmocollin family: a new gene and expression patterns reflecting epithelial cell proliferation and differentiation. *J. Cell Biol.* 126:507–518.

Mahoney, M.G., Z. Wang, K. Rothenberger, P.J. Koch, M. Amagai, and J.R. Stanley. 1999. Explanation for the clinical and microscopic localization of lesions in pemphigus foliaceus and vulgaris. *J. Clin. Invest.* 103:461–468.

Mann, S.J. 1971. Hair loss and cyst formation in hairless and rhino mutant mice. *Anat. Rec.* 170:485–500.

Marcozzi, C., I.D.J. Burdett, R.S. Buxton, and A.I. Magee. 1998. Coexpression of both types of desmosomal cadherin and plakoglobin confers strong intercellular adhesion. *J. Cell Sci.* 111:495–509.

Marshall, D., M.J. Hardman, and C. Byrne. 2000. SPRR1 gene induction and barrier formation occur as coordinated moving fronts in terminally differentiating epithelia. *J. Invest. Dermatol.* 114:967–975.

Messent, A.J., M.J. Blisset, G.L. Smith, A.J. North, A. Magee, D. Foreman, D.R. Garrod, and M. Boulton. 2000. Expression of a single pair of desmosomal glycoproteins renders the corneal epithelium unique amongst stratified epithelia. *Invest. Ophthalmol. Vis. Sci.* 41:8–15.

Montagna, W., H.B. Chase, and H.P. Melarango. 1952. The skin of hairless mice. The formation of cysts and the distribution of lipids. *J. Invest. Dermatol.* 19: 83–94.

North, A.J., M.A.J. Chidgey, J.P. Clarke, W.G. Bardsley, and D.R. Garrod. 1996. Distinct desmocollin isoforms occur in the same desmosomes and show reciprocally graded distributions in bovine nasal epidermis. *Proc. Natl. Acad. Sci. USA.* 93:7701–7705.

Nuber, U.A., S. Schafer, S. Stehr, H.-R. Rackwitz, and W.W. Franke. 1996. Patterns of desmocollin synthesis in human epithelia: immunolocalization of desmocollins 1 and 3 in special epithelia and in cultured cells. *Eur. J. Cell Biol.* 71:1–13.

Osada, K., M. Seishima, and Y. Kitajima. 1997. Pemphigus IgG activates and translocates protein kinase C from the cytosol to the particulate/cytoskeleton fractions in human keratinocytes. *J. Invest. Dermatol.* 108:482–487.

Panteleyev, A.A., C. van der Veen, T. Rosenbach, S. Müller-Röver, V. Sokolov, and R. Paus. 1998. Towards defining the pathogenesis of the *hairless* phenotype. *J. Invest. Dermatol.* 110:902–907.

Parrish, E.P., P.V. Steart, D.R. Garrod, and R.O. Weller. 1987. Antidesmosomal monoclonal antibody in the diagnosis of intracranial tumors. *J. Pathol.* 153: 265–273.

Porter, R.M., A.M. Hutcheson, E.L. Rugg, R.A. Quinlan, and E.B. Lane. 1998a. cDNA cloning, expression, and assembly characteristics of mouse keratin 16.

J. Biol. Chem. 273:32265–32272.

Porter, R.M., J. Reichelt, D.P. Lunny, T.M. Magin, and E.B. Lane. 1998b. The relationship between hyperproliferation and epidermal thickening in a mouse model for BCIE. *J. Invest. Dermatol.* 110:951–957.

Proksch, E., K.R. Feingold, M. Mao-Qiang, and P.M. Elias. 1991. Barrier function regulates epidermal DNA synthesis. *J. Clin. Invest.* 87:1668–1673.

Prowse, D.M., D. Lee, L. Weiner, N. Jiang, C.M. Magro, H.P. Baden, and J.L. Brissette. 1999. Ectopic expression of the *nude* gene induces hyperproliferation and defects in differentiation: implications for the self-renewal of cutaneous epithelia. *Devl. Biol.* 212:54–67.

Robinson, N.A., S. Lapic, J.F. Welter, and R.L. Eckert. 1997. S100A11, S100A10, annexin1, desmosomal proteins, small proline-rich proteins, plasminogen activator inhibitor-2, and involucrin are components of the cornified envelope of cultured human epidermal keratinocytes. *J. Biol. Chem.* 272:12035–12046.

Schermer, A., J.V. Jester, C. Hardy, D. Milano, and T.-T. Sun. 1989. Transient synthesis of K6 and K16 keratins in regenerating rabbit corneal epithelium: keratin markers for an alternative pathway of keratinocyte differentiation. *Differentiation.* 42:103–110.

Sellheyer, K., J.B. Bickenbach, J.A. Rothnagel, D. Bundman, M.A. Longley, T. Krieg, N.S. Roche, A.B. Roberts, and D.R. Roop. 1993. Inhibition of skin development by overexpression of transforming growth factor β_1 in the epidermis of transgenic mice. *Proc. Natl. Acad. Sci. USA.* 90:5237–5241.

Selvaratnam, L., A.T. Cruchley, H. Navsaria, P. Wertz, E. Hagi-Pavli, I.M. Leigh, C.A. Squier, and D.M. Williams. 2001. Oral keratinocytes develop a functional and biochemical permeability barrier similar to intact oral mucosa. *Oral Diseases.* 7:252–258.

Shimizu, H., T. Masunaga, A. Ishiko, A. Kikuchi, T. Hashimoto, and T. Nishikawa. 1995. Pemphigus vulgaris and pemphigus foliaceus sera show an inversely graded binding pattern to extracellular regions of desmosomes in different layers of human epidermis. *J. Invest. Dermatol.* 105:153–159.

Shinohara, M., A. Hiraki, T. Ikebe, S. Nakamura, S.-I. Kurahara, K. Shirasuna, and D.R. Garrod. 1998. Immunohistochemical study of desmosomes in oral squamous cell carcinoma: correlation with cytokeratin and E-cadherin staining, and with tumour behaviour. *J. Pathol.* 184:369–381.

Suga, Y., M. Jarmick, P.S. Attar, M.A. Longley, D. Bundman, A.C. Steven, P.J. Koch, and D.R. Roop. 2000. Transgenic mice expressing a mutatant form of loricrin reveal the molecular basis of the skin diseases, Vohwinkel syndrome and progressive symmetric erythrokeratoderma. *J. Cell Biol.* 151: 401–412.

Tselepis, C., M. Chidgey, A. North, and D. Garrod. 1998. Desmosomal adhesion inhibits invasive behavior. *Proc. Natl. Acad. Sci. USA.* 95:8064–8069.

Wallis, S., S. Lloyd, I. Wise, G. Ireland, T.P. Fleming, and D. Garrod. 2000. The α isoform of protein kinase C is involved in signaling the response of desmosomes to wounding in cultured epithelial cells. *Mol. Biol. Cell.* 11:1077–1092.

Whitby, D.J., and M.W.J. Ferguson. 1991. The extracellular matrix of lip wounds in fetal, neonatal and adult mice. *Development.* 112:651–668.

Whittock, N.V., D.M. Hunt, L. Rickman, S. Malhi, A.P. Vogazianou, L.F Dawson, R.A.J. Eady, R.S Buxton, and J.A. McGrath. 2000. Genomic organisation and amplification of the human desmosomal cadherin genes *DSC1* and *DSC3*, encoding desmocollin types 1 and 3. *Biochem. Biophys Res. Comm.* 276:455–460.

Neuron, Vol. 33, 789–804, February 28, 2002, Copyright ©2002 by Cell Press

Decreased Synaptic Vesicle Recycling Efficiency and Cognitive Deficits in Amphiphysin 1 Knockout Mice

Gilbert Di Paolo,[1,2]
Sethuraman Sankaranarayanan,[5]
Markus R. Wenk,[1,2] Laurie Daniell,[1,2] Ezio Perucco,[6]
Barbara J. Caldarone,[4] Richard Flavell,[1,3]
Marina R. Picciotto,[4] Timothy A. Ryan,[5]
Ottavio Cremona,[6,7] and Pietro De Camilli[1,2,8]
[1]Howard Hughes Medical Institute
[2]Department of Cell Biology
[3]Sections of Immunology
[4]Department of Psychiatry
Yale University School of Medicine
New Haven, Connecticut 06510
[5]Department of Biochemistry
The Weill Medical College of Cornell University
New York, New York 10021
[6]Dipartimento di Scienze Mediche
Università del Piemonte Orientale "A. Avogadro"
28100 Novara
[7]Università Vita-Salute San Raffaele
Milano, San Raffaele Scientific Institute
20132 Milano
Italy

Summary

The function of the clathrin coat in synaptic vesicle endocytosis is assisted by a variety of accessory factors, among which amphiphysin (amphiphysin 1 and 2) is one of the best characterized. A putative endocytic function of amphiphysin was supported by dominant-negative interference studies. We have now generated amphiphysin 1 knockout mice and found that lack of amphiphysin 1 causes a parallel dramatic reduction of amphiphysin 2 selectively in brain. Cell-free assembly of endocytic protein scaffolds is defective in mutant brain extracts. Knockout mice exhibit defects in synaptic vesicle recycling that are unmasked by stimulation and suggest impairments at multiple stages of the cycle. These defects correlate with increased mortality due to rare irreversible seizures and with major learning deficits, suggesting a critical role of amphiphysin for higher brain functions.

Introduction

Neurotransmission relies on a tightly regulated balance between synaptic vesicle exocytosis and endocytosis to maintain a pool of functional synaptic vesicles. A major pathway through which synaptic vesicle membranes can be recycled is clathrin-mediated endocytosis (Cremona and De Camilli, 1997; Brodin et al., 2000). Following depolarization-mediated synaptic vesicle fusion at active zones, membrane retrieval occurs either by the formation of individual clathrin-coated vesicles or by bulk invagination of the plasmalemma to generate endosome-like structures from which clathrin-coated vesicles originate. Once clathrin-coated vesicles have pinched off, they rapidly shed their coat and are directed back to the cluster of synaptic vesicles, from where they can be mobilized for subsequent rounds of release. Recently, a variety of accessory factors thought to assist the clathrin coat in its function have been identified. These include proteins that affect membrane dynamics by direct physical interaction, lipid metabolizing enzymes, regulatory components of the actin cytoskeleton, signaling proteins, and adaptor proteins that link these factors to each other and to the clathrin coat (reviewed in Marsh and McMahon, 1999; Owen and Luzio, 2000; Slepnev and De Camilli, 2000).

In nerve terminals, clathrin-mediated endocytosis occurs at sites that are spatially segregated from sites of exocytosis (Heuser and Reese, 1973; Gad et al., 1998; Teng and Wilkinson, 2000). These endocytic zones form a belt around the active zones of secretion and are regions where components of the endocytic machinery are concentrated (Roos and Kelly, 1999). They are also enriched in actin (Gad et al., 2000; Dunaevsky and Connor, 2000), consistent with evidence that several clathrin accessory factors may be components of protein scaffolds that regulate the actin cytoskeleton (reviewed in Geli and Riezman, 1998; Qualmann et al., 2000; Slepnev and De Camilli, 2000). For instance, the GTPase dynamin, which plays a critical role in fission, also interacts with actin binding proteins and may affect actin dynamics at the synapse through these interactions (Witke et al., 1998; Qualmann et al., 1999; McNiven et al., 2000; Ochoa et al., 2000). The polyphosphoinositide phosphatase synaptojanin 1 hydrolyzes a pool of phosphatidylinositol-4,5-bisphosphate [PI(4,5)P_2] that participates both in clathrin coat recruitment and in actin polymerization at endocytic zones in nerve terminals (Cremona et al., 1999; Gad et al., 2000; Harris et al., 2000). Syndapin/pacsin and DAP160/intersectin, which bind dynamin 1 and synaptojanin 1, are also involved in actin function via an interaction with regulatory components (WASP and Cdc42, respectively) of the Arp2/3 actin nucleating complex (Roos and Kelly, 1998; Qualmann et al., 1999; Modregger et al., 2000; Hussain et al., 2001; Wasiak et al., 2001).

One of the best characterized clathrin accessory factors is amphiphysin (reviewed in Wigge and McMahon, 1998). The amphiphysin protein family is conserved from yeast to man and has a three domain structure (see Figure 3A): an NH_2-terminal BAR (Bin-Amphiphysin-Rvs) domain (Elliott et al., 1999), which mediates binding to acidic phospholipids (Takei et al., 1999; Farsad et al., 2001) and homo/heterodimerization (Wigge et al., 1997a; Slepnev et al., 1998; Ramjaun et al., 1999), a central variable domain, and a COOH-terminal Src homology 3 (SH3) domain that interacts with dynamin 1 and synaptojanin 1 (David et al., 1996; McPherson et al., 1996). Two isoforms of amphiphysin, amphiphysin 1 and 2, are expressed in mammals. Amphiphysin 1 is primarily expressed in brain and is the dominant target of autoimmunity in human paraneoplastic Stiff-man syndrome (De Camilli et al., 1993). Amphiphysin 2 is more widely ex-

*Correspondence: pietro.decamilli@yale.edu

pressed as alternatively spliced isoforms, with the highest levels found in brain and striated muscle (Butler et al., 1997; Leprince et al., 1997; Ramjaun et al., 1997; Wechsler-Reya et al., 1997; Wigge et al., 1997a). The predominant neuronal isoforms of amphiphysin 2 form heterodimers with amphiphysin 1 and the heterodimer is concentrated in nerve terminals (Wigge et al., 1997a; Ramjaun et al., 1997), where it is localized in the presynaptic cytomatrix and is further enriched on coated endocytic intermediates (Bauerfeind et al., 1997). Both components of this heterodimer contain in their central region binding sites for clathrin and AP-2 (McMahon et al., 1997; Ramjaun and McPherson, 1998; Slepnev et al., 2000), while the muscle isoform of amphiphysin 2 lacks the clathrin and AP-2 binding sites, suggesting functions for these isoforms independent of the clathrin coat. Similarly, *Drosophila* amphiphysin lacks clathrin coat binding sites (Razzaq et al., 2000; Leventis et al., 2001). Additional proteins that contain a BAR domain, but are otherwise different from amphiphysin in their domain structure, are expressed in mammals and other organisms (Crouzet et al., 1991; Ge and Prendergast, 2000; Routhier et al., 2001).

A function for amphiphysin in synaptic vesicle endocytosis is supported by several lines of evidence in addition to its localization and biochemical interaction with other endocytic proteins. Expression or microinjection of amphiphysin fragments that compete for the binding of this protein to any of its major partners, such as dynamin, AP-2, and clathrin, strongly inhibits clathrin-mediated endocytosis, possibly by titrating out these factors, thus demonstrating that these interactions can occur in vivo (Shupliakov et al., 1997; Wigge et al., 1997b; Slepnev et al., 2000). More importantly, presynaptic microinjection of peptides that bind the SH3 domain of amphiphysin, and therefore compete its SH3-dependent interactions, also severely impair synaptic vesicle endocytosis (Shupliakov et al., 1997). The interaction of amphiphysin with dynamin affects dynamin's enzymatic activity and oligomeric state (Wigge et al., 1997a; Owen et al., 1998; Takei et al., 1999). Furthermore, the interaction of amphiphysin with dynamin and other endocytic partners in enhanced by nerve terminal depolarization via Ca^{2+}-dependent dephosphorylation, when a burst of endocytic activity is needed (Bauerfeind et al., 1997; Slepnev et al., 1998). Finally, amphiphysin binds and deforms lipid bilayers and may, therefore, facilitate membrane deformations that accompany vesicle budding (Takei et al., 1999; Farsad et al., 2001).

Additional evidence for a role of amphiphysin in endocytosis comes from studies in *Saccaromyces cerevisiae*. In this organism, the homolog of amphiphysin, Rvs167, forms a heterodimer with Rvs161—a protein that comprises a BAR domain only (Crouzet et al., 1991; Lombardi and Riezman, 2001). Although neither gene is essential, mutations in either one of them produce endocytic defects that correlate with a disruption of the actin cytoskeleton (Sivadon et al., 1995). Collectively, these observations suggest that amphiphysin may have an important role in the physiology of endocytic zones of synapses. It may act as a multifunctional adaptor that links cytosolic proteins to the membranes and coordinates the function of clathrin coat proteins, other accessory factors, and the actin cytoskeleton.

In this study, we have used a genetic approach to investigate the role of amphiphysin in synaptic physiology. We have generated mice that lack the expression of amphiphysin 1 and, as an unexpected consequence, also lack brain amphiphysin 2. These mice exhibit synaptic vesicle recycling defects that are compatible with the basic function of the nervous system. However, the mice are prone to seizures, which dramatically decrease their viability, and exhibit severe learning deficits.

Results

Inactivation of the Amphiphysin 1 Gene and Resulting Loss of Both Amphiphysin 1 and 2 in Brain

The amphiphysin 1 gene was disrupted by insertion of a gene encoding a selection marker (neo cassette) in the first coding exon (Figure 1A). The occurrence of correct recombination events was confirmed by Southern blot analysis of ES cells and F2 mice (Figure 1B). Homozygous mutant animals were born, and their genotypes had normal mendelian distribution, revealing lack of embryonic lethality. They did not exhibit any obvious anatomical or histological changes and appeared to develop and reproduce normally, although they displayed an increased mortality rate after reaching adulthood (see below). The expression of the amphiphysin 1 protein was completely abolished in homozygous mutant animals, as shown by Western blotting analysis of brain extracts using a panel of poly- and monoclonal antibodies directed against either the COOH- or the NH_2-terminal region of amphiphysin 1 (Figure 1C and data not shown; see also Figure 2B).

Interestingly, Western blot analysis revealed that expression of amphiphysin 2 was also nearly abolished in the brain of amphiphysin 1-deficient animals (Figure 1C), regardless of the developmental stage of mutant animals (data not shown). No change in the expression level of a variety of other synaptic proteins was observed, including the major interacting partners of amphiphysin such as dynamin 1, synaptojanin 1, clathrin, and the clathrin adaptor AP-2. Levels of intrinsic membrane proteins of synaptic vesicles were also unchanged (Figure 1C and data not shown). The parallel disappearance of amphiphysin 1 and 2 was confirmed by immunofluorescence staining of brain frozen sections (data not shown) and of cortical neurons in culture (Figure 1D). While amphiphysin 1 and 2 colocalize with the synaptic marker synaptophysin in wild-type neurons, the immunoreactivity for both proteins, but not for synaptophysin, is absent in knockout neurons (Figure 1D and data not shown). By Northern blot analysis expression levels of the 2.2 kb transcript encoding amphiphysin 2 were comparable in wild-type and knockout brain (Figure 2A), suggesting that transcriptional mechanisms do not account for the downregulation of amphiphysin 2 in mutant brain. In skeletal muscle, where a shorter isoform of amphiphysin 2 is expressed and where amphiphysin 1 is undetectable (Figure 2B and see also Butler et al., 1997; Wigge et al., 1997a), amphiphysin 2 protein levels were not affected (Figure 2B). These data suggest that amphiphysin 1 is required for the stability of amphiphysin 2 only in neurons, where the two isoforms are primarily found as heterodimers and colocalize accordingly (Figure 2C; see also Ramjaun et al., 1997; Wigge et al., 1997a; Slepnev et al., 1998).

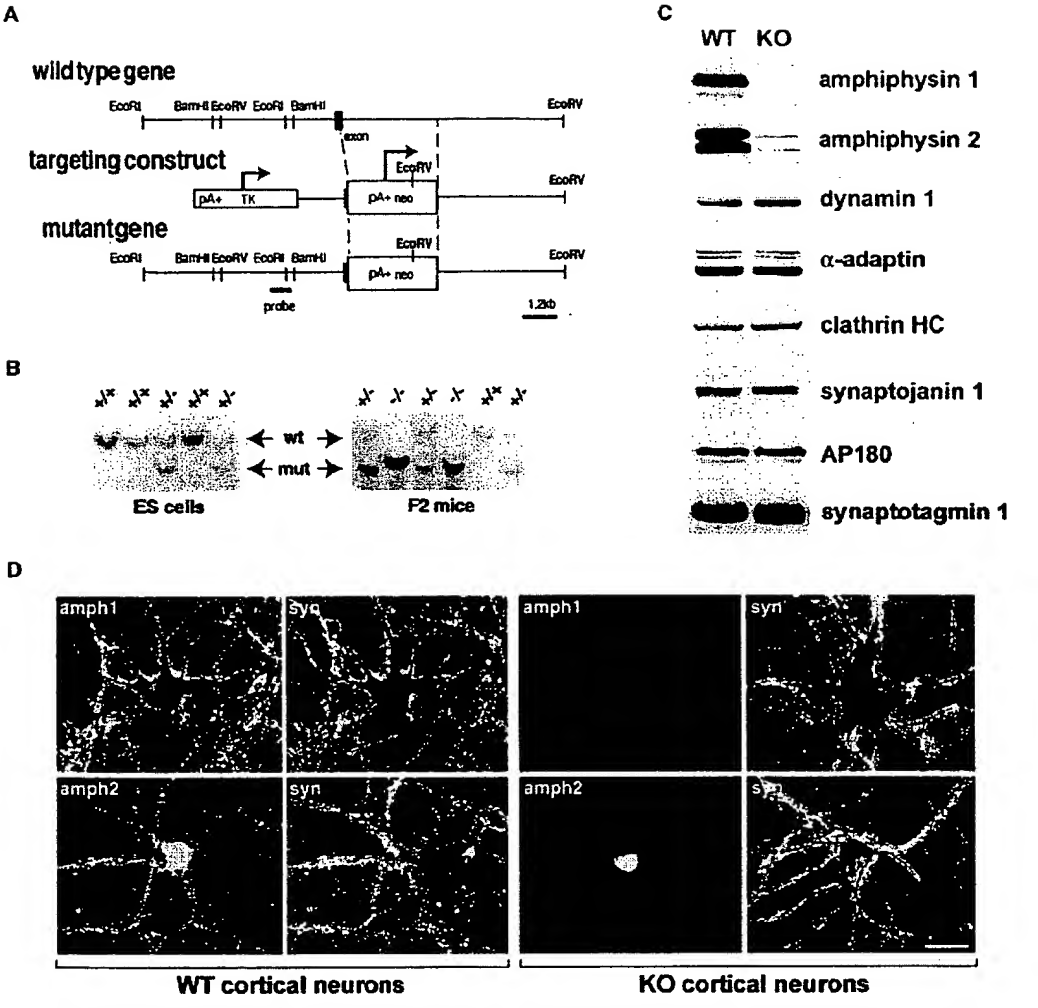

Figure 1. Generation of Amphiphysin 1 Knockout Mice and Downregulation of Amphiphysin 2 Expression

(A) Schematic diagram showing the amphiphysin 1 gene locus, the targeting vector, and the mutant allele following homologous recombination. The neo cassette substitutes part of the first coding exon and part of the following intron. The EcoRV restriction sites and the probe used for the Southern blot analysis are indicated.

(B) Southern blot of EcoRV-digested genomic DNA from wild-type (+/+) and heterozygous (+/−) ES cell clones and from wild-type (+/+), heterozygous (+/−), and homozygous mutant mice (−/−) of the F2 generation.

(C) Western blot of brain extracts from wild-type and knockout mice with antibodies directed against either amphiphysin 1 or 2 or several other synaptic proteins, including major interacting partners of amphiphysin 1 (HC, heavy chain). The knockout extract contains no amphiphysin 1 and drastically reduced levels of amphiphysin 2.

(D) Double immunofluorescence of primary cultures of cortical neurons prepared from the brain of wild-type and knockout mice. Sections were stained for either amphiphysin 1 or 2 (amph) and counterstained for the presynaptic marker synaptophysin (syn). Lack of amphiphysin 1 expression correlates with loss of amphiphysin 2 immunoreactivity in knockout neurons. Residual immunoreactivity found in the nucleus may represent a nuclear pool of amphiphysin 2 (Wechsler-Reya et al., 1997). Scale bar = 15 μm.

Defective Cell-Free Assembly of Endocytic Protein Complexes in Brain Extracts of Amphiphysin 1 Knockout Mice

The properties of the amphiphysin 1/2 heterodimer to bind and deform lipid bilayers (Takei et al., 1999) and to interact with several endocytic proteins (Figure 3A; see also Wigge and McMahon, 1998) suggest that it functions as a multifunctional adaptor at the membrane. We tested this putative function of amphiphysin by determining in cell-free reactions whether the formation of complexes among these proteins, or between these proteins and lipid bilayers, was affected by the lack of the amphiphysin 1/2 heterodimers from brain cytosol. Liposomes composed of total brain lipids were incubated with cytosol from wild-type and mutant brain in the presence of nucleotides (Cremona et al., 1999; Gad et al., 2000). Proteins bound to membranes were then isolated by ultracentrifugation and analyzed by quantita-

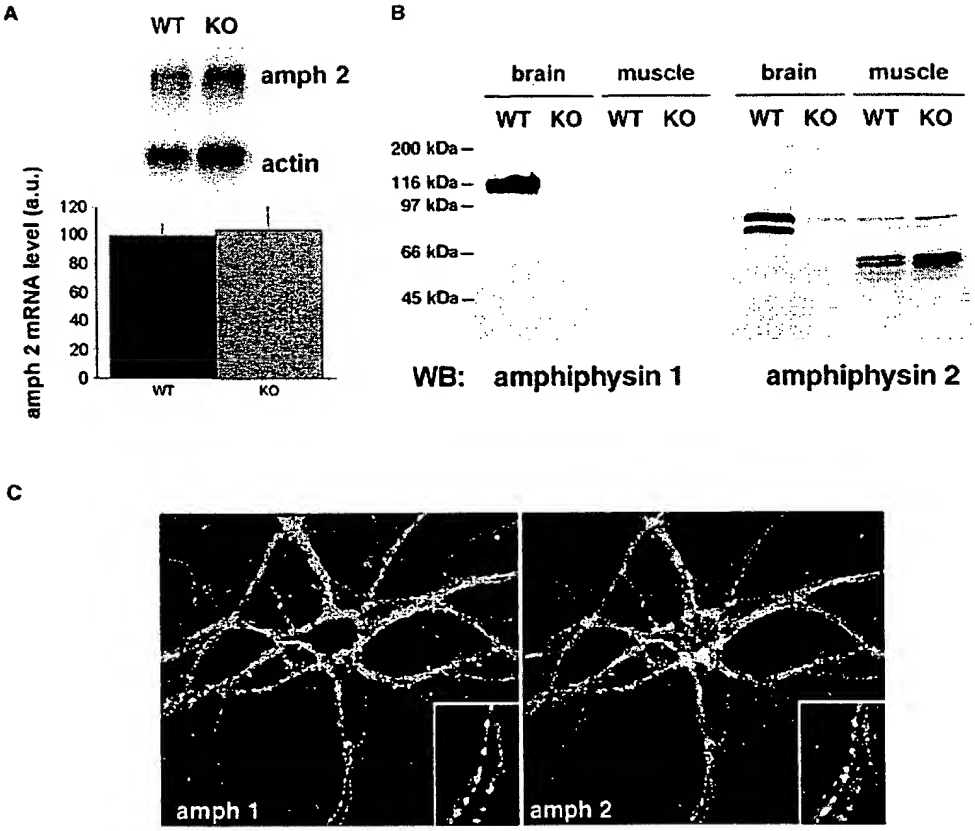

Figure 2. Selective Loss of Amphiphysin 2 in Brain where Amphiphysin 1 and 2 Form Heterodimers and Colocalize

(A) Northern blot analysis showing normal levels of amphiphysin 2 mRNA in knockout brain. Actin mRNA was used as a control for loading. mRNA levels were quantified by phosphoimaging, and amphiphysin 2 mRNA levels were normalized to those of actin mRNA (n = 2).

(B) Western blot analysis of brain and skeletal muscle extracts from wild-type and knockout mice using anti-amphiphysin 1 and anti-amphiphysin 2 antibodies. While amphiphysin 1 is only detected in brain, amphiphysin 2 is expressed at high levels in both brain and skeletal muscle, but as isoforms of different molecular weight. In mutant mice, the downregulation of amphiphysin 2 expression levels occurs selectively in brain.

(C) Double immunofluorescence of cultured cortical neurons from wild-type mice showing precise colocalization of amphiphysin 1 with amphiphysin 2 at synaptic sites. Inset: higher magnification.

tive immunoblotting along with proteins in the starting cytosols. While levels of all proteins examined were the same in the starting cytosol (data not shown), the recovery of clathrin (heavy chain) and AP-2 (α-adaptin) in the "bound" fraction was reduced by 40% and 25%, respectively, in mutant extract relative to wild-type extract (Figures 3B and 3C). A 40% decrease in the recovery of the polyphosphoinositide phosphatase synaptojanin 1 was also observed. Accordingly, incubation of the pelleted liposomes in the presence of ^{32}P-labeled ATP after the binding reaction resulted in an increased level of [^{32}P]-PI(4,5)P_2, most likely reflecting altered PI(4,5)P_2 turnover due to decreased synaptojanin 1-mediated PI(4,5)P_2 hydrolysis (Figure 3D). The recovery of dynamin 1 in the "bound" fraction of liposomes was not affected by the lack of amphiphysin 1 (Figure 3B and 3C). This observation most likely reflects, at least in part, the direct binding of dynamin to lipid membranes via both its pleckstrin homology (PH) domain and the recently identified additional lipid binding site (Burger et al., 2000). As it was shown previously, although amphiphysin does not enhance dynamin recruitment to liposomes, it affects the morphology and the properties of dynamin oligomers at the surface of liposomes (Takei et al., 1999).

We further investigated the potential adaptor function of amphiphysin in the assembly of endocytic proteins in brain, by performing affinity chromatography of a detergent brain extract from wild-type and knockout mice on the COOH-terminal proline-rich tail of dynamin 1 (GST-PRD)—i.e., the amphiphysin binding domain of dynamin. The use of wild-type extracts for these experiments leads to the affinity purification not only of amphiphysin 1 and 2 and other direct interactors of dynamin's tail, such as endophilin and intersectin, but also of clathrin and AP-2 (Figure 3A; see also Slepnev et al., 1998). Immunoblotting of the affinity-purified material revealed a reduction in AP-2 (α-adaptin) and clathrin

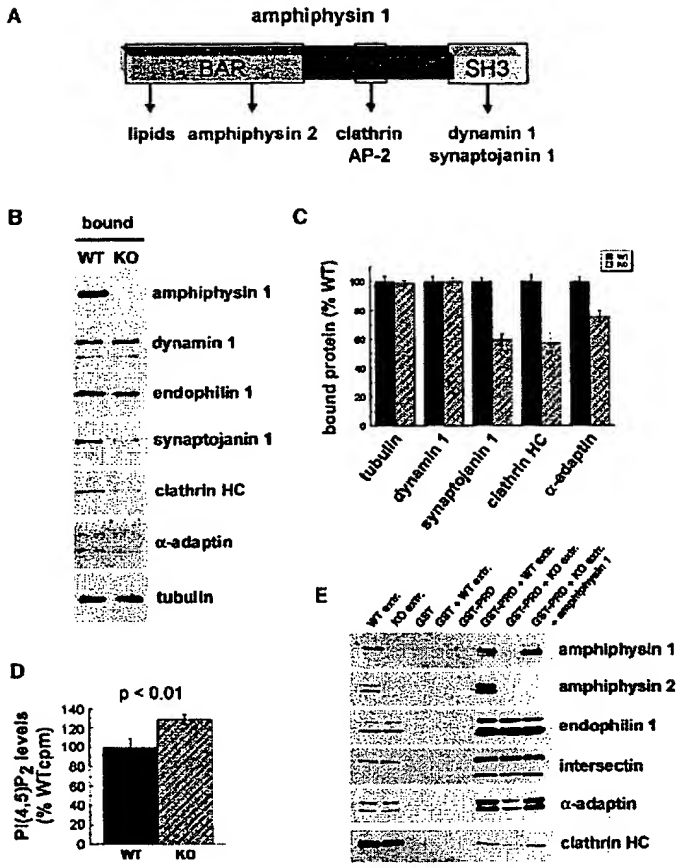

Figure 3. Evidence for a Role of Amphiphysin as an Adaptor Protein in the Recruitment of Cytosolic Endocytic Complexes

(A) Schematic drawing depicting the structure of amphiphysin 1 and its interactors.

(B and C) Recovery of endocytic proteins on liposomes following their incubation with brain cytosol from wild-type and knockout mice in the presence of ATP and GTP. Representative Western blots are shown in (B), and a quantification by phosphoimaging of results from three experiments is shown in (C). Note the absence of amphiphysin 1 and the selective decrease of clathrin, AP-2 (α-adaptin subunit), and synaptojanin 1 in the "bound" material from knockout animals.

(D) Quantification of ^{32}P incorporation into $PI(4,5)P_2$ in liposomes that were first incubated with brain cytosol in the presence of GTP and cold ATP, washed, and subsequently incubated with [$\gamma^{32}P$]ATP. Decreased recovery of synaptojanin 1 in membranes shown in (B) and (C) correlates with increased labeling of $PI(4,5)P_2$.

(E) Western blot analysis of a representative affinity chromatography experiment from wild-type and mutant brain extracts on GST alone, or GST fused to the proline-rich domain (PRD) of dynamin 1. The first two lanes show starting material from both genotypes. Mock affinity purifications (lack of extract) are included as indicated. The knockout brain extract used for the last lane was supplemented with recombinant amphiphysin 1 at physiological concentration. The PRD of dynamin affinity purifies less clathrin and AP-2 from knockout cytosol and exogenous amphiphysin 1 rescues the effect.

Values in (C) and (D) denote means ± SD. The p value from a Student's t test analysis is indicated.

binding, but not in that of endophilin and intersectin, when brain extracts from knockout animals were used (Figure 3E), consistent with a bridging function of amphiphysin. This decrease was rescued by the addition to the knockout extract of recombinant amphiphysin 1 at physiological concentration prior to affinity purification. Collectively, these results provide strong evidence for a role of amphiphysin in the assembly of endocytic complexes at the membrane.

Decreased Stimulus-Dependent Labeling of Synaptic Vesicles Following a "Pulse" Incubation with an Endocytic Tracer

In spite of the biochemical results described above, no obvious ultrastructural differences were observed by electron microscopy in synapses of wild-type and mutant neurons both in brain tissue or in cultures. No accumulation of endocytic intermediates was observed in mutant synapses and the number of synaptic vesicles per synapse was the same in the two genotypes (data not shown). To assess the possible occurrence of synaptic vesicle recycling defects that could be unmasked by stimulation, we used two distinct and complementary approaches.

First, we performed experiments on cerebral cortex synaptosomes. This preparation allows for the analysis of exo- and endocytosis on a global synaptic population, thus avoiding possible bias due to uneven neuronal sampling. Furthermore, synaptosomes, in contrast to neuronal cultures (see below), reflect the properties of synapses in the adult brain. Using a well established fluorimetry-based glutamate release assay (Nicholls and Sihra, 1986), we found no difference in the kinetics or amount of glutamate release between wild-type and knockout synaptosomes upon high K^+ stimulation, which points to a normal exocytic function in knockout synapses (Figures 4A and 4B). Fluorescent amphipathic styryl dyes were then used to study synaptic vesicle recycling. We employed FM2-10 for these experiments, because it has the fastest "off rate" among commonly used styryl dyes and was shown to give a good signal-to-noise ratio in synaptosomes (Cousin and Robinson, 1998; Marks and McMahon, 1998; Cousin and Robinson, 2000). We started by determining the ability of synaptosomes to internalize the dye into vesicular compartments in a stimulation-dependent fashion. Briefly, synaptosomes were preincubated with FM2-10 and depolarized for 90 s by the addition of high K^+ in the continued presence of dye. Then, after a brief wash, synaptosomes were hypotonically lysed, subjected to low-speed centrifugation, and the fluorescence trapped

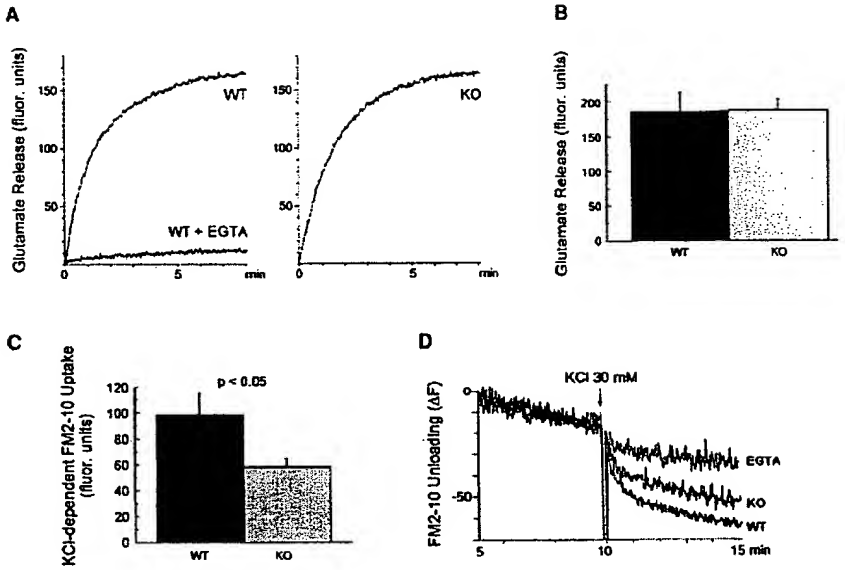

Figure 4. Normal Glutamate Release but Defective Recycling of FM2-10 in Knockout Mice

(A) Fluorimetric tracings of wild-type and knockout synaptosomes showing comparable Ca^{2+}-dependent glutamate release for both genotypes after stimulation with 30 mM KCl.

(B) Quantification of total glutamate release after stimulation with 30 mM KCl for 8 min.

(C) Recovery of FM2-10 in a low speed supernatant of lysed synaptosomes after a first round of stimulation with 30 mM KCl in the presence of dye. The amount of dye trapped in this fraction (endosomes and small vesicles) was smaller in mutant synaptosomes.

Values in (B) and (C) denote means ± SEM (n = 3). The p value from a Student's t test analysis is indicated.

(D) Fluorimetric tracing of wild-type and knockout synaptosomes showing high K^+-dependent unloading of FM2-10 following a first round of stimulation in the presence of dye and a 10 min incubation in dye-free low K^+ to allow for recycling of the dye into the releasable vesicle pool. A tracing showing dye unloading of wild-type synaptosomes in the presence of 2 mM EGTA is also shown.

within membranous organelles of the supernatant, which include primarily endosomes and small vesicles, was measured by fluorimetry. This assay revealed a 40% decrease in the depolarization-dependent internalization of dye in knockout synaptosomes, compared to wild-type synaptosomes (Figure 4C). In the next series of experiments, synaptosomes were stimulated for 90 s in the presence of dye, further incubated for 10 min in dye-free medium to allow for chasing of the dye into releasable synaptic vesicles, and finally exposed to a second high K^+ incubation to induce exocytotic release of the dye. Under these assay conditions, knockout synaptosomes released significantly less FM2-10 than wild-type synaptosomes (Figure 4D), suggesting that synaptic vesicle recycling efficiency is also reduced in amphiphysin 1-deficient nerve terminals.

Second, we used electron microscopy in combination with the fluid-phase uptake of the endocytic marker horseradish peroxidase (HRP) to monitor formation of endocytic intermediates in cultured cortical neurons (Heuser and Reese, 1973). Neurons were grown in culture for at least 2 weeks to allow for the formation of numerous synaptic contacts (see Figure 1D). They were then preincubated with HRP for 3 min, stimulated with high K^+ for 90 s (or mock-incubated in low K^+) in the continued presence of the tracer, fixed, and processed for electron microscopy analysis. High K^+ stimulation produced a significant increase in the HRP labeling of synaptic vesicles and endosomal structures as expected (Figure 5A). However, morphometric analysis indicated that the fraction of HRP-labeled synaptic vesicles and endosome-like structures was significantly reduced in knockout synapses relative to wild-type after stimulation, demonstrating the occurrence of a recycling defect in knockout animals (Figures 5B and 5C). No statistical difference in the number of labeled organelles was found under resting conditions (Figures 5B and 5C).

Smaller Recycling Vesicle Pool Size, Slower Destaining Kinetics, and Delayed Vesicle Repriming in Mutant Nerve Terminals

The reduced stimulus-dependent dye uptake into vesicular compartments described above could be explained by a delayed endocytic uptake of the tracers but also by a smaller size of the recycling pool of synaptic vesicles. Although the number of vesicles per synapse appears to be normal, the functional recycling pool could be smaller. To determine the possible contribution of a smaller functional recycling vesicle pool and to validate the results described above with a more physiological stimulus, we performed styryl dye uptake and release studies in paired cortical cultures from wild-type and mutant animals using action potential trains of variable duration at 20 Hz. Cultures were first exposed to an initial dye-staining step with FM1-43 using a variable number (x) of action potentials (where x ranges from 20

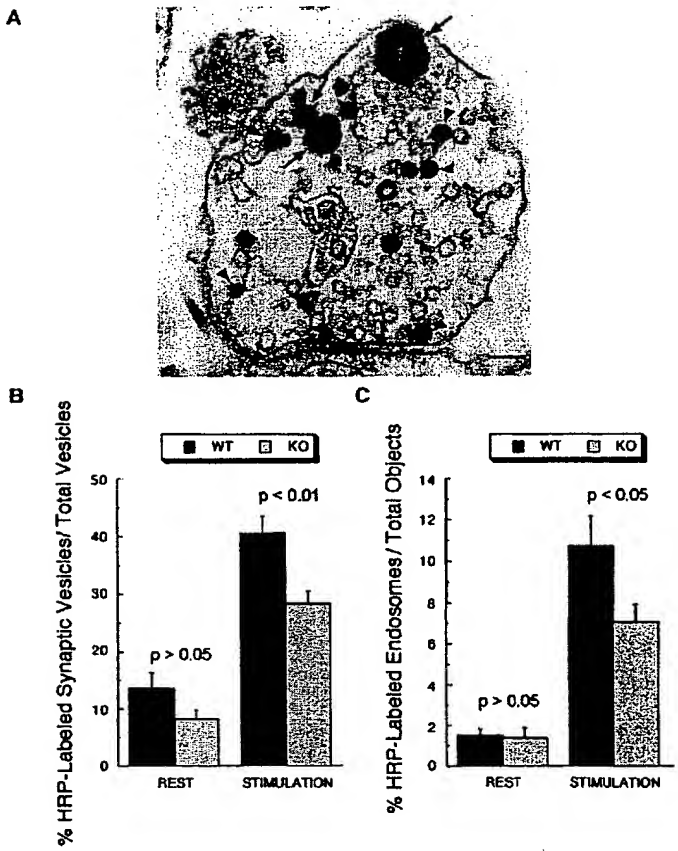

Figure 5. Decreased Labeling of Synaptic Vesicles and Endosome-like Structures after a "Pulse" Incubation with the Fluid Phase Tracer HRP in Synapses of Mutant Cortical Neurons in Culture

(A) Electron micrograph of wild-type synapse stimulated with 90 mM KCl for 90 s in the presence of tracer. A fraction of synaptic vesicles is labeled by HRP (arrowsheads). HRP-labeled objects defined as endosome-like structures are indicated by arrows. Scale bar = 100 nm.

(B) Morphometric analysis indicating the percentage of total small vesicles that are labeled by HRP. The stimulation-dependent increase in the labeling of synaptic vesicles is greater for wild-type synapses than for knockout synapses.

(C) Percentage of HRP-labeled endosomal structures over total number of objects (small vesicles plus labeled endosomal structures). Even in this case, the stimulation-dependent increase in the labeling of endosomes is less pronounced in the case of mutant synapses. Values denote means ± SEM, and p values according to ANOVA are indicated.

to 800) followed by an additional 90 s incubation in the continued presence of the dye in order to label endocytic vesicles whose formation lags behind the interruption of the stimulus. Then, after a 10 min washing period to allow for the chasing of the dye into the releasable pool vesicles, internalized dye was released by a stimulus protocol previously shown to result in maximal destaining (Ryan, 1999). The amount of released dye gives an estimate of the dye taken up in the staining period and thus an estimate of the fraction of synaptic vesicles that underwent exocytosis during a particular action potential stimulus in the dye-loading step.

The total amount of dye uptake with different number of action potentials was normalized to the uptake at 600 action potentials in wild-type terminals and plotted as a function of action potential numbers (Figure 6A). As expected, there was clearly an increase in the size of the vesicle pool that is mobilized with a longer stimulus train in both wild-type and knockout cultures. However, the recycling vesicle pool was 25%–30% smaller in the knockout cultures compared to the wild-type cultures over the entire range of action potential stimuli.

The experiments described in Figure 6A, which showed a smaller total recycling vesicle pool size in knockout cultures, also allowed us to determine whether there was a difference in the fraction of the recycling pool that is engaged by a given duration of action potential train in knockout cultures. To this aim, each of the FM1-43 uptake values from Figure 6A was normalized to the uptake at 600 action potentials for both wild-type and knockout cultures. Comparison of the two sets of values revealed a statistically significant defect in the fractional pool of vesicles mobilized at intermediate AP stimuli in knockout synapses. The fractional pool mobilized at 200 and 300 AP was 0.61 ± 0.02 and 0.74 ± 0.02 for wild-type cultures (n = 265 boutons, three experiments) and 0.54 ± 0.01 and 0.61 ± 0.02 for knockout cultures (n = 288 boutons, three experiments).

We also measured the destaining kinetics of synaptic terminals loaded with FM1-43 during a 600 action potential stimulus. A delay in the delivery of newly internalized vesicles to the releasable vesicle pool would be reflected in a greater time constant for dye release. Onset of the stimulus was associated with a decline in fluorescence in both wild-type and knockout synaptic terminals (Figure 6B). The decline in fluorescence was identical until 100 action potentials, the fifth time point measured. However, at later time points (>200 action potentials), there was a statistically significant delay in the destaining kinetics of knockout terminals relative to wild-type terminals. The time constant of destaining was 17.6 ± 0.6 s in wild-type compared to 21.1 ± 0.5 s in knockout terminals ($p < 0.02$, n = 3).

The slower destaining kinetics of FM1-43-loaded syn-

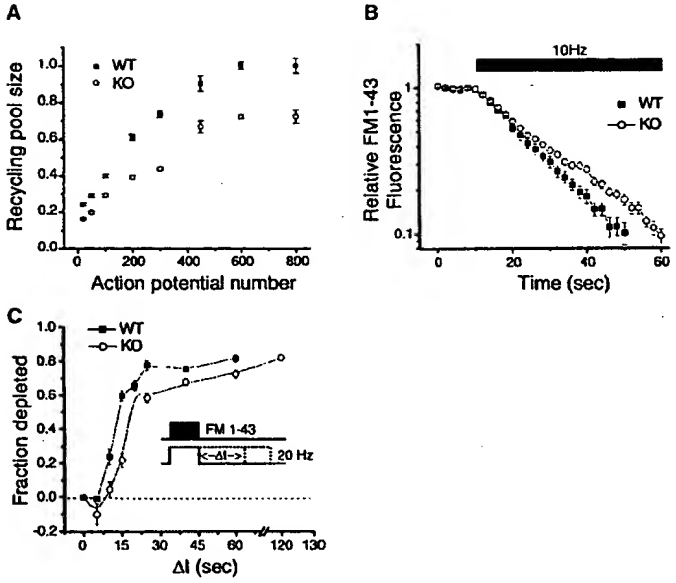

Figure 6. Defects in Synaptic Vesicle Dynamics Revealed by FM1-43 Studies in Synapses of Knockout Mice

(A) Measurement of synaptic vesicle functional pool size in response to action potential (AP) trains of variable duration at 20 Hz. Cortical cultures were first loaded with FM1-43 during a train of APs (abscissa), then, after a 10 min wash-out period, they were subjected to two rounds of AP trains at 20 Hz (separated by a 2 min rest period) to ensure complete dye release. The total amount of dye released during the destaining period gives an estimate of dye uptake into synaptic vesicles during the staining period, and, indirectly, of the vesicle pool size engaged in exo-endocytosis during the same period. Values of FM1-43 uptake at different AP stimuli for both wild-type and mutant synapses were normalized to the uptake at 600 APs in wild-type synapses. Mutant cultures have a smaller vesicle pool size. The total FM1-43 uptake at 600 AP stimuli was 3969 ± 73 (a.u.) in wild-type cultures (n = 635 boutons, five experiments) compared to 2867 ± 45 (a.u.) in knockout cultures (n = 725 boutons, six experiments), statistically significant at $p < 0.001$, Student's t test.

(B) Following FM1-43 loading with 600 APs at 10 Hz, the time course of destaining differs between wild-type and mutant nerve terminals. Destaining of knockout synapses lags behind wild-type. Comparable results were obtained in six other experiments.

(C) Time course of vesicle repriming. The inset shows the experimental protocol. Nerve terminals were stimulated, during a 5 s exposure to FM1-43, by a train of action potentials at 20 Hz that exceeded the period of dye exposure by an amount of time Δt. The resulting dye uptake was measured during a subsequent destaining stimulus at 20 Hz after a 10 min rest. The dye uptake at Δt = 0s (F_0) represents the total number of releasable vesicles engaged by the stimulus. The dye uptake measured in runs where Δt > 0s ($F_{\Delta t}$) provides an estimate of vesicle depletion, due to fusion of reprimed vesicles, during the additional action potential stimulation after dye washout. The data points represents the fraction depleted ($F_0 - F_{\Delta t}/F_0$) as a function of Δt. The data are from a total of 80–165 boutons for each time point in both wild-type and knockout cultures. Error bars are ± SEM.

aptic terminals could be due to a delay in repriming time, defined as the time that elapses before newly endocytosed vesicles become available for a new round of release (Ryan and Smith, 1995). We tested this hypothesis by directly measuring the repriming time course in cultured cortical neurons (Figure 6C). Nerve terminals were loaded with FM1-43 for a fixed period of 5 s, during a train of action potentials at 20 Hz that exceeded the period of dye exposure by an amount of time Δt (inset in Figure 6C). The total fluorescence incorporated into vesicles was measured 10 min later using a maximal destaining stimulus ($F_{\Delta t}$). These data were normalized to the average fluorescence in bracketed control and recovery runs, when the stimulation was terminated at exactly the same time as the washout of dye (Δt = 0, F_0). The ratio ($F_0 - F_{\Delta t}/F_0$) represents the fraction of the fluorescence that was depleted during the additional period of stimulation and reflects the time course of gain in rerelease-competence of recently endocytosed vesicles. Any delay in the endocytic journey of the vesicle will prolong this time. Results of such analyses show that both wild-type and amphiphysin 1-deficient nerve terminals released about 80% of the endocytosed vesicles in the next 120 s of continuous stimulation. However, mutant nerve terminals showed a significant delay in dye depletion compared to wild-type terminals (at Δt = 15 s, wild-type was 60% depleted compared to 20% in knockout cultures, $p < 0.001$). The time to deplete 40% of dye taken up was 12 s in the wild-type terminals compared to 17 s in the knockout cultures. Thus, a delay in repriming of vesicles may at least partially account for the slower destaining kinetics observed in knockout cultures (Figure 6B).

Collectively, these results demonstrate the occurrence of complex recycling defects in amphiphysin knockout terminals, which range from a decreased functional recycling pool size to delayed recycling and repriming rates.

Reduced Viability and Increased Susceptibility to Seizures in Amphiphysin 1 Knockout Mice

Given the cell biological defects described above at synapses of knockout animals, we further investigated changes at the organismal level. A significant decrease in survival rate was observed in the amphiphysin 1 knockout colony, such that only 50% of the animals survived to 10 months of age, as compared with 95% for wild-type mice (Figure 7A). Animals were found dead, mainly between 2 and 5 months of age, with no previous decrease in body weight or other noticeable health problems. To document what appeared to be sudden death, continuous digital camera monitoring of a small group of animals was performed. This approach revealed the occurrence of rare spontaneous seizures. Death resulted from seizures that reached a tonic extension and failed to resolve. Such an observation suggested that amphiphysin 1 knockout mice may exhibit a lower threshold to seizures compared to wild-type animals.

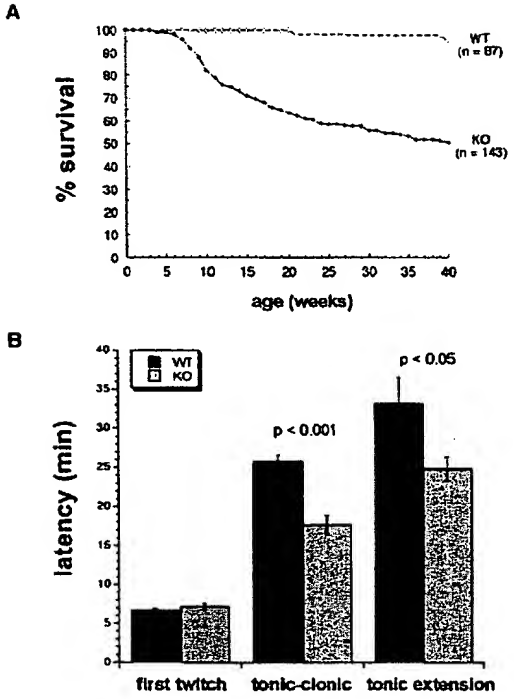

Figure 7. Amphiphysin 1 Knockout Mice Exhibit Increased Mortality and a Higher Propensity to Seizures

(A) Survival curves showing reduced viability of knockout mouse colonies at adult age. Animals die from rare irreversible seizures.

(B) Time (latency) required for wild-type and knockout mice to develop three phases of epilepsy after repeated intraperitoneal injections of pentamethylenetetrazole (metrazol), an epileptogenic $GABA_A$ receptor antagonist. No difference is observed for the first phase (first twitch), but amphiphysin 1 knockout mice progress significantly faster to the hyperkinetic tonic-clonic phase and finally to tonic extension and death. Values denote means ± SEM (n = 7 for wild-type; n = 10 for knockout). P values from a Student's t test analysis are indicated.

To test this hypothesis, we investigated the response of the animals to intraperitoneal injections of pentamethylenetetrazole (metrazol), an epileptogenic $GABA_A$ receptor antagonist (Tecott et al., 1995). Increasing blood levels of the drug results in a series of well-defined responses that start with intermittent body twitches, leading to hyperkinetic tonic-clonic seizures and finally to a tonic extension and death. Whereas the time lag to the first neurological symptoms (first twitch) was comparable in both genotypes, knockout mice progressed significantly faster to the next two phases (tonic-clonic and tonic extension, respectively), demonstrating an increased propensity to seizures (Figure 7B).

Amphiphysin 1 Knockout Mice Exhibit Cognitive Defects

Considering the synaptic vesicle recycling defects revealed by our studies, the lack of impairment in nervous tissue function, besides occasional seizures, was puzzling. Behavioral tests were therefore performed to assess higher brain function. We first examined the spatial learning ability of amphiphysin 1 knockout mice using the Morris water maze task (Morris, 1989). Mice were trained on a task in which they searched for a hidden submerged platform in order to escape from water, using visual cues from the environment. The escape latency, recorded over several sessions, revealed a progressive improvement of the performance in all animals. However, a striking learning deficit in the mutant animals was detected (Figure 8A). After training in the hidden platform test, the transfer test in which mice were allowed to swim freely for 60 s following removal of the platform, was performed. A measurement of quadrant occupancy revealed that wild-type mice spent significantly more time in the quadrant where the platform had been originally located, whereas mutant mice did not (Figure 8C). Moreover, crossings of amphiphysin 1 knockout mice over the original platform location were significantly lower compared to wild-type animals (Figure 8D). No difference in path length was observed between the two genotypes (Figure 8E), indicating that swimming ability is not impaired in knockout mice. To rule out any differences in visual acuity, locomotor activity, or motivation, mice were trained on a visible platform test, in which the platform was placed above the surface of the water with a prominent "flag" attached to it. The escape latency was recorded over the course of 4 days. During this time, the performance of mice from both genotypes improved, although less dramatically in the case of mutant mice (Figure 8B). These results strongly suggest that amphiphysin 1 knockout mice exhibit deficits in learning that may not be only restricted to spatial learning.

To assess whether other forms of learning are impaired in mutant mice, we performed a fear-conditioning test (Paylor et al., 1994), which measures an amygdala-dependent form of associative emotional learning (reviewed in LeDoux, 2000). In this paradigm, an innocuous conditioned stimulus (tone) elicits fear response after being associatively paired with an aversive unconditioned stimulus (footshock). The fear response is measured by the frequency of freezing behaviors, which is defined as a stereotyped motionless crouching posture. Amphiphysin 1 knockout mice exhibited very mild fear responses in both the context test and the auditory cue test compared to their wild-type littermates. In contrast, the fear response generated by a novel context was comparable for both genotypes (Figure 8F). As a control, nociceptive reactions to footshocks were also investigated for both genotypes and were found to be comparable (data not shown). Altogether, our data indicate that amphiphysin 1 knockout mice exhibit major learning deficits, which are not restricted to spatial learning deficits.

Discussion

The results of this study show that in mammals amphiphysin function is required for efficient synaptic vesicle recycling. The data further demonstrate that a partial impairment of this process, and possibly of other membrane recycling pathways at the synapse, is compatible with the basic operation of the nervous system, although

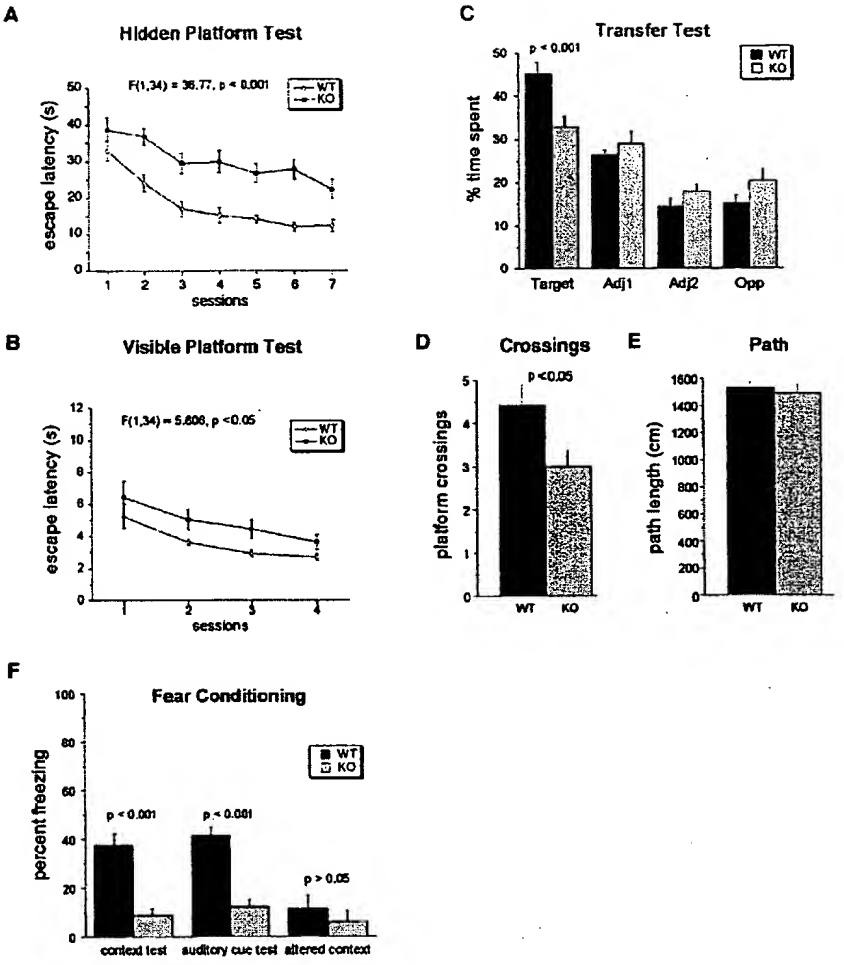

Figure 8. Amphiphysin 1 Knockout Mice Exhibit Learning Deficits in the Morris Water Maze Task (A–E) and in the Fear Conditioning Task (F)

5- to 7-month-old wild-type or knockout animals were used. All values denote means ± SEM.

(A) Learning curve indicating the time required to reach the hidden platform over seven days (n = 18 for each genotype). Statistical analysis was performed by two-way ANOVA for repeated measures.

(B) Latency to find the visible platform over the course of four sessions.

(C–E) Transfer test performance after the acquisition trials of the hidden platform task.

(C) Bars represent the time spent in the four quadrants (target, adjacent 1, adjacent 2, and opposite). Wild-type animals spent significantly more time in the quadrant that originally contained the platform than in each of the other quadrants. This was not the case for knockout animals.

(D) Number of crosses over the area that originally contained the platform during the transfer test were significantly lower for knockout animals relative to wild-type. P values from Mann-Whitney *U*-test are indicated.

(E) Path length (cm) during the transfer test. No statistical difference was observed between the two genotypes.

(F) Freezing responses in the fear conditioning test (n = 9 for each genotype). Amphiphysin 1 knockout mice exhibited significantly less freezing behavior than wild-type mice in both the context test and the auditory cue test. Comparable responses to altered context were observed for both genotypes. Statistical analysis was performed according to Student's t test, and p values are indicated.

it is associated with decreased viability and with defects in higher brain function.

At the molecular level, a striking consequence of the lack of amphiphysin 1 expression in brain was the nearly complete disappearance of amphiphysin 2. Since levels of amphiphysin 2 mRNA are unchanged in the brain of mutant mice, this phenomenon is likely to result from decreased stability of amphiphysin 2 and is consistent with the reported occurrence of amphiphysin 1 and 2 primarily as stable heterodimers in brain (Wigge et al., 1997a; Ramjaun et al., 1997; Slepnev et al., 1998). No downregulation of amphiphysin 2 occurs in skeletal muscle where this protein is normally expressed at very high levels without amphiphysin 1 (Butler et al., 1997). It remains to be determined whether the stability of this skeletal muscle isoform, which differs from the major

brain amphiphysin 2 isoform (Butler et al., 1997), is accounted for by its greater intrinsic resistance to proteolytic degradation or different proteolytic machinery in muscle, by heterodimerization with another BAR domain-containing protein, or by its localization in a subcellular compartment which protects it from high turnover.

The property to form dimers, which resides in the BAR domain, is a conserved feature in the amphiphysin family of proteins, since it also applies to yeast Rvs167, which heterodimerizes with Rvs161 (Navarro et al., 1997; Lombardi and Riezman, 2001). Furthermore, deletion of either the *RVS167* or the *RVS161* gene leads to a significant decrease in the half-life of the protein encoded by the other gene. Interestingly, overexpression of the Rvs161 protein in the *RVS167* knockout strain aggravates, rather than rescues the abnormal phenotype, indicating that the stoichiometry of interaction between related amphiphysin isoforms is a critical parameter for their function (Wigge et al., 1997a; Lombardi and Riezman, 2001).

Our biochemical results strongly support the hypothesis that one of the functions of brain amphiphysin is to act as a multifunctional adaptor connecting various cytosolic components of the endocytic machinery to each other and to the lipid bilayer (Takei et al., 1999). They suggest that amphiphysin may contribute to the recruitment of clathrin, AP-2, and synaptojanin 1 to the membrane. Moreover, although binding of dynamin to lipid bilayers was not dependent upon amphiphysin under our in vitro conditions, affinity purification experiments on the proline-rich tail of dynamin demonstrated that amphiphysin can indeed act as a bridge between clathrin coat components and dynamin. Thus, amphiphysin may help to coordinate the function of all these proteins at the membrane. Furthermore, the direct binding of dynamin to membrane in situ may undergo regulation, and a contribution of amphiphysin to dynamin recruitment in vivo cannot be ruled out.

The defects revealed by our cell-free approaches did not correlate with obvious morphological changes in mutant synapses. However, changes in the efficiency of synaptic vesicle recycling were demonstrated by a variety of physiological approaches after synapse stimulation. These include decreased uptake of extracellular tracers into small vesicles after an endocytic labeling pulse and a slower recycling time as demonstrated by a delay in styryl dye unloading, both during a prolonged stimulus (minimum repriming time) and after recovery from a stimulus (destaining kinetics). Consistent changes were observed both in synaptosomes and in synapses of cultured cortical neurons. Based on FM1-43 experiments in cultured neurons, the pool size of recycling synaptic vesicles also appeared to be smaller. This finding cannot merely be accounted for by a difference in the number of synaptic vesicles per synapse, based on both biochemical (comparable levels of synaptic proteins in brain homogenates) and morphometric results. Thus, the lack of amphiphysin seems to affect several stages of recycling. It seems likely, that although the kinetics of endocytosis is not perturbed (data not shown), the fate of vesicles endocytosed in the absence of amphiphysin is altered such that capacity for subsequent reuse of synaptic vesicles is diminished. This could arise for example if amphiphysin plays a role in mediating the correct sorting of components necessary for efficient postendocytic trafficking to the budding membrane. Although some data could also be explained by the occurrence of a partial defect in exocytosis (for example, the delay in dye unloading after stimulation), the normal glutamate release observed in synaptosomes argues against a significant impairment of this process. It remains possible that the upregulation of a putative "kiss-and-run" recycling pathway partially compensates for recycling defects in knockout animals and contributes to glutamate release stability during prolonged stimulation.

The complex recycling defects may be the results of adaptive changes triggered by an endocytic defect. They may also depend on actions of amphiphysin that are linked to its proposed, albeit not yet understood, function in actin cytoskeleton dynamics. Such a function is suggested by the severe disruption of actin cytoskeleton that is observed in *rvs167* and *rvs161* yeast mutants, in addition to endocytic defects (Sivadon et al., 1995; Lombardi and Riezman, 2001). So far, evidence for a role for amphiphysin in actin dynamics in mammalian cells is only indirect (Mundigl et al., 1998), but the putative role in actin function of some of its partners, dynamin and synaptojanin, support this possibility (Sakisaka et al., 1997; Gad et al., 2000; McNiven et al., 2000). Furthermore, the occurrence of amphiphysin 2 isoforms that lack clathrin and AP-2 binding sites points to functions of amphiphysin that are unrelated to the clathrin coat.

Interestingly, acute disruption of amphiphysin function at synapses of stimulated giant lamprey axons by microinjection either of peptides that bind specifically the SH3 domain of amphiphysin (Shupliakov et al., 1997) or of anti-lamprey amphiphysin antibodies (N. Tomilin, M. Marcucci, H. Gad, P. Löw, V. Slepnev, L. Brodin, P.D.C., and O. Shupliakov, unpublished data) produce more severe vesicle recycling defects than those reported here. Compensatory changes dependent upon the presence of proteins whose function is partially redundant with that of amphiphysin may explain the lack of a dramatic cellular phenotype in neurons of mice that develop in the absence of amphiphysin. It is of note that an acute antisense-mediated inhibition of amphiphysin 1 expression in cultured neurons results in major defects of neurite outgrowth (Mundigl et al., 1998), whereas this process occurs normally in mutant neurons. A puzzling observation is the lack of biochemical evidence for an interaction between amphiphysin and dynamin in *Drosophila* (Razzaq et al., 2001), where the synaptic dynamin interacting network seems to be at least partially different from the corresponding mammalian one (Roos and Kelly, 1998). In *Drosophila*, the single amphiphysin gene lacks clathrin and AP-2 binding sites and is abundantly expressed in skeletal muscle (Razzaq et al., 2001). Accordingly, amphiphysin-deficient flies predominantly show a muscle phenotype (Razzaq et al., 2001; Zelhof et al., 2001). In mammals, the presence of two neuronal isoforms of amphiphysin (amphiphysin 1 and the neuronal form of amphiphysin 2) in brain underlines their importance for nervous system function.

A striking observation is that the subtle vesicle recycling defects observed in amphiphysin 1 knockout mice produce important defects at the organismal levels.

While amphiphysin 1 knockout mice develop and reproduce normally, suggesting a basic normal functioning of the nervous system, some important neurological and behavioral defects were also observed. The death rate of mutant animals is significantly increased compared to normal littermates, in particular during the first few months of adulthood. Death was caused by rare irreversible seizures and, accordingly, mutant mice have a lower threshold to seizures. It was shown that synaptic depression during high-frequency stimulation occurs much faster at excitatory synapses than at inhibitory synapses, and this difference may be a critical mechanism protecting the nervous system from seizures (Galarreta and Hestrin, 1998; Varela et al., 1999; Kraushaar and Jonas, 2000). In turn, the remarkable stability of inhibitory synapses during ongoing stimulation is critically dependent upon the vesicle cycle, as shown by the loss of this stability in synaptojanin 1 knockout mice (Cremona et al., 1999; Lüthi et al., 2001). Thus, an increased susceptibility to seizures is consistent with the occurrence of a recycling defect in amphiphysin 1 knockout mice.

Another consequence of the lack of amphiphysin is a cognitive deficit, as defined by a significant impairment in learning tasks. Mutant animals exhibited severe learning disabilities in the Morris water maze test as well as in the fear-conditioning task, which rely on distinct neuronal circuitries. Although we cannot rule out that subthreshold seizures interfered with these experiments, it appears unlikely that seizure activity accounted for the defects observed. First, other knockout mouse models which experience severe seizures, such as synapsin 1 knockout mice, do not show impaired learning (Silva et al., 1996). Second, we used 5- to 7-month-old animals for our behavioral experiments, and we found that in this age category as well as in older animals, the death rate drops dramatically compared to younger adult animals. Since knockout animals die from seizures, we may have selected for our experiments a category of animals that is less prone to epilepsy.

Many mouse models with abnormal function of signaling pathways show learning deficits (Mayford and Kandel, 1999). A role of amphiphysin in signaling pathways cannot be excluded given the strong interconnections between endocytosis and signaling (Di Fiore and De Camilli, 2001; McPherson et al., 2001). Indeed some interactions of amphiphysin with signaling proteins have been reported (Kadlec and Pendergast, 1997; Leprince et al., 1997). Furthermore, in view of growing evidence for a critical role of clathrin-mediated endocytosis in the internalization of postsynaptic receptors (Turrigiano, 2000; Carroll et al., 2001; Kittler et al., 2000), it is possible that postsynaptic vesicle recycling changes may contribute to the cognitive defects of amphiphysin 1 knockout animals. However, we can at least conclude from our study that amphiphysin is indeed an effector in synaptic vesicle recycling and in the physiology of endocytic zones of mammalian synapses and that a perturbation of this function is likely to play a role in the cognitive deficits observed in mutant animals.

Several human conditions involve substantial cognitive defects that are not associated with major neurological impairments. In most cases, responsible genes have not yet been identified. An inherited mental retardation syndrome was mapped to the gene encoding a Rab GDP-dissociation inhibitor (GDI), a protein that controls the Rab cycle, and therefore the vesicle cycle, in nerve terminals and possibly also postsynaptically (D'Adamo et al., 1998). The learning defects observed in amphiphysin 1 knockout mice provide another example of a gene which functions in vesicle recycling and whose mutation underlies learning defects in a mammalian organism. Other human psychiatric conditions may be due to defects in membrane trafficking at the synapse.

Experimental Procedures

Generation of Amphiphysin 1 Knockout Mice

A λFIXII genomic library from 129SV/J mice was screened with a 250 bps DNA fragment corresponding to the 5′ end of the rat amphiphysin 1 cDNA. Phage clones containing the first coding exon of amphiphysin 1 gene were isolated and identified. A replacement targeting vector was constructed as shown in Figure 1A. In the targeting vector, most of the 3′ end of the first coding exon and a fragment of the following intron were replaced by the selection cassette (neomycin resistance gene under the PGK promoter [neo cassette]). The herpes simplex virus-1 thymidine kinase gene under the PGK promoter (TK cassette) was added at the end of the short arm of the construct. Both the neo and the TK cassette have a transcription direction that is the same as the amphiphysin 1 gene. The vector was linearized and electroporated into embryonic stem (ES) cells (129/Sv agouti ES cells) that were then selected according to standard procedures (Yang et al., 1997). Recombination events were identified by Southern blot screening using a PCR-generated probe corresponding to a fragment outside the recombination site but inside the restriction fragment generated by EcoRV digestion (Figure 1A). Chromosomal counting on recombinant ES cell clones was performed before blastocyst microinjection, in order to increase the chances of germline transmission. Positive clones were independently microinjected into blastocysts, which were then reimplanted into pseudopregnant foster mothers. Several chimeras were generated and independently bred with C57BL/6 mice. Germline transmission was achieved, and heterozygous animals were produced. Knockout mice were generated by successive breedings and identified by Southern blot analysis using the same screening strategy as for the identification of recombinant ES cell clones (Figure 1B). For Northern blot analysis, probes consisting of full length amphiphysin 2 and actin sequences, respectively, were obtained by PCR amplification from a mouse brain cDNA library and were labeled by random priming.

Antibodies, Immunoblotting, and Immunofluorescence

Brains from wild-type and knockout mice were homogenized in a lysis buffer containing 25 mM HEPES (pH 7.4), 150 mM KCl, 2 mM EGTA supplemented with a cocktail of proteinase inhibitors. Postnuclear supernatants (50 μg) were processed for SDS-PAGE and immunoblotting using ECL procedures (Amersham Pharmacia Biotech, Inc., Piscataway, NJ). The following antibodies were generated in our lab: rabbit antisera to synaptojanin 1, amphiphysin 1 and 2, endophilin 1, synaptophysin, as well as mouse mAb to amphiphysin 1 and AP180. Other antibodies are from commercial sources: Bin 1 (Upstate Biotechnology, Lake Placid, NY), dynamin 1 (Transduction Laboratories, Lexington, KT), α-adaptin (Affinity BioReagents, Golden, CO), a mouse hybridoma producing antibodies to clathrin heavy chain (ATCC, Rockville, MD), and α-tubulin (Sigma, St. Louis, MO). The mAb to synaptotagmin was a kind gift from Dr. R. Jahn (University of Göttingen, Germany). Immunofluorescence was performed on 2- to 3-week-old cultures of cortical neurons as previously described (Mundigl et al., 1998).

Biochemical Procedures

The experiment using liposomes was performed as previously described (Cremona et al., 1999; Gad et al., 2000). Quantification was performed using a phosphoimaging. For the lipid experiment, liposomes (0.25 mg/ml) were incubated with brain cytosol (0.5 mg/ml) for 15 min at 37°C in the presence of 2 mM ATP and 0.2 mM GTP.

Liposomes were then isolated by ultracentrifugation, washed three times, and incubated in the presence of 20 μCi [γ^{32}P]ATP for 10 min at 37°C. Lipids were extracted and processed for analysis by thin layer chromatography, and the identity of lipids was confirmed by high performance liquid chromatography as described previously (Cremona et al., 1999). Using phosphoimaging, counts for PI(4,5)P2 were normalized to total counts, which mainly included those of phosphatidic acid. The affinity chromatography using GST fused to the proline-rich region of dynamin was performed as in Slepnev et al. (1998), with slight modifications. 15 mg detergent extracts from wild-type and knockout brains were incubated for 4 hr at 4°C in the presence of 0.8 mg GST or GST fused to the proline-rich region of human dynamin 1 prebound to 150 μl Sepharose 4B beads (Amersham Pharmacia Biotech, Inc., Piscataway, NJ) in a buffer containing 25 mM HEPES (pH 7.4), 150 mM KCl, 1 mM EGTA, 1% Triton X-100, and a cocktail of protease inhibitors. In one experimental condition, 15 mg knockout extract were supplemented with 30 μg purified recombinant amphiphysin 1 prior to affinity chromatography. Following five washes with the same buffer, proteins were eluted in sample buffer and processed for immunoblotting.

FM2-10 Uptake in Synaptosomes

Synaptosomes were prepared from four mouse cortices as previously described (Marks and McMahon, 1998). For each experiment, 500 μg synaptosomes were used. In the "unloading" experiment, synaptosomes were incubated for 5 min at 37°C in low K^+ saline solution prior to transfer to the 1 ml cuvette preheated at 37°C in a Hitachi F-3010 fluorimeter. Synaptosomes were preincubated for 3 min with FM2-10 (Molecular Probes, Inc., Eugene, OR) at 100 μM final concentration and stimulated with 30 mM KCl for 90 s. Synaptosomes were washed twice with 1 ml low K^+ saline solution containing 1 mg/ml BSA, resuspended in low K^+ buffer, and transferred back to the cuvette. Following a 10 min incubation, a second stimulation with 30 mM KCl was applied, and fluorescence was measured at 467/550 nm as a function of time. In the FM2-10 internalization experiment, a similar protocol was used except that, following the first stimulation with 30 mM KCl and the washes, synaptosomes were lysed in a hypotonic solution containing 20 mM HEPES (pH 7.4), vortexed for 10 s, supplemented with KCl to 150 mM final concentration, and centrifuged for 2 min in a microfuge at maximal speed. Fluorescence associated with the supernatant, containing FM2-10 labeled internal membranes, was subsequently measured with the fluorimeter. The glutamate release was performed as previously described (Nicholls and Sihra, 1986).

Electron Microscopy and Morphometry of HRP-Labeled Cortical Neurons in Culture

Primary cultures of cortical neurons were prepared according to procedures previously described (Banker and Goslin, 1991; Cremona et al., 1999). Cells were maintained up to 3 weeks in Neurobasal/B27 medium (Life Technologies/Gibco-BRL, Gaithersburg, MD) at 37°C in a 5% CO_2 humidified incubator. Neurons were labeled with the fluid-phase marker HRP (Sigma, St Louis, MO) at 10 mg/ml for 3 min at 37°C before stimulation in a low K^+ saline solution containing 130 mM NaCl, 5 mM KCl, 2 mM $CaCl_2$, 2 mM $MgCl_2$, 25 mM HEPES (pH 7.33), 30 mM glucose, 10 μM CNQX, and 50 μM AP-V (Research Biochemicals, Inc., Natick, MA). Neurons were then either kept in low K^+ for another 90 s ("rest") or stimulated for 90 s with a solution containing 90 mM KCl and 45 mM NaCl in the presence of HRP ("stimulation"). Cells were fixed in 2% glutaraldehyde/2% sucrose in 0.1M sodium phosphate buffer (pH 7.4) for 2 hr at 4°C and processed for electron microscopy as described (Cremona et al., 1999). For morphometry, 37–54 synapses were analyzed at a final magnification of 63,000×. For each condition, 2000–4000 objects were scored. They included labeled or unlabeled synaptic vesicles and clathrin-coated vesicles as well as labeled endosome-like structures. Endosome-like structures were defined as HRP-labeled compartment larger than synaptic vesicles. Statistics were performed using ANOVA. Results of two independent experiments were pooled.

FM1-43 Uptake and Release in Cultured Cortical Neurons

Cortical cultures were generated from 1- to 2-day-old amphiphysin 1 knockout and wild-type mice. Brains were dissected; cerebral cortices were separated from the hippocampus and basal ganglia and dissociated using protocols similar to those used for hippocampal cultures (Ryan, 1999). Confocal laser scanning microscopy, electrical field stimulation, FM1-43 uptake, and release experiments were performed as described (Ryan, 1999) in 2- to 3-week-old cultures. FM1-43 (Molecular Probes, Eugene, OR) was stored at 4°C as 3 mM aliquots and used at a final concentration of 15 μM.

Metrazol Injection

12-week-old mice were injected intraperitoneally with a solution of pentamethylenetetrazole at 15 mg/kg every 5 min until observation of the last phase of seizure. The time required to reach the various phases of seizure was recorded. The first twitch was generally detectable in the ear; the tonic-clonic phase was defined as repeated hyperkinetic movements of forelimbs followed by a loss of postural control and falling, after which both the forelimbs and hindlimbs were characterized by clonic movements; the tonic extension phase began when animals arched their body and their limbs, after which, in most cases, they stopped breathing and died. Seven wild-type and ten knockout mice were used for the experiment. Statistics were performed using ANOVA.

Behavioral Paradigms

The Morris water maze test was performed as described previously (Morris, 1989; Wickman et al., 2000). In total, 18 mice (nine males, nine females) of 5–7 months of age were used for the experiments for both wild-type and knockout genotypes. A circular white plastic tub 1 min in diameter was filled with water (21°–22°C) and divided into four quadrants of equal surface. Swim times, path length, and all other measurements were made using the Poly-track Video Tracking System (San Diego Instruments). For the hidden platform test, a 10 cm^2 transparent Plexiglas platform was submerged 0.5 cm beneath the surface and positioned consistently over the course of the test. Mice were allowed to swim until they encountered the platform or for a maximal duration of 60 s, after which they were placed on the platform for 15 s. Mice began each of the four daily trials from a different quadrant, and the time required to find the platform was recorded and averaged. The intertrial interval was 3.5 min. The test was performed for 7 consecutive days, always in the afternoon. On day 8, the transfer test was performed. Briefly, the platform was removed, and mice were allowed to swim for 60 s, starting from the center of the pool. The time spent in every quadrant, the number of entries into the area where the platform had been originally located, and the swimming distance were measured. On days 9–12, in the visible platform test, trials were performed like in the hidden platform test, except that the platform was flagged.

The fear-conditioning test was performed as described (Paylor et al., 1994; Caldarone et al., 2000). In total, nine mice (five males, four females) of 5–7 months of age were used for the experiments for both wild-type and knockout genotypes. On the first day of training, each mouse was placed in a training chamber and freezing behavior was assessed every 10 s. After 2 min, the conditioned stimulus, a tone, was applied for 30 s and terminated by a 2 s unconditioned stimulus, a footshock of 0.5 mA. This sequence was repeated a second time, after which animals were kept for 30 s in the chamber and returned to their original cages. On the second day, animals were first tested for contextual fear. Each mouse was placed in the training chamber, and freezing behavior was assessed for 5 min in the absence of tone. One hour later, animals were tested for their fear response to the auditory stimulus. Each mouse was placed in a different training chamber and exposed to a smell of orange extract. During the first 3 min, freezing to altered context was measured, after which the tone was continuously presented for another 3 min, and freezing behavior to the auditory stimulus was scored.

Acknowledgments

We would like to thank David A. McCormick, Anita Lüthi, and Fabio Benfenati for helpful discussions and preliminary work; Lijuan Liu and Wayne Yan for excellent technical assistance; Khashayar Farsad, Sergei Voronov, Raani Punglia, and Sarah L. King for help at various stages of the study; and Reinhard Jahn (Gottingen, Germany) for the kind gift of antibodies. This work was supported in

part by National Institutes of Health grants (NS36251 and CA46128) and a grant from the United States Army Medical Research and Development Command to P.D.C., by NIH grants to T.A.R. (NS24692 and GM61925) and to M.R.P. (DA00436 and MH25642), by Telethon (project D.11) and COFIN2000 grants to O.C. T.A.R. is an Alfred P. Sloan Research Fellow.

Received August 6, 2001; revised January 9, 2002.

References

Banker, G.A., and Goslin, K. (1991). Culturing Nerve Cells (Cambridge, MA: MIT Press).

Bauerfeind, R., Takei, K., and De Camilli, P. (1997). Amphiphysin I is associated with coated endocytic intermediates and undergoes stimulation-dependent dephosphorylation in nerve terminals. J. Biol. Chem. *272*, 30984–30992.

Brodin, L., Low, P., and Shupliakov, O. (2000). Sequential steps in clathrin-mediated synaptic vesicle endocytosis. Curr. Opin. Neurobiol. *10*, 312–320.

Burger, K.N., Demel, R.A., Schmid, S.L., and de Kruijff, B. (2000). Dynamin is membrane-active: lipid insertion is induced by phosphoinositides and phosphatidic acid. Biochemistry *39*, 12485–12493.

Butler, M.H., David, C., Ochoa, G.C., Freyberg, Z., Daniell, L., Grabs, D., Cremona, O., and De Camilli, P. (1997). Amphiphysin II (SH3P9; BIN1), a member of the amphiphysin/Rvs family, is concentrated in the cortical cytomatrix of axon initial segments and nodes of ranvier in brain and around T tubules in skeletal muscle. J. Cell Biol. *137*, 1355–1367.

Caldarone, B.J., Duman, C.H., and Picciotto, M.R. (2000). Fear conditioning and latent inhibition in mice lacking the high affinity subclass of nicotinic acetylcholine receptors in the brain. Neuropharmacology *39*, 2779–2784.

Carroll, R.C., Beattie, E.C., von Zastrow, M., and Malenka, R.C. (2001). Role of AMPA receptor endocytosis in synaptic plasticity. Nat. Rev. Neurosci. *2*, 315–324.

Cousin, M.A., and Robinson, P.J. (1998). Ba^{2+} does not support synaptic vesicle retrieval in rat cerebrocortical synaptosomes. Neurosci. Lett. *253*, 1–4.

Cousin, M.A., and Robinson, P.J. (2000). Two mechanisms of synaptic vesicle recycling in rat brain nerve terminals. J. Neurochem. *75*, 1645–1653.

Cremona, O., and De Camilli, P. (1997). Synaptic vesicle endocytosis. Curr. Opin. Neurobiol. *7*, 323–330.

Cremona, O., Di Paolo, G., Wenk, M.R., Luthi, A., Kim, W.T., Takei, K., Daniell, L., Nemoto, Y., Shears, S.B., Flavell, R.A., et al. (1999). Essential role of phosphoinositide metabolism in synaptic vesicle recycling. Cell *99*, 179–188.

Crouzet, M., Urdaci, M., Dulau, L., and Aigle, M. (1991). Yeast mutant affected for viability upon nutrient starvation: characterization and cloning of the RVS161 gene. Yeast *7*, 727–743.

D'Adamo, P., Menegon, A., Lo Nigro, C., Grasso, M., Gulisano, M., Tamanini, F., Bienvenu, T., Gedeon, A.K., Oostra, B., Wu, S.K., et al. (1998). Mutations in GDI1 are responsible for X-linked non-specific mental retardation. Nat. Genet. *19*, 134–139.

David, C., McPherson, P.S., Mundigl, O., and De Camilli, P. (1996). A role of amphiphysin in synaptic vesicle endocytosis suggested by its binding to dynamin in nerve terminals. Proc. Natl. Acad. Sci. USA *93*, 331–335.

De Camilli, P., Thomas, A., Cofiell, R., Folli, F., Lichte, B., Piccolo, G., Meinck, H.M., Austoni, M., Fassetta, G., Bottazzo, G., et al. (1993). The synaptic vesicle-associated protein amphiphysin is the 128-kD autoantigen of Stiff-Man syndrome with breast cancer. J. Exp. Med. *178*, 2219–2223.

Di Fiore, P.P., and De Camilli, P. (2001). Endocytosis and signaling. Cell *106*, 1–4.

Dunaevsky, A., and Connor, E.A. (2000). F-actin is concentrated in nonrelease domains at frog neuromuscular junctions. J. Neurosci. *20*, 6007–6012.

Elliott, K., Sakamuro, D., Basu, A., Du, W., Wunner, W., Staller, P., Gaubatz, S., Zhang, H., Prochownik, E., Eilers, M., and Prendergast, G.C. (1999). Bin1 functionally interacts with Myc and inhibits cell proliferation via multiple mechanisms. Oncogene *18*, 3564–3573.

Farsad, K., Ringstad, N., Takei, K., Floyd, S.R., Rose, K., and De Camilli, P. (2001). Generation of high curvature membranes mediated by direct endophilin bilayer interactions. J. Cell Biol. *155*, 193–200.

Gad, H., Low, P., Zotova, E., Brodin, L., and Shupliakov, O. (1998). Dissociation between Ca^{2+}-triggered synaptic vesicle exocytosis and clathrin-mediated endocytosis at a central synapse. Neuron *21*, 607–616.

Gad, H., Ringstad, N., Low, P., Kjaerulff, O., Gustafsson, J., Wenk, M., Di Paolo, G., Nemoto, Y., Crun, J., Ellisman, M.H., et al. (2000). Fission and uncoating of synaptic clathrin-coated vesicles are perturbed by disruption of interactions with the SH3 domain of endophilin. Neuron *27*, 301–312.

Galarreta, M., and Hestrin, S. (1998). Frequency-dependent synaptic depression and the balance of excitation and inhibition in the neocortex. Nat. Neurosci. *1*, 587–594.

Ge, K., and Prendergast, G.C. (2000). Bin2, a functionally nonredundant member of the BAR adaptor gene family. Genomics *67*, 210–220.

Geli, M.I., and Riezman, H. (1998). Endocytic internalization in yeast and animal cells: similar and different. J. Cell Sci. *111*, 1031–1037.

Harris, T.W., Hartwieg, E., Horvitz, H.R., and Jorgensen, E.M. (2000). Mutations in synaptojanin disrupt synaptic vesicle recycling. J. Cell Biol. *150*, 589–600.

Heuser, J.E., and Reese, T.S. (1973). Evidence for recycling of synaptic vesicle membrane during transmitter release at the frog neuromuscular junction. J. Cell Biol. *57*, 315–344.

Hussain, N.K., Jenna, S., Glogauer, M., Quinn, C.C., Wasiak, S., Guipponi, M., Antonarakis, S.E., Kay, B.K., Stossel, T.P., Lamarche-Vane, N., and McPherson, P.S. (2001). Endocytic protein intersectin-l regulates actin assembly via Cdc42 and N-WASP. Nat. Cell Biol. *3*, 927–932.

Kadlec, L., and Pendergast, A.M. (1997). The amphiphysin-like protein 1 (ALP1) interacts functionally with the cABL tyrosine kinase and may play a role in cytoskeletal regulation. Proc. Natl. Acad. Sci. USA *94*, 12390–12395.

Kittler, J.T., Delmas, P., Jovanovic, J.N., Brown, D.A., Smart, T.G., and Moss, S.J. (2000). Constitutive endocytosis of GABAA receptors by an association with the adaptin AP2 complex modulates inhibitory synaptic currents in hippocampal neurons. J. Neurosci. *20*, 7972–7977.

Kraushaar, U., and Jonas, P. (2000). Efficacy and stability of quantal GABA release at a hippocampal interneuron-principal neuron synapse. J. Neurosci. *20*, 5594–5607.

LeDoux, J.E. (2000). Emotion circuits in the brain. Annu. Rev. Neurosci. *23*, 155–184.

Leprince, C., Romero, F., Cussac, D., Vayssiere, B., Berger, R., Tavitian, A., and Camonis, J.H. (1997). A new member of the amphiphysin family connecting endocytosis and signal transduction pathways. J. Biol. Chem. *272*, 15101–15105.

Leventis, P.A., Chow, B.M., Stewart, B.A., Iyengar, B., Campos, A.R., and Boulianne, G.L. (2001). Drosophila amphiphysin is a post-synaptic protein required for normal locomotion but not endocytosis. Traffic *2*, 839–850.

Lombardi, R., and Riezman, H. (2001). Rvs161p and Rvs167p, the two yeast amphiphysin homologs, function together in vivo. J. Biol. Chem. *276*, 6016–6022.

Lüthi, A., Di Paolo, G., Cremona, O., Daniell, L., De Camilli, P., and McCormick, D.A. (2001). Synaptojanin 1 contributes to maintaining the stability of GABAergic transmission in primary cultures of cortical neurons. J. Neurosci. *21*, 9101–9111.

Marks, B., and McMahon, H.T. (1998). Calcium triggers calcineurin-dependent synaptic vesicle recycling in mammalian nerve terminals. Curr. Biol. *8*, 740–749.

Marsh, M., and McMahon, H.T. (1999). The structural era of endocytosis. Science *285*, 215–220.

Mayford, M., and Kandel, E.R. (1999). Genetic approaches to memory storage. Trends Genet. *15*, 463–470.

McMahon, H.T., Wigge, P., and Smith, C. (1997). Clathrin interacts specifically with amphiphysin and is displaced by dynamin. FEBS Lett. *413*, 319–322.

McNiven, M.A., Kim, L., Krueger, E.W., Orth, J.D., Cao, H., and Wong, T.W. (2000). Regulated interactions between dynamin and the actin-binding protein cortactin modulate cell shape. J. Cell Biol. *151*, 187–198.

McPherson, P.S., Garcia, E.P., Slepnev, V.I., David, C., Zhang, X., Grabs, D., Sossin, W.S., Bauerfeind, R., Nemoto, Y., and De Camilli, P. (1996). A presynaptic inositol-5-phosphatase. Nature *379*, 353–357.

McPherson, P.S., Kay, B.K., and Hussain, N.K. (2001). Signaling on the endocytic pathway. Traffic *2*, 375–384.

Modregger, J., Ritter, B., Witter, B., Paulsson, M., and Plomann, M. (2000). All three PACSIN isoforms bind to endocytic proteins and inhibit endocytosis. J. Cell Sci. *113*, 4511–4521.

Morris, R.G. (1989). Synaptic plasticity and learning: selective impairment of learning rats and blockade of long-term potentiation in vivo by the N-methyl-D-aspartate receptor antagonist AP5. J. Neurosci. *9*, 3040–3057.

Mundigl, O., Ochoa, G.C., David, C., Slepnev, V.I., Kabanov, A., and De Camilli, P. (1998). Amphiphysin I antisense oligonucleotides inhibit neurite outgrowth in cultured hippocampal neurons. J. Neurosci. *18*, 93–103.

Navarro, P., Durrens, P., and Aigle, M. (1997). Protein-protein interaction between the RVS161 and RVS167 gene products of Saccharomyces cerevisiae. Biochim. Biophys. Acta *1343*, 187–192.

Nicholls, D.G., and Sihra, T.S. (1986). Synaptosomes possess an exocytotic pool of glutamate. Nature *321*, 772–773.

Ochoa, G.C., Slepnev, V.I., Neff, L., Ringstad, N., Takei, K., Daniell, L., Kim, W., Cao, H., McNiven, M., Baron, R., and De Camilli, P. (2000). A functional link between dynamin and the actin cytoskeleton at podosomes. J. Cell Biol. *150*, 377–389.

Owen, D.J., and Luzio, J.P. (2000). Structural insights into clathrin-mediated endocytosis. Curr. Opin. Cell Biol. *12*, 467–474.

Owen, D.J., Wigge, P., Vallis, Y., Moore, J.D., Evans, P.R., and McMahon, H.T. (1998). Crystal structure of the amphiphysin-2 SH3 domain and its role in the prevention of dynamin ring formation. EMBO J. *17*, 5273–5285.

Paylor, R., Tracy, R., Wehner, J., and Rudy, J.W. (1994). DBA/2 and C57BL/6 mice differ in contextual fear but not auditory fear conditioning. Behav. Neurosci. *108*, 810–817.

Qualmann, B., Roos, J., DiGregorio, P.J., and Kelly, R.B. (1999). Syndapin I, a synaptic dynamin-binding protein that associates with the neural Wiskott-Aldrich syndrome protein. Mol. Biol. Cell *10*, 501–513.

Qualmann, B., Kessels, M.M., and Kelly, R.B. (2000). Molecular links between endocytosis and the actin cytoskeleton. J. Cell Biol. *150*, F111–F116.

Ramjaun, A.R., and McPherson, P.S. (1998). Multiple amphiphysin II splice variants display differential clathrin binding: identification of two distinct clathrin-binding sites. J. Neurochem. *70*, 2369–2376.

Ramjaun, A.R., Micheva, K.D., Bouchelet, I., and McPherson, P.S. (1997). Identification and characterization of a nerve terminal-enriched amphiphysin isoform. J. Biol. Chem. *272*, 16700–16706.

Ramjaun, A.R., Philie, J., de Heuvel, E., and McPherson, P.S. (1999). The N terminus of amphiphysin II mediates dimerization and plasma membrane targeting. J. Biol. Chem. *274*, 19785–19791.

Razzaq, A., Su, Y., Mehren, J.E., Mizuguchi, K., Jackson, A.P., Gay, N.J., and O'Kane, C.J. (2000). Characterisation of the gene for Drosophila amphiphysin. Gene *241*, 167–174.

Razzaq, A., Robinson, I.M., McMahon, H.T., Skepper, J.N., Su, Y., Zelhof, A.C., Jackson, A.P., Gay, N.J., and O'Kane, C.J. (2001). Amphiphysin is necessary for organization of the excitation-contraction coupling machinery of muscles, but not for synaptic vesicle endocytosis in Drosophila. Genes Dev. *15*, 2967–2979.

Roos, J., and Kelly, R.B. (1998). Dap160, a neural-specific Eps15 homology and multiple SH3 domain- containing protein that interacts with Drosophila dynamin. J. Biol. Chem. *273*, 19108–19119.

Roos, J., and Kelly, R.B. (1999). The endocytic machinery in nerve terminals surrounds sites of exocytosis. Curr. Biol. *9*, 1411–1414.

Routhier, E.L., Burn, T.C., Abbaszade, I., Summers, M., Albright, C.F., and Prendergast, G.C. (2001). Human BIN3 complements the F-actin localization defects caused by loss of Hob3p, the fission yeast homolog of Rvs161p. J. Biol. Chem. *276*, 21670–21677.

Ryan, T.A. (1999). Inhibitors of myosin light chain kinase block synaptic vesicle pool mobilization during action potential firing. J. Neurosci. *19*, 1317–1323.

Ryan, T.A., and Smith, S.J. (1995). Vesicle pool mobilization during action potential firing at hippocampal synapses. Neuron *14*, 983–989.

Sakisaka, T., Itoh, T., Miura, K., and Takenawa, T. (1997). Phosphatidylinositol 4,5-bisphosphate phosphatase regulates the rearrangement of actin filaments. Mol. Cell. Biol. *17*, 3841–3849.

Shupliakov, O., Low, P., Grabs, D., Gad, H., Chen, H., David, C., Takei, K., De Camilli, P., and Brodin, L. (1997). Synaptic vesicle endocytosis impaired by disruption of dynamin-SH3 domain interactions. Science *276*, 259–263.

Silva, A.J., Rosahl, T.W., Chapman, P.F., Marowitz, Z., Friedman, E., Frankland, P.W., Cestari, V., Cioffi, D., Sudhof, T.C., and Bourtchuladze, R. (1996). Impaired learning in mice with abnormal short-lived plasticity. Curr. Biol. *6*, 1509–1518.

Sivadon, P., Bauer, F., Aigle, M., and Crouzet, M. (1995). Actin cytoskeleton and budding pattern are altered in the yeast rvs161 mutant: The Rvs161 protein shares common domains with the brain protein amphiphysin. Mol. Gen. Genet. *246*, 485–495.

Slepnev, V.I., and De Camilli, P. (2000). Accessory factors in clathrin-dependent synaptic vesicle endocytosis. Nat. Rev. Neurosci. *1*, 161–172.

Slepnev, V.I., Ochoa, G.C., Butler, M.H., Grabs, D., and De Camilli, P. (1998). Role of phosphorylation in regulation of the assembly of endocytic coat complexes. Science *281*, 821–824.

Slepnev, V.I., Ochoa, G.C., Butler, M.H., and De Camilli, P. (2000). Tandem arrangement of the clathrin and AP-2 binding domains in amphiphysin 1 and disruption of clathrin coat function by amphiphysin fragments comprising these sites. J. Biol. Chem. *275*, 17583–17589.

Takei, K., Slepnev, V.I., Haucke, V., and De Camilli, P. (1999). Functional partnership between amphiphysin and dynamin in clathrin-mediated endocytosis. Nat. Cell Biol. *1*, 33–39.

Tecott, L.H., Sun, L.M., Akana, S.F., Strack, A.M., Lowenstein, D.H., Dallman, M.F., and Julius, D. (1995). Eating disorder and epilepsy in mice lacking 5-HT2c serotonin receptors. Nature *374*, 542–546.

Teng, H., and Wilkinson, R.S. (2000). Clathrin-mediated endocytosis near active zones in snake motor boutons. J. Neurosci. *20*, 7986–7993.

Turrigiano, G.G. (2000). AMPA receptors unbound: membrane cycling and synaptic plasticity. Neuron *26*, 5–8.

Varela, J.A., Song, S., Turrigiano, G.G., and Nelson, S.B. (1999). Differential depression at excitatory and inhibitory synapses in visual cortex. J. Neurosci. *19*, 4293–4304.

Wasiak, S., Quinn, C.C., Ritter, B., de Heuvel, E., Baranes, D., Plomann, M., and McPherson, P.S. (2001). The Ras/Rac guanine nucleotide exchange factor mammalian Son-of-sevenless interacts with PACSIN 1/syndapin I, a regulator of endocytosis and the actin cytoskeleton. J. Biol. Chem. *276*, 26622–26628.

Wechsler-Reya, R., Sakamuro, D., Zhang, J., Duhadaway, J., and Prendergast, G.C. (1997). Structural analysis of the human BIN1 gene. Evidence for tissue- specific transcriptional regulation and alternate RNA splicing. J. Biol. Chem. *272*, 31453–31458.

Wickman, K., Karschin, C., Karschin, A., Picciotto, M.R., and Clapham, D.E. (2000). Brain localization and behavioral impact of the

G-protein-gated K+ channel subunit GIRK4. J. Neurosci. *20*, 5608–5615.

Wigge, P., and McMahon, H.T. (1998). The amphiphysin family of proteins and their role in endocytosis at the synapse. Trends Neurosci. *21*, 339–344.

Wigge, P., Kohler, K., Vallis, Y., Doyle, C.A., Owen, D., Hunt, S.P., and McMahon, H.T. (1997a). Amphiphysin heterodimers: potential role in clathrin-mediated endocytosis. Mol. Biol. Cell *8*, 2003–2015.

Wigge, P., Vallis, Y., and McMahon, H.T. (1997b). Inhibition of receptor-mediated endocytosis by the amphiphysin SH3 domain. Curr. Biol. *7*, 554–560.

Witke, W., Podtelejnikov, A.V., Di Nardo, A., Sutherland, J.D., Gurniak, C.B., Dotti, C., and Mann, M. (1998). In mouse brain profilin I and profilin II associate with regulators of the endocytic pathway and actin assembly. EMBO J. *17*, 967–976.

Yang, D., Tournier, C., Wysk, M., Lu, H.T., Xu, J., Davis, R.J., and Flavell, R.A. (1997). Targeted disruption of the MKK4 gene causes embryonic death, inhibition of c-Jun NH2-terminal kinase activation, and defects in AP-1 transcriptional activity. Proc. Natl. Acad. Sci. USA *94*, 3004–3009.

Zelhof, A.C., Bao, H., Hardy, R.W., Razzaq, A., Zhang, B., and Doe, C.Q. (2001). Drosophila Amphiphysin is implicated in protein localization and membrane morphogenesis but not in synaptic vesicle endocytosis. Development *128*, 5005–5015.

Neuron, Vol. 39, 163–176, July 3, 2003, Copyright ©2003 by Cell Press

Synaptic Transmission and Plasticity in the Absence of AMPA Glutamate Receptor GluR2 and GluR3

Yanghong Meng,[1,3] Yu Zhang,[1,3] and Zhengping Jia[1,2,*]
[1]Program in Brain and Behavior
The Hospital for Sick Children
555 University Avenue
Toronto, Ontario M5G 1X8
[2]Department of Physiology
University of Toronto
Toronto, Ontario M5S 1A8
Canada

Summary

The AMPA glutamate receptor (AMPAR) subunits GluR2 and GluR3 are thought to be important for synaptic targeting/stabilization of AMPARs and the expression of hippocampal long-term depression (LTD). In order to address this hypothesis genetically, we generated and analyzed knockout mice deficient in the expression of both GluR2 and GluR3. We show here that the double knockout mice are severely impaired in basal synaptic transmission, demonstrating that GluR2/3 are essential to maintain adequate synaptic transmission in vivo. However, these mutant mice are competent in establishing several forms of long-lasting synaptic changes in the CA1 region of the hippocampus, including LTD, long-term potentiation (LTP), depotentiation, and dedepression, indicating the presence of GluR2/3-independent mechanisms of LTD expression and suggesting that AMPA receptor GluR1 alone is capable of various forms of synaptic plasticity.

Introduction

AMPA glutamate receptors (AMPARs) are the principle mediators of the fast excitatory synaptic transmission in the mammalian central nervous system (CNS), and they are important for the expression of several forms of long-lasting synaptic plasticity, including LTP and LTD, extensively studied forms of synaptic plasticity thought to be critical to learning and memory (Bliss and Collingridge, 1993; Malenka and Nicoll, 1999; Bear and Abraham, 1996). In the CA1 region of the hippocampus, while the induction of LTP and LTD requires activation of NMDA receptors (NMDARs) and the subsequent calcium influx, the expression mechanisms appear much more complex, possibly involving both presynaptic and postsynaptic modifications. However, recent studies indicate that activity-dependent AMPAR insertion and internalization at the postsynaptic membrane play a critical role in the expression of LTP and LTD, respectively (Shi et al., 1999; 2001; Hayashi et al., 2000; Carroll et al., 1999; 2001; Beattie et al., 2000; Lin et al., 2000; Man et al., 2000; Wang and Linden, 2000). Thus, regulation of AMPAR trafficking may represent a key mechanism for the modification of synaptic efficacy (Luscher et al., 2000; Malinow and Malenka, 2002)

AMPARs are heteromeric complexes assembled from four distinct subunits GluR1–GluR4 (also referred to as GluRA–GluRD) encoded by four separate genes (Hollmann and Heinemann, 1994). Several studies suggest that these receptor subunits may play distinct roles in the regulation of AMPAR trafficking and synaptic plasticity. For example, the GluR1 subunit is required for NMDAR-dependent synaptic delivery of AMPARs, a process thought to be responsible for adding new receptors to increase synaptic transmission during LTP (Shi et al., 1999; 2001; Hayashi et al., 2000; Passafaro et al., 2001). In contrast, the GluR2/3 subunits are thought to be important for activity-independent movements of AMPARs, a constitutive process thought to be essential for stable basal synaptic responses (Shi et al., 2001; Passafaro et al., 2001). Although the molecular mechanisms underlying these subunit-specific functions are unknown, the protein-protein interactions between the AMPAR subunits and adjacent postsynaptic proteins may play an important role (see reviews by Barry and Ziff, 2002; Song and Huganir, 2002; Sheng and Kim, 2002).

Ample biochemical studies indicate that the C-terminal tails of the GluR2/3 subunits can selectively interact with a number of intracellular proteins (e.g., GRIP1, ABP, NSF, and PICK1) and that these interactions are important for targeting and accumulating GluR2-containing AMPARs at specific subcellular sites, either at the postsynaptic membrane or inside the cell (Dong et al., 1997; 1999; Nishimune et al., 1998; Osten et al., 1998, 2000; Srivastava et al., 1998; Song et al., 1998; Dev et al., 1999; Xia et al., 1999; Perez et al., 2001). Consistent with these biochemical data, postsynaptic injection of synthetic peptides designed to disrupt protein interactions between GluR2 and AMPAR-interacting proteins causes a rapid and selective change in AMPAR-mediated synaptic responses (Nishimune et al., 1998; Noel et al., 1999; Luscher et al., 1999; Luthi et al., 1999; Daw et al., 2000; Lee et al., 2002). Furthermore, some of these peptides or deletions of the C-terminal tail of GluR2 also interfere with activity-dependent AMPAR internalization and the expression of LTD both in the hippocampus and cerebellum (Luscher et al., 1999; Luthi et al., 1999; Daw et al., 2000; Xia et al., 2000; Lin et al., 2000; Lee et al., 2002). Therefore, it has been hypothesized that the expression of hippocampal LTD and AMPAR internalization from the postsynaptic surface involve interactions between GluR2/3 and AMPAR-interacting proteins (Kullmann, 1999; Luthi et al., 1999; Daw et al., 2000; Xia et al., 2000).

In this study, we took genetic approaches to address the in vivo function of GluR2/3 in synaptic regulation by conducting hippocampal slice recordings in three genetically manipulated mouse strains. First, as an extension to our previous studies (Jia et al., 1996), we analyzed LTD and depotentiation in knockout mice lacking GluR2 and found that both LTD and depotentiation could be established in these mice. Since GluR3 is closely related to GluR2 in the protein sequence and in

*Correspondence: jia@sickkids.ca
[3]These authors contributed equally to this work.

fact GluR3 can interact with a number of GluR2-interacting proteins (Braithwaite et al., 2000), we then explored the possibility that GluR3 may play a similar role in synaptic plasticity by generating and analyzing knockout mice lacking GluR3. We showed that the GluR3 knockout mice exhibited normal basal synaptic transmission and LTD but enhanced LTP, indicating that GluR3 was not critical for the expression of LTD. Finally, to address the possibility that GluR2/3 may have redundant functions, we analyzed double knockout mice lacking both GluR2 and GluR3. We demonstrated that the double knockout mice exhibited a dramatic reduction in the mean amplitude of basal synaptic transmission, indicating that GluR2/3 are essential to maintain high levels of synaptic transmission in vivo. However, in spite of a severe reduction in basal synaptic function, the double knockout mice were capable of establishing and maintaining several forms of long-lasting synaptic changes, including LTP, LTD, depotentiation, and dedepression. These results provide genetic evidence for the existence of GluR2/3-independent mechanisms for the expression of hippocampal LTD and depotentiation and suggest that the GluR1 subunit is sufficient for expressing hippocampal synaptic plasticity.

Results

Hippocampal LTD and Depotentiation in GluR2 Knockout Mice

If GluR2 is important for the expression of hippocampal LTD by regulating AMPAR trafficking, one would expect that LTD or depotentiation is affected in GluR2 knockout mice (Jia et al., 1996). To test this possibility, we carried out electrophysiological recordings in the CA1 region of the hippocampus. Previously, we found no significant differences in the degree of LTD of field excitatory postsynaptic potential (fEPSPs) between the wild-type and the knockout mice in an 129XCD1 genetic background (Jia et al., 1996). Since the present study focused on GluR3 and GluR2/3 double knockout mice which were generated in an 129XC57/BL6 genetic background, we therefore backcrossed the GluR2 null mutation into a C57/BL6 genetic background and further verified that both LTD and depotentiation were present in the absence of GluR2. As shown in Figure 1A, no significant differences were found in the degree of LTD induced by low-frequency stimulation (LFS; 1 Hz lasting 15 min) between the two groups of mice (79.2 ± 2.3% for $GluR2^{+/+}$ versus 77.2 ± 4.2% for $GluR2^{-/-}$, $p = 0.66$; Figure 1A). Although LTP induced by high-frequency stimulation (HFS; 100 Hz lasting 1 s) was enhanced in GluR2 knockout mice (155.3% ± 3.2% for $GluR2^{+/+}$ versus 181.6% ± 3.9% for $GluR2^{-/-}$, $p = 0.006$), depotentiation induced by LFS was not significantly altered (87.9% ± 2.2% for $GluR2^{+/+}$ versus 76.3% ± 13.5% for $GluR2^{-/-}$, $p = 0.18$; Figure 1B). In adult hippocampal slices, depotentiation could not be induced by LFS in either wild-type or GluR2 knockout mice (Figure 1C). These results indicate that GluR2 is not essential for the expression of hippocampal LTD or depotentiation. However, because GluR3 is closely related to GluR2 in the structure and biochemical properties (Hollmann and Heinemann, 1994; Braithwaite et al., 2000, Shi et al., 2001) and is expressed in the hippocampus, it is possible that the GluR3 subunit is involved in the expression of hippocampal LTD. Alternatively, GluR3 may have a redundant function sufficient to compensate for the loss of GluR2 so that LTD and depotentiation can be established in the GluR2 knockout mice. It is also important to note that despite the fact that GluR3 is abundantly expressed in many regions of the CNS and that it can form functional heteromeric receptors with other AMPA receptor subunits, there have been very few studies directly focusing on the GluR3 subunit. Therefore, we set out to investigate the in vivo function of GluR3 by generating and analyzing knockout mice deficient in the expression of GluR3.

Normal CNS Anatomy and Synaptic Structures in GluR3 Knockout Mice

The GluR3 knockout mice were generated by standard homologous recombination techniques using R1 ES line (Figures 2A and 2B) (Jia et al., 1996; Nagy et al., 1993). The *GluR3* gene is X chromosome linked; therefore, only one copy is present in the male mice. Since the male knockout animals (X^-Y, $GluR3^-$) bred poorly, all experiments were performed using male offspring (X^-Y as GluR3 knockout and X^+Y littermate as wild-type control) generated from F1 X^+Y ($GluR3^+$) and X^+X^- ($GluR3^{+/-}$) breeding. The GluR3 knockout mice were viable and showed no apparent behavioral deficits, including normal locomotor activities. The whole-brain lysate from the GluR3 knockout mice showed no detectable expression of GluR3 mRNA, but normal levels of mRNA for GluR1 and GluR2 (data not shown). Since there are no commercially available antibodies specific to the GluR3 subunit, we generated GluR2/3 double knockout mice by crossing the GluR3 knockout mice to GluR2 knockout mice. Using antibodies that recognize both GluR2 and GluR3, we showed that the double knockout mice had no expression of GluR2 or GluR3 protein, confirming the absence of GluR3 protein in the GluR3 knockout mice (Figure 2C). The protein levels for other glutamate receptors and postsynaptic proteins, including GluR1, GluR2, GluR4, NR1, NR2A/B, and CaMKIIα(CKIIα) were not altered in GluR3 knockout mice (Figure 2C). The GluR3 knockout mice showed no detectable abnormalities in the gross anatomy or synaptic structures of the CNS (Figures 2Db and 2Df).

Normal Basal Synaptic Transmission in GluR3 Knockout Mice

To further investigate the effect of GluR3 deletion on the properties of synaptic transmission and plasticity, we conducted field and whole-cell recordings in the CA1 region of the hippocampus in the GluR3 knockout mice. Analysis of evoked fEPSPs revealed no differences in the stimulus intensity/response curve, maximal response, and fEPSP waveform (Figure 3A). The passive membrane properties of CA1 pyramidal neurons, including resting membrane potential, input resistance, threshold to fire action potential, and its amplitude were not altered in GluR3 knockout mice (data not shown). Analysis of spontaneous miniature excitatory postsynaptic currents (mEPSCs) of CA1 pyramidal neurons also showed no differences in the frequency (Figure 3B), amplitude (Figure 3C), and kinetics between the wild-type and GluR3 knockout mice. Similarly, evoked EPSCs of

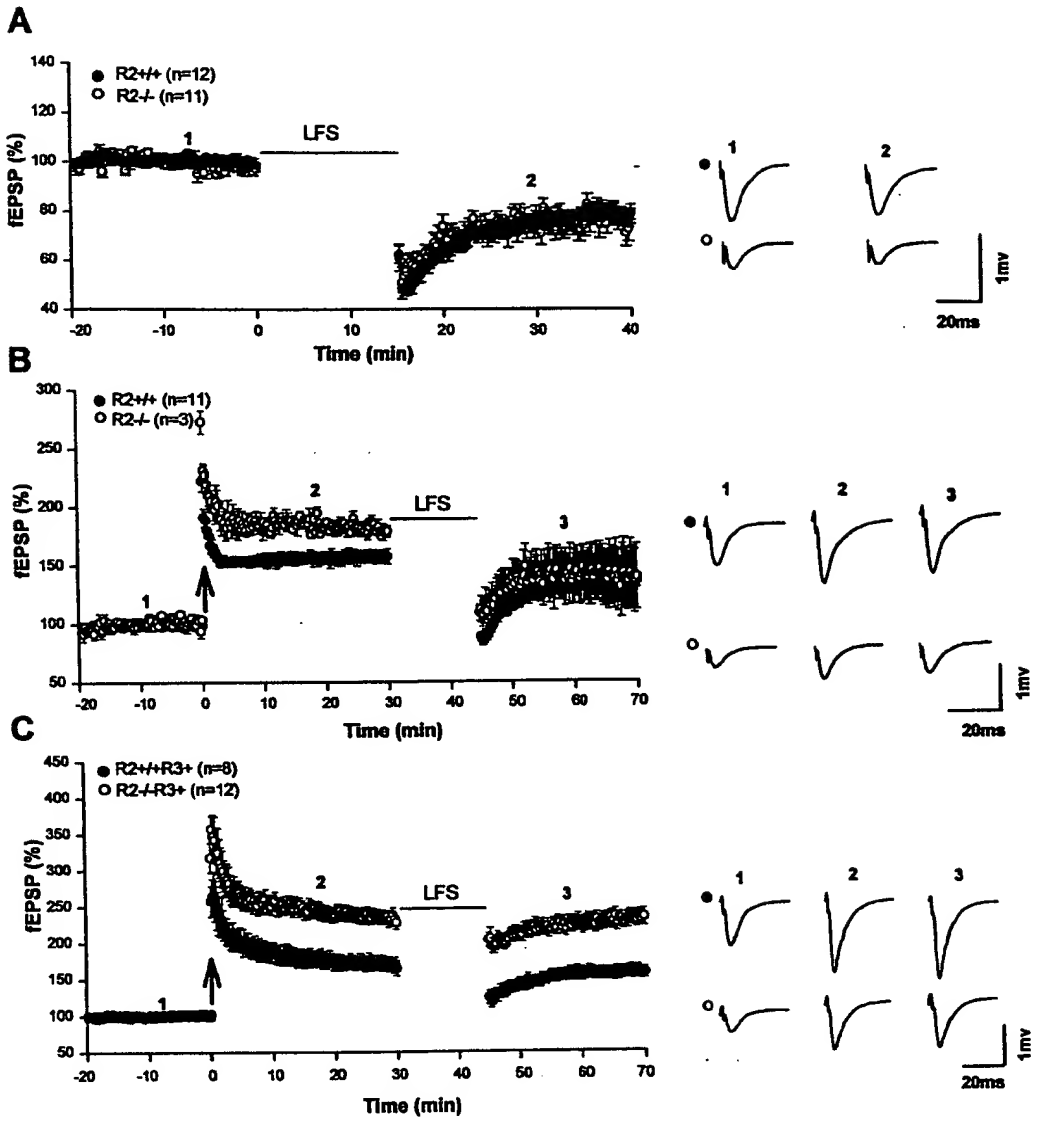

Figure 1. Normal Hippocampal LTD and Depotentiation in GluR2 Knockout Mice

(A) LTD induced by LFS (1 Hz stimulation, 15 min) was indistinguishable between the wild-type and GluR2 knockout mice (12–16 days).

(B) Depotentiation induced by LFS (1 Hz stimulation, 15 min) after establishment of LTP induced by HFS (100 Hz, 1s, upward arrow) showed no differences between the wild-type and GluR2 knockout mice (2–3 weeks).

(C) Depotentiation could not be induced by LFS in hippocampal slices from adult animals (2–3 months) of either the wild-type or GluR2 knockout mice. LTP was enhanced in the knockout mice.

CA1 pyramidal neurons showed no differences in the amplitude, current/voltage relation, and reversal potential between these two groups of mice (Figure 3D). These results indicate that synaptic targeting and function of AMPARs were not significantly disrupted by genetic deletion of GluR3 alone.

Enhanced LTP but Normal LTD in GluR3 Knockout Mice

To examine the role of GluR3 in the regulation of synaptic plasticity, we analyzed LTP and LTD in the CA1 region of the hippocampus. While LTD induced by LFS was indistinguishable between the wild-type and knockout mice (79.1% ± 3.8% for GluR3$^+$ versus 83.7% ± 2.5% for GluR3$^-$, p = 0.33; Figure 4B), the magnitude of LTP induced by HFS was significantly enhanced in the GluR3 knockout mice (128.2% ± 4.5% for GluR3$^+$ versus 152.5% ± 5.0% for GluR3$^-$, p = 0.0039; Figure 4C). The saturated level of LTP induced by multiple HFS trains was also enhanced in the knockout mice (162.8% ± 6.5% for GluR3$^+$ versus 205.2% ± 10.0% for GluR3$^-$, p = 0.0073; Figure 4D). While LTP was enhanced, depotentiation after establishment of LTP was not significantly altered in GluR3 knockout mice (85.0% ± 1.4%

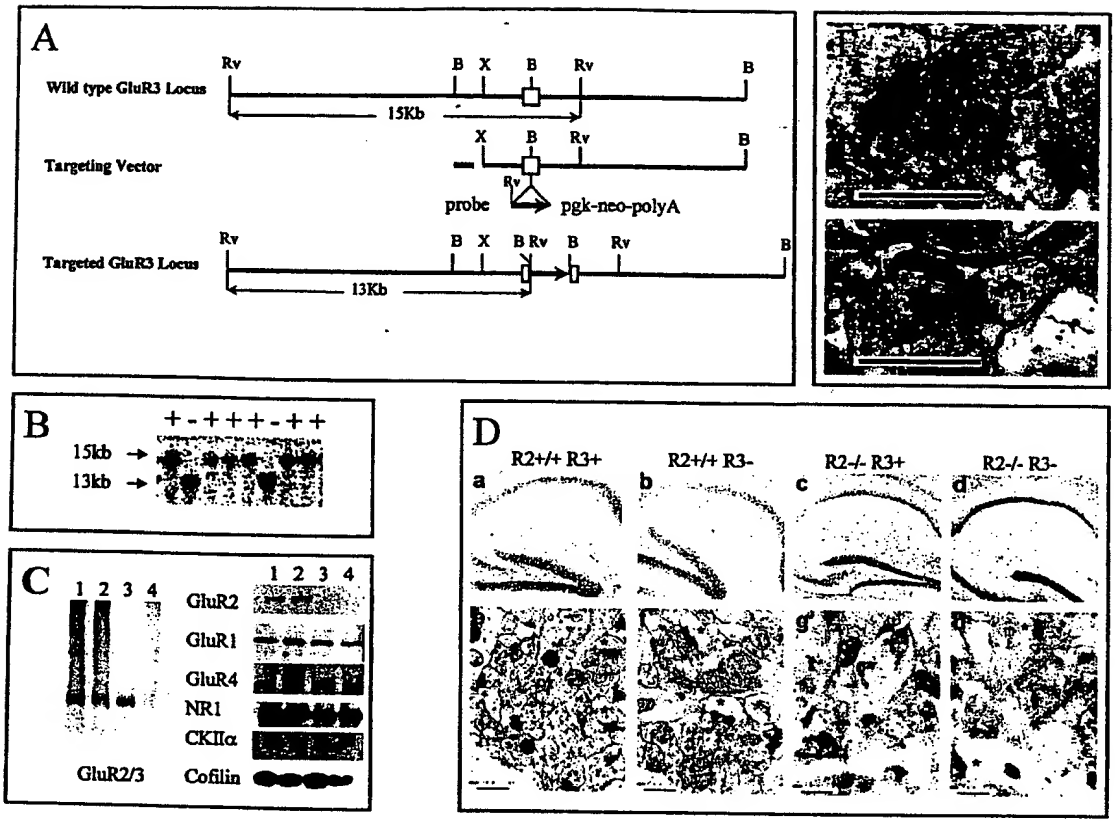

Figure 2. Creation of GluR3 and GluR2/3 Double Knockout Mice

(A) Schematic representation of the wild-type *GluR3* genomic locus, the targeting vector, and the targeted *GluR3* locus. The open box indicates the position of the exon containing the second TM where the insertion of pgk-neo-polyA cassette was made in the targeted *GluR3* locus. Upstream and downstream exons were not mapped.

(B) Representative Southern blot analysis of tail DNA of GluR3 knockout mice. Genomic DNA was isolated from male mice, digested by EcoRV (Rv), and hybridized with the external probe shown in (A). As expected, the probe detected a 15 kb fragment in the wild-type (X^+Y) and a 13 kb fragment in the knockout (X^-Y) mice.

(C) Absence of GluR2 and GluR3 proteins in the GluR2/3 double knockout mice. The GluR2/3 double knockout mice were obtained by intercrossing between mice heterozygous for both GluR2 and GluR3 ($GluR2^{+/-}$ $GluR3^{+/-}$). Total brain lysates were isolated from 12- to 16-day-old male animals of various genotypes (lane 1, $GluR2^{+/+}$ $GluR3^{+}$; lane 2, $GluR2^{+/+}$ $GluR3^{-}$; lane 3, $GluR2^{-/-}$ $GluR3^{+}$; lane 4, $GluR2^{-/-}$ $GluR3^{-}$), immunoblotted, and detected by indicated antibodies. The GluR2/3 antibodies detected no signals in the GluR2/3 double knockout mice, confirming the absence of both GluR2 and GluR3 in the double knockout mice (left panel). The level of GluR1 and GluR4 was quantified (see Experimental Procedures) and showed no differences between the wild-type and the double knockout mice.

(D) Normal hippocampal formation and synaptic structure in GluR2, GluR3, and GluR2/3 double knockout mice. Nissl staining (a–d) and EM (e–h) micrographs of fixed brain sections showed normal anatomy of hippocampus (a–d) and the density of asymmetric synapses (e–h) identified by the presence of postsynaptic density (asterisks) and presynaptic vesicles in CA1 area.

(E) High magnifications of EM micrographs showed apparently normal distribution of presynaptic vesicles and postsynaptic density. Scale bar in (D) and (E), 500 nm.

for $GluR3^{+}$ versus 82.5% ± 9.2% for $GluR3^{-}$; Figure 4E). NMDA receptor antagonist DL-APV (100 μM) completely blocked LTP in both the wild-type and knockout mice (data not shown). Therefore, the enhanced LTP in the GluR3 knockout mice does not involve NMDAR-independent mechanisms. To test whether GluR3 plays a role in presynaptic functions, we compared paired-pulse facilitation and found no differences between the wild-type and knockout mice (Figure 4A). Therefore, hippocampal synaptic plasticity can occur in the absence of GluR3.

Normal Gross CNS and Synaptic Structures in GluR2/3 Double Knockout Mice

To address the possibility that GluR2 and GluR3 are functionally redundant and that only one of them is required for the expression of synaptic plasticity, we generated and analyzed knockout mice lacking both GluR2 and GluR3. The double knockout mice ($GluR2^{-/-}$ $GluR3^{-}$, males) were born indistinguishable from the wild-type littermates, but during postnatal weeks 2–4 displayed an increased mortality (approximately 20%–30%) and gradual appearance of global abnormalities, including smaller body sizes, reduced locomotor activities, and severe tremors upon movements. Surprisingly, the double knockout mice showed no detectable abnormalities in the gross anatomy of the CNS, including hippocampus (Figure 2D). In addition, the synaptic structures in the CA1 region of the hippocampus appeared unchanged in the double knockout mice (Figures 2Dd, 2Dh, and 2E). There were no significant differences in

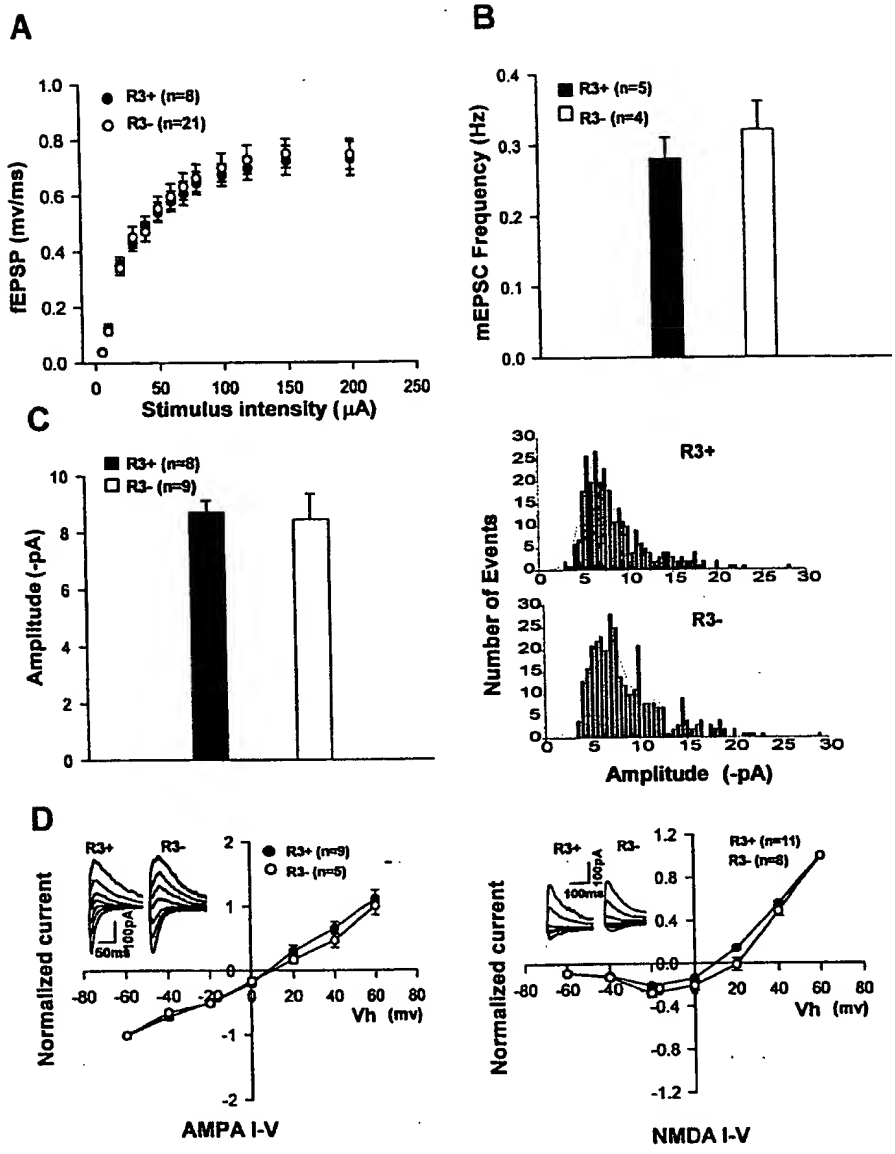

Figure 3. Normal Basal Synaptic Transmission in GluR3 Knockout Mice

(A) fEPSP slopes plotted as a function of stimulus intensity. The distance between the stimulating and recording electrodes was kept constant between slices.

(B) Summary histogram showing the frequency of mEPSCs of CA1 pyramidal neurons recorded under whole-cell voltage clamp mode in the presence of TTX (1 μM) and picrotoxin (100 μM). mEPSCs were blocked by AMPA receptor antagonist CNQX (5 μM).

(C) Summary histogram showing averaged (left) and distribution of mEPSC amplitudes of one representative neuron from each genotype (right).

(D) Averaged amplitudes of evoked AMPA receptor- (left) and NMDA receptor- (right) mediated EPSCs recorded from CA1 pyramidal neurons showing no differences between the wild-type ($R3^+$) and GluR3 knockout ($R3^-$) mice. The AMPAR-mediated EPSCs were estimated at indicated holding potentials in the presence of 100 μM picrotoxin 5 ms after the stimulus and normalized to the EPSC at −60mV. The NMDAR-mediated EPSCs were measured with peak amplitudes in the presence of 100 μM picrotoxin and 10 μM CNQX and normalized to the EPSC at 60mV. The representative EPSC traces at various holding potentials were averages of four successive sweeps.

the numbers of asymmetric synapses and the lengths of postsynaptic density between the wild-type and the double knockout mice (see Experimental Procedures). These results indicate that the excitatory synapses are formed and maintained in the absence of GluR2/3.

Reduced Basal Synaptic Transmission in GluR2/3 Double Knockout Mice

To investigate the properties of basal synaptic function in GluR2/3 double knockout mice, we analyzed fEPSPs evoked by various stimulus intensities. In these experi-

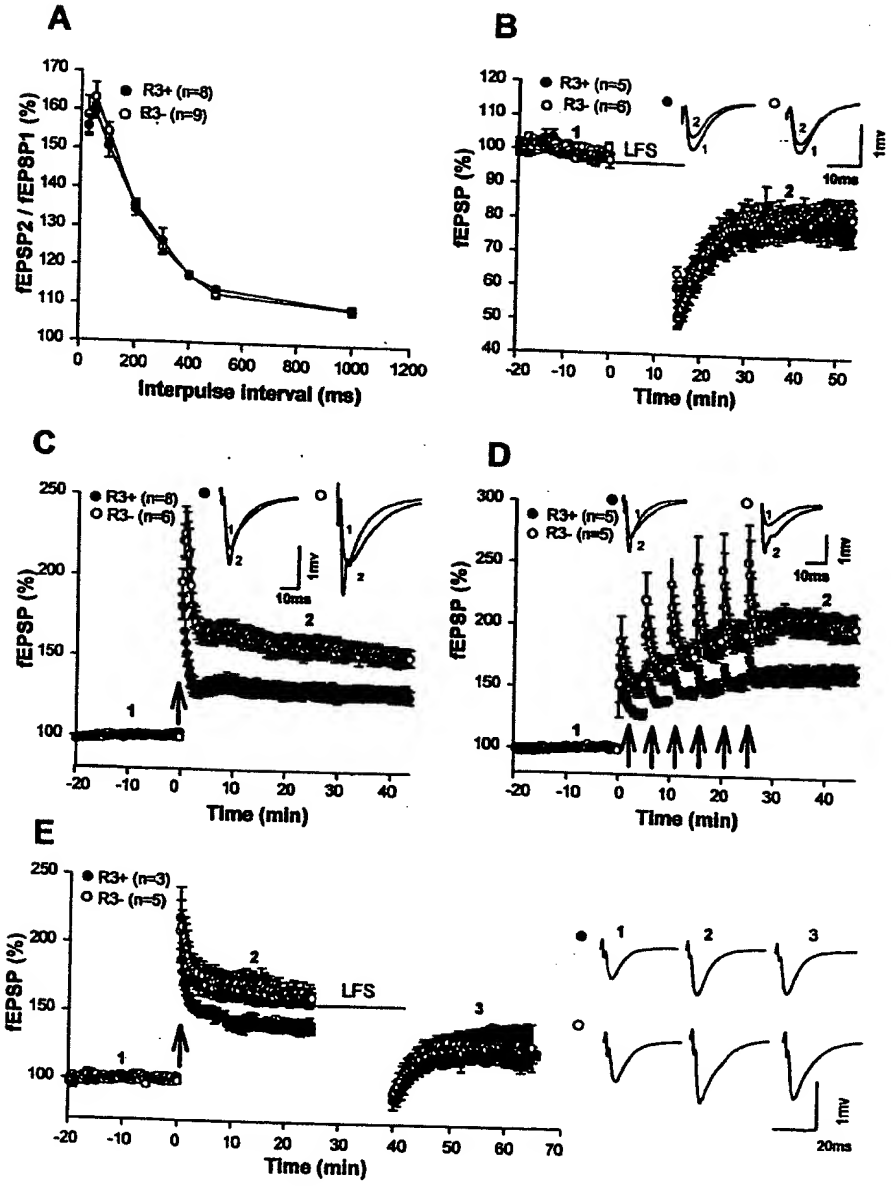

Figure 4. Normal Presynaptic Function and LTD but Enhanced LTP in GluR3 Knockout Mice

(A) Normal paired-pulse facilitation. The plot summarizes facilitation of the second fEPSP slope compared to the first one as a function of the interpulse interval.

(B) Normal hippocampal LTD. LTD induced by LFS showed no differences between the wild-type ($R3^+$) and GluR3 knockout ($R3^-$) mice (12–16 days).

(C) Enhanced hippocampal LTP. LTP induced by single HFS train was higher in GluR3 knockout than the wild-type mice (2–3 months).

(D) Enhanced level of saturated LTP. LTP induced by six trains of HFS (5 min intertrain intervals, upward arrows) was significantly enhanced in GluR3 knockout mice (2–3 months).

(E) Normal depotentiation. Depotentiation induced by LFS following establishment of LTP showed no differences between the wild-type ($R3^+$) and GluR3 knockout ($R3^-$) mice (2–3 weeks).

ments, we used adult mice to minimize the effect of GluR4 on synaptic transmission. As shown in Figure 5A, the mean amplitudes of fEPSPs in the double knockout mice were significantly smaller over a wide range of stimulus intensities (data not shown) or presynaptic fiber volley compared to those of the wild-type or GluR2 knockout mice. The maximal amplitude of fEPSPs in the double knockout slices was only 10%–20% of that in the wild-type control. To investigate the mechanisms underlying this reduced synaptic response, we recorded

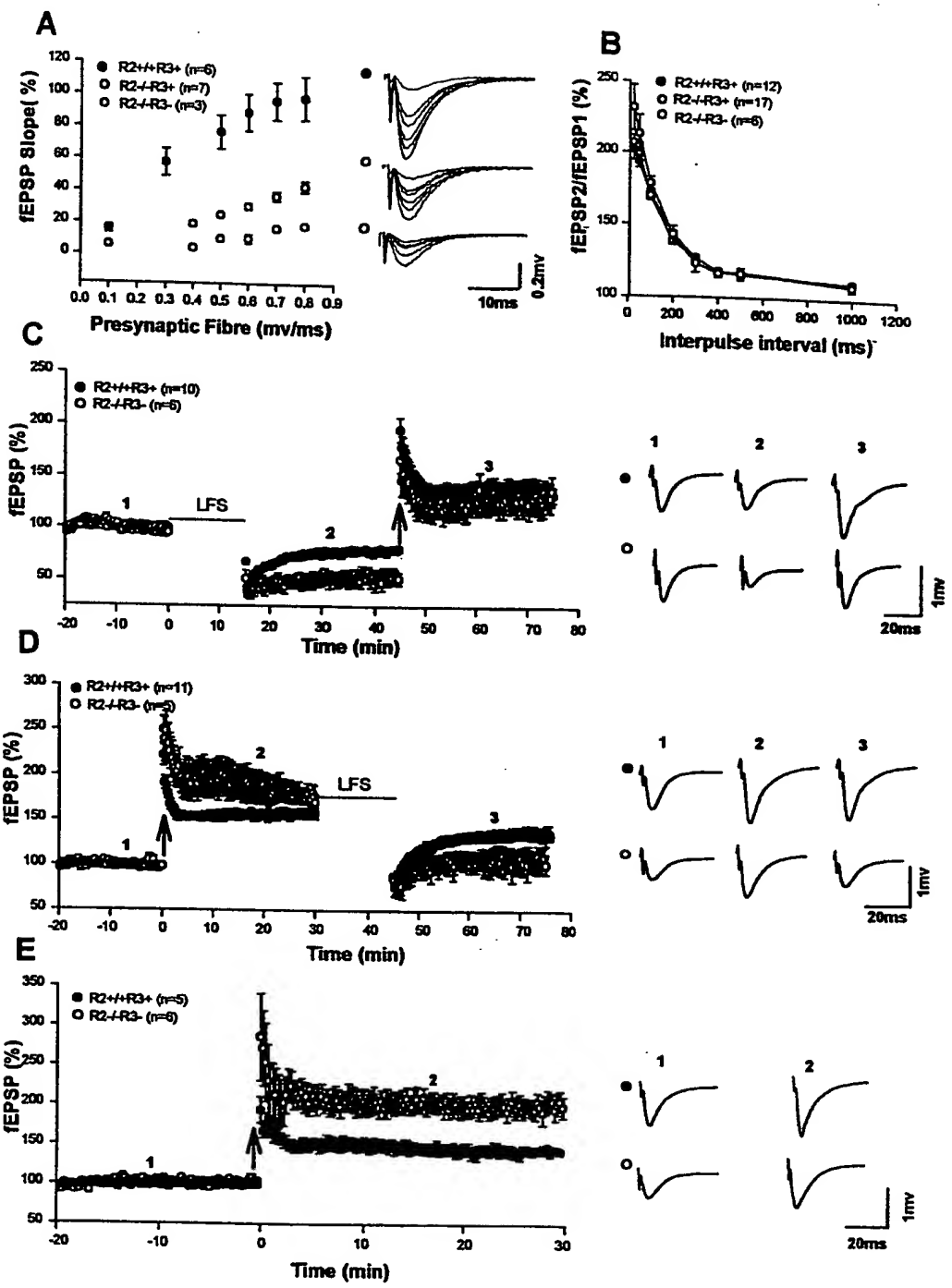

Figure 5. Enhanced Synaptic Plasticity in GluR2/3 Double Knockout Mice

(A) Reduced synaptic response. fEPSP slopes were plotted as function of presynaptic fiber volley. The maximal fEPSP slopes were significantly smaller in the double knockout mice ($GluR2^{-/-}$ $GluR3^{-}$) than those in the wild-type ($GluR2^{+/+}$ $GluR3^{+}$) and GluR2 knockout ($GluR2^{-/-}$ $GluR3^{+}$) mice (2–3 months). The traces show typical fEPSPs evoked with various stimulus intensities.

(B) Normal paired-pulse facilitation. The plot summarizes the facilitation of the second fEPSPs compared with the first one as a function of interpulse interval. No differences were found between these three groups of mice (2–3 months).

(C) Enhanced LTD and dedepression. Both LTD induced by LFS and dedepression induced by HFS (upward arrow) after establishment of LTD were significantly higher in the double knockout ($GluR2^{-/-}$ $GluR3^{-}$) than the wild-type ($GluR2^{+/+}$ $GluR3^{+}$) mice (12–16 days).

(D) Enhanced LTP and depotentiation. Both LTP induced by HFS (upward arrow) and depotentiation induced by LFS after the establishment of LTP were significantly enhanced in the GluR2/3 double knockout mice (2–3 weeks).

(E) Sufficiency of GluR1 for LTP. LTP induced by HFS (upward arrow) in hippocampal slices prepared from adult mice (3–6 months) was also significantly higher in the GluR2/3 double knockout than the wild-type mice. The traces on the right are averages of four successive sweeps at indicated time points.

mEPSCs from CA1 pyramidal neurons and found no significant differences in either the frequency (0.23% ± 0.01% Hz for GluR2$^{+/+}$ GluR3^{+} versus 0.25% ± 0.02% Hz for GluR2$^{-/-}$ GluR3^{-}, n = 9 neurons, p = 0.5) or amplitude (10.61% ± 0.58% pA for GluR2$^{+/+}$ GluR3^{+} versus 10.92% ± 0.19% pA for GluR2$^{-/-}$ GluR3^{-}, n = 9 neurons, p = 0.63) between the wild-type and double knockout mice. To test whether presynaptic function was altered, we analyzed paired-pulse facilitation and found no differences in the degree of facilitation between the wild-type and the double knockout mice (Figure 5B). Therefore, the reduction in basal synaptic responses in the double knockout mice was not likely caused by presynaptic changes.

Synaptic Plasticity in GluR2/3 Double Knockout Mice

To address the role of GluR2/3 in the regulation of hippocampal synaptic plasticity, we compared several forms of long-lasting synaptic changes between the wild-type and the double knockout mice. First, we induced LTD with LFS and after LTD was stabilized, delivered HFS to induce LTP or dedepression. As shown in Figure 5C, both LTD (79.2% ± 3% for GluR2$^{+/+}$ GluR3^{+} versus 51.4% ± 8.0% for GluR2$^{-/-}$ GluR3^{-}, p = 0.0026) and dedepression (189.3% ± 8.3% for GluR2$^{+/+}$ GluR3^{+} versus 237.3% ± 16.5% for GluR2$^{-/-}$ GluR3^{-}, p = 0.014) were present and clearly enhanced in the double knockout mice. Second, we induced LTP by HFS and then depotentiation by LFS following establishment of LTP (Figure 5D). Again, both LTP (155.3% ± 4.0% for GluR2$^{+/+}$ GluR3^{+} versus 181.0% ± 10.4% for GluR2$^{-/-}$ GluR3^{-}, p = 0.013), and depotentiation (88.0% ± 8.3% for GluR2$^{+/+}$ GluR3^{+} versus 60.6% ± 5.7% for GluR2$^{-/-}$ GluR3^{-}, p = 0.00015) could be elicited and significantly enhanced in the double knockout mice. Since GluR4 is only expressed in developing hippocampus, we then tested whether LTP could be established in adult hippocampal slices (2–3 months) of the double knockout mice (which should have GluR1 only AMPARs). As shown in Figure 5E, LTP was present and significantly higher in the double knockout mice (141.9% ± 5.5% for GluR2$^{+/+}$ GluR3^{+} versus 198.6% ± 11.5% for GluR2$^{-/-}$ GluR3^{-}, p = 0.0025).

To address the possibility that hippocampal LTP and LTD in the double knockout mice may differ from those of the wild-type animals, we conducted following experiments. First, we induced LTD in the presence of 100 μM DL-APV and showed that LTD was largely abolished by APV in both genotypes (102.3% ± 2.6% for GluR2$^{+/+}$ GluR3^{+} versus 92.1% ± 3.7% for GluR2$^{-/-}$ GluR3^{-}; Figures 6A and 6B). Therefore, the induction of hippocampal LTD in the double knockout mice was mainly through NMDAR-dependent mechanisms. This conclusion was consistent with the finding that LTD in the double knockout mice was insensitive to the application of MCPG (0.5 mM) or bicuculline (20 μM) (Figure 6C). Both of these drugs have been shown to block metabotropic glutamate receptor (mGluR)-dependent LTD, which is known to coexist with NMDAR-dependent LTD in CA1 pyramidal neurons under certain conditions (Oliet et al., 1997). Second, we recorded fEPSPs from two independent pathways and induced LTP or LTD in one pathway. As shown in Figures 7A–7C, synapse-specific LTP (Figure 7B) or LTD (Figure 7C) of the conditioned pathway was obtained in the double knockout mice. After stabilization of LTP or LTD, we applied AMPAR antagonist CNQX (10 μM) and found that fEPSPs were completely abolished, indicating that all synaptic responses during LTP or LTD were mediated by AMPARs. Then the extracellular solution was changed to low Mg^{2+} (0.1 mM) plus CNQX to isolate NMDAR-mediated synaptic responses in both pathways (Mainen et al., 1998; Kullmann et al., 1996). In these experiments, we found little changes in NMDAR-mediated transmission associated with LTP (111.4% ± 2.99% for GluR2$^{+/+}$ GluR3^{+} versus 120.6% ± 5.5% for GluR2$^{-/-}$ GLuR3^{-}) or LTD (99.1% ± 3.25% for GluR2$^{-/-}$ GluR3^{-}) (Figures 7B and 7C), indicating predominant changes in AMPAR-mediated synaptic transmission during LTP or LTD both in the wild-type and the double knockout mice. Finally, we examined the effect of a 15 amino acid peptide (D15) corresponding the PRD domain of the dynamin (dynamin 828–842) on synaptic transmission and LTD in the double knockout mice. This peptide is known to interfere with the binding of amphiphysin with dynamin, an interaction that is important for endocytosis and has been shown to block the expression of LTD (Luscher et al., 1999). Postsynaptic injections of D15 blocked LTD in 8 out of 12 neurons recorded, whereas LTD was obtained in all 10 recorded neurons filled with control peptide S15. The averaged LTD was 82.9% ± 5.9% for neurons filled with D15 and 69.8% ± 4.5% filled with control peptide S15 (p < 0.05). These peptides had similar effects on LTD of the wild-type neurons (data not shown). Collectively, these results indicate that hippocampal LTD in the double knockout mice requires NMDAR activation and postsynaptic endocytosis.

Discussion

Previous studies using cultured hippocampal neurons and inhibitory peptides indicate that the GluR2/3 subunits are important for synaptic trafficking of AMPARs and the expression of LTD. In this study, we demonstrate that knockout mice deficient in the expression of both GluR2 and GluR3 are severely affected in basal synaptic function. However, in spite of a dramatic reduction in the mean amplitude of basal synaptic responses, the double knockout mice are capable of undergoing several forms of long-lasting synaptic plasticity, including LTD and depotentiation in the CA1 region of the hippocampus. These results demonstrate that GluR2/3 are critically involved in maintaining basal synaptic transmission and suggest that GluR1 is sufficient for the expression of synaptic plasticity in vivo.

Importance of GluR2/3 for Basal Synaptic Transmission

In GluR2/3 double knockout mice, the mean amplitude of evoked fEPSP with a wide range of stimulation intensities is much smaller compared to the wild-type animals, indicating that GluR2/3 are critical for maintaining high levels of basal synaptic responses. This difference is most significant in adult hippocampus where the expression of GluR4 is absent, suggesting that GluR4 may

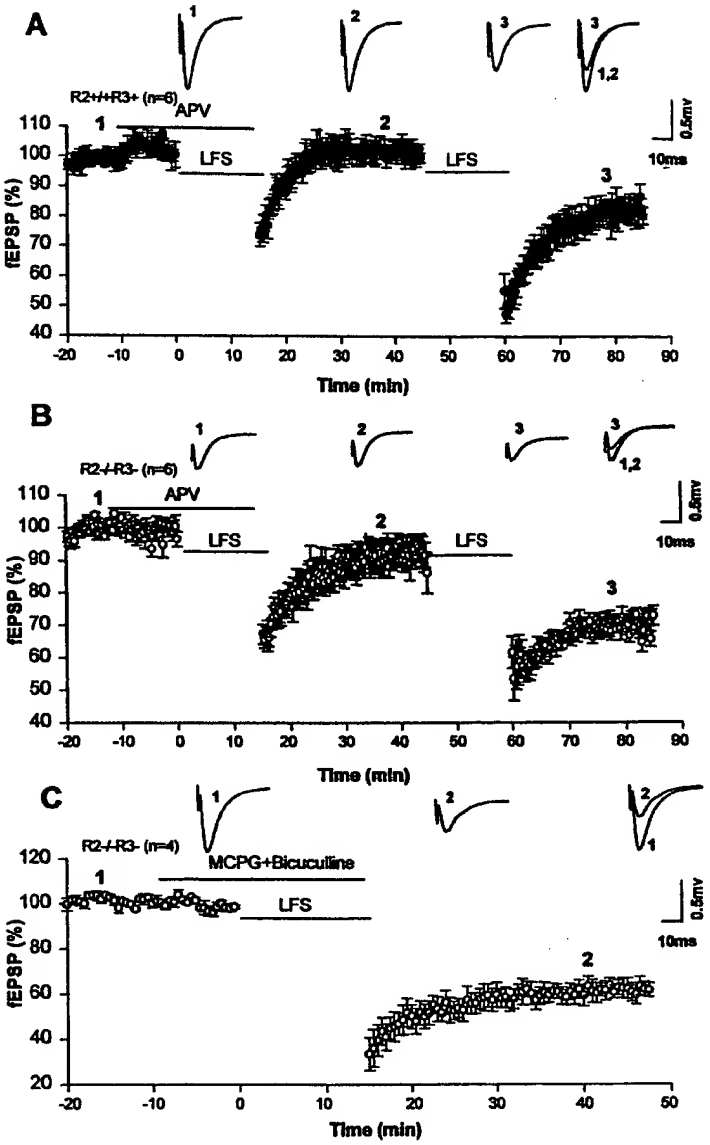

Figure 6. Dependence of LTD on NMDA Receptors in GluR2/3 Double Knockout Mice

(A) LTD was blocked by DL-APV in the wild-type mice (12–16 days). Bath application of DL-APV (100 μM) blocked the induction of LTD. Subsequent LFS after washout of DL-APV produced LTD in the same slices.

(B) LTD was also largely blocked by DL-APV (100 μM) in the GluR2/3 double knockout mice (12–16 days). The experiments were performed as described in (A).

(C) LTD was not affected by MCPG and bicuculline. Bath application of mGluR antagonist MCPG (1 mM) and $GABA_A$ inhibitor bicuculline (20 μM) had no significant effect on LTD in the double knockout mice (12–16 days). Traces are averages of four successive sweeps at indicated time points.

partially compensate for the loss of GluR2/3 in developing brain. It is unlikely that a reduction in the size of fEPSPs is caused by structural perturbations, as there is no evidence that the number of neurons, the density of excitatory synapses, the length of PSD, or the number of presynaptic vesicles is altered in the double knockout mice. The simplest explanation is that GluR2/3 are required for synaptic targeting and stabilization of AMPARs in vivo. Thus, in the absence of GluR2/3, AMPARs would not be sufficiently targeted or stabilized, resulting in a smaller number of synaptic AMPARs and reduced synaptic transmission. This possibility is consistent with the results obtained from in vitro biochemical studies and cultured hippocampal neurons demonstrating that the C-terminal tails of GluR2/3 are capable of interacting with several postsynaptic proteins and that disruption of the interaction causes a selective reduction in AMPAR-mediated basal synaptic transmission and surface expression of AMPARs (see reviews by Braithwaite et al., 2000; Barry and Ziff, 2002; Song and Huganir, 2002). The smaller fEPSPs in the double knockout mice are also consistent with the idea that GluR2/3-containing AMPARs may undergo constitutive recycling, a process considered to be important for preserving stability of basal synaptic transmission (Shi et al., 2001; Passafaro et al., 2001). However, even in adult hippocampus where GluR1 is likely the only remaining AMPAR subunit in the double knockout mice, synaptic transmission occurs and sufficiently high for the establishment of various forms of long-lasting synaptic changes, indicating that GluR1 alone AMPARs are capable of synaptic targeting and dynamic changes.

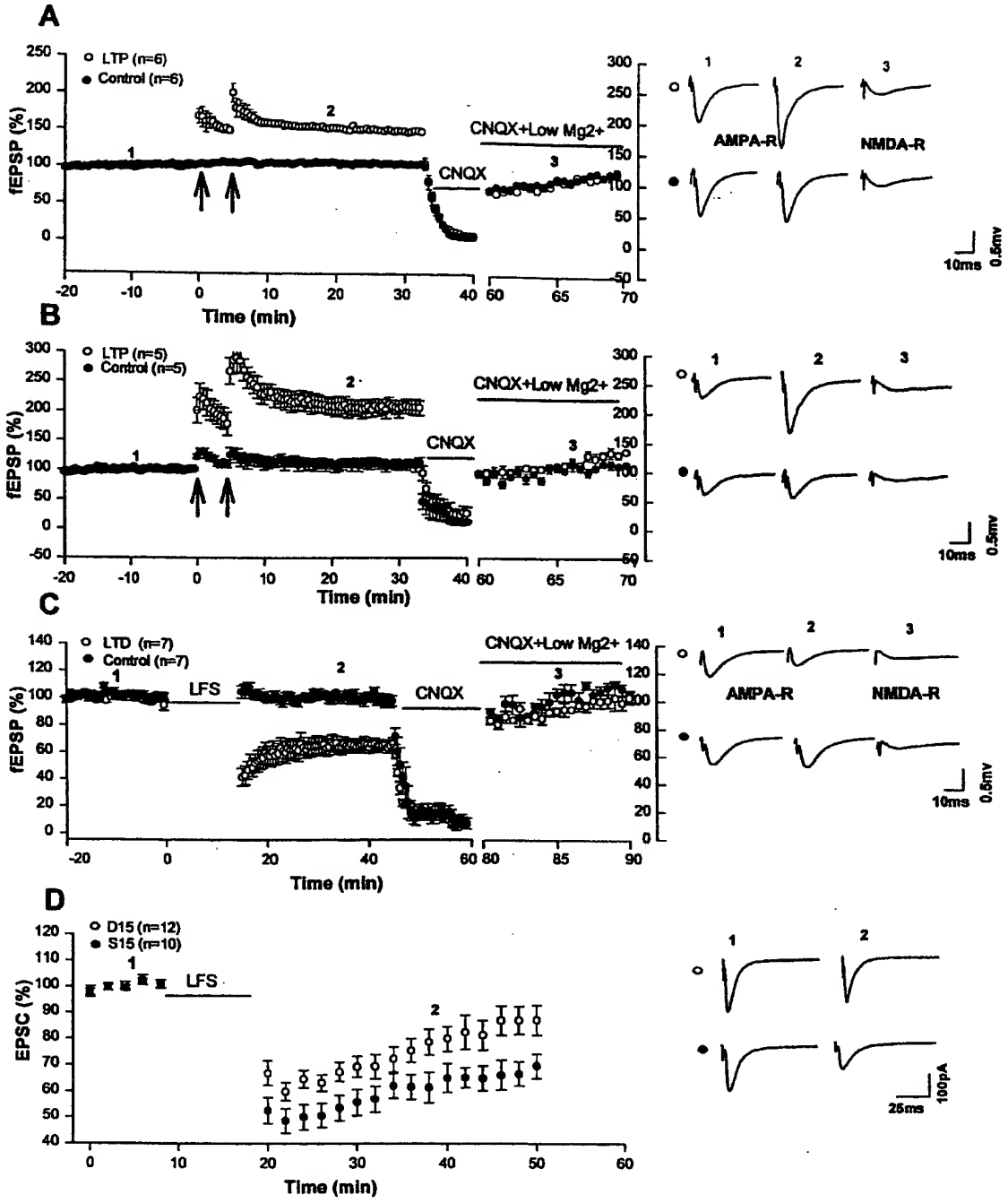

Figure 7. Expression Mechanisms of LTP and LTD in GluR2/3 Double Knockout Mice

(A) Field recordings from two independent pathways (LTP or tetanized pathway and control pathway) showed predominant changes in AMPAR-mediated synaptic transmission during LTP in the wild-type animals (2 months).

(B) Field experiments showed predominant changes in AMPAR-mediated synaptic transmission in LTP pathway in GluR2/3 double knockout mice (2 months).

(C) Field experiments showed predominant changes in AMPAR-mediated synaptic responses in LTD pathway in GluR2/3 double knockout mice (12–16 days). Traces on the right in (A)–(C) are sample fEPSPs from the LTP or LTD and control pathways evoked before HFS or LFS (1), 30 min after first HFS or LFS (2), and after bath application of an extracellular solution containing CNQX (10 μM) and low Mg^{2+} (0.1 mM) to isolate NMDAR-mediated synaptic responses (3). NMDAR responses were normalized to AMPAR-mediated responses before LTP or LTD (Kullmann et al., 1996). The absolute mean fEPSP slope of NMDAR responses is 0.046% ± 0.01% mV/ms for $GluR2^{-/-}$ $GluR3^{+}$ (n = 6) and 0.037% ± 0.004% mV/ms for $GluR2^{-/-}$ $GluR3^{-}$ (n = 5). The ratio of NMDAR- versus AMPAR-mediated fEPSPs is 0.13 ± 0.02 for $GluR2^{-/-}$ $GluR3^{+}$ (n = 6) and 0.15 ± 0.02 for $GluR2^{-/-}$ $GluR3^{-}$ (n = 5).

(D) Whole-cell recordings showed inhibition of LTD by postsynaptic injection of D15 but not by S15 in the double knockout mice (13–16 days). Active peptide D15 or its control peptide S15 was included in the intracellular solution and LTD was induced by LFS (1 Hz lasting 10 min at −40mV) after 15 min of baseline recording. Traces on the right were averages of four successive EPSCs at indicated time points.

Synaptic Plasticity in the Absence of GluR2/3

An intriguing and rather surprising finding of the present study is that various forms of hippocampal synaptic plasticity can be established in the double knockout mice. In particular, the presence of hippocampal LTD and depotentiation in the absence of GluR2/3 is not predicted by the hypothesis that GluR2/3 are necessary for AMPAR endocytosis and LTD (Luthi et al., 1999; Daw et al., 2000; Xia et al., 2000). One possible interpretation for this discrepancy is that the mechanisms of synaptic plasticity in our genetically altered mice may differ from those of the wild-type animals. This appears unlikely because hippocampal LTD in the double knockout mice is (1) largely blocked by NMDAR antagonist APV; (2) insensitive to MCPG or bicucullin, therefore mGluR-independent; (3) expressed predominantly via changes in AMPAR-mediated synaptic transmission; and (4) still inhibited by perturbations of endocytosis, although to a less degree compared to the wild-type animals. These results indicate that GluR2/3-independent AMPAR endocytosis contributes significantly to hippocampal LTD in the double knockout mice. However, we cannot rule out the possibility that some aspects of synaptic plasticity are distinct in the double knockout mice. Indeed, LTD was only partially blocked by D15 peptide, the same peptide that has been shown to completely abolish LTD in other preparations from the wild-type animals (e.g., Luscher et al., 1999), suggesting that a component of LTD is endocytosis independent in these knockout mice. Further experiments are needed to determine exactly what proportion of LTD is contributed by endocytosis-dependent or endocytosis-independent processes. Since most AMPARs exist as heteromeric assemblies of GluR1/2 or GluR2/3, not as GluR1 homomeric receptors present in the double knockout mice, it also remains to be investigated whether (or under what conditions) GluR2/3-independent AMPAR endocytosis operates and how much it contributes to synaptic changes in the wild-type animals.

In the absence of GluR2/3, the relative amount (as compared to basal synaptic response) of synaptic plasticity is significantly greater (Figures 5–7). This enhancement, in particular of LTD and depotentiation (Figures 5C and 5D), cannot be accounted for simply by an increased Ca^{2+} influx during the induction phase because (1) LTD is blocked by APV and (2) the relative amount of NMDAR- versus AMPAR-mediated fEPSPs is not much greater in the double knockout than in the wild-type mice (Figures 7A–7C). These results suggest that one of the in vivo functions of the GluR2/3 subunits may be to inhibit synaptic changes. It is reasonable to hypothesize that the interaction between GluR2/3- and AMPAR-interacting proteins also function to retain and/or stabilize the receptors either at synaptic surface (Noel et al., 1999; Osten et al., 2000; Lee et al., 2002) or inside the cell (Daw et al., 2000; Perez et al., 2001; Greger et al., 2002) during synaptic changes as proposed for basal synaptic transmission. Thus, disruption of the interaction, for example, by protein phosphorylation/dephosphorylation (Matsuda et al., 1999; 2000; Xia et al., 2000; Kim et al., 2001; Daw et al., 2000; Chung et al., 2000) may facilitate receptor trafficking and synaptic changes.

However, it should be emphasized that because basal synaptic transmission is so drastically reduced in the absence of GluR2/3, the absolute amount of changes in synaptic transmission during LTP/LTD in most experiments is actually smaller in the double knockout mice. Therefore, one interpretation of the results is that GluR2/3 may normally participate in facilitating and/or stabilizing synaptic changes by interacting with AMPAR-interacting proteins as mentioned above. Thus, disruption of these interactions or deletion of GluR2/3 would lead to reduced synaptic plasticity. As indicated earlier, this possibility is supported by results from many previous studies using cultured hippocampal neurons (Nishimune et al., 1998; Luthi et al., 1999; Daw et al., 2000; Xia et al., 2000; Kim et al., 2001; Lee et al., 2002). Given the complexity of protein interactions that occur at the GluR2/3 C termini (e.g., Braithwaite et al., 2002; Hanley et al., 2002; see reviews by Barry and Ziff, 2002; Malinow and Malenka, 2002), it is likely that these interactions have differential and potentially opposing effects on AMPAR trafficking and synaptic plasticity. Targeted deletions or mutations of individual protein binding sites in GluR2/3 C-terminal tails in mice would be important to address the specific function of each interaction.

GluR1 Sufficiency for Hippocampal LTP

In the adult hippocampus where most AMPARs are made of GluR1/2 or GluR2/3 (Wenthold et al., 1996), LTP could be established and also dramatically enhanced in the absence of GluR2/3, indicating that GluR1 is sufficient for the expression of hippocampal LTP. These results are consistent with the observations that LTP is impaired in GluR1 knockout mice (Zamanillo et al., 1999) and that GluR1 is necessary for NMDAR-dependent synaptic targeting of AMPARs in cultured hippocampal slices (Shi et al., 1999, 2001). The C-terminal tail of GluR1 can also interact with a number of proteins, including SAP97 (Leonard et al., 1998), actin binding protein 4.1N (Shen et al., 2000), and AP2 (Lee et al., 2002). Disruption of the interaction between GluR1 and these proteins blocks the activity-dependent synaptic delivery of GluR1 and LTP (Shi et al., 2001). Since LTD experiments were performed using mice at postnatal days 12–15 when GluR4 is also expressed in the hippocampus, it is not clear whether GluR1 is sufficient for the expression of LTD. However, since depotentiation could be established and enhanced in the double knockout animals at postnatal week 3 when the expression of GluR4 is diminishing in the hippocampus (Zhu et al., 2000), our results also suggest that GluR1 may be sufficient for the expression of synaptic depression.

In conclusion, by employing genetic approaches in mice, we provide evidence that the primary function of GluR2/3 is to stabilize synaptic transmission. Thus, in the absence of GluR2/3, both basal synaptic transmission and synaptic plasticity are affected. The complex interactions between GluR2/3 and various cytosolic proteins may provide multiple mechanisms to ensure the stability of synaptic transmission. We suggest that GluR1 contains all the necessary molecular determinants to allow long-lasting synaptic plasticity to occur. Important issues remain to be investigated, including the analysis of the synaptic properties such as AMPAR trafficking in the double knockout mice and to define the in vivo function of specific protein binding sites of GluR2/3 C-terminal tails.

Experimental Procedures

Creation of GluR3 and GluR2/3 Double Knockout Mice

A genomic clone containing the TM1 and TM2 domains of the *GluR3* gene was isolated from a genomic 129/sv library. The targeting vector for generating GluR3 knockout mice was constructed by inserting a 1.8 kb PGK-neo cassette into the BamHI site of exon 12 in a sense direction with creation of an additional EcoRV site for the purpose of diagnostic restriction digestion of the genomic DNA. The G418 resistant ES clones were tested for a targeted event by Southern blot analysis. The procedures for culturing and screening ES cells and for generation of chimeric mice were described previously (Nagy et al., 1993; Jia et al., 1996). The chimeric mice were backcrossed to C57/BL6 to generate the F1 population. The *GluR3* gene is X chromosome linked; therefore, only one copy is present in male mice. Since the male GluR3 knockout animals (X^-Y, $GluR3^-$) bred poorly, most experiments for GluR3 knockout mice were performed using male offsprings (X^-Y as knockout and X^+Y littermate as wild-type control) generated from F1 X^+Y (wild-type male, $GluR3^+$) and X^+X^- (heterozygous female, $GluR3^{+/-}$) breeding. The GluR2/3 double knockout mice ($GluR2^{-/-}$ $GluR3^-$, male) were generated by intercrossing between $GluR2^{+/-}$ $GluR3^+$ males and $GluR2^{+/-}$ $GluR3^{+/-}$ females. All the mice used in the present study had a genetic background of 129XC57/BL6. The genotype of the double knockout mice was determined by Southern blot analysis using three independent DNA probes: an external probe for GluR2 (Jia et al., 1996), an external probe for GluR3 (Figure 2), and an internal neo-probe. The absence of GluR2 and GluR3 proteins in the double knockout mice was confirmed by Western blot analysis using anti-GluR2/3 antibodies. The observed number for GluR2/3 double knockout mice was consistent with the expected Mendelian ratio (1/16), suggesting no embryonic lethality for the double knockout mice.

Immunoblotting, Histochemistry, and Electron Microscopy

The procedures for Western blot analysis of total brain or hippocampal lysates and for Nissl staining of fixed brain sections were described previously (Jia et al., 1996; Meng et al., 2002). The primary antibodies used were: anti-NMDAR1 (Chemicon, Temeculo, CA), anti-NMDAR2A/B (Upstate, Charlottesville, VA), anti-GluR1 (Chemicon), anti-GluR2 (Chemicon), anti-GluR2/3 (Upstate and Chemicon), anti-GluR4 (Upstate and Chemicon), anti-CaMKIIα (gift of Dr. Bill Trimble), and anti-cofilin (Santa Cruz, Santa Cruz, CA). The levels of GluR1 and GluR4 were estimated and normalized against the amount of cofilin using the enhanced chemiluminescence (Amersham) method in more than ten separate experiments from three animals of each genotype and showed no significant differences (GluR1: 94% ± 17% arbitrary unit for wild-type and 153% ± 21% for double knockout, $p = 0.1$; GluR4: 104% ± 10% for wild-type and 80% ± 15% for double knockout, $p = 0.3$). For electron microscopy, the transcardially fixed brain samples were sliced (500 μm) on a vibratome and 1 × 1 mm CA1 areas isolated from comparable sections of each genotype. The blocks were then postfixed for an additional 3 hr and processed according to standard methods. For each block, 1 μm thick sections were cut and stained with 1% toluidine blue to guide further trimming to isolate equivalent CA1 subfields. Thin sections (60 nm) were then cut and stained with uranyl acetate and Reynolds lead citrate. The numbers of the synapses (wild-type: 0.324 ± 0.016%/μm², $n = 33$ images; GluR2/3 double knockout: 0.359 ± 0.014%/μm², $n = 55$ images, $p = 0.11$) and the lengths of postsynaptic density (wild-type: 171.3% ± 3.9% [nm], $n = 208$ synapses; GluR2/3 double knockout: 175.7% ± 0.34% [nm], $n = 227$ synapses, $p = 0.33$) were estimated on thin-section images covering neuropil regions totaling 4000–7000 μm² from two animals for each genotype (Meng et al., 2002).

Electrophysiology

The procedures for electrophysiological recordings were described previously (Jia et al., 1996; Meng et al., 2002). Briefly, hippocampal slices (400 μm) were prepared from 10 days to 6-month-old mice (the age of the mice was indicated in each experiment) and allowed to recover in a holding chamber for at least 1 hr. A single slice was then transferred to the recording chamber and submerged and superfused with 95% O_2-5% CO_2 saturated artificial CSF (ACSF, 2 ml/min). The ACSF contained 120 mM NaCl, 2.5 mM KCl, 1.3 mM $MgSO_4$, 1.0 mM NaH_2PO_4, 26 mM $NaHCO_3$, 2.5 mM $CaCl_2$, and 11 mM D-glucose. For field EPSPs, the recording pipette (3 MΩ) was filled with ACSF solution. For whole-cell voltage-clamp recordings, the patch pipette (3–5 MΩ) contained the following: 132 mM Cs gluconate, 17.5 mM CsCl, 0.05 mM EGTA, 10 mM HEPES, 2 mM Mg-ATP, 0.2 mM Na-GTP, QX-314, pH7.4 (292 mOsm); for current clamp, it contained 150mM K_2MeSO_4, 0.1 mM EDTA, 10 mM HEPES, and 2 mM Mg-ATP, pH 7.4 (290 mOsm). Synaptic responses were evoked by bipolar tungsten electrodes placed 200–400 μm from the cell body layer in the CA1 area. fEPSPs were measured by taking the slope of the rising phase between 5% and 60% of the peak response. Unless otherwise indicated, LTP and dedepression were induced with two trains (intertrain interval of 10 s) of 100 Hz stimulation each lasting 1 s. LTD and depotentiation were induced by low-frequency stimulation (LFS) at 1 Hz lasting 15 min for field experiments and lasting 10 min at a holding potential of −40mV for whole-cell experiments. Peptides were synthesized and purified by the Advanced Protein Technology Center at the University of Toronto, Toronto, Ontario, CAN. The amino acid sequence for D15 was PPPQVPSRPNRAPPG and the corresponding scrambled peptide (S15) was ANVRRGPPPPPQPPS. Peptides (1.0 mM) were added to the intracellular solution immediately before experiments. All data acquisition and analysis were done using pCLAMP 7 software (Axon instruments). When average data were plotted, data were normalized to the average of the baseline responses unless indicated otherwise. All data were statistically evaluated by Student's t test.

Acknowledgments

We are indebted to J. Hwang and Y.M. Heng for electron microscopy assistance and to Dr. S. Heinemann for providing the GluR3 cDNA. This work was supported by grants to Z.P.J. from Heart and Stroke Foundation of Canada, Canadian Institutes of Health Research (CIHR), and The Hospital For Sick Children Foundation. Y.H.M is supported by an HSC Trainee Fellowship, and Z.P.J. is a New Investigator of CIHR.

Received: November 11, 2002
Revised: April 17, 2003
Accepted: May 23, 2003
Published: July 2, 2003

References

Barry, M.F., and Ziff, E.B. (2002). Receptor trafficking and the plasticity at excitatory synapses. Curr. Opin. Neurobiol. *12*, 279–286.

Bear, M.F., and Abraham, W.C. (1996). Long-term depression in the hippocampus. Annu. Rev. Neurosci. *19*, 437–462.

Beattie, E.C., Carroll, R.C., Yu, X., Morishita, W., Yashuda, H., von Zastrow, M., and Malenka, R.C. (2000). Regulation of AMPA receptor endocytosis by a signaling mechanism shared with LTD. Nat. Neurosci. *3*, 1291–1300.

Bliss, T.V.P., and Collingridge, G.L. (1993). A synaptic model of memory: long-term potentiation in the hippocampus. Nature *361*, 31–39.

Braithwaite, S.P., Meyer, G., and Henley, J.M. (2000). Interactions between AMPA receptors and intracellular proteins. Neuropharmacology *39*, 919–930.

Braithwaite, S.P., Xia, H., and Malenka, R.C. (2002). Differential roles for NSF and GRIP/ABP in AMPA receptor cycling. Proc. Natl. Acad. Sci. USA *99*, 7096–7101.

Carroll, R.C., Lissin, D.V., von Zastrow, M., Nicoll, R.A., Malenka, R.C., and Zastrow, M. (1999). Dynamin-dependent endocytosis of ionotropic glutamate receptors. Proc. Natl. Acad. Sci. USA *96*, 14112–14117.

Carroll, R.C., Beattie, E.C., von Zastrow, M., and Malenka, R.C. (2001). Role of AMPA receptor endocytosis in synaptic plasticity. Nat. Rev. Neurosci. *2*, 315–324.

Chung, H.J., Xia, J., Scannevin, R.H., Zhang, X., and Huganir, R.L.

(2000). Phosphorylation of the AMPA receptor subunit GluR2 differentially regulates its interaction with the PDZ domain-containing proteins. J. Neurosci. *20*, 7258–7267.

Daw, M., Chittajalu, R., Bortolotto, Z.A., Dev, K.K., Duprat, F., Henley, J.M., Collingridge, G.L., and Isaac, J.T.R. (2000). PDZ proteins interacting with C-terminal GluR2/3 are involved in a PKC-dependent regulation of AMPA receptors at hippocampal synapses. Neuron *28*, 873–886.

Dev, K.K., Nishimune, A., Henley, J.M., and Nakanishi, S. (1999). The protein kinase C binding protein PICK1 interacts with short but not long form alternative splice variants of AMPA receptor subunits. Neuropharmacology *38*, 635–644.

Dong, H., O'Brien, R.J., Fung, E.T., Lanahan, A.A., Worley, P.F., and Huganir, R.L. (1997). GRIP: a synaptic PDZ-containing protein that interacts with AMPA receptors. Nature *386*, 279–284.

Dong, H., Zhang, P., Song, I., Petralia, R.S., Liao, D., and Huganir, R.L. (1999). Characterisation of the glutamate receptor-interacting proteins GRIP1 and GRIP2. J. Neurosci. *19*, 6930–6941.

Greger, I.H., Khatri, L., and Ziff, E.B. (2002). RNA editing at Arg607 controls AMPA receptor exit from the endoplasmic reticulum. Neuron *34*, 759–772.

Hanley, J.G., Khatri, L., Hanson, P.I., and Ziff, E.B. (2002). NSF ATPase and alpha/beta-SNAPs disassemble the AMPA receptor-PICK1 complex. Neuron *34*, 53–67.

Hayashi, Y., Shi, S.H., Esteban, J.A., Poncer, J.C., and Malinow, R. (2000). Driving AMPA receptors into synapses by LTP and CaMKII: requirement for GluR1 and PDZ domain interaction. Science *287*, 2262–2267.

Hollmann, M., and Heinemann, S. (1994). Cloned glutamate receptors. Annu. Rev. Neurosci. *17*, 31–108.

Jia, Z., Agopyan, N., Miu, P., Xiong, Z., Henderson, J., Gerlai, R., Taverna, F.A., Velumian, A., MacDonald, J., Carlen, P., et al. (1996). Enhanced LTP in mice deficient in the AMPA receptor GluR2. Neuron *17*, 945–956.

Kim, C.H., Chung, H.J., Lee, H.K., and Huganir, R.L. (2001). Interaction of the AMPA receptor subunit GluR2/3 with PDZ domains regulates long-term depression. Proc. Natl. Acad. Sci. USA *98*, 11725–11730.

Kullmann, D.M. (1999). AMPA receptor attrition in long-term depression. Neuron *24*, 288–290.

Kullmann, D.M., Erdemli, G., and Asztely, F. (1996). LTP of AMPA and NMDA receptor-mediated signals: evidence for presynaptic expression and extrasynaptic glutamate spill-over. Neuron *17*, 461–474.

Lee, S.H., Liu, L., Wang, Y.T., and Sheng, M. (2002). Clathrin adaptor AP2 and NSF interact with overlapping sites of GluR2 and play distinct roles in AMPA receptor trafficking and hippocampal LTD. Neuron *36*, 661–674.

Leonard, A.S., Davare, M.A., Horne, M.C., Garner, C.C., and Hell, J.W. (1998). SAP97 is associated with the alpha-amino-3-hydroxy-5-methylisoxazole-4-propionic acid receptor GluR1 subunit. J. Biol. Chem. *273*, 19518–19524.

Lin, J.W., Ju, W., Foster, K., Lee, S.H., Ahmadian, G., Wyszynski, M., Wang, Y.T., and Sheng, M. (2000). Distinct molecular mechanisms and divergent endocytic pathways of AMPA receptor internalization. Nat. Neurosci. *3*, 1282–1290.

Luscher, C., Xia, H., Beattie, E.C., Carroll, R.C., von Zastrow, M., Malenka, R.C., and Nicoll, R.A. (1999). Role of AMPA receptor cycling in synaptic transmission and plasticity. Neuron *24*, 649–658.

Luscher, C., Nicoll, R.A., Malenka, R.C., and Muller, D. (2000). Synaptic plasticity and dynamic regulation of the postsynaptic membrane. Nat. Neurosci. *3*, 545–550.

Luthi, A., Chittajallu, R., Duprat, F., Palmer, M.J., Benke, T.A., Kidd, F.L., Henley, J.M., Isaac, J.T.R., and Collingridge, G.L. (1999). Hippocampal LTD expression involves a pool of AMPARs regulated by the NSF-GluR2 interaction. Neuron *24*, 389–399.

Mainen, Z.F., Jia, Z.P., Roder, J., and Malinow, R. (1998). Use-dependent AMPA receptor block in mice lacking GluR2 suggests postsynaptic site for LTP expression. Nat. Neurosci. *1*, 579–586.

Malenka, R.C., and Nicoll, R.A. (1999). Long-term potentiation—a decade of progress? Science *285*, 1870–1874.

Malinow, R., and Malenka, R.C. (2002). AMPA receptor trafficking and synaptic plasticity. Annu. Rev. Neurosci. *25*, 103–126.

Man, Y.H., Lin, J.W., Ju, W.H., Ahmadian, G., Liu, L., Becker, L.E., Sheng, M., and Wang, Y.T. (2000). Regulation of AMPA receptor-mediated synaptic transmission by clathrin-dependent receptor internalization. Neuron *25*, 649–662.

Matsuda, S., Mikawa, S., and Hirai, H. (1999). Phosphorylation of serine-880 in GluR2 by protein kinase C prevents its C terminus from binding with glutamate receptor-interacting protein. J. Neurochem. *73*, 1765–1768.

Matsuda, S., Launey, T., Mikawa, S., and Hirai, H. (2000). Disruption of AMPA receptor GluR2 clusters following long-term depression induction in cerebellar Purkinje neurons. EMBO J. *9*, 2765–2774.

Meng, Y.H., Zhang, Y., Tregoubov, V., Janus, C., Cruz, L., Jackson, M., Lu, W.Y., MacDonald, J.F., Wang, J., Falls, D.L., et al. (2002). Abnormal spine morphology and enhanced LTP in LIMK-1 knockout mice. Neuron *35*, 121–133.

Nagy, A., Rossant, J., Nagy, R., Abramow-Newerly, W., and Roder, J.C. (1993). Derivation of completely cell culture-derived mice from early passage embryonic stem cells. Proc. Natl. Acad. Sci. USA *90*, 8424–8428.

Nishimune, A., Isaac, J.T.R., Molnar, E., Noel, J., Nash, S.R., Tagaya, M., Collingridge, G.L., Nakanishi, S., and Henley, J.M. (1998). NSF binding to GluR2 regulates synaptic transmission. Neuron *21*, 87–97.

Noel, J., Ralph, G.S., Pickard, L., Williams, J., Molnar, E., Uney, J.B., Collingridge, G.L., and Henley, J.M. (1999). Surface expression of AMPA receptors in hippocampal neurons is regulated by an NSF-dependent mechanism. Neuron *23*, 365–376.

Oliet, S.H.R., Malenka, R.C., and Nicoll, R.A. (1997). Two distinct forms of long-term depression coexist in CA1 hippocampal pyramidal cells. Neuron *18*, 969–982.

Osten, P., Srivastava, S., Inman, G.J., Vilim, F.S., Khatri, L., Lee, L.M., States, B.A., Einheber, S., Milner, T.A., Hanson, P.I., et al. (1998). The AMPA receptor GluR2 C terminus can mediate a reversible, ATP-dependent interaction with NSF and alpha- and beta-SNAPs. Neuron *21*, 99–110.

Osten, P., Khatri, L., Kohr, G., Giese, G., Daly, C., Schulz, T.W., Wensky, A., Lee, L.M., and Ziff, E.B. (2000). Mutagenesis reveals a role for ABP/GRIP binding to GluR2 in synaptic surface accumulation of the AMPA receptor. Neuron *27*, 313–325.

Passafaro, M., Piech, V., and Sheng, M. (2001). Subunit-specific temporal and spatial patterns of AMPA receptor exocytosis in hippocampal neurons. Nat. Neurosci. *4*, 917–926.

Perez, J.L., Khatri, L., Chang, C., Srivastava, S., Osten, P., and Ziff, E.B. (2001). PICK1 targets activated protein kinase C alpha to AMPA receptor clusters in spines of hippocampal neurons and reduces surface levels of the AMPA-type glutamate receptor subunit 2. J. Neurosci. *21*, 5417–5428.

Shen, L., Liang, F., Walensky, L.D., and Huganir, R.L. (2000). Regulation of AMPA receptor GluR1 subunit surface expression by a 4.1N-linked actin cytoskeletal association. J. Neurosci. *20*, 7932–7940.

Sheng, M., and Kim, M.J. (2002). Postsynaptic signaling and plasticity mechanisms. Science *298*, 776–780.

Shi, S.-H., Hayashi, Y., Petralia, R.S., Zaman, S.H., Wenthold, R.J., Svoboda, K., and Malinow, R. (1999). Rapid spine delivery and redistribution of AMPA receptors after synaptic NMDA receptor activation. Science *284*, 1811–1816.

Shi, S.-H., Hayashi, Y., Esteban, J.A., and Malinow, R. (2001). Subunit-specific rules governing AMPA receptor trafficking to synapses in hippocampal pyramidal neurons. Cell *105*, 331–343.

Song, I., and Huganir, R.L. (2002). Regulation of AMPA receptors during synaptic plasticity. Trends Neurosci. *25*, 578–588.

Song, I., Kamboj, S., Xia, J., Dong, H., Liao, D., and Huganir, R.L. (1998). Interaction of the N-ethylmaleimide-sensitive factor with AMPA receptors. Neuron *21*, 393–400.

Srivastava, S., Osten, P., Vilim, F.S., Khatri, L., Inman, G., States,

Studying Gene Function: Creating Knockout Mice

Hubert Walinski
Graphics:Fan Sozzi

Construction a knockout mouse

For decades researchers have tried to create tools that allowed for precise control over a specific gene in order to study its function. In the early 1980's a breakthrough technology known as transgenics or gene transfer was developed[1]. This new technology involved the process of pronuclear microinjection, a method involving the injection of genetic material into the nuclei of fertilized eggs. Following injection, DNA would incorporate into the genome of the cell. The transformed fertilized eggs were then injected back into pregnant females and brought to term. A major downfall of this technique is that researchers could neither predict nor control where in the genome the foreign genetic material would be inserted. Since a gene's location in the genome is important for its expression pattern, mouse lines carrying the same transgene could display wildly varying phenotypes.

An innovative solution that resolved this conflict was originated by a team of scientists led by Martin Evans, Oliver Smithies and Mario Capecchi who created what is known as a genetic "knockout". By creating a knockout they proved that it was possible to aim the inserted gene at a precise location in the mouse genome. This gave scientists the ability to replace, or knock out, a specific gene with an inactive or mutated allele. Therefore, knockout animals are considered an investigative technique that allows for a particular gene of interest to be removed, and define exactly what effect that gene has in the life of an organism. The gene knockout is created by selectively disabling a specific target gene in a particular type of cells called embryonic stem cells. The three scientists received the Lasker Award in 2001 for this achievement. The technique has been used to make several thousand different knockout mice. Knockout mice have become one of the most useful scientific tools in helping to understand the human genome and its roles in disease.

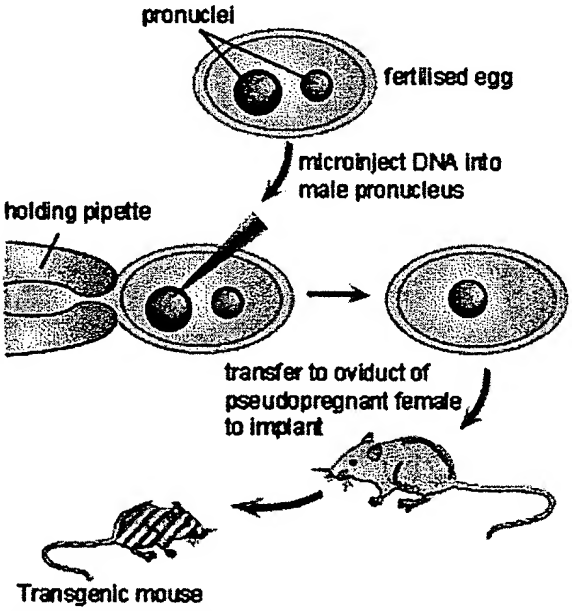

Figure 1. Pronuclear microinjection. Genetic material is injected directly into the fertilized egg which is then implanted back into a mouse and allowed to come to term.

The process of gene targeting involves two processes. First a vector must be constructed. Once this has been done, the vector must be put into embryonic stem cells and a new mouse made from these cells[1]. The vector consists of two regions of homology at either end, the disrupted gene of interest and two additional genes to allow for quality control in the process. The regions of homology are located at either end of the vector and are complementary to specific sites on the genome surrounding the gene of interest. The vector binds to the genome at these two points of homology. This technology then takes

advantage of the process of recombination to swap the disrupted gene for the real one. Here the two additional genes are used. In order to make sure that the vector has been inserted into the genome, the neomycin resistance gene is included. If the vector has not been inserted then all cells will die when the cells are grown in neomycin. It is also possible that the vector has been inserted into the genome in the wrong place. To make sure this has not happened, the thymidine kinase (tk) gene is also added into the construct outside the region of homology. If recombination has taken place then the tk gene will not be in the genome and so cells will be insensitive to gancyclovir. However if the vector has been inserted into the genome completely then the cell will die when grown in gancyclovir. Thus through positive and negative selection, cells with the correct insert can be isolated. Figure 2 illustrates this process.

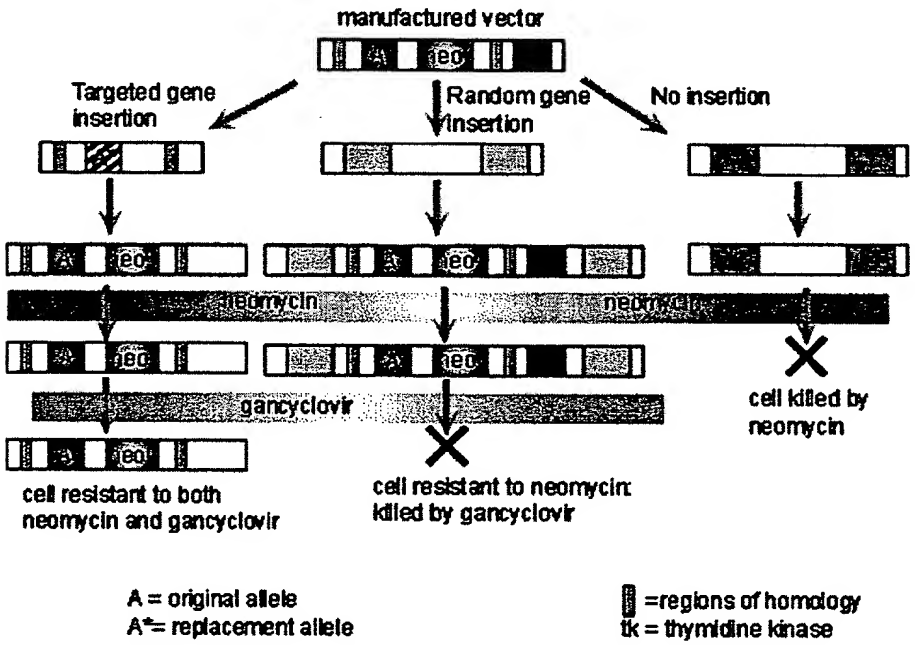

Figure 2. Construction of a vector. The vector consists of two homologous regions which have complementary strands of DNA either side of the targeted gene in the genome. The disrupted gene along with a gene coding for neomycin resistance are included between the homologous regions. A thymidine kinase gene is included outside the homologous region. Once the vector is introduced into the host cell, it can either be incorporated into the genome by homologous recombination (the desired result), undergo complete insertion into the genome at an undesirable point or not be taken up by the cell at all. Neomycin resistance is used to select for cells in which the vector has been taken up and then gancyclovir sensitivity is used to select for cells which have undergone recombination.

Embryonic stem cells are used as the target cells for the insertion of these vectors because they are pluripotent, meaning that they can give rise to every different type of cell in the adult body. Scientists interested in examining a specific gene will remove or "knock out" the gene in an embryonic stem cell as described above, then put the cell into a recently fertilized embryo. The manipulated cell then divides and eventually develops into many different tissues. The result is a mouse in which some of the cells have developed from the knocked-out embryonic stem cells. Often embryonic stem cells which give rise to mice with a brown coat colour are injected into blastocysts which give rise to mice with a white coat colour. This allows the researcher an easy way to see which mice have contributions from both the injected cells and the blastocyst: if a mouse is completely white, then no injected cells grafted with the blastocyst. On the other hand if the mouse has both brown and white markings on its coat, then the injection of knockout embryonic stem cells was successful. After finding mice which have contributions from both cell types, the mice are bred to propagate the knockout gene to a certain percentage of the progeny, a process known as germ-line transmission. Once germ-line transmission is achieved, it is possible to breed mice where some are missing the knocked-out gene while others are not. In this case the latter group can act as a control group to see if the

experiment has worked. Figure 3 illustrates the process of making knockout mice once the vector has been taken up by the cells.

Uses of knockout mice

Knockout mice are used in a variety of ways. They allow to test the specific functions of particular genes and to observe the processes that these particular genes could regulate. What actions does this gene it turn off and on Examining what is happening in an *in vivo* (inside the body) model, we are able to determine the effects a particular gene may have, that would otherwise be impossible to observe in a culture dish. However, to completely establish and assign an action to a particular gene is very challenging and requires an incredible amount of work.

One of the most exciting applications of knockout technology is in biomedical research. Scientists are using these models to study the progress of thousands of genetically based diseases at the molecular level. The hope is that by better understanding how a certain gene contributes to a particular disease, researchers can then take the knowledge a step further and look for drugs that act on that gene. Another essential application of knockout mice is in drug development. The knockout technology defines a path forward for the biopharmaceutical industry to discover the next generation of blockbuster potential therapies for curing numerous diseases based on novel targets from the human genome[4].

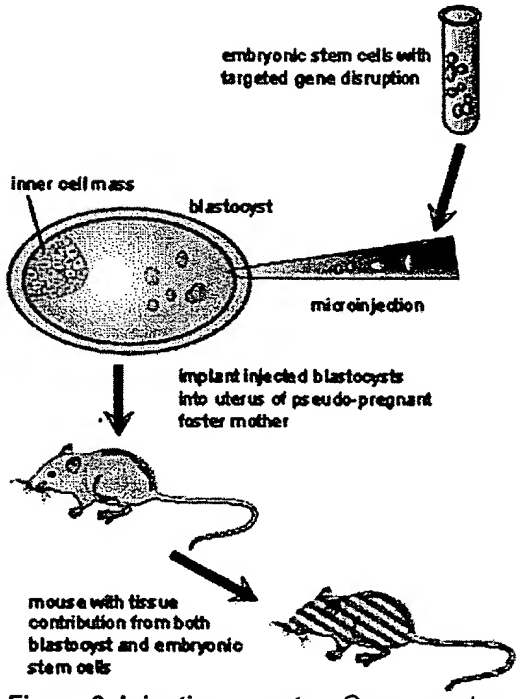

Figure 3. Injecting a vector. Once a vector has been incorporated correctly into the embryonic stem cells genome, the cells are expanded in culture and injected into 3.5 day old mouse blastocysts. The blastocysts are injected into the uterus of a pregnant female and the embryos allowed to come to term. Following selection of mouse with brown coat colour, these are bred to make pure knockout mice.

Although knockout technology is highly advantageous for both, biomedical research and drug development it also contains a number of limitations. For example, because of developmental defects, many knockout mice die while they are still embryos before the researcher has a chance to use the model for experimentation. Even if a mouse survives, several mouse models have somewhat different physical and physiological (or phenotypic) traits than their human counterparts. An example of this phenomenon is the *p53* knockout. Gene *p53* has been implicated in as many as half of all human cancers. However *p53* knockout mice develop a completely different range of tumors than do humans. In particular, mice develop lymphomas and sarcomas, whereas humans tend to develop epithelial cell-derived cancers[2]. Because such differences exist it cannot be assumed that a particular gene will exhibit identical function in both mouse and human, and thus limits the utility of knockout mice as models of human disease.

More advanced types of knockouts

Recently newer technologies have been developed which allow for conditional knockout or tissue-specific gene targeting. The goal of conventional knockout technology is to knock out both alleles so that the gene is entirely absent from all cells. The purpose of conditional knockouts, in contrast, is to delete a gene in a particular organ, cell type, or stage of development[3]. Researchers can use the technique to knock out certain portions of specific genes at particular times when it is important for them to do so. Conditional knockout mice have several benefits over the conventional technique. Not only do they typically survive longer than traditional knockout mice but also conditional knockout methods are more precise. There are several different ways to make conditional knockout models, however the most widely used method is the Cre-*loxP* recombinase system. Cre recombinase is an enzyme that works like scissors to cut out a gene that is in between two target sequences called *loxP*. Because this enzyme is expressed only in certain cell types, the

targeted gene will be knocked out of only those cells and only when the researcher wants them to be.

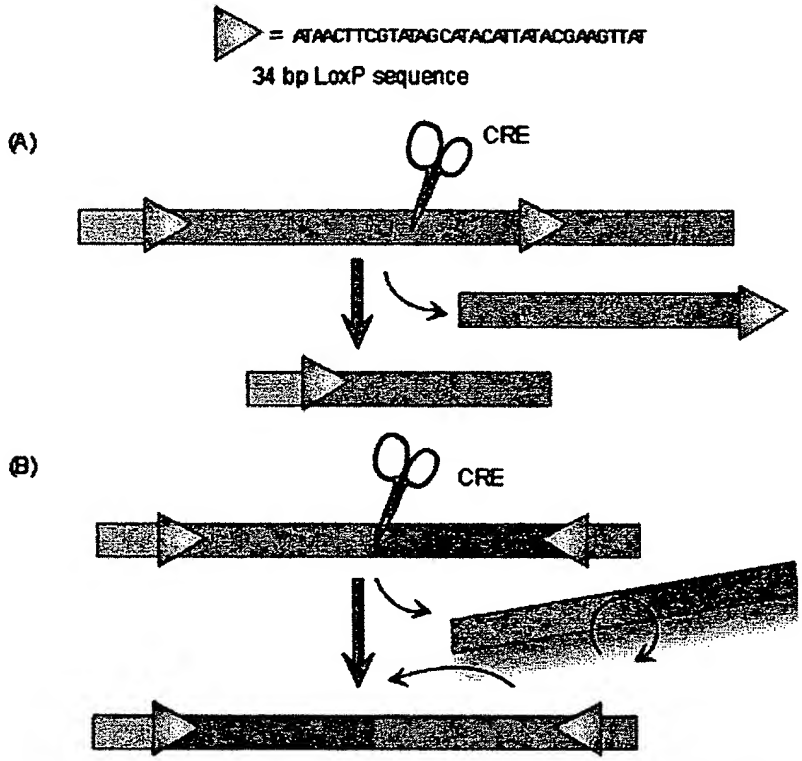

Figure 4. The Cre-*LoxP* system. The *loxP* site can be inserted either side of a piece of DNA. (A) If Cre recombinase is then expressed in the cell, the *loxP* site will be cut and joined together, removing the piece of DNA between the two sites. (B) Since the *loxP* site is directional, it can also be used to invert pieces of DNA which are between it. Here two *loxP* sites which are inserted either side of a piece of DNA in opposite directions. Once Cre is expressed, the *loxP* sites are both cut and the piece of DNA inverted and reattached.

Disadvantages of knockout technology

Although knockout mice are extremely useful in studying gene function, producing custom knockout mice is very expensive. Typical cost ranges anywhere from $3,000 to as much as $30,000. There are hundreds of knockout mice commercially available. These can be purchased from a variety of companies, one being The Jackson Laboratory (Jax) in Bar Harbor, Maine.

It is also important to consider the cost of care for genetically altered animals, as they require special transgenic core facilities where staff can assist researchers with housing and taking proper measures to keep these knockout animals at optimal conditions for research purposes. The cost of equipping and maintaining such a facility is usually very high and may be a limiting factor.

Conclusions

In conclusion, knockout mice are a wonderful tool used to study the function of specific genes in a system. Despite numerous concerns and limitations applying this technique, it provides tremendous insight into understanding the disease process. The development of a gene knockout mouse has been a massive advance to the biomedical and pharmaceutical field presenting researchers with a very powerful tool for analyzing gene function during development, as well as in disease. In short, gene knockout technologies have

become invaluable experimental tools for modeling genetic disorders, assigning functions to genes, evaluating drugs and toxins, and for helping to answer fundamental questions in basic and applied research. On top of it all, with constant evolution in biotechnology the future of knockout mice looks even friendlier!

References

1. (2002). The life history of the mouse in genetics. *Nature* 420: 510.
2. Pray L. (2002). Refining Transgenic Mice. *The Scientist* 16(13): 34.
3. Smith C.M. (2000). Technical Knockout. *The Scientist* 14(15): 32.
4. Zambrowicz B.P., Sands A.T. (2003). Knockouts Model the 100 Best-Selling Drugs—Will They Model the Next 100? *Nature Reviews Drug Discovery* 2: 38-51. PubMed

Additional Reading

1. Nagy A. (2000). Cre recombinase: The universal reagent for genome tailoring. *Genesis* 26(2): 99-109. PubMed

Contact us: ambl@interchange.ubc.ca

Related Articles	Related Resources
Restriction Endonucleases a description of the discovery and use of restriction enzymes.	MacGyver Project an experiment that allows you to isolate DNA using supplies found in your local IGA.
The Cre/*LoxP* System How Cre/*lox* works and why it is important.	Doogie Mouse using genetics to create smart mice
Serial Analysis of Gene Expresson a rapid means of providing scientists with a functional profile of gene expression.	Immortal Mouse references and a discussion on a hoax that was publish in the prestigous journal *Nature*.

Refining Transgenic Mice

Emerging technologies allow researchers to make tissue- and developmental stage-specific knockouts | **By Leslie Pray**

Mice have been freeloading on humans for millennia. Now, in laboratories around the world, scientists are returning the favor. Model systems such as the fruit fly *Drosophila melanogaster* and the nematode *Caenorhabditis elegans* are actually easier to work with than mice, but mice are more closely related to humans, making them better models of human physiology. "For modeling genetic diseases like breast cancer, you definitely need mammals," says **Kay-Uwe Wagner**, a molecular biologist at the Eppley Institute for Research in Cancer and Allied Diseases, Omaha, Neb.

Early in the 20th century, geneticists used inbred mouse strains for much of their work.[1] Long before the true nature of a gene was understood, geneticists were using inbred mice—genetically identical animals, akin to identical twins—to map murine genes. These early mice had other uses, too: they served as xenograft hosts and helped researchers tease apart the nuances of the immune system.

In the 1970s and 1980s, as molecular biology ascended, transgenic technology gave researchers the power to insert exogenous, human genes into mice. *Mus musculus* became the preferred model organism for investigators keen to understand the functions of human genes. But transgenic technology, while elegant, was crude by comparison with the gene "knockout" strategies that emerged later. This gene-targeting technology—also known as targeted mutagenesis and gene replacement technology—gave investigators a powerful new tool to study the genetic basis of mammalian development and disease. Most recently, researchers have refined these tools and begun exercising ever more precise control over the changes they make as they seek to discern a specific gene's function.

BREAKTHROUGH TECHNOLOGY Transgenic or gene transfer technology originated in the early 1980s with the development of a technique known as pronuclear microinjection: the transfer of genetic material into rodent embryos.[2] Researchers needed only an inverted microscope and a microinjector (see table), and by the end of the decade, hundreds of transgenic mouse lines were being produced in laboratories worldwide. The problem was, researchers could neither predict nor control where in the genome the foreign genetic material would insert. As a result, mouse lines carrying the same transgene could display wildly varying phenotypes. Then, **Mario Capecchi**, a human geneticist at the University of Utah, changed all that.[3]

"There was a breakthrough in altering the gene in the late '80s, early '90s, when the gene targeting technique was pioneered by Capecchi," explains Wagner. Using homologous recombination—the exchange of equivalent DNA sequences between the host genome and the introduced genetic material—Capecchi proved it was possible to aim the transgenic insertion, or transgene, at a precise location in the mouse genome.[4,5] This gave scientists the ability to replace, or knock out, a specific gene with an inactive or mutated allele. By comparing the phenotypes of these knockout mice to those of wild-type mice that still have all their genes intact, researchers can readily deduce the function of the targeted gene. Conversely, scientists can also "knock in" a wild-type gene to test whether a particular mutation causes a given phenotype. Last year, Capecchi, **Oliver Smithies**, and **Martin Evans** shared the Lasker Award for their seminal work in the development of knockout technology in mice.[3]

One of the most exciting applications of murine knockout technology is in biomedical research. Scientists are using the models to study the molecular pathologies of a variety of genetically based diseases, from colon cancer to mental retardation. The hope is that by better understanding how a certain gene contributes to a particular disease, researchers can then take the knowledge a step further and look for drugs that act on that gene.

Still, knockout technology has its limitations. Because of developmental defects, many knockout mice die as embryos before the researcher has a chance to use the model for experimentation. Even if a mouse survives, several mouse models have "somewhat different phenotypes" from their human counterparts, says Wagner. The *p53* knockout is a good example. *p53* has been implicated in as many as half of all human cancers, but *p53* knockout mice develop a different spectrum of tumors than do humans. In particular, mice develop lymphomas and sarcomas, whereas humans tend to develop epithelial cell-derived cancers. This phenotypic difference limits the utility of knockout mice as models of human disease.[6] Now, a new technology known as conditional knockout or tissue-specific gene targeting is providing a way around these limitations.

MOUSE HOUSE: *Scientists at Taconic's Molecular Analysis Laboratory genotype transgenic rat and mouse lines.*

THE NEXT GENERATION The goal of conventional knockout technology, explains Wagner, is to knock out both alleles so that the gene is entirely absent from all cells. The purpose of conditional knockouts, in contrast, is to delete a gene in a particular organ, cell type, or stage of development. Researchers can use the technique to knock out certain portions of specific genes. These conditional knockout mice offer at least two benefits. First, they typically survive longer than traditional knockout mice. In addition, if knockout mouse technology is more precise than transgenic technology, conditional knockout methods are even more so.

For more than a decade, for example, researchers have known of the link between *BRCA1* mutation and breast cancer. But *BRCA1* knockout mice, in which the entire gene was deleted, did not survive, hindering efforts to understand this gene's function. It was not until **Chu-Xia**

IMAGE: COURTESY OF TACONIC FARMS

SUPPLIERS OF MICROINJECTORS AND MICROMANIPULATORS

Applied Scientific Instrumentation
www.asiimaging.com

BioLogic Science Instruments
www.bio-logic.fr

Burleigh Instruments (now EXFO)
www.burleigh.com

Carl Zeiss
www.zeiss.com

Drummond Scientific
www.drummondsci.com

Eppendorf
www.eppendorf.com

Harvard Apparatus
www.harvardapparatus.com

Intracel
www.intracel.co.uk

Leica Microsystems
www.leica-microsystems.com

MicroData Instrument
www.microdatamdi.com

Micro Instruments
www.m-i.co.uk

Multi Channel Systems
www.multichannelsystems.com

Narishige International
www.narishige.co.jp

Nikon Instruments
www.nikon.com

Olympus
www.olympus.com

Research Instruments
www.research-instruments.com

Singer Instruments
www.singerinst.co.uk

Stoelting
www.stoeltingco.com

Sutter Instrument
www.sutter.com

Tritech Research
www.tritechresearch.com

World Precision Instruments
www.wpiinc.com

Editor's Note: To the best of our knowledge, these are comprehensive listings of suppliers.

Deng and his colleagues at the National Institutes of Health engineered *BRCA1* knockout mice with a disabled exon 11, that scientists began to understand the gene's precise function and role in tumorigenesis.[7] Indeed, Deng says that much of the attention that his work has received is from scientists who are just as, if not more, interested in his animal model than the results of his research.

There are several different ways to make conditional knockout models, but the most widely used method is the Cre-*lox*P recombinase system. Scientists use Cre recombinase like scissors, Wagner explains, to excise a gene that has been flanked by two *lox*P target sequences. Because Cre recombinase is expressed only in certain cell types, the targeted gene will be knocked out of only certain cells.

Like Deng, Wagner and his colleagues have been using the Cre-*lox*P recombination system to generate transgenic mice with mammary tissue-specific gene deletions. "You can narrow the window down even further to a particular time frame you want to study," says Wagner. "You can really refine the whole technology to do exactly what you want to do."

Wagner and his colleagues are using the Cre system to target and knock out transcriptional stop sequences as a way to permanently activate genes, enabling their use as cellular labels. By staining for the gene activity of these constitutive genes, says Wagner, researchers can follow the cells at any physiological stage.

Wagner's team is using this genetic labeling system in its search for cellular clues to why women who have been pregnant are at lower risk for breast cancer.[8] "We have identified a certain population of cells in the mammary gland that genetically are different but morphologically the same. Maybe these are the cells that protect." Wagner says that by labeling cells and making them traceable, researchers can learn much more about the kinds of cells that give rise to cancer. "It is very exciting," he concludes.

MICE FOR SALE Conventional knockout technology has become so well established that its methods are described in cookbook-style manuals. Conditional knockouts, on the other hand, are "a bit more complicated to make," says Wagner. Technical challenges aside however, there are two good reasons to obtain knockout mice from a third party, commercial or otherwise: time and money. **Donna Gulezian**, product manager at New York-based **Taconic**, estimates that it takes at least one to two years to make a new knockout mouse, and then the animals must be carefully scrutinized. Commercially available mice, on the other hand, tend to be fairly well characterized, she says. "If you're building on work that someone else has done," says Gulezian, "you can use the same mice without a loss of integrity."

Custom knockout mice are also big-ticket items. "Making a knockout is very, very expensive," explains Wagner. A core facility might charge from $3,000 to $10,000 to make a knockout mouse, while a contractor might charge as much as $30,000. Commercially available mice, in contrast, generally sell for several hundred dollars.

One of the primary suppliers is the not-for-profit **The Jackson Laboratory** (Jax) in Bar Harbor, Maine. With more than two million mice from over 2,700 different strains shipped to thousands of labs worldwide every year, Jax (**www.jax.org**) is the world's largest supplier of laboratory mice. And with more than 300 knockout mice already available or currently under development, they are also the largest supplier of knockouts.

Taconic (**www.taconic.com**) is the largest commercial supplier of transgenic mice and rats. According to Gulezian, the company sells about 40 different knockout lines to hundreds of institutions worldwide. About a third of their clients are academic institutions, one-third are government, and the remainder are for-profit institutions.

Except for about 30 of the in-house knockout strains that come from Jax, neither Jax nor Taconic actually creates the mouse models themselves. Rather, they work in collaboration with outside investigators who are engineering the models, says Gulezian. Most, but not all, of these investigators are in academia. Taconic then imports the line and does additional work to stabilize the genome and ensure the health of the line. Despite some overlap with lines from Jax, Taconic's aim is to produce unique lines. "Our *p53* knockout is definitely our top selling model," says Gulezian, finding wide use in short-term carcinogenicity studies. The MDR [multidrug resistance] knockouts, which are used for drug transport and availability studies, are also popular.

Although Jax and Taconic are the primary suppliers of already-engineered knockout mice, the UK-based **B & K Universal** (**www.bku.com**) also offers knockout mice commercially; they sell about a dozen different strains. And the MMHCC (Mouse Models of Human Cancers Consortium) Repository at the National Cancer Institute in Frederick, Md., which was founded just last year, has about 10 knockout strains currently available

PHOTO: COURTESY OF TACONIC FARMS

(web.ncifcrf.gov/researchresources/mmhcc/information/about.asp).

MOUSE HOUSES ON CAMPUS Many universities have on-campus transgenic core facilities, where staff can assist researchers with everything from engineering the knockouts to housing them. Washington State University's (WSU) Center for Reproductive Biology, for example, has a transgenic core facility for which space was set aside in one of the campus vivariums, according to **Eric Nilsson**, a researcher at WSU and one of the staff who oversees the facility. The core has existed for about two years, according to Nilsson, with usually three or four researchers using it at any one time. Most of the knockouts that the core scientists use come from Jax and Taconic, but the core also subsidizes researchers who develop their own knockouts.

One of the primary advantages to having this kind of for-hire resource on campus is that scientists need not know anything about knockout technology to use the facility. If the prospect of incorporating knockout technology into your research program is too daunting to set out on your own, you just ask for help. "That's part of my job," says Nilsson. "To help lead you through."

But before committing the resources to make a knockout mouse, researchers should be certain that nobody has beaten them to the punch. Contact the primary mouse vendors, as well as prominent researchers in the field. A small bit of legwork could save months or even years of bench work. "I would bet lots of animal models are shipped between researchers for collaboration," observes Wagner. Indeed, he says, many researchers don't make their models commercially available at all. ⊗

Leslie Pray (lpray@nasw.org) is a freelance writer in Leverett, Mass.

References

1. B.A. Maher, "Test tubes with tails," *The Scientist*, 16[3]:22–4, Feb. 4, 2002.
2. Taconic Transgenic Models and Services Division, Access to Transgenic Technologies, Taconic, NY, 1997.
3. B.A. Maher, "Lasker ceremony: Homage amidst angst," *The Scientist*, 15[20]:10, Oct. 15, 2001.
4. M.R. Capecchi, "The new mouse genetics: altering the genome by gene targeting," *Trends in Genetics*, 5:70–6, 1989.
5. M.R. Capecchi, "Altering the genome by homologous recombination," *Science*, 244:1288–92, 1989.
6. J.M. Perkel, "Telomeres as the key to cancer," *The Scientist*, 16[11]:38–40, May 27, 2002.
7. L. Pray, "The role of BRCA1 in breast cancer," *The Scientist*, 15[12]:23, June 11, 2001.
8. K.U. Wagner et al., "An adjunct mammary epithelial cell population in parous females: Its role in functional adaptation and tissue renewal," *Development*, 129:1377–86, March 2002.

USPS, Biotech Forge Alliance

Companies vie for lucrative pathogen-detection system contracts | **By Jim Kling**

In its ongoing efforts to ensure the safety of the mail system, the US Postal Service (USPS) is turning to PCR-based pathogen-detection systems. On May 13, USPS announced a $3.7 million (US) agreement with the Baltimore, Md.-based Automation and Information Systems division of **Northrup Grumman**, to test a multicompany system in one of the USPS's central processing facilities. At the core of the technology is the GeneXpert® system developed by Sunnyvale, Calif.-based **Cepheid**. A competing device from **Lockheed Martin** is undergoing prequalifying evaluations.

Soon after the October 2001 anthrax attacks, USPS decided to install a biological detection system to head off future attacks. It consulted the military, which suggested PCR-based approaches over immunoassays or mass spectroscopy-based instruments. "It's a proven technology, and the military has been using it since the Gulf War for field-testing of anthrax in a combat environment," says USPS spokesman **Gerry Kreienkamp**.

But surveying the USPS presents very different challenges from the battlefield. The threat comes from powder-laden letters sorted along with harmless envelopes through pinch rollers, which sort them into appropriate bins in central processing facilities. Last October, those pinch rollers liberated anthrax spores from letters intended for Sens. **Tom Daschle** (D–SD) and **Patrick Leahy** (D–Vt.), causing a cross-contamination that officials now believed killed two women in New York City and Connecticut.

"So our strategy is this: We want to [identify] a release at these pinch points... so we know if we detect the presence of a biohazard in some piece of mail at the first piece of equipment that it's run through, then we can isolate it. That letter will not have left the building," says Kreienkamp.

Northrop's system is based on Cepheid's GeneXpert technology, which boasts a turnaround time of less than 30 minutes. According to **Kurt Petersen**, Cepheid's president, its efficiency is due to two key improvements over other systems—ultrasonic lysing and freeze-dried PCR components. Ultrasonic lysing obviates the need for harsh lysing chemicals, which otherwise must be removed from the sample prior to PCR analysis. The freeze-dried components are particularly vital for a system that gets used on the battlefield, though not as critical in a post office. "There is no practical way of having refrigerated reagents in a field situation," says Petersen.

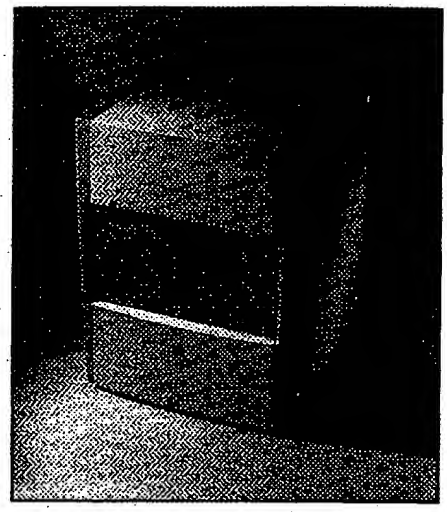

SILENT SENTINEL: *Cepheid's GeneXpert system, core of a developmental bio-hazard detection system intended for use in postal processing facilities.*

For security reasons, Lockheed Martin is remaining tight-lipped about the nature of its system, saying only that it is very early in the testing process with USPS and that it differs substantially from the BioMail™ system that is currently in use to screen mail systems in both government and commercial applications.

The company that comes out on top can expect a big payoff, as USPS will install systems into about 290 processing facilities. But the competition is intense. "I can't say enough about the dedication of the post office employees," comments Petersen. "The testing was grueling. You arrived at 7 am and you left at 8 pm at the earliest, and the postal service people were still there." ⊗

Jim Kling (jkling@nasw.org) is a freelance writer in Washington, DC.

PHOTOS: COURTESY OF CEPHEID

The life history of the mouse in genetics

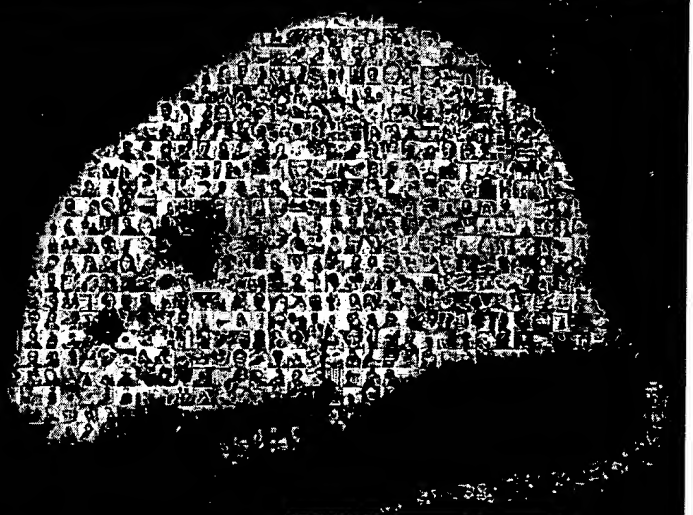

1999
The Mouse Genome Sequencing Consortium

At its inception in 1990, the Human Genome Project included the mouse as one of its five central model organisms to have its genome sequenced. In 1999, with the human genome sequence well under way, three major sequencing centres (the Wellcome Trust Sanger Institute, the Whitehead Center for Genome Research and Washington University Genome Sequencing Center) launch a concerted effort to sequence the mouse genome, under the title of the Mouse Genome Sequencing Consortium. By 2002, the consortium has expanded to embrace scientists from 26 institutes in six countries.

2001 Feb
The human genome

The first drafts of the human genome are published. The publicly funded International Human Genome Sequencing Consortium publishes its draft sequence in *Nature*, going head-to-head with Celera Genomics, a US-based company led by Craig Venter, which publishes in *Science*. Both of these milestone achievements provide a panoramic view of our genomic landscape, estimating a

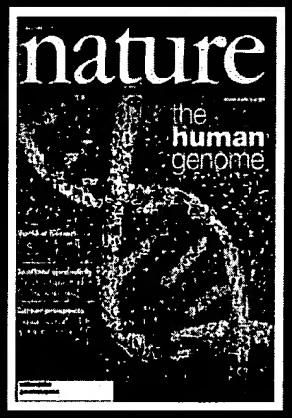

size of 3.2 billion base pairs (Gb) and predicting some 31,000 genes. Much work needs to be done to produce a complete sequence, but the collaborative effort of the public consortium coupled with the Celera sequence reflect an unprecedented achievement.

2001 June
The private shotgun mouse genome

Celera sells its draft mouse sequence, which has been generated by whole-genome shotgun sequencing — a technique in which the entire genome is sequenced at once. Five-fold coverage of the mouse genome is made available to private customers for $45,000 for a three-year contract. Celera's sequence is made up of four strains of mouse, including DBA, but not C57BL/6J — the subject of the publicly funded sequencing effort.

2002 May
Mouse chromosome 16

Using the sequence generated by Celera's private mouse genome, Richard Mural *et al.* publish an analysis of the sequence of mouse chromosome 16 in *Science*. They find that there is a large region with high genetic similarity to human chromosome 21, which has already been well characterized.

2002 Aug
Physical map of the mouse genome

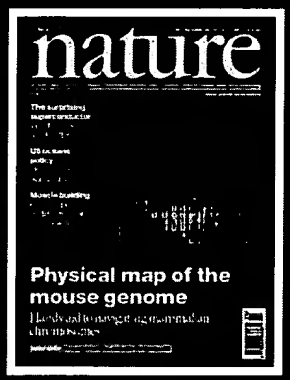

An international consortium provides the framework for the full determination of the mouse DNA sequence by building a physical map of the genome. Large blocks of correspondence between mouse and human sequences make it possible to lay out chunks of decoded mouse sequence and, conversely, the mouse map can be used to fill gaps in the human genome.

2002 Dec
The mouse genome

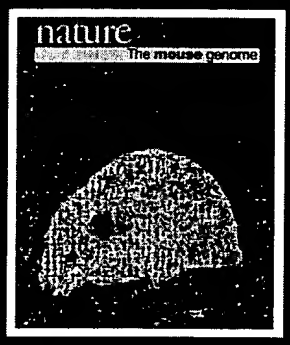

The Mouse Genome Sequencing Consortium publishes the culmination of international efforts — a high-quality draft sequence and analysis of the genome of the C57BL/6J mouse strain. The estimated size is 2.5 Gb, smaller than the human genome, with less than 30,000 genes. About 40% of the human and mouse genomes can be directly aligned with each other, and about 80% of human genes have one corresponding gene in the mouse genome. Accompanying papers detail various other aspects of the genetic make-up of the mouse, and through the efforts of the RIKEN Genome Science Laboratory in Japan, many essential resources are made freely available.

For an extended, interactive version of this timeline, visit our Mouse Genome Web Focus at ▸ www.nature.com/nature/mousegenome, which also contains all of the articles on the mouse genome from this special issue, available free. These are accompanied by related articles from the archives of *Nature* and *Nature Reviews Genetics*, available free until 5 March 2003.

timeline

The house mouse, *Mus musculus*, has been inextricably linked with humans since the beginning of civilization — wherever farmed food was stored, mice would be found. Many of the advances in twentieth-century biology owe a huge debt to the mouse, which has become the favoured model animal in most spheres of research. With the completion of the draft sequence of its genome published in this issue, the mouse promises to continue to provide us with an essential resource for all aspects of biology. In this timeline, we chart the key events in the history of the mouse that led to this landmark achievement.

75–125 million years ago
A common ancestor of mice and humans

M. A. KLINGENIUS

The common ancestor of mice and humans — a creature about the size of a small rat — lives alongside the dinosaurs. The picture above is 125-million-year-old *Eomaia scansoria*, the earliest known representative of the Eutheria lineage, which gave rise to all modern placental mammals.

~6 million years ago
Mus

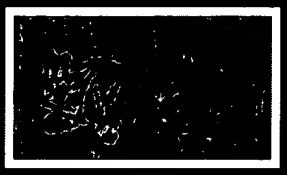

PRINCETON UNIVERSITY DUNHUANG PROJECT

The genus *Mus* is established, although the name comes much later, via Latin, from the ancient Sanskrit word 'mush', meaning to steal. *Mus musculus*, the house mouse, does not appear as a distinct species until after the end of the last ice age, at about 8,000 BC. The picture shows an early depiction of the mouse in a detail from a Chinese zodiac dating from AD 877.

1900
Fancy mice become lab mice

Generations of 'fancy mice' are created during the nineteenth century, as hobbyists selectively breed the house mouse. These mice have a range of different coat colours, and among the mutations created are agouti and satin, both still used in research today. In 1900, Abbie Lathrop, a retired schoolteacher, turns her hobby of breeding fancy mice into a business, selling the animals from her farm in Granby, Massachusetts. Within two years, biologist William Ernest Castle (above) has begun buying mice from her to conduct experiments in his lab in nearby Harvard, testing Mendel's laws of inheritance on coat colours.

1909
Birth of the lab mouse

Clarence Cook Little (above), a Harvard biologist from William Castle's lab, develops the first inbred mouse strain, known as DBA (dilute brown non-agouti). He is convinced that studying a genetically pure breed will unlock the secrets of human diseases such as cancer. This event is subsequently hailed as the birth of the modern lab mouse, and DBA mice are still used in genetics labs today.

1921
C57BL

Clarence Little breeds the mouse strain C57BL from a female mouse code-numbered 57 bought from Abbie Lathrop's farm. C57BL becomes one of the most widely used and important mice to geneticists, and is the strain that will have its genome sequence completed and published in 2002.

1929
The Jackson Laboratory

Two car barons, Edsel Ford (son of Henry) and Roscoe Jackson, head of the Hudson Motorcar Company, provide backing for Clarence Little to set up the Jackson Laboratory in Bar Harbor, Maine. The lab grows into one of the world's most important research centres for mouse genetics.

1972
First computer database for mouse genetics

The Jackson Laboratory updates its card-file database for mouse genetics by designing the first computer database for mammalian genetics. It forms the precursor to the Mouse Genome Database, which will serve as the hub of mouse-genome sequencing projects.

1982
First transgenic mouse

JACKSON LAB

A team led by Richard Palmiter and Ralph Brinster fuse elements of a gene that can be regulated by dietary zinc to a rat growth-hormone gene, and inject it into fertilized mouse embryos. The resulting mice, when fed with extra zinc, grow to be huge, and the technique paves the way for a wave of genetic analysis using transgenic mice.

1987–89
The first knockout mouse

Teams led by Martin Evans, Oliver Smithies and Mario Capecchi create the first 'knockout' mice, by selectively disabling a specific target gene in embryonic stem cells. The three receive the Lasker Award in 2001 for this achievement, and the technique goes on to be used to create several thousand knockout mice.

1998
Mouse clones

After Dolly the cloned sheep in 1997, a team in Hawaii produces Cumulina and her clones, the first cloned mice.

Technical Knockout

Gene-targeting strategies provide an avenue for studying gene function

By Christopher M. Smith

A few years ago, a scholarly scientific society published an anecdote in its monthly newsletter that described the different approaches to scientific discovery taken by geneticists and biochemists. In the story, a geneticist and a biochemist are on a hill overlooking an auto manufacturing plant, observing parts and workers going into one end of the plant and a finished product moving out of the other. The two are intrigued and want to find out how the familiar-looking product, a metal shell with transparent solid parts sitting on round rubber rings, works. The biochemist's approach is to steal one of the finished products, then take it apart and analyze each part separately. The geneticist's approach is to tie up certain workers or steal certain parts before assembly, then observe (from afar!) the effect on the product exiting the plant.

The latter approach essentially describes what is referred to as "knockout" or "gene-targeting" technology: the targeted removal of a specific gene or cassette of genes from an organism's genome. The organism of choice in modern biomedical research is the mouse, *Mus musculus*. For genes without a known function, researchers can attempt to define a function by knocking the gene out of the genomic repertoire of a mouse, then observing the resultant phenotype. In this synopsis of knockout technology, techniques and biologicals as they apply to generation of knockout or "null" mice will be emphasized instead of gene therapy of mammalian genetic disorders and diseases. But keep in mind that many technological principles and methods apply to both.

The Embryonic Years

Historically, researchers studying gene function have used various natural and induced mutant organisms, including bacteria, insects, plants, and mammals (especially mice). Over the last decade, researchers have made major inroads in understanding human development by studying mice with unusual, mutant phenotypes and analyzing the gene or genes contributing to that phenotype. Mice are perfect models for human development. Biologically speaking, they have many of the same genes, and hence many of the same genetic diseases as humans. They also have a short lifespan, enabling study of the full developmental cycle of various genes. A variety of mice bearing a broad spectrum of phenotypes are easily obtainable in the laboratory through various crossings or through animal research suppliers such as The Jackson Laboratory of Bar Harbor, Maine, a not-for-profit research institution and international repository for mouse models for biomedical research. Unfortunately, the classical method for generating mutants is rather laborious and time consuming, and the majority of potentially biologically important cloned genes do not have a corresponding mutation in the mouse stocks.[1] The intensity of research up to the early 1980s had for the most part exhausted the supply of unique and useful mutants, and the technology at the time could not meet the growing need for genetically defined mutant mouse strains. The advent of gene-targeting technology overcame many of these hurdles.

Gene-targeting technology was the product of two critical scientific discoveries during the early 1980s. The first was development of a cultured line of pluripotent mouse embryonic stem (ES) cells by Gail Martin of the University of California, San Francisco.[2] These cells could be maintained indefinitely in the undifferentiated state, but if the culture conditions were changed or the cells returned to their natural environment, they were capable of differentiating into all the cell types of the embryo. The second scientific advance was the demonstration that foreign DNA (a vector construct bearing a marker gene) transfected into ES cells became part of the genetic makeup of all

Above, embryonic stem cells cultured with Life Technologies' Knockout Serum Replacement

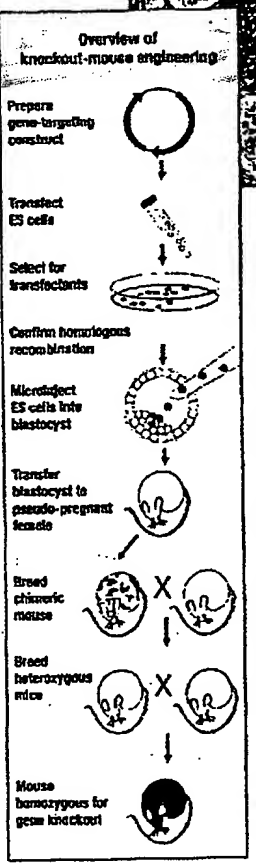

embryonic cell types after injection into a mouse blastocyst.[3] Subsequently, R.D. Palmiter and colleagues demonstrated the first phenotypic change in a transgenic mouse.[4] They created a targeting vector containing the gene for a rat growth hormone under the control of a heterologous promoter. The resultant transgenic mice expressed massive amounts of the growth hormone and thus grew and grew and grew! The image of these "super" mice attracted media attention, and the mice quickly became the poster children for what the technology could accomplish. Many other researchers were also able to demonstrate the inheritance (germ line transmission) of marker genes introduced into a mouse through this technology.[5] The heritability of introduced genes was the last biological hurdle to overcome in the generation of new, genotype-defined mutant mice for research.

Right on Target

The process of creating a transgenic mouse follows six basic steps: 1) creating a gene-targeting construct; 2) transfecting this construct into ES cells; 3) selecting for transfected cells and confirming homologous recombination; 4) microinjecting the transgenic ES cells into a blastocyst; 5) transferring the blastocyst to a pseudopregnant female; and 6) performing various back- and self-crosses to ensure the generation of a mouse homozygous for the target gene. Although these steps may seem straightforward, each has its own set of difficulties.

Designing the targeting vector is perhaps one of the most important procedures in generating a knockout mouse. The vector's composition will have a major impact on transfection and targeting efficiency and the ability to select and screen for ES cell transformants. The typical targeting vector is composed of a plasmid backbone, selection markers, and target DNA (homologous to the target gene chromosomal integration site) derived from the host genome. The plasmid backbone provides the framework with which to manipulate and produce target vector in a microbial host. It usually contains an origin of replication and an antibiotic marker to select for the targeting construct. Positive selection markers allow discrimination between transformed and nontransformed ES cells based on antibiotic resistance. For example, the *neo* gene encodes neomycin phosphotransferase, which mediates host cell resistance to the antibiotic G418.

One inherent problem with positive selection is that it does not differentiate between ES cell transformants that are the product of random (nonhomologous) recombination events and those derived from homologous events. S.L. Mansour and colleagues, who introduced the concept of positive-negative selection, resolved this.[6] In a nutshell, a targeting construct bearing a positive-negative selection cassette contains a standard positive selection marker and a negative selection marker positioned at each end of the target DNA. Negative selection markers include the human or herpes simplex virus *TK* (thymidine kinase) genes and the *HPRT* (hypoxanthine-guanine phosphoribosyltransferase) gene. During homologous recombination, the negative marker gene is not incorporated into the host genome, whereas in random (nonhomologous) recombination the marker is transferred. Thus, by selecting against the marker, one can specifically isolate homologous recombination-generated transformants.

Stratagene of La Jolla, Calif., in collaboration with Lexicon Genetics Inc. of The Woodlands, Texas, provides a comprehensive suite of molecular and cell biology products specifically developed to generate knockout mice. The pKO Scrambler Series® of gene-targeting vectors provides two "scrambled" polylinkers for bidirectional subcloning of mouse genomic fragments as well as insertion sites for selection markers. The scrambled polylinkers, designated "Scrambler A" and "Scrambler B," contain unique restriction sites and are located upstream and downstream of the selection cassette. The polylinker combinations provide a wide variety of restriction-ligation options for incorporating target genomic DNA. Positive, negative, and conditional selection may easily be incorporated into the parent pKO Scrambler-based targeting construct through use of selection elements from any one of a series (pKO Select) of selection plasmids. The pKO SelectNeo and pKO SelectPuro plasmids provide positive selection (neomycin and puromycin resistance, respectively); pKO SelectTK (thymidine kinase) provides negative selection; and pKO SelectHPRT (hypoxanthine-guanine phosphoribosyltransferase) provides conditional selection. Also available is the pKO Scrambler NTKV vector series, which contains both *neo* and *TK* genes for built-in positive-negative selection. Once a researcher has created a pKO targeting vector, a collection of tools called The Mouse Kit™ provides all the necessary ES and feeder cell lines, cell culture/growth media, reagents, and detailed technical protocols for transfecting ES cells and selecting transformants. Once ES transformants are identified and targeted clones verified, they can be microinjected into the blastocysts of mice.

Researchers may also construct a targeting vector from scratch using a plasmid backbone, polylinker, and selection cassettes from the cloning vectors offered by number of major molecular biology suppliers. Although many providers do not specifically label their products for gene knockout or gene therapy research, it is important to note that many of their products or derivatives of their products have extensive applications in this area. For example, H. Leblois and colleagues report using sequence elements from various vectors: pBS246 from Life Technologies of Rockville, Md.; pCEP4 and pCMV-EBNA from Invitrogen of Carlsbad, Calif.; pUT641 from Cayla of Toulouse, France; and pCITE2a from Novagen of Madison, Wis., to construct their novel targeting vector.[7]

Products & Services for Knockout Gene Technology

Company	Cloning Vectors	ES & Feeder Cell	Cell Culture Media	Mouse Strains	Comments
American Type Culture Collection (703) 365-2700, www.atcc.org		✔	✔		
BD PharMingen (877) 232-8995, www.pharmingen.com	✔				
Charles River Laboratories (800) 522-7287, www.criver.com				✔	Offers breeding, genotyping, and phenotyping services, supplies superovulated mice, offers backcrossing to well-characterized background strains
CLONTECH Laboratories (800) 662-2566, www.clontech.com	✔	✔			Tet-On & Tet-Off Expression Systems, RevTet-On & RevTet-Off Systems, Retro X Systems, MSCV Retroviral Systems
DNX Transgenic Sciences (509) 860-0806, www.dnxsciences.com	✔	✔		✔	Mouse models sold through Taconic
Gene Therapy Systems (888) 428-0558, www.genetherapysystems.com	✔	✔	✔		gWiz high expression vectors, pGeneGrip vectors
Harlan (317) 894-7521, www.harlan.com				✔	
HyClone Laboratories (800) 492-5663, www.hyclone.com			✔		Fetal Bovine Serum screened for ES cells
Incyte Genomics (800) 430-0030, www.incyte.com	✔	✔			Custom model production, including gene cloning, mapping, sequencing, vector construction, targeting in ES cells, generation of chimeras, phenotype assessment, morphological analysis, ISH, GEM
Invitrogen (800) 955-6288, www.invitrogen.com	✔				pBC1 MAR Expression Vector Kit
The Jackson Laboratory (207) 288-5000, www.jax.org		✔		✔	
Lexicon Genetics Inc. (281) 364-0100, www.lexgen.com		✔	✔	✔	The Mouse Kit (marketed in collaboration with Stratagene)
Life Technologies (800) 828-6686, www.lifetech.com	✔		✔		Cre-lox® vectors, Knockout SR (Serum Replacement)
New England Biolabs Inc. (800) 632-5227, www.neb.com	✔				
Novagen (800) 252-0144, www.novagen.com	✔				Anti-Cre Antibody to monitor the presence of Cre protein in mammalian systems
Promega Corp. (800) 356-9526, www.promega.com	✔		✔		TransFast, Tfx-10, Tfx-20, Tfx-50, and ProFection Transfection Reagents; pSI, pCI, pCI-neo, pALTER-MAX, and pTarget Vectors
Qiagen (800) 424-6101, www.qiagen.com	✔				AdEasy Adeno-Quest, AdenoExpress Reporter (LacZ, GFP)
Sigma (800) 325-3010, www.sigma-aldrich.com	✔		✔		
Specialty Media (800) 543-6029, www.specialtymedia.com		✔	✔		
Stem Cell Technologies Inc. (800) 667-0322, www.stemcell.com		✔	✔		ES-Cult Products: a comprehensive product line of reagents for the in vitro differentiation of murine embryonic stem cells
Stratagene (800) 424-5444, www.stratagene.com	✔	✔	✔		pBD Scrambler Series and pBD Select Vectors, Gene Knockout Product Line
Taconic (800) 822-6642, www.taconic.com				✔	

"Gene trapping" is another strategy used to enhance selection for homologous recombination-derived transformants.[8] This strategy capitalizes upon chromosomal elements near the target locus that are not part of the targeting vector. These chromosomal elements drive the transcription of a positive selection marker located within a targeting cassette that has been specifically position-inserted into the chromosomal DNA by homologous recombination.

Perhaps the most important element of a targeting vector is the target DNA—that is, the DNA that flanks the chromosomal locus of the gene being replaced (replacement vectors) or at the site where one wishes to insert a gene (insertional vector). Two critical factors that come into play here are the sequence identity between the target vector and the genome of the target cell and the length of the homologous regions.[5,9] Ideally, the flanking chromosomal DNA used in constructing the targeting vector should be obtained from the genome of the ES cell line into which the targeting construct will be transfected. The longer the homologous regions, the greater the targeting efficiency and hence the success rate in developing knockout strains. Generally, 5–8 kb of homologous DNA flanking the selection cassette should be included in the targeting construct.

Planting a Seed

The standard transfection host for the targeting vector is the pluripotent ES cell isolated from mice.[7] ES cell lines from other organisms (monkey, hamster, human) are now also available. Most mouse ES cell lines are derived from the 129Sv mouse strain and can be self-prepared or obtained from several research animal and cell providers.

ES cells are typically maintained on a layer of nondividing feeder cells (mouse embryonic fibroblasts). The feeder cells produce growth factors used by the ES cells and provide a matrix for ES cell adhesion. It is recommended that researchers use feeder cells that are resistant to the selection agents (e.g., antibiotics) used in the post-transfection screening for transformed ES cells. Feeder and ES cells are generally maintained in a growth medium composed of supplemented Dulbecco's Modified Eagle Medium (DMEM) and fetal bovine serum (FBS). Most feeder cells and culture media may be prepared independently or obtained from a commercial supplier.[10] Both the Stratagene-Lexicon Mouse Kit system and the EmbryoMax Mouse Cloning Kit from Specialty Media of Phillipsburg, N.J., include ES cells, feeder cells, and culture media. Researchers wishing to circumvent potential problems with undefined ES cell differentiation factors in FBS may substitute Life Technologies' KNOCKOUT™ Serum Replacement.

Insertion of the linearized targeting cassette into ES cells is accomplished via a number of transfection techniques.[10] The transfected cells are then returned to plates of feeder cells and ES culture medium to recover. After a day or two, selection agents are added to the growth media and transformants identified through cell growth in the presence of these agents. Selected transformants are then subjected to PCR and/or Southern blot analysis to verify homologous recombination. Replacement and insertion recombination will yield transformants lacking the targeted endogenous gene, or carrying a targeted exogenous gene, respectively.

Historically, ES cell transformants have been inserted into a blastocyst through microinjection techniques. This process requires much manual dexterity and sophisticated (i.e., expensive!) equipment. This hurdle has recently been circumvented through "coculture" or "clumping needle aggregation" techniques.[11,12] These techniques simply require the researcher to cocultivate the transformed ES cells with denuded eight-cell embryos (morulae lacking the zona pellucida glycoprotein sphere), then recover the transformed blastocyst and implant it into a pseudopregnant female mouse. This technique allows many researchers to embrace gene-targeting technology.

Chimeric mice produced from the blastocyst implant will be heterozygous for the target gene. Through a series of back- and self-crosses, a mouse homozygous for the targeted gene can be generated. This genetically defined, stable, transgenic mouse can then be used for any number of biochemical and physiological studies. These tests usually aim to decipher the intricate details of the function of the targeted gene and/or its gene product, and its relationship to other genes and gene products.

Old Problems, New Solutions

Knockout mice have been instrumental in assessing mammalian reproductive and developmental physiology. In the not so distant future, medicine may also benefit from knockout technology. A research team at the Massachusetts General Hospital in Boston has reported a gene knockout that prolongs ovarian lifespan in mice, a finding that may have implications for human reproductive therapy.[13] Knockout strategies are also being used to investigate sickle cell disease.[14]

One of the biggest limitations of knockout technology is that embryos with defects in early developmental genes often do not survive gestation. Although this provides clues that the altered gene is involved in the earliest stages of development, downstream consequences of the knockout are not observable. One experimental approach to combat this involves introducing a construct expressing a particular portion of the knockout gene into the null background to rescue the developmental defect but not downstream functions. Recently *GATA-2* null mice, which succumb to midgestational death from hematopoietic failure, were rescued with a yeast artificial chromosome bearing *GATA-2* sequences.[15] Restored hematopoietic function allowed full gestation, but the rescued pups were found to have genitourinary abnormalities, suggesting that *GATA-2* also plays a role in urogenital development.

One of the long-standing concerns of gene targeting with selection cassettes has been the possibility that expression of the selection markers may interfere in unpredictable ways with the phenotype of the knockout organism. Researchers have developed a mechanism to excise the selection cassette from transformed, selected ES cells prior to incorporation into the blastocyst.[16] During construction of the targeting vector, the selection cassette is bracketed at both ends by a 34 bp sequence motif, *loxP*. After selection of recombinant transformed ES cells, the selected cells are transiently transfected with a vector expressing the Cre recombinase. The Cre protein excises sequences between the *loxP* sites; thus the selection cassette is easily removed from the target site in the host cell chromosomal DNA. This same system can also potentially be used to modify the target gene (via deletions, replacements, insertions, and point mutations), in a cell type-specific and inducible manner.

Additional resources for gene targeting/knockout technology information can be found at www.the-scientist.com/yr2000/jul/index_000724.html. The list includes practical guides (books), journals, organizations, databases, and other Web resources.

Christopher M. Smith (csmith@sdsc.edu) is a freelance writer in San Diego.

References

1. T.W. Mak (ed.), *The Gene Knockout Factsbook*, New York, Academic Press, 1998.
2. G.R. Martin, "Isolation of a pluripotent cell line from early mouse embryos cultured in medium conditioned by teratocarcinoma stem cells," *Proceedings of the National Academy of Sciences*, 78:7634–8, 1981.
3. R.L. Brinster et al., "Somatic expression of herpes thymidine kinase in mice following injection of a fusion gene into eggs," *Cell*, 27:223–31, 1981.
4. R.D. Palmiter et al., "Dramatic growth of mice that develop from eggs microinjected with metallothionein-growth hormone fusion genes," *Nature*, 300:611–5, 1982.
5. K.R. Thomas, M.R. Capecchi, "Site-directed mutagenesis by gene targeting in mouse embryo-derived stem cells," *Cell*, 51:503–12, 1987.
6. S.L. Mansour et al., "Disruption of the proto-oncogene *int-2* in mouse embryo-derived stem cells: a general strategy for targeting mutations to non-selectable genes," *Nature*, 336:348–52, 1988.
7. H. Leblois et al., "Stable transduction of actively dividing cells via a novel adenoviral/episomal vector," *Molecular Therapy*, 1:314–22, April 2000.
8. K. Kitajima, T. Tokuoshi, "Mouse gene trap approach: identification of novel genes and characterization of their biological functions," *Biochemistry and Cell Biology*, 76:1029–37, 1998.
9. L.A. Galli-Taliadoros et al., "Gene knockout technology: a methodological overview for the interested novice," *Journal of Immunological Methods*, 181:1–15, 1995.
10. A.L. Joyner, *Gene Targeting: A Practical Approach*, 2d ed., Oxford, U.K., Oxford University Press, 2000.
11. S.A. Wood et al., "Simple and efficient production of embryonic stem cell-embryo chimeras by co-culture," *Proceedings of the National Academy of Sciences*, 90:4582–5, 1993.
12. A. Nagy et al., "Derivation of completely cell culture-derived mice from early-passage embryonic stem cells," *Proceedings of the National Academy of Sciences*, 90:8424–8, 1993.
13. G. Perez et al., "Prolongation of ovarian life span into advanced chronological age by *Bax*-deficiency," *Nature Genetics*, 21:200–3, February 1999.
14. T.M. Ryan et al., "Knockout-transgenic mouse model of sickle cell disease," *Science*, 278:873–6, 1997.
15. Y. Zhou et al., "Rescue of the embryonic lethal hematopoietic defect reveals a critical role for *GATA-2* in urogenital development," *The EMBO Journal*, 17:6689–700, 1998.
16. K. Rajewsky et al., "Conditional gene targeting," *Journal of Clinical Investigation*, 98:600–3, 1996.

Perspectives Series: Molecular Medicine in Genetically Engineered Animals

Conditional Gene Targeting

Klaus Rajewsky, Hua Gu, Ralf Kühn, Ulrich A.K. Betz, Werner Müller, Jürgen Roes, and Frieder Schwenk
Institute for Genetics, University of Cologne, Cologne, Germany

Gene targeting: The classical approach

Central to an understanding of the in vivo function of genes is their analysis by mutation, that is, inactivation or modification of a gene by mutation and the study of the consequences of the mutation in the mutant organism. In mammals, before gene targeting, this approach was limited to the rare spontaneous mutations reflected in obvious phenotypes, as in the case of inheritable diseases in the human. The targeted mutagenesis of the mouse germline was thus a fundamental breakthrough in this area of research. In its original form, gene targeting involves the inactivation of a given gene in the genome of embryonic stem (ES) cells by homologous recombination (1–3).

Address correspondence to Klaus Rajewsky, Institute for Genetics, University of Cologne, Weyertal 121, D-50931 Cologne, Germany. Phone: 49-221-470-4586; FAX: 49-221-470-5185. Hua Gu's present address is Laboratory of Immunology, National Institutes of Health, Rockville, MD. Jürgen Roes' present address is University College London, Ryne Institute, London, WC1E, UK.

Received for publication 19 June 1996.

1. *Abbreviation used in this paper:* ES, embryonic stem.

ES cells derive from an early stage of mouse development and have retained their totipotency, thus they can participate in the generation of cell lineages of the mouse (including germ cells) if transferred into an early mouse embryo. Transfer of mutant ES cells into mouse embryos thus allows the transmission of the mutation in question into the mouse germline.

In the classical experiment of Thomas and Capecchi (3) gene inactivation was achieved by replacing a predetermined gene segment with a mutant version of this segment, through homologous recombination. Since the latter is infrequent in mammalian cells, the isolation of the mutant ES cells requires stringent selection. This was achieved by placing a selectable gene (in that case the neomycin resistance gene) into the targeted locus in a manner that allows its expression (and hence cellular selection) while inactivating the target gene.

Refining classical gene targeting by the Cre-loxP recombination system

A limitation of classical gene targeting comes from the presence of a selection marker gene in the targeted locus. Since this gene must be active in order to allow ES cell selection, it must always be considered that through its expression it might affect the mutant phenotype in an unpredictable way. A par-

"Molecular Medicine in Genetically Engineered Animals"
Series Editor, Kenneth R. Chien

January 1	Gene modification via "plug and socket" gene targeting	Jada Lewis, Baoli Yang, Pete Detloff, and Oliver Smithies
January 15		Edward M. Rubin and Gregory S. Barsh
February 1	In vitro differentiation of murine embryonic stem cells: new approaches to old problems	Mitchell J. Weiss and Stuart H. Orkin
February 15	Genes and physiology: molecular physiology in genetically engineered animals	Kenneth R. Chien
March 1	Animal models of human disease for gene therapy	James M. Wilson
March 15	Targeted mutagenesis: analysis of phenotype without germ line transmission	Andras Nagy and Janet Rossant
April 1	Transgenesis in the rat and larger mammals	Linda Mullins and John Mullins
April 15	The zebrafish: heritable diseases in transparent embryos	Wolfgang Driever and Mark Fishman
May 1	Recent advances in gene mutagenesis by site-directed recombination	Jamey Marth
August 1	Conditional gene targeting	Klaus Rajewsky, Hua Gu, Ralf Kühn, Ulrich A.K. Betz, Werner Müller, Jürgen Roes, and Frieder Schwenk

J. Clin. Invest.

0021-9738/96/08/0600/04 $2.00
Volume 98, Number 3, August 1996, 600–603

ticularly serious problem arises if gene targeting is used for the modification or elimination of regulatory DNA sequences, as the selectable gene brings in its own promoter and enhancer. For this reason, attempts have been made to eliminate the selection marker genes from the targeted locus (4–7).

We have used the bacteriophage-derived Cre-loxP recombination system (8, 9) for this purpose which had been shown to perform well in mouse cells in vitro (10) and in vivo (11, 12) and which appeared to offer a broad range of applications in gene targeting. The Cre enzyme, a member of a large family of recombinases (13), recognizes a sequence motif of 34 bp, called loxP (9). If a DNA segment is flanked by two loxP sites in the same orientation, Cre excises that segment from the DNA, leaving a single loxP site behind. (A piece of DNA flanked by loxP sites in opposite orientations will be inverted by the enzyme, a reaction that waits to be exploited in the gene targeting field [14, 15].) Considering this site as innocent, "clean" deletions can thus be produced. If in a gene targeting experiment the selection marker gene on the targeting vector (subsequently inserted into the target locus by homologous recombination) is flanked by loxP sites, it can later be removed from the ES cell genome via transient transfection of a Cre-expression vector into these cells. By appropriately positioning the two loxP sites, one can use this system as a general system of mutagenesis, producing deletions (16–18), gene replacements, insertions (often called "knock-ins") (19, 20), point mutations, (21) etc. However, we shall focus here on yet another and perhaps the most important aspect of Cre-loxP–mediated targeted mutagenesis, namely conditional (rather than general) gene targeting.

Conditional gene targeting

Why do we want to achieve conditional, i.e., cell-type–specific and/or inducible, gene targeting beyond targeted mutagenesis of the mouse germline? There are several reasons. First, germline mutations may be lethal, in which case there is no mouse to study gene function. Second, genes may exert their function at several stages of ontogeny and in different cell types. In the latter case, complex phenotypes may result, where it is difficult to distinguish cell-autonomous from more complex lesions. In the former case, classical gene targeting will allow one to identify the initial stage at which the target gene plays a critical role, but not necessarily later stages. Finally, in medical research, conditional gene targeting could allow one to generate models of somatically acquired genetic diseases (such as most forms of cancer) rather than of inherited ones.

The strategy of conditional targeting of endogenous genes that we have developed (16) consists of flanking a target gene or gene segment with loxP sites in ES cells by classical gene targeting and deleting the selection marker gene by transient transfection with a Cre-encoding plasmid. This protocol yields ES cell mutants in which the gene segment of interest is either flanked by loxP sites or deleted. Either mutation can be transmitted into the germline. In the former case, the mutant mice carry a functional, but loxP-flanked gene in their genome (Fig. 1 *A*). In the latter the gene is deleted in all cells of the body,

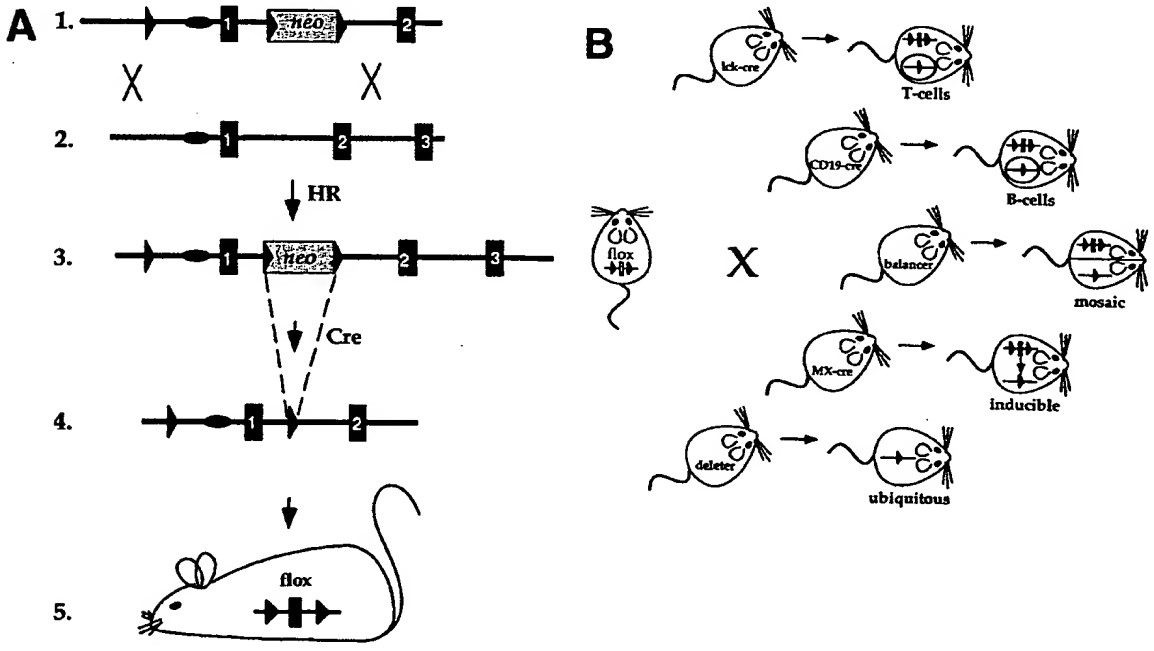

Figure 1. (*A*) Generation of mice with loxP-flanked target genes (flox). (*1*) Gene targeting vector containing three loxP sites (*filled triangles*), two of them flanking the Neomycin resistance (neo) gene. The HSV-tk gene, often used for negative selection, is not shown. (*2*) Target gene in the genome of ES cells (exons drawn as filled boxes). (*3*) Genomic locus modified by homologous recombination (*HR*) between vector and target gene. (*4*) Deletion of the loxP-flanked neo gene by transient Cre expression in ES cells. Two loxP sites remain in the target gene. (*5*) Generation of a loxP-containing mouse line from modified ES cells. (*B*) Utilization of Cre transgenic mice for conditional gene targeting. The mouse strain harboring two loxP sites in the target gene (see *A*) can be crossed to various strains expressing Cre recombinase. The target gene becomes inactivated only in cells expressing Cre but remains active in all other cells of the body. The Cre-expressing strains are described in the text.

generating the situation of a classical knockout experiment, except that no selection marker gene remains in the mutant locus.

Conditional targeting of loxP-flanked genes or gene segments can be achieved by crossing into the mutant animal a Cre-transgene from which Cre recombinase is expressed in a cell-type–specific or inducible manner (Fig. 1 *B*). The initial experiment, done in collaboration with J. Marth's group, established that in principle, cell-type–specific gene targeting can be successfully performed in this manner (lck-cre; 16). We subsequently generated a Cre transgene under the control of an interferon α/β (IFNα/β) inducible promoter and showed that in this system 100% deletion of a loxP-flanked gene segment could be achieved in the liver upon injection of IFNα/β and up to 98% in lymphocytes, whereas lower degrees of deletion were seen in other tissues (MX-cre; 22). Thus, both cell-type–specific and inducible gene targeting are feasible using the Cre-loxP recombination system, the efficiency in the system can reach 100% (as also recently shown by J. Marth and colleagues for T cell–specific gene targeting [23]) and Cre recombinase can do its job in resting cells such as the liver. Note also that conditional as well as classical gene targeting can be used not only for gene inactivation, but also, by appropriately constructing targeting vectors, for the introduction of subtle mutations (21) and also the activation of a gene (see reference 12).

The extent to which conditional gene targeting can be applied in biological and medical research depends at this point, at a technical level, on the availability of Cre-transgenic strains in which Cre is expressed at sufficiently high levels, but under strict cell-type–specific and/or inducible control. Indeed, if Cre expression could be induced specifically in any given cell type, that would for many purposes represent an ideal system of conditional gene targeting. While this goal has not yet been reached, fusion proteins in which Cre is fused to the ligand binding domain of a steroid receptor and which can be activated inside the cell by a steroid antagonist may allow for a successful approach to this problem (24–26). Alternatively, one may consider using systems of inducible, cell-type–specific transcriptional control like that developed by Bujard and colleagues, with tetracycline as the inducer (27, 28).

At present, a limited number of Cre transgenic animals is available which allows gene targeting in T cells (23), B cells (CD19-cre; 29 and R. Rickert, J. Roes, and K. Rajewsky, unpublished data), and, inducible by IFNα/β, in a variety of tissues but predominantly liver and lymphocytes (22). Many other such strains are presently being generated worldwide, so that one can expect that a large set of Cre transgenics will soon be at the disposition of the scientific community, making conditional gene targeting a routine approach in the analysis of mammalian gene function in vivo.

We have recently generated two Cre transgenic mouse lines which behaved unexpectedly, but still turn out to be particularly useful in this context. The first is a strain, designated balancer, which allows partial gene inactivation in essentially all tissues of the body, generating a mosaic situation in which competition between wild-type and mutant cells can be studied in situ. In a situation in which Cre-mediated deletion results in homozygous mutant cells, a simple Southern analysis of the extent of deletion in various tissues of the mosaic mutant animal allows one to pinpoint the sites at which the gene in question plays a functionally critical role (Betz, U.A.K., C. Voßhenrich, K. Rajewsky, and W. Müller, manuscript submitted for publication). The second Cre-transgenic strain, called deleter, mediates deletion of loxP-flanked gene segments in essentially all cells of the body, including germ cells (30). Crossing this strain to a strain in which a target gene is flanked by loxP sites on one or both homologous chromosomes, one obtains ubiquitous deletion which can also be transmitted into the germline, producing a classical knockout, again without a selection marker gene in the mutant locus.

Given these options of targeted mutagenesis through transgenes encoding Cre under various kinds of genetic control, we now mostly perform gene targeting experiments such that only a single mutation of the target gene is transmitted into the germline, namely a loxP-flanked, functional version of the wild-type locus. The resulting animals are healthy and indistinguishable from the wild-type. However, by crossing them to the various Cre-transgenics, any type of conditional mutagenesis as well as a classical (general) knockout can be obtained. Since the production of a strain carrying a loxP-flanked allele represents only little more effort than that of a classical knockout, we recommend that this protocol be generally considered when gene targeting experiments are being planned.

References

1. Capecchi, M.R. 1989. The new mouse genetics: altering the genome by gene targeting. *Trends Genet.* 5:70–76.
2. Koller, B.H., and O. Smithies. 1992. Altering genes in animals by gene targeting. *Annu. Rev. Immunol.* 10:705–730.
3. Thomas, K.R., and M.R. Capecchi.1987. Site-directed mutagenesis by gene targeting in mouse embryo-derived stem cells. *Cell.* 51:503–512.
4. Hasty, P., R. Ramirez-Solis, R. Krumlauf, and A. Bradley. 1991. Introduction of a subtle mutation into the Hox-2.6 locus in embryonic stem cells. *Nature (Lond.).* 350:243–246.
5. Valancius, V., and O. Smithies. 1991. Testing an "in-out" targeting procedure for making subtle genomic modifications in mouse embryonic stem cells. *Mol. Cell. Biol.* 11:1402–1408.
6. Wu, H., X. Liu, and R. Jaenisch. 1994. Double replacement: strategy for efficient introduction of subtle mutations into the murine Col1a-1 gene by homologous recombination in embryonic stem cells. *Proc. Natl. Acad. Sci. USA.* 91:2819–2823.
7. Stacey, A., A. Schnieke, J. McWhir, J. Cooper, A. Colman, and D.W. Melton. 1994. Use of double replacement gene targeting to replace the murine alpha-lactalbumin gene with its human counterpart in embryonic stem cells and mice. *Mol. Cell. Biol.* 14:1009–1016.
8. Sternberg, N., and D. Hamilton. 1981. Bacteriophage P1 site-specific recombination. I. Recombination between loxP sites. *J. Mol. Biol.* 150:467–486.
9. Hoess, R.H., M. Ziese, and N. Sternberg. 1982. P1 site-specific recombination: nucleotide sequence of the recombining sites. *Proc. Natl. Acad. Sci. USA.* 79:3398–3402.
10. Sauer, B., and N. Henderson. 1988. Site-specific DNA recombination in mammalian cells by the Cre recombinase of bacteriophage P1. *Proc. Natl. Acad. Sci. USA.* 85:5166–5170.
11. Orban, P.C., D. Chui, and J.D. Marth. 1992. Tissue- and site-specific DNA recombination in transgenic mice. *Proc. Natl. Acad. Sci. USA.* 89:6861–6865.
12. Lakso, M., B. Sauer, B. Mosinger, Jr., E.J. Lee, R.W. Manning, S.H. Yu, K.L. Mulder, and H. Westphal. 1992. Targeted oncogene activation by site-specific recombination in transgenic mice. *Proc. Natl. Acad. Sci. USA.* 89:6232–6236.
13. Argos, P., A. Landy, K. Abremski, J.B. Egan, E. Haggard-Ljungquist, R.H. Hoess, M.L. Kahn, B. Kalionis, S.V.L. Narayana, L.S. Pierson III, et al. 1986. The integrase family of site-specific recombinases: regional similarities and global diversity. *EMBO (Eur. Mol. Biol. Organ.) J.* 5:433–440.
14. Abremski, K., R. Hoess, and N. Sternberg. 1983. Studies on the properties of P1 site-specific recombination: evidence for topologically unlinked products following recombination. *Cell.* 32:1301–1311.
15. Hamilton, D.L., and K. Abremski. 1984. Site-specific recombination by the bacteriophage P1 lox-Cre system. Cre-mediated synapsis of two lox sites. *J. Mol. Biol.* 178:481–486.
16. Gu, H., J.D. Marth, P.C. Orban, H. Mossmann, and K. Rajewsky. 1994. Deletion of a DNA polymerase beta gene segment in T cells using cell type specific gene targeting. *Science (Wash. DC).* 265:103–106.
17. Gu, H., Y.R. Zou, and K. Rajewsky. 1993. Independent control of immunoglobulin switch recombination at individual switch regions evidenced through Cre-loxP-mediated gene targeting. *Cell.* 73:1155–1164.

18. Ramirez-Solis, R.R., P. Liu, and A. Bradley. 1995. Chromosome engineering in mice. *Nature (Lond.)*. 378:720–724.

19. Zou, Y.R., W. Müller, H. Gu, and K. Rajewsky. 1994. Cre-loxP-mediated gene replacement: a mouse strain producing humanized antibodies. *Curr. Biol.* 4:1099–1103.

20. Hanks, M., W. Wurst, L. Anson-Cartwright, A.B. Auerbach, and A.L. Joyner. 1995. Rescue of the En-1 mutant phenotype by replacement of En-1 with En-2. *Science (Wash. DC)*. 269:679–682.

21. Torres, R.M., H. Flaswinkel, M. Reth, and K. Rajewsky. 1996. Aberrant B cell development and immune response in mice with a compromised BCR complex. *Science (Wash. DC)*. 272:1804–1808.

22. Kühn, R., F. Schwenk, M. Aguet, and K. Rajewsky. 1995. Inducible gene targeting in mice. *Science (Wash. DC)*. 269:1427–1429.

23. Hennet, T., F.K. Hagen, L.A. Tabak, and J.D. Marth. 1995. T-cell-specific deletion of a polypeptide *N*-acetylgalactosaminyl-transferase gene by site-directed recombination. *Proc. Natl. Acad. Sci. USA*. 92:12070–12074.

24. Metzger, D., J. Clifford, H. Chiba, and P. Chambon. 1995. Conditional site-specific recombination in mammalian cells using a ligand-dependent chimeric Cre recombinase. *Proc. Natl. Acad. Sci. USA*. 92:6991–6995.

25. Zhang, Y., C. Riesterer, A.-M. Ayral, F. Sablitzky, T.D. Littlewood, and M. Reth. 1996. Inducible site-directed recombination in mouse embryonic stem cells. *Nucleic Acids Res.* 24:543–548.

26. Kellendonk, C., F. Tronche, A.-P. Monaghan, P.-O. Angrand, F. Steward, and G. Schütz. 1996. Regulation of Cre recombinase activity by the synthetic steroid RU 486. *Nucleic Acids Res.* 24:1404–1411.

27. Furth, P.A., L. St. Onge, H. Böger, P. Gruss, M. Gossen, A. Kistner, H. Bujard, and L. Henninghausen. 1994. Temporal control of gene expression in transgenic mice by a tetracycline-responsive promoter. *Proc. Natl. Acad. Sci. USA*. 91:9302–9306.

28. Schultze, N., Y. Burki, Y. Lang, U. Certa, and H. Bluethmann. 1996. Efficient control of gene expression by single step integration of the tetracycline system in transgenic mice. *Nat. Biotechnol.* 14:499–503.

29. Rickert, R., K. Rajewsky, and J. Roes. 1995. Impairment of T-cell-dependent B-cell responses and B1 cell development in CD19-deficient mice. *Nature (Lond.)*. 376:352–355.

30. Schwenk, F., U. Baron, and K. Rajewsky. 1995. A cre-transgenic mouse strain for the ubiquitous deletion of loxP-flanked gene segments including deletion in germ cells. *Nucleic Acids Res.* 23:5080–5081.

Proc. Natl. Acad. Sci. USA
Vol. 91, pp. 2819–2823, March 1994
Genetics

Double replacement: Strategy for efficient introduction of subtle mutations into the murine *Col1a-1* gene by homologous recombination in embryonic stem cells

(gene targeting/point mutations/mutant mice)

HONG WU, XIN LIU, AND RUDOLF JAENISCH

Whitehead Institute for Biomedical Research, 9 Cambridge Center, Cambridge, MA 02142

Communicated by Salome G. Waelsch, December 14, 1993

ABSTRACT **A subtle mutation that rendered type I collagen resistant to mammalian collagenase has been introduced into the murine *Col1a-1* (recently redesignated *Col a-1*) gene by homologous recombination in embryonic stem (ES) cells. Initially, a "hit and run" procedure was used. Since two steps were required for introducing each mutation and more than one mutation was to be introduced in the same genomic region independently, we have developed a streamlined procedure that involves two sequential replacement-type homologous recombination events. In the first step, an internal deletion was introduced into the *Col1a-1* locus along with the positive and negative selectable markers, *neo* and *tk*, to mark the region of interest. G418-resistant homologous recombinants were isolated and used in the second step in which the deleted *Col1a-1* allele was replaced with a construct containing the desired mutation. Homologous recombinants containing the mutation were identified among the Tk⁻ ES clones after selection with FIAU [1-(2-deoxy-2-fluoro-β-D-arabinofuranosyl)-5-iodouracil (called fialuridine)]. Approximately 10% of such clones contained the desired mutation. The double replacement procedure greatly reduces the time and amount of work required to introduce mutations independently into the same or closely linked regions. Once the homologous recombinants derived from the first step are established, the introduction of other mutations into the deleted region becomes a one-step procedure. For *X* number of introduced mutations, 2*X* selections are required with the "hit and run" approach, but only *X* + 1 are required with the double-replacement method. This innovative procedure could be very useful in studies of gene structure and function as well as gene expression and regulation.**

Recently, homologous recombination in mammalian embryonic stem cells (ES cells) has become a powerful tool for functional studies of genes *in vivo* (1). Mice carrying various null alleles have been generated by disrupting the endogenous gene in ES cells, and valuable information has been obtained by analysis of animals carrying these mutations. However, introduction of subtle mutations into a gene of interest without alteration of the rest of the genome is still a very difficult task. Since most genes in the mammalian genome have no phenotypes that allow direct selection of mutations in ES cells, several methods with varying efficiencies have been developed, such as microinjection of a targeting construct into ES cells and identification of homologous events by PCR analysis (2) or coelectroporation of a targeting construct with an unlinked selectable marker into ES cells (3, 4). The two-step in–out (5) or "hit-and-run" (6) procedure is probably the most promising method developed so far. This procedure allows one to introduce a site-specific mutation into the mammalian genome very efficiently. Point mutations have been introduced into the murine *Hprt* gene (5) and the *Hox-2.6* gene (6) by this procedure.

We are interested in the role of type I collagen turnover in animal development and disease. Collagenases are the only enzymes characterized so far that are capable of degrading nondenatured types I, II, and III collagen extracellularly at neutral pH. Collagenase recognition sequences are well defined in these collagens and are conserved among different species. They cleave the peptide bond between Gly-775 and Ile-776 (or Leu-776) in the triple helical region. Previously, we have generated three mutations in the *Col1a-1* locus (recently redesignated *Col a-1*) that rendered type I collagen resistant to collagenase cleavage (7). To address the role of type I collagen turnover *in vivo*, it was necessary to introduce these mutations into the endogenous *Col1a-1* gene so that the pattern and the level of the mutant gene expression would mimic that of the endogenous gene.

In this study, one of the mutations was introduced into the *Col1a-1* gene by two different procedures, a hit-and-run procedure and the "double-replacement" procedure described herein. Both approaches have been compared as to the ease and efficiency of introducing subtle mutations into endogenous genes.

MATERIALS AND METHODS

129 (J1) Genomic Library and *Col1a-1* Locus. Genomic DNA from a 129/Sv mouse strain was partially digested with *Mbo* I, size-selected (17–21 kb; provided by Doug Gray, University of Ottawa), and ligated into the *Bam*HI site of λ DASH II arms (Stratagene). Isogenic *Col1a-1* clones were isolated from this library. Two clones that cover the entire *Col1a-1* locus, pCol1a1-22 and pCol1a1-25, were isolated and used to construct targeting vectors.

DNA Constructions. *pPGKneopA-PGKtkpA*. A 1.9-kb *Xho* I–*Sal* I fragment containing the mouse phosphoglycerate kinase 1 gene (*Pgk-1*) promoter, bacterial neomycin phosphotransferase (*neo*) cassette, and the *Pgk-1* polyadenylylation signal was isolated from the pGEM7(KJ1)R plasmid (8). This fragment was then inserted into the *Xho* I site of the pGEM7(tk)SalI plasmid, in which the herpes simplex virus thymidine kinase (*tk*) cassette is driven by the *Pkg-1* promoter in a tail-to-head orientation.

pPGKneoNTRtkpA. Three steps were involved in making the construct. First, a 0.58-kb *Eco*RI–*Bal* I fragment containing the 5′ nontranslated region (NTR) of the encephalomyocarditis virus (ECMV; ref. 9) was isolated from plasmid pBS-ECAT (provided by H.-S. Shin of POSTECH, Republic

The publication costs of this article were defrayed in part by page charge payment. This article must therefore be hereby marked "*advertisement*" in accordance with 18 U.S.C. §1734 solely to indicate this fact.

Abbreviations: ES cells, embryonic stem cells; NTR, nontranslated region; FIAU, 1-(2-deoxy-2-fluoro-β-D-arabinofuranosyl)-5-iodouracil (fialuridine); FIAU^r and G418^r, FIAU and G418 resistant; G418^s, G418 sensitive; *tk*, viral thymidine kinase gene; *neo*, bacterial gene for neomycin phosphotransferase.

of Korea) and end-modified with a *Bgl* II linker at the 5′ end and a *Bam*HI linker at the 3′ end. This *Bgl* II–*Bam*HI NTR fragment was then inserted into the *Bam*HI site, which is located at the 3′ end of the *neo* gene between a translational stop codon and a polyadenylylation signal of pGEM7(KJ1)R plasmid, to generate the plasmid pGEM7(KJ1)R-NTR. Finally, a 2.1-kb *Bgl* II fragment isolated from pGEM7(TK)-SalI, which includes the *tk* gene and polyadenylylation signal sequences from both *tk* and *Pgk-1* genes, was used to replace the *Bam*HI fragment at the 3′ end of pGEM7(KJ1)R-NTR plasmid.

pCol1a1-22-MIV. A 0.5-kb *Kpn* I–*Nco* I fragment from pCol1a1-22 was replaced by the same fragment in mutant IV (7). This plasmid carried double substitutions of proline for Gln-744 and Ala-777 and a single substitution of methionine for Ile-776 at the collagenase cleavage site, resulting in an additional *Sph* I site (S* in Fig. 2).

pNT-S-I. A 7-kb *Hinc*II–*Bam*HI fragment from pCol1a1-22-MIV was inserted into a plasmid vector containing the PGKneoNTRtkpA cassette.

pNT-S-II. A 2.2-kb *Nsi* I–*Xba* I fragment from pCol1a1-25 plasmid was replaced by a 4-kb PGKneoNTRtkpA fragment with orientation of the *Pgk-1* promoter opposite to that of the *Col1a-1* gene.

ES Cell Culture, Drug Selections, and DNA Preparation. J1 ES cells were cultured essentially as described (10). To introduce the targeting construct into the endogenous *Col1a-1* gene, 25 μg of linearized plasmid DNA was electroporated into 1×10^7 J1 ES cells (in a volume of 0.8 ml) at 400 V and 25 μF (Bio-Rad). After 24 hr, the ES medium was supplemented with 400 μg of G418 per ml (GIBCO/BRL), and colonies were isolated after 7–9 days of selection.

To isolate revertants in the hit-and-run procedure or to replace the "marked" allele with the mutant construct in the double replacement procedure, 0.2 μM FIAU (a kind gift from the Bristol–Myers Squibb Company) was added to the medium 24 hr after plating or electroporation. Selection was continued for 8–10 days.

The counter selection step with FIAU often yielded drug-resistant clones in which the selectable cassette had not been looped out or replaced by the mutant construct. To reduce this background, we used a prescreening procedure. Targeted ES cells from the first step were selected in FIAU-containing medium 24 hr after plating. Individual ES clones were isolated. After trypsinization, cells from each clone were divided and replated in ES medium containing FIAU (I) or G418 (II) or in embryonic fibroblast medium containing FIAU (III). Cells grown in the first set of plates (I) were frozen in the plate after reaching confluence and kept as a source. Cells grown in the second set of plates (II) were G418-resistant ($G418^r$) and recorded. Cells grown in the third set of plates (III) but absent in the second set of plates were G418-sensitive/FIAU-resistant ($G418^s$/$FIAU^r$). DNA was prepared from these cells according to the method described (11).

RESULTS

General Scheme of the Hit-and-Run and Double-Replacement Procedures and Construction of pPGKneoNTRtkpA Vector. Fig. 1 shows a schematic diagram illustrating the hit-and-run and double-replacement procedures. Both hit-and-run and double-replacement procedures consist of two steps of homologous recombination events that are facilitated by positive and negative selections, respectively. In a previous report, Hasty *et al.* (6) used two promoters to drive the *neo* and *tk* genes individually. To assure that both markers were expressed efficiently, we have constructed a pPGKneo-NTRtkpA vector in which a single strong promoter, the *Pgk-1* promoter, was used to drive both the *neo* and *tk* genes. The 5′ NTR fragment from encephalomyocarditis virus (9) was inserted between the stop codon of the *neo* gene and the start codon of the *tk* gene so that a bicistronic mRNA was generated. Since the NTR fragment contains an internal ribosomal entry site (IRES), the *tk* gene is translated efficiently in a cap-independent manner (12, 13). This vector was electroporated into ES cells. The number of ES colonies surviving after G418 selection or G418/FIAU selection was compared. The enrichment of FIAU selection obtained with pPGKneoNTRtkpA was approximately 10 times higher than that obtained with the pMC1neopA-MC1tkpA vector (a gift from M. A. Rudnicki), in which the *neo* and *tk* genes were driven individually by the *tk* promoter, and was 3–5 times higher than that obtained with the pPGKneopA-PGKtkpA vector (see *Materials and Methods*), in which the *neo* and *tk* genes were driven individually by the *Pgk-1* promoter (data not shown). Therefore, the pPGKneoNTRtkpA vector was used in all subsequent experiments.

Introduction of a Collagenase-Resistant Mutation by the Hit-and-Run Procedure. For the "hit" step, we constructed

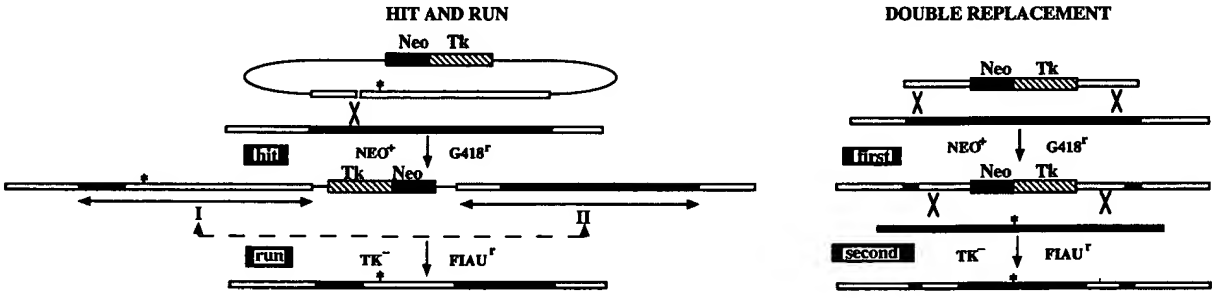

FIG. 1. A general scheme of the hit-and-run and double-replacement procedures. The hit-and-run strategy involves two single reciprocal homologous recombination events. The vector used for the hit-and-run procedure includes sequences homologous to the target gene with a desired mutation and two selectable markers, the *neo* and *tk* genes located outside the homologous region for positive and negative selection, respectively. The construct is first linearized in the homologous region, then introduced into ES cells. In the "hit" step, a duplication of the homology (I and II), separated by the vector sequence and the selectable markers, is generated by a simple insertion type of homologous recombination event. In the "run" step, the selectable cassettes, the vector sequence, and a copy of the duplicated homologous fragment are looped out by a single reciprocal intrachromosomal recombination event. ES clones carrying either the desired mutation or the wild-type allele could be isolated after FIAU selection for the loss of the *tk* gene. In contrast, the double-replacement strategy involves two replacement types of homologous recombination events. In the first step, an internal deletion and a selectable cassette containing the *neo* and *tk* genes are introduced into the target gene by a replacement type of homologous recombination to "mark" the gene of interest. In the second step, sequences homologous to the target gene carrying a desired mutation are used to replace the marked allele. Similar to the hit-and-run procedure, ES clones containing either the introduced mutation or the wild-type allele could be isolated in this step by FIAU selection for loss of the *tk* gene.

pNT-S-I, an insertion-type of targeting vector carrying nucleotide changes that result in double substitutions of proline for Gln-744 and Ala-777 and a single substitution of methionine for Ile-776 at the collagenase cleavage site. These changes also introduced an additional *Sph* I (S* in Fig. 2) site, which could facilitate screening for the mutation by Southern analysis. The plasmid was linearized with *Nhe* I. The distance between the *Nhe* I and mutation sites (*Sph* I site) was 0.67 kb. After electroporation and G418 selection, G418^r ES clones were screened for homologous recombinants by Southern analysis as shown in Fig. 2 *A* and *B*. Of 97 G418^r clones tested, 29 had undergone homologous integration, corresponding to a frequency of 30% (Table 1). Of these 29 clones, 17 recombinant clones carried a single insert and 12 carried multiple inserts, probably in tandem arrays (data not shown). Four of the 17 clones had the *Sph* I site in the 5′ duplication, 2 had the *Sph* I site in the 3′ duplication, and one clone had the mutation in both 5′ and 3′ duplications. The remaining 10 clones had apparently lost the *Sph* I site. This was probably due to gene conversion or mismatch repair during the process of homologous recombination (14).

To select for excision and to obtain ES clones carrying the desired mutation, clone 94 carrying the *Sph* I site in the 5′ duplication was subjected to *tk* counter selection at a density of 1×10^5 cells per 10-cm plate. FIAU^r clones were isolated and genotyped. Approximately 32% of phenotypically FIAU^r clones, however, still carried the *neo* and *tk* genes, indicating that FIAU selection alone was not sufficient to eliminate all of the cells carrying the *tk* gene.

Table 1. Frequency of introducing a point mutation by the hit-and-run or double-replacement procedure

Measurements	Hit and run	Double replacement
First step		
G418^r clones, no.	97	363
Recombinants, no. (%)	29 (30)	14 (3.9)
Recombinants carrying the mutation, no. (%)	7 (7)	14 (3.9)
Second step		
G418^s/FIAU^r clones,* no.	5	115
Revertants carrying the mutation, no. (%)	2 (40)	11 (10)

*Clones obtained after prescreening procedure.

To reduce this background, we used a prescreening procedure as described in *Materials and Methods*. Only DNAs from G418^s/FIAU^r clones were harvested and genotyped. In this experiment, five of five such ES clones genotyped were "loop-out" clones, two of which contained the desired mutation (Fig. 2*C* and Table 1). Thus, the prescreening procedure greatly reduced the amount of work in analyzing FIAU^r clones and made the detection of revertants much easier. This procedure was also used in the double-replacement procedure described below.

Introduction of a Collagenase-Resistant Mutation by the Double-Replacement Procedure. The murine *Col1a-1* locus spans approximately 24 kb of genomic region. The second

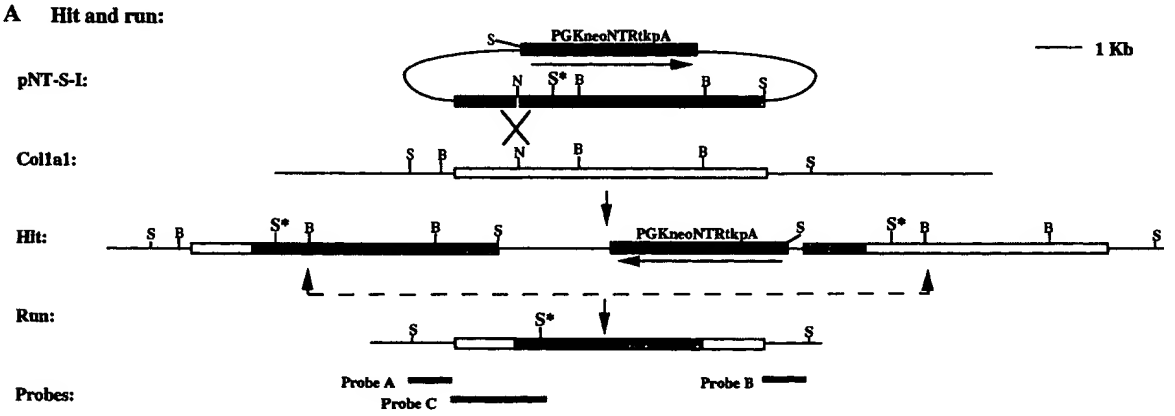

B Targeted locus: SphI Digestion BamH I Digestion

Genotype:	Probe A	Probe B	Probe C
Wild Type:	9.0 Kb	9.0 Kb	2.85 Kb
Mutation at 5':	2.8 Kb	8.3 Kb	2.85 Kb, 11.3 Kb
Mutation at 3':	7.7 Kb	6.0 Kb	2.85 Kb, 11.3 Kb

C Loop-out Locus: SphI Digestion

Genotype	Probe C
Clone 94:	9.0 Kb, 8.3 Kb, 2.8 Kb
Mutant:	9.0 Kb, 2.8 Kb
Wild Type:	9.0 Kb

FIG. 2. Introduction of a collagenase-resistant mutation by the hit-and-run procedure. (*A*) The hit-and-run steps were as described in Fig. 1. B, *Bam*HI; N, *Nhe* I; S, *Sph* I; S*, *Sph* I polymorphism corresponding to a collagenase-resistant mutation; open box, the endogenous homology; stippled boxes, the homology in the targeting vector and the selective cassette; and horizontal bars, probes used in the Southern analysis. (*B*) The expected sizes of restriction fragments detected by the probes indicated for the wild-type and targeted alleles. DNAs were digested with *Sph* I. A 9-kb band corresponding to the wild-type allele could be detected by probes A and B. If the *Sph* I polymorphic site were present in the 5′ duplication, a 2.8-kb and a 8.3-kb fragment would be detected by probes A and B, respectively. On the other hand, if the *Sph* I site were present in the 3′ duplication, a 7.7 kb and a 6.0 kb band would be detected by probes A and B, respectively. To detect possible multiple integration events, DNAs were digested with *Bam*HI and probed with an internal probe C. A 2.85-kb band from the wild-type allele, a 2.85-kb band from the 5′ duplication of the targeted allele, and a 11.3-kb band from the targeted allele should be detected. If the recombinant carried more than one copy of the insert, the intensity ratio between the 2.85-kb and 11.3-kb bands would be <2:1. (*C*) Detecting the "loop-out" revertants in the "run" step. DNA was digested by *Sph* I and hybridized with probe C. Three bands of 9, 8.3, and 2.8 kb were detected in the parental ES cells (clone 94); two bands of 9 and 2.8 kb were detected in the "loop-out" revertant carrying the mutation. In revertants which lost the *Sph* I site, only the 9-kb wild-type band could be detected.

*Eco*RI fragment contains several functional domains including two integrin binding sites, a collagenase cleavage site, a fibronectin binding site, and a C-proteinase cleavage site. A replacement-type of targeting vector, pNT-S-II, was used in the first step. This vector consisted of 7.2 kb of 5′ *Col1a-1* sequence, a 2.2-kb *Nsi* I–*Xba* I deletion that encoded several functional domains including the collagenase cleavage site, the PGKneoNTRtkpA cassette, and 3.2 kb of 3′ *Col1a-1* sequence (Fig. 3*A*). The construct was linearized with *Sal* I in the plasmid backbone and electroporated into ES cells. Of the 363 G418^r clones tested, 14 (3.9%) carried the targeted allele at the *Col1a-1* locus (Fig. 3 *A* and *B*; Table 1).

After "marking" the *Col1a-1* locus with the PGKneoNTRtkpA cassette, the introduction of mutations in the deleted region became a one-step procedure. Plasmid pCol1a1-22-MIV was linearized with *Sal* I and electroporated into targeted ES cells generated in the first step. Of 384 clones isolated after FIAU selection, 231 clones were grown up and were sensitive to G418 selection (60%). These G418^s/FIAU^r clones were further screened by Southern analysis for the presence of the desired mutation at the *Col1a-1* locus. Of the 115 clones tested, all had the "marked" allele replaced, but only 11 clones (9.6%) contained the new *Sph* I site (Fig. 3 *A* and *C*; Table 1).

To test whether ES clones that lacked *Sph* I polymorphism contained small deletions or rearrangements in the *Col1a-1* locus, DNAs were digested with *Eco*RI, and filters were probed with probes II and III, which are located at the 5′ and 3′ ends of the *Col1a-1* locus, respectively. Only 14-kb and 4.5-kb bands (data not shown), corresponding to the wild-type allele, were detected in Sph I$^-$ clones. Since probes I, II, and III cover the entire *Col1a-1* locus and no aberrant banding patterns were found in Sph I$^-$ ES clones, the lack of the *Sph* I site in the collagenase cleavage site was not due to deletions or rearrangements in the *Col1a-1* locus.

We further tested by Southern analysis whether the chromosome carrying the "marked" *Col1a-1* allele was randomly lost during FIAU selection. This was achieved by comparing the intensity of a fragment corresponding to the *Col1a-1* locus with that of a fragment corresponding to the *Col3a-1* locus, which is located on a different chromosome. DNAs were digested with *Eco*RI, and filters were probed with probes II and B31, an 0.8-kb *Bam*HI fragment derived from the *Col3a-1* gene. More than 97% of Sph I$^-$ clones showed a 1:1 ratio between the *Col1a-1* and *Col3a-1* locus (data not shown). Thus, random loss of the chromosome carrying the "marked" allele during FIAU selection occurred infrequently. The possible explanations for Sph I$^-$ clones obtained in the second step will be discussed later.

DISCUSSION

We have successfully introduced a subtle mutation into the endogenous *Col1a-1* gene by homologous recombination in ES cells, which rendered type I collagen molecules resistant to collagenase digestion. This was accomplished first by the

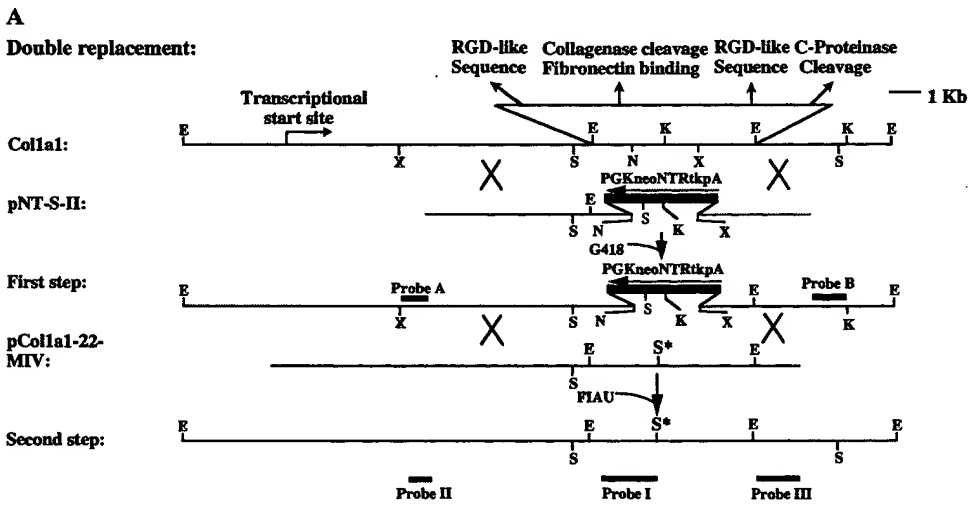

B

Target the Col1a1 locus with the pNT-S-II vector:

	XbaI Digestion	KpnI Digestion
Genotype:	*Probe A*	*Probe B*
Wild type:	10 Kb	6.8 Kb
Targeted:	12 Kb	7.1 Kb

C

Replace the "marked" allele with the mutant construct:

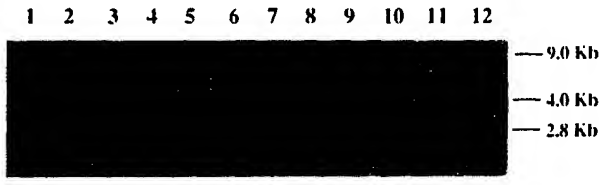

FIG. 3. Introduction of a collagenase-resistant mutation by the double-replacement procedure. (*A*) The double-replacement procedure was described in Fig. 1. E, *Eco*RI; K, *Kpn* I; N, *Nsi* I; X, *Xba* I; S, *Sph* I; and S*, same as in Fig. 2*A*. (*B*) First replacement: DNAs were digested with either *Xba* I or *Kpn* I, and filters were probed with probes A or B, respectively. Probe A could hybridize to a 10-kb band from the wild-type allele and a 12-kb band from the targeted allele. Probe B could detect a 6.8-kb band from the wild-type allele and a 7.1-kb band from the targeted allele (data not shown). (*C*) Second replacement: DNAs were digested with *Sph* I, and filters were probed with probe I. This probe hybridized (*i*) to a 9-kb band from the wild-type allele (lane 1), (*ii*) to a 4-kb band from a "marked" allele containing the PGKneoNTRtkpA cassette (lane 2), and (*iii*) to a 2.8-kb band when the "marked" allele was replaced by the mutation (lanes 4–6 and 9–12). Revertants that lost the *Sph* I site contained the wild-type band only (lanes 3, 7, and 8).

hit-and-run procedure and then by the double-replacement procedure described in this paper.

The hit-and-run procedure involves an insertion-type of homologous recombination event followed by a single reciprocal intrachromosomal recombination event (5, 6). In contrast, the double-replacement procedure involves two replacement-type homologous recombination events. Since the frequency of homologous recombination with insertion-type targeting vectors has been reported to be much higher than with replacement-type vectors (15), the first step—i.e., the insertion of the vector into the gene—is likely to be more efficient in the hit-and-run procedure. However, if the objective is to introduce different mutations into the same genomic region individually, the hit-and-run procedure would be very time and labor intensive compared with the double-replacement procedure described in this study.

In the hit-and-run procedure, each introduced mutation requires two homologous recombination events and two drug selections. In the double-replacement procedure, however, the construct used in the first step is designed to delete the region of interest and replace it with a selectable cassette. Once the targeted ES clones are established in the first step, the introduction of any mutation into the deleted region becomes a one-step procedure. This design reduces the amount of work required to generate the second and subsequent mutations in the same region. The targeting vector used in the second step is simple and easy to construct, since it requires only genomic DNA sequences carrying the desired mutation. Therefore, constructs used in *in vitro* assays or in transgenic experiments could be used in this step without change.

The double-replacement procedure would be useful in studies of gene structure and function. Since the deletion introduced in the first step could span a large genomic region, mutations could be generated individually or in combination in one or more functional domains within the deleted region. This strategy also offers an opportunity to introduce efficiently a series of deletions or point mutations into the regulatory elements of a gene so that the regulation of gene expression can be directly studied in its native chromosomal context. Furthermore, this method could be used to generate a partial "knock out" mouse by mutating a tissue-specific regulatory element so that the gene expression would be abolished in a particular tissue but would be regulated normally in others.

It was expected that the majority of the Neo^-/Tk^- ES clones derived from the second step of the double-replacement procedure would carry the desired mutation ($Sph\ I^+$). Surprisingly, however, approximately 90% of these clones were $Neo^-/Tk^-/Sph\ I^-$. These $Sph\ I^-$ clones could have arisen by different mechanisms—e.g., deletion or rearrangement in the *Col1a-1* locus, random loss of the chromosome containing the "marked" *Col1a-1* allele, or gene conversion. We have tested these possibilities by restriction enzyme mapping of the whole *Col1a-1* locus by Southern analysis and by quantitation of the *Col1a-1* locus with a probe derived from another chromosome. No rearrangement in the *Col1a-1* locus could be detected in the 115 clones analyzed. In only three cases was the ratio of intensity between the *Col1a-1* allele and the allele from the other chromosome changed. These results suggest that gene rearrangement, gene deletion, or random chromosomal loss were not the main reasons for the presence of the $Neo^-/Tk^-/Sph\ I^-$ clones. Instead, nonreciprocal transfer of information from the wild-type to the mutant chromatid, or gene conversion, is the likely explanation. A high frequency of gene conversion has been observed and well studied in yeast (14). This mechanism has also been used to explain some phenomena observed in the process of homologous recombination in ES cells (6, 16–18). To prove that the $Neo^-/Tk^-/Sph\ I^-$ clones were derived from gene conversion requires differentially marking the two alleles so that gene conversion events can be directly studied.

While this manuscript was under preparation, Askew *et al.* (19) published a paper describing introduction of point mutations into the $\alpha 2$ Na,K-ATPase gene in ES cells. The procedure they used, termed "tag-and-exchange," is very similar to the double-replacement procedure described in this study except for the following two differences. (*i*) In the tag-and-exchange procedure, the selectable cassette was simply inserted into the $\alpha 2$ Na,K-ATPase gene. This limits the region into which subsequent mutations could be introduced. In our procedure, however, a deletion along with the selectable cassette was introduced into the region of interest so that multiple individual mutations could be introduced into a large region of the *Col1a-1* locus. (*ii*) In the *tk* counter selection step, we obtained $G418^s/FIAU^r$ clones in which the selectable cassette had been looped out or replaced with a much higher frequency than that of Askew *et al.* (60–68% vs. 10%). Approximately 10% of these clones carried the desired mutation when selection was applied 1 day after electroporation. In the case of Askew *et al.*, no ES clone carrying the desired mutation was obtained when selection was applied 0–3 days after electroporation, and 1.4% of these clones were obtained when selection was applied 4–5 days after electroporation. The different results could be due to the different expression levels of *tk* gene from these two constructs. As discussed earlier, a strong *Pgk-1* promoter was used to drive both the *neo* and the *tk* genes in our study. Instead, Askew *et al.* used the weaker *tk* promoter to drive the two selectable markers independently.

We have injected BALB/c and C57BL/6 embryos at blastocyst stage with one of the ES clones carrying the desired mutation and have derived mice carrying the mutation in the germ line.

We thank Dr. Philippe Soriano for the initial discussions of the double-replacement strategy. We thank Drs. Paul Bornstein, Jordon Kreidberg, Peter Laird, and Paul Soloway for critical comments on this manuscript. This work was supported by National Institutes of Health Grants P01-HL41484 and 5R35-CA44339 to R.J. and a Leukemia Society of America grant to X.L.

1. Koller, B. H. & Smithies, O. (1992) *Annu. Rev. Immunol.* **10**, 705–730.
2. Zimmer, A. & Gruss, P. (1989) *Nature (London)* **338**, 150–153.
3. Reid, L. H., Shesely, E. G., Kim, H.-S. & Smithies, O. (1991) *Mol. Cell. Biol.* **11**, 2769–2777.
4. Davis, A. C., Wims, A. & Bradley, A. (1992) *Mol. Cell. Biol.* **12**, 2769–2776.
5. Valancius, V. & Smithies, O. (1991) *Mol. Cell. Biol.* **11**, 1402–1408.
6. Hasty, P., Ramirez-Solis, R., Krumlauf, R. & Bradley, A. (1991) *Nature (London)* **350**, 243–246.
7. Wu, H., Byrne, M. H., Stacey, A., Goldring, M. B., Birkhead, J. R., Jaenisch, R. & Krane, S. M. (1990) *Proc. Natl. Acad. Sci. USA* **87**, 5888–5892.
8. Rudnicki, M. A., Braun, T., Hinuma, S. & Jaenisch, R. (1992) *Cell* **71**, 383–390.
9. Jang, S. K., Davies, M. V., Kaufman, R. J. & Wimmer, E. (1989) *J. Virol.* **63**, 1651–1660.
10. Li, E., Bestor, T. H. & Jaenisch, R. (1992) *Cell* **69**, 915–926.
11. Laird, P. W., Zijderveld, A., Linders, K., Rudnicki, M. A., Jaenisch, R. & Berns, A. (1991) *Nucleic Acids Res.* **19**, 4293.
12. Jang, S. K. & Wimmer, E. (1990) *Genes Dev.* **4**, 1560–1572.
13. Ghattas, I. R., Sanes, J. R. & Majors, J. E. (1991) *Mol. Cell. Biol.* **11**, 5848–5859.
14. Orr-Weaver, T. & Szostak, J. W. (1985) *Microbiol. Rev.* **49**, 33–58.
15. Hasty, P., Rivera-Perez, J. & Bradley, A. (1991) *Mol. Cell. Biol.* **11**, 4509–4517.
16. Doetschman, T., Gregg, R. G., Maeda, N., Hooper, M. L., Melton, D., Thompson, S. & Smithies, O. (1987) *Nature (London)* **330**, 576–578.
17. Valancius, V. & Smithies, O. (1991) *Mol. Cell. Biol.* **11**, 4389–4397.
18. Mortensen, R. M., Conner, D. A., Chao, S., Geisterfer-Lowrance, T. & Seidman, J. G. (1992) *Mol. Cell. Biol.* **12**, 2391–2395.
19. Askew, G. R., Doetschman, T. & Lingrel, J. B. (1993) *Mol. Cell. Biol.* **13**, 4115–4124.

Proc. Natl. Acad. Sci. USA
Vol. 90, pp. 8424–8428, September 1993
Developmental Biology

Derivation of completely cell culture-derived mice from early-passage embryonic stem cells

(pluripotency/tetraploid embryos/chimeras)

ANDRÁS NAGY*†‡, JANET ROSSANT*§, RÉKA NAGY¶, WANDA ABRAMOW-NEWERLY¶, AND JOHN C. RODER§¶

*Division of Molecular and Developmental Biology and ¶Division of Neuro- and Immunobiology, Samuel Lunenfeld Research Institute, Mount Sinai Hospital, 600 University Avenue, Toronto, ON, Canada M5G 1X5; †Department of Biochemistry, Loránd Eötvös University, Budapest, Hungary; and §Department of Molecular and Medical Genetics, University of Toronto, Toronto, ON, Canada M5S 1A8

Communicated by Philip Leder, June 3, 1993

ABSTRACT **Several newly generated mouse embryonic stem (ES) cell lines were tested for their ability to produce completely ES cell-derived mice at early passage numbers by ES cell ↔ tetraploid embryo aggregation. One line, designated R1, produced live offspring which were completely ES cell-derived as judged by isoenzyme analysis and coat color. These cell culture-derived animals were normal, viable, and fertile. However, prolonged *in vitro* culture negatively affected this initial totipotency of R1, and after passage 14, ES cell-derived newborns died at birth. However, one of the five subclones (R1-S3) derived from single cells at passage 12 retained the original totipotency and gave rise to viable, completely ES cell-derived animals. The total *in vitro* culture time of the sublines at the time of testing was equivalent to passage 24 of the original line. Fully potent early passage R1 cells and the R1-S3 subclone should be very useful not only for ES cell-based genetic manipulations but also in defining optimal *in vitro* culture conditions for retaining the initial totipotency of ES cells.**

Embryonic stem (ES) cells are now widely used for introducing targeted mutations and other genetic alterations into the mouse germ line (1, 2). One of the basic requirements for the successful application of these new techniques is to maintain ES cell lines in a state compatible with germ-cell formation, when the cells are introduced back into a host embryo. Germ-line contribution is most likely to occur when cells retain broad developmental potential, contributing extensively to a wide variety of somatic tissues. We have recently developed a system to characterize the full developmental potential of ES cells (3); the system is based on aggregation of ES cells with developmentally compromised tetraploid embryos. In such chimeras the tetraploid component is selected against in all lineages where ES cells are able to differentiate normally, allowing the ES cells to take over the embryo proper and relegating the tetraploid component to the extraembryonic membranes.

We tested the developmental potential of several commonly used ES cell lines, such as D3 (4) and AB1 (5), in this system and found that they were able to support fetal development up to term. However, all such completely ES cell-derived newborns died perinatally (3, 6). To investigate whether this failure to generate viable offspring was intrinsic to all cell lines at all stages of culture, we established four new ES cell lines and tested their pluripotency at different stages from very early passage number. One of the lines (designated R1) produced viable, completely ES cell-derived animals at early passages but lost this ability with extended culture *in vitro*. This cell line was used to study different aspects of maintenance of totipotency during *in vitro* culture.

The publication costs of this article were defrayed in part by page charge payment. This article must therefore be hereby marked "*advertisement*" in accordance with 18 U.S.C. §1734 solely to indicate this fact.

MATERIALS AND METHODS

Strains of Mice Used for Embryos. CD1 mice purchased from Charles River Laboratories were preselected for *Gpi-1^b/Gpi-1^b* genotype and set up for breeding to produce GPI-BB albino CD1 animals. Embryos for the tetraploid component of the chimeras were obtained from this stock. To establish ES cell lines, chinchilla 129/Sv females were mated with agouti 129/Sv-CP males, and blastocysts were obtained by flushing the uterus at postcoitum day 3.5.

Establishment of ES Cell Lines. Thirty-eight 129/Sv × 129/Sv-CP embryos were plated individually onto a feeder layer of mitomycin C-treated SNL (5) fibroblasts in Dulbecco's modified Eagle's medium supplemented with 20% fetal calf serum (FCS; Hyclone) and 2000 units of leukemia inhibitory factor (LIF; ESGRO) per ml in 4-well plates (Nunc). Most embryos hatched and attached to the feeders by day 2 after plating. The inner cell masses (ICMs) were left to grow for 4 more days, when they were mechanically disaggregated in their own wells by using drawn-out Pasteur pipettes. Four to five days later, the cells were transferred into new wells either by trypsinizing or by mechanically disaggregating the undifferentiated colonies. We started counting passage number when we were first able to pass the cells into 35-mm plates (passage 1). The cells were first frozen at passage 5, which was ≈3 weeks after the blastocyst stage. Four cell lines were established, designated R1, R2, R6, and R13.

Production of Tetraploid Embryos. The oviducts of superovulated and mated CD1 (GPI-BB) females were flushed 44–46 hr after treatment with human chorionic gonadotropin to collect late two-cell-stage embryos. The embryos were placed one at a time between two platinum electrodes laid 250 μm apart in M2 medium (7) in the electrode chamber (8). The blastomeres were fused by a short electric pulse (9) (90 V for 100 μsec in M2 medium) applied by a pulse generator (CF 100; manufactured by Biochemical Laboratory Service, Budapest, Hungary).

Production of ES Cell–Tetraploid Embryo Aggregation Chimeras. The fused, tetraploid embryos were cultured in M16 microdrops under paraffin oil at 37°C in 95% air/5% CO_2. Twenty-four hours after fusion, most of the tetraploid embryos developed to the four-cell stage. Only these four-cell-stage embryos were used for aggregation. Zonae pellucidae of the embryos were removed by treatment with acid Tyrode's buffer (10). ES cells (plated at low density 2 days prior to aggregation) were briefly trypsinized to form clumps of loosely connected cells. Clumps of 10–15 ES cells were then sandwiched between two tetraploid embryos in aggregation wells made by pressing a darning needle into the plastic

Abbreviations: ES cells, embryonic stem cells; GPI, glucose phosphate isomerase; LIF, leukemia inhibitory factor; FCS, fetal calf serum.

‡To whom reprint and cell line requests should be addressed.

Table 1. Developmental potentiality of ES cell lines at early-passage numbers (passages 6–8) tested by ES cell–tetraploid embryo aggregates

Cell line	Tetraploid aggregates transferred, no.	Resorptions, no.	Midgestation dead embryos,* no.	Newborns, no.	Recovered newborns, no.
R1	53	21	6	9	3†
R2	31	7	7	0	0
R6	40‡				
R13	37	17	5	2	0

*Resorptions above 4 mm in diameter at term were considered in this category.
†Two of the three recovered newborns survived and reached adulthood.
‡Uteruses with obvious signs of early abortion were recovered from these recipients at term.

bottom of the culture plate (3). The aggregates were cultured overnight in microdrops of M16 before transfer into the uterus of 2.5-day pseudopregnant recipients.

Caesarean Section and Data Collection. Pregnant recipients were routinely subject to a Caesarean section on day 18.5 of pregnancy. Live fetuses were counted as well as the number of early postimplantation resorptions and embryos dying at or after midgestation. Fetuses that were alive at delivery but failed to survive the early postnatal period were subject to complete glucose phosphate isomerase (GPI) analysis. Fetuses that recovered after the Caesarean section were placed with foster mothers, and a small sample of blood and the tip of the tail were taken for GPI analysis. Adult ES cell-derived mice were mated with CD1 females to test for germ-line transmission. After test breeding, two mice were killed and various tissues were dissected for GPI analysis.

Genetic Markers. The polymorphic *Gpi-1* gene was used to distinguish between the tetraploid embryo and ES cell-derived components of the chimeras; the ES cell lines were derived from GPI-AA 129 and the tetraploid components were produced from GPI-BB CD-1 embryos. The isoenzyme analysis was performed as described earlier (11). Briefly, tissue homogenates were diluted in sample buffer and run on cellulose acetate membranes (Helena Laboratories) in Supraheme electrophoresis buffer (Helena Laboratories) for 90 min at 300 V. A 1% agarose overlay containing 15 mg of fructose 6-phosphate, 2 mg of nicotinamide-adenine dinucleotide phosphate, 1 unit of glucose-6-phosphate dehydrogenase, 2 mg of dimethylthiazol-diphenyltetrazolium bromide, and 0.4 mg of phenazine methosulfate per ml of 0.1 M Tris·HCl, pH 7.2/15 mM sodium citrate/30 mM $MgCl_2$ was poured over the gel and incubated at 37°C until the GPI isoenzyme bands appeared. The intensity difference between GPI-AA and GPI-BB electrophoretic bands reflected the composition of chimeric tissues. Coat color also indicated the ES cell origin of the viable ES cells–tetraploid embryo chimeras, since tetraploid embryos were albino, while the ES cell lines were derived from agouti embryos.

Karyotype Analysis. ES cells ($\approx 2 \times 10^6$ cells) were arrested in metaphase by adding colcemid (0.2 mg/ml) to the culture medium for 1 hr at 37°C. The cells were collected after trypsin/EDTA treatment and centrifuged at 900 × *g*; the pellet was exposed to hypotonic shock by using prewarmed 0.075 M KCl for 19 min at 37°C. After gentle centrifugation, the hypotonic solution was aspirated, and the pellet was fixed with cold methanol/acetic acid, 3:1 (vol/vol), at least three times prior to spreading on cold microscope slides. The slides were rinsed with Hanks' solution, stained in freshly made 1% Giemsa for 3 min and 50 sec, rinsed with distilled H_2O, and mounted in Permount.

Southern Blot Analysis. DNA was isolated from cell lines by standard procedures and digested with *Eco*RI. The digests were run on a 0.7% agarose gel and blotted onto GeneScreen-*Plus* (DuPont). The blots were hybridized with a Y chromosome-specific probe, pT353/B (12) labeled by random priming, and washed in 15 mM NaCl/1.5 mM sodium citrate, pH 7.0/0.1% SDS at 65°C before exposure to x-ray film.

RESULTS

Developmental Potential of R1, R2, R6, and R13 ES Cells at Early Passages. The cell lines did not differ from each other in their undifferentiated morphology, all of them showing the typical ES cell morphology (13). Differentiation capabilities and developmental potential of cells at passage 6–8 were tested *in vitro* by differentiating the cells into embryoid bodies (4) or *in vivo* by aggregating them with tetraploid embryos (3). All of them developed cystic embryoid bodies at similar frequency *in vitro* (data not shown). However, their *in vivo* developmental potential showed differences (Table 1). R2 and R6 were not able to support development to term. Recipients containing R6 chimeras had only signs that implantation occurred, but no remnants of either fetus or decidual tissue remained. Two of 37 R13–tetraploid embryo aggregates developed to term. Both were completely R13-derived as judged by GPI assay of their main organs. They had extremely high birth weight (*ca.* 3g) and swollen edemic skin. They failed to oxygenize their lungs and died shortly after birth. No detailed pathology was performed. The nine newborns from R1–tetraploid embryo aggregates showed no sign of apparent anatomical abnormalities, although only three of them recovered from Cesarean section. Two of these three reached adulthood. GPI assay of their blood and tail indicated pure R1 origin of one of the survivors. However, the other had about 10–15% tetraploid contribution (data not shown).

Southern blot analysis of the DNA (Fig. 1) prepared from R1, R2, R6, and R13 with a Y chromosome-specific probe (12) revealed that only R1 was a male line.

Developmental Potential of R1 as a Function of Different Culture Conditions and *in Vitro* Culture Time. To investigate the effect of culture conditions on the developmental poten-

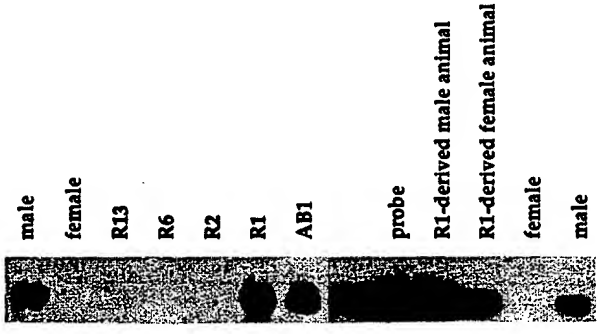

FIG. 1. Southern blot analysis of DNA derived from different cell lines and R1-derived animals. The blots were hybridized with a Y chromosome-specific probe.

Table 2. Prenatal developmental potential of R1 cultured under different conditions between passages 6 and 24 and tested by R1–tetraploid embryo aggregates

Passages, no.	Conditions	Tetraploid aggregates transferred, no.	Implantations, no.	Resorptions, no.	Midgestation dead embryos, no.	Newborns, no.	Recovered newborns, no.	Survivors, no.
6	Feeders + LIF	53	36	21	6	9	3	2
10	Feeders + LIF	15	11	6	1	4	2	1
14	Feeders + LIF	25	13	7	5	1	1	1
	Feeders	13	8	4	3	1	1	1
	LIF	24	19	7	7	5	2	0
16	Feeders + LIF	6	3	2	0	1	0	0
17	Feeders + LIF	18	13	9	3	1	0	0
	Feeders	20	9	5	4	0	0	0
	LIF	15	7	4	2	1	0	0
20	Feeders + LIF	24	20	10	9	1	0	0
	Feeders	25	19	6	10	3	0	0
	LIF	32	24	7	13	4	1	0
24	Feeders + LIF	22	14	8	5	1	0	0

tial of ES cells, we cultured R1 from passage 8 under three different conditions.

Condition 1: feeder layers + LIF. Cells were kept on SNL fibroblast feeders in DME medium supplemented with 20% FCS and 2000 units of LIF per ml. (These were the original conditions used when establishing the cell line.)

Condition 2: feeders alone. The cells were gradually weaned off LIF by decreasing the concentration by 500-unit steps at the first four passages and then maintained on SNL feeders in DME medium supplemented with 20% FCS.

Condition 3: LIF alone. The cells were kept on gelatinized plates in DME medium supplemented with 20% FCS and 2000 units of LIF per ml.

Aggregates with tetraploid embryos were prepared by using cells from passages 6–24. Raw data on the prenatal and perinatal development of these aggregates are shown in Table 2. There was no obvious difference between the different culture conditions in their ability to support development to term. Thus, to obtain a clear idea on the effect of *in vitro* culture time on developmental potential, data from the three culture conditions were pooled into two age groups: early (6–14) and late passages (Table 3).

Interestingly, the groups did not differ in implantation (67%) and resorption rate (35% and 31%, respectively), but the percentage of dead embryos at midgestation increased and the rate of newborns at term decreased significantly by late passage. In the late-passage group, only 1 of the 12 newborns recovered after the Caesarean section, whereas almost 50% of the newborns of the early-passage groups started breathing normally. No animal survived to adulthood from passages later than 14.

Karyotype of R1 at Early and Late Passages. To see if gross karyotypic changes could explain the decrease of developmental potentiality as a function of *in vitro* culture time, chromosome spreads were prepared from an early and a late passage, 11 and 33, respectively. A slight decrease was detected in the frequency of spreads with the normal number of chromosomes (Fig. 2), but the modal number was still 40.

Characterization of Completely ES Cell-Derived Animals. Since the tetraploid component was produced from albino and preselected GPI-BB CD1 embryos and R1 was agouti and GPI-AA, both the coat color and the GPI served as markers to detect occasional tetraploid contribution in the animals derived from R1–tetraploid embryo aggregates. The coat color of all five animals indicated only agouti contribution (Fig. 3). However, GPI analysis of blood from adult animals showed that one animal contained detectable tetraploid contribution (*ca.* 5–10%). This animal was the same one showing tetraploid contribution at birth. The remaining four animals showed no evidence of tetraploid cells in the blood. Further, GPI assay of the organs of two of the five animals—analyzed at 10 months of age—showed exclusive R1 contribution (Fig. 4 shows one of the two analyzed). Thus, within the limits of sensitivity of the GPI analysis, which allowed detection of contributions as low as 2%, no tetraploid cells remained in these animals. A minor contribution (<2%) from tetraploid cells cannot be excluded. The remaining three animals are more than 1 year old. They do not show any signs of premature aging or tumor development. It is likely that the life span of completely ES-derived animals is not affected by their cell culture origin.

The two newborns derived from R13 were female as predicted from Southern blot analysis of the cell line. Nearly all of the completely R1-derived newborns were male as predicted. However, two of these total 32 newborns (Table 3) were female. One of these two newborns reached adulthood but was not fertile. The existence of an R1-derived female may indicate some degree of Y chromosome loss in this cell line even at this early passage number. Y-chromosome loss could not have been complete, Southern blot analysis showed Y-specific sequences in this animal (Fig. 4).

Table 3. Prenatal developmental potential of R1 tested by R1–tetraploid embryo aggregates as a function of *in vitro* culture time (passage number)

No. of passages	Tetraploid aggregates transferred, no.	Implantations, no.	Resorptions, no.	Midgestation dead embryos, no.	Newborns, no.	Recovered newborns, no.	Survivors, no.
6–14	130	87 (67)	45 (35)	22 (17)	20 (15)	9	5
16–24	162	109 (67)	51 (31)	46 (28)	12 (7)	1	0
	χ^2	0.002	0.22	4.10	4.19	8.37	6.23
	P (df = 1)	$\gg$0.2	$\gg$0.2	<0.05	<0.05	<0.01	<0.02

The numbers in parentheses are percentages of aggregates transferred.

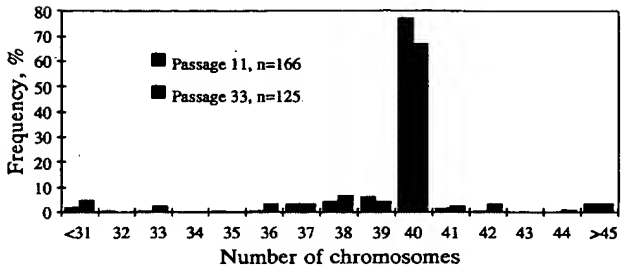

FIG. 2. Distribution of metaphase spreads with different chromosome numbers at passage 11 and passage 33 of R1.

The R1-derived males were all fertile, producing normal-size litters, and exclusively transmitted the R1 genotype to their offspring.

Developmental Potential of Subclones Derived from an Early Passage of R1. *In vitro* culture time negatively affected the developmental potential of R1 ES cells. To further investigate this phenomenon, we tried to distinguish between two models of the changes that may happen during culture. One possibility is that ES cells are not able to replicate exactly their stem-cell state during successive rounds of cell division and gradually lose their full potential. This loss is strictly related to the *in vitro* culture time or the number of cell divisions. The other possibility is that a certain proportion of cells replicate the fully potent stem-cell state at each cell division. The remaining cells move away from this state and form a developmentally restricted compartment. In time this restricted compartment gradually takes over the culture. However, at any time point, there are cells with intact potential. If the first model were true, it should not be possible to retain the full potential of later passage cell cultures by subcloning; but if the second model should be true, it should be possible to establish subclones of the parent cell line that retain full potential after prolonged passage *in vitro*.

To test the two models, we established subclones from single cells of passage 12 by using the original culture conditions and maintained them *in vitro* for a period equivalent to that of passage 24–25 of the original R1 stock before testing for pluripotency by tetraploid embryo aggregation. Table 4 shows the developmental potential of these lines. One of the five sublines, R1-S3, supported completely ES cell-derived development to term and gave rise to viable animals with similar efficiency to the parental R1 cell line at very early passages.

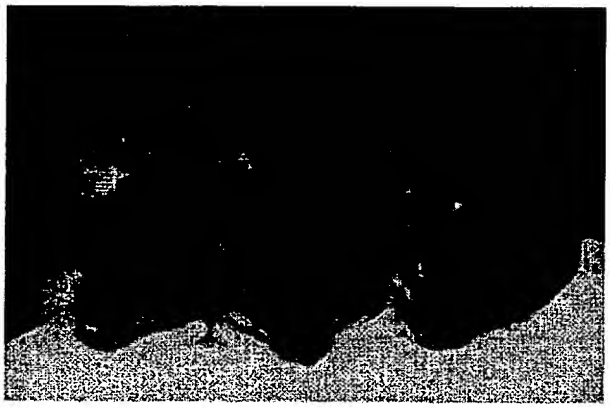

FIG. 3. Group of five R1-derived animals produced by R1–tetraploid embryo aggregates.

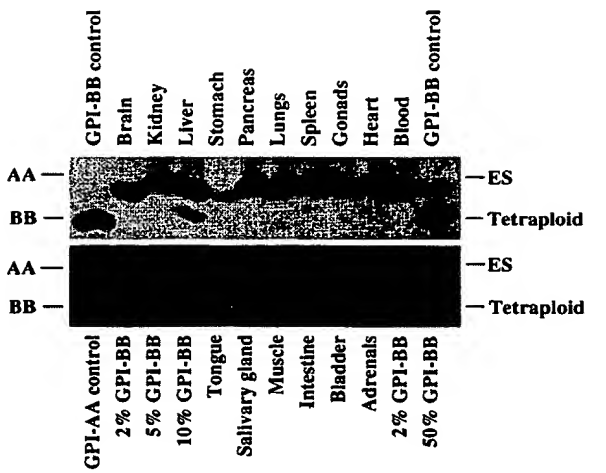

FIG. 4. GPI analysis of the major organs of one of the two R1–tetraploid embryo chimera. The tetraploid component had GPI-BB phenotype, while R1 was GPI-AA. The assay shows the complete R1 origin of the organs. The minor band in the liver sample does not line up with the band of GPI-BB and might be a degradative product of GPI-AA. By overdeveloping the stain, the sensitivity of our GPI test was estimated at 2% on the control samples.

DISCUSSION

Using ES cell–tetraploid aggregates, we have produced viable mice that are entirely ES cell-derived, as judged by GPI and coat color phenotype and germ-line transmission. This success was achieved with a newly derived ES cell line (R1) at early passage number (up to passage 14) and is the fullest demonstration to date of the remarkable potential of these tissue culture cells. Previous experiments using established cell lines had resulted in perinatal death of any totally ES cell-derived fetuses (3, 6). The same effect was observed here with later passages of R1, suggesting that prolonged passage in culture reduces the potential of the ES-cell population as a whole. However, one subclone of R1 isolated at passage 12 and maintained in culture until the equivalent of passage 24 was still able to produce viable ES cell-derived mice after aggregation with tetraploid embryos. This indicates that loss of full developmental potential is not a necessary consequence of passage in culture, but rather that the proportion of cells that retains full potential diminishes with extended passage. Some cell lines lose potential more quickly than others; three cell lines established in parallel with R1 failed to produce viable ES cell-derived embryos even at early passage.

The nature of the factors that cause this variable decline in developmental potential is still unclear. Both genetic and epigenetic changes can accumulate with passage in culture and may vary from line to line. It seems unlikely that major karyotypic changes are the main cause of the decline, since we only observed a small increase in the proportion of aneuploid cells in the R1 population with extended passage, and other established cell lines similarly retain a high proportion of euploid cells. It seems more likely that minor genetic changes or changes in DNA methylation and imprinting underlie the phenomenon. It will be interesting to compare the properties of the apparently stable subline with the parent cell line to see if subtle changes in DNA modification, gene expression, or differentiation capacity can be detected.

Although the R1 cell line can produce viable ES cell-derived mice, this is still an inefficient process; many ES cell–tetraploid aggregates die before reaching term, even when early passage cells are used. Therefore, this approach cannot be considered as a feasible approach for routinely

Table 4. Prenatal developmental potential of R1 sublines tested by ES cell–tetraploid aggregates

Subline of R1	Tetraploid aggregates transferred, no.	Resorptions, no.	Midgestation dead embryos, no.	Newborns, no.	Recovered newborns, no.	Animals reached adulthood, no.
R1-S1	19	7	3	0	0	0
R1-S2	45	9	3	1	0	0
R1-S3	20	6	5	5	3	2
R1-C3	10	4	3	2	0	0
R1-B1	23	9	5	2	1	0
Total	117	35	19	10	4	2

achieving germ-line transmission from genetically manipulated ES cells. However, a cell line, like R1, which retains full developmental potential for extended passage in at least one subclone, is likely to contribute well to the germ line after standard blastocyst injection or morula aggregation. Indeed, the R1 cell line has proved to be an efficient vehicle for transmitting genetic alterations through the germ line after either injection into C57BL/6 blastocysts or aggregation with diploid CD1 eight-cell stage embryos (unpublished data).

Understanding more about the factors that affect the developmental potential of ES cells in tetraploid aggregates may help to improve the technology of genetic manipulation of the mammalian genome.

We thank Dr. Robert Gerlai for useful discussions. This work was supported by Bristol-Myers Squibb and the Networks of Centres of Excellence Program on Neural Regeneration and Functional Recovery. J.R. is a Terry Fox Research Scientist of the National Cancer Institute of Canada and an International Scholar of the Howard Hughes Medical Research Institute. J.C.R. is a Medical Research Council (Canada) scientist.

1. Rossant, J., Moens, C. B. & Nagy, A. (1993) *Philos. Trans. R. Soc. London B* **339**, 207–215.
2. Koller, B. H. & Smithies, O. (1992) *Annu. Rev. Immunol.* **10**, 705–730.
3. Nagy, A., Gócza, E., Diaz, E. M., Prideaux, V. R., Iványi, E., Markkula, M. & Rossant, J. (1990) *Development* **110**, 815–821.
4. Doetschman, T., Eistetter, H., Katz, M., Schmidt, W. & Kemler, R. (1985) *J. Embryol. Exp. Morphol.* **87**, 27–45.
5. McMahon, A. P. & Bradley, A. (1990) *Cell* **62**, 1073–1085.
6. Rossant, J., Merentes-Diaz, E., Gócza, E., Iványi, E. & Nagy, A. (1991) in *Serono Symposium on Preimplantation Embryo Development*, ed. Bavister, B. (Springer, New York), pp. 157–165.
7. Quinn, P., Barros, C. & Whittingham, D. G. (1982) *J. Reprod. Fertil.* **66**, 161–168.
8. Nagy, A. & Rossant, J. (1992) in *Practical Approach Series: Gene Targeting*, ed. Joyner, A. (Oxford Univ. Press, New York), in press.
9. Kubiak, J. Z. & Tarkowski, A. K. (1985) *Exp. Cell Res.* **157**, 561–566.
10. Hogan, B., Constantini, F. & Lacy, E. (1986) *Manipulating the Mouse Embryo* (Cold Spring Harbor Lab. Press, Plainview, NY).
11. Forrester, L. M., Bernstein, A., Rossant, J. & Nagy, A. (1991) *Proc. Natl. Acad. Sci. USA* **88**, 7514–7517.
12. Bishop, C. E., Boursot, P., Baron, B., Bonhomme, F. & Hatat, D. (1985) *Nature (London)* **315**, 70–72.
13. Evans, M. J. & Kaufman, M. (1981) *Nature (London)* **292**, 154–156.

Proc. Natl. Acad. Sci. USA
Vol. 89, pp. 6861–6865, August 1992
Genetics

Tissue- and site-specific DNA recombination in transgenic mice

PAUL C. ORBAN*, DANIEL CHUI*, AND JAMEY D. MARTH*†‡

*Biomedical Research Centre and †Departments of Medical Genetics and Biochemistry, 2222 Health Sciences Mall, University of British Columbia, Vancouver, BC V6T 1Z3 Canada

Communicated by Richard D. Palmiter, April 28, 1992

ABSTRACT **We have developed a method of specifically modifying the mammalian genome *in vivo*. This procedure comprises heritable tissue-specific and site-specific DNA recombination as a function of recombinase expression in transgenic mice. Transgenes encoding the bacteriophage P1 Cre recombinase and the *loxP*-flanked β-galactosidase gene were used to generate transgenic mice. Genomic DNA from doubly transgenic mice exhibited tissue-specific DNA recombination as a result of Cre expression. Further characterization revealed that this process was highly efficient at distinct chromosomal integration sites. These studies also imply that Cre-mediated recombination provides a heritable marker for mitoses following the loss of Cre expression. This transgene-recombination system permits unique approaches to *in vivo* studies of gene function within experimentally defined spatial and temporal boundaries.**

Bacteriophage P1 encodes the 38-kDa Cre recombinase that catalyzes site-specific DNA recombination between 34-base-pair (bp) repeats termed *loxP* (1). Cre is a member of the integrase family of recombinases. These enzymes recognize specific nucleotide sequences and function through a transient DNA-protein covalent linkage (reviewed in refs. 2 and 3). Cre activity appears mechanistically identical to that of yeast FLP recombinase and can function *in vitro* in the absence of high-energy cofactors, topoisomerase activity, and DNA replication (4, 5). In Cre-mediated recombination, resultant DNA structures are dependent upon the orientation of *loxP* sites. Direct repeats of *loxP* dictate an excision of intervening sequences whereas inverted repeats specify inversion (4). Cre and FLP have been shown to mediate site-specific DNA recombination in tissue-cultured eukaryotic cells, *Drosophila*, and transgenic plants (6–12).

With the aim of applying Cre recombinase function to molecular studies of normal and abnormal mammalian physiology, we sought to generate a transgenic mouse system that would establish whether Cre could effectively mediate chromosomal DNA recombination. As a foundation for future applications, we devised a nondeleterious transgene strategy that would provide an assessment of the efficiency, position dependence, and heritability of Cre-mediated chromosomal DNA recombination in mammals.

MATERIALS AND METHODS

Transgene Construction and Transgenic Mouse Production. The Cre transgene expression vector was constructed by inserting the 1.5-kilobase (kb) *Xho* I–*Xba* I fragment of pBS31 (7), containing the Cre coding sequence, into the unique *Bam*HI site of p1017 (ref. 13 and Fig. 1*A*). A second transgene vector, in which the *Escherichia coli* β-galactosidase (β-gal) gene was flanked by *loxP* sites (Fig. 1*B*), was constructed as follows. The β-gal gene, obtained as a 3.5-kb *Not* I fragment from pCMVβ (14), was blunt-end ligated into the *Bam*HI site residing between two direct repeats of *loxP* in plasmid plox² (derived from pBS64, 7). In plox², two direct repeats of *loxP* are flanked by polylinker-derived *Eco*RI and *Hin*dIII restriction enzyme sites. Isolation of the *loxP*–β-gal–*loxP* fragment was followed by blunt-ended ligation into the *Bam*HI site of p1017. Transgene vectors were purified away from plasmid sequences following *Not* I digestion and are represented as those *Not* I fragments in Fig. 1 *A* and *B*. Transgenic mice were produced following harvest of ICR × ICR zygotes (albino outbred, Harlan–Sprague–Dawley), DNA microinjection, and implantation. The presence of transgene DNA was assessed by hybridizing mouse tail DNA with either Cre or β-gal DNA probes (depicted in Fig. 1). In surgical procedures, 0.5 ml of 2.5% avertin was used as an anesthetic.

Southern and Northern Analysis. Thymocytes and splenocytes were harvested as single-cell suspensions by gently teasing freshly removed tissue. DNA was prepared from tissues and cells by incubation with proteinase K (100 μg/ml; Bethesda Research Laboratories) in 100 mM Tris, pH 8.0/50 mM EDTA for 24 hr at 55°C followed by extraction with phenol/chloroform and ethanol precipitation. Purified DNA was subjected to restriction enzyme digestion and Southern blot analyses (15). For Northern analyses, RNA was prepared from freshly homogenized tissue or single-cell suspensions in 6 M guanidinium isothiocyanate and fractionated through a CsCl cushion (16). The RNA was denatured with formamide/formaldehyde for agarose gel electrophoresis, blotting, and hybridization (15). DNA fragments for use as probes were nick-translated in the presence of random oligonucleotides to a specific activity of 10^8 cpm/μg. Densitometric analyses were performed with a Molecular Dynamics scanning densitometer (Sunnyvale, CA).

Flow Cytometry. Spleen-derived T cells were stained for surface expression of CD4 or CD8 antigens with phycoerythrin-conjugated anti-CD4 and fluorescein-conjugated anti-CD8 (anti-L3T4 and anti-Lyt-2, respectively; Becton Dickinson). Sorted populations were obtained by using a Becton Dickinson FACStar Plus flow cytometer (Becton Dickinson). The sorted population was >97% pure as judged by subsequent FACScan analysis.

RESULTS

Creation of Transgenic Lines. In transgene vector constructs derived from p1017, expression is regulated by the mouse proximal *lck* promoter, while the hGH gene contributes exon–intron splicing and polyadenylylation signals. Transgene expression from this vector is generally obtained in a thymocyte-specific manner (13, 17–19). Following thymocyte development in the thymus, emigration of mature T cells to peripheral compartments, including the spleen, coincides with loss of proximal *lck* promoter activity.

The publication costs of this article were defrayed in part by page charge payment. This article must therefore be hereby marked "*advertisement*" in accordance with 18 U.S.C. §1734 solely to indicate this fact.

Abbreviations: β-gal, β-galactosidase; hGH, human growth hormone.

‡To whom reprint requests should be addressed.

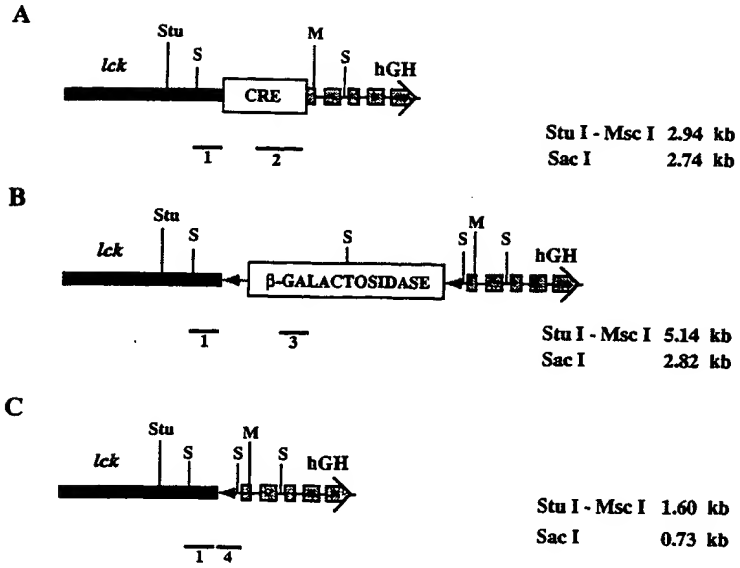

FIG. 1. Structures of transgene vector constructs and the Cre-mediated recombination event. (*A*) The Cre transgene represented as the microinjected *Not* I restriction fragment. The black bar represents 3.0 kb and contains the mouse thymus-specific proximal *lck* promoter. Human growth hormone (hGH) gene sequence (2.1 kb) is denoted by boxes (exons) and lines (introns) and contributes the polyadenylylation signal. Restriction enzyme sites used in Southern blotting analyses are depicted: S, *Sac* I; Stu, *Stu* I; M, *Msc* I. Probes used in Southern analyses are represented by numbered lines. Probe 1 is the 0.6-kb *Sac* I–*Bam*HI fragment of the *lck* promoter region. Probe 2 is a 900-bp *Bam*HI fragment of Cre. (*B*) The *loxP*-flanked β-gal transgene represented as the microinjected *Not* I restriction enzyme fragment. *loxP* sites are denoted by small arrows (represented at 10× relative construct size) flanking the β-gal gene as direct repeats. Probe 3 is a 600-bp *Hpa* I fragment of the β-gal gene. (*C*) Cre-mediated recombination structure resulting from excision of the *loxP*-flanked β-gal gene. A single *loxP* site is resolved following recombination. Probe 4 consists of the 180-bp *Hin*dIII–*Eco*RI fragment of plox^2 containing two *loxP* sites and a small contribution of plasmid polylinker sequence. Expected Southern blot fragment sizes are indicated.

A Cre transgenic line (I-57) was derived from zygotes injected with the Cre expression vector depicted in Fig. 1*A*. Two independent transgenic lines (I-86 and I-87) were derived from zygotes injected with the *loxP*–β-gal–*loxP* vector (Fig. 1*B*). As the β-gal gene is flanked by direct repeats of *loxP*, a Cre-mediated recombination event would be predicted to excise the β-gal gene, generating the structure depicted in Fig. 1*C*. These Cre and *loxP*–β-gal–*loxP* transgenic mouse lines bred as expected for unique single-site integration events and harbored the specific transgenes oriented as "head-to-tail" tandem arrays (data not shown), as is common for most transgene integration structures (reviewed in refs. 20–22). Transgenic mice from the Cre and *loxP*–β-gal–*loxP* lines were then bred to generate doubly transgenic progeny.

Genomic DNA was prepared from thymocytes and tails of Cre transgenic mice, *loxP*–β-gal–*loxP* transgenic mice, and doubly transgenic mice for Southern blot analyses. The Cre gene was visualized as the expected 2.94-kb *Stu* I–*Msc* I restriction fragment within the parental Cre transgenic mouse and a doubly transgenic offspring (Fig. 2*A*, lanes 3 and 5, respectively). With a β-gal-specific probe and the same thymocyte DNAs, the expected 2.82-kb *Sac* I fragment was observed in both the I-86 and the I-87 line (Fig. 2*B* and data not shown). Densitometric analysis of tail DNA (see below) revealed that the I-57 Cre line harbored the transgene at high copy number relative to the levels in the I-86 and I-87 *loxP*–β-gal–*loxP* transgenic lines (Fig. 2 *A* and *B* and see below).

Cre-Mediated Recombination Occurs *in Vivo* in Transgenic Mice. Southern analysis of thymocyte DNA from double transgenic mice revealed that the β-gal gene hybridization signal was eliminated (Fig. 2*B*, lane 5). This is the expected result following Cre-mediated recombination resulting in an excision of the β-gal gene situated between direct repeats of *loxP* (Fig. 1*C*). Evidence for the predicted Cre-mediated recombination structure was obtained by using a *loxP*-specific DNA probe (Fig. 2*C*). Hybridization was observed to a novel 1.60-kb *Stu* I–*Msc* I DNA fragment in the doubly transgenic thymocyte sample. Recombination was not detected in tail DNA derived from the same doubly transgenic mouse (Fig. 2*C*, lane 5). This new DNA structure was not present in parental thymocyte DNA derived from either the Cre or the *loxP*–β-gal–*loxP* transgenic mice (Fig. 2*C*, lanes 2 and 3). As would also be expected, there was a loss of the 5.14-kb DNA fragment (the double *loxP*-containing β-gal transgene).

Using the polymerase chain reaction (PCR), we have cloned the recombination structure residing within the 5′ *lck* untranslated sequence and the second exon of hGH. Analyses with this DNA revealed the expected structural attributes, including the exact size predicted, presence of a single *loxP* sequence, and the expected unique polylinker-derived restriction enzyme sites flanking this novel Cre-generated *loxP* site (data not shown).

The β-gal gene was incorporated as a second marker to ascertain Cre-mediated recombination by loss of β-gal enzymatic activity, but neither the I-86 nor the I-87 *loxP*–β-gal–*loxP* transgene allele was sufficiently active to allow protein detection (data not shown). However, RNA expression was observed following quantitative PCR assays (data not shown). These studies revealed, on average, three to five molecules of transgene-derived RNA per cell. Lack of high-level RNA expression in low-transgene-copy-number p1017-derived transgenic mice is routinely observed (unpublished observations) and does not reflect a specific inhibition mediated by *loxP* sites. Furthermore, studies in eukaryotic cells *in vitro* have shown substantial *loxP*-flanked gene expression at the level of both RNA and protein (6, 8, 12).

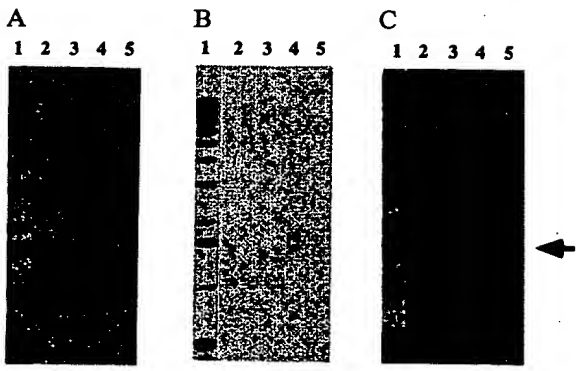

FIG. 2. Evidence of Cre-mediated recombination in genomic thymocyte DNA derived from doubly transgenic mice. (*A*) Southern blot analysis of *Stu* I/*Msc* I-digested thymocyte DNAs probed with ^{32}P-labeled Cre DNA (probe 2). Lane 1, ^{32}P-labeled 1-kb ladder (Bethesda Research Laboratories); lane 2, nontransgenic; lane 3, Cre parental transgenic; lane 4, *loxP*–β-gal–*loxP* parental transgenic; lane 5, doubly transgenic offspring 57/86-2. (*B*) Southern analysis of *Sac* I-digested thymocyte DNAs (identical to those used above) probed with ^{32}P-labeled β-gal DNA (probe 3). Lane 1, 1-kb ladder; lane 2, nontransgenic; lane 3, Cre parental transgenic; lane 4, *loxP*–β-gal–*loxP* parental transgenic; lane 5, doubly transgenic. (*C*) Southern blot analysis of *Stu* I/*Msc* I-digested genomic DNA (identical to those used above) hybridized with ^{32}P-labeled *loxP* fragment (probe 4). Lane 1, 1-kb ladder; lane 2, Cre parental thymocyte DNA; lane 3, *loxP*–β-gal–*loxP* parental thymocyte DNA; lane 4, doubly transgenic thymocyte DNA; lane 5, doubly transgenic tail DNA. Arrow, Cre-mediated recombination-derived fragment. A low level of hybridization to polylinker DNA sequence is seen in Cre-transgene-containing samples (*C*, lanes 2, 4, and 5), representing limited polylinker sequence residing within the Cre transgene fragment and the *loxP* probe. Five micrograms of DNA was loaded per lane.

Cre Recombinase Activity Can Be Tissue-Specific and Heritable in Transgenic Mice. Evidence of the tissue specificity of Cre-mediated recombination was obtained following RNA and Southern blot analyses of multiple tissue samples. Cre-specific RNA was detected in the thymus but not in the brain, kidney, liver, spleen, or tail (Fig. 3*A* and data not shown). The predominant Cre RNA species migrated with an apparent molecular size of ≈3.9 kb. Analyses of these RNA samples with hGH probes, and the obvious presence of multiple Cre RNA species, provided evidence that the 3.9-kb transcripts reflected incomplete splicing of the hGH gene (data not shown). More completely spliced Cre transgene RNA was observed migrating slightly larger than 18S (≈2.4 kb; Fig. 3*A*, lane 2). In immunoblotting experiments using a polyclonal anti-Cre antibody (provided by Brian Sauer, DuPont) with total cellular protein derived from these tissues, we observed the predicted 38-kDa Cre recombinase specifically expressed within the thymocyte population (data not shown). This Cre expression profile is identical to that obtained from all transgenic descendents of the Cre transgenic founder animal. DNA samples from these tissues were also subjected to Southern blot analysis. In brain, kidney, liver, and tail DNAs, β-gal gene hybridization remained constant and the 1.60-kb recombination structure was not present (Fig. 3*B*).

Although Cre expression was undetectable in splenocyte RNA (Fig. 3*A*, lane 4), evidence of the recombination event was apparent in splenocyte DNA (Fig. 3*C*, lane 2). Southern analyses of the purified splenic T-cell subpopulation (≈20% of total splenocytes) revealed an enrichment for the recombination structure at the expense of the nonrecombined *loxP*–β-gal–*loxP* transgene allele (Fig. 3*C*, lane 3). The expected *loxP*-hybridizing recombination product, as displayed in Fig. 2*C*, was also observed in this and other blotting analyses (see below). As Cre expression was not detected in either the total splenocyte or the splenic T-cell subpopulation (Fig. 3*A* and data not shown), the high degree of recombination within the *loxP*–β-gal–*loxP* transgene array (a loss of ≈95% of β-gal DNA; see below) implies that this Cre-mediated recombination occurred in the thymus, the natural site of T-cell ontogeny. In experiments that expanded the number of spleen-derived T cells by using the polyclonal lectin concanavalin A and interleukin 2, the recombined transgene allele frequency was retained following multiple mitoses (over at least 14 cell division cycles) in the absence of detectable Cre RNA (data not shown). These data indicate that Cre-mediated recombination can be a stable and heritable chromosomal alteration *in vivo* but do not rule out the possibility that undetected levels of splenic T-cell Cre recombinase are mediating *loxP*-flanked DNA recombination.

Transgenic Cre-Mediated Recombination Is Highly Efficient. For assessments of transgene copy number and recombination efficiency, Southern blot analyses were performed on *Stu* I/*Msc* I-digested DNAs hybridized to *lck* promoter sequence (probe 1) in a strategy that provided stoichiometric

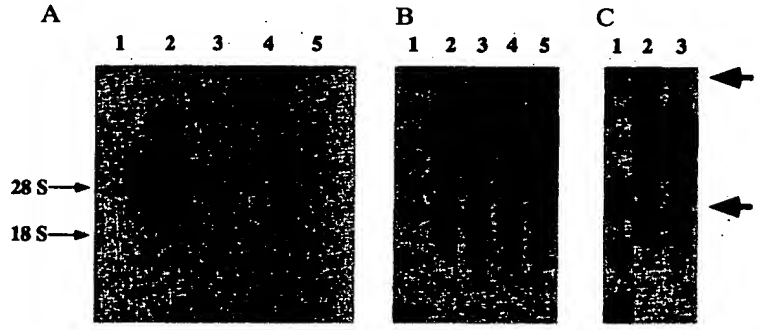

FIG. 3. Distribution of Cre RNA expression and *loxP*–β-gal–*loxP* transgene structure provides evidence of tissue-specific and heritable Cre-mediated recombination *in vivo*. (*A*) RNA blot analysis of Cre expression among normal tissues in a doubly transgenic offspring (57/86-4). Lane 1, brain; lane 2, thymus; lane 3, kidney; lane 4, spleen; lane 5, liver. RNA preparation and blotting procedures were performed as described (9). Blot was probed with ^{32}P-labeled Cre DNA (probe 2). Positions of 28S and 18S rRNAs are indicated. (*B* and *C*) Southern blot analyses of *Stu* I/*Msc* I-digested tissue DNAs, from the same animal analyzed in *A*, hybridized to *lck* promoter sequence (probe 1). In *B*: lane 1, 1-kb ladder; lane 2, tail; lane 3, liver; lane 4, brain; lane 5, kidney. In *C*: lane 1, 1-kb ladder; lane 2, spleen; lane 3, spleen-derived T cells. The Cre transgene is observed as the high-copy 2.9-kb fragment. The 2.5-kb fragment represents an aberrant integration event derived from p1017 sequence contained within the I-57 Cre transgene array (data not shown). Upper arrow, nonrecombined β-gal transgene fragment; lower arrow, 1.60-kb Cre-mediated recombination-derived fragment. The 1.40-kb fragment represents the endogenous *lck* gene. In the experiments above, 5 μg of either total cellular RNA or genomic DNA was loaded per lane.

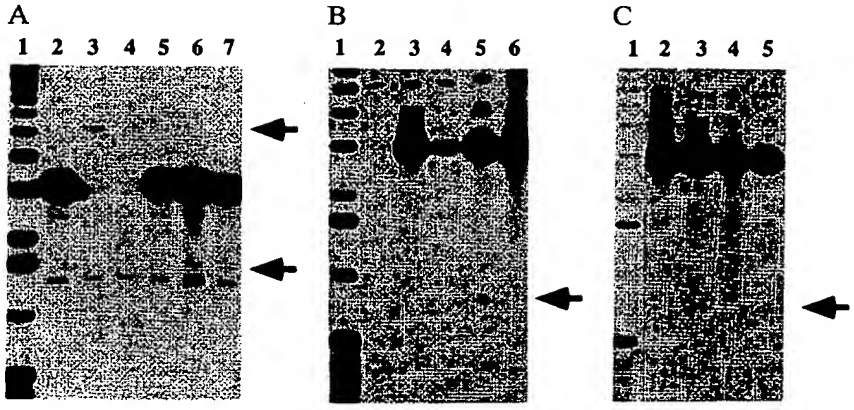

FIG. 4. Transgene-encoded Cre recombinase is highly efficient and can function at distinct chromosomal sites. These Southern blot analyses used the *lck* promoter fragment (probe 1). (*A*) *Stu* I/*Msc* I-digested thymocyte DNA. Lane 1, 1-kb ladder; lane 2, Cre parental transgenic; lane 3, *loxP*–β-gal–*loxP* parental transgenic; lane 4, nontransgenic; lanes 5–7, individual doubly transgenic progeny (57/86-8, 57/86-10, and 57/86-18, respectively). (*B*) *Sac* I-digested thymocyte DNA. Lane 1, 1-kb ladder; lane 2, nontransgenic; lane 3, Cre parental; lane 4, *loxP*–β-gal–*loxP* parental transgenic; lane 5, doubly transgenic thymocytes (57/86-10); lane 6, doubly transgenic tail from the same animal as in lane 5. An additional *lck*-hybridizing fragment at 4.2 kb represents an aberrant integration event derived from p1017 sequence contained within the I-57 Cre transgene array (data not shown). (*C*) *Sac* I-digested DNA derived from doubly transgenic mice produced by a cross between Cre transgenic line I-57 and the *loxP*–β-gal–*loxP* transgenic line I-87. Lane 1, 1-kb ladder; lane 2, tail DNA from offspring 57/87-3; lane 3, thymocyte DNA from 57/87-3; lane 4, tail DNA from offspring 57/87-7; lane 5, thymocyte DNA from 57/87-7. In the *Sac* I digest, the endogenous *lck* gene is apparent as a 5.3-kb fragment. Upper arrow, intact β-gal transgene fragment; lower arrow, Cre-mediated recombination fragment. An additional *lck*-hybridizing band at 1.7 kb reflects an aberrant integration event derived from truncated p1017 sequence contained within the I-87 *loxP*–β-gal–*loxP* transgene array (data not shown).

detection of the Cre transgene, the *loxP*–β-gal–*loxP* transgene, the endogenous *lck* gene, and the recombination structure (as in Fig. 3 *B* and *C*). In comparison to the single-copy (per haploid genome) *lck* gene (15), the I-57 Cre line was estimated to contain 110 copies of the transgene while both the I-86 and I-87 *loxP*–β-gal–*loxP* transgenic lines harbored ≈8 copies each (Fig. 4*A*). Southern analyses of doubly transgenic mice from multiple matings revealed that thymocyte Cre-mediated recombination produced the expected fragment sizes in all animals surveyed, as exemplified in Fig. 4 *A* and *B*. However, variation in the degree of Cre-mediated recombination among doubly transgenic mice was observed.

To assess this variation in Cre-mediated recombination among doubly transgenic progeny, densitometric comparisons were performed using the endogenous *lck* gene hybridization levels as internal controls. In these experiments, the extent of recombination was approximately 87%, 99%, and 97% in three doubly transgenic mice, as measured by loss of β-gal DNA (Fig. 4*A*, lanes 5–7, respectively). In spleen-derived T-cell DNA analyses, a >95% deletion of the β-gal gene was routinely observed (Fig. 3*C*, lane 3, and data not shown). In identical analyses using hGH sequence as a probe, similar results were obtained (data not shown). These results represent an average of analyses undertaken on >20 doubly transgenic mice generated from seven litters.

As the *loxP*–β-gal–*loxP* lines harbor 8 copies of transgene per cell, removal of >88% of the total β-gal transgene level would indicate that some cells have lost all copies of the β-gal gene. The efficacy of transgenic Cre-mediated recombination may be greater than evaluated here, as remaining levels of β-gal hybridization may indicate the presence of prothymocytes or contamination of thymocytes with B cells, thymic epithelial cells, and dendritic cells during cell preparation. These cells do not express *lck* and hence presumably would not express the Cre recombinase.

Cre-Mediated Recombination Excises the Transgene Array. The length of DNA between two *loxP* sites is a variable that may influence the efficiency of transgenic Cre-mediated recombination. In thymocyte DNA of doubly transgenic mice, the copy number of the resultant Cre-mediated DNA recombination structure is approximately half that of the endogenous *lck* gene (Figs. 3 and 4). Combined with the observations that β-gal and hGH DNA elimination can be virtually complete, and must be totally complete in some cells (perhaps those expressing the highest levels of Cre), these data imply that Cre-mediated recombination reduces the eight copies of the *loxP*–β-gal–*loxP* transgene array to a recombined allele consisting of a single copy of the *lck* promoter, the residual *loxP* site, and the hGH gene (Fig. 1*C*). This requires recombination between *lck* and hGH sequences within the transgene array, as may be expected since a "head-to-tail" transgene structure would contain direct repeats of *loxP* flanking the 3.0-kb *lck* promoter and the 2.1-kb hGH minigene. Thus at least 5.1 kb of chromosomal DNA can be excised in a single event. However, the exact distance between specific recombination events could be in integrals of 3.5 and 5.1 kb up to ≈70 kb, the estimated length of the transgene array.

The excised β-gal DNA is degraded, as hybridization to β-gal sequences is not observed at other chromosomal sites. Further, we were unable to detect the presence of intermediates that would reveal a sequential recombination process in transgene array reduction (data not shown). While those intermediates may nevertheless exist, they would be relatively short-lived species. These findings show that transgenic Cre-mediated recombination can be highly efficient in excising multiple DNA sequences flanked by direct repeats of *loxP* at a single chromosomal integration site.

Cre Can Function at Different Chromosomal Sites *in Vivo*. The efficiency of Cre function may also depend upon the chromosomal context of *loxP* sites. In this regard, a second *loxP*–β-gal–*loxP* transgene line (I-87) was mated with the Cre transgenic line I-57. Breeding experiments revealed that in the I-87 line, the *loxP*–β-gal–*loxP* transgene is at a different chromosomal site from that of the I-86 transgenic line (data not shown). Tissue-specific Cre-mediated recombination was also detected in the progeny of the I-57 × I-87 cross (Fig. 4*C*). Thus, in two transgene integrations that occurred at distinct chromosomal sites, Cre recombinase was able to access the transgenic *loxP* sites and function in producing chromosomal DNA recombination. While there may be some mammalian chromosomal sites at which Cre is unable to generate recombination, further studies will be required to address this in a spatially and statistically significant manner.

DISCUSSION

These studies provide a basis for the use of DNA recombination strategies in transgenic animal technology. Although one experimental approach initially considered included generating specific developmental phenotypes, we reasoned that modifying cellular fate, proliferative status, or viability would alter the validity of recombinase efficacy measurements. We find that the Cre recombinase can function in a highly efficient manner in directing tissue-specific, site-specific, and heritable chromosomal DNA recombination events *in vivo* in transgenic mice. Although, like FLP, Cre does not contain a canonical nuclear localization signal, Cre could access chromatin either through diffusion or following the transient breakdown of the nuclear membrane during mitosis.

Cre activity can be observed at both chromosomal sites assayed in this study, suggesting that the majority of the mammalian genome may be accessible to Cre function. From the transgene constructs used in this study we conclude that Cre can effectively recombine at least 5.1 kb of DNA in a single event. However, the reduction of the entire transgene array described herein (≈70 kb) suggests that Cre may mediate larger recombination events. The ability of Cre recombinase to recombine DNA over large distances in the mammalian genome may provide an experimental method of directing specific chromosomal translocations *in vivo*. This activity can be inferred from studies of FLP in *Drosophila* (23).

This technological advance allows studies of various aspects of gene function *in vivo* that could not be addressed hitherto. For example, current methodologies for gene ablation in transgenic mice, following embryonic stem-cell manipulations, produce null alleles in all cells of animals bred to homozygosity (reviewed in ref. 24). However, with the recombinase approach described in this study, null alleles could be generated in a tissue-specific and developmentally regulated manner. *loxP* sites could be positioned, by homologous recombination, to flank the target gene/exon in a nondeleterious manner; alternatively, *loxP* sites could be inserted to flank a gene replacement vector for complementation of the null background. When bred into a Cre transgenic line with a predefined Cre expression profile, the exact spatial and temporal pattern of recombination would be known. This would permit reproducible studies of the immediate metabolic alterations taking place following recessive genetic lesions and also reveal tissue-specific functions for genes shown to be expressed in multiple spatial and temporal patterns. Additionally, this methodology can generate transgene ablation. A requirement for constitutive transgene expression in the evolution of developmental and pathologic phenotypes could be addressed.

The heritable nature of Cre-mediated recombination allows a significant advance in the methodology for cell fate determination in mammals. Expression of a marker gene could be engineered to be dependent upon a Cre-mediated recombination event that would excise a *loxP*-flanked "stop" sequence (for example a transcriptional stop and RNA splice donor site) placed between a pan-specific promoter and the marker gene. Following recombination, marker gene expression would commence. In this way daughter cells could be identified by virtue of the initial activity from the Cre transgene promoter, irrespective of subsequent Cre expression. We expect that these applications of this transgene-recombination system will greatly enhance the information gained in gene function and disease modeling research employing transgenic animals.

We thank Drs. John Schrader, Kevin Leslie, and Stuart Berger for helpful comments on the manuscript and Dr. Brian Sauer for providing the Cre gene- and *loxP*-containing plasmids. FACStar Plus operation was performed by Dan Zecchini. P.C.O. is supported by a grant from the National Cancer Institute of Canada to John Schrader. This research was supported by the National Centers of Excellence "Genetic Basis of Human Disease" programme (to J.D.M.). J.D.M. is a recipient of a Medical Research Council of Canada scholarship.

1. Sternberg, N. & Hamilton, D. (1981) *J. Mol. Biol.* **150**, 467–486.
2. Argos, P., Landy, A., Abremski, K., Egan, J. B., Haggard-Ljunquist, E., Hoess, R. H., Kahn, M. L., Kalionis, B., Narayana, S. V. L., Pierson, L. S., III, Sternberg, N. & Leong, J. M. (1986) *EMBO J.* **5**, 433–440.
3. Craig, N. L. (1988) *Annu. Rev. Genet.* **22**, 77–105.
4. Abremski, K., Hoess, R. & Sternberg, N. (1983) *Cell* **32**, 1301–1311.
5. Abremski, K. & Hoess, R. (1984) *J. Biol. Chem.* **259**, 1509–1514.
6. Sauer, B. (1987) *Mol. Cell. Biol.* **7**, 2087–2096.
7. Sauer, B. & Henderson, N. (1988) *Proc. Natl. Acad. Sci. USA* **85**, 5166–5170.
8. Sauer, B. & Henderson, N. (1989) *Nucleic Acids Res.* **17**, 147–161.
9. Golic, K. G. & Lindquist, S. (1989) *Cell* **59**, 499–509.
10. Sauer, B. & Henderson, N. (1990) *New Biol.* **2**, 441–449.
11. O'Gorman, S., Fox, D. T. & Wahl, G. M. (1991) *Science* **251**, 1351–1355.
12. Dale, E. & Ow, D. W. (1991) *Proc. Natl. Acad. Sci. USA* **88**, 10558–10562.
13. Chaffin, K. E., Beals, C. R., Wilkie, T. M., Forbush, K. A., Simon, M. I. & Perlmutter, R. M. (1990) *EMBO J.* **9**, 3821–3829.
14. MacGregor, G. R. & Caskey, C. T. (1989) *Nucleic Acids Res.* **17**, 2365.
15. Marth, J. D., Peet, R., Krebs, E. G. & Perlmutter, R. M. (1985) *Cell* **43**, 393–404.
16. Chirgwin, J. M., Przybyla, A. E., MacDonald, R. J. & Rutter, W. J. (1979) *Biochemistry* **18**, 5294–5299.
17. Garvin, A. M., Abraham, K. M., Forbush, K. A., Farr, A. G., Davison, B. L. & Perlmutter, R. M. (1990) *Int. Immunol.* **2**, 173–180.
18. Abraham, K. M., Levin, S. D., Marth, J. D., Forbush, K. A. & Perlmutter, R. M. (1991) *Proc. Natl. Acad. Sci. USA* **88**, 3977–3981.
19. Cooke, M. P., Abraham, K. M., Forbush, K. A. & Perlmutter, R. M. (1991) *Cell* **65**, 281–291.
20. Brinster, R. L. & Palmiter, R. D. (1986) in *The Harvey Lectures Series 80* (Liss, New York), pp. 1–38.
21. Jaenisch, R. (1988) *Science* **240**, 1468–1474.
22. Hanahan, D. (1989) *Science* **246**, 1265–1274.
23. Golic, K. G. (1991) *Science* **252**, 958–961.
24. Capecchi, M. R. (1989) *Science* **244**, 1288–1292.

Transgenic Animals

Index to this page

A transgenic animal is one that carries a foreign gene that has been deliberately inserted into its genome. The foreign gene is constructed using recombinant DNA methodology. In addition to a **structural gene**, the DNA usually includes other sequences to enable it

- to be incorporated into the DNA of the host and
- to be expressed correctly by the cells of the host.

- Transgenic **sheep** and goats have been produced that express foreign proteins in their milk.
- Transgenic chickens are now able to synthesize human proteins in the "white" of the eggs.

These animals should eventually prove to be valuable sources of proteins for human therapy.

In July 2000, researchers from the team that produced Dolly reported success in producing transgenic lambs in which the transgene had been inserted at a specific site in the genome and functioned well. [More]

Transgenic **mice** have provided the tools for exploring many biological questions.

An example:

Normal mice cannot be infected with polio virus. They lack the cell-surface molecule that, in humans, serves as the receptor for the virus. So normal mice cannot serve as an inexpensive, easily-manipulated model for studying the disease. However, transgenic mice expressing the human gene for the polio virus receptor

- can be infected by polio virus and even
- develop paralysis and other pathological changes characteristic of the disease in humans.

Two methods of producing transgenic mice are widely used:

- transforming **embryonic stem cells** (**ES** cells) growing in tissue culture with the desired DNA;
- injecting the desired gene into the **pronucleus** of a fertilized mouse egg.

The Embryonic Stem Cell Method (Method "1")

Embryonic stem cells (**ES** cells) are harvested from the **inner cell mass** (ICM) of mouse blastocysts. They can be grown in culture and retain their full potential to produce all the cells of the mature animal, **including its gametes**.

Link to discussion of embryonic stem cells.

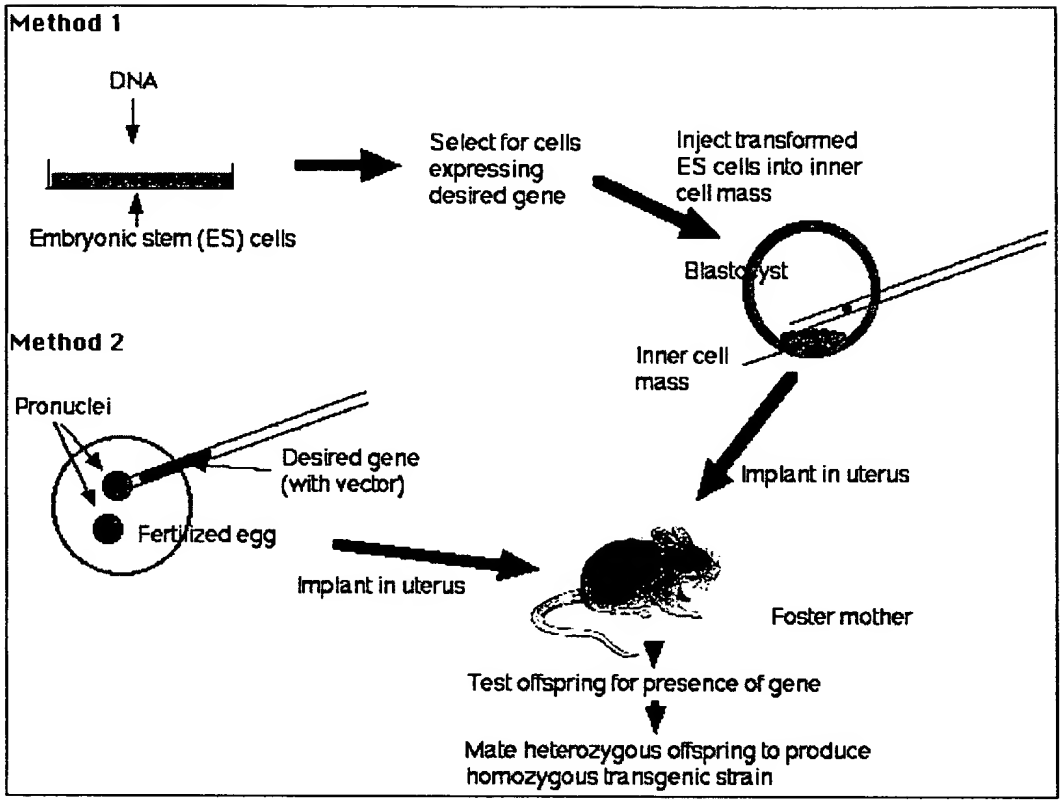

1. Make your DNA

Using recombinant DNA methods, build molecules of DNA containing

- the structural gene you desire (e.g., the insulin gene)
- **vector** DNA to enable the molecules to be inserted into host DNA molecules
- **promoter and enhancer sequences** to enable the gene to be expressed by host cells

2. Transform ES cells in culture

Expose the cultured cells to the DNA so that some will incorporate it.

3. Select for successfully transformed cells. [Method]

4. Inject these cells into the inner cell mass (ICM) of mouse blastocysts.

5. Embryo transfer

- Prepare a **pseudopregnant** mouse (by mating a female mouse with a vasectomized male). The stimulus of mating elicits the hormonal changes needed to make her uterus receptive.
- Transfer the embryos into her uterus.
- Hope that they **implant** successfully and develop into healthy pups (no more than one-third will).

6. Test her offspring

- Remove a small piece of tissue from the tail and examine its DNA for the desired gene. No more than 10-20% will have it, and they will be heterozygous for the gene.

7. Establish a transgenic strain

- Mate two heterozygous mice and screen their offspring for the 1:4 that will be **homozygous** for the transgene.
- Mating these will found the transgenic strain.

The Pronucleus Method (Method "2")

1. Prepare your DNA as in Method 1

2. Transform fertilized eggs

- Harvest freshly fertilized eggs before the sperm head has become a pronucleus.
- Inject the male pronucleus with your DNA.
- When the pronuclei have fused to form the diploid zygote nucleus, allow the zygote to divide by mitosis to form a 2-cell embryo.

3. Implant the embryos in a pseudopregnant foster mother and proceed as in Method 1.

An Example

This image (courtesy of R. L. Brinster and R. E. Hammer) shows a transgenic mouse (right) with a normal littermate (left). The giant mouse developed from a fertilized egg transformed with a recombinant DNA molecule containing:

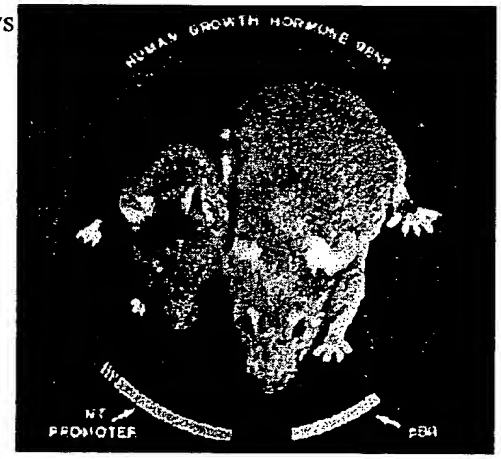

- the structural gene for **human growth hormone**
- a strong mouse gene **promoter**

The levels of growth hormone in the serum of some of the transgenic mice were several hundred times higher than in control mice.

Random vs. Targeted Gene Insertion

The early vectors used for gene insertion could, and did, place the gene (from one to 200 copies of it) anywhere in the genome. However, if you know some of the DNA sequence flanking a particular gene, it is possible to design vectors that replace that gene. The replacement gene can be one that

- restores function in a mutant animal or
- knocks out the function of a particular locus.

In either case, targeted gene insertion requires

- the desired gene
- ***neo***^{r}, a gene that encodes an enzyme that inactivates the antibiotic neomycin and its relatives, like the drug G418, which is lethal to mammalian cells;
- ***tk***, a gene that encodes **thymidine kinase**, an enzyme that phosphorylates the nucleoside analog **gancyclovir. DNA polymerase** fails to discriminate against the resulting nucleotide and inserts this nonfunctional nucleotide into freshly-replicating DNA. So ganciclovir kills cells that contain the *tk* gene.

Step 1

Treat culture of ES cells with preparation of vector DNA.

Results:

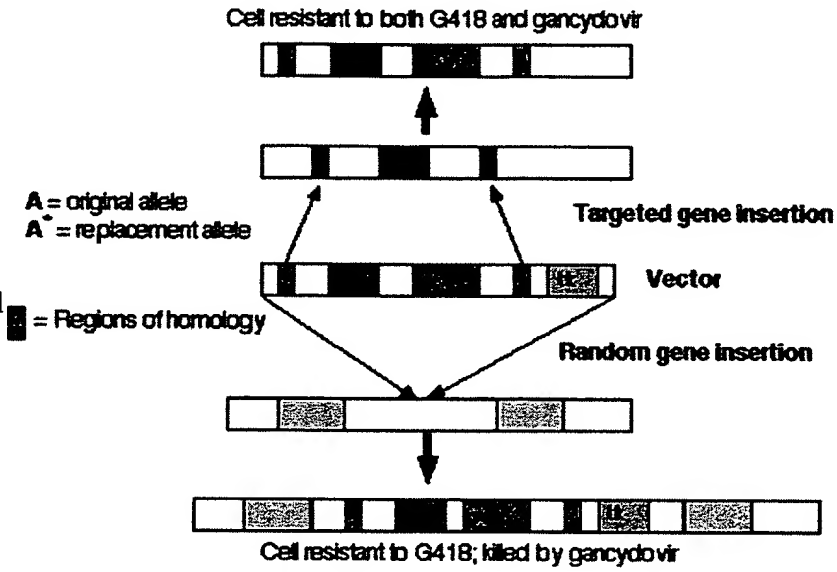

- **Most cells** fail to take up the vector; these cells will be killed if exposed to G418.
- In a **few cells**: the vector is inserted randomly in the genome. In random insertion, the entire vector, including the ***tk*** gene, is inserted into host DNA. These cells are resistant to G418 but killed by gancyclovir.
- In **still fewer cells**: **homologous recombination** occurs. Stretches of DNA sequence in the vector find the homologous sequences in the host genome and the region between these homologous sequences replaces the equivalent region in the host DNA.

Step 2

Culture the mixture of cells in medium containing both G418 and ganciclovir.

- The cells (the majority) that failed to take up the vector are killed by G418.
- The cells in which the vector was inserted randomly are killed by gancyclovir (because they contain the *tk* gene).
- This leaves a population of cells transformed by homologous recombination (enriched several thousand fold).

Step 3

Inject these into the inner cell mass of mouse blastocysts.

Knockout Mice: What do they teach us?

If the replacement gene (**A*** in the diagram) is nonfunctional (a "null" allele), mating of the heterozygous transgenic mice will produce a strain of "**knockout mice**" homozygous for the nonfunctional gene (both copies of the gene at that locus have been knocked out").

Knockout mice are valuable tools for discovering the function(s) of genes for which mutant strains were not previously available. Two generalizations have emerged from examining knockout mice:

- Knockout mice are often surprisingly unaffected by their deficiency. Many genes turn out not to be indispensable. The mouse genome appears to have sufficient redundancy to compensate for a single missing pair of alleles.
- Most genes are **pleiotropic**. They are expressed in different tissues in different ways and at different times in development.

Transgenic Sheep

Until recently, the transgenes introduced into sheep inserted randomly in the genome and often worked poorly. However, in July 2000, success at inserting a transgene into a specific gene locus was reported. The gene was the human gene for **alpha1-antitrypsin**, and two of the animals expressed large quantities of the human protein in their milk.

This is how it was done.

Sheep fibroblasts (connective tissue cells) growing in tissue culture were treated with a vector that contained these segments of DNA:

1. 2 regions homologous to the sheep *COL1A1* gene. This gene encodes Type 1 collagen. (Its absence in humans causes the inherited disease osteogenesis imperfecta.)

   This locus was chosen because fibroblasts secrete large amounts of collagen and thus one would expect the gene to be easily accessible in the chromatin.

2. A neomycin-resistance gene to aid in isolating those cells that successfully incorporated the vector. [Link to technique]
3. The human gene encoding alpha1-antitrypsin.

   Some people inherit two non- or poorly-functioning genes for this protein. Its resulting low level or absence produces the disease **Alpha1-Antitrypsin Deficiency (A1AD** or **Alpha1)**. The main symptoms are damage to the lungs (and sometimes to the liver).

4. Promoter sites from the **beta-lactoglobulin** gene. These promote hormone-driven gene expression in milk-producing cells.
5. Binding sites for ribosomes for efficient translation of the mRNAs.

Successfully-transformed cells were then

- fused with enucleated sheep eggs [Link to description of the method] and
- implanted in the uterus of a ewe (female sheep).
- Several embryos survived until their birth, and two young lambs have now lived over a year.
- When treated with hormones, these two lambs secreted milk containing large amounts of alpha1-antitrypsin (650 μg/ml; 50 times higher than previous results using random insertion of the transgene).

On June 18, 2003, the company doing this work abandoned it because of the great expense of building

a facility for purifying the protein from sheep's milk.

Transgenic Chickens

Chickens

- grow faster than sheep and large numbers can be grown in close quarters;
- synthesize several grams of protein in the "white" of their eggs.

Two methods have succeeded in producing chickens carrying and expressing foreign genes.

- Infecting embryos with a viral vector carrying
  - the human gene for a therapeutic protein
  - promoter sequences that will respond to the signals for making proteins (e.g. lysozyme) in egg white.
- Transforming rooster sperm with a human gene and the appropriate promoters and checking for any transgenic offspring.

Preliminary results from both methods indicate that it may be possible for chickens to produce as much as 0.1 g of human protein in each egg that they lay.

Not only should this cost less than producing therapeutic proteins in culture vessels, but chickens will probably add the correct sugars to glycosylated proteins - something that E. coli cannot do.

Transgenic Pigs

Transgenic pigs have also been produced by fertilizing normal eggs with sperm cells that have incorporated foreign DNA. This procedure, called sperm-mediated gene transfer (SMGT) may someday be able to produce transgenic pigs that can serve as a source of transplanted organs for humans. [More]

Welcome&Next Search

19 August 2003

Kimball's Biology Pages

The server for this site has been changed. The new URL can be either
http://biology-pages.info or
http://users.rcn.com/jkimball.ma.ultranet/BiologyPages

About These Pages	More on Navigating Through Them	About The Author

How You Can Help Support this Site with a Voluntary Contribution

1 May 2004

News

Search: GO

search tips sitemap

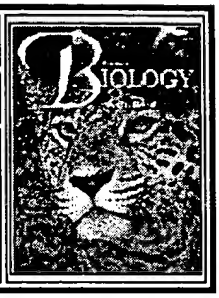

Ways to Search These Pages

- **Search Engine** Enter desired term(s) in box above (advantage: finds all occurrences; disadvantages: may return trivial hits, your choice of term may not match mine). Suggestion: Click on search tips link to help you get the most useful results.
- **Link To Individual Index Pages**

  A-B-C-D-E-F-G-H-I-J-K-L-M-N-O-P-Q-R-S-T-U-V-W-X-Y-Z

- **Frames Version** (places this clickable alphabet across the top of all windows)
- **Consolidated Index (A-Z)** Enables you to search the entire index using the "Find" function of your browser. Some browsers take so long to load this large file that you may wish to open a link from it in a **new window** (thus keeping the index open in the background).
- **Table Of Contents** (list of topic pages grouped by category)

NEWS

The News: A team of Japanese and Korean scientists reports creating the first mammal (a mouse) by parthenogenesis ("virgin birth").

The Background: Link to a discussion of how they did it and the obstacles they had to overcome; includes links to related pages.

News archives

About These Pages

The pages represent an **online biology textbook**.

It has always seemed to me that the many parts that make up the subject of biology are related to each other more like the nodes of a web than as a linear collection of independent topics. So I believe that the power of hypertext will be better suited to learning about biology than is the linear structure of a printed textbook.

Another disadvantage of printed textbooks is the inevitable delay between

the time that new advances in biology are reported and the time that they can become incorporated in a printed book (often several years). Material here can be updated promptly.

So although some of this information has been drawn from the sixth edition of the author's text **Biology** published in 1994 by Wm. C. Brown, every effort has been made to adapt the material to the opportunities provided by an online text.

Your comments, criticisms, and suggestions are always welcome. Send them to:

Dr. John W. Kimball 89 Prospect Road Andover, MA 01810	or send them by e-mail to **jkimball@envoy.mcb.harvard.edu** Because of the children (in mindset if not in years) who created the Klez-type viruses, you will have to type this address (in this gif image) into your message header. I would also appreciate it if you would NOT add this address to the address book in your e-mail program.

Navigating These Pages

Using the search engine

Return to top of page, type your desired term(s) into the box, and click on "GO". (Suggestion: Click on search tips link to help you get the most useful results.)

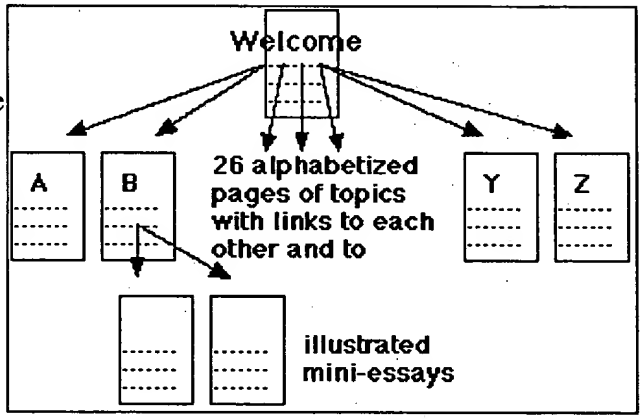

Not using the search engine

1. Click the first letter of your desired term in the alphabet at the **top** of **this page** or **any** of the index/glossary pages

2a. scroll down to your desired item **or**, alternately,

2b. Open the "**Find**" dialog box from your browser's tool bar and enter the word you seek. If you begin with an uppercase letter AND choose "case sensitive" or "match case", you will increase your chance of hitting the topic item itself rather than hitting the same word appearing within other items.

Note that unless you have chosen the consolidated index, the **Find** function of your browser will only work for terms beginning with the letter of the page you are on (because each alphabetized section is on a separate page).

Moving on..

3a.A link at the bottom of **every page** returns you to this welcome page (where you can then link to the first letter of a new item).

3b. Each **index/glossary** page also has a link ("**Next Search**") to the alphabet at the top of that page.

3c. You can pull down the history list ("**Go**" on the Netscape and Internet Explorer menus) and release on the welcome page ("Kimball's Biology Pages") or any other earlier page.

3d. If you are using a frames-capable browser, you can use the link at the top of this page ("FRAMES VERSION") to place a clickable alphabet that will remain at the top of each window.

How You Can Help Support This Site With A Voluntary Contribution

This site continues to be free. However, if you find it useful and would like to help support it, Amazon.com has provided a mechanism with you can make a voluntary contribution (of as little as $1).

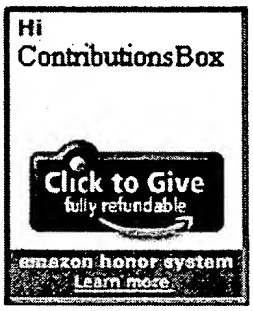

- Clicking on the box at the right takes you briefly to Amazon.com where you can indicate your wishes.
  - If you are already an Amazon customer, another click will do it.
  - Otherwise, you will have to enter credit card data (their site is secure).
- If you change your mind, you can cancel.
- Then a click returns you to this welcome page.
- Later you (but not I) will be notified by e-mail of your contribution (and given another opportunity to cancel it).

About the Author

John W. Kimball has retired from a lifetime of teaching biology. A graduate of Harvard College, he began his teaching career at the secondary level, teaching chemistry and biology to students at Phillips Academy, an independent school in Andover, Massachusetts. In 1969, he returned to Harvard to study immunology with the late Professor A. M. Pappenheimer. After receiving his Ph.D. there, he went on to teach introductory biology (in both majors and nonmajors courses) and immunology at Tufts University where he became a tenured professor. In 1982 he returned again to Harvard where he taught immunology and also participated in teaching the introductory course for majors.

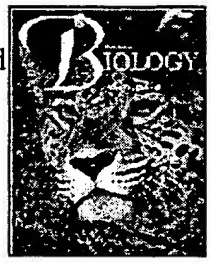

The first edition of Kimball's general biology text was published in 1965. Since that time it has gone through five revisions, the most recent being the sixth edition, which appeared in 1994 (that's its cover on the right). He has also published books on cell biology and a widely-used text on immunology. His biology books have also been published in Spanish, German, Japanese, Arabic, Polish, Korean and Bahasian (Indonesian) versions.

COPYRIGHT

Return to top of page

IMMUNOLOGY

Janis Kuby

Professor of Biology,
San Francisco State University

Faculty,
Joint Medical Program,
University of California at Berkeley

W. H. Freeman and Company
New York

Cover illustration of AIDS viruses budding from an infected T cell was provided by L. Montagnier/CNRI, Science Photo Library.

Library of Congress Cataloging-in-Publication Data

Kuby, Janis.
Immunology / Janis Kuby.
p. cm.
Includes bibliographical references and index.
ISBN 0-7167-2257-7
1. Immunology. I. Title.
[DNLM: 1. Immune System. 2. Immunity. QW 504 K95i]
QR181.K83 1992
616.07'9—dc20
DNLM/DLC
for Library of Congress
91-44429
CIP

Printed in the United States of America

3 4 5 6 7 8 9 RRD 9 9 8 7 6 5 4 3

inbred strain whose progeny are homozygous at more than 98% of all loci. There are currently over 150 different inbred strains of mice, which are designated by a series of letters and/or numbers (Table 2-1). Most of these strains are purchased by immunologists from such suppliers as Jackson Laboratory in Bar Harbor, Maine. Inbred strains have also been produced in rats, guinea pigs, hamsters, rabbits, and domestic fowl.

Since inbred animals are genetically identical (*syngeneic*), they make it possible to study the immune response in the absence of variables that can be introduced by genetic differences among animals. Once inbred strains became available, immunologists could isolate lymphocyte subpopulations from one animal and inject them into another animal of the same strain. It was with this type of experimental system that immunologists were first able to show that lymphocytes from an antigen-primed animal could transfer immunity to an unprimed syngeneic recipient.

Adoptive-Transfer Systems

In some cases it is important to eliminate the immune responsiveness of the syngeneic host so that the response of only the transferred lymphocytes can be studied in isolation. In adoptive-transfer experiments this is achieved by inactivating the immune cells of the syngeneic recipient. Inactivation can be achieved by exposure to x-rays, to which lymphocytes have been shown to be extremely sensitive. Subjecting a mouse that will serve as host to sublethal doses of x-rays (650–750 rads) can kill 99.99% of its lymphocytes, after which the lymphocytes from the spleen of a syngeneic donor can be studied without interference. In some adoptive-transfer experiments higher x-ray levels are used (900–1000 rads) to eliminate the entire hematopoietic system. This is sometimes necessary if the recipient's hematopoietic cells might influence the adoptive-transfer experiment. The x-irradiated mice will die unless reconstituted with bone marrow from a syngeneic donor.

The adoptive-transfer system has enabled immunologists to study the development of injected lymphoid stem cells in various organs of the recipient. Adoptive-transfer experiments have also facilitated the study of various populations of lymphocytes and of the cellular interactions required to generate an immune response. For example, it was through such experiments that immunologists were first able to show that a T helper cell is necessary for B-cell activation in the humoral response.

Cell-Culture Systems

The complexity of the cellular interactions that generate an immune response has led immunologists to rely heavily on various types of in vitro cell-culture system A variety of cells can be cultured including prima lymphoid cells, cloned lymphoid cell lines, and hybr cells.

Primary Lymphoid Cell Cultures

Primary lymphoid cell cultures can be obtained by is lating lymphocytes directly from blood or lymph or fro various lymphoid organs by tissue dispersion. The lyn phocytes can then be grown in a chemically define basal medium containing saline, sugars, amino acids, v tamins, trace elements, and various other nutrients, which various serum supplements are added. Becau in vitro culture techniques require from 10- to 100-fo fewer lymphocytes than typical in vivo techniques, the have enabled immunologists to assess the function properties of minor subpopulations of lymphocytes. was by means of cell-culture techniques, for exampl that immunologists were first able to define the fun tional differences between $CD4^+$ T helper cells ar $CD8^+$ T cytotoxic cells.

Cell-culture techniques have also been used to ide tify various cytokines involved in the activation, growt and differentiation of various cells involved in the in mune response. Early experiments showed that med conditioned by the growth of various lymphocytes antigen-presenting cells would support the growth other lymphoid cells. Many of the individual cytokin that characterized various conditioned media have sul sequently been identified and purified, and in many cas the genes encoding them have been cloned. The solub growth factors elaborated by monocytes and macr phages are called *monokines*, and the ones elaborate by lymphocytes are called *lymphokines*. These cyt kines, which play a central role in the activation an regulation of the immune response, are discussed mo fully in Chapter 11.

Cloned Lymphoid Cell Lines

Primary lymphoid cell cultures comprise a heterog neous group of cells which can be propagated only fo a limited time. This heterogeneity complicates inte pretation of experiments aimed at understanding th molecular and cellular mechanisms by which lymph cytes generate an immune response. To avoid thes problems immunologists use cloned lymphoid cell line and hybrid cells.

Normal mammalian cells generally have a finite life span in culture; that is, after a number of populatio doublings characteristic of the species and cell type, th cells stop dividing. Tumor cells or normal cells tran formed with chemical carcinogens or viruses, howeve

1: Clin Diagn Lab Immunol. 1997 Sep; 4(5): 630-2.

Antibodies to the hepatitis B e antigen (HBeAg) can be induced in HBeAg-transgenic mice by adoptive transfer of a specific T-helper 2 cell clone.

Hultgren C, Milich DR, Sallberg M.

Division of Clinical Virology, Huddinge University Hospital, Sweden.

Production of antibody to hepatitis B e antigen (HBeAg); i.e., anti-HBe antibody,) in HBeAg-transgenic mice is believed to be mediated by T-helper (Th2) cells. Injection of an HBeAg-specific Th2 clone into HBeAg-transgeni H-2k mice induced anti-HBe antibody production, confirming the function o Th2 cells in this model system.

PMID: 9302220 [PubMed - indexed for MEDLINE]

1: Proc Natl Acad Sci U S A. 2000 Jul 18; 97(15): 8473-8. Related Articles, Lin

FREE full text article at www.pnas.org

FREE full text article in PubMed Central

Comparative T cell receptor repertoire selection by antigen afte adoptive transfer: a glimpse at an antigen-specific preimmune repertoire.

Attuil V, Bucher P, Rossi M, Mutin M, Maryanski JL.

Institut National de la Sante et de la Recherche Medicale, Unit 503, Ecole Normale Superieure de Lyon, 69007 Lyon, France.

The low frequency of precursor cells specific for any particular antigen (Ag) makes it difficult to characterize preimmune T cell receptor (TCR) repertoire and to understand repertoire selection during an immune response. We have undertaken a combined adoptive transfer single-cell PCR approach to probe the Ag-specific preimmune repertoires of individual mice. Our strategy was t inject paired irradiated recipient mice with normal spleen cells prepared from individual donors and to compare the TCR repertoires subsequently selected during a CD8 response to a defined model Ag. We found that although some TCRs were shared, the TCR repertoires selected by mice receiving splenocytes from the same donor were not identical in terms of the TCRs selected and their relative frequencies. Our results together with computer simulations imply that individual mice express distinct Ag-specific preimmune TCR repertoires composed of expanded clones and that selection by Ag is a random process.

PMID: 10900008 [PubMed - indexed for MEDLINE]

1: Eur J Immunol. 2000 May; 30(5): 1297-307.

Tumor size at the time of adoptive transfer determines whether tumor rejection occurs.

Cordaro TA, de Visser KE, Tirion FH, Graus YM, Haanen JB, Kioussis D, Kruisbeek AM.

Division of Immunology, The Netherlands Cancer Institute, Amsterdam, The Netherlands.

Here we investigate the minimal requirements for induction of an anti-tumor response in CD8 T cells in vivo. We compare the efficacy of adoptive transfe of CD8 T cells with a transgenic TCR specific for the main cytotoxic T lymphocyte epitope of the influenza virus nucleoprotein (NP) on the growth NP-expressing EL4 tumors under different conditions. In a setting in which tumor rejection is solely dependent on tumor-specific CD8 T cells, small immunogenic tumors fail to induce a rejection response, despite the fact that they are not ignored: tumor-specific CD8 T cells are activated, differentiate into effector cells and infiltrate the tumor bed. Nevertheless, tumor rejection does not occur. In sharp contrast, the same immunogenic tumor, when growing as a large tumor mass, is rejected by transferred tumor-specific CD8 T cells. The main features which distinguish the rejection response to a large tumor mass from the response to a small tumor is that, in the latter case, activated CD8 T cells appear much later, and in much smaller numbers. Efficacy of adoptive transfer is thus dictated by the size of the tumor mass at the time of transfer. These findings predict that treatment of minimal residua disease with adoptive transfer will fail, unless vaccination is also provided at the time of transfer.

PMID: 10820375 [PubMed - indexed for MEDLINE]

1: Hum Gene Ther. 1993 Oct; 4(5): 659-80. Related Articles, Lin

A study of the safety and survival of the adoptive transfer of genetically marked syngeneic lymphocytes in HIV-infected identical twins.

Walker R, Blaese RM, Carter CS, Chang L, Klein H, Lane HC, Leitman SF, Mullen CA, Larson M.

This phase I/II pilot project will evaluate the survival, tolerance, safety, and efficacy of infusions of activated, gene marked, syngeneic T lymphocytes obtained from HIV seronegative identical twins on the functional immune status of HIV infected twin recipients. T cells from each seronegative twin will be obtained by periodic apheresis, separated into CD4 and CD8 enriched populations by monoclonal antibody affinity binding techniques, induced to polyclonal proliferation with anti-CD3 and rIL-2 stimulation, transduced with distinctive neoR retroviral vectors, and expanded 10-1,000 fold in numbers during approximately 2 weeks of culture. These marked T cell fractions will then be infused into the seropositive twins and the survival of the uniquely marked T cell populations will be monitored by vector-specific PCR, while the recipients' functional immune status is monitored by standard in vitro and in vivo testing protocols. A total of 3 cycles of treatment will be given at intervals of 6 weeks between infusions.

Publication Types:
- Clinical Trial
- Clinical Trial, Phase I
- Clinical Trial, Phase II

PMID: 8280803 [PubMed - indexed for MEDLINE]

1: Scand J Immunol. 1996 Mar; 43(3): 283-8. Related Articles, Lin

Cancer prevention by adoptive transfer of antigen 60-activated immunocompetent cells.

Maes H, Cocito C.

Laboratory of Microbiology and Molecular Genetics, Medical School, University of Louvain, Brussels, Belgium.

The authors have already shown that A60, the thermostable macromolecular antigen complex of Mycobacterium bovis BCG, induced resistance to tumou challenge in several murine systems. In the present work, the authors provide evidence that activated macrophages played a major role, and cytolytic T lymphocytes a minor one, in both in vivo and in vitro A60-promoted cancer cell cytolysis. To identify the types of immunocompetent cells involved in th protective effect, macrophages and T lymphocytes from A60-primed mice donors were adoptively transferred to irradiated recipients prior to EMT 6 tumour challenge. In some groups, A60-primed donors were survivors of previous tumour challenges. Transfer of T lymphocytes from the spleen or lymph-nodes of A60-immunized mice induced 80-90% protection against tumour challenge. Conversely, transferred macrophages, although cytolytically active, did not induce resistance to tumour implantation. Furthermore, adoptive transfer with T lymphocytes from A60-immunized an EMT 6 challenge-surviving donors induced 100% protection. It is concluded that stimulation of T lymphocytes by A60 is the key step which leads to activation of the immunocompetent cells involved in tumour rejection.

PMID: 8602462 [PubMed - indexed for MEDLINE]

1: J Autoimmun. 1994 Dec; 7(6): 819-31. Related Articles, Lin

ELSEVIER FULL-TEXT ARTICLE

Adoptive transfer of autoimmune diabetes mellitus to athymic rats: synergy of CD4+ and CD8+ T cells and prevention by RT6 T cells.

Whalen BJ, Greiner DL, Mordes JP, Rossini AA.

Department of Medicine, University of Massachusetts Medical School, Worcester 01655.

We describe the induction and prevention of autoimmune insulin dependent diabetes mellitus (IDDM), and its pathological substrate, insulitis, in congenitally athymic nude rats following injections of major histocompatibility complex (MHC) compatible lymph node T cells. The cells capable of adoptive transfer of autoimmunity were obtained from diabetes resistant (DR) BB rats that had been rendered hyperglycemic by in vivo depletion of the RT6+ regulatory T cell subset. We first established that our adoptive transfer assay system is cell dose- and time dependent and therefore amenable to quantitative analysis. It was also observed that both CD4+ and CD8+ T cells are required for efficient transfer of autoimmunity. The data indicate that, as in the NOD mouse, a synergistic interaction between CD4+ and CD8+ T cells is important for beta cell destruction. Finally, we demonstrated that the admixture of equal numbers of lymph node T cells, 60% of which were RT6+, from intact, non-diabetic DR rats prevented the adoptive transfer of IDDM mediated by diabetogenic T cells from RT6-depleted DR-BB rats. We conclude that an equilibrium between autoreactive and regulatory cells determines the expression of autoimmunity in the DR-BB rat and in the adoptive transfer of diabetes in quantitative analytical systems.

PMID: 7888038 [PubMed - indexed for MEDLINE]

Display Abstract Show: 20 Sort Send to Text

1: Immunology. 1992 Apr; 75(4): 693-9. Related Articles, Lin

Adoptive transfer of the generalized lymphoproliferative disease (gld) syndrome in nude beige mice.

Froidevaux S, Rosenblatt N, Loor F.

Laboratoire d'immunologie, Universite Louis Pasteur, Strasbourg, France.

C57BL/6 nude beige mice (B6 nubg) were used as recipients for the transfer of haematopoietic cells from either B6 wild as control mice, or systemic lupu erythematous B6 mice homozygous for the recessive generalized lymphadenopathy disease (gld) locus. Both gld and wild cell grafts prolonge survival of the short-living B6 nubg recipients and restored some T-cell functions, as monitored by the presence of T-dependent Ig isotypes in the serum and responsiveness of spleen cells to a T-cell mitogen. Moreover, the [gld----nubg] chimeras but not the [wild----nubg] chimeras showed several similarities with gld control mice, particularly, a spleen and lymph node hyperplasia, elevated anti-single-stranded DNA antibody titres and a hyperglobulinaemia. This hyperglobulinaemia was however qualitatively different from the gld-type hyperglobulinaemia with an important contributic of the IgG1 isotype; the lymph node hyperplasia was also less marked than i B6 gld mice.

PMID: 1592442 [PubMed - indexed for MEDLINE]

1: Adv Immunol. 1991; 50: 303-25.

Adoptive transfer of human lymphoid cells to severely immunodeficient mice: models for normal human immune function, autoimmunity, lymphomagenesis, and AIDS.

Mosier DE.

Division of Immunology, Medical Biology Institute, La Jolla, California 92037.

Though the development of human-to-mouse xenotransplant models is in its infancy, astonishing progress has been made in a short period of time. Two experimental applications have been developed: short-term transfer of humar lymphocytes to generate models for autoimmunity and infectious diseases, and long-term engraftment of tissues with self-renewal potential. Human PBL-SCID mice have been used by multiple laboratories to study normal anc autoimmune antibody responses, and have been shown to be readily infectab with HIV-1. SCID mice grafted with fetal tissue have been developed for studies of HIV-1 infection and its therapy as well as for studies of human hematopoietic cell differentiation. Human tumors appear to grow better in SCID mice than in nude mice, and hu-PBL-SCID mice can develop EBV-related B cell lymphoproliferative disease that resembles the immunoblastic lymphomas appearing in immunosuppressed transplant recipients. There is some evidence of mouse NK cells responding to the human xenograft, and of human T and B cells responding to mouse xenoantigens in these models, but these responses are not generally strong enough to have a major impact on human immune function. The use of these surrogate human models is expected to have a major impact on the understanding and treatment of huma disease.

Publication Types:
- Review
- Review, Tutorial

PMID: 1950798 [PubMed - indexed for MEDLINE]

1: Proc Natl Acad Sci U S A. 1990 Oct; 87(19): 7618-22. Related Articles, Lin

FREE full text article at www.pnas.org

FREE full text article in PubMed Central

Adoptive transfer of autoimmune diabetes and thyroiditis to athymic rats.

McKeever U, Mordes JP, Greiner DL, Appel MC, Rozing J, Handler ES Rossini AA.

Department of Medicine, University of Massachusetts Medical School, Worcester 01655.

We describe the induction of autoimmune diabetes, insulitis, and thyroiditis i athymic rats following injections of major histocompatibility complex compatible spleen cells. Lymphocytes with these capabilities were found in normal rats of the YOS, WAG, PVG, and diabetes-resistant BB strains, and i diabetes-prone BB rats. Adoptive transfer was facilitated by prior in vivo depletion of RT6.1+ regulatory T cells and in vitro mitogen activation of donor spleen cells. By RT6 depleting diabetes-resistant donors and using nuc recipients, transfer of diabetes and thyroiditis was accomplished by using fresh, unstimulated spleen cells. The data suggest that organ-specific autoreactive cells may be present to various degrees but suppressed to a variable extent in many rat strains. The equilibrium between autoreactive anc regulatory cells appears to determine the expression of autoimmunity.

PMID: 2217193 [PubMed - indexed for MEDLINE]

1: Cancer Res. 1990 Dec 1; 50(23): 7450-6. Related Articles, Lin

Adoptive transfer of tumor cytotoxic macrophages generated in vitro from circulating blood monocytes: a new approach to cancer immunotherapy.

Andreesen R, Scheibenbogen C, Brugger W, Krause S, Meerpohl HG, Leser HG, Engler H, Lohr GW.

Medizinische Klink I, Albert-Ludwigs-Universitat Freiburg im Breisgau, We Germany.

Cells of the macrophage lineage are considered to be of special importance ir the defense of the host against tumor development and spread. Immunotherapeutic strategies to stimulate macrophage (MAC) tumor cytotoxicity make use of activating compounds such as gamma-interferon which are given systemically. However, there are several lines of evidence that in malignant disease the generation of cytotoxic effector MACs is impaired. Both defective cell maturation and loss of responsiveness to activation are described. Here, a first clinical phase I trial of adoptive immunotherapy in cancer patients using autologous MACs generated in vitro from blood monocytes (MOs) is reported. Mononuclear cells were isolated b cytapheresis and density centrifugation and cultured in hydrophobic Teflon bags for 7 days with 2% autologous serum and recombinant human gamma-interferon being present for the last 18 h. Cytotoxic MO-derived MACs were then purified by countercurrent elutriation and reinfused into the patient. A total of 72 therapies have been performed with patients being treated i.v. (n = 8) and i.p. (n = 7). In vitro generated MACs proved to be mature as judged b the expression of maturation-associated surface molecules (MAX antigens, CD16, CD51, CD71), were cytotoxic to U937 tumor cells, and were efficient secretory cells. Cell dose escalation was performed in the first patients beginning with 10(8) MACs to finally infuse the total number of cells recovered from one single cycle of isolation and culture. MAC yield varied from 1 to 17 x 10(8) representing 13-79% of MOs initially seeded. Adoptive MAc transfer was well tolerated. Side effects observed were low-grade fever (less than 38.5 degrees C), induction of the coagulation cascade, and abdominal discomfort after i.p. application. The procoagulant activity of MA autografts was cell dose dependent and demonstrated by detection of circulating fibrin monomers and thrombin-antithrombin complexes. Biological responses observed included elevated serum neopterin levels and

the appearance of interleukin-6 in sera and ascitic fluids. Indication of a possible therapeutic effect was only observed in i.p.-treated patients and consisted of disappearance of malignant ascites in 2 of 7 patients.

Publication Types:
- Clinical Trial

PMID: 1701343 [PubMed - indexed for MEDLINE]

1: J Immunol. 1983 Mar; 130(3): 1478-82.

Adoptive transfer of resistance to growth of an idiotype-secretin hybridoma by T cells from idiotypically suppressed mice.

Kresina TF, Baine Y, Nisonoff A.

A/J or CAF1 mice that are suppressed with respect to an idiotype, CRIA, associated with anti-Ar antibodies, and hyperimmunized develop high concentrations of idiotype-suppressor T cells. In this paper we show that sucl CAF1 mice are resistant to the growth of a CRIA-positive hybridoma that is lethal in normal or in immunized non-suppressed mice. No resistance was observed to the growth of a hybridoma secreting anti-Ar antibodies that lack CRIA. The state of resistance could be adoptively transferred to naive syngeneic recipients with spleen cells or T-enriched spleen cells from suppressed hyper-immunized mice; B-enriched cells were ineffective.

PMID: 6600485 [PubMed - indexed for MEDLINE]

1: J Gen Virol. 1981 Sep; 56(Pt 1): 25-31.

Recovery from experimental rabies by adoptive transfer of immune cells.

Prabhakar BS, Fischman HR, Nathanson N.

The transient, sublethal infection produced by intracerebral inoculation of the Flury high egg passage (HEP) strain of rabies virus into adult mice was converted into a lethal one (approx. 80 to 100% mortality) by administering 150 mg/kg cyclophosphamide (CY) 2 days after infection. Immunosuppressed, infected animals showed no immunological response to rabies and died 15 to 20 days after infection. However, mortality was reduce to 12% when suppressed mice were adoptively immunized, 4 days after infection, with an intravenous injection of 60 X 10(6) spleen cells from rabie immune syngeneic donors. The lymphocytes obtained early after donor immunization (4 to 11 days) reduced mortality, whereas those obtained late (16 to 32 days after immunization) were not effective. The ability of donor cells to protect animals corresponded very closely with donor cytotoxic T lymphocyte (CTL) activity. Within 4 days after immune cell transfer, serum neutralizing antibody and CTL levels in recipients were comparable to those found in virus-infected control animals. Immune donor cells were fractionate into thymus-derived (T-enriched) and bone marrow-derived (B-enriched) subsets. The T and B subsets reduced mortality to 32% and 34% respectively CTL and serum neutralizing antibody responses could be detected in these animals, although they appeared later than in mice treated with unfractionate immune spleen cells. The present study demonstrates that both B and T lymphocytes are required for optimum clearance of rabies from the central nervous system (CNS) and suggests a functional role for rabies-specific CTL in vivo.

PMID: 6975354 [PubMed - indexed for MEDLINE]

Contact Us Site Map

You think it up and we knock it out.

inGenious Targeting Laboratory, Inc.

inGenious Targeting Laboratory specializes in providing mouse gene knockout services. iTL's goal is to make genetically altered mice available to researchers in various fields at low cost and with fast turn around time.

- ***Gene Targeting***
- ***DNA Sequencing***

Services
About iTL
Clients
FAQ's

Contact Us ▸
Find out more about our services.

Services | About iTL | Clients | FAQ's | Contact Us | Site Map

inGenious Targeting Laboratory, Inc.
LIHTI Building, Suite 106
25 East Loop Road
Stony Brook, NY 11790-3350
Phone: 631.444.6640
Fax: 631.444.6645
E-mail: info@genetargeting.com

Web Site Development By Innovative Internet Marketing Solutions

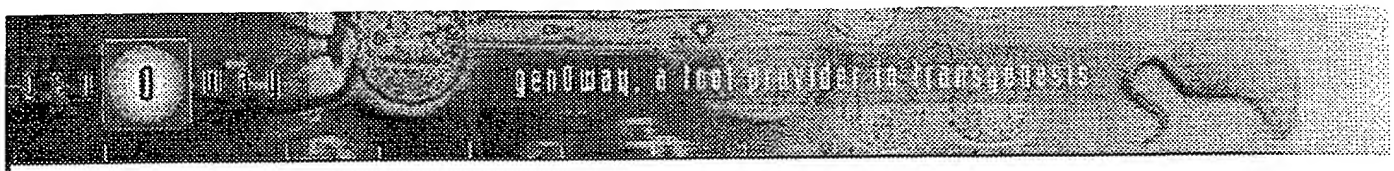

Home
Service offer
Scientific background
R&D pipeline
Rat models
Partnership
Corporate overview
We are seeking for...
News room
Contact us

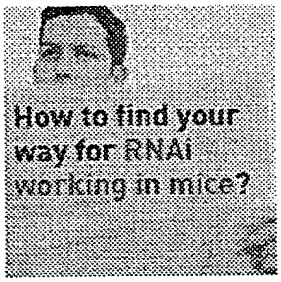

Technology releases "Safe RNAiTransgenesis ™"

Corporate mission

Tool provider in transgenesis:
knock out mouse, knock-in mouse and transgenic mouse or rat

Provide every scientist with solutions that optimise value of scientific results obtained from transgenic models. Increase predictability & reliability and reduce development time and scientific uncertainly of transgenesis.

Service offer

Tailor-made knock out mouse, knock-in mouse and transgenic mouse or rat.

Product range

Proprietary models currently in development

News

December 2003, Bayer HealthCare AG and genOway announce an agreement in the field of genetically modified mouse models

Reliability is our commitment

A provider in Transgenesis: knock out mouse, knock-in mouse and transgenic mouse

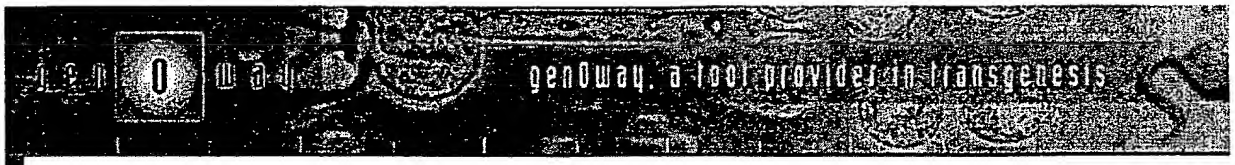

Home
Service offer
Gene overexpression
Gene deletion
Achievements
Offer description
Scientific background
R&D pipeline
Rat models
Partnership
Corporate overview
We are seeking for...
News room
Contact us

Service offer

genOway provides its customers with a high quality service, exemplified by the following

- **Consultancy**
- **Fully customized service**
- **Flexibility**
- **Clear-cut guaranties**
- **Exclusive property of the model to the customer**
- **Animal facility subcontracted to a professional breeder: *Charles River Laborato***
- **Complementary services**

Focusing its effort on the mouse and rat models, genOway has developed a compl technological solutions to overexpress (transgenic mouse, knock-in mouse,...) ar (constitutive knock out / knockout, conditional knock out / knockout,...) genes.

- The **overexpression** can be achieved by **random integration** of the gene in the mouse and rat (transgenic mouse and rat), or by targeted **insertion in a selected** mouse or rat genome (knock-in).
- The **deletion** of the gene occurs in all tissues in **constitutive knock out** (knockou **conditional knock out** (knockout) models, the inactivation happens only in selected a certain time during the animal development.

Inactivation (knock out / knockout) of genes and targeted overexpression (knock- important strategies for animal models. These strategies are only available in the mouse genOway is currently developing a **rat knock out / knock-in program** .

A provider in Transgenesis: knock out mouse, knock-in mouse .

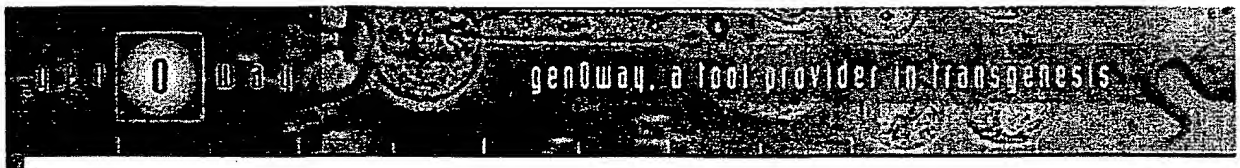

Home
Service offer
Gene overexpression
Gene deletion
Constitutive Knock out
Conditional Knock out
Achievements
Offer description
Scientific background
R&D pipeline
Rat models
Partnership
Corporate overview
We are seeking for...
News room
Contact us

Service offer

Ge
Constitutive knock

Gene deletion is based on the inactivation at the genetic level of a gene of interest. This can be achieved through random mutation (gene trap approach, chemical mutage targeted insertion (homologous recombination). genOway has developed an offer base of a homologous recombination vector and embryonic stem cells. Homologous re provides the customer with the best adapted model and the lowest risk. All con laboratories including those that have heavily invested in random mutagenesis r solutions.

The constitutive "knock out" (knockout) approach has the following characteristics.

Advantages	Drawbacks
Total inactivation of the gene in any cell	Phenotypes can be complex since all or affected

The constitutive "knock out" (knockout) model provides a broad overview of gene functio

The offer genOway has developed can include the following steps, but the service is flex limited to part of this offer and/or adapted to customer requirements) :

Step 1:	Subcloning and characterization of the locus of interest
Step 2 :	Knock out / knockout vector construction (targeting vector)
Step 3 :	Homologous recombination in Embryonic Stem cells (ES cell)
Step 4 :	Blastocyst injection and chimera generation
Step 5 :	Breeding of F1 and F2 generation

The development of the first cloned rat reported by genOway in Science (Qi et al. 200 way for the development of knock out rat models and allows new opportunities for res focused on **rat models**. This technology is not yet available as a service. On **partnerships** may be established.

For more information, please e-mail us at **info@genoway.com**
or visit our **information request page**

A provider in Transgenesis: knock out mouse, knock-in mouse

GENOMATIX

Modular Vectors for Complex Genomics™

Need a knockout vector? We specialize in constitutive and inducible knockout transgenes

Price Estimation Form

Home
Transgene Services
Ancillary Services
Vector System
Vector Frameworks
Key Benefits
Info Request
Privacy Policy

SEARCH

Genomatix is a global service provider of modular vectors for complex genomics applications. We use our patent-pending UltraVector™ System, coupled with our advanced Transgene Services, to provide our R&D customers a faster and more affordable way to acquire transgenes that will meet their application requirements.

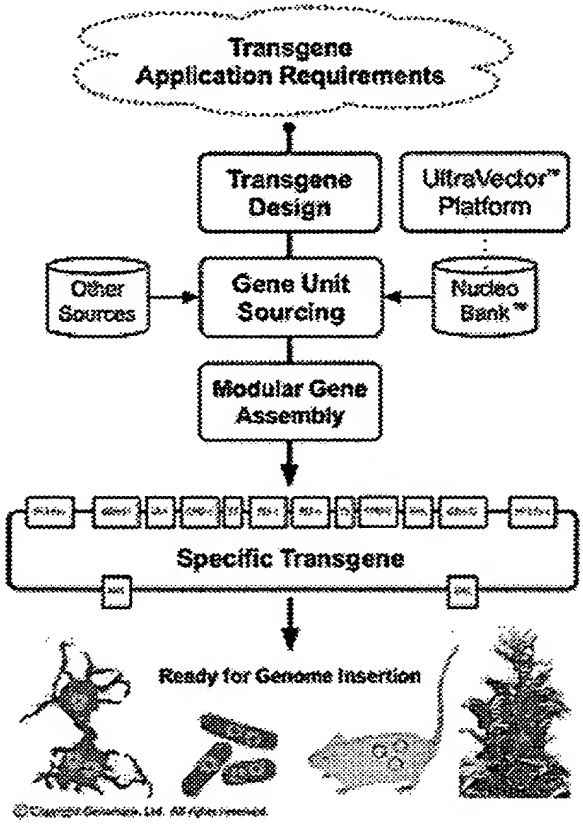

"The rapidly growing complexity o functional genomics demands a shift to modular vectors - in much the same way increasing complexity of computer applications forced a shift from monolithic software programming to modular, object-oriented strategies."

Thomas Reed, Ph.D.
Chief Science Officer
Genomatix, Ltd.

Transgene Applications
Knockout targeting
Codon-optimized expression
Reporter constructs
Tissue-specific gene expression
Adenoviral shuttle vectors
Probe templates
Combinations of above
Other specialized applications

Key Benefits
Improved accuracy for lower cost
Faster production of transgenes
Multiple gene units per transgene
Rapid reuse with new gene units
Higher success rates
Stock vector frameworks
NucleoBank™ storage/retrieval

Detailed information on Genomatix technologies and services is available on the following pages:

UltraVector™ System	Transgene Services	Ancillary Services
UltraVector™ Technology UltraVector™ Frameworks Licensing Approach	Design & Assembly Pricing Information	NucleoBank™ Storage/Retrieval Genotyping BAC Isolation

Information Request Form:
For more information please use our Information Request Form, or call us within the United States at **888-236-3029**. International callers please use 513-

631-4362.

Information Email Addresses:
info@genomatix.com (general info)
science@genomatix.com (scientific info)

Top of Page

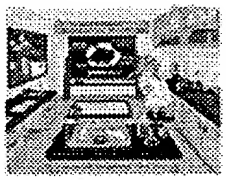

Click here to download a PDF version of our "Project Rudolph" holiday card

[redacted]

GENOMATIX

Modular Vectors for Complex Genomics™

Price Estimation Form

Home
Transgene Services
- Design & Assembly
- Pricing Information
- Price Estimation Form

Ancillary Services
Vector System
Vector Frameworks
Key Benefits
Info Request
Privacy Policy

SEARCH

HOME > TRANSGENE SERVICES > Design & Assembly

Genomatix scientists and technicians are highly proficient at using our modular UltraVector System to rapidly design and assemble complex transgenes for life science researchers and bio-production companies across industry, academia and government. The extensive experience of our services team, combined with the unique advantages of our modular UltraVector System, allows Genomatix to offer a far more productive alternative to slower, more traditional methods of designing and building complex transgenes.

- **Knockout Targeting Vectors**
  - Constitutive knockouts
  - Inducible knockouts
  - Tissue-specific inducible knockouts
- **Multi-Function Combinations**
  - Knockouts with reporter constructs
  - Exon replacement knock-ins
  - Locus-specific multi-genic integration
- **Tissue-Specific Gene Expression**
- **Reporter Constructs**
- **Adenoviral Shuttle Vectors**
- **Codon-Optimized Expression**

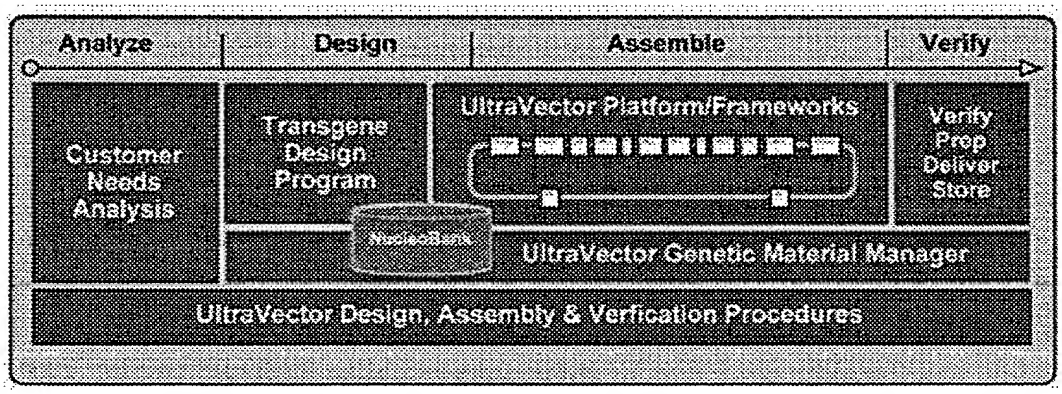

The Genomatix transgene design and assembly process consists of four distinct phases:

1 - Analyze	Genomatix scientists analyze the performance and application criteria to be encoded within the customer's desired transgene.
2 - Design	A Genomatix scientist takes the resulting analysis and designs an UltraVector transgene that will meet those criteria.
3 - Assemble	Genomatix technicians assemble the actual transgene using the selected UltraVector framework, modules and customer-specific genetic units.
4 - Verify & Prep	Genomatix technicians verify the encoded sequence integrity and prepare the transgene for delivery and storage.

Please see our 2004 Price Schedule and Price Estimation Form. Please contact us at **888-236-3029** or info@genomatix.com if you need more information or assistance.

GENOMATIX

Modular Vectors for Complex Genomics™

Price Estimation Form

Need a knockout vector? We specialize in constitutive and inducible knockout transgenes

Home
Transgene Services
Ancillary Services
Vector System
Vector Frameworks
Key Benefits
Info Request
Privacy Policy

SEARCH

Genomatix is a global service provider of modular vectors for complex genomics applications. We use our patent-pending UltraVector™ System, coupled with our advanced Transgene Services, to provide our R&D customers a faster and more affordable way to acquire transgenes that will meet their application requirements.

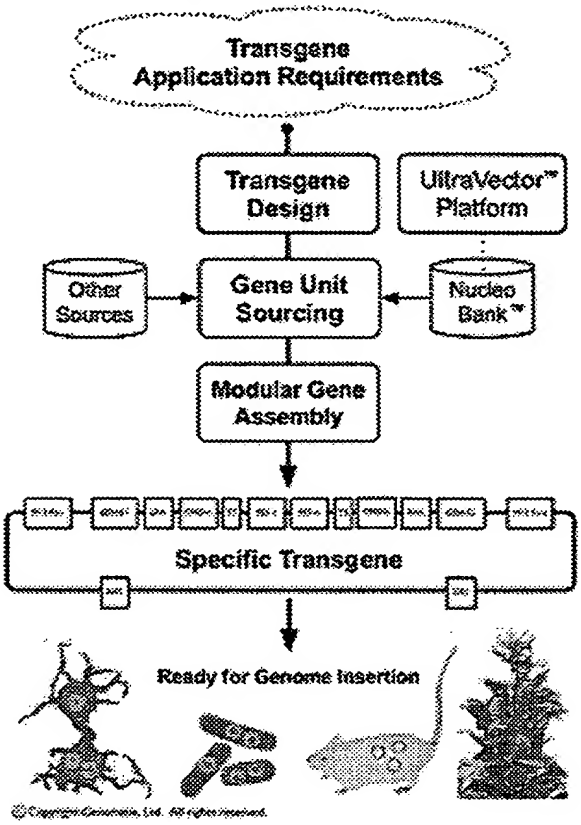

"The rapidly growing complexity o functional genomics demands a shift to modular vectors - in much the same way increasing complexity of computer applications forced a shift from monolithic software programming to modular, object-oriented strategies."

Thomas Reed, Ph.D.
Chief Science Officer
Genomatix, Ltd.

Transgene Applications
Knockout targeting
Codon-optimized expression
Reporter constructs
Tissue-specific gene expression
Adenoviral shuttle vectors
Probe templates
Combinations of above
Other specialized applications

Key Benefits
Improved accuracy for lower cost
Faster production of transgenes
Multiple gene units per transgene
Rapid reuse with new gene units
Higher success rates
Stock vector frameworks
NucleoBank™ storage/retrieval

Detailed information on Genomatix technologies and services is available on the following pages:

UltraVector™ System	Transgene Services	Ancillary Services
UltraVector™ Technology UltraVector™ Frameworks Licensing Approach	Design & Assembly Pricing Information	NucleoBank™ Storage/Retrieval Genotyping BAC Isolation

Information Request Form:
For more information please use our Information Request Form, or call us within the United States at **888-236-3029**. International callers please use 513-

631-4362.

Information Email Addresses:
info@genomatix.com (general info)
science@genomatix.com (scientific info)

Top of Page

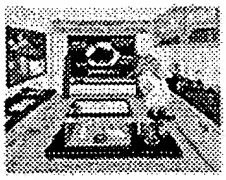

Click here to download a PDF version of our "Project Rudolph" holiday card

[redacted]

LECTURE

Pemphigus as a paradigm of autoimmunity and cell adhesion

Masayuki Amagai

Department of Dermatology, School of Medicine, Keio University, Tokyo, Japan

(Received for publication on April 15, 2002)

Abstract. Pemphigus is a group of autoimmune blistering diseases of the skin and mucous membranes that are characterized histologically by intraepidermal blisters due to the loss of cell-cell adhesion of keratinocytes and immunopathologically by the finding of pathogenic IgG autoantibodies directed against the cell surface of keratinocytes. Identification of the target antigens has redefined pemphigus as an autoimmune disease against desmosomal cadherin or desmoglein. The IgG autoantibody-mediated functional inhibition of desmoglein which plays an important role in the cell-cell adhesion of keratinocytes results in blister formation. Patients with pemphigus vulgaris and pemphigus foliaceus have IgG autoantibodies against desmoglein3 and desmoglein1, respectively. Even complex clinical variations of pemphigus vulgaris and foliaceus are now logically explained by the desmoglein compensation theory. As an extension of this theory, the exfoliative toxin produced by *Staphylococcus aureus*, which causes staphylococcal scalded skin syndrome and bullous impetigo, was found to specifically cleave desmoglein1 and induce the identical histology to pemphigus foliaceus. Another recent innovation has been the development of an active disease mouse-model for pemphigus using autoantigen knockout mice, in which self-tolerance of the defective gene product is not acquired. When splenocytes from desmoglein3 knockout mice are adoptively transferred into mice expressing desmoglein3, anti-desmoglein3 IgG is stably produced in the recipient mice that develop the phenotype of pemphigus vulgaris. This model will be valuable not only for dissecting the cellular and molecular mechanisms in pathogenic antibody production but also for developing novel therapeutic strategies.
(Keio J Med 51 (3): 133–139, September 2002)

Key words: cadherin, autoantibody, mouse model, desmoglein

Pemphigus as an Autoimmune Disease Against Desmosomal Cadherin

The term pemphigus stems from the Greek *pemphix* meaning blister or bubble and describes a group of chronic blistering skin diseases in which autoantibodies are directed against the cell surface of keratinocytes, resulting in the loss of cell-cell adhesion of keratinocytes through a process called acantholysis.[1] Pemphigus can be divided into three major forms; pemphigus vulgaris, pemphigus foliaceus, and paraneoplastic pemphigus (Table 1).

In pemphigus vulgaris, essentially all patients have mucosal membrane erosions and more than half of them also have skin blisters and erosions. The blisters of pemphigus vulgaris develop in the deeper part of the epidermis, just above the basal cell layer. In pemphigus foliaceus, patients have only cutaneous involvement without mucosal lesions and the splits occur in the superficial part of the epidermis, mostly at the granular layer. Pemphigus vegetans is a vegetative variant of pemphigus vulgaris, and pemphigus erythematosus and fogo selvagem are localized and endemic variants of pemphigus erythematosus, respectively. Paraneoplastic pemphigus was more recently recognized as a disease distinct from the classic forms of pemphigus.[2] Patients with paraneoplastic pemphigus have a known or occult associated neoplasm, usually of lymphoid tissue. Painful severe oral and conjunctival erosions are a prominent feature of paraneoplastic pemphigus.

The hallmark of pemphigus is the finding of IgG autoantibodies against the cell surface of keratinocytes.[3] The pemphigus autoantibodies found in patients' sera play a primary pathogenic role in inducing the loss of

Presented at the 2001 Keio Medical Science Prize Symposium, November 30, 2001.
Reprint requests to: Dr. Masayuki Amagai, Department of Dermatology, School of Medicine, Keio University, 35 Shinanomachi, Shinjuku-ku, Tokyo 160-8582, Japan, e-mail: amagai@sc.itc.med.keio.ac.jp

Table 1 Target Autoantigens in Pemphigus

Subtypes	Antigens	MW
Pemphigus vulgaris		
Mucosal dominant type	desmoglein3	130 kD
Mucocutaneous type	desmoglein3	130 kD
	desmoglein1	160 kD
Pemphigus foliaceus	desmoglein1	160 kD
Paraneoplastic pemphigus	desmoglein3	130 kD
	desmoglein1	160 kD
	plectin/HD1	500 kD
	desmoplakinI	250 kD
	desmoplakinII	210 kD
	BPAG1	230 kD
	envoplakin	210 kD
	periplakin	190 kD
	?	170 kD

* Pemphigus vegetans is a variant of pemphigus vulgaris. Pempigus erythematosus and Brazilian pemphigus (fogo selvagem) is a variant of pemphigus foliaceus.

cell adhesion of keratinocytes with resultant blister formation. Immunochemical characterization of pemphigus antigens by immunoprecipitation or immunoblotting with extracts from cultured keratinocytes or epidermis has demonstrated that the pemphigus vulgaris and foliaceus antigens are 130 kDa and 160 kDa transmembrane glycoproteins, respectively (Table 1).[4–8] Molecular cloning of cDNA encoding pemphigus antigens indicates that both these molecules are members of the cadherin supergene family.[9,10] Pemphigus foliaceus and vulgaris antigens are termed desmoglein1 (Dsg1) and desmoglein 3 (Dsg3), respectively. Thus, pemphigus was discovered to be an anti-cadherin autoimmune disease. The basic pathophysiology of pemphigus is that autoantibodies inhibit the adhesive function of desmogleins and lead to the loss of cell-cell adhesion of keratinocytes with resultant blister formation.

Compelling evidence has accumulated that IgG autoantibodies against Dsg1 and Dsg3 are pathogenic and play a primary role in inducing the blister formation in pemphigus. IgG that is affinity-purified from pemphigus vulgaris sera on the extracellular domain of Dsg3 can cause suprabasilar acantholysis, the typical histologic finding of pemphigus vulgaris, when injected into neonatal mice.[11] Furthermore, when anti-Dsg3 IgG is immunoadsorbed with the extracellular domains of Dsg3 from pemphigus vulgaris sera, those sera no longer have the pathogenic activity to cause blisters in neonatal mice.[12] Similarly, immunoadsorption of pemphigus foliaceus sera with the extracellular domains of Dsg1 eliminates the pathogenic activity of those sera and anti-Dsg1 IgG bound on the column can cause superficial blisters in neonatal mice.[13]

Desmoglein Compensation Theory as an Explanation for Localization of Blisters

The disruption of desmoglein-dependent cell adhesion by autoantibodies is the basic pathophysiology in blister formation of pemphigus, but the clinical spectrum of pemphigus is more complex than this. Splits associated with pemphigus foliaceus occur in the superficial layer of the epidermis, while those of pemphigus vulgaris occur deep in the epidermis. Oral erosions are developed in patients with pemphigus vulgaris, but not in patients with pemphigus foliaceus. Some patients with pemphigus vulgaris have only oral involvement, but others have extensive lesions on both skin and mucous membranes. These complex clinical features of pemphigus are explained logically by the desmoglein compensation theory: *i.e.* Dsg1 and Dsg3 compensates for their adhesive function when they are coexpressed in the same cell (Fig. 1).[14–16]

When pemphigus vulgaris is divided into two subgroups, the mucosal dominant type which is demonstrated by mucosal lesions with minimal skin involvement and the mucocutaneous type which is demonstrated by extensive skin blisters and erosions in addition to mucosal involvement, each subtype of pemphigus has its own anti-desmoglein antibody profile (Table 1). Patients with pemphigus foliaceus have only anti-Dsg1 IgG autoantibodies. Patients with the mucosal dominant type of pemphigus vulgaris have only anti-Dsg3 IgG autoantibodies, while the mucocutaneous type of pemphigus vulgaris has both anti-Dsg3 and anti-Dsg1 IgG autoantibodies.[17] The intraepithelial expression pattern of Dsg1 and Dsg3 are different between skin and the mucous membranes. In the skin, Dsg1 is expressed throughout the epidermis, but more intensely in the superficial layers, while Dsg3 is expressed in the lower part of the epidermis, mainly in the basal and parabasal layers.[18] In contrast, in the mucous membranes, Dsg1 and Dsg3 are expressed throughout the squamous mucosal epithelia, but Dsg1 is expressed at a much lower level than Dsg3.[14]

When sera contain only anti-Dsg1 IgG which interferes with the function of Dsg1, those sera cause blisters only in the superficial epidermis because that is the only area in which Dsg1 is present without coexpression of Dsg3 (Fig. 1A). In the unaffected deep epidermis, the presence of Dsg3 compensates for the loss of function of Dsg1. Although the anti-Dsg1 IgG binds to the mucosa, no blisters are formed because of the coexpression of Dsg3. Thus, sera containing only anti-Dsg1 IgG cause superficial blisters in the skin without mucosal involvement as seen in patients with pemphigus foliaceus. When sera contain only anti-Dsg3 IgG, those sera do not effectively cause blisters in the skin because the co-expressed Dsg1 compensates for

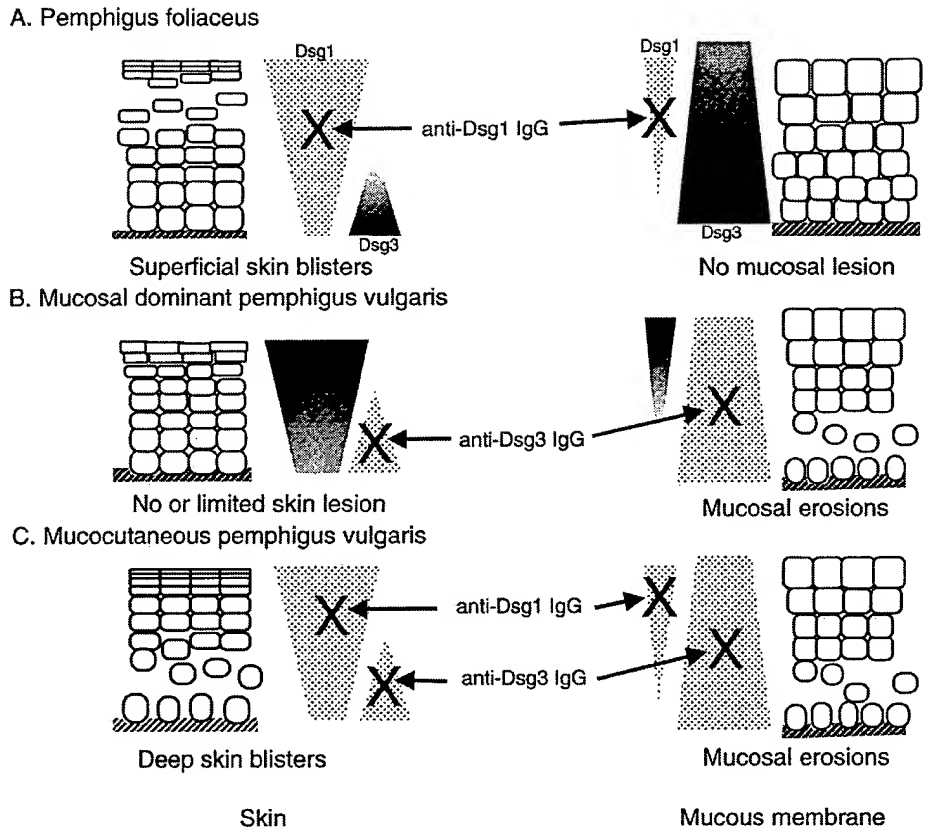

Fig. 1 Explanation of the sites of blisters in pemphigus by the desmoglein compensation theory. The triangles represent the distribution of desmoglein1 (Dsg1) and desmoglein3 (Dsg3) in the skin and mucous membranes. Pemphigus foliaceus sera contain only anti-Dsg1 IgG and cause superficial blisters in the skin because Dsg3 functionally compensates for the impaired Dsg1 in the lower part of the epidermis, while these sera do not cause blisters in the mucous membrane because cell-cell adhesion is mainly mediated by Dsg3 (A). Sera containing only anti-Dsg3 IgG cause no or only limited blisters in the skin because Dsg1 compensates for the loss of the Dsg3-mediated adhesion, whereas those sera induce separation in the mucous membrane where the low expression of Dsg1 will not compensate for the loss of the Dsg3-mediated adhesion (B). When sera contain both anti-Dsg1 and anti-Dsg3 IgG, the function of both Dsgs are compromised and blisters occur both in the skin and mucous membranes (C).

the impaired function of Dsg3, resulting in no or only limited skin blisters (Fig. 1B). In contrast, in mucous membranes, Dsg1 cannot compensate for the impaired Dsg3 function because of its low expression. Therefore, sera containing only anti-Dsg3 IgG cause oral erosions without apparent skin involvement as seen in patients with the mucosal dominant type of pemphigus vulgaris. When sera contain both anti-Dsg1 and anti-Dsg3 IgG, they interfere with the function of both Dsg1 and Dsg3, resulting in extensive blisters and erosions in the skin as well as the mucous membranes, as seen in patients with the mucocutaneous type of pemphigus vulgaris (Fig. 1C). It is not clear why splits occur just above the basal layer instead of the whole keratinocyte falling apart, it is however speculated that the cell-cell adhesion between the basal and parabasal layers might be weaker than the other parts of the epidermis because there are fewer desmosomes. In addition, the lower part of the epidermis might offer better access for autoantibodies penetrating from the dermis.

In pregnant women with pemphigus, autoantibodies cross the placenta and bind to the fetal epidermis. Neonates develop blisters from mothers with pemphigus vulgaris, but very rarely from mothers with pemphigus foliaceus. The reason for this paradoxical observation is also explained by the desmoglein compensation theory.[19] The distribution of Dsg3 in the neonatal epidermis is unlike that in the adult epidermis and is found on the surface of keratinocytes throughout the epidermis, which is more like the distribution in mucous membranes because the neonatal skin was in amnio. Therefore, pemphigus foliaceus sera containing only anti-Dsg1 IgG cannot induce blisters in neonatal skin.

Staphylococcus Aureus Exfoliative Toxin Directly Digests Desmoglein1 in SSSS And Bullous Impetigo

Staphylococcal scalded skin syndrome (SSSS) is a generalized, confluent, superficially exfoliative disease that is caused by the exfoliative toxin (ET, also known as epidermolytic toxin, epidermolysin, and exfoliatin) of *Staphylococcus aureus*. The splits occur in the superficial epidermis, at the level of the granular layer. ET has two major serotypes: A and B (ETA and ETB, respectively). In SSSS, *S. aureus* is present at a distant focus, such as the pharynx, nose, ear, or conjunctiva, and ET produced by *S. aureus* enters the circulation and causes exfoliation at remote sites, while in bullous impetigo, a localized form of SSSS, *S. aureus* is present in the lesions. In 1970, Melish and Glasgow identified the toxin responsible by injecting newborn mice with broth cultures of *S. aureus* isolated from patients with SSSS, resulting in blister formation.[20] However, its mode of action *in vivo* remained an unanswered question for more than three decades.

One day, we realized that SSSS and pemphigus foliaceus share many similar features. Both diseases involve only the skin, and not mucous membranes or other tissues. The histology of both diseases shows superficial epidermal separation where Dsg3 is not co-expressed. Pathology textbooks actually say that the histology of both diseases is indistinguishable. When IgG from PF is injected into neonatal mice, the mice develop blisters. When ET is injected into neonatal mice, the mice also develop blisters. The histology in both mice is essentially identical. These similarities caused us to consider whether the molecular mechanism of blister formation in SSSS was actually similar to that in PF, and we started to investigate the fate of Dsg1 after ET treatment.[21]

We first stained Dsg1 and Dsg3 in mouse skin one hour after injecting ETA into neonatal mice. ETA caused substantial changes in Dsg1 staining, which was much less intense on keratinocyte cell surfaces, while there was no apparent change in Dsg3 staining. We next examined whether Dsg1 is degraded after ETA treatment. We performed an immunoblot analysis for Dsg1, Dsg3, and E-cadherin on extracts of skin from the mice that developed blisters. The 160-kDa Dsg1 was degraded into a peptide of approximately 113 kDa, while there was no degradation of Dsg3 or E-cadherin. To demonstrate direct proteolysis of the extracellular domain of Dsg1 by ETA, we incubated a soluble recombinant form of the extracellular domains of Dsg1 and Dsg3 with ETA *in vitro* (Fig. 2). ETA cleaved the recombinant mouse and human Dsg1 in a dose-dependent fashion, while ETA did not cleave Dsg3 at all. Combined, these findings indicate that ETA specifically recognizes and cleaves the extracellular domain of both mouse and human Dsg1. Subsequently, we also demonstrated that ETB, another major serotype of ET, specifically cleaved Dsg1 in a manner identical to ETA.[22]

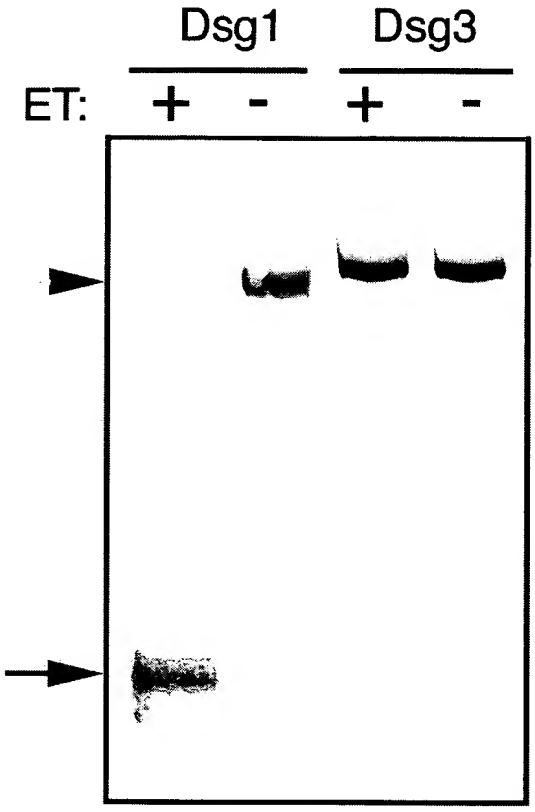

Fig. 2 *In vitro* digestion of the recombinant extracellular domains of human Dsg1 by exfoliative toxin. Dsg1 and Dsg3 extracellular domains produced in baculovirus were incubated with or without exfoliative toxin A (ET) and subjected to immunoblotting to visualize Dsg1 and Dsg3. The toxin cleaved the extracellular domain of Dsg1, but not that of Dsg3. The arrowhead and arrow indicate intact recombinant Dsg1 and the cleaved product, respectively.

These findings provide an important framework to understand the molecular mechanism of blister formation in these diseases, as well as cell-to-cell adhesion of keratinocytes in the epidermis. By bringing dermatological tools to bear on our observations we were thus able to clarify of the molecular mechanism of an exfoliative toxin, which had remained unsolved for three decades after its identification.

A Novel Autoimmune Mouse Model Using the Autoantigen Knockout Mouse

To investigate the pathophysiological mechanisms and to develop therapeutic strategies, animal disease models have been playing important roles in the study

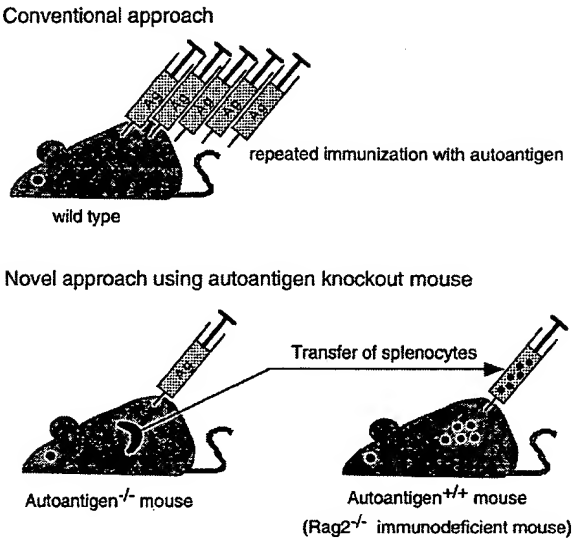

Fig. 3 Methods to develop an active disease mouse models for autoimmune diseases. In the conventional approach (A), various strains of wild type mice are repeatedly immunized with various adjuvants to break their immunological tolerance. In a novel approach (B), splenocytes of autoantigen knockout mice which do not acquire tolerance against the defective gene product are adoptively transferred to mice that express the autoantigen.

of various conditions including autoimmune diseases. To examine the cellular mechanisms of autoantibody production in pemphigus, specimens from patients are naturally the best clinical material, but it is not easy to obtain sufficient amounts with proper controls. To overcome this problem an active disease model is required. The conventional approach to develop an autoimmune mouse model is forced immunization of autoantigens in various strains of mice (Fig. 3A). However, this approach is empirical and immune responses are largely dependent on the strains of mice or types of adjuvant used. Furthermore, any autoimmune reaction in those mice may be transient, unlike that found in patients, and the immune system is systemically stimulated.

The major difficulty in the development of an autoimmune reaction in mice is because of the self-tolerance factor inherent in homeostasis, which prevents the immune system from reacting destructively against self-components. When lymphocytes are exposed to self-components during the development of the immune system, auto-reacting lymphocytes are eliminated or inactivated. We have taken a novel approach to overcome this problem. Because self-tolerance is a technical barrier to the development of autoimmune mouse models we thought of generating a condition where self-tolerance is not established in an antigen-specific way. If it were possible to remove the antigen during the development of the immune system, or if were not present from the start, tolerance against the removed or absent molecule would not be acquired (Fig. 3B). In the autoantigen knockout mouse, lymphocytes are not exposed to the defective gene product, and self-tolerance against that particular autoantigen is not established. Upon immunization with the autoantigen, the autoantigen knockout mice should elicit an immune reaction against the autoantigen. However, in the immunized knockout mice, the antigen-antibody reaction is not expected because the mice lack the target antigen. Therefore, lymphocytes from the immunized autoantigen knockout mice are adoptively transferred to wild type mice that express the autoantigen. The transferred lymphocytes from the autoantigen knockout mice should be persistently stimulated by the endogenous autoantigen in the recipient mice and should therefore produce antibodies against the autoantigen with resultant phenotypes of the human disease.

Pemphigus Mouse Model with Persistent Pathogenic Antibody Production

To develop an active disease mouse model for pemphigus vulgaris, we took this novel approach of using autoantigen knockout mice, in the case of pemphigus vulgaris, $Dsg3^{-/-}$ mice.[23] When we immunized $Dsg3^{-/-}$ mice with mouse recombinant Dsg3, anti-Dsg3 IgG was indeed produced. These sera were able to bind to the cell surfaces of living cultured mouse keratinocytes, indicating that the anti-Dsg3 IgG produced in $Dsg3^{-/-}$ mice is capable of binding to the native Dsg3 on living keratinocytes. In contrast, sera from $Dsg3^{+/-}$ littermates or wild type mice failed to bind to the surface of living keratinocytes. These findings confirmed that $Dsg3^{-/-}$ mice and mice expressing Dsg3 have a clear difference in their ability to produce anti-Dsg3 IgG that can bind to the native Dsg3.[24]

Despite the production of anti-Dsg3 IgG, no autoimmune reaction is expected in the immunized $Dsg3^{-/-}$ mice because they lack the target antigen. To allow the anti-Dsg3 IgG to be exposed to the antigen, we isolated splenocytes from the immunized $Dsg3^{-/-}$ mice and transferred them into $Rag\text{-}2^{-/-}$ immunodeficient mice that do express Dsg3. $Rag\text{-}2^{-/-}$ mice have no mature T or B cells due to the inability to rearrange T cell receptors or immunoglobulin genes and thus are unable to produce antibodies or reject the transferred splenocytes. Circulating anti-Dsg3 IgG was detected in the sera of recipient $Rag\text{-}2^{-/-}$ mice as early as day 4 after the transfer of $Dsg3^{-/-}$ splenocytes, and its titer increased rapidly without further boosting by recombinant Dsg3, and reached a plateau around day 21. The circulating anti-Dsg3 IgG was detected for as long as 6

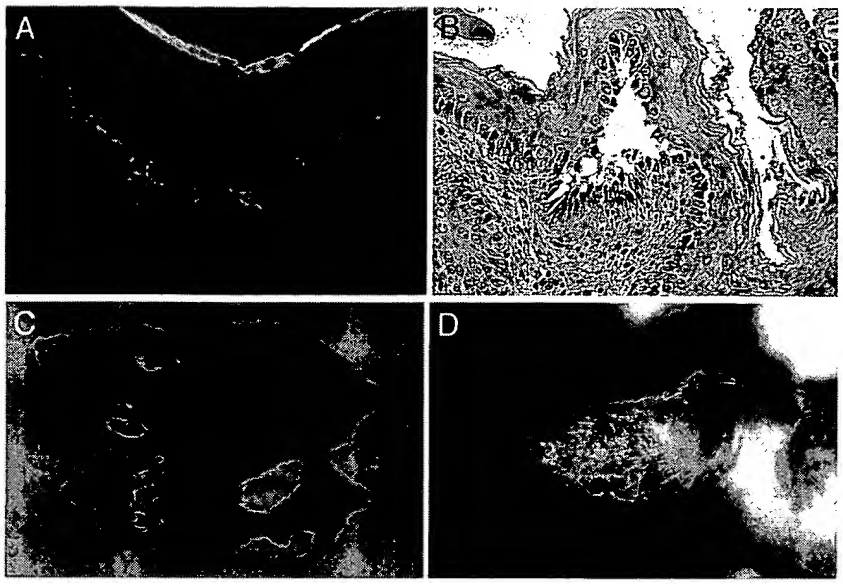

Fig. 4 Phenotype of active disease model mice for pemphigus vulgaris. Recipient mice with Dsg3$^{-/-}$ splenocytes show *in vivo* mouse IgG deposition on keratinocyte cell surfaces (A) and suprabasilar acantholysis (B) just as in patients with pemphigus vulgaris. The recipient mice with Dsg3$^{-/-}$ splenocytes (the lower mouse in C) are smaller than control mice with Dsg3$^{+/-}$ splenocytes (the upper mouse in C) because oral erosions inhibit food intake. Some recipient mice with Dsg3$^{-/-}$ splenocytes show crusted erosions around the snout and cheeks, where mice normally scratch (D).

months or more. No significant reactivity against Dsg1, another desmosomal cadherin targeted in pemphigus foliaceus, was observed in these recipient mice during this period. In contrast, no circulating anti-Dsg3 IgG was detected in Rag-2$^{-/-}$ mice given Dsg3$^{+/-}$ splenocytes. The persistent anti-Dsg3 IgG production indicates that endogenous Dsg3 in the recipient mice stimulated the transferred Dsg3-specific lymphocytes from the immunized Dsg3$^{-/-}$ mice *in vivo*.

In recipient mice with Dsg3$^{-/-}$ splenocytes, *in vivo* IgG deposition was found on keratinocyte cell surfaces in stratified squamous epithelia, including the skin and oral and esophageal mucous membranes, just as seen in patients with pemphigus vulgaris (Fig. 4A). In these mice, no IgG deposition was found in other tissues, including heart, lung, liver, kidney, stomach, and small and large intestines. These IgG binding sites correspond to the known tissue distribution of Dsg3. Histological examination of the recipient mice revealed an intraepithelial loss of cell-cell adhesion just above the basal layers, *i.e.*, suprabasilar acantholysis, in the buccal mucosa, hard palate, oropharyngeal areas, and the upper part of the esophagus, just as in human patients (Fig. 4B). These oral erosions likely inhibited food intake, resulting in the weight loss (Fig. 4C). Some of the recipient mice developed crusted erosions on the skin around the snout, an area that is normally traumatized by scratching (Fig. 4D). Close histological examination revealed that the recipient mice with Dsg3$^{-/-}$ splenocytes also exhibited eosinophilic spongiosis which is often found in patients with early lesions.[25] We also observed patchy hair loss in the recipient mice with Dsg3$^{-/-}$ splenocytes. This hair loss phenotype also persisted for over 6 months. Skin biopsy showed intense IgG deposition on the cell surface of keratinocytes surrounding the telogen hair club. Cleft formation was observed between the cells surrounding the telogen club and the basal layer of the outer root sheath epithelium. In contrast, no phenotypic or pathological changes were observed in recipient mice with Dsg3$^{+/-}$ splenocytes. These results indicate that the Rag-2$^{-/-}$ recipient mice given immunized Dsg3$^{-/-}$ splenocytes developed clinical, histologic and immunopathologic phenotypes similar to those of patients with pemphigus vulgaris.[24]

A major hurdle in developing animal models of autoimmune diseases has been overcoming the self-tolerance component of the homeostatic system. We circumvented this problem by immunizing autoantigen knockout mice with the autoantigen, then transferring their splenocytes to Rag-2$^{-/-}$ mice that expressed the autoantigen. Although this model does not reflect the actual triggers of autoimmune diseases, it does provide a means to investigate the roles of T and B lymphocytes in perpetuating autoantibody production in the autoimmune response.[26] We are also attempting to isolate

a panel of monoclonal anti-Dsg3 IgG antibodies from pemphigus model mice, and investigate their pathogenic strength to clarify what factor(s) determines the severity of the disease. In addition, this active animal model should be beneficial for evaluating various therapeutic strategies that could modulate the autoimmune response. Finally, our approach is widely applicable to various antibody-mediated and T cell-mediated autoimmune diseases, unless the relevant autoantigen knockout mice are embryonicaly lethal or show gross abnormalities in their immune systems.

Acknowledgements: I acknowledge a deep debt of gratitude to Dr. Takeji Nishikawa for his generous support and guidance and Dr. John R. Stanley for his collaboration and stimulating discussion throughout the course of the studies mentioned in this manuscript. The pemphigus mouse model was developed with collaboration with Dr. Shigeo Koyasu. The works mentioned in this article were supported by Keio Gijuku Academic Development Funds, Health Sciences Research Grants for Research on Specific Diseases from Ministry of Health, Labour and Welfare, and a Grant-in-Aid for Scientific Research from the Ministry of Education, Culture, Sports, Science and Technology of Japan.

References

1. Stanley JR: Pemphigus. In: Freedberg IM, Eisen AZ, Wolff K, *et al*, eds, Dermatology in General Medicine, 4th ed., New York, McGraw-Hill, 1998; 654–666
2. Anhalt GJ, Kim S, Stanley JR, Korman NJ, Jabs DA, Kory M, Izumi H, Ratrie H, Mutasim D, Ariss AL *et al*: Paraneoplastic pemphigus. An autoimmune mucocutaneous disease associated with neoplasia. N Engl J Med 1990; 323: 1729–1735
3. Beutner EH, Jordon RE: Demonstration of skin antibodies in sera of pemphigus vulgaris patients by indirect immunofluorescent staining. Proc Soc Exp Biol Med 1964; 117: 505–510
4. Stanley JR, Yaar M, Hawley NP, Katz SI: Pemphigus antibodies identify a cell surface glycoprotein synthesized by human and mouse keratinocytes. J Clin Invest 1982; 70: 281–288
5. Stanley JR, Koulu L, Thivolet C: Distinction between epidermal antigens binding pemphigus vulgaris and pemphigus foliaceus autoantibodies. J Clin Invest 1984; 74: 313–320
6. Eyre RW, Stanley JR: Human autoantibodies against a desmosomal protein complex with a calcium-sensitive epitope are characteristic of pemphigus foliaceus patients. J Exp Med 1987; 165: 1719–1724
7. Eyre RW, Stanley JR: Identification of pemphigus vulgaris antigen extracted from normal human epidermis and comparison with pemphigus foliaceus antigen. J Clin Invest 1988; 81: 807–812
8. Hashimoto T, Ogawa MM, Konohana A, Nishikawa T: Detection of pemphigus vulgaris and pemphigus foliaceus antigens by immunoblot analysis using different antigen sources. J Invest Dermatol 1990; 94: 327–331
9. Koch PJ, Walsh MJ, Schmelz M, Goldschmidt MD, Zimbelmann R, Franke WW: Identification of desmoglein, a constitutive desmosomal glycoprotein, as a member of the cadherin family of cell adhesion molecules. Eur J Cell Biol 1990; 53: 1–12
10. Amagai M, Klaus-Kovtun V, Stanley JR: Autoantibodies against a novel epithelial cadherin in pemphigus vulgaris, a disease of cell adhesion. Cell 1991; 67: 869–877
11. Amagai M, Karpati S, Prussick R, Klaus-Kovtun V, Stanley JR: Autoantibodies against the amino-terminal cadherin-like binding domain of pemphigus vulgaris antigen are pathogenic. J Clin Invest 1992; 90: 919–926
12. Amagai M, Hashimoto T, Shimizu N, Nishikawa T: Absorption of pathogenic autoantibodies by the extracellular domain of pemphigus vulgaris antigen (Dsg3) produced by baculovirus. J Clin Invest 1994; 94: 59–67
13. Amagai M, Hashimoto T, Green KJ, Shimizu N, Nishikawa T: Antigen-specific immunoadsorption of pathogenic autoantibodies in pemphigus foliaceus. J Invest Dermatol 1995; 104: 895–901
14. Shirakata Y, Amagai M, Hanakawa Y, Nishikawa T, Hashimoto K: Lack of mucosal involvement in pemphigus foliaceus may be due to low expression of desmoglein1. J Invest Dermatol 1998; 110: 76–78
15. Mahoney MG, Wang Z, Rothenberger KL, Koch PJ, Amagai M, Stanley JR: Explanation for the clinical and microscopic localization of lesions in pemphigus foliaceus and vulgaris. J Clin Invest 1999; 103: 461–468
16. Amagai M: Autoimmunity against desmosomal cadherins in pemphigus. J Dermatol Sci 1999; 20: 92–102
17. Amagai M, Tsunoda K, Zillikens D, Nagai T, Nishikawa T: The clinical phenotype of pemphigus is defined by the anti-desmoglein autoantibody profile. J Am Acad Dermatol 1999; 40: 167–170
18. Amagai M, Koch PJ, Nishikawa T, Stanley JR: Pemphigus vulgaris antigen (Desmoglein3) is localized in the lower epidermis, the site of blister formation in patients. J Invest Dermatol 1996; 106: 351–355
19. Wu H, Wang ZH, Yan A, Lyle S, Fakharzadeh S, Wahl JK, Wheelock MJ, Ishikawa H, Uitto J, Amagai M *et al*: Protection against pemphigus foliaceus by desmoglein3 in neonates. N Engl J Med 2000; 343: 31–35
20. Melish ME, Glasgow LA: The staphylococcal scalded skin syndrome: Development of an experimental model. N Engl J Med 1970; 282: 1114–1119
21. Amagai M, Matsuyoshi N, Wang ZH, Andl C, Stanley JR: Toxin in bullous impetigo and staphylococcal scalded skin syndrome targets desmoglein1. Nature Medicine 2000; 6: 1275–1277
22. Amagai M, Yamaguchi T, Hanakawa Y, Nishifuji K, Sugai M, Stanley JR: Staphylococcal Exfoliative Toxin B Specifically Cleaves Desmoglein1. J Invest Dermatol 2002; 118: 845–850
23. Koch PJ, Mahoney MG, Ishikawa H, Pulkkinen L, Uitto J, Shultz L, Murphy GF, Whitaker-Menezes D, Stanley JR: Targeted disruption of the pemphigus vulgaris antigen (desmoglein3) gene in mice causes loss of keratinocyte cell adhesion with a phenotype similar to pemphigus vulgaris. J Cell Biol 1997; 137: 1091–1102
24. Amagai M, Tsunoda K, Suzuki H, Nishifuji K, Koyasu S, Nishikawa T: Use of autoantigen knockout mice to develop an active autoimmune disease model of pemphigus. J Clin Invest 2000; 105: 625–631
25. Ohyama M, Amagai M, Tsunoda K, Ota T, Koyasu S, Umezawa A, Hata J, Nishikawa T: Immunologic and histopathologic characterization of active disease mouse model for pemphigus vulgaris. J Invest Dermatol 2002; 118: 199–204
26. Tsunoda K, Ota T, Suzuki H, Ohyama M, Nagai T, Nishikawa T, Amagai M, Koyasu S: Pathogenic autoantibody production requires loss of tolerance against desmoglein 3 in both T and B cells in experimental pemphigus vulgaris. Eur J Immunol 2002; 32: 627–633